JOURNAL OF ATMOSPHERIC AND TERRESTRIAL PHYSICS

EDITORIAL ADVISORY BOARD

H. O. G. ALFVÉN-STOCKHOLM · **J. BARTELS**-GÖTTINGEN **W. J. G. BEYNON**-ABERYSTWYTH · **P. M. S. BLACKETT**-LONDON · **E. G. BOWEN**-SYDNEY · **SIR DAVID BRUNT**-LONDON · **R. BUREAU**-BAGNEUX · **S. CHAPMAN**-ALASKA · **J. EGEDAL**-COPENHAGEN · **V. F. HESS**-NEW YORK · **E. O. HULBURT**-WASHINGTON, D.C. **H. ISRAEL**-AACHEN · **D. K. MENZEL**-CAMBRIDGE, MASS. · **S. K. MITRA**-CALCUTTA · **M. NICOLET**-UCCLE · **E. H. NORINDER**-UPSALA · **B. van der POL**-GENEVA · **N. V. PUSHKOV**-MOSCOW · **J. A. RATCLIFFE**-CAMBRIDGE · **O. E. H. RYDBECK**-GOTHENBURG · **SIR GEORGE SIMPSON**-LONDON · **H. SOLBERG**-OSLO · **J. VELDKAMP**-DE BILT · **M. WALDMEIER**-ZÜRICH · **J. ZENNECK**-ALTHEGNENBERG

VOL.
13
58/59

EDITOR-IN-CHIEF

SIR EDWARD APPLETON, F.R.S.

EDINBURGH

VOLUME 13

1958–9

PERGAMON PRESS

LONDON • NEW YORK • PARIS • LOS ANGELES

J. Atmosph. Terr. Phys.

VOL.
13
1958/5

CONTENTS

Nos. 1/2

E. Harnischmacher and K. Rawer: Drift observations evaluated by the method of "similar fades" 1

J. E. Titheridge: Variations in the direction of arrival of high-frequency radio waves . . 17

V. Marasigan, S.J.: Bifurcations in the *F*-region at Baguio, 1952–1957 26

M. W. Chiplonkar and V. N. Athavale: Simultaneous recording of atmospherics on four different frequency bands in the low-frequency region 32

B. A. P. Tantry and R. S. Srivastava: Waveforms of atmospherics with superimposed pulses recorded with an automatic atmospheric recorder 38

J. C. Bhattacharyya: Non-uniformity in the brightness of the sun's disc at sunspot minimum 43

A. Vallance Jones and A. W. Harrison: $^1\Delta_g$–$^3\Sigma_g^-$ O_2 Infrared emission band in the twilight airglow spectrum 45

G. R. Ellis: The trapping of cosmic radio waves beneath the ionosphere 61

H. A. Whale and L. M. Delves: Some relations between the bearing and amplitude of a fading radio wave 72

S. Chapman and K. Davies: On the approximate daytime constancy of the absorption of radio waves in the lower ionosphere 86

J. C. Brandt and J. W. Chamberlain: Resonance scattering by atmospheric sodium—V. Theory of the day airglow 90

J. C. Brandt: Resonance scattering by atmospheric sodium—VI. The analytic solution for the twilight intensity 99

V. Marasigan, S.J.: Height-gradient of electron-loss in the *F*-region 107

F. E. Roach, E. Tandberg-Hanssen and L. R. Megill: The characteristic size of airglow cells 113

F. E. Roach, E. Tandberg-Hanssen and L. R. Megill: Movements of airglow cells . . 122

J. O. Thomas and A. Robbins: The electron distribution in the ionosphere over Slough—II. Disturbed days 131

F. Horner: The relationship between atmospheric radio noise and lightning 140

J. L. Wolfe: Satellite tracking by H.F.D.F. 155

Research Notes:

T. M. Donahue and D. M. Hunten: The correction of sodium twilight-glow observations 165

W. Stoffregen: Radio reflections on low frequencies from 75 to 90 km height during intense aurora activity 167

N. C. Gerson: Very long-distance ionospheric propagation 169

H. G. Möller: Further results of sweep frequency oblique incidence experiments . . . 173

H. J. Albrecht: On instrument effects in ionospheric data 173

S. A. Bowhill: The Faraday-rotation rate of a satellite radio-signal 175

M. R. Kundu and J. R. Denisse: Solar radiation on decimeter waves as an index for ionospheric studies 179

W. J. G. Beynon and G. L. Goodwin: Horizontal drifts and temperature in the lower part of region-*E* 180

R. S. Macmillan, W. V. T. Rusch and R. M. Golden: A new antenna to eliminate ground-wave interference in ionospheric sounding experiments 183

B. Maehlum: The diurnal variation of f_0F2 near the auroral zone during magnetic disturbances 187

B. N. Singh and R. L. Ram: A peculiar type of periodic fading 190

W. Dieminger, H. G. Möller and G. Rose: Long-distance single *F*-hop transmission . 191

K. A. Sarada: Sudden cosmic noise absorption associated with the solar event of 23rd March, 1958 192

D.S.I.R., Slough: Electron density profiles in the ionosphere during the I.G.Y. . . . 195

K-indices of geomagnetic activity from the observatories at Hartland, Eskdalemuir and Lerwick for March to June, 1958 198

Papers to be published in future issues 200

Nos. 3/4

R. Satyanarayana, K. Bakhru and S. R. Khastgir: Triple-splitting of the *F*-echoes . . 201

E. B. Armstrong: The temperature in the atmospheric region emitting the nightglow OI 5577 line and in regions above faint auroral arcs 205

R. W. Wright and N. J. Skinner: Lunar tides in the sporadic *E*-layer at Ibadan . . . 217

C. A. Onwumechilli: A study of the equatorial electrojet—I. An experimental study . . 222

C. A. Onwumechilli: A study of the equatorial electrojet—II. A model electrojet that fits H observations 235
H. A. Whale: The effects of ionospheric irregularities and the auroral zone on the bearings of short-wave radio signals 258
M. N. Rao and A. P. Mitra: Effect of vertical drifts on the nocturnal ionization of the lower ionosphere 271
A. W. Harrison and A. Vallance Jones: Observations of Meinel N_2 bands near 1·5 μ in the auroral spectrum 291
J. A. Thomas and E. K. Smith: A survey of the present knowledge of sporadic-*E* ionization . 295
C. Collins and P. A. Forsyth: A bistatic investigation of radio-aurora 315
C. M. Minnis: Ionospheric changes at Singapore during the solar eclipse of 14th December 1955 346
B. Peters: Cosmic ray produced radioactive isotopes as tracers for studying large-scale atmospheric circulation 351

Research Notes:

H. Helm, J. W. King and A. M. van Wijk: Measurements of magnetic declination during the solar eclipse of October 23rd 1957 371
C. H. Cummack: A comparison of the critical frequency of the *F2*-layer between Rarotonga and Maui 372
J. Verö: Earth current variations of different period in the observatorium near Nagycenk . 375
J. A. Thomas and F. Hibberd: Satellite Doppler measurements and the ionosphere . . 376
A. Haubert: Le renforcement du champ en ondes longues et les evanouissements en ondes courtes 379

Letter to the Editor:

R. Silberstein: The origin of the current nomenclature for the ionospheric layers . . 382

Book Reviews:

"Handbuch der Physik, Band XXII" Edited by S. Flügge (Reviewed by W. E. J. Farvis) 383
"Fundamentals of Sonar" by J. W. Horton (Reviewed by W. A. Lynch) 383
"Advances in Geophysics, Volume 4" Edited by H. E. Landsberg and J. van Mieghem (Reviewed by E. V. Appleton) 384

K-indices of geomagnetic activity for July, August and September 1958 385
Papers to be published in future issues 387

VOL.
13
1958/5

AUTHOR INDEX

(B.R.) denotes a book review

Albrecht H. J. 173
Appleton E. V. (B.R.) 384
Armstrong E. B. 205
Athavale V. N. 32
Bakhru K. 201
Beynon W. J. G. 180
Bhattacharyya J. C. 43
Bowhill S. A. 175
Brandt J. C. 90, 99
Chamberlain J. W. 90
Chapman S. 86
Chiplonkar M. W. 32
Collins C. 315
Cummack C. H. 372
Davies K. 86
Delves L. M. 72
Denisse J. R. 179
Dieminger W. 191
Donahue T. M. 165
Ellis G. R. 61
Farvis W. E. J. (B.R.) 383
Forsyth P. A. 315
Gerson N. C. 169
Golden R. M. 183
Goodwin G. L. 180
Harnischmacher E. 1
Harrison A. W. 45, 291
Haubert A. 379
Helm H. 371
Hibberd F. 376
Horner F. 140
Hunten D. M. 165
Jones A. Vallance 45, 291
Khastgir S. R. 201
King J. W. 371
Kundu M. R. 179
Lynch W. A. (B.R.) 383
Macmillan R. S. 183
Maehlum B. 187
Marasigan V. 26, 107
Megill L. R. 113, 122
Minnis C. M. 346
Mitra A. P. 271
Möller H. G. 173, 191
Onwumechilli C. A. 222, 235
Peters B. 351
Ram R. L. 190
Rao M. N. 271
Rawer K. 1
Roach F. E. 113, 122
Robbins A. 131
Rose G. 191
Rusch W. V. T. 183
Sarada K. A. 192
Satyanarayana R. 201
Silberstein R. 382
Singh B. N. 190
Skinner N. J. 217
Smith E. K. 295
Srivastava R. S. 38
Stoffregen W. 167
Tandberg-Hanssen E. 113, 122
Tantry B. A. P. 38
Thomas J. A. 295, 376
Thomas J. O. 131
Titheridge J. E. 17
Verö J. 375
Whale H. A. 72, 258
Wijk A. M. van 371
Wolfe J. L. 155
Wright R. W. 217

Journal of Atmospheric and Terrestrial Physics, 1958, Vol. 13, pp. 1 to 16. Pergamon Press Ltd., London

Drift observations evaluated by the method of "similar fades"

E. HARNISCHMACHER and K. RAWER
Ionosphären-Institut
im Fernmeldetechnischen Zentralamt der Deutschen Bundespost
Breisach b. Freiburg im Br., Germany

(*Received* 24 *January* 1958)

Abstract—A regular interference model of the fading pattern is considered as opposed to the usually accepted purely random model. It would appear that some of the observed features are well explained by a model which is intermediate between these two types insofar as regular interference perturbations are concerned, but one in which a finite lifetime for the irregularities is supposed. It appears that with the "similar fade" analysis there is a marked tendency to select those periods where the interference is quite regular and the rather small angular dispersion found in most sets of observations can thus be explained.

The observed big dispersion of the speed is at least partially due to a small vertical component of the movement.

INTRODUCTION: "METHOD OF SIMILAR FADES" AND "CORRELATION METHOD"

FOR the analysis of ionospheric drift observations with the KRAUTKRÄMER (1950) arrangement two basically different methods are used. That of KRAUTKRÄMER himself starts with the identification of certain typical forms of fading maxima or minima in the three traces and from the differences between the times of their appearance in the traces the apparent drift vector is obtained. The second method is a statistical approach in which the auto- and cross-correlations between the amplitude functions obtained at the three antennae are compared. For an accurate application, correlation functions with variable time-shift must be calculated (BRIGGS, 1950) but this is very troublesome; since one obtains not only the apparent drift vector but also the mean turbulent motion of the fading pattern. YERG (1955, 1956) has introduced a simplified form of this method in which only one time difference is involved which may correspond to that obtained from the distance of antennae and the mean drift velocity. We may call the first method the "similar fade method" and the second the "correlation method".

The great majority of actual observations has been evaluated with the "similar fade method" because of its simplicity. On the other hand the "correlation method" is a more general approach, its basis being a random distribution of amplitudes which is only assumed to be isotropic (SALES, 1956). Such a distribution will result from the interference of many rays slightly different in direction. On the contrary the "similar fade method" will be adequate in the case of the interference of only a few rays, say two or three. In this case clear field strength minima appear as a result of interference and the corresponding pattern differs from a random pattern by a certain regularity in the interference fringes.

One might anticipate that experience would easily distinguish between the two forms of analysis but unfortunately, practically all observations have been obtained with the KRAUTKRÄMER method using three antennae only. This is the minimum number required to obtain the wind vector and further information on

the pattern could only be deduced by statistical methods. A direct check of the form of the pattern could be obtained with four or more antennae.

Another point seems to us to be most important. When using the "similar fade method" on the recorded traces over a period of, say, 10 or 12 min, one selects between six and twelve typical forms. Now it may well be that for the selected features some simple form of interference is actually present which is not characteristic of the whole period. Hence although the general behaviour of the pattern during the period as a whole may often be nearly random we feel that by sampling distinct minima, one may in fact be selecting just those features which do not fit with a random model. Hence it may be that the application of both methods can

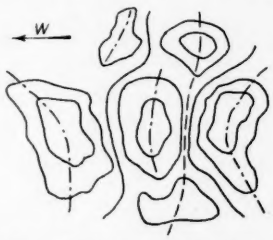

Fig. 1. Random field strength pattern (full lines) and extremal line (broken lines)

be justified, the more general "statistical" one corresponding to the overall behaviour whilst the "selected fading method" applies just to those cases for which a more simple model is appropriate. It must also be admitted that instantaneously well-defined fading fringes which vary rapidly during the period of observation may behave like a random pattern for a statistical analysis covering the whole period.

1. The Method of Similar Fades

It is of interest to discuss both models and their results for the case in which the simple "method of similar fades" is used.

1.1. *Random patterns*

The case of the random pattern which is obtained by interference of many rays has been considered by Ratcliffe (1954) and Pütter (1954). This analysis shows that the observed characteristic amplitude features depend on the movement of the so-called "extremal lines" of the pattern. The apparent drift is only that component of the real velocity of the pattern which is orthogonal to the direction of the "extremal lines". Thus the "direction error" (difference between the apparent direction and the real one) may be as much as $\pm 90°$; furthermore the end-points of the apparent drift vectors should lie on a circle the diameter of which is the real drift vector ("Ratcliffe–Pütter-circle"). As the "extremal lines" are not independent of the direction of the real movement there will be some preference for smaller direction errors (Berg, 1957) (Fig. 1). A "Monte Carlo test" with artificial random patterns (Briggs and Page, 1954) gives an error probability function of approximately Gaussian type with quartile ranges of $\pm 26°$. Some trials have been made with actual observations of selected fading to test whether

VOL
13
1958/

the "Ratcliffe–Pütter-circle" (BERG, 1957; HARNISCHMACHER and RAWER, 1956) is obtained, but these have completely failed, since only a small percentage of all cases correspond to a circle. Thus some other influence must exist. This cannot merely be a perturbation effect such as a general turbulent motion because in that case the dispersion of observed values should increase, in any case it should not be inferior to that of the random model. However, at least insofar as direction is concerned, this is just what is observed. The dispersion of the direction error has been found to be (HARNISCHMACHER and RAWER, 1956) $\pm 20°$ for the quartile ranges and $\pm 41°$ for the decile ranges and this is somewhat smaller than would be expected from a random model (BRIGGS and PAGE, 1954).

1.2. *Fringe patterns*

Consider now the case of interference fringes. We take an over simplified model with two rays only, one vertical and another slightly different in direction coming from some deformation of the reflecting layer. Geometrical ray considerations are adopted and diffraction effects are neglected.

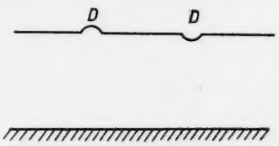

Fig. 2. Two simple types of deformation: "hole" and "blob"

1.2.1. *The range of interference.* In the first place the range over which such a deformation can give rise to an oblique ray path is delineated by the form of the deformation itself. This at least is valuable within the limits of geometrical optics. It is improbable that large deformation will be of frequent occurrence, and we therefore suppose that in the distorted region of the ionosphere, the normal to the surface of constant ionization is not inclined to the vertical by an angle greater than γ. We consider two different types of deformations of the surfaces of equal ionization, one which may be approximated by a point and another which resembles a straight line. The first may be thought of as having the form of part of a sphere forming a "hole" or a "blob" in an otherwise plane surface of constant ionization (Fig. 2). The second type of irregularity has the same section but is of cylindrical form with its axis horizontal.

The deformation will of course affect every ray which reaches the required level. With the first type the effect on a narrow bundle of rays will give rise to a diffuse cone of reflected rays, the width of which, for a given direction of the incident beam, will be $\pm 2\gamma$. With the second type of irregularity the reflected rays from each incident narrow-bundle will form a diffuse flat fan in the plane of incidence, the width being also $\pm 2\gamma$. Since there is an infinity of incident rays this irregularity will result in a straight band on the ground. Thus at oblique incidence a deformation is effective if it is situated in the vicinity of the "normal reflection point" and it will give rise to an elliptical pattern in the first case, and to a straight line in the second. In drift work we are concerned with nearly vertical incidence. The intersection of the diffuse cone or fan with the ground

plane defines the range where an interference pattern is observed. For the first type the limit is practically a circle (BERG, 1957) [(Fig. 3(a)]; in the second case it is a straight line [Fig. 3(b)]. The position of the range at which interference occurs varies with the position of the irregularity relative to the transmitter. No interference is observed in the vicinity of the transmitter if the direct ray to the irregularities has a greater angle of incidence than γ (Fig. 4): The condition for the existence of an interference pattern is thus that the deformation be not

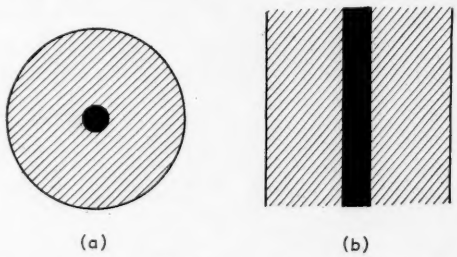

Fig. 3. Effective range of a deformation (a: point b: line-deformation)

too far distant: $d \leqslant h \tan \gamma = d_{\max}$. With the usual arrangement, in which the receiving antennae are very near to the transmitter, irregularities outside the circle of radius $d_{\max}$ drawn around the transmitter are not observed.

The size of the interference range depends essentially on γ. From the work of BRAMLEY and ROSS (1951) on the direction of the reflected beam we may take a value of this limiting angle which is of the order of 0·1 (6°). (A value of 0·2

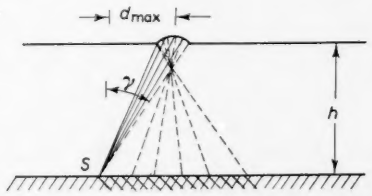

Fig. 4. Scatter-cone from the deformation (limiting angle γ)

will be rather rare). Thus $d_{\max}$ is about 10 km for reflections from the E-layer.

1.2.2. *The fringe system.* If an irregularity is present in the range considered, then there will be two rays reflected from the ionosphere, a "normal" one and another coming from the irregularity. With both rays an interference pattern forms which is essentially a system of fringes. The form of these fringes depends on the type of the irregularity. With the first type a system of ellipses appears; as the rays are nearly vertical it can well be approximated by a system of concentric circles with the "image" of the transmitter as centre (Fig. 5). The distance ϵ of subsequent zero-fringes is given by (see Appendix A):

$$\epsilon = \sqrt{(r_n^2 + 2h \,.\, \lambda)} - r_n \simeq 2d \left\{ \sqrt{\left(1 + \frac{h \,.\, \lambda)}{2d^2}\right)} - 1 \right\}$$

Thus in the vicinity of the transmitter the fringes on the ground are normal to

the direction from the transmitter to the projection of the deformation. The distance between subsequent fringes, ϵ increases if the distance d between the transmitter and the deformation decreases (with $H = 100$ km, $\lambda = 0{\cdot}2$ km we have $\epsilon = 1$ km for $d = 10$ km but $\epsilon = 6{\cdot}3$ km for $d = 0$).

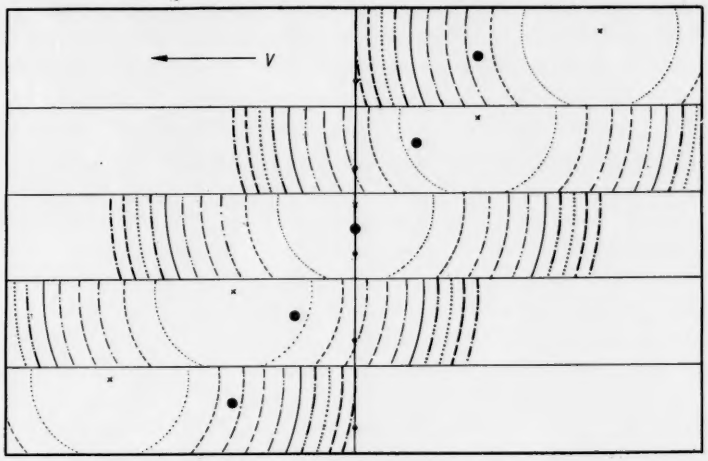

Fig. 5. Transition of a point-deformation (large black point, going from right to left) and corresponding interference lines: subsequent phases are given by the five pictures (beginning with the top picture). (Small circle: transmitter; small star: centre of interference figure)

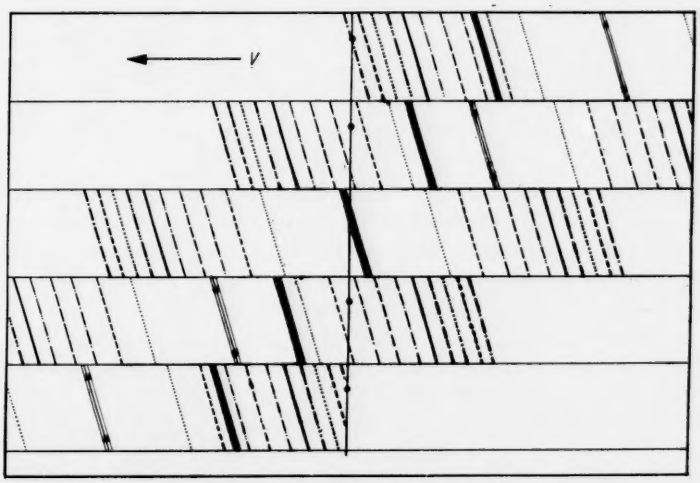

Fig. 6. Transition of a line-deformation (details see Fig. 5)

Similar results are obtained in the second case (Appendix B), only the fringes are now straight lines parallel to the deformation (Fig. 6). The distance between successive fringes in the vicinity of the transmitter is the same as with the first model.

1.2.3. *Travelling irregularities.* Let us now consider an irregularity of the

first type which travels with constant horizontal velocity v across the effective range of the transmitter. The fringes appear only when the irregularity reaches the distance d_{max}. Then initially we have a rather dense fringe system which gradually becomes less and less dense until the irregularity comes nearest to the transmitter and then becoming denser again as it moves away. Thus the most interesting fading pattern occurs with the deformation at a rather large distance (Fig. 5). The form of the pattern undergoes systematic changes during the period of observation and this is an important difference from a pure random model.

Now what is observed is the apparent movement of the interference minima (or maxima) across the antenna system, and one sees at once from our model that only the component which is perpendicular to the interference fringes can be observed; this has been stated in a general form by RATCLIFFE (1954) and PÜTTER (1954). At large distances the angle between the fringes and the drift of the pattern is nearly $\frac{1}{2}\pi$ but when the irregularity is at the minimum distance, it is zero. This is characteristic for the "point-type" irregularity; with the "line-type" there is no variation at all of this angle (Fig. 6).

The *apparent direction* of the movement of the pattern, w, is deduced from the time differences at different antennae; it is orthogonal to the fringes (Appendices A and B). The same result is obtained, whether the calculation is made for three antennae in a fixed position, or whether a system of two antennae which can be directed normally to the fringes is assumed. With the latter system, calculations are much simpler. For the first model it follows that the apparent direction is not at all the direction of the movement of the irregularity but simply the direction from the transmitter to the projection on the ground of the irregularity. Hence, the apparent direction is dependent on the path of the irregularity through the effective range. It is nearest to the real direction of the movement, v, at the beginning and at the end of this path and only for an irregularity which goes straight across the transmitter is the direction of w always the same as that of v.

In the case of the other model, w is always perpendicular to the line of the irregularity (Fig. 6); the apparent direction is thus constant depending only upon the angle between the real movement v and the line of the irregularity. It is clear that only the component of v which corresponds to a right angle can be observed, and a movement along the line cannot be detected. If the real movement were perpendicular to the extension of the deformation, w and v would have the same direction. In any case, for the second model a smaller dispersion of observed direction values will be obtained if some preference or relation existed between the direction of the real movement, v, and the direction of the axis of the irregularities. The amplitude of the apparent drift vector also appears to be dependent on the position of the irregularities, at least for our first model. In this case the apparent direction and amplitude show a clear relation corresponding exactly to the Ratcliffe–Pütter-circle (Appendix A). With the second model no variation at all is found, the apparent drift vector being equal to that component of the real movement which is orthogonal to the axis of the irregularity.

1.2.4. *The statistics of apparent drift movement.* Consider now a constant, uniform movement v. Deformations form and disappear again in the layer;

VOL
13
1958/

the corresponding interference fringes move over the ground, and their apparent movement, w, is observed. There is no reason why the position of a disturbance should not be random, its movement being supposed to correspond to the constant velocity v. Hence for the first model we have equal probability for all values of the polar distance, d_0. On the other hand the density of the interference lines depends markedly on the position of the deformation. Thus the probability of obtaining a fading minimum is roughly proportional to cos χ where χ is the angle between v and w (Appendix A). We now suppose that the deformations are not stable over a long time but have a finite lifetime. For a mean lifetime T, the

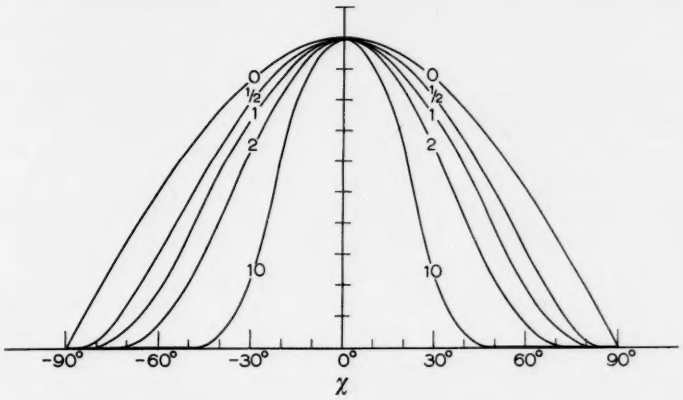

Fig. 7. Probability of observing an angle χ between w and v. (Parameter of the curves: $1/2v\ T$, T mean lifetime of a deformation The curves have been reduced to 1 at $\chi = 0$)

probability of observing two interference minima (with a time difference τ) is exp $(-\tau/\mathrm{T})$. On the average we may use this factor to take account of the decrease of probability. The method of calculating the probability w, of observing a minimum is given in Appendix A, and the result is given in Fig. 7 as an integrated probability for different values of the parameter T. With our model, to each value of χ there corresponds a certain value of the apparent velocity w and the probability of the direction χ may be transformed into that of the amplitude $|w|$. The distribution of directions, as given by one of the curves of Fig. 7 corresponds quite closely to the observations where a quartile range of $\pm 21°$ has been found. (At least this is the case if no account is taken of the random amplitude dispersion which has not yet been explained.)

The same calculation has been made for the second model (Appendix B). Here the direction and amplitude of w vary according to the Ratcliffe–Pütter-circle, provided the direction of the different deformation lines is at random. In this special case, the fringe density, being dependent only on the distance d from the sender, cannot give different probabilities for different directions of w, but some differentiation is introduced by the lifetime of the irregularity since the apparent velocity varies with cos χ. We do not think that a random distribution of the deformation lines is the only possible hypothesis. According to their physical origin some relation between their direction and that of v, i.e. between

w and v, should not be excluded and in such cases a further concentration of w-values somewhere on the Ratcliffe–Pütter-circle should result.

1.3. *Vertical movement of deformations*

In our study of interference patterns we have always found that the Ratcliffe–Pütter-circle should, in principle, be valuable for w but as shown in Section (2) the probability distribution has been found to be dependent on the type of model, giving a statistical preference for the higher w-values with directions near that of v (i.e. for small values of χ).

Now the observations show a high degree of amplitude dispersion of w which has not been explained, either by random or by fringe models. Such a variation could of course be explained by turbulent motions or also by a vertical velocity gradient, if the deformation appeared at different heights. [This latter hypothesis is only helpful if a considerable gradient is assumed but in this connexion it is to be noted other observations show that quite rapid vertical movements of deformations exist (BIBL, 1953)]. These of course, must influence the movement of the interference pattern on the ground but an important effect only occurs if the normal echo and that coming from the deformation behave in a different manner. In Appendix C we have considered the case in which the normal echo comes from a constant height and the second ray from a rapidly downwards moving deformation. (This is the observed direction of vertical movements.) The analysis shows that $|w|$ must be multiplied by:

$$\left(1 + \zeta^2 + \frac{h_0}{d} \cdot \zeta\right)$$

where ζ is the ratio of vertical to horizontal velocity of the deformation, d the distance of the projection of the deformation from the sender and h_0 the height of reflexion of the reference ray. It appears that the linear term causing a decrease of the apparent velocity is more important and it will be seen that a large error occurs, even if the vertical movement is only 3 per cent of the horizontal one (Appendix C).

Vertical movements of quite large amplitude, with a velocity comparable to that of the observed drift, occur very regularly in the F-region and also between E- and F-regions (BIBL, 1953).

It must be assumed that the amplitude of these movements decreases with decreasing height as a consequence of increasing air density but nevertheless it seems not improbable that they should even reach the lower part of the E-layer, but with such small amplitudes that they are not directly visible in the ionograms. We think that all three influences, turbulence, height gradient of v and vertical movements may be responsible for the observed dispersion of the apparent velocity $|w|$.

2. SOME EXPERIMENTAL RESULTS

On observation days, every half hour, we make three track observations on a frequency between 2 and 3 MHz with a recording period of 10 to 12 min. On the average for each of these periods between ten and twenty fades are used and the speeds and directions individually determined. Median and quartile values

VOL.
13
1958/5

are given on a daily sheet of the type shown in Fig. 8. In this sheet different trends in the direction are clearly to be seen. The velocity magnitude (speed) usually appears to be less regular. A reproduction of the trends found for 15 days of 1 month is shown in Fig. 9. A more statistical description is given by a probability diagram and Fig. 10 corresponds to the same month as Fig. 9.* It is evident

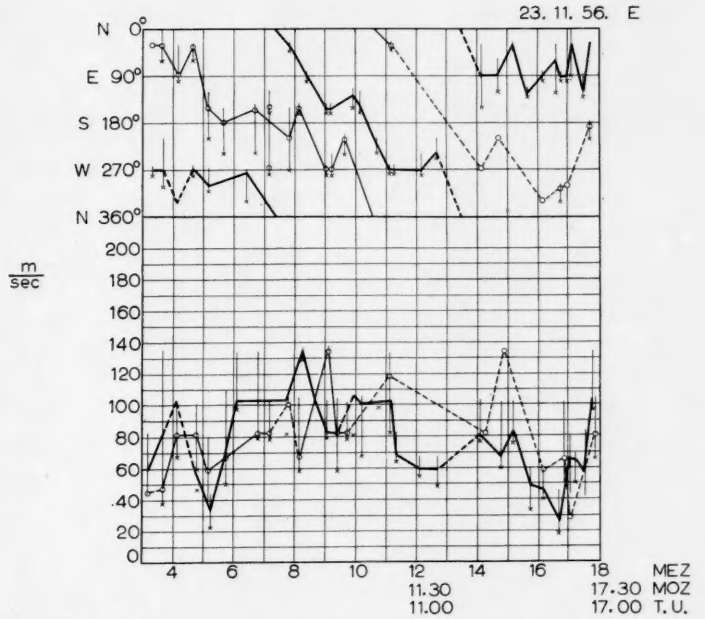

Fig. 8. Results of 1 day (direction on the upper diagram, speed on the lower one; vertical lines indicate quartile range. Thick curve: main trend. Thin curve: Secondary trend corresponding to second accumulation point)

from these figures that for full information a large number of observation days and many observations must be made. The rate of 3 days/month which has been applied by many stations during recent years is not sufficient. As things actually stand, only the method of similar fades is simple enough to permit use on a large mass of observations but our observations are now made with at least 10 observation days/month and the results are regularly published (HARNISCHMACHER and RAWER, 1957).

Some general results will be discussed in another publication but one final point may be mentioned here. In the normal case in which a single fixed frequency is used, the height of the reflexion level is somewhat dependent on ionospheric changes (such as the incidence E_s) and it seems worthwhile to use alternatively two or more frequencies as we do now. It is also desirable to have available more accurate information on the reflexion height from a separate echo recorder.

* These observations have been made at Neuf-Brisach Ht. Rh. under contract with the French "Centre National d'Etudes des Télécommunications".

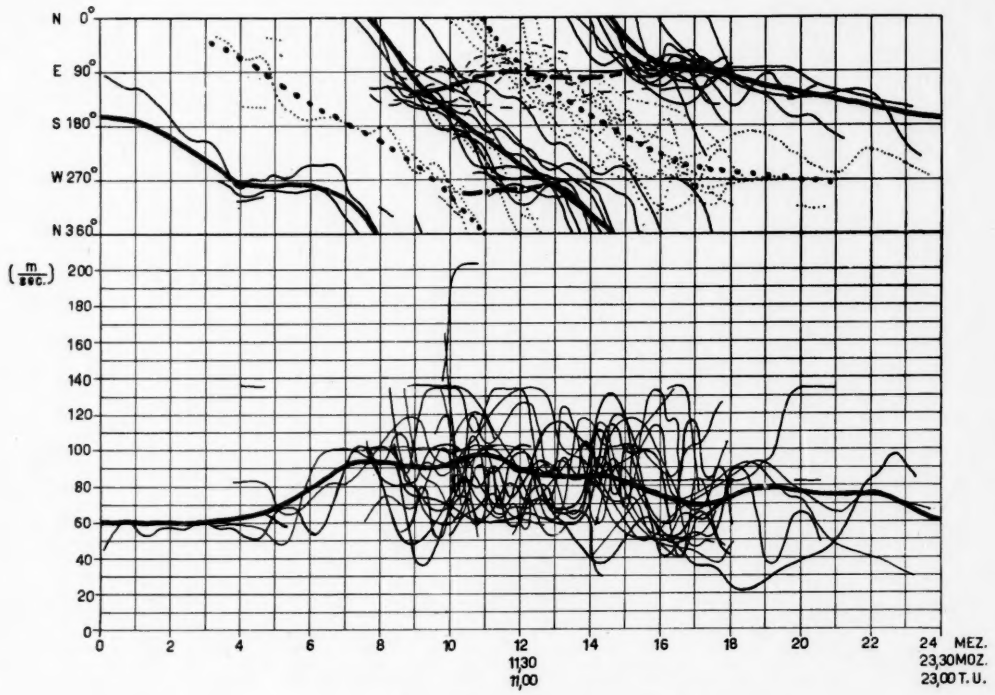

Fig. 9. Results (trends) for 1 month, (Thin curves: daily main trends. Pointed curves: daily secondary trends. Thick full curve: median rotating trend; thick pointed curve: median secondary trend. Thick broken curve: median constant direction)

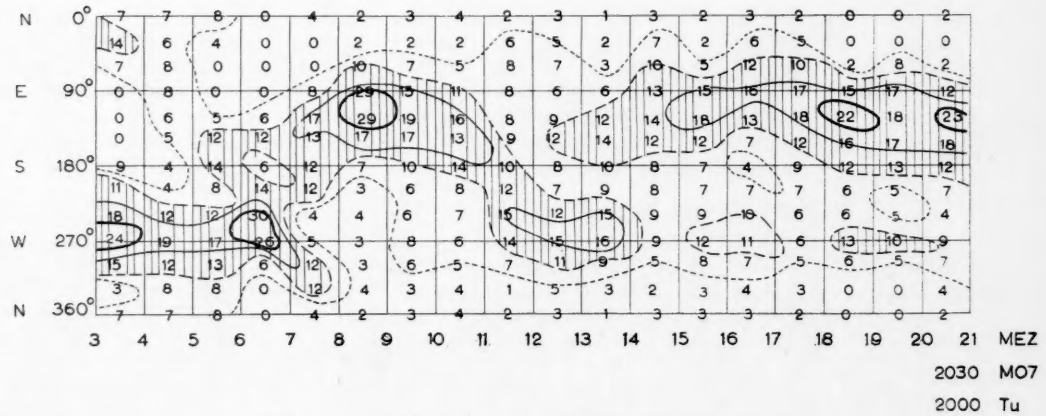

Fig. 10. Statistics of observed directions (probability in %)

Appendix A

Point Deformation, Horizontal Movement

We consider the normally reflected ray (Fig. 11, thick line) and another one being reflected by the deformation D (thin line). The path difference Δ is found from Fig. 11:

$$\Delta = \sqrt{(h^2 + d^2)} + \sqrt{\{h^2 + (d - x)^2 + y^2\}} - 2\sqrt{\{h^2 + (x/2)^2 + (y/2)^2\}}$$

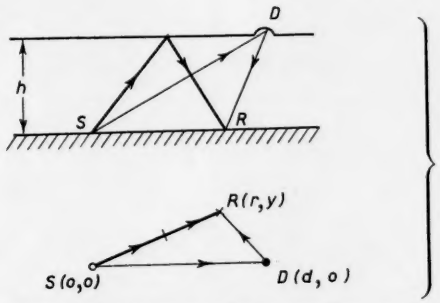

Fig. 11. Interfering rays for point deformation
(S sender, R receiver, D deformation)

For nearly vertical incidence we have approximately:

$$h \,.\, \Delta = d^2 - d \,.\, x + \tfrac{1}{4}x^2 + \tfrac{1}{4}y^2 \qquad (1)$$

The curves $\Delta = \text{const}$ (interference curves) are circles with the centre $(x - 2d)$ and radius $2 \,.\, \sqrt{(\Delta \,.\, h)}$. The amplitude distribution as given by interference of both rays is:

$$F(x, y) = \cos^2 \left\{ \frac{\pi}{h \,.\, \lambda} (d^2 - d \,.\, x + \tfrac{1}{4}x^2 + \tfrac{1}{4}y^2) \right\} \qquad (2)$$

Let us now suppose that the deformation is moving with the velocity v on a straight line, the minimum distance between this line and the sender being d_0. We take the zero of the time t such that the deformation is just at this point for $t = 0$, then $d(t) = \sqrt{({d_0}^2 + v^2t^2)}$

$$F(x, y) = \cos^2 \left[\frac{\pi}{h \,.\, \lambda} \{{d_0}^2 + v^2t^2 - x\sqrt{({d_0}^2 + v^2t^2)} + \tfrac{1}{4}x^2 + \tfrac{1}{4}y^2\} \right] \qquad (3)$$

The coordinates x, y had been fixed with respect to the direction sender-deformation, they are rotating with $\chi(t)$ $\{\sin \chi = y/\sqrt{(x^2 + y^2)} = y/R\}$. We transform to co-ordinates which are invariable with respect to the earth, X, Y by a rotation by the angle χ and obtain:

$$F(x, y) = \cos^2 \left[\frac{\pi}{h\lambda} \{{d_0}^2 + v^2t^2 - (d_0X + vtY) + \tfrac{1}{4}(X^2 + Y^2)\} \right] \qquad (4)$$

The movement of the interference lines on the ground is observed with three antennae. Let us first consider a steerable system of two antennae (1) and (2) which shall be directed perpendicularly to the interference lines. This corresponds

to one antenna at (0, 0) and the other one at (l, 0) in the X, Y system. The phase of the interference function F is different at both antennae. The time difference Δt is given by the condition that the phase at antenna (1) at time t_1 shall be equal to that at antenna (2) at time $t_2 = t_1 + \Delta t$. This condition gives with (3):

$$v^2\Delta t^2 + 2v^2 \,.\, t_1 \,.\, \Delta t - l\sqrt{\{d_0{}^2 + v^2(t_1 + \Delta t)^2\}} + \tfrac{1}{4}l^2 = 0 \qquad (5)$$

As l is usually small, Δt is also small provided $t_1 \gg \Delta t$. In this case we can also neglect l^2 compared with ($v^2 \,.\, t_1{}^2 + d_0{}^2$) and we find finally for Δt after approximation of the square root:

$$\Delta t = \frac{l}{v^2 t_1} \cdot \frac{d_0{}^2 + v^2 t_1{}^2}{2\sqrt{(d_0{}^2 + v^2 t_1{}^2)} - l} \simeq l \,.\, \sqrt{(d_0{}^2 + v^2 t_1{}^2)}$$

This is the time difference corresponding to two antennae at the distance l. The apparent velocity is then:

$$w = \frac{l}{\Delta t} = \frac{2\sqrt{(d_0{}^2 + v^2 t_1{}^2)} - l}{d_0{}^2 + v^2 t_1{}^2} \,.\, v^2 \,.\, t_1 \simeq \frac{2v \,.\, vt_1}{\sqrt{(d_0{}^2 + v^2 t_1{}^2)}} = 2v \sin \chi \qquad (6)$$

This is the "Pütter–Ratcliffe-circle". As the apparent velocity is perpendicular to the fringes, the corresponding direction is given by χ. The lines $\chi = \text{const}$ are also lines $w = \text{const}$.

With a fixed antenna system we find the same result. The calculation has been made in the X,Y-system for two pairs of antennae (0,0) ($0,l$) and (0,0) (l,0) respectively. The time difference is, for the first system: $\Delta t_Y = l/2v$ whence we find a velocity $w_Y = 2v$ and for the second system:

$$\Delta t_X = \sqrt{\left\{t^2 + \frac{l}{v}\left(\frac{d_0}{v} - \frac{1}{4}\frac{l}{v}\right)\right\}} - t$$

If $t \gg \Delta t$ this reduces to:

$$\frac{1}{2}\frac{l}{vt}\left(\frac{d_0}{v} - \frac{1}{4}\frac{l}{v}\right)$$

if $d_0 \gg l$ we have:

$$\Delta_X \simeq \frac{l}{2v} \cdot \frac{d_0}{v \,.\, t} = \frac{l}{2v} \cot \chi$$

whence

$$w_X \simeq 2v \tan \chi$$

The apparent velocity components w_X and w_Y must be related to the apparent velocity w by the expression:

$$|w|^{-2} = |w_X|^{-2} + |w_Y|^{-2}$$

Thus we finally have w with amplitude:

$$w = 2v \sin \chi \text{ and direction } \chi$$

the same result as obtained above.

Our approximations are invalid near $t = 0$ since there is a change of sign of Δt_x and even a discontinuity with the rigorous formulae.

VOL
13
1958/

For the statistics of the observations and results it must be supposed that all values of d_0 are equally probable. The probability of an observation depends at first on the density of the interference lines. This is roughly given by the derivative d/dt of the argument of the interference function F near the sender (0,0); as $d^2 = {d_0}^2 + v^2t^2$, the derivative of $(\pi/h\lambda)\ d^2$ [see equation (2)] is $(2\pi v/h\lambda)\ .\ (vt)$. But vt is just the actual Y-co-ordinate of the deformation.

From the density of interference lines we obtain the probability $W(\chi)$ that a certain direction χ is observed (by comparison with a constant probability distribution):

$$W(\chi) = \overline{Y}_{\text{dist}}/\bar{R} = \overline{R \sin \chi}/\bar{R} = \sin \chi \tag{7}$$

Another factor $\sin \chi$ should perhaps be valuable if the reading accuracy is supposed to influence the chance of observing a fade. Shallow fadings, as obtained with small χ, are more difficult to observe.

This discussion would be incomplete if the limited lifetime of the deformations was not considered. If only successive minima are used we should introduce a weight factor $\exp(-\tau_1/\mathrm{T})$ where τ_1 is the time difference between successive minima and T the mean lifetime of the irregularities. If, as is usual, isolated fades are used in the reduction of records, irregularities with a smaller lifetime can then be observed. Nevertheless there is a limitation imposed by the distance of the three receiving antennae: the fade must be observable on all three of them. If we take l as the corresponding distance, τ is given by

$$F(l\ .\ \cos \chi,\ l\ .\ \sin \chi;\ t) = F(0,\ 0;\ t - \tau)$$

$$-l(d_0\ .\ \cos \chi + vt\ .\ \sin \chi) + \tfrac{1}{4}l^2 = \tau(-2t + \tau)v^2$$

Quadratic terms in l and τ can be neglected, if the Y-co-ordinate of the irregularity (R,χ) is not too small:

$$\tau \simeq \frac{l}{2v}\left(\frac{d_0}{v\ .\ t}\cos \chi + \sin \chi\right)$$

As $vt = R\ .\ \sin \chi$ and $d_0 = R\ .\ \cos \chi$

$$\tau \simeq \frac{l}{2v}\ .\ \frac{1}{\sin \chi},\ \text{independent of } R \tag{8}$$

By introducing a factor $\exp(-\tau/\mathrm{T})$ into the probability distribution we take account of the finite lifetime:

$$W(\chi) = \overline{R \sin \chi\ .\ \exp\left(-\tau/\mathrm{T}\right)}/\bar{R} = \sin \chi\ .\ \exp\left(\frac{-B}{\sin \chi}\right) \tag{9}$$

$$B = l/2v\mathrm{T} \text{ is the time ratio}$$

Appendix B

Line Deformation, Horizontal Movement

We suppose a deformation in the form of a cylindrical reflector of small radius. If the angle of incidence at the reflector is less than α, the reflected rays form a

cone of aperture angle 2α and the deformation line is the axis of this cone. Thus the angle between any reflected ray and the deformation is $-\alpha$ and the intersection of the cone with the plane of the ground is the locus of all points which can be reached with the given incoming ray after reflection from the deformation.

By purely geometrical considerations it follows (see Fig. 12) that:

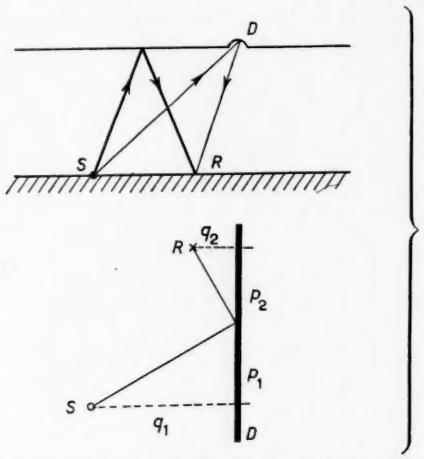

Fig. 12. Interfering rays for line-deformation (see Fig. 11)

$$\cot\alpha = \frac{p_1}{\sqrt{({q_1}^2 + h^2)}} = \frac{-p_2}{\sqrt{({q_2}^2 + h^2)}};\ |p_2| = \sqrt{\left(\frac{{q_2}^2 + h^2}{{q_1}^2 + h^2}\right)} \cdot |p_1|$$

As the rays are nearly vertical $h \gg q_1, q_2$ and approximately:

$$|p_2| \simeq [1 + \tfrac{1}{2}(q_2/h)^2 - \tfrac{1}{2}(q_1/h)^2] \cdot |p_1|$$

From Fig. 12 the path difference against the normally reflected ray is obtained:

$$\Delta = \sqrt{\left\{h^2 + d^2 + \left(\frac{y}{2}\right)^2\left(1 + \frac{x(2d - x)}{h^2}\right)^2\right\}} + \sqrt{\left\{h^2 + d^2 + \left(\frac{y}{2}\right)^2 \cdot \left(1 - \frac{x(2d - x)}{4h^2}\right)^2\right\}} - 2\sqrt{\left\{h^2 + \left(\frac{x}{2}\right)^2 + \left(\frac{y}{2}\right)^2\right\}} \qquad (10)$$

which is approximated by:

$$h \cdot \Delta = d^2 - d \cdot x + \tfrac{1}{4}x^2 \qquad (11)$$

The interference pattern thus consists of straight lines parallel to the y-axis.

$$F(x, y) = \cos^2\left\{\frac{\pi}{h\lambda} \cdot (v^2t^2 - xvt + \tfrac{1}{4}x^2)\right\} \qquad (12)$$

The x, y system is not rotating relative to the earth, if the direction of the deformation line is not changed during its movement.

With a steerable system of two antennae (0, 0) (l, 0) we find from the condition of equal phase:

$$v^2 \cdot \Delta t^2 + 2v^2t_1 \cdot \Delta t - lv\Delta t - lvt_1 + \tfrac{1}{4}l^2 = 0 \qquad (13)$$

VOL
13
1958/

It follows exactly:

$$t = \frac{l}{2} \cdot v$$

and the apparent velocity is

$$w = 2v$$

This result corresponds to the maximum value of the Pütter–Ratcliffe-circle. There is no dispersion in direction if the deformation line moves parallel to itself.

Appendix C
Line Deformation, Horizontal and Vertical Movement

In this case the height of reflection is supposed to be constant (h_0) for the normally reflected ray, but to be variable for the deformation:

$$h = h_0 + ut$$

Then

$$h_0\Delta = (2h_0 + ut)ut + d^2 - dx + \tfrac{1}{4}x^2 \qquad (14)$$

Supposing a steerable antenna system (0, 0) (l, 0) we find now as the condition of equal phase:

$$(u^2 + v^2)(2t_1 \,.\, \Delta t + \Delta t^2) + 2h_0 \,.\, u \,.\, \Delta t - lv(t_1 + \Delta t) + \tfrac{1}{4}l^2 = 0 \qquad (15)$$

If $t_1 \gg \Delta t$ and $\gg l/v$ we have ($\zeta = u/v$):

$$\Delta t \simeq \frac{l/2v}{1 + h_0\zeta/vt + \zeta^2} = \frac{l/2v}{1 + h_0\zeta/d + \zeta^2}$$

the apparent velocity is:

$$|w| = 2v(1 + h_0\zeta/d + \zeta^2) \qquad (16)$$

The importance of the correction term may be seen from the following table ($h_0 = 100$ km); the "error" introduced by the vertical movement is given as a percentage.

$\zeta = u/v$	−0·001	−0·003	−0·01	−0·03	−0·1
(d = 10 km)	−1	−3	−10	−30	−100
(d = 1 km)	−10	−30	−100	−300	−1000

References

Berg H. 1954 In *The Physics of the Ionosphere* Cambridge Meeting 104–112; 1957 *Beitr. z. Phys. der Atmos.* **29,** 276–289.

Bibl K. 1952 *C. R. Acad. Sci., Paris* **235,** 734–736; 1953 *Z. Geophys.* **18,** 136–141.

Bramley E. N. and Ross W. 1951 *Proc. Roy. Soc.* A **207,** 251.

BRIGGS B. H. and PAGE E. S.	1954	In *The Physics of the Ionosphere.* Cambridge Meeting 119–122.
BRIGGS B. H., PHILLIPS G. J. and SHINN D. H.	1950	*Proc. Phys. Soc. Lond.* B **63,** 106.
HARNISCHMACHER E. and RAWER K.	1956	*C. R. Acad. Sci., Paris* **243,** 747–750.
HARNISCHMACHER E. and RAWER K.	1957	*Beitr. z. Phys. der Atmos.* **29,** 253–268 (To be continued).
KRAUTKRÄMER J.	1950	*Arch. elektr. Ubertr.* **4,** 133.
RATCLIFFE J. A.	1954	*J. Atmosph. Terr. Phys.* **5,** 173.
ST. PÜTTER P.	1954	*The Physics of the Ionosphere.* Cambridge Meeting 191–201.
SALES G. S.	1956	*Sci. Rep.* **88,** Pennsylvania State Univ.,
YERG D. G.	1955	*J. Geophys. Res.* **60,** 173; 1956 *J. Atmosph. Terr. Phys.* **8,** 247–259.

VOL.
13
1958/5

Journal of Atmospheric and Terrestrial Physics, 1958, Vol. 13, pp. 17 to 25. Pergamon Press Ltd., London

Variations in the direction of arrival of high-frequency radio waves

J. E. TITHERIDGE*
Auckland University College, New Zealand

(*Received* 23 *January* 1958)

Abstract—A general relation is derived for determining the effect of a non-horizontally uniform ionosphere on the propagation of short radio waves. The deviations for linear and parabolic layers are evaluated and the results generalized to include an ionosphere with several layers. Some experimental results showing large diurnal changes in apparent bearing are discussed and shown to be consistent with the foregoing theory.

INTRODUCTION

MEASUREMENTS of the apparent heights of reflection of fixed-frequency radio-waves transmitted vertically upwards from different points on the earth's surface frequently indicate an apparent tilt of several degrees in the effective reflecting surface. This may be due to an overall tilt of the ionospheric layer, and the effect on oblique-incidence transmission is then simply obtained by considering the radio-waves to be reflected at a surface with this tilt. However, much of the observed variation in virtual height is often due to variations in the rate of increase of ionization with height above the base of the reflecting layer. The calculations in this case are less straightforward, and it will be shown that the deviations of a reflected wave are less than one-third as large as those obtained on the simple assumption of a uniformly tilted layer.

RAWER (1951) showed that the horizontal gradients of electron density known to exist could cause appreciable distortion of ray paths. He evaluated the deviation to be expected for one particular form of ionosphere for which the differential equation of the ray-path was integrable. WALDO-LEWIS (1953) considered two more general cases of a parabolic layer varying in the direction of propagation. By approximating to the ray-path integral he obtained expressions giving the change in range and elevation angle of the reflected ray with an accuracy of 5–25 per cent. ARGENCE (1955) obtained expressions for the deviation at grazing incidence by approximate integration in some further cases. The present work is an attempt to provide a general relation which may be readily applied to any particular case including that of penetration of a layer, the main cause of the experimentally observed deviations described later.

General relations for lateral deviation

Consider a ray with angle i to the vertical incident at O on a plane boundary between media of refractive index n and $n + dn$ (Fig. 1). The boundary is taken at any angle α to the horizontal, the horizontal direction Ox in the plane making an angle ε with the vertical plane containing the ray direction. Oy is the line of greatest slope in the boundary.

* Now at the Cavendish Laboratory, Cambridge.

If dn, di, $d\varepsilon$ are the (infinitesimal) changes in n, i, ε over the boundary, applications of Snell's law in the directions Ox and Oy give:

$$dn \sin i \cos \varepsilon + n \cos i \cos \varepsilon \, di - n \sin i \sin \varepsilon \, d\varepsilon = 0 \qquad (1)$$

and

$$-dn(\sin i \sin \varepsilon + \cos i \tan \alpha)$$
$$= n \sin i \cos \varepsilon \, d\varepsilon + n \cos i \sin \varepsilon \, di - n \sin i \tan \alpha \, di \qquad (2)$$

Eliminating dn we get:

$$d\varepsilon(1 + \alpha_1 \cot i) = \frac{di}{\sin^2 i} \alpha_2$$

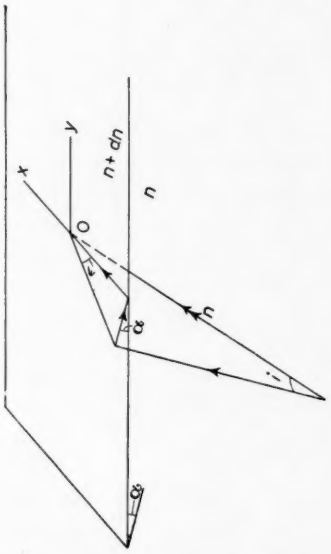

Fig. 1.

where α_1 and α_2 are the lateral and longitudinal components ($\tan \alpha \sin \varepsilon$ and $\tan \alpha \cos \varepsilon$) of the tilt $\tan \alpha$.

For the downcoming ray, the deviation is in the same direction and is given by:

$$d\varepsilon(1 - \alpha_1 \cot i) = \frac{di}{\sin^2 i} \alpha_2 \qquad \text{(replacing } i \text{ by } \pi - i\text{)}$$

(When α_1 is not zero the values of i applicable to the upgoing and downcoming rays at a given electron density will differ slightly and the following formulae apply to some mean value.) The mean change in the horizontal direction of propagation over two corresponding sections of the ray-path is therefore:

$$d\varepsilon = \frac{1}{1 - \alpha_1^2 \cot^2 i} \frac{di}{\sin^2 i} \alpha_2 \fallingdotseq \frac{di}{\sin^2 i} \alpha_2$$

Cot i is zero at reflection and, in practice, is less than one at the base of the layer where $\alpha = 0$ (measuring tilts from this plane). So the above approximation gives a mean error of less than 0·06 per cent for a mean longitudinal tilt of less than 3°.

Writing $u = \cot i / \cot i_0$ we get $d\varepsilon = -\cot i_0 \, . \, \alpha_2 \, du$ where u varies from 1 at the base of the layer to 0 at reflection, and is in fact the refractive index for the equivalent vertical ray of frequency $f \cos i_0$, i_0 being the angle of incidence of the

VOL.
13
1958/5

ray on the base of the layer. The total deviation in the bearing of a received signal is then

$$\Delta\varepsilon = \cot i_0 \int_0^1 \alpha_2 \, du \tag{3}$$

In the presence of longitudinal tilt, i_0 should be taken as the mean of the angles of incidence and emergence. Reflection at a plane surface tilted at an angle ψ to the horizontal about a horizontal line in the direction of propagation causes a bearing deviation of $\psi \cot i_0$. This may be shown from geometrical considerations or by equation (3) for an ionosphere with a constant lateral tilt ψ. Thus an ionosphere in which the tilt α of the planes of constant ionization varies with height causes the same deviation in the bearing of a reflected radio-wave as a constant lateral tilt ψ given by:

$$\psi = \Delta\varepsilon \tan i_0 = \int_0^1 \alpha_2 \, du \tag{4}$$

This result is applicable to any type of layer, any variation of tilt α with height and any angle of incidence. It is exact when the tilt is entirely perpendicular to the direction of propagation. When the tilt (with respect to the base of the layer) has a maximum longitudinal component of about 5°, it is correct to within about 0·1 per cent except for near-vertical propagation with $i_0 < 20°$. The mean variation of i with n may still be taken as $n \sin i = \sin i_0$, i, being as before a mean value, giving:

$$\cos^2 i_0(1 - u^2) = 1 - \frac{\sin^2 i_0}{\sin^2 i} = 1 - n^2 = \frac{Ne^2}{\pi m f^2} \tag{5}$$

where N is the mean electron density at a given height. When α_2 is given as any polynomial in N the effective tilt of the reflecting layer is then given by equations (4) and (5) as an immediately integrable function of the parameter u.

Changes in the angle of elevation

Eliminating $d\varepsilon$ between equations (1) and (2) gives:

$$-\frac{dn}{n} = di \frac{1 - \alpha_1 \tan i}{\tan i + \alpha_1} = F(i)\, di, \text{ say.}$$

Thus the variation of i is, as assumed earlier, entirely independent of any sideways tilt of the refracting layer. Tan i and dn change sign for the downcoming ray, and the above relation is unchanged except for the sign of α_1. The deviation due to the tilt is then in the opposite direction, and the net deviation at any height is small except near reflection where tan i is large and the ray-path is asymmetrical.

If i_0 is the mean of the angles of incidence and emergence, i increases from $i_0 - \psi$ to $\pi - (i_0 + \psi)$ over the ray path, where ψ is the effective tilt of the ionosphere in the direction of propagation. The integral of dn/n over the complete ray-path must be zero, giving:

$$\int_{i_0-\psi}^{\pi/2} F(i)\, di = \int_{\pi-(i_0+\psi)}^{\pi/2} F(i)\, di = -\int_{i_0+\psi}^{\pi/2} F(\pi - i)\, di$$

and therefore

$$-\int_{i_0}^{\pi/2} \{F(i) + F(\pi - i)\}\, di = \int_{i_0-\psi}^{i_0} F(i)\, di - \int_{i_0}^{i_0+\psi} F(\pi - i)\, di$$
$$\doteqdot \psi \{F(i_0) - F(\pi - i_0)\} \tag{6}$$

Since any small tilt α near the base of the layer decreases $F(i)$ and $F(\pi - i)$ equally, the error in (6) is small and corresponds to an error of much less than ψ in i_0.

Substituting for $F(i)$ in (6) gives:

$$\psi = \frac{\tan i_0}{1 - \alpha_1^2 \cot^2 i} \int_{i_0}^{\pi/2} \alpha_1 \frac{di}{\sin^2 i}$$

$$\fallingdotseq \int_0^1 \alpha_1 \, du \tag{7}$$

where $u = \cot i / \cot i_0$ as before. This result is exactly equivalent to, and involves the same error as, equation (4) although the two tilts are quite independent.

Changes in range and critical frequency

Consider refraction at a plane boundary with a small tilt $\alpha^1 = \tan^{-1} \alpha$ in the direction of propagation. Then with the notation of Fig. 1, $n \sin (i + \alpha^1)$ is constant over the boundary giving:

$$-n \frac{di}{dn} = \tan (i + \alpha^1) \fallingdotseq \tan i \{1 - \alpha(\tan i + \cot i)\}^{-1}$$

since, as before, $\cot i$ is small. If h is measured vertically, the total range for a ray incident at angle i_0 on a layer with effective tilt ψ in the direction of propagation is given by:

$$l = \int_{i=i_0}^{i=\pi-i_0-2\psi} dh \tan i$$

$$= -\int_{i_0}^{\pi-i_0} n \frac{dh}{dn} di + \int_{i_0}^{\pi-i_0} \alpha n \frac{dh}{dn} (\tan i + \cot i) \, di$$

$$+ \int_{\pi-i_0-2\psi}^{\pi-i_0} n \frac{dh}{dn} \{1 - \alpha(\tan i + \cot i)\} di$$

The first integral is the range l_0 obtained when $\psi = 0$. The second integral is zero, since the integrand changes sign over the second half of the range of integration. Thus the third term represents the increase in range due to the tilt, and gives:

$$\Delta l \fallingdotseq 2\psi \left(\frac{dh}{dn}\right)_0 \tag{8}$$

since $\alpha \to 0$, $n \to 1$ at the base of the layer.

Now
$$l_0 + \Delta l = -2\int_{i_0}^{\pi/2} n \frac{dh}{dn} di + 2\left(n \frac{dh}{dn}\right)_0 \psi$$

$$\fallingdotseq -2\int_{i_0+\psi}^{\pi/2} n \frac{dh}{dn} di$$

and the range is very nearly the same as for a flat ionosphere and an angle of incidence $i_0 + \psi$, the mean of the actual angles of incidence and emergence. For small tilts the effective virtual height of reflection h' is also the same, for the range is:

$$h' \tan i_0 + h' \tan (i_0 + 2\psi) \fallingdotseq 2h' \tan (i_0 + \psi)$$

VOL
13
1958/

The critical ray which has an infinite virtual height will have a frequency equal to the oblique incidence critical frequency under these equivlent conditions. So the layer is again equivalent, to a first approximation, to one with an overall tilt ψ as given by (7). This is the result which would be expected, since as for the angular deviations the changes in range and critical frequency due to a tilt α increasing with height must be slightly less than if the layer had a constant tilt equal to that at the maximum height of reflection.

Application of the general relation

Equations (4) and (7) show that for any direction of propagation the ionosphere behaves as if it had an overall vector tilt $\boldsymbol{\psi} = \int_0^1 \boldsymbol{\alpha}\, du$ where $\boldsymbol{\alpha}$ represents the tilt of a plane of constant ionization in magnitude and (horizontal) direction and is measured with respect to the base of the ionospheric layer. Any tilt $\boldsymbol{\alpha}_0$ of this base may then be exactly allowed for by supposing the reflecting plane to have a total tilt $\boldsymbol{\psi} + \boldsymbol{\alpha}_0$. This is the result which would be obtained by measuring α from the horizontal. Similarly the components in any direction or from any particular cause may be separately evaluated, the overall tilt and the resulting deviations being simply the linear sum of such components. Thus curvature of the ionosphere need not be explicitly taken into account when calculating the effects of any departure from spherical symmetry.

If the tilt of a plane of constant ionization is supposed to increase linearly with electron density N, equation (5) gives $\alpha = K^1N = K \cos^2 i_0\,(1-u^2)$ and the overall effective tilt is $\frac{2}{3}K \cos^2 i_0$, or two-thirds of the tilt at the maximum height reached ($u = 0$). This is a general result applicable to any shape of reflecting layer and any angle of incidence. For a linear layer, ψ is one-third of the tilt of virtual heights.

For a parabolic layer of semi-thickness y_m variations of critical frequency (f_c) will produce an apparent tilt. Measuring h from the base of the layer, we have:

$$\cos^2 i_0(1 - u^2) = 1 - n^2 = \frac{f_c^2}{f^2}\left\{1 - \left(1 - \frac{h}{y_m}\right)^2\right\}$$

On a plane of constant ionization, $dn = 0$ and therefore:

$$dh = -y_m \frac{df_c}{f_c} \frac{z^2(1 - u^2)}{\sqrt{(1 - z^2 + z^2u^2)}}$$

where $z = \dfrac{f \cos i_0}{f_c}$.

If f_c varies by df_c in a horizontal distance ds, the overall effective tilt in the direction of ds is then:

$$\psi = \int_0^1 \frac{dh}{ds}\, du = y_m \frac{df_c}{f_c ds}\, B(z) \qquad (9)$$

where $B(z) = \dfrac{1}{4}\left(z + \dfrac{1}{z}\right) \ln\left|\dfrac{1 + z}{1 - z}\right| - \dfrac{1}{2}$

This function is infinite at $z = 1$, but drops rapidly and for z between 0·8 and

0·9 the effective tilt is 0·5 to 1·0 times $y_m(df_c/f_c ds)$. For z in 0·75 to 0·95 (the normal range for oblique incidence transmission) the effective tilt causing deviations is only about one-fifth of the tilt of the apparent or virtual reflecting plane.

The resultant deviation in the horizontal direction of propagation of a reflected ray is $2\Delta\varepsilon = 2\psi \cot i_0$. For a transmitted ray ($z > 1$) this relation may be used to define the equivalent tilt ψ. Equation (9) then remains valid, the form of $B(z)$ given being unaltered by the change of limits. For the layer model considered the deviations throughout the layer for both the upgoing and the downcoming portions of a complete ray path are in the same direction, the layer acting as a prism, and the overall change corresponds to reflection at a surface with tilt 2ψ. The changes in direction when a ray penetrates several layers 1, 2, ... and is reflected from a layer r are thus described by an overall effective tilt:

$$\psi = 2\psi_1 + 2\psi_2 + \ldots + \psi_r + \psi_{0r}$$

where ψ_{0r} is the tilt of the base of the reflecting layer and:

$$\psi_n = \int_{u_0}^{1} \alpha_n \, du$$

with $u_0 = 0$ for reflection and $\sqrt{[1 - (1/z^2)]}$ for penetration. α is here measured with respect to the base of the layer, any overall tilt of a penetrated layer having no net effect.

EXPERIMENTAL RESULTS

A rotating interferometer has for the past few years been operated at Auckland, New Zealand by the Auckland University College. The apparatus has been described elsewhere (WHALE, 1954); the foregoing theory was developed in an attempt to explain the large diurnal variations in the recorded directions of arrival of high frequency radio-waves. The records analysed covered distances of from 2000 to 10,000 km and frequencies of from 5 to 15 Mc, bearing and elevation angles being continuously recorded with an accuracy of about 0·5° and 1° respectively.

Some typical curves illustrating the diurnal variations in the mean monthly bearings are shown in Fig. 2. The dashed lines for *ZQD* (9·3 Mc; 2000 km at 10°E) for April and March 1954, were obtained by subtracting from the solid variations the deviation calculated from the apparent lateral tilt of the reflecting layer as given by the published monthly minimum virtual heights. Since the *ZQD* signal travels in a (magnetically) north–south direction, this tilt was approximately calculated from the changing value of $h'F_2$ at the centre of the path (obtained as the mean of the figures for Canberra and Raratonga). The effect is seen to be far too small to explain the observed diurnal changes, but the remaining variation is smoother and shows to within the experimental accuracy (about 0·2°) a continuous linear variation of about 0·09°/hr per hop. The 10 Mc signal from *WWVH* (7000 km at 30°E) also shows this change, while on 15 Mc this figure is reduced to 0·062, and records of *ZQD* on 6 Mc give a figure of 0·17. There is thus a change in apparent bearing of about $(1/f)$°/hr per hop throughout the day, observed for all months and all northerly stations recorded.

The 9·3 Mc signal from *ZQD* was clearly recorded on 8 days in April, the measured elevation angles showing that daytime propagation was almost entirely

VOL
13
1958/

due to 2-hop F_2-reflection. The effects of the horizontal gradients of ionization were calculated for this month assuming semi-thicknesses of 60 and 100 km for the F_1- and F_2-layers. The effective tilts ψ_1 and ψ_2 and the resultant bearing deviations $(2\psi_1 + \psi_2)$ cot i_0 were then obtained from the experimental values of i_0 and the variations of the monthly mean critical frequencies. The calculated deviations are

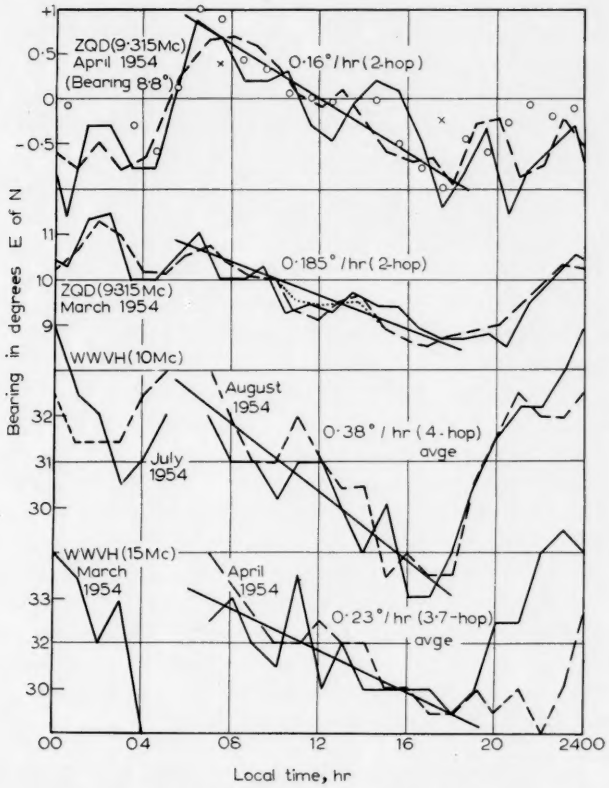

Fig. 2. Diurnal variations in the direction of arrival of radio signals received at Auckland.

shown as circles in Fig. 2, and from 0800 to 1700 are mainly due to the smooth variation of the F_1-layer critical frequency, the linear change representing the changing slope of the normal hourly f_cF_1 records. The deviations just outside this time are due to the relatively sudden changes in f_cF_2; the time of these changes has always been observed to define the limits of the large regular variation.

The crosses represent the deviations calculated from the effective F_2-tilt immediately after the disappearance (and before the appearance) of the F_1-layer. However at this time $h'F_2$ is still dropping and the vanishing F_1-ionization may still be exerting a noticeable effect. The circles at 0730 and 1730 show the deviations obtained if we assume that the effective tilts of the F_1-layer persist for 1 hr outside the period during which F_1 is recorded as a separate layer. The

correspondence with the observed values is improved, although the correction may be too large.

The dashed curve was obtained by subtracting the effects of the variations in $h'F_2$. These variations will be due in part to the changing critical frequencies, so the calculated deviations due to the variations in f_c only should lie between the two curves of Fig. 2. More exact calculations show that the observed afternoon variations of $h'F_2$ at Brisbane during April 1954 would be entirely due to the variations in f_cF_1/f_cF_2 if the semithickness of the F_2-layer was about 250 km. This is probably about twice too large, and the large corrections for the changing height of the base of the reflecting layer from 1400 to 1600 should be halved. The deviations calculated from equation (9) then fully explain the observed variation from sunrise to sunset.

The records for March 1954 do not show the small bearing angles observed in the early morning during April (when records were only obtained on two nights) and the mean bearings over the 2 months follow the calculated nightime values fairly closely. Calculations for other months and other stations yield similar results, with a linear daytime variation due to the changing critical frequencies combined with a smaller and more irregular variation largely due to changes in the height of the reflecting layer.

The bearing deviations are given by $\psi \cot i_0$, where at a given time ψ depends only on the ratios $f \cos i_0/f_c$ for the various ionospheric layers. The experimental results show that the elevation angle of the strongest received ray is generally such that the equivalent vertical frequency $f \cos i_0$ is mid-way between the layer critical frequencies. Thus in normal short wave transmission $f \cos i_0$ is approximately constant and the bearing deviations are proportional to $\cot i_0$ and therefore to $1/f$ since $\cot i_0$ is small and approximately equal to $\cos i_0$. Deviations calculated for F_1-layer reflection are of about the same magnitude and show the same diurnal variation as those for propagation via the F_2-layer. Thus there is little seasonal effect other than that due to a change in the number of hops n, the uniform change in bearing over a north–south path being always about $(n/f_{Mc})°$/hr. For a 5 Mc wave transmitted over a distance of 10,000 km the diurnal change could amount to 20°.

Consideration of the elevation angles recorded at Auckland leads to some further general conclusions which may be summarized as follows. During the day the virtual height of reflection giving the strongest signal is within ± 5 km of the least possible height for the layer concerned. This is greater than the minimum virtual height recorded at vertical incidence by from 10 to 30 km, due to the curvature of the earth. At night the virtual height of reflection generally exceeds the minimum recorded at vertical incidence by less than 10 km. Strong signals are normally only received when the elevation angle required for reflection at the minimum virtual height of an ionospheric layer gives equivalent vertical frequencies at the centres of the various layers differing by at least 5 per cent from the layer critical frequencies.

These considerations enable the possibility and the probable modes of propagation, and the elevation angles of the received rays, to be readily determined by a graphical method. The earth's magnetic field has very little effect on normal short

VOL
13
1958/

wave transmission; the magnitudes of the perturbations are calculated in another paper. Sporadic *E*-ionization can considerably effect the transmission. The effect is normally to reduce the signal strength, but it occasionally enables transmission which would otherwise be impossible.

References

Argence E.	1955	Report on *Physics of Ionosphere* p. 288. Physical Society, London.
Waldo-Lewis R. P.	1953	*Proc. Phys. Soc. Lond.* B **66,** 308.
Whale H. A.	1954	*Proc. Phys. Soc. Lond.* B **67,** 553.
Rawer K.	1951	*Z. angew. Phys.* **3,** 226.

VOL. 13 58/59

Journal of Atmospheric and Terrestrial Physics, 1958, Vol. 13, pp. 26 to 31. Pergamon Press Ltd., London

Bifurcations in the *F*-region at Baguio, 1952-1957

V. MARASIGAN, S.J.
Manila Observatory, Mirador, Baguio, Philippines

(*Received* 23 *December* 1957)

Abstract—A 5-year statistical survey of bifurcations in the *F*-region at Baguio is presented and analysed in the light of a parametric mechanism of the v–R relations of the *F1*- and *F2*-layers. The conclusion is reached that two of the features of bifurcation-statistics are mainly due to variations in layer heights and thicknesses with season and solar activity respectively.

INTRODUCTION

IT has often been noticed in some places, e.g. Lindau (BECKER, 1956) and Slough (PIGGOTT, 1956), that bifurcations occur more often at sunspot-minimum than at sunspot-maximum. But this does not seem to be true at other places, e.g. Singapore (PIGGOTT, 1956). Since bifurcation occurrence evidently varies with place as well as with solar-cycle epoch, this brings up the problem of establishing these variations on a theoretical basis in conformity with the current physical theories of the ionosphere. As an approach to this problem, an initial survey is made at Baguio, Philippines, near the magnetic equator. A statistical picture of bifurcations for the 5 year period 1952–1957 is presented and examined for its most prominent features. By setting up a parametric mechanism, these features are examined and qualitatively correlated with solar-cycle variations. It is hoped that this approach, if satisfactory, would be used at other locations, and perhaps make available to theoreticians the vast accumulation of untapped data on bifurcations, as an additional convenient semi-empirical check on physical theories of the *F*-region.

VOL.
13
1958/5

PRESENTATION OF DATA

Bifurcation is defined as the clear separation of the *F1*- and *F2*-layers such that the *F1* critical frequency can be accurately measured. The monthly day-by-hour records at Baguio provide a rapid way of obtaining the percentage-occurrence of bifurcations for each month. Nine daytime hourly records, 0800 to 1600, are considered each day. The total number of numerical entries for *F1* critical frequency for each month—divided by the total number of daytime-hourly records of that month (usually 270 or 279)—is the percentage-occurrence for that month. The sixty-six such values from May 1952 to October 1957 are presented graphically in Fig. 1. The graph reveals two outstanding features: (1) the decrease of bifurcation-occurrence during sunspot-maximum, and (2) the seasonal variations, producing two maxima each year, one in summer and another in winter, the former being higher than the latter.

DISCUSSION

Mechanism of bifurcation

The first step towards explaining the above features is to consider the mechanism of bifurcation. Following APPLETON's suggestion as later developed by RATCLIFFE

(1951), the *F1*- and *F2*-layers are represented as intersecting parabolae, each with three varying dimensions, the height of the maximum ion-density h_m, the layer semi-thickness y_m and the critical frequency f_0. A certain relation between five of these six parameters defines the necessary and sufficient condition for

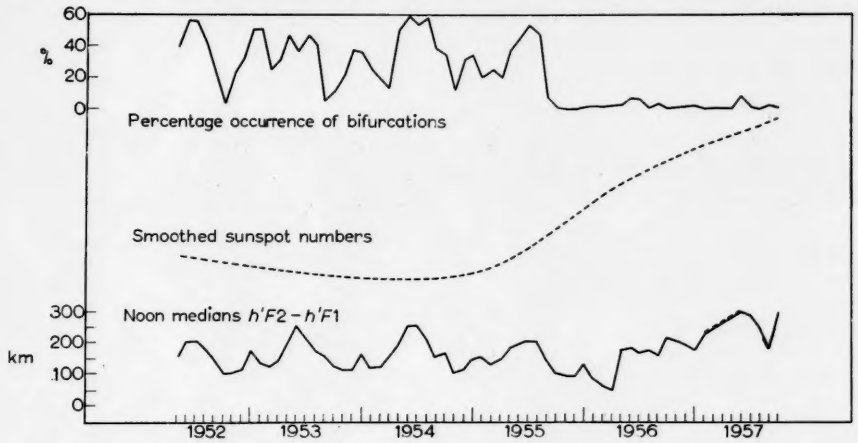

Fig. 1. Comparison of bifurcation-occurrence with solar-cycle and with layer-separation.

bifurcation, which relation may be worded thus: bifurcation occurs if and only if the upper parabola (*F2*) intersects the lower parabola (*F1*) at a point no lower than h_mF1 (see Fig. 2). In symbols:

$$\Delta h_m \geqq y_mF2 - z \tag{1}$$

where z is the point of intersection of the two parabolae, measured from the

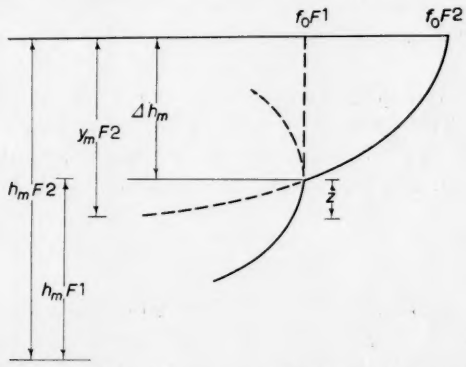

Fig. 2. Bifurcated *F*-region represented by intersecting parabolae

bottom of the *F2*-layer. To reduce (1) to parameters directly measurable on an ionogram, let

$$v = \frac{h_mF2 - h_mF1}{y_mF2}$$

and

$$R = f_0F1/f_0F2$$

Then, equation (1) may be expressed in terms of v and R thus:

$$v \geqslant \sqrt{(1 - R^2)}$$

as the necessary and sufficient condition for bifurcation.

Fig. 3 shows the curve of the minimum values of v against R.

The v–R plot of bifurcations

To check this hypothetical mechanism, random cases of bifurcation may be examined and plotted on the chart of Fig. 3. If all their v–R plots fall above the limiting curve, and no case of bifurcation falls under the curve, then the mechanism may validly be used. Unfortunately, cases of single F-layer or L-condition cannot

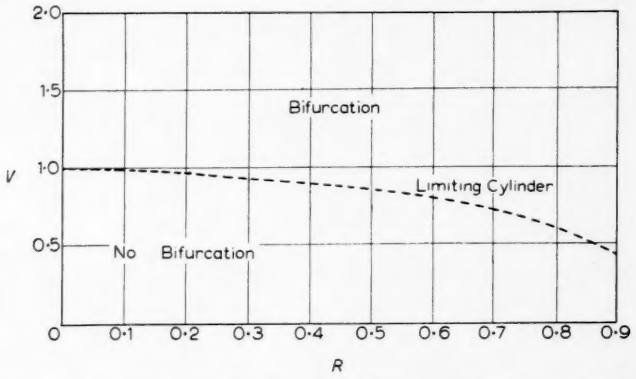

Fig. 3. Curve indicates lower limit of parameters of bifurcated F-region on the assumption of parabolic distribution.

be plotted in a similar manner, since by definition, their f_0F1 values are not measurable.

About twenty-five ionograms with bifurcated F-regions were scaled for their h_m, y_m and f_0 values. The scaling was carried out according to RATCLIFFE's (1951) method, supplemented in certain cases by a cosine distribution following the suggestion of KELSO (1954). The earth's magnetic field was neglected. The results are indicated in Fig. 4.

Significant parameters

It will readily be noticed that the R-values fall within a relatively narrow range, converging at a median of $R = 0{\cdot}5$. It is probable that the R-values for non-bifurcated cases would also fall within this range. On the other hand, the v-values show a range of variation that is considerably larger, even after generous allowance is made for errors in scaling vertical parameters. This strongly suggests that the mechanism of bifurcation is more subject to the control of the vertical parameters h_mF2, h_mF1 and y_mF2, than to critical frequencies. However, there certainly is a mutual dependence between critical frequencies and vertical parameters, as when a layer expands vertically without changing its total ion content, a process already described by APPLETON (1955).

VOL
13
1958/

The above considerations lead to an investigation of two variables: (1) the vertical separation of *F1*- and *F2*-peak levels, Δh_m, and (2) the semi-thickness of the *F2*-layer, $y_m F2$. These two, respectively, are the numerator and denominator of the parameter v.

Variation of Δh_m

It would really be better, for the sake of accuracy, to obtain the Δh_m values by scaling the $h_m F1$ and $h_m F2$ directly from the ionograms. However, since this

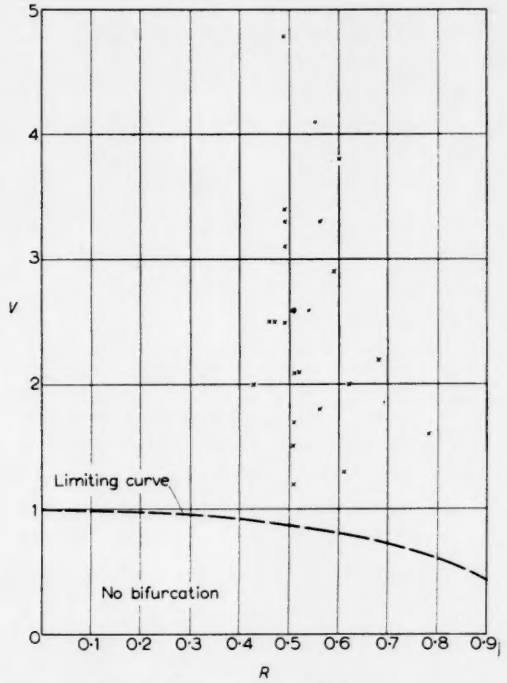

Fig. 4. The v–R plot of bifurcations.

investigation is mainly qualitative, and since the monthly medians for the minimum virtual heights of *F1* and *F2* are at hand, this less laborious procedure is followed. Assuming that the thickness of *F1* and *F2* are approximately equal and that their differential retardation is negligible (Appleton, 1950), the running differences of the noon monthly medians of $h'F1$ and $h'F2$ may be taken as a fair index of the annual variation of Δh_m. These values are represented by the lowest curve in Fig. 1. A comparison with the plot of bifurcation-percentages immediately explains the two maxima bifurcation-percentages in summer and in winter as being due to a correspondingly large separation of *F1*- and *F2*-layers. As the *F1*-height is fairly constant throughout the year, it would seem, then, that these annual variations of bifurcation-percentages are mainly due to variations of $h_m F2$.

In relation to the ionospheric equator, defined by Appleton (1950), the observed annual variations of $h'F2$ for 1953–1955 (period of low solar activity)

would characterize Baguio as a low-north latitude station. And in fact, its magnetic latitude is 9·5°N. However, the picture changes in 1956–57, a period of high solar activity; but this may be due to increased retardation effects on $h'F2$ values by the $F1$-layer, which may be expected to thicken with increase of solar activity.

The noon monthly medians also show an increase of $F2$-heights with solar activity. This is in disagreement with the generalization by CHATTERJEE (1955) that $F2$ heights decrease with increasing solar activity at low latitude stations.

Variation of y_mF2

Referring again to Fig. 1, it will be noticed that as the sunspot number increases in 1956–57, the bifurcation-percentage *decreases*, and this despite the continued increase of h_mF2. The apparent anomaly is readily clarified upon consideration of y_mF2 variations, which, as has been mentioned, is the denominator of the parameter v. There is a definite thickening of $F2$ with the approach of sunspot-maximum. This is shown (Fig. 5) by comparing the average daytime values of y_mF2 for two

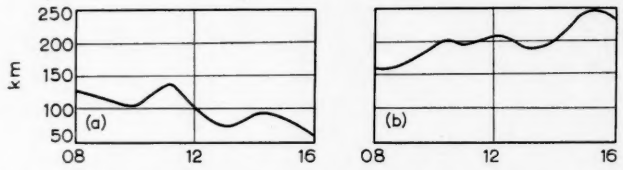

Fig. 5. Average semi-thickness of $F2$-layer for (a) low solar activity, June 1945, and (b) high solar activity, June 1957.

magnetically quiet days of June 1954 with those of two similar days of June 1957. The increase is by a factor of 2. This more than compensates for the increase in vertical separation (factor of 1·2). There results an overall decrease of v by a factor of $\frac{3}{5}$, tending to bring the imaginary v–R plot below the limiting curve, i.e. lowering the probability of bifurcation-occurrence.

The increase of y_mF2 with increasing solar activity is to be expected, since the semi-thickness is proportional to the scale-height, which is a linear function of radiation-intensity, and therefore, of solar activity, as has been pointed out by CHATTERJEE (1955).

It may be of interest to add the fact that there is a corresponding increase of noon values of f_0F2 from June 1954 to June 1957 by a factor of 1·73. This agrees very well with the findings of APPLETON and PIGGOTT (1954) obtained for the epoch 1944–47 for different latitudes. Now, taking n, the total ion-content of $F2$, to be proportional to $y_mf_0^2$, it would seem that at Baguio n increases from sunspot-minimum to -maximum by a factor of 6. This is higher than the estimated factor of 2 for Huancayo (RATCLIFFE, 1951) during an earlier solar cycle, i.e. cycle 17. However, cycle 17 reached a maximum Zurich sunspot count of 125 in May 1939, whereas cycle 19 had already reached 206 by June 1957 and was still rising.

Moreover, the fact that v changes with the solar cycle agrees with the findings of SKINNER and WRIGHT (1954) at Ibadan that h_m and y_m are not linearly dependent. If they were, v would be more or less constant. Actually, it is observed to vary widely and as a function of solar activity.

VOL
13
1958/

Conclusion

The above considerations in general lead to the conclusion that bifurcations are conditioned mainly by the vertical parameters h_m and y_m of the *F2*-layers—annual variations by h_m dependent upon ionospheric latitude, and solar-cycle variations by y_m dependent upon activity. This parametric mechanism is evidently an over-simplification of the total picture, but quite adequate for the present study. The diurnal, lunar and magnetic variations, though of great interest, are not included. If they are to be included, the basic parametric relations will have to undergo profound modifications in the light of the theory of vertical drift and diffusion as proposed by Martyn (1955); the vertical relations of *F1* and *F2* must obey the law of layer-formation as developed by Appleton and Lyon (1955); finally, the two fluctuating heights of ionization must reasonably agree with data from rockets and satellites, as well as with the theory that solar radiation ionizes the *F*-region in two distinct bands, one below 200 Å responsible for the *F1*-layer, and the other above 200 Å producing the *F2*-layer (Havens, Friedman and Hulbert, 1955). However, this last-mentioned theory has been called into question by Bates (1956).

Acknowledgements—The author is grateful to Rev. J. J. Hennessey, S.J., Director of the Manila Observatory, whose stimulating discussions and helpful suggestions inspired this study. Father Hennessey personally scaled and recorded the daily ionograms of the 5-year period considered in this study.

VOL. 13 58/59

References

Appleton E.	1950	*J. Atmosph. Terr. Phys.* **1,** 106.
	1955	*Endeavour* **14,** 25.
Appleton E. and Lyon A. J.	1955	*Conference on Physics of the Ionosphere* p. 31. Physical Society, London.
Appleton E. and Piggott W. R.	1955	*Conference on Physics of the Ionosphere* p. 221. Physical Society, London.
Bates D. R.	1956	*Solar Eclipses and the Ionosphere* (Edited by Brown W. J. G. and Beynon G. M.) p. 184. Pergamon Press, London.
Becker W.	1956	*Solar Eclipses and the Ionosphere* (Edited by Brown W. J. G. and Beynon G. M.) p. 148. Pergamon Press, London.
Chatterjee B.	1955	*J. Geophys. Res.* **60,** 325.
Havens R. J. Friedman H. and Hulbert E. O.	1955	*Conference on Physics of the Ionosphere* p. 240. Physical Society, London.
Kelso J. M.	1954	*J. Atmosph. Terr. Phys.* **5,** 117.
Martyn D. F.	1955	*Conference on Physics of the Ionosphere* p. 254. Physical Society, London.
Piggott W. R.	1956	*Solar Eclipses and the Ionosphere* (Edited by Beynon W. J. G. and Brown G. M.) p. 148. Pergamon Press, London.
Ratcliffe J. A.	1951	*J. Geophys. Res.* **56,** 463 and 487.
Skinner N. J. and Wright R. W.	1954	*J. Atmosph. Terr. Phys.* **5,** 296.

Journal of Atmospheric and Terrestrial Physics, 1958, Vol. 13, pp. 32 to 37. Pergamon Press Ltd., London

Simultaneous recording of atmospherics on four different frequency bands in the low-frequency region

M. W. Chiplonkar and V. N. Athavale
University Department of Physics, University of Poona, Poona 7, India

(*Received* 10 *April* 1957)

Abstract—With a view to studying the variations in the intensity and the number of atmospherics received in the low-frequency region, four narrow band t.r.f. receivers were designed and constructed. The bands are 85 kc/s, 125 kc/s, 175 kc/s and 455 kc/s respectively. The output of the receivers were given to the X-deflecting plates of four identical cathode ray tubes. A moving plate camera with an $f/2{\cdot}5$ coated lens recorded simultaneously the deflections of all the c.r.t. spots. Records of 1 min duration were taken at two fixed hours (2000 and 2200 hours) during the night. In all over seventy plates were obtained during the period March–June 1956. The plates were measured to give intensities and number of atmospherics on the four bands. The results were analysed statistically and summarized in tables and presented in the form of histograms and curves. It is found that: (a) atmospherics with relatively large field strengths are less frequent than those with smaller field strengths on each band; (b) the field strength of atmospherics received on 125 kc/s band has maximum values as compared with those on the other bands and in fact is the seat of maximum activity of atmospherics with both large field strengths and number.

Introduction

With a view to carrying out an all-round study of the nature and origin of atmospherics in the low-frequency region (from 50 kc/s to 500 kc/s) an experimental station has been established in the University Department of Physics, University of Poona, since 1954. One of the objects is to study the variations in the number and the intensity of atmospherics *simultaneously* received on some narrow frequency bands in this region.

As far as our information goes such simultaneous observations of atmospherics, especially in the low-frequency region, have not been carried out by many workers so far. For instance, for a comparative study of the pulse durations of atmospherics in two different frequency regions Norinder (1947) employed a double-beam cathode-ray oscillograph and a recording camera. He obtained simultaneous measurements on two frequencies at a time, one of which was always in the low-frequency region and the other in the high-frequency region (e.g. 33 kc/s and 300 kc/s, 150 kc/s and 1500 kc/s, etc.). He found that "the disturbances on 33 kc/s band were all of a short total duration; while those on the 150 kc/s, 300 kc/s and 500 kc/s bands were composed of coherent groups of durations sometimes extending even up to one second."

Horner (1953, 1956) on the other hand, selected two frequencies at a time in the high-frequency region, 1–3 Mc/s apart. From the simultaneous measurements of the intensities of atmospherics and considerations of the ground wave propagation and skip distance he was able to obtain the distances of the sources of atmospherics from the place of observation.

For a comparative study of the waveforms of atmospherics Bowe (1951) applied a single atmospheric simultaneously to four narrow-band receivers tuned to different very low frequencies between 2 kc/s and 10 kc/s. He found that "waves of frequency below about 8 kc/s are heavily attenuated during the daytime

VOL
13
1958/

but are propagated freely at night. The attenuation is greater during a sudden ionospheric disturbance." (See also CHAPMAN and EDWARDS, 1950; CHAPMAN and MACARIS, 1956.)

For our study of the number and intensity of atmospherics we have selected at our station four well separated narrow frequency bands, viz. 85 kc/s, 125 kc/s, 175 kc/s and 455 kc/s, lying in the low-frequency region. Some of the interesting results of the preliminary observations carried out during the period March to June 1956 are presented in this paper.

EXPERIMENTAL TECHNIQUE

Four tuned radio-frequency receivers with almost identical electrical and electronic characteristics were designed and constructed for the purpose of this investigation [see Fig. 1(a)]. The choice of the present frequencies was made in order to avoid any interference with the frequencies of nearby broadcasting stations. It was seen that no nearby transmitting station was operating on any of the frequencies we have selected. All the receiver components used were identical as far as possible. The receivers were frequently tested and defects such as hum, oscillations, motorboating, etc., removed. The receiver characteristics were checked periodically by means of standard instruments (such as standard signal generator, vacuum tube voltmeter and a c.r.o.) and maintained constant within the practical limits throughout the period of observation.

VOL. 13 58/59

Each receiver was calibrated by means of the proper radio-frequency carrier signal which was modulated at 30 per cent by 400 c/s. This signal was derived from the standard signal generator (Marconi, T.F. 144 G) and was fed to the receiver input terminal through an equivalent dummy antenna. A vacuum tube voltmeter was used to measure the various radio-frequencies and audio-frequency voltages. The characteristics of the receivers are given in Table 1.

Table 1

Test \ Receiver	85 kc/s	125 kc/s	175 kc/s	455 kc/s
Sensitivity (μV)	30–60	30–50	30–50	20–45
Band width between half power points	6 kc/s	4·8 kc/s	5·4 kc/s	4·8 kc/s

Four identical cathode-ray tubes (ECR 35, Mullard) with screen diameter 3·5 in. and medium persistence green fluorescence were mounted side by side on a rack. The screens were arranged in a vertical plane in a row and at the same time maximum advantage of space in the photographic record was retained. The power supply circuit was specially designed and built for the purpose of supplying the required H.T. and L.T. power to all the cathode-ray tubes. The tubes were carefully shielded from stray electric and magnetic fields by proper shielding arrangements. The Y-(vertical deflecting) plates were earthed, together with

other electrodes not in use. One of the X (horizontal deflecting) plates was fed with the signal while the other was earthed. The deflexion sensitivity of each tube was determined separately and was found to be constant for a range of from 400 to 1400 V on the third anode.

Time-base circuit was not used. Intensity and focus controls were manually operated. A diode clipper circuit was used in parallel with X-deflecting plates. Due to this circuit the unwanted negative portion of the trace was clipped off and the deflexion made unidirectional only. Due to its very high input impedance the cathode-ray tube could be used as a voltmeter giving a direct record of the strength of atmospherics received. The outputs from the first audio frequency stages of the four receivers* were supplied to the X-deflecting plates of the four cathode-ray tubes respectively. The reception of atmospherics was indicated by the horizontal deflexions of the spot of the cathode-ray tubes. In order to avoid 50 c/s pickup from a.c. mains a circuit supplying the required voltage equal in magnitude but opposite in phase was occasionally employed.

A moving plate camera with an $f/2{\cdot}5$ coated lens (Taylor, Taylor and Hobson, $f = 16$ cm) was specially constructed for the purpose. Kodak P1200 photographic plates were found suitable.

Method of observation

All the electrical circuits were switched on for at least 10 min before a record was taken. This helped in stabilizing the electronic conditions of the receiver and adjusting the cathode-ray tube spots for their brightness, fineness and alignment. The record was made by moving the plate vertically downwards with a uniform speed for a period of one minute. The records were made at two fixed hours (2000 and 2200 hours) during the night-time, when it is found that the number of atmospherics received is relatively fairly large.

VOL
13
1958/

Results and Discussion

In all about seventy to seventy-five photographic records were obtained during the period March to June 1956. Some of the defective plates were rejected because of defocusing of the cathode-ray tube spots, inadequate exposures or even accidental recording of man-made noise. After eliminating these defective plates some fifty good plates were retained. Two typical records have been reproduced in Figs. 1(b) and (c). The number of atmospherics and their intensities were measured according to the following schemes and the numerical results thus obtained have been statistically analysed.

1.1. *Histograms of field strengths*

In this method of analysis the frequencies of occurrence of various impulse groups having different field strengths were considered. For this purpose the numbers of deflexions with their peak values lying in the various field-strength intervals (viz. 0–0·2 mV, 0–0·4 mV, etc.) were counted. The same procedure

* N.B. These receivers were also used for a study of the number of atmospherics received throughout the 24 hr by using mechanical counters and for which an additional amplifying stage was necessary.

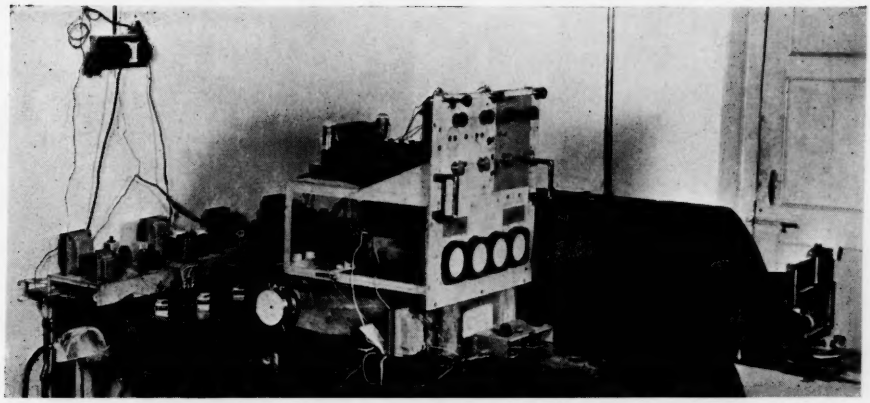

Fig. 1(a). Showing the four receivers at the extreme left, the four cathode-ray tubes in the middle and the recording camera at the extreme right.

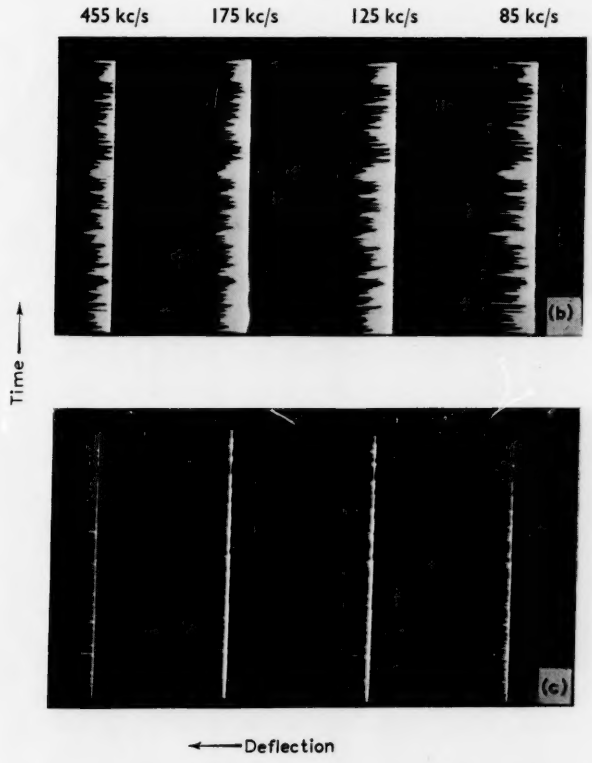

Fig. 1(b) and (c). Two typical records of atmospherics on four frequency bands each obtained during 1 min. Note the large deflexions and number of atmospherics in (b) in contrast to those in (c).

VOL.
13
1958/5

was adopted for all the four bands and for all the plates. It may be noted that it was not possible to count the exact number of pulses with their peaks lying in the low range group (0–0·2 mV) for all the bands, as the atmospherics recorded were too numerous to be resolved by the present speed of movement of the plate. This kind of situation extends up to 0·6 mV in the case of 125 kc/s band, indicating a greater strength of activity. The different field strength groups which show the unresolved atmospherics are given in the following table.

Table 2

Band (kc/s)	The unresolved groups (mV)
85	0–0·2
125	0–0·6
175	0–0·2
455	0–0·2

While drawing the histograms in Fig. 2, the first unresolved groups were seen to contain 100 per cent distribution of the number and in each case histograms based on measurements of resolved pulses only are prepared and shown after

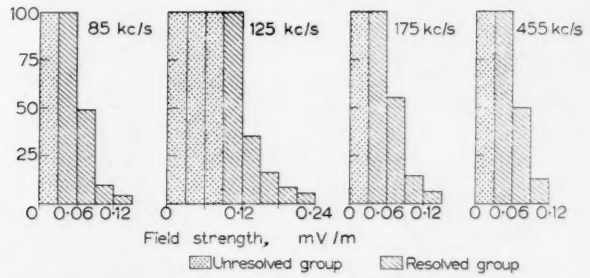

Fig. 2. Histograms showing the distribution of the number of atmospherics in the different field strength groups received on each of the frequency bands.

the unresolved group ranges. Naturally the countable numbers alone were used and shown as percentages, taking the value in the first *resolved* group for each band to be 100.

The general trend of each histogram is more or less identical and shows that there is a steep exponential fall in the number of atmospherics with the increase in the field strength, indicating that atmospherics with relatively greater field strength are less frequent.

1.2. *Monthly variation of the average peak field strength*

The plates were grouped according to the month. The *peak field strength* of atmospherics received on each band and for each plate was separately noted and all such readings were averaged for each band. A graph showing the relation between the average peak field strength in mV and the month was then plotted

(Fig. 3); it is seen that the relative peak field strength of atmospherics steadily increased from March to May and slightly decreased for the month of June. The figure also shows that the order of magnitudes of average peak field strength on the different frequency bands is 125 kc/s, 85 kc/s, 175 kc/s and 455 kc/s.

1.3. *Distribution of the peak field strengths*

In this method of analysis, as in (1.2), the peak field strength values observed for each separate band during 1 min intervals were selected. These field-strength values ranged from about 0·3 mV to 8 mV for all the bands and for all the plates.

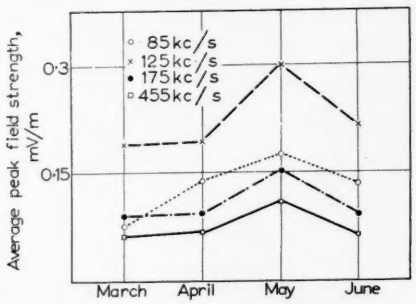

Fig. 3. Monthly variations of the average peak field strength of atmospherics.

They were grouped into three groups for each band separately and their numbers were noted according to the following scheme:

Group A: Large field strength 6·1–9·0 mV
Group B: Medium field strength 3·1–6·0 mV
Group C: Small field strength 0·0–3·0 mV

The results are shown in Table 3.

Table 3

Group	No.				
	85 kc/s	125 kc/s	175 kc/s	455 kc/s	Total
A	02	09	04	—	15
B	16	29	14	09	68
C	25	05	25	34	89
Total	43	43	43	43	172

It will be seen from this table that there is a systematic distribution of these peak-field-strength values amongst the four bands studied. On the whole the occasions of small field strengths are much more numerous than those of large field strengths. As before atmospherics with large field strengths (Groups A and B) are confined to the 125 kc/s band and those with the small field strengths (Group C) to the 455 kc/s band. The 125 kc/s band is seen to be the seat of maximum activity of atmospherics with large field strengths, as was mentioned in connexion with the unresolved values in Table 2.

VOL. 13 1958/5

1.4. *Comparison of simultaneous field strengths*

In this method of analysis the field strengths of atmospherics received simultaneously on all the four bands were compared. For the purpose of comparison the deflexion showing the peak value on any particular band was located and corresponding deflexions occurring at the same instant on the other three remaining bands were found. Naturally these latter deflexions were not necessarily the maximum on those bands recorded during the interval of 1 min. The values of the deflexions were noted and averaged for each band separately. A relation between the relative field strengths of atmospherics and the carrier frequency of the band is shown graphically in Fig. 4. This figure also shows that the field strength of

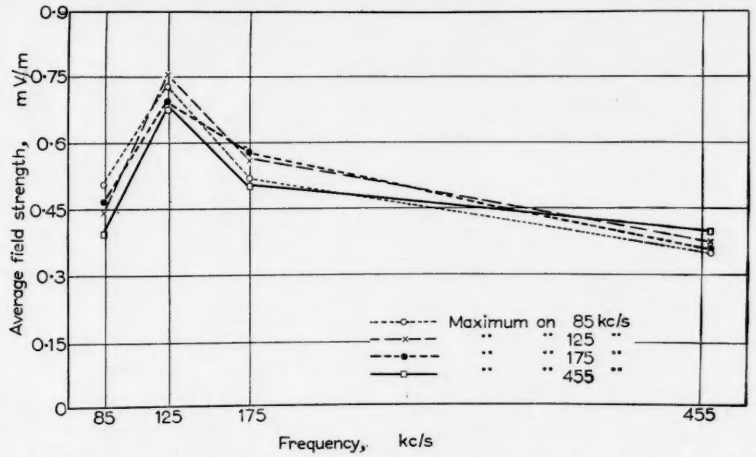

Fig. 4. Shows the relative field strength of atmospherics received simultaneously on different carrier frequencies.

atmospherics received on the 125 kc/s band has maximum values as compared with those received on the other bands. Also the order of carrier-frequency bands according to the decreasing magnitude of field strength of atmospherics is 125 kc/s, 175 kc/s, 85 kc/s and 455 kc/s which is only slightly different from the one observed in Section (1.2) above.

Conclusions

In concluding this short preliminary account we would like to point out that the work is being continued with some modifications in the present set-up in order to obtain a better time resolution in the record and more frequent observations during the 24 hr period. Arrangements are also being made to add at least one more receiver with a carrier-frequency band round about 300 kc/s.

References

Bowe P. W. A.	1951	*Phil. Mag.* **42,** 121.
Chapman F. W. and Edwards A. G.	1950	*Proc. Un. Radio. Sci. Int.* **8,** 351.
Chapman F. W. and Macaris R. C. V.	1956	*Nature, Lond.* **177,** 930–933.
Horner F.	1953	*J. Atmosph. Terr. Phys.* **4,** 129–140.
Horner F. and Harwood J.	1956	*Proc. Instn. Elect. Engrs.* **103,** No. 12, III.
Norinder H.	1947	*J. Franklin Inst.* **244,** 109; *J. Franklin Inst.* **244,** 167.

Journal of Atmospheric and Terrestrial Physics, 1958, Vol. 13, pp. 38 to 42. Pergamon Press, Ltd. London

Waveforms of atmospherics with superimposed pulses recorded with an automatic atmospherics recorder

B. A. P. Tantry and R. S. Srivastava
Banaras Hindu University, Banaras 5, U.P., India

(*Received 5 September* 1957)

Abstract—The automatic atmospheric recorder constructed and used by the authors has been briefly described. Of the various types of superimposed pulses recorded with its help, the "stepped" pulses from a lightning source, superimposed on the waveform due to a different lightning discharge has not been observed by previous investigators. Superimposed pulses, reflected successively from the ionosphere have been shown, where the superimposed pulses and the waveform on which they are superimposed originate from two different lightning sources or from the same lightning discharge. The "hook"–components of Malan and Schonland have also been recorded.

1. Introduction

The stepped structure in an "air-discharge" or in a β-leader gives rise to "pre-discharges" of an isolated type, whereas the "steps" and discontinuities in an α-leader give "pre discharges" followed by the features characteristic of the return-stroke of a lightning discharge. Norinder (1951) recorded some observations of superimposed "pre-discharges" from lightning discharges other than the one responsible for the recorded waveform. In the present paper we shall report some oscillographic observations of "stepped" pulses from a lightning source, superimposed on the waveform of an atmospheric pulse originating from a different lightning discharge. We shall also present oscillograms showing *separately* the "stepped" pulses from a lightning discharge and the waveform of the type similar to the one on which the "stepped" pulses were found superimposed. It is well known that an atmospheric pulse successively reflected from the ionosphere often gives rise to short or long wave-trains superimposed on the slow field-change or on the "slow-tail" component. In such superimposed waveforms, it has been shown in the paper that there are two distinct varieties. In one, the reflected pulses and the waveform on which they are superimposed originate from the same lightning discharge, and in the other, they are produced by two different lightning discharges. Typical records of the two varieties of superimposed reflected pulses have been shown. We shall also present a representative oscillogram out of a number of oscillographic records, showing the "hook-components" of Malan and Schonland (1947) on the slow field-change of an atmospheric pulse. For the lightning discharges of very near origin, the "hook"-components are in the form of small discontinuities (or minor depressions) in the c-field change; for discharges which are not so near, they assume the form of small radiative pulses.

The paper also describes the essential parts of the automatic atmospheric recorder which was designed and constructed by the authors. The details of the experimental arrangements have been published elsewhere Tantry (1958).

VOL
13
1958/

2. The Automatic Atmospherics Recorder

The different units in the automatic atmospherics recorder are briefly described below.

2.1. *Aerial unit*

A suitable damped antenna consisting of a long open air horizontal wire was employed, the time-constant of the antenna being small as compared with the duration of the atmospheric pulses.

2.2. *Main amplifier*

A wide-band linear voltage amplifier of the resistance-capacitance type, having a flat frequency-response characteristic from 100 c/s to 100 kc/s was constructed. The total gain obtainable was from 0 to 80 dB.

2.3. *Square-wave trigger*

The intensity-modulation of the cathode-ray oscillograph required for making it operative only at the incidence of the atmospherics, was effected with the help of a positive square-wave trigger unit in the following manner:

A part of the output voltage from the main amplifier, adjustable by means of a potentiometer, was fed into a single stage R/C-coupled triode amplifier, the output of which was connected to a cathode-follower phase-inverter. The input of the latter could be adjusted to any desired level without disturbing the gain of the main amplifier. The balanced output voltages (with respect to the ground) from the phase-inverter were fed into a double diode via two peak clippers, so that whatever be the polarity (positive or negative) and the amplitude of the initial portion of the atmospheric pulse, a positive voltage of almost fixed value (nearly 40 V) was developed between the cathode of the diode and the ground. The output from this double diode was then applied to a univibrator which remained quiescent until its action was initiated by a positive voltage of about 40 V at its input. The output from the univibrator gave a rectangular pulse of about 50 V. The univibrator was so arranged as to have a *quasi*-stable state of controllable time from 0·5 to 2·0 sec. This rectangular pulse was differentiated and then applied to a diode-clamping circuit from which only the sharp positive pulse was derived. This sharp positive pulse was utilized to trigger another univibrator, the ouput of which gave a rectangular pulse of about 40 V with a quasi-stable state of about 6 msec. This was applied to the modulating grid (normally kept at a high negative potential with respect to the ground) of the cathode-ray oscillograph causing the modulating grid to become *just* positive with respect to the cathode, thus allowing the cathode-ray beam to reach its full brilliance.

During the *quasi*-stable state of the first univibrator, lasting for a time 0·5–2·0 sec, no further intensity-modulating pulse could be derived from the subsequent atmospherics. The entire triggering circuit would thus have a quiescent time of the same duration after each triggering pulse, preventing thereby overlapping of oscillograms.

2.4. *Delay-line unit*

As a square-wave pulse generator would require a positive voltage of predetermined value, there must be a definite time-lapse between the arrival of the

atmospheric pulse and the restoration of the brilliancy of the cathode-ray beam, the magnitude of this time-delay depending upon the initial rise-time of the waveform of an atmospheric pulse. Hence in order to restore the initial portion of the waveform lost in the oscillographic record before triggering, it was necessary to delay the signal by about 60 μsec, whereas the undelayed signal was used for triggering the square-wave pulse generator.

The delay line was of negligible time-rise and was of the form of a low-pass, ladder-type filter having thirty sections, with negligible phase distortion. A suitable impedance matching amplifier was inserted between the main amplifier and the delay line.

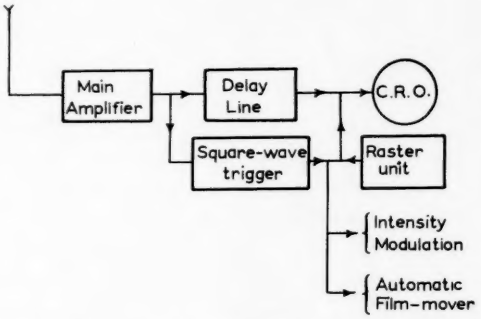

Fig. 1. Block diagram of the automatic atmospherics recorder.

VOL 13 1958/

2.5. *Automatic film-moving unit*

The intensity-modulating pulse derived from the square-wave trigger was differentiated once again and applied to another diode-clamping circuit, the output of which gave a positive pulse which was used to trigger another univibrator. A solenoidal relay placed in the plate circuit of the cut-off valve of the univibrator was energized during its *quasi*-stable state, thus completing the power supply line of a suitable electric motor fitted with a reducing gear system. The motor-drive was transmitted to the spindle of the camera, to that the exposed film could be automatically moved forward about 2 cm distance within a fraction of a second in the quiescent period of the first univibrator.

2.6. *Raster unit*

In this unit there was a thyratron linear time-base followed by a two-stage R/C-coupled amplifier. The first stage of the latter worked as a voltage amplifier and the second stage was an impedance-matching amplifier. The linear time-base of the cathode-ray oscillograph would by itself deflect the cathode-ray spot horizontally. When the raster linear time base with a period which was an integral multiple of that of the horizontal sweep was applied simultaneously to the vertical deflector plates of the cathode-ray oscillograph, several horizontal lines, one above another, were swept out and exhibited on the fluorescent screen of the oscillograph. Since the output from the main amplifier was applied to the same vertical deflector plates of the oscillograph through the delay-line unit, any electrical field-change

due to an atmospheric discharge would produce a corresponding vertical deflexion on the raster lines.

The purpose of the raster arrangement has been to provide for the longer duration of the oscillographic records without overlappings, at the same time permitting a greater time-resolution in the wave-form observations.

A block diagram of the automatic atmospherics recorder indicating its various units is shown in Fig. 1.

3. Oscillograms of the Waveforms of Atmospherics with Superimposed Pulses

Out of all the oscillograms of the waveforms of atmospherics with superimposed pulses, recorded at Banaras with the automatic atmospherics recorder during the course of our investigations on the waveforms of atmospherics, we shall *first* show, in Fig. 2, a typical record of the waveform of an atmospheric pulse from one lightning discharge with superimposed "stepped" pulses from a different lightning source. In each waveform, the superimposed pulses were invariably preceded by an "aperiodic" pulse of large amplitude (about 0·1 V/m). The striking feature in these waveforms was the uniform step-like structure on the slow field-changes. The time-interval between the successive "stepped" pulses of small amplitude were found to be about 50 μsec. Very few oscillograms of this type were recorded and they were observed when the lightning discharges were not very far.

VOL. 13 58/59

In Fig. 3(a) is shown a typical oscillogram of the "stepped" pulses, either from an "air-discharge" or from a β-leader. The "stepped" pulses from an α-leader are, however, followed by return-stroke pulses. Such "stepped" pulses were also recorded by us. The waveform in which the "stepped" pulses were found superimposed, as shown in Fig. 2, had a characteristic shape with initial sharp positive and negative peaks, followed by a rapid rise and a subsequent slow fall. Such form is usually associated with a lightning discharge at a distance of 15–300 km (*vide* Schonland *et al.*, 1940). A typical record of such a waveform, taken during the daytime, without any superimposition, is shown in Fig. 3(b).

With regard to the pulses reflected successively from the ionosphere and superimposed on the slow field-change, it was found that in most cases, the reflected pulses and the waveform on which they were superimposed belonged to two different lightning discharges. The time-interval between the successive reflected pulses superimposed on the slow field-change, shown in Fig. 4(a), gave the distance of the lightning discharge which was responsible for the reflected train. The distance was estimated as nearly 2000 km, whereas the characteristic shape of the waveform on which the reflected pulses were superimposed, suggested that the origin of the lightning discharge responsible for this waveform was not farther than 300 km. The superimposed reflected pulses, shown in Fig. 4(b) strongly suggested that the reflected train and the waveform on which they were superimposed belonged to one and the same lightning source. The observed time-interval between the successive crests in the reflected train gave the distance of the lightning discharge as 300 km.

The height at which an atmospheric pulse is reflected from the ionosphere and

the distance of the source can be determined from the formula:

$$h = 150 \cdot \frac{t_1 t_2 (t_1 + t_2)}{t_1(r^2 - q^2) - t_2(q^2 - p^2)}$$

$$D = \frac{d}{1 - h/R} = \sqrt{\left[\left\{\frac{1}{150} \cdot \frac{h^2(q^2 - p^2)}{t_1} - 150\, t_1\right\}^2 - 4p^2h^2\right]}$$

where h is the height of the ionospheric layer (km), d the great-circle distance on the earth's surface (km) between the source and the receiver, R the radius of the earth (km), $t_1 = t_q - t_p$ and $t_2 = t_r - t_q$, t_p, t_q, t_r being the time-intervals (msec) of the three pulses of the pth, qth, and rth orders of reflections. For evaluating h and D from the observed time-intervals of the reflected pulses, a graphical method similar to the one followed by CATON and PIERCE (1952) has been found convenient.

In Fig. 5, is shown a representative oscillogram showing the "hook"-components of MALAN and SCHONLAND (1947) on the slow field-change of an atmospheric pulse.

The dates and time when the waveforms of atmospherics were recorded are mentioned under the oscillograms.

Acknowledgements—Our sincere thanks are due to Prof. S. R. KHASTGIR, D.Sc., F.N.I., for guidance in this investigation. We are also indebted to the Council of Scientific and Industrial Research for sponsoring a research scheme on atmospherics, of which the present work forms only a part of the programme.

VOL. 13 1958/5

REFERENCES

CATON P. G. F. and PIERCE E. T.	1952	*Phil. Mag.* **43,** 393.
MALAN D. J. and SCHONLAND B. F. J.	1947	*Proc. Roy. Soc.* A **191,** 485.
NORINDER H.	1951	*Proceedings of the Second Meeting of the Joint Commission on Radio-Meteorology held in Brussels.* International Council of Scientific Unions.
SCHONLAND B. F. J., ELDER J. S., HODGES D. B., PHILLIPS W. E. and VAN WYK J. W.	1940	*Proc. Roy. Soc.* A **176,** 180.
TANTRY B. A. P.	1958	*Ind J. Phys.* **33,** No. 6, 267.

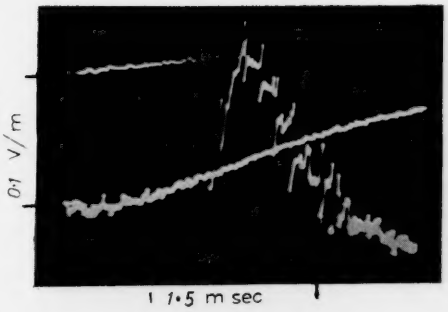

Fig. 2. A typical record of the waveform of an atmospheric pulse from one lightning discharge with superimposed "stepped" pulses from a different lightning discharge.
(Date: 19 June 1955; time: 10.30 p.m.)

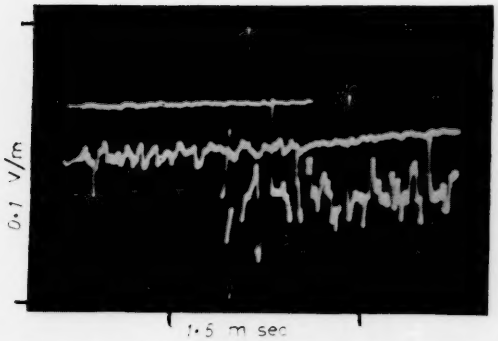

Fig. 3(a). A typical oscillogram of the "stepped" pulses either from an "air discharge" or from a β-leader.
(Date: 4 August 1955; time: night)

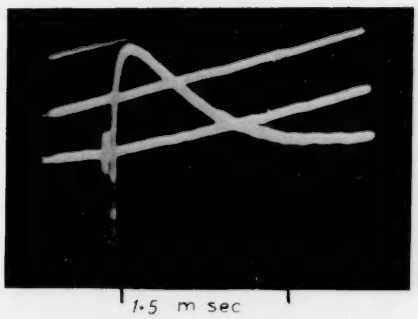

Fig. 3(b). A typical waveform of an atmospheric pulse without any superimposition.
(Date: 26 July 1957; time: 2.10 p.m.)

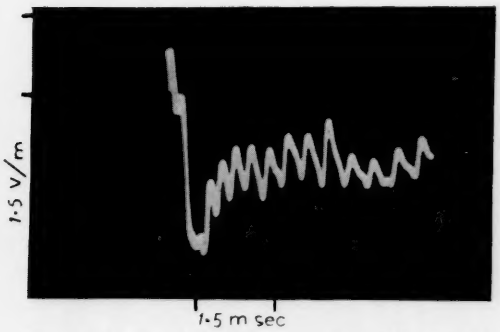

Fig. 4(a). Waveform with superimposed reflected pulses—the superimposed pulses and the waveform on which they were superimposed originating from two different lightning sources.
(Date: 9 July 1952; time: 8.40 p.m.)

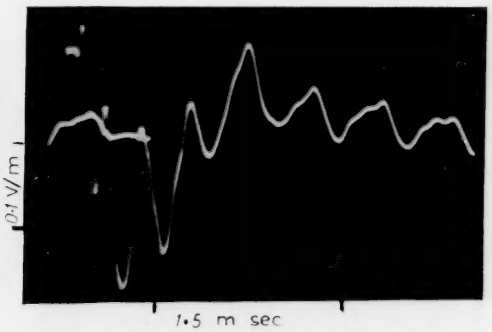

Fig. 4(b). Waveform with superimposed reflected pulses—the superimposed pulses and the waveform on which they were superimposed originating from the same lightning source.
(Date: 25 August 1952; time: 6.50 p.m.)

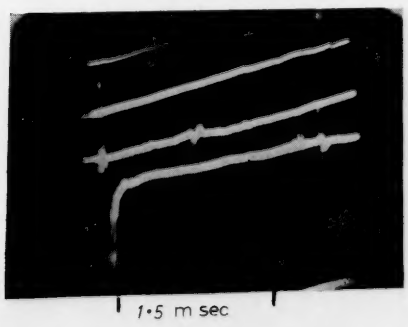

Fig. 5. A typical oscillogram showing the "hook" components of MALAN and SHONLAND.
(Date: 3 August 1957; time: 4.15 p.m.)

VOL.
13
1958/5

Journal of Atmospheric and Terrestrial Physics, 1958, Vol. 13, pp. 43 to 44. Pergamon Press Ltd., London

Non-uniformity in the brightness of the sun's disk at sunspot minimum

J. C. BHATTACHARYYA*
D.S.I.R. Radio Research Station, Slough

(*Received* 26 *February* 1958)

Abstract—Ionospheric changes during solar eclipses show that, even at sunspot minimum, the brightness of the sun's disk is not uniform. The brightness model derived by MITRA for the 1944 eclipse includes a complete bright ring round the disk, but that given by MINNIS for the 1954 eclipse does not. It is shown that the 1944 data can be explained in terms of an alternative model which does not include a bright ring but significant differences between the models for 1944 and 1954 still remain.

THE ionospheric changes which accompanied the solar eclipse of 20 July 1944 were first reported by BARAL and MITRA (1944) but they have recently been subjected to a more critical examination by MITRA (1957). At the outset it should be pointed out that the ionospheric parameters discussed by MITRA refer to the *F1* and not to the *E*-layer as stated; the critical frequencies quoted are consistent with those for the *F1*-layer at other stations during the same period.

The eclipse of 1944 occurred near sunspot minimum and for this reason it is interesting to compare the eclipse results obtained by MITRA with those for the 1954 minimum described by MINNIS (1956) and by LANDMARK *et al.* (1956). In spite of the low level of solar activity during both the 1944 and 1954 eclipses, all these investigators have concluded that the *F1*-layer ionizing radiation is not emitted uniformly from the whole area of the sun's disk. The models representing brightness distribution are not, however, identical for the 1944 and 1954 eclipses.

According to MITRA, the 1944 data can best be fitted to a model which includes the following sources of radiation:

J_D: background radiation emitted uniformly from the whole disk.

J_R: radiation from a thin circular bright rim on the visible disk.

J_E, J_W: additional radiation from the east and west limbs.

MINNIS (1958), has shown that, in spite of superficial differences between his model for the 1954 eclipse and that of LANDMARK *et al.*, both sets of results are consistent with a common model consisting of J_D, J_E and J_W, as in the Mitra model, with an elliptical central bright source, J_C, which extends to the east and west limbs but not to the poles. The poles are, therefore, assumed to be less bright than the centre of the disk.

Unless a bright rim around the disk is assumed to contribute a large fraction of the total radiation, ionospheric data are generally not accurate enough to make it easy to distinguish between a uniformly bright disk and such a disk surrounded by a bright rim. Thus it seems worth considering whether it would be possible to replace MITRA's 1944 model by an alternative model which excludes the bright rim and is in

* Permanent address: India Meteorological Department, Poona, India.

better agreement with the 1954 model. It has been found that this is possible, but only provided that the east and west limb sources are assumed to be much more intense than in 1954. It seems possible that a somewhat better fit between the observed and calculated data could be obtained by tapering off the brightness of the J_E and J_W sources towards the poles and by assuming slight darkening near the poles, but this has not been investigated in detail.

Table 1. Intensity of sources of ionizing radiation (per cent)

Eclipse	Source				Size of JE or JW	
	JD	$JE + JW$	JR	JC	r/R	θ
20 July 1944						
MITRA	48	27	25	—	?	?
BHATTACHARYYA	40	60	—	—	~0·1	105°
30 June 1954						
MINNIS	72	18	—	10	~0·2	60°

The numerical values for the contribution of the different sources for all three models are given in Table 1. There is nothing to choose between the two 1944 models as regards the closeness of the agreement with the experimental data. It is not known whether, on physical grounds, the original MITRA model, which includes a complete bright rim, is preferable to the alternative which necessitates the postulation of very bright sources at the east and west limbs. It is evident that whichever is assumed to be the more acceptable model, the ionospheric data appear to indicate significant differences between the characteristics of the sun in 1944 and 1954.

Acknowledgement—The work has been carried out as part of the programmes of the Radio Research Board. The author takes this opportunity of thanking the British Council for the award of a fellowship enabling him to visit various research establishments in the United Kingdom. This paper is published with the permission of the Director of Radio Research of the Department of Scientific and Industrial Research.

REFERENCES

BARAL S. S. and MITRA S. N.	1944	*Sci. & Cult.* **10,** 175.
LANDMARK B. *et al.*	1956	*Geofys. Publ.* **19,** No. 8.
MINNIS C. M.	1956	*J. Atmosph. Terr. Phys.* **9,** 201.
MINNIS C. M.	1958	*J. Atmosph. Terr. Phys.* In press.
MITRA N.	1957	*Indian J. Phys.* **31,** 69.

VOL 13 1958/

Journal of Atmospheric and Terrestrial Physics 1958, Vol. 13, pp. 45 to 60. Pergamon Press Ltd., London

$^1\Delta_g$–$^3\Sigma_g^-$ O_2 Infrared emission band in the twilight airglow spectrum*

A. Vallance Jones and A. W. Harrison
University of Saskatchewan, Saskatoon, Sask., Canada

(*Received* 22 *February* 1958)

Abstract—The 0,1 $^1\Delta_g$–$^3\Sigma_g^-$ O_2 emission band has been observed at 1·58 μ in the evening twilight spectrum obtained with a PbS infrared spectrometer. The band is absent in the morning twilight. The absolute brightness and decay of the emission for a constant zenith distance in the sun–zenith plane has been measured. The measurements have been compared with calculations of the brightness of the bands to be expected as a result of either a resonance phosphorescence excited by infrared solar radiation or by the reaction between atomic oxygen and ozone. A definite decision between these two mechanisms is not yet possible.

1. Introduction

The 1·2 μ to 2·0 μ wavelength region of the auroral and airglow spectrum has become accessible within recent years as a result of the development of a suitable PbS cell infrared spectrometer (Gush and Vallance Jones, 1955). The night airglow spectrum from 1·2 to 2·0 μ has been the subject of several studies which have shown that the predominant emissions are the Meinel OH vibration–rotation bands. Various authors (Krassovsky, 1954; Meinel, 1953) have suggested the possibility that the $A\,^1\Delta_g - X\,^3\Sigma_g^-$ system of O_2 might be observable in the night airglow emission since the related $B\,^1\Sigma_g$–$X\,^3\Sigma_g^-$ bands are prominent features of the photographic infrared spectra of the aurora and night airglow. Attention was therefore directed, at first, to the 1·27 μ region where the 0,0 band of the $^1\Delta_g$–$^3\Sigma_g^-$ system should lie. No emission has been detected, as yet, at this wavelength. In this paper an account is given of the discovery of an emission at 1·58 μ in the evening twilight airglow which proved to be the 0,1 band of the $^1\Delta_g$–$^3\Sigma_g^-$ system.

2. Experimental

The spectrometer used in this work has been described by Gush and Vallance Jones (1955). Spectra were obtained in the first order and the higher orders were eliminated with a 7–56 Corning filter. The resolving power is energy limited so that it is difficult to achieve resolution better than 100 Å because a decrease in the spectral slit width causes an intolerable decrease in the signal to noise ratio. However a very considerable improvement in resolution has been made possible by a condenser memory unit designed and constructed by Dr. D. M. Hunten. This apparatus stores and effectively averages a large number of successive spectra from the spectrometer; in this way the random noise fluctuations are averaged out so that a representation of the true spectrum is obtained. In this way is was possible to obtain spectra with a spectral slit width of 25 Å over a range of 250 Å.

Absolute brightness measurements were made by comparison with a secondary

* The research reported in this paper has been sponsored by the Geophysics Research Directorate of the Air Force Cambridge Research Center, Air Research and Development Command, under Contract AF 19(604)–1831

standard low brightness source which had been calibrated against a black body source according to the method described by HARRISON and VALLANCE JONES (1957).

3. OBSERVATIONS

The investigations of GUSH and VALLANCE JONES (1955) showed that the vibration rotation bands of OH predominate in the wavelength region between 1·0 μ and 2·0 μ. HARRISON and VALLANCE JONES (1957) studied the diurnal variation of the intensity of the OH bands in this region. In the course of these observations it was found that the Q-branch of the 4,2 OH band seemed to be

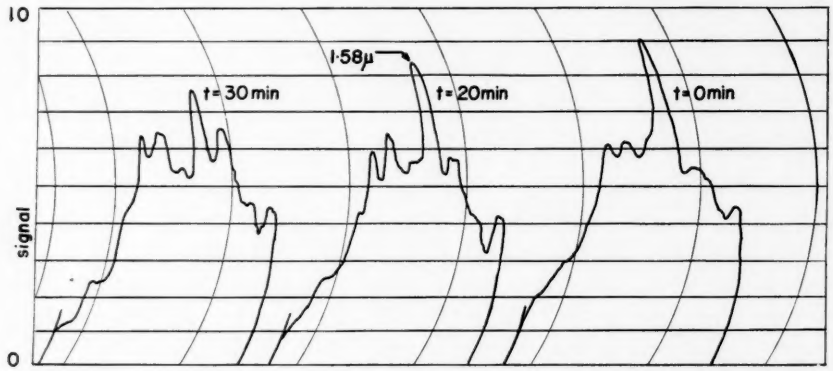

Fig. 1. Decay of 1·58 μ emission feature. Times given are measured from the time of sunset at a height of 70 km, on the line of sight of the spectrometer. The spectrometer was directed at an azimuth angle equal to that of the sun and at a zenith distance of 80°. This sunset time is calculated for a screening height of 40 km.

intensified during the evening twilight. This enhancement was found to be greatest in the early twilight and was most clearly defined when the line of sight of the spectrometer was directed to have the same azimuth angle as the sun and a zenith angle of 80°.

Twelve evening twilight runs were made in this way during January and February 1957; on each occasion the twilight enhancement at 1·58 μ was observed with about the same intensity. Six morning twilight runs were made during the same period but none showed any sign of the enhancement. All these observations were made when the sky was relatively free from haze and consequently there can be no doubt that the intensification of the emission at 1·58 μ is characteristic of the evening twilight only. A typical set of spectra observed at different times during the evening twilight is shown in Fig. 1; the spectral slit width was 200 Å. These spectra show that the enhancement at 1·58 μ decays slowly throughout the twilight until the normal night airglow spectrum due to OH remains.

The enhancement of intensity occurs at 1·58 μ only. This observation rules out the possibility that the effect is due to an intensification of the 4,2 OH band because this would lead to a corresponding increase of intensity in the P- and R-branches of this band. An alternative explanation is that some other emission feature at 1·58 μ appears with comparatively high intensity during the evening twilight. A study of the lines and bands which could occur in this region of the

VOL
13
1958/

spectrum showed that the hitherto unobserved 0,1 band of the $^1\Delta_g - ^3\Sigma_g^-$ atmospheric O_2 bands should occur at 1·58 μ. The wavelength of this band can be predicted exactly since the 0,0 and the 1,0 bands of this system have been studied in the terrestrial atmospheric absorption spectrum by HERZBERG and HERZBERG (1947). Therefore, the twilight enhancement at 1·58 μ was ascribed provisionally to this band and further observations were carried out to test the hypothesis.

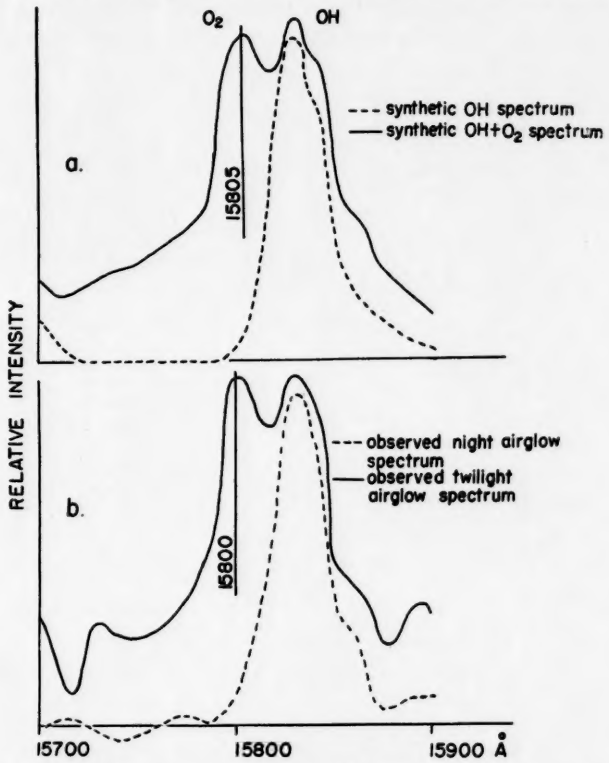

Fig. 2. (a) Synthetic OH spectrum and combined OH/O_2 spectrum from 1·57 to 1·59 μ for a spectral slit width of 25 Å.
(b) Observed nightglow and twilight spectra for spectral slit width of 25 Å.

The first test was a comparison between the observed twilight spectrum near 1·58 μ and a calculated synthetic spectrum. To make this test the more decisive a higher resolution spectrum of the twilight emission was obtained with the help of the condenser memory unit. A spectrum obtained with a spectral slit width of 25 Å is shown in Fig. 2(b). In this spectrum the twilight emission feature and the Q-branch of the OH band are resolved from one another; this provides conclusive evidence for the presence of a new emission feature peculiar to the evening twilight. The resolution attained is still insufficient to resolve the individual rotational lines of the overlapping OH bands and the O_2 band. Therefore synthetic spectra were calculated for the $^1\Delta_g - ^3\Sigma_g^-$ O_2 band superposed on the 3,1; 4,2; and 5,3 OH bands. A triangular transmission function of spectral slit width 25 Å was assumed

for the spectrometer. The intensities of the rotational lines of the O_2 band were calculated for a Boltzmann distribution for 250°K among the rotational levels; this temperature was chosen since it is shown later that the emission probably arises from the 60 km level at which height the temperature is about 250°K. The wavelengths of the rotational lines of the O_2 band were calculated from the data of HERZBERG and HERZBERG. All lines for $K'' \leqslant 30$ were considered; the line strength factors were calculated from the formulae of VAN VLECK (1934). The intensities of the rotational lines of the OH bands were calculated assuming a Boltzmann distribution for 260°K which is the vibrational temperature observed by MEINEL

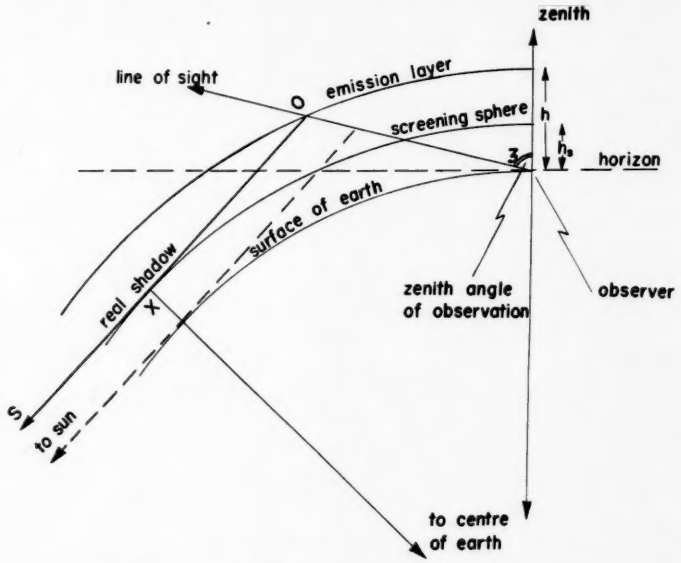

Fig. 3. Diagram showing geometry of twilight emission process.

for OH bands in the photographic infrared region. The relative OH band intensities of HEAPS and HERZBERG were used. A suitable choice of the intensity ratio between the $^1\Delta_g$–$^3\Sigma_g^-$ O_2 band and the OH bands led to the synthetic spectra shown in Fig. 2(a). It can be seen that the synthetic and observed spectra are almost identical. This similarity provides very strong evidence that the O_2 band is indeed present in twilight. A synthetic spectrum (not reproduced here) was calculated also for a spectral slit width of 200 Å. This calculated spectrum is very similar to Fig. 1 and in particular shows that at this spectral slit width the two peaks are not resolved.

A second test of the postulated identity of the twilight emission is provided by a comparison of its observed absolute intensity and rate of disappearance with theoretical values of these quantities calculated on the basis of the excitation mechanism proposed below. Consequently careful measurements were made of the absolute brightness of the twilight emission during the period over which it was observable. For these observations the line of sight of the spectrometer was directed at a zenith angle of 80° and at an azimuth angle equal to that of the sun.

VOL
13
1958/

The centre of the earth then lies in the same plane as the sun and the line of sight of the spectrometer as illustrated in Fig. 3. Since the decaying O_2 band is superposed on the night airglow OH bands the absolute brightness of the former must be determined from the difference between the areas under the curves for the twilight spectrum and the pure night airglow spectrum. The night airglow spectrum was obtained well after the twilight enhancement at 1·58 μ had vanished. The results obtained for a typical night are shown in Fig. 4. The ordinates in this figure are brightnesses in rayleighs* referred to the zenith. The zero of the time scale corre-

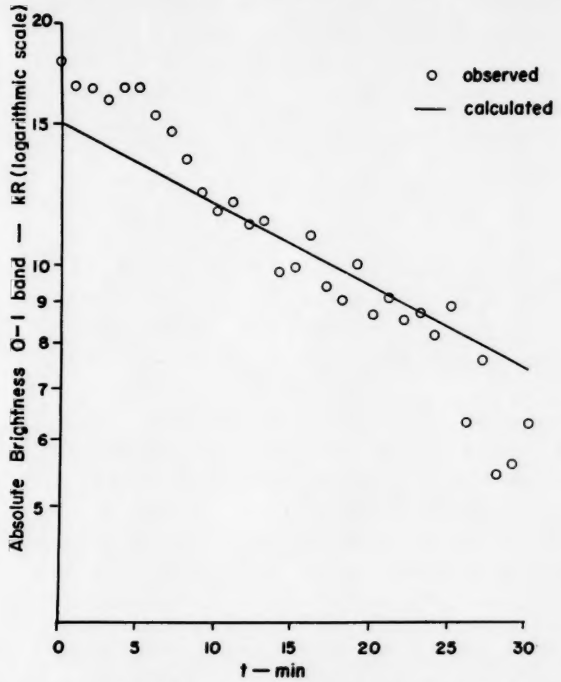

Fig. 4. Observed and calculated decay of 0,1 $^1\Delta_g - ^3\Sigma_g^- O_2$ band in twilight. The calculations are for the resonance phosphorescence process.

sponds to that time at which the shadow surface cast by a layer in the earth's atmosphere at a height of 40 km intersects the line of sight of the spectrometer at the 70 km level (i.e. when $h = 70$ km for $h_s = 40$ km and $\mathscr{Z} = 80°$ in Fig. 3). In Table 1 are given the results of a series of measurements for different evenings measured for the same zero time as for Fig. 4.

The discussion of the interpretation of the results of Fig. 4 and Table 1 will be taken up in the next section.

Since the twilight feature at 1·58 μ has been identified as the 0,1 O_2 ($^1\Delta_g - ^3\Sigma_g^-$) band the question arises as to whether the 0,0 band of this system should be observable at 1·27 μ. Several attempts were made to observe this band in the

* The brightness in rayleighs (R) (HUNTEN, ROACH and CHAMBERLAIN, 1956) equals $4\pi B$, where B is the angular surface brightness of the emitting layer in units of 10^6 photons/cm^2 steradian sec.

Table 1. Absolute brightness of 0–1 $^1\Delta_g$–$^3\Sigma_g^-$ O_2 band referred to zenith

Date (1957)	Jan. 12	Feb. 1	Feb. 7	Feb. 17	Feb. 18	Feb. 22	Mean
Brightness (kR)	18·3	12·2	19·6	17·1	19·8	18·1	17·6

evening twilight airglow but they were without success. The reasons for this failure will be discussed in Section (5).

4. EXCITATION MECHANISM OF ($^1\Delta_g$–$^3\Sigma_g^-$) O_2 BAND

Molecules of oxygen excited to the $^1\Delta_g$ state could be formed by a number of processes of which reactions (1), (2) and (3) are the most probable.

$$O + O + M \rightarrow O'_2 + M \quad (1)$$

$$O_2(^3\Sigma_g^-) + h\nu \rightarrow O'_2 \quad (2)$$

$$O + O_3 \rightarrow 2\,O'_2 \quad (3)$$

The symbol O'_2 will be used to denote an O_2 molecule excited to the $^1\Delta_g$ state. While reaction (1) can be eliminated it does not seem possible to decide definitely between reactions (2) and (3). A full discussion has been given of both reactions to provide a starting point for further work. These processes will be discussed in turn:

VOL. 13 1958/5

4.1. *Three body recombination of atomic oxygen* [*reaction* (1)]

In this process atomic oxygen formed by dissociation during the day would recombine through reaction (1) and it is reasonable to expect that a substantial fraction of the O_2 molecules formed would be excited to the $^1\Delta_g$ state. If this reaction is responsible for the twilight emission then this emission should be concentrated in the region between 80 km and 90 km where the product $n^2(O)\cdot n(M)$ has its maximum value. At this level however the concentration of atomic oxygen remains almost constant throughout the night (BATES, 1954) so that the twilight emission as observed cannot be ascribed to reaction (1).

4.2. *Phosphorescent excitation of molecular oxygen* [*reaction* (2)]

In this case the oxygen is excited directly by absorption of solar radiation. This process is analogous to that responsible for the excitation of sodium in the twilight except that the radiative half-life of the oxygen molecule is about 60 min. As is pointed out below this long lifetime can account for the absence of the oxygen band from the morning twilight. Evidence that reaction (2) may be responsible for the twilight emission is provided by the agreement between the absolute brightness and rate of decay of the O_2 emission and the values of these quantities calculated on the basis of this reaction.

In making this calculation the following factors must be taken into account:

4.2.1. The long radiative half-life of the $^1\Delta_g$ state.

4.2.2. Collisional deactivation of excited $^1\Delta_g$ O_2 molecules.

4.2.3. The effect of atmospheric refraction and absorption on the location of the solar shadow surface in the atmosphere.

4.2.4. The movement of the solar shadow surface through the atmosphere.

The effect of these factors will now be discussed in turn:

4.2.1. *Radiative lifetime of the* $^1\Delta_g$ *state of* O_2. The half-life of the $^1\Delta_g$ state for spontaneous radiative emission is given by the expression:

$$t_{\frac{1}{2}} = 0{\cdot}69/\sum_{v''} A'(0,v'') \simeq 0{\cdot}69/A'(0,0) = 3{\cdot}6 \times 10^3 \text{ sec} = 60 \text{ min}$$

where $A'(v',v'')$ is the Einstein transition probability for v',v'' vibrational transition of the $^1\Delta_g - ^3\Sigma_g^-$ system. $\sum_{v''} A'(0,v'')$ is approximately equal to $A'(0,0)$ because the internuclear distance of O_2 in the $^1\Delta_g$ state is almost identical with the value for the $^3\Sigma_g^-$ state. When this is so the Franck–Condon parabola degenerates into a straight line and consequently $A'(0,0) \gg A'(0,1) \gg A'(0,2)$, etc.

This long half-life would, in the absence of other effects lead to a much slower decay of the emission than is observed. The results given in Fig. 4 show that the emission in fact falls to half its initial intensity in 20 min.

4.2.2. *Collisional deactivation.* A very plausible explanation of the accelerated decay of the emission is collisional deactivation of the excited $^1\Delta_g$ state. This effect causes the half-life of the excited O_2 molecules and the daytime equilibrium ratio of excited to unexcited molecules to become functions of height. In order to treat the problem quantitatively it is convenient to introduce a constant, F, which expresses the probability that a two-body collision involving a $^1\Delta_g$ molecule will result in the deactivation of that molecule.

4.2.3. *Atmospheric absorption and refraction.* Since the exciting solar radiation must traverse the lower atmosphere at X (Fig. 3) before reaching the region from which the phosphorescence is observed, there will be a very considerable pre-absorption of the exciting radiation. Consequently one cannot consider the surface of the earth as casting the shadow, at the wavelengths responsible for the excitation process; instead one can consider that the shadow is cast by a level in the lower atmosphere at the so-called "screening height", h_s, above the surface. Radiation capable of exciting the $^1\Delta_g$ state, traversing a path which has a minimum height equal to h_s will then be attenuated by a factor $1/e$. Although the shadow in the exciting radiation cast by the screening layer will be somewhat diffuse it should be a reasonable approximation to treat it as a sharp shadow surface. The screening height was calculated by the method given in Appendix I; the result obtained was 40 km.

Atmospheric refraction causes the shadow surface to be bent downwards to lower heights. However for a screening height of 40 km this refraction effect is negligible.

4.2.4. *Motion of shadow surface.* The observations reported here were commenced when the shadow surface arising from the screening height intersected the line of sight of the spectrometer at a height of 70 km. During the course of the evening twilight observations the shadow surface rises. The position of the shadow surface can be specified by introducing a function $t(h)$ which specifies the time at which sunset occurs at different heights, h, along the line of sight of the spectrometer. A plot of this function for $h_s = 40$ km and $\mathscr{Z} = 80°$ is given in Fig. 6. Since the time required for the shadow layer to traverse the effective emitting

region is appreciable in comparison with the lifetime of the excited oxygen molecules it is clear that account must be taken of this factor in calculating the rate of decay of the twilight emission.

The rate of production of excited $^1\Delta_g$ O_2 molecules by reaction (2) is:

$$dn'/dt = n.B''(0,0) \,.\, \rho(0,0) \tag{7}$$

while the rate of loss from the $^1\Delta_g$ state is:

$$-dn'/dt = n'[A'(0,0) + B'(0,0) \,.\, \rho(0,0) + z \,.\, F] \tag{8}$$

where

n is concentration of ground state O_2 molecules,
n' is the concentration of $^1\Delta_g$ O_2 molecules in $v' = 0$ vibrational level,
z is the two-body collision rate experienced by a single molecule,
$\rho(0,0)$ is the solar radiation density for the wavelengths capable of exciting the 0,0 band of the $^1\Delta_g$–$^3\Sigma_g^-$ system and
$A'(v',v'')$, $B'(v',v'')$, and $B''(v',v'')$ are the Einstein transition probabilities for spontaneous emission, induced emission and absorption respectively.

For daytime equilibrium:

$$n \,.\, B''(0,0) \,.\, \rho(0,0) = n'[A'(0,0) + B'(0,0) \,.\, \rho(0,0) + z \cdot F] \tag{9}$$

Values of $A'(0,0)$, $B'(0,0)$ and $B''(0,0)$ were estimated from the equivalent widths of lines of the 1·27 μ terrestrial O_2 absorption band which appears in the solar spectrum. The details of this calculation are given in Appendix II. The magnitude of F is very uncertain; it was found in the present work that a value of 8×10^{-11} led to a reasonably correct prediction of both the observed decay rate and the absolute brightness of the twilight emission. Since these two observed quantities are largely independent of each other, the agreement obtained still provides a test of the theory.

The equilibrium values of n' as a function of height were calculated from equation (9). The numerical values of n and z were calculated from the ROCKET PANEL (1952) data. $\rho(0,0)$ was calculated to be $2{\cdot}34 \times 10^{-9}$ erg/cm^2, from the data of MINNAERT (1954) for the differential brightness of the sun in the infrared. A plot of n', the equilibrium concentration of excited $^1\Delta_g$ O_2 molecules against height is shown in Fig. 5. When the solar shadow surface rises through the atmosphere the production of excited oxygen molecules ceases in the dark regions and the instantaneous concentration of excited molecules is governed by equation (8). At any time, t, the interval for which the region at height, h, has been dark is given by $t - t(h)$, where $t(h)$ is the sunset function plotted in Fig. 6. Consequently the concentration of excited molecules is obtained by integrating equation (8). The result obtained is:

$$n'(h,t) = n'_e(h) \exp\,[-\{A'(0,0) + z(h).F\}\{t - t(h)\}] \tag{10}$$

where $n'_e(h)$ is the daytime equilibrium value of $n'(h)$. Plots of $n'(h,t)$ are given in Fig. 5 for a set of values of t; the heights for which the shadow surface intersects the line of sight are indicated for each value of t. The emission per cm^2

VOL.
13
1958/5

(column) at any time t, can then be found by numerical integration from Fig. 5 to find the total number of $^1\Delta_g$ O_2 molecules/cm^2 (column) at that time and subsequent multiplication by the transition probability; thus:

$$4\pi B(t) = A'(0,1)\int_0^\infty n'(h,t)\,dh$$

Numerical integration gave the results in Table 2. It should be noted that the results of this integration give values of a fictitious quantity which is the brightness which would be observed in the zenith if the sunset function $t(h)$ had

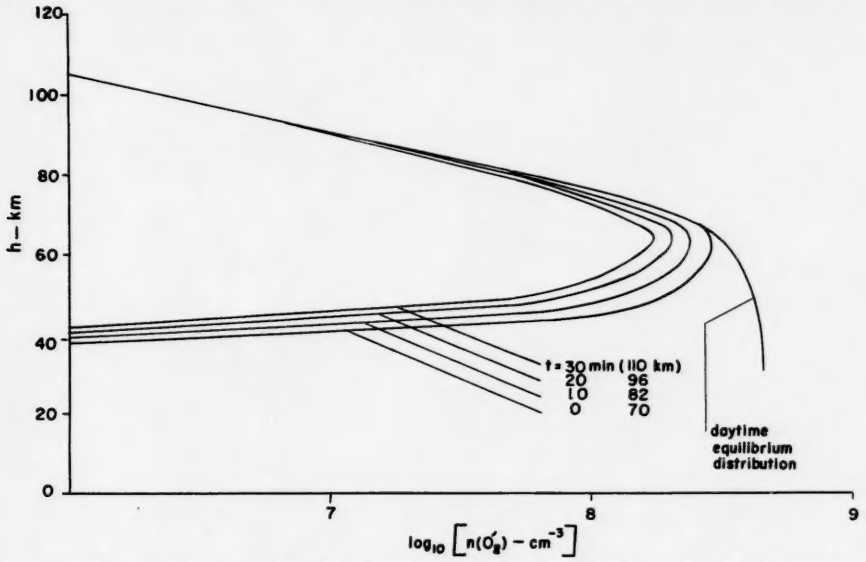

Fig. 5. Concentrations of $^1\Delta_g$ O_2 molecules as a function of height calculated for the resonance phosphorescence process. The time scale is the same as that described in the caption for Fig. 1.

the same values in the zenith as it has along the actual direction of observation at a zenith angle of 80°. However, these fictitious brightnesses should be directly comparable with the results in Fig. 4, which have been referred to the zenith by dividing by the van Rhijn factor.

Table 2. Calculated decay of absolute brightness on basis of reaction (2). Time measured from sunset at 70 km height for $h_s = 40$ km and $\mathscr{Z} = 80°$

Time (min)	0	10	20	30
Brightness (kR) (referred to zenith)	15	11·7	9·4	7·4

A curve corresponding to the theoretical results of Table 2 is plotted in Fig. 4. It will be seen that the agreement between the theoretical curve and the observed points is fairly good. This agreement provides some support for the phosphorescence theory for the origin of the observed emission.

4.3. *Ozone–oxygen reaction* (*reaction* 3)

Serious consideration must be given to this reaction because, in the first place, the rate at which excited oxygen is produced in this way may be comparable with the rate at which it is produced by reaction (2) and, secondly, the production of excited oxygen ceases fairly quickly after sunset, since at the 60–70 km level the atomic oxygen is removed by the reaction:

$$O + O_2 + M \rightarrow O_3 + M \qquad (4)$$

An estimate was therefore made, of the distribution of excited $^1\Delta_g$ molecules which would be found as a consequence of reaction (3).

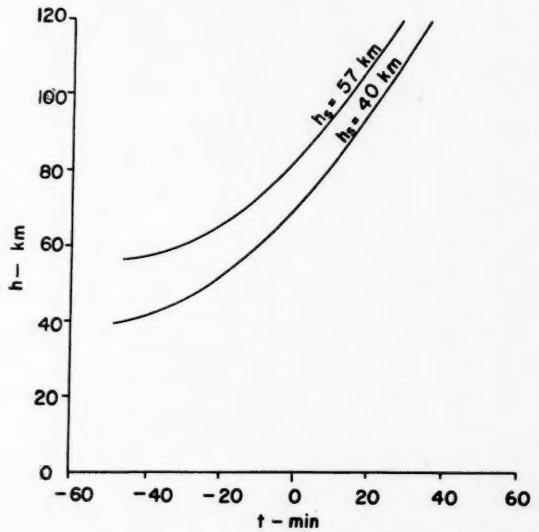

Fig. 6. Times of sunset as a function of height, h, along the line of sight of the spectrometer (as specified in caption to Fig. 1) calculated for screening heights of 40 km and 57 km.

The rate of production of excited molecular oxygen, O'_2, as determined by reaction (3) and by radiative and collisional deactivation is:

$$dn(O'_2)/dt = 2p \,.\, k_3 \,.\, n(O) \,.\, n(O_3) - [A'(0,0) + z \,.\, F] \,.\, n(O'_2) \qquad (11)$$

where p is the factor giving the efficiency of reaction (3) for excitation of O_2 into the $^1\Delta_g$ state, and the other symbols have their previously defined meaning. Simultaneously the concentration of atomic oxygen is decreasing by reaction (4) so that

$$dn(O)/dt = -k_4 \,.\, n(O_2) \,.\, n(M) \,.\, n\,(O) \qquad (12)$$

Solution of equations (11) and (12) for the instantaneous concentration of excited oxygen at a time, t, after sunset gives the result:

$$n(O'_2) = \frac{2p \,.\, k_3 n_e(O) \,.\, n_e(O_3)}{A'(0,0) + z \,.\, F - k_4 n(O_2) \,.\, n(M)} [\exp\{-k_4 \,.\, n(O_2) \,.\, n(M) \,.\, (t - t(h))\}$$

$$- \exp\{-(A'(0,0) - z \,.\, F) \,.\, (t - t(h))\}] + n_e(O_2') \exp\{-(A'(0,0) + z \,.\, F) \,.\, (t - t(h))\} \qquad (13)$$

VOL
13
1958/

where $n_e(O'_2)$ gives the daytime equilibrium concentration, which can be inferred from equation (11) to be given by the expression

$$n_e(O'_2) = \frac{2p \,.\, k_3 \,.\, n_e(O) \,.\, n_e(O_3)}{A'(0,0) + z \,.\, F} \tag{14}$$

$n_e(O)$ and $n_e(O_3)$ are the equilibrium daytime concentrations of atomic oxygen and ozone respectively.

Rough estimates of the values of k_3 and k_4 are available (BATES, 1954). The values adopted were $k_3 = (1{\cdot}8 \times 10^{24}) \exp(-3070/T) k_4$ and $k_4 = 5 \times 10^{-36} T^{\frac{1}{2}}$

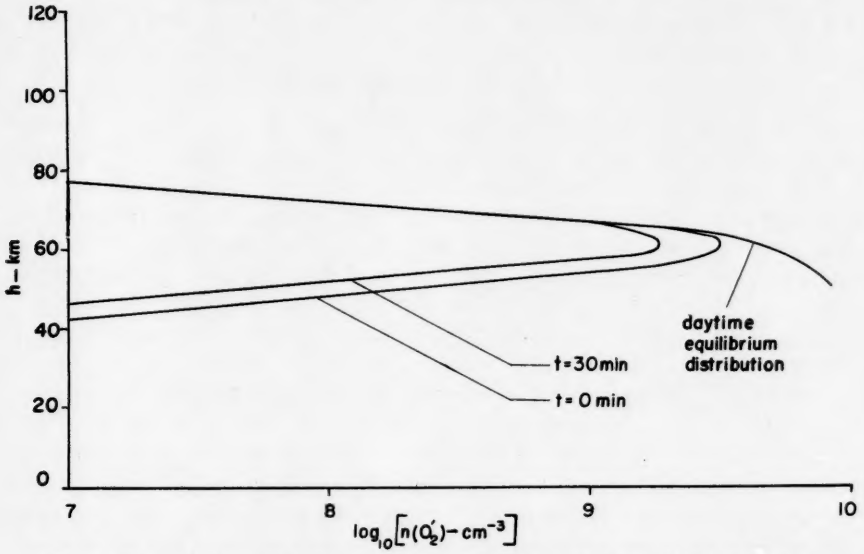

Fig. 7. Concentration of $^1\Delta_g$ O_2 molecules as a function of height calculated for the ozone–oxygen reaction. The time-scale is the same as that described in the caption for Fig. 1.

cm^6/sec. Calculated values of the daytime equilibrium concentrations of atomic oxygen and ozone were taken from the work of NICOLET (1957). In the application of equation (13) it is however necessary to know the time of sunset for the radiation which is effective in the dissociation of molecular oxygen. In the 60 to 80 km height range the effective dissociating radiation is that of the Herzberg continuum. An approximate estimate (Appendix I) suggested that a screening height of 57 km should be taken for this radiation (2000–2400 Å). The sunset function $t(h)$ for $h_s = 57$ km is also given in Fig. 6. As a consequence of the greater screening height for the ultraviolet light the sunset occurs earlier at these wavelengths and therefore the decline in the concentration of excited oxygen begins sooner.

In Fig. 7 are plotted the results for the concentrations of excited $^1\Delta_g$ oxygen molecules as a function of height for the daytime equilibrium value, for a time when the 1·27μ shadow surface is at 70 km and for a time when this layer reaches 110 km. These results were obtained using equations (13) and (14) taking $p = 1$. The values in Fig. 7 are directly comparable with those of Fig. 5. The integrated

brightness of the 0,1 band to be expected at $t = 0$ would then be 65 kR compared to 15 kR for the phosphorescence mechanism. However the efficiency factor, p, is unlikely to be greater than 0·5 and might be much smaller. Therefore it seems that the yield from the ozone–oxygen reaction may be less than that from the phosphorescence. However it must be noted that the uncertainties in the values of the rate constants for the reactions (3) and (4) and for p make it difficult to make reliable calculations for the ozone–oxygen reaction.

A similar calculation was carried out using the values of $n_e(O)$ and $n_e(O_3)$ calculated by Bates and Witherspoon (1952). The result obtained was 4 kR compared to the 65 kR obtained above. The difference between these two results illustrates the difficulties involved in deciding the contribution of reaction (3) to the observed emission.

5. Discussion of Results

The experimental and theoretical results of the two previous sections provide the basis of an explanation of the appearance of the oxygen band in the evening twilight. In this section some additional points will be considered.

The failure to observe the 1·58μ band in the morning twilight can be understood as a consequence of the long lifetime of the $^1\Delta_g$ state in the height range from which the principal contribution to the emission is obtained. In the morning twilight the concentration of excited oxygen molecules does not have time to build up to a high enough value to give an observable emission before lower levels of the atmosphere are illuminated. Consequently the emission is masked by scattered light from the denser atmosphere below before it is bright enough to be detected.

The absence of the 0,0 band in twilight emission is to be attributed to reabsorption by oxygen of the lower atmosphere. The emission rate of the 0,0 band should be about ten times that of the 0,1 band. On the other hand the central optical depth of the atmospheric oxygen for the strongest line of the 0,0 band, the $^RR(K'' = 3)$ rotational line was calculated to be about 12. Consequently the transmission at the centre of the line would be about 0·006 per cent so that the transmitted intensity for this line of the band would be about 0·06 per cent of that of the corresponding line of the 0,1 band. Since it is unlikely that an emission with less than 10 per cent of the intensity of the 1·58 μ feature could be distinguished from background noise it is not surprising that no trace of an emission at 1·27 μ was discovered.

Acknowledgements—The authors would like to acknowledge the kindness of Dr. D. M. Hunten in making available the condenser memory unit and also the value of many useful discussions.

Appendix I

Screening heights must be calculated for the direct excitation of O_2 to the $^1\Delta_g$ level and for the dissociation of oxygen by absorption in the Herzberg continuum. If $k(\lambda)$ represents the total extinction coefficient of air at N.T.P. at wavelength, λ, and $k'(\lambda)$ represents the extinction coefficient attributable to the process in question, then if l is the equivalent path at N.T.P. through the

VOL
13
1958/

atmosphere along the path SO (Fig. 3) the screening height, h_s, may be defined to be such that:

$$\frac{\int I_0 \cdot \exp(-kl)\, k' \cdot d\lambda}{\int I_0, k' d\lambda} = 1/e \tag{1}$$

where I_0 is the incident intensity of solar radiation outside the earth's atmosphere. This must be so, since the denominator is proportional to the rate of the excitation process in unit volume of air exposed to direct solar radiation. The numerator is proportional to the rate of excitation produced under the same conditions by solar radiation which has been attenuated by passage through an equivalent path, l, of air.

For direct excitation in the 0,0 $^1\Delta_g - ^3\Sigma_g^-$ band, $k'(\lambda) = k(\lambda)$ and I_0 may be taken as constant across the band. k however varies rapidly over the rotational lines of the band. The absorption coefficient for each line (for Doppler broadening) can be written $k = k(n,m) \exp(-x^2)$ where x is proportional to the wavelength difference from the line centre and $k(n,m)$ is the peak absorption coefficient of the mth line of the nth branch of the band. Consequently the left-hand side of (1) becomes:

$$\frac{\sum_n \sum_m k(n,m) \int_0^\infty \exp\{-k(n,m) e^{-x^2} l\} \exp(-x^2)\, dx}{\sum_n \sum_m k(n,m) \int_0^\infty \exp(-x^2)\, dx} \tag{2}$$

The analysis of a similar problem by HUNTEN (1956) shows that (2) is approximately equivalent to:

$$\frac{\sum_n \sum_m k(n,m) \exp\{-k(n,m) l/\sqrt{2}\}}{\sum_n \sum_m k(n,m)} \tag{3}$$

For the lines of the branches of the bands of the $^1\Delta_g - ^3\Sigma_g^-$ system, $k(n,m) \simeq k(n) m \exp(-\beta m^2)$. The summation over m can be replaced by an integration so that (3) becomes:

$$\frac{\sum_n k(n) \int_0^\infty m \exp(-\beta m^2) \exp[-\gamma m \cdot e^{-\beta m^2}] dm}{\sum_n k(n) \int_0^\infty m \exp(-\beta m^2) dm} \tag{4}$$

where $\gamma = k(n) l/\sqrt{2}$

The integral in the denominator equals $1/2\beta$. It is easy to show by expanding the integrand in series and integrating term by term that the integral in the numerator is approximated by:

$$\exp\left[-\gamma \sqrt{\left(\frac{\pi}{32\beta}\right)}\right] \Big/ 2\beta$$

so that (4) becomes:

$$\frac{\sum_n k(n) \exp\left[-\gamma \sqrt{\left(\frac{\pi}{32\beta}\right)}\right]}{\sum_n k(n)} \tag{5}$$

The $^1\Delta_g {}^3\Sigma_g^-$ bands have branches for which $k(n)$ has the following approximate values:

$$^RR,\ ^RQ,\ ^RP,\ ^PQ, \qquad k(n) = \sqrt{(2\beta e)} \cdot k_0$$

$$^QR,\ ^QP,\ ^OP,\ ^SR, \qquad k(n) = 1/2\sqrt{(2\beta e)} \cdot k_0$$

$$^QQ, \qquad k(n) = 2\sqrt{(2\beta e)} \cdot k_0$$

where k_0 is the peak absorption coefficient of the strongest line of the ^RR branch. When these expressions are substituted into expression (5) and the exponential terms expanded in series it is found that again to a good approximation that (5) equals:

$$\exp\left\{-\frac{9}{8} \cdot \frac{1}{\sqrt{2}} \sqrt{\left(\frac{\pi e}{16}\right)} \cdot k_0 l\right\}$$

Hence for equation (1) to be satisfied:

$$l = \frac{8}{9} \cdot \sqrt{2} \sqrt{\left(\frac{16}{\pi e}\right)} \cdot \frac{1}{k_0}$$

In Appendix II it is shown that $k_0 \simeq 1{\cdot}0\ \text{km}^{-1}$, $l = 2{\cdot}2$ km and hence with the help of the relationship developed by HUNTEN (1954) the screening height, h_s, is found to be 40 km.

The screening height for the dissociation of O_2 in the Herzberg continuum was found by numerical integration of (1). In this case I_0 was derived for a black body at 5000°K. The data of NICOLET and MANGE (1954) were used for $k'(\lambda)$ while absorption both in the Herzberg continuum and also by ozone was considered in evaluating k. The value found for h_s was 60 km. The value adopted in the calculations was 57 km; the reduction takes into account the fact that the absorbing path is reduced when the screening height approaches the height of the emitting region.

APPENDIX II

Calculation of transition probabilities for $^1\Delta_g$–$^3\Sigma_g^-$ transition

The equivalent width, W, of the $^SR_{(K''=21)}$ line of the 0,0 band was measured from the tracings of the McMath–Hulbert *Atlas of the Solar Spectrum* (1950) and was found to be $9 \times 10^{-3}\ \text{cm}^{-1}$. Since this line is weak, the Einstein transition probability for absorption, B'', may be calculated directly from the relation:

$$W = NB''h\bar{\nu}$$

where N is the number of lower state O_2 molecules ($^3\Sigma_g^-$, $v'' = 0 K'' = 21\ J'' = 22$) per cm^2 along the absorption path and $\bar{\nu}$ is the wavenumber of the transition. N was calculated for a reduced height of 8 km and a temperature of 0°C. In this way B'' was calculated to be $1{\cdot}1 \times 10^{-2}\ \text{sec}^{-1}\ \text{erg}^{-1}\ \text{cm}^2$ for the line measured and the transition probability A', for the corresponding spontaneous emission becomes $2{\cdot}7 \times 10^{-5}\ \text{sec}^{-1}$.

The relationship between the transition probability A' for a single rotational line to that, $A'(0,0)$, for the 0,0 vibrational band is:

$$A'(0,0) = [2(2J' + 1)/S_J] \cdot A' \qquad (1)$$

VOL
13
1958/

where S_J is the line strength factor for the rotational line of which J' is the quantum number of the upper state. Values of S_J have been given by VAN VLECK (1934).

The corresponding transition probabilities for induced emission and absorption $B'(0,0)$ and $B''(0,0)$ are related to $A'(0,0)$ by the relations:

$$B'(0,0) = B''(0,0)(Q_r''/Q_r')$$
$$B''(0,0) = A'(0,0)(1/8\pi hc\,\bar{\nu}_0^3)(Q_r'/Q_r'')$$

where Q'_r and Q''_r are the rotational partition functions of the upper and lower states respectively.

To a good approximation, Q_r'/Q_r'' for the 0,0 band of the $^1\Delta_g - ^3\Sigma_g^-$ O_2 system is equal to $\frac{2}{3}$. From the above equations the following values of the transition probabilities were calculated:

$$A'(0,0) = 1{\cdot}9 \times 10^{-4}\ \text{sec}^{-1}$$
$$B'(0,0) = 7{\cdot}5 \times 10^{-2}\ \text{sec}^{-1}\ \text{erg}^{-1}\ \text{cm}^2$$
$$B''(0,0) = 5{\cdot}0 \times 10^{-2}\ \text{sec}^{-1}\ \text{erg}^{-1}\ \text{cm}^2$$

The value of $A'(0,1)$ is also required in the calculations. Application of the "r_e-shift" method of JARMAIN and FRASER (1953) gave the result that $A'(0,0)/A'(0,1) \simeq 10$.

The central absorption coefficient k_0, of the $^RR_{(K''=3)}$ line was calculated from the measured equivalent width, W, of the $^SR_{(K''=21)}$ line. The central absorption coefficient of a Doppler broadened line is given by the relation (e.g. BENEDICT *et al.* 1956):

$$k_0 = (Sc/\bar{\nu})(m/2\pi kt)^{\frac{1}{2}} \qquad (2)$$

where $\bar{\nu}$ is the wavenumber of the line and S $(= \int k_{\bar{\nu}}\, d\bar{\nu})$ is the line strength. Now:

$$S \propto S_J \,.\, \exp\,(-F''hc/kT) \qquad (3)$$

where S_J is the line strength factor and F'' is the lower state rotational term value. For a weak line such as the $^SR_{(K''=21)}$ line it is possible to calculate S directly from the measured equivalent width from the relation $Sl = W$ where l is the equivalent atmospheric path at N.T.P. S may then be found for the $^RR_{(K''=3)}$ line with the help of equation (3) and finally from (2) the central absorption coefficient for air at N.T.P. may be calculated. The value calculated was $1{\cdot}0\ \text{km}^{-1}$.

REFERENCES

BATES D. R.	1954	*The Earth As a Planet* (Edited by KUIPER G. P). University of Chicago Press.
BATES D. R. and WITHERSPOON AGNES E.	1952	*Mon. Not. R. Astr. Soc.* **112,** 101.
BENENDICT W. S., HERMAN R., MOORE G. E. and SILVERMAN S.	1956	*Canad. J. Phys.* **34,** 830.
HUNTEN D. M.	1954	*J. Atmosph. Terr. Phys.* **5,** 44.
HUNTEN D. M.	1956	*J. Atmosph. Terr. Phys.* **9,** 179.
GUSH H. P. and VALLANCE JONES A.	1955	*J. Atmosph. Terr. Phys.* **7,** 285.
HARRISON A. W. and VALLANCE JONES A.	1957	*J. Atmosph. Terr. Phys.* In press.

Heaps H. S. and Herzberg G.	1952	*Z. Phys.* **133,** 48.
Herzberg G. and Herzberg L.	1947	*Astrophys. J.* **105,** 356.
Hunten D. M., Roach F. E. and Chamberlain J. W.	1956	*J. Atmosph. Terr. Phys.* **8,** 345.
Jarmain W. R. and Fraser P. A.	1953	*Proc. Phys. Soc. Lond.* A **66,** 1153.
Krassovsky V. I.	1954	*Usp. Fiz. Nauk, Mosk.* **54,** 469.
Mohler O. C., Pierce A. K., McMath R. R. and Goldberg L.	1950	*Photometric Atlas of the Near Infrared Solar Spectrum* λ8465 *to* λ25242. University of Michigan Press.
Meinel A. B.	1953	Discussion at joint meeting of International Scientific Radio Union and Institute of Radio Engineers, Ottawa.
Minnaert M.	1954	*The Sun* (Edited by Kuiper G. P.) p. 88. University of Chicago Press.
Nicolet M.	1957	*Paper presented at Symposium on Aeronomy.* International Association of Geomagnetism and Aeronomy, Toronto.
Nicolet M. and Mange P.	1954	*J. Geophys. Res.* **59,** 15.
Rocket Panel.	1952	*Phys. Rev.* **88,** 1027.
van Vleck J. H.	1934	*Astrophys. J.* **80,** 161.

VOL.
13
1958/5

Journal of Atmospheric and Terrestrial Physics, 1958, Vol. 13, pp. 61 to 71. Pergamon Press Ltd., London

The trapping of cosmic radio waves beneath the ionosphere

G. R. Ellis
Radio Research Laboratories, C.S.I.R.O., Camden, N.S.W., Australia

(*Received* 1 *March* 1958)

Abstract—The observation of cosmic radio noise at frequencies less than the local ionospheric critical frequency is discussed. It is shown that this effect may adequately be explained in terms of the trapping of the radiation between the ionosphere and the ground. Wherever there is a horizontal gradient of critical frequency in an ionospheric layer, incoming extra terrestrial radiation may be reflected by the layer after one ground reflection and may subsequently propagate by hop transmission for large horizontal distances beneath the layer.

A method of calculating the amplitude of the trapped radiation at any distance is given, allowing for all possible modes.

1. Introduction

A characteristic and unexpected feature of observations of cosmic radio noise with low resolution antennae is the detection of the noise at wave frequencies somewhat less than the local ionospheric critical frequency. This effect was first observed by Reber and Ellis (1956) who reported that in typical circumstances cosmic noise could be observed with a full wave antenna at 2·13 Mc/s when the critical frequency was less than about 3 Mc/s. In addition the noise intensity appeared to reach prematurely a maximum value when the critical frequency had fallen only to about 1·6 Mc/s.

These results should be contrasted with those of Shain and Higgins (1954) who, using a relatively higher resolution antenna (beam width 17°) found that the cosmic noise intensity at 18·3 Mc/s decreased more rapidly than expected when the critical frequency rose. During their observations the critical frequency was normally less than about 10 Mc/s. They suggested that absorption, scattering and refraction in the outer ionosphere might account for the discrepancy. Similarly, Kerr and Shain (1951) using moon echoes found that the echo intensity was always reduced, apparently by refraction, to less than the expected value.

Providing the cosmic noise can be considered to come from a uniformly bright sky, refraction due to the curvature of the ionosphere will neither increase nor decrease the observed intensity at the ground. The intensity of discrete sources on the other hand is always reduced by refraction. It is thus necessary to look elsewhere for an explanation of the effects observed by Reber and Ellis, and it will be shown here that the noise excess can be due to the reception of cosmic noise penetrating the ionosphere at places remote from the observer, and where the critical frequency is less than in his vicinity.

Providing there is a horizontal gradient of critical frequency, the extra-terrestrial radiation can be trapped between the ionosphere and the ground and can spread by hop transmission into areas of higher critical frequency. The observation of this trapped radiation will normally depend on the use of antennae with an acceptance pattern which extends to large zenith angles in circumstances when the area of sky directly observed is limited by the ionosphere and not the antenna.

With higher resolution antennae such as Shain and Higgins used and with relatively low critical frequencies an excess of noise due to trapping would not be observed. These ideas are illustrated in Fig. 1.

2. Theoretical

In the absence of trapping and absorption the cosmic noise power S observed at the ground will be a function of the distribution of radio brightness across the sky $P(\theta, \phi)$, the antenna acceptance pattern $K(\theta, \phi)$ and the maximum angles of

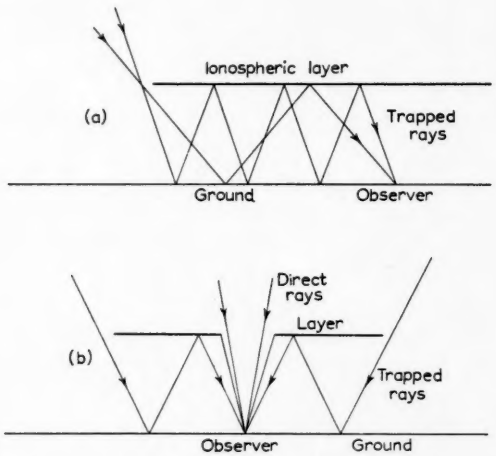

Fig. 1. Propagation of trapped radiation when the local critical frequency is: (a) greater than the observing frequency; (b) less than the observing frequency.

incidence θ_0, θ_x for which transmission through the ionosphere is possible by the ordinary and extraordinary modes respectively. That is

$$S = \frac{1}{2}\left[\int_0^{2\pi}\int_0^{\theta_0} K(\theta,\phi)P(\theta,\phi)\sin\theta\, d\theta\, d\phi + \int_0^{2\pi}\int_0^{\theta_x} K(\theta,\phi)\,P(\theta,\phi)\sin\theta\, d\theta\, d\phi\right] \quad (1)$$

If the effect of the earth's magnetic field is neglected:

$$\theta_0 = \theta_x = \cos^{-1}\frac{f_0}{f} \quad (2)$$

where f_0 = critical frequency and f = wave frequency

Figure 2 shows the variation of S for the particular case of a horizontal full wave antenna, one-sixth wavelength above the ground, a wave frequency of 2·13 Mc/s, a gyro frequency of 1·5 Mc/s, and for the ordinary mode only. The sky was

VOL 13 1958/

assumed to be uniformly bright. These were essentially the conditions of the observations of REBER and ELLIS (1956). Also shown are the relative cosmic noise intensities which they observed during the period May to August 1955 at times near midnight when f_0F2 was varying only slowly. On many occasions the noise could be observed at wave frequencies below the critical frequency and also the noise intensity often increased to a limiting maximum value when the critical frequency had fallen to only about 1·6 Mc/s, contrary to equation (1).

Both of these effects were also observed at times when the critical frequency was

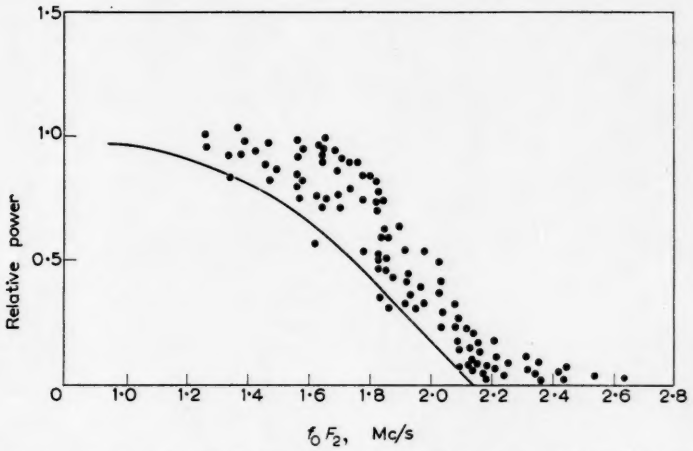

Fig. 2. Amplitude of 2·13 Mc/s cosmic noise at Hobart observed from May to September 1955, at times near midnight. The curve shows the relative intensity expected in the absence of trapping and absorption.

changing rapidly, usually near dawn. Figure 3 shows a typical record. Here the noise could still be observed when the critical frequency had increased to twice the wave frequency.

Figure 4 shows the variation of cosmic noise amplitude with critical frequency for a number of occasions during the dawn period. The noise could always be observed to some extent when f_0F2 was greater than the wave frequency although there was considerable variation from day to day.

To determine whether these anomalies could be explained in terms of the trapping of the noise at distant places would require a knowledge of the instantaneous critical frequency within a radius of several thousand kilometres of the observer. This information is not normally available but may be estimated in certain circumstances.

During the winter months at middle latitudes the rapid increase in critical frequency during the dawn period travels from east to west at the speed of rotation of the earth and the variation of critical frequency with time at any one place may be transformed, without great error, into a corresponding spatial variation along an east–west line. This situation is similar to that illustrated in Fig. 3.

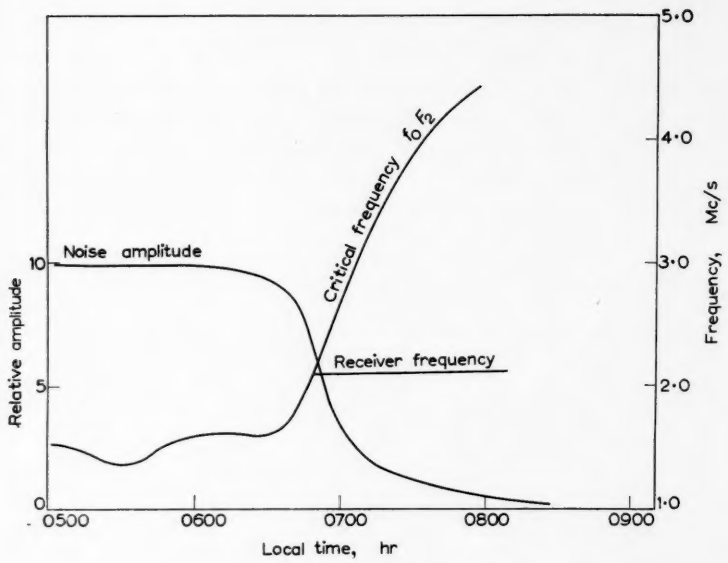

Fig. 3. Record of cosmic noise at 2·13 Mc/s at Hobart, Tasmania on 10 August 1955, showing the continued observation of the noise for 1¼ hr after the critical frequency rose above the observing frequency. Full wave antenna.

VOL
13
1958/

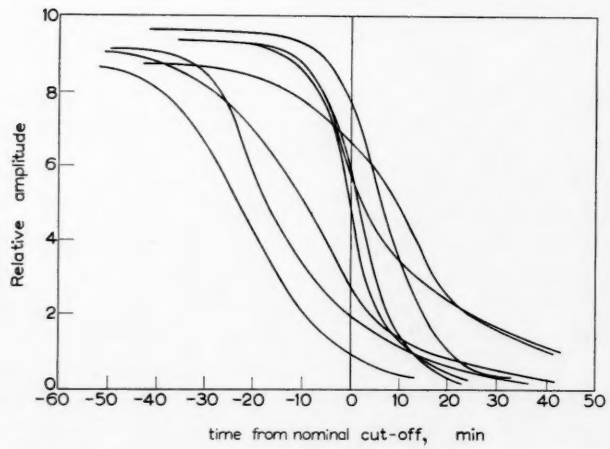

Fig. 4. Records of dawn cut-off in cosmic noise at 2·13 Mc/s, August 1955

Suppose then that the distribution of critical frequency is known. We wish to calculate the total radiation intensity due to trapping at any point A, distance d from the nominal cut-off point in the front, at which the critical frequency is equal to the wave frequency. To do this it is necessary to calculate all the ray paths ending at A for which propagation through the ionosphere at some point is possible, allowing for any given number of hops between the point of penetration and A.

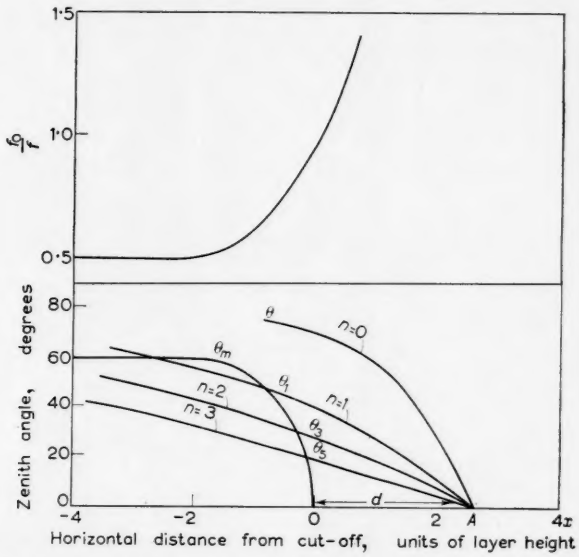

Fig. 5. Variation across a critical frequency front of the maximum allowable angle of incidence θ_m and of the actual angle of incidence θ for rays which reach A.

These calculations may be performed with the aid of a simple graphical technique. Consider a frontal change in critical frequency in a flat thin ionospheric layer, in which the critical frequency varies with distance x across the front as in Fig. 5. On the same distance scale we may plot the variation in the maximum angle of incidence θ_m for penetration of the layer, using equation (2). Also, the angle of incidence θ of a ray which penetrates the layer and arrives at the observing point A after n hops will be given by:

$$\tan \theta = \frac{d - x}{(2n + 1)h} \tag{3}$$

where h is the layer height, and $d - x$ is the horizontal distance between the penetration point and A.

Clearly, if the curve expressed by equation (2) for a given value of n, does not intersect that of equation (3) then no rays ending at A will penetrate the layer, since their angle of incidence will always be greater than θ_m, the maximum allowable value.

If there is a pair of intersections between the two curves, the two values of θ_m

obtained will form the limits to the range of angles of incidence for which penetration is possible, with the given number of hops. For greater numbers of hops there will be corresponding ranges of θ, with the limitation that no particular value of θ may be associated with more than one value of n. For example, if we obtain solutions:

$$\theta_1, \theta_2 \quad \text{for} \quad n = 1$$
$$\theta_3, \theta_4 \quad \text{for} \quad n = 2$$
$$\theta_5, \theta_6 \quad \text{for} \quad n = 3, \text{ etc.}$$

then the allowed angles of incidence will be:

One hop θ_2 to θ_1,
two hops θ_4 to θ_2, θ_1 to θ_3,
three hops θ_6 to θ_4, θ_3 to θ_5, and so on.

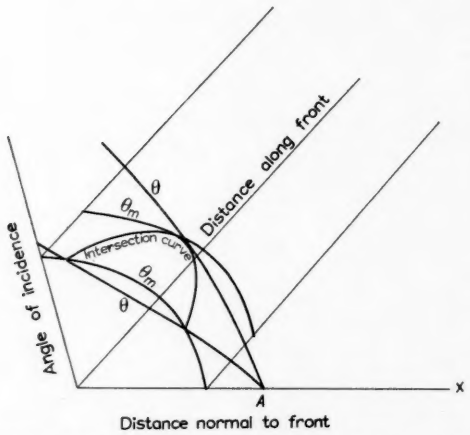

Fig. 6. Three-dimensional generalization of Fig. 3 to include rays of all azimuths.

A two hop ray with an angle of incidence in the range θ_2 to θ_1 would pass back through the layer after one ground reflection. We can thus determine all rays which will penetrate the ionosphere and arrive at the observing point. Also, rays are grouped according to the number of hops and it is simple to allow for the effect of attenuation if the reflection coefficient is known or can be assumed.

This graphical technique may be extended to include rays of all azimuths and not only those normal to the critical frequency front, by using a three-dimensional coordinate system instead of the two-dimensional one of Fig. 5. The $\theta(x)$ curves then become conical surfaces, and the $\theta_m(x)$ curve a cylindrical surface. The curve of intersection between these two surfaces then defines the limits of allowable angles of incidence for all azimuths (Fig. 6).

Figure 7 shows examples of the solutions obtained for the angle of incidence as a function of azimuth for different values of the distance of the observing point from the front. The actual radiation power received at any distance can be obtained

VOL
13
1958/

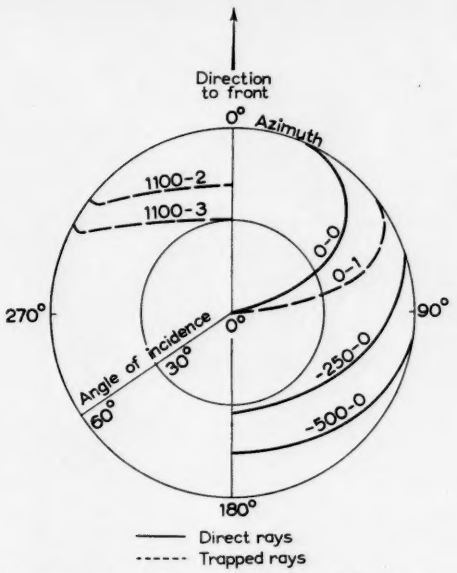

Fig. 7. Solutions obtained for the angle of incidence at different distances from the front of Fig. 3. The distance d (km) and the hop number is shown thus: 1100–2. Layer height 250 km. Ordinary mode only.

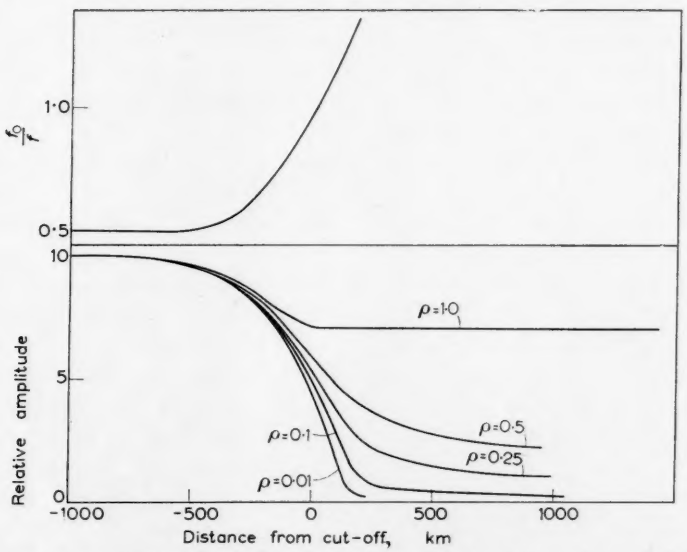

Fig. 8. Change in radiation amplitude with distance calculated from Fig. 5, for different values of the power reflection coefficient. Half wave antenna.

from these solutions by summing over all possible modes. That is, at a distance d the power is:

$$F = \sum_{n=n_1^o}^{\infty} \iint [\rho_0(\theta)]^n P(\theta, \phi)\, K(\theta, \phi) \sin\theta\, d\theta\, d\phi + \sum_{n=n_1^x}^{\infty} \iint [\rho_x(\theta)]^n P(\theta, \phi)\, K(\theta, \phi) \sin\theta\, d\theta\, d\phi \quad (4)$$

where $\rho_{0,x}(\theta)$ are the power reflection coefficients and $n_1^{o,x}$ the smallest hop numbers for the ordinary and extraordinary modes respectively. Figures 8 and 9 show typical curves of the variation in radiation amplitude with distance, obtained by

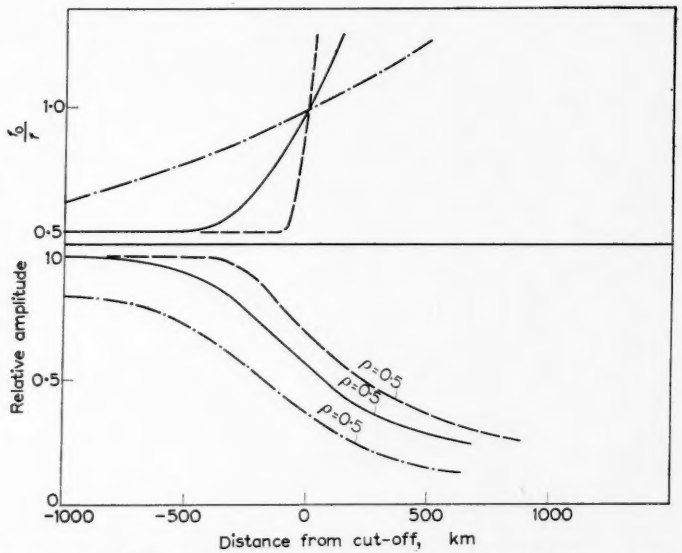

Fig. 9. Change in radiation amplitude with distance from fronts of different horizontal gradient. Layer height 250 km. Half wave antenna.

graphical integration. For simplicity it is assumed that the reflection coefficient is independent of angle of incidence and that the sky is uniformly bright. As might be expected, the amplitude at any distance is strongly dependent on the reflection coefficient, and on the horizontal gradient of critical frequency in the front.

Other ionospheric models may be analysed in the same way, and in particular it is simple to allow for the curvature and thickness of the ionospheric layer by slightly altering the shape of the angle of incidence curves $\theta(x)$. The corrections obtained however, are small and of opposite sign, and are neglected in the present analysis.

3. Discussion

3.1. *Comparison with observations*

To test the theory quantitatively a number of records of the dawn cut-off in cosmic noise were analysed. The critical frequency versus time curve was transformed to the corresponding critical frequency distance curve using the relation

$$\Delta d = V \sin\alpha\, \Delta t$$

where α is the azimuth of the sun at sunrise and V is the rotational speed of the earth. At the latitude of Hobart this is 1210 km/hr.

The theoretical value of relative noise amplitude at several distances from the front was then calculated as outlined in Section 2, for different values of the reflection coefficient. The variation of reflection coefficient and of reflection height with distance were neglected.

Figure 10 shows a typical record obtained on 11 May 1955 at Hobart and the calculated relative amplitudes for a reflection coefficient of 0·3. Measured reflection

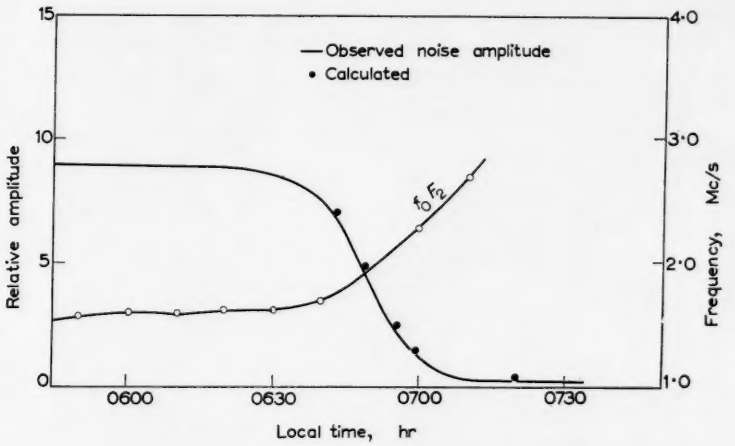

Fig. 10. Record of cosmic noise at 2·13 Mc/s at Hobart on the 11 May 1955, together with the calculated amplitudes for a reflection coefficient of 0·3. Layer height 310 km. Ordinary mode only.

coefficients during the observations varied from about 0·2 to 0·4 for vertical incidence reflection from the F-layer at night at 2 Mc/s. For this and similar records good agreement between the experimental and theoretical points was obtained and it appears that the trapping mechanism can produce a cosmic noise intensity at a distance from a front which is commensurate with that actually observed.

When there is only a slow change of local critical frequency with time it is reasonable to suppose that noise observed below the critical frequency is also due to trapping at distant places. The observed noise intensities shown in Fig. 2 for frequencies above 2·13 Mc/s for example could be accounted for by distant critical frequencies between 1·5 Mc/s and 2·0 Mc/s if absorption is neglected and the critical frequency distribution is independent of azimuth. For other distributions the required distant critical frequency would be less.

The reason for the premature limiting of the noise amplitude with decreasing critical frequency is more a matter for speculation at this stage since it is not known whether the limiting is due to excess of noise caused by trapping or to a deficit caused by some other process. Nevertheless it would be expected that at least part of the observed noise above the critical frequency would be due to trapping. In Fig. 2 the theoretical and experimental intensity scales are arranged as if all the

discrepancy above the critical frequency results from excess noise. In this case the difference between the local and distant critical frequencies would need to be about the same as that required to explain the observed noise below the critical frequency. An analogous discrepancy can be seen in the frontal records of Fig. 4. Some show noise amplitudes at cut-off, greater than 0·7 times the maximum value before cut-off. For a simple model like that Fig. 5 where the critical frequency

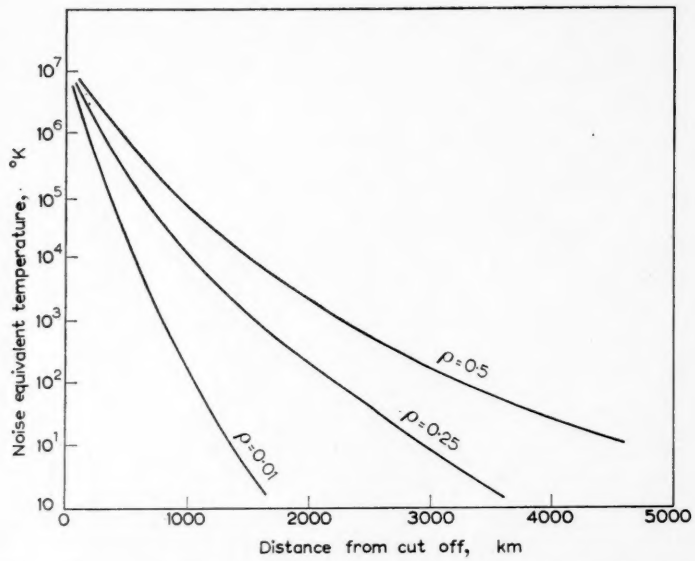

Fig. 11. Variation of noise equivalent temperature with distance for model of Fig. 3. Layer height 250 km. Half wave antenna. Assumed initial noise temperature 2×10^7 °K.

increases monotonically from some minimum value, the cut-off amplitude must always be less than this. If, however, trapping due to low distant critical frequencies contributes to the noise maximum before cut-off then this limitation need not apply.

3.2. *Ionospheric thermal radiation*

It is of some interest to consider whether the propagation of trapped radiation from the night side of the dawn twilight zone would be likely to interfere with daytime observations of thermal radiation from the ionosphere. At frequencies of a few megacycles per second the equivalent temperature of cosmic noise is of the order of 10^7 °K (Ellis, 1957) while the equivalent temperature of ionospheric radiation is about 260°K and changes of about 10°K are considered significant (Gardner, 1954). Clearly, observations just after dawn at a frequency above the lowest pre-dawn critical frequency could be contaminated by cosmic noise. Nevertheless, the relatively small reflection coefficient during the day would produce rapid attenuation of the trapped radiation, particularly where successive reflections occurred at the *E*-layer instead of the *F*-layer. Figure 11 shows the

VOL.
13
1958/5

theoretical curves of Fig. 8 extended to lower radiation levels and greater distances. For this particular model an attenuation by a factor of 10^7 would occur within a few thousand kilometres.

Acknowledgements—Part of the work reported here was done while the author was with the Australian Ionospheric Prediction Service and the University of Queensland.

References

Ellis G. R.	1957	*J. Geophys. Res.* **62**, 229.
Gardner F. F.	1954	*J. Atmosph. Terr. Phys.* **5**, 298.
Kerr F. J. and Shain C. A.	1951	*Proc. Inst. Radio Engrs., N.Y.* **39**, 230.
Reber G. and Ellis G. R.	1956	*J. Geophys. Res.* **61**, 1.
Shain C. A. and Higgins C. S.	1954	*Aust. J. Phys.* **7**, 130.

OL.
13
8/59

Journal of Atmospheric and Terrestrial Physics, 1958, Vol. 13, pp. 72 to 85. Pergamon Press Ltd., London

Some relations between the bearing and amplitude of a fading radio wave

H. A. WHALE and L. M. DELVES*
Seagrove Radio Research Station, Auckland, New Zealand

(*Received* 1 *March* 1958)

Abstract—A correlation ratio connecting the changes in amplitude with the changes of bearing of a fading radio wave made up of a number of randomly phased components is derived. The modifications necessary when specular components are also present are indicated. Experimental measurements of the correlation ratio for waves reflected from the ionosphere are compared with the theory.

INTRODUCTION

AN initially uniform, plane radio wave which has encountered a changing non-uniform medium exhibits, in consequence, variations in amplitude (fading) and in apparent wave normal direction. In the case of short radio waves reflected from the ionosphere, some of the variations arise from large scale changes in ionospheric conditions but most of the rapid variations are effects arising from the interference of the various scattered waves produced by the non-uniform (or "rough") ionosphere. The analysis and experimental results given in this paper represent an approach to an understanding of the relations existing between the variations of amplitude and the associated variations in bearing of a short-wave radio signal. Since the design of aerials for the reception of short-waves is aided by a knowledge of the variation of average signal level with direction these results may be of some importance, especially when the signal involved contains a large amount of scattered radiation.

The present analysis starts from equations arising in the statistics of random noise as given by RICE (1945). From these, several probability distributions relating the signal amplitude to the wave-normal direction are here derived and it is found that most of these distributions are symmetrical about some mean wave normal direction. Some of our experimental distributions, however, are asymmetrical and this is attributed to the presence of two groups of waves with different mean directions, each containing an appreciable specular component.

1. SYMMETRICAL FAN OF RAYS

The voltages v_1 and v_2 received on two aerials P_1 and P_2 may be represented in phase and amplitude by:

$$v_1 = B_{1c} \cos \omega t + B_{1s} \sin \omega t$$

$$v_2 = B_{2c} \cos \omega t + B_{2s} \sin \omega t$$

where $\omega = 2\pi$ times the nominal frequency of the incoming waves and the B's are the inphase and quadrature components of the voltages.

If the incoming signal is made up of a large number of plane waves of random phase with coplanar wave normals (i.e. a *fan* of rays) it has been shown (RICE,

* Now at Wadham College, Oxford.

1945; BRAMLEY, 1951) that the joint probability distribution of B_{1c}, B_{1s}, B_{2c}, B_{2s} is given by:

$$p(B_{1c}, B_{1s}, B_{2c}, B_{2s}) = \frac{dB_{1c} \cdot dB_{1s} \cdot dB_{2c} \cdot dB_{2s}}{4\pi^2(P_0^2 - \mu_{13}^2 - \mu_{14}^2)}$$

$$\times \exp\left\{ - \frac{P_0(B_{1c}^2 + B_{1s}^2 + B_{2c}^2 + B_{2s}^2) - 2\mu_{13}(B_{1c}B_{2c} + B_{1s}B_{2s}) - 2\mu_{14}(B_{1c}B_{2s} - B_{2c}B_{1s})}{2(P_0^2 - \mu_{13}^2 - \mu_{14}^2)} \right\} \quad (1)$$

where P_0 = total power in the incoming waves

$$= \int_0^{2\pi} P(\alpha) \cdot d\alpha$$

$P(\alpha)$ = power in those waves with directions between α and $\alpha + d\alpha$

α = wave-normal direction of a component wave measured from the line P_1P_2

$$\mu_{13} = \int_0^{2\pi} P(\alpha) \cdot \cos\left(\frac{2\pi x \cos\alpha}{\lambda}\right) \cdot d\alpha$$

$$\mu_{14} = \int_0^{2\pi} P(\alpha) \cdot \sin\left(\frac{2\pi x \cos\alpha}{\lambda}\right) \cdot d\alpha$$

x = distance P_1P_2, $\quad \lambda = 2\pi c/\omega$

The amplitudes A_1, A_2 and the phases ψ_1, ψ_2 of the signals at the two aerials may be obtained from the relations:

$$B_{1c} = A_1 \cos\psi_1, \quad B_{2c} = A_2 \cos\psi_2, \quad B_{1s} = A_1 \sin\psi_1, \quad B_{2s} = A_2 \sin\psi_2$$

whence, by a change of variables in equation (1), we obtain

$$p(A_1, A_2, \psi_1, \psi_2) = \frac{A_1A_2 \cdot dA_2 d\psi_1 d\psi_2}{4\pi^2(P_0^2 - \mu_{13}^2 \simeq \mu_{14}^2)}$$

$$\times \exp\left\{ - \frac{P_0(A_1^2 + A_2^2) - 2A_1A_2\{\mu_{13}\cos(\psi_2 - \psi_1) + \mu_{14}\sin(\psi_2 - \psi_1)\}}{2(P_0^2 - \mu_{13}^2 - \mu_{14}^2)} \right\} \quad (2)$$

The measurements to be described in this paper are made on a small-aperture direction-finder so that A_1 will be nearly equal to A_2 and the measured amplitude may be taken as $A_1 = A$, say. Let the phase difference between the signals from the two aerials be $\psi_1 - \psi_2 = \psi$ so that the indicated bearing θ is given by $\psi = 2\pi x \sin\theta/\lambda$. By further change of variables and successive integrations with respect to ψ_2 and A_2 we obtain:

$$p(A,\psi) = \left[\frac{A}{2\pi P_0} \cdot \exp\left(-\frac{A^2P_0}{2M^2}\right) + \frac{NA^2}{2\sqrt{(2\pi)}M \cdot P_0^{3/2}} \left(1 + \operatorname{erf}\frac{NA}{MP_0^2}\right) \right.$$

$$\left. \times \exp\left\{ - \frac{A^2}{2M^2}\left(P_0 - \frac{N^2}{P_0}\right)\right\}\right] \cdot dA \cdot d\psi \quad (3)$$

where $N = \mu_{13}\cos\psi - \mu_{14}\sin\psi$

$M^2 = P_0^2 - \mu_{13}^2 - \mu_{14}^2$

1.1. *Narrow symmetrical fan of rays*

If, now, the incoming fan of rays is concentrated near one direction α_0 we may write $\alpha = \alpha_0 + \phi$, where ϕ is small. The expressions for P_0, μ_{13} and μ_{14} then become:

$$P_0 = \int_{-\infty}^{\infty} P(\phi) \, . \, d\phi$$

$$\mu_{13} = \cos\left(\frac{2\pi x}{\lambda} \cos \alpha_0\right) \, . \int_{-\infty}^{\infty} P(\phi) \, . \cos\left(\frac{2\pi x}{\lambda} \sin \alpha_0\right) \, . \, d\phi$$

$$\mu_{14} = -\sin\left(\frac{2\pi x}{\lambda} \cos \alpha_0\right) \, . \int_{-\infty}^{\infty} P(\phi) \, . \cos\left(\frac{2\pi x}{\lambda} \sin \alpha_0\right) \, . \, d\phi$$

Since ϕ, x are both small, the trigonometrical functions may be expanded to give:

$$\left.\begin{aligned} \mu_{13} &= P_0\left\{1 - \frac{2\pi^2 x^2}{\lambda^2}(\cos^2 \alpha_0 + \overline{\phi^2} \, . \sin^2 \alpha_0)\right\} \\ \mu_{14} &= -P_0 \, . \frac{2\pi x}{\lambda} \, . \cos \alpha_0 \\ \text{therefore } M^2 &= {P_0}^2 - {\mu_{13}}^2 - {\mu_{14}}^2 = \frac{4\pi^2 x^2}{\lambda^2} \, . \, {P_0}^2 \, . \, \overline{\phi^2} \, . \, \sin^2 \alpha_0 \end{aligned}\right\} \quad (4)$$

The direction-finder used in these measurements (WHALE and ROSS, 1956) aligns itself along the wavefront of the incoming wave so that $\alpha_0 = 90°$. Substituting the values obtained in (4) into equation (3), changing the variables ψ to S (where $S = \sin \theta = \lambda\psi/2\pi x$) and A to the normalized $R = A/\sqrt{P_0}$, we obtain:

$$p(R, S) = \frac{R^2}{\sqrt{2\pi} \, . \, (\overline{\phi^2})^{1/2}} \, . \exp\left\{-\frac{R^2}{2\overline{\phi^2}}(\overline{\phi^2} + S^2)\right\} \, . \, dR \, . \, dS \quad (5)$$

An expression equivalent to this has been obtained previously (WOODING, 1955) in connexion with the distribution of amplitude and frequency of water waves.

A normalized form of equation (5) may be obtained by changing the variable S to a new variable T (where $T = S/\sqrt{\overline{\phi^2}}$) obtaining:

$$p(R, T) = \frac{R^2}{\sqrt{2\pi}} \, . \exp\left\{-\frac{R^2}{2}(1 + T^2)\right\} dR \, . \, dT \quad (5a)$$

The probability contours derived from expression (5) for $\overline{\phi^2} = 0{\cdot}1^2$ and $0{\cdot}01^2$ are drawn in Figs. 1A, 1B.

2. NARROW ASYMMETRICAL FAN OF RAYS

If the incoming fan of rays is asymmetrical, expressions (4) become (where $\alpha_0 = 90°$):

$$\mu_{13} = P_0\left(1 - \frac{2\pi^2 x^2}{\lambda^2}\overline{\phi^2}\right)$$

$$\mu_{14} = -P_0 \, . \frac{\pi x}{\lambda} \, . \frac{\overline{\phi^3}}{3}$$

$$M^2 = \frac{4\pi^2 x^2}{\lambda^2} \, . \, {P_0}^2 \, . \, \{\overline{\phi^2} - \overline{\phi^3}^2/36\}$$

VOL
13
1958/

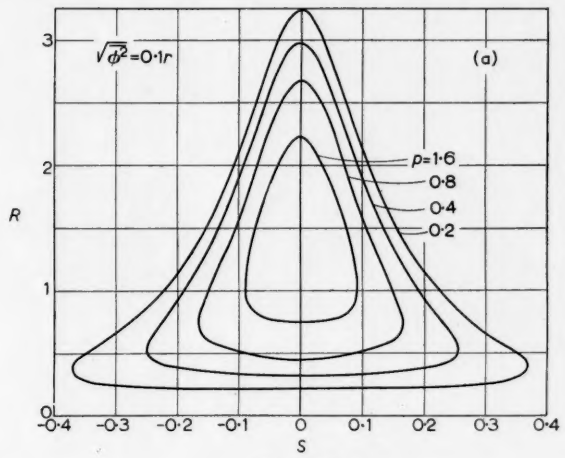
$\sqrt{\phi^2}=0{\cdot}1r$
(a)
p=1·6
0·8
0·4
0·2
R
S
3
2
1
0
-0·4
-0·3
-0·2
-0·1
0
0·1
0·2
0·3
0·4

Fig. 1(a)

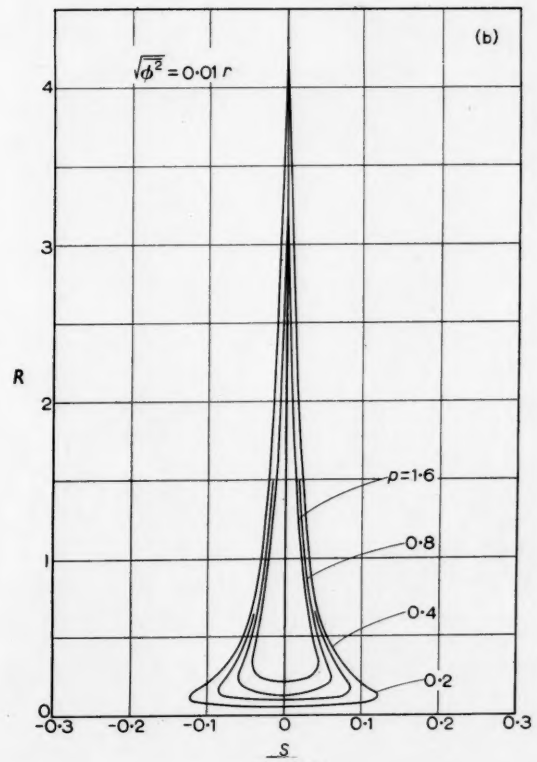
$\sqrt{\phi^2}=0{\cdot}01\,r$
(b)
p=1·6
0·8
0·4
0·2
R
S
4
3
2
1
0
-0·3
-0·2
-0·1
0
0·1
0·2
0·3

Fig. 1(b)

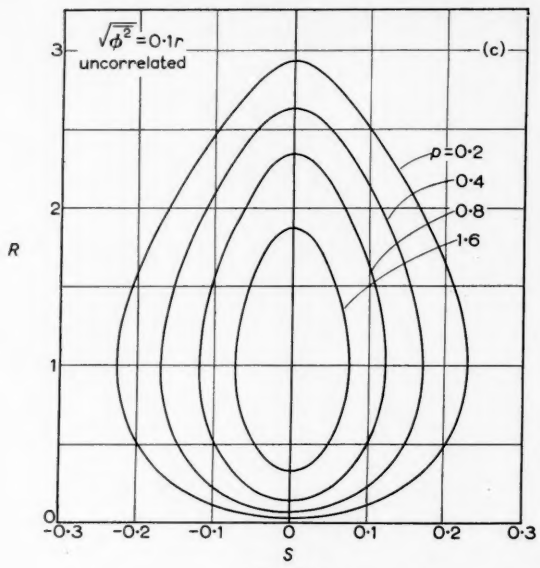

Fig. 1(c)

Fig. 1. Two-dimensional joint-probability contour diagrams for symmetrically or asymmetrically distributed groups of waves with no specular component. $p = p(R, S)dR \,.\, dS$, where R = relative amplitude and S = sine of instantaneous bearing; $\overline{\phi^2}$ = mean square distribution of the directions of the incoming waves.

VOL
13
1958/

$$\text{Hence } p(R,S) = \frac{R^2}{\sqrt{\{2\pi(\overline{\phi^2} - \overline{\phi^3}^2/36)\}}} \exp\left\{-\frac{R^2(\overline{\phi^2} + S^2 - S\overline{\phi^3}/3)}{2(\overline{\phi^2} - \overline{\phi^3}^2/36)}\right\} . dR \,.\, dS \qquad (6)$$

which, for all practical values of $\overline{\phi^3}$ is a distribution symmetrical in S but with the centre shifted slightly from $S = 0$.

3. Statistical Relations Between Amplitude and Bearing

The probability distributions of R and S separately may be obtained from equation (5). By integrating with respect to R we obtain:

$$p(S) = \frac{\overline{\phi^2}}{2(\overline{\phi^2} + S^2)^{3/2}} \,.\, dS \qquad (7)$$

This expression may also be obtained from BRAMLEY's equation (35) which gives the probability of the phase difference between the voltage in two aerials.

The distribution, which may be regarded as one of STUDENT's distributions, is more sharply peaked than a normal distribution and has been confirmed experimentally by Ross (1955), who obtained the relation in this form.

Similarly, the distribution of amplitude can be shown to be given by:

$$p(R) = R \,.\, \exp\,(-R^2/2) \,.\, dR \qquad (8)$$

the well-known RAYLEIGH distribution.

For comparison with the distribution given in equation (5) plotted as a contour

diagram in Fig. 1A the equivalent diagram when the amplitude and bearing are uncorrelated [obtained by multiplying together equations (7) and (8)] is drawn in Fig. 1C.

The mean value $\bar{R}$ and the variance $\overline{(R-\bar{R})^2}$ are given by

$$\bar{R} = \sqrt{\frac{\pi}{2}}, \quad \overline{(R-\bar{R})^2} = 2 - \frac{\pi}{2}$$

The mean value $\bar{S}$ is zero for the symmetrical case; the variance $\overline{S^2}$ is found from equation (7) to be given by:

$$\overline{S^2} = \frac{\overline{\phi^2}}{2}\left\{\ln\frac{\sqrt{(1+\overline{\phi^2})}+1}{\sqrt{(1+\overline{\phi^2})}-1} - \frac{2}{\sqrt{(1+\overline{\phi^2})}}\right\}$$

$$= -\frac{\overline{\phi^2}}{2}\ln\frac{\overline{\phi^2}}{4}, \text{ if } \overline{\phi^2} \text{ is small enough}$$

A more direct connexion is obtained from the mean deviation given by:

$$\overline{|S|} = -(\overline{\phi^2})^{1/2}, \text{ nearly}$$

The usual correlation coefficient between the two variables R and S, defined by:

$$\rho_{RS} = \int\int (R-\bar{R}) \,.\, (S-\bar{S}) \,.\, p(R,S)\, dR \,.\, dS / \overline{(R-\bar{R})^2}^{1/2} \,.\, \overline{(S-\bar{S})^2}^{1/2}$$

is zero for the distribution given by equation (5). This arises since the regression line obtained by averaging R in equation (5) is symmetrical about the vertical axis.

In such a case we may use PEARSON's *correlation ratios* η_{RS}, η_{SR} (WEATHERBURN, 1946; CRAMÉR, 1945) defined by:

$$\eta_{RS}^2 = \int (\bar{R}_S - \bar{R})^2 \,.\, p(S) \,.\, dS / \overline{(R-\bar{R})^2} \tag{9}$$

and a similar expression for η_{SR}^2 obtained by interchanging the variables.

In these expressions, $\bar{R}_S$ is the mean value of R for a given value of S and is thus given by:

$$\bar{R}_S = \int R \,.\, p\,(R,S)\, dR / p(S)$$

$$= 4\overline{\phi^2}^{1/2} / \sqrt{2\pi} \,.\, (\overline{\phi^2} + S^2)^{1/2}$$

Carrying out the integration in (9):

$$\eta_{RS}^2 = \left(\frac{16}{3\pi} - \frac{\pi}{2} - \frac{\pi\overline{\phi^2}}{4}\right) \Big/ \left(2 - \frac{\pi}{2}\right)$$

$$= 0{\cdot}296\,(1 - 6{\cdot}18\,\overline{\phi^2})$$

and thus $$\eta_{RS} = 0{\cdot}544\,(1 - 3{\cdot}09\,\overline{\phi^2}), \text{ since } \overline{\phi^2} \text{ is small} \tag{10}$$

This correlation ratio is a quantity which may be obtained from an analysis of the experimental records.

The correlation ratio η_{SR} is zero since, in the equation corresponding to (9), $\overline{S}_R = 0$ and $\bar{S} = 0$ while the denominator is finite.

4. SPECULAR COMPONENT IN THE INCOMING WAVE

From analyses of the fading of radio signals it is well known (MACNICOL, 1949) that the incoming distribution of waves often consists of a fairly steady (or specular)

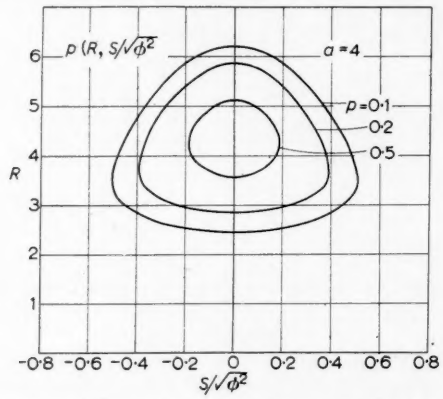

Fig. 2. Probability contour diagram for group of waves containing a specular component. The amplitude of the specular component is a times the effective amplitude of the random components.

VOL. 13 1958/5

component together with random components such as those considered in Section 1. If a plane wave of amplitude I in the direction α_0, the mean direction of the random waves, is included in the distribution of waves, equation (1) is unchanged but the coefficients become:

$$B_{1c} = A_1 \cos \psi_1 - I, \qquad B_{2c} = A_2 \cos \psi_2 - I$$

$$B_{1s} = A_1 \sin \psi_1, \qquad B_{2s} = A_2 \sin \psi_2$$

On carrying through the integrations as before, we obtain:

$$p(R, S) = I_0(aR) \,.\, \exp\left\{-\frac{a^2}{2} \,.\, \frac{R^2}{\sqrt{(2\pi.\overline{\phi^2})}}\right\} \,.\, \exp\left\{-\frac{R^2\,(\overline{\phi^2} + S^2)}{2\overline{\phi^2}}\right\} \,.\, dR \,.\, dS \quad (11)$$

where $a = I/\sqrt{P_0}$ (equivalent to a "signal to noise" or "coherence" ratio) and I_0 is the Bessel function of zero order and imaginary argument. This expression is very similar to equation (5) apart from a multiplying factor not involving S. For comparison with the case in which there is no specular component, some typical contour curves corresponding to equation (11) (for $a = 4$) are drawn in Fig. 2. The probability distribution for R obtained by integrating equation (11) over S is:

$$p(R) = I_0\,(aR) \,.\, R \,.\, \exp\{-(R^2 + a^2)/2\} \,.\, dR \quad (12)$$

in agreement with an expression given by RICE (1951) for the amplitude distribution in the corresponding noise problem.

The probability distribution of S is given by:

$$p(S) = \frac{\overline{\phi^2}}{2(\overline{\phi^2} + S^2)^{3/2}} \cdot \exp\left(-\frac{a^2}{2}\right) \cdot \exp\left(\frac{z}{2}\right) \cdot \left\{(1+z)I_0\left(\frac{z}{2}\right) + z.\, I_1\left(\frac{z}{2}\right)\right\} \cdot dS$$

where $z = a^2\overline{\phi^2}/2(\overline{\phi^2} + S^2)$

For moderate a this becomes, on expanding the Bessel functions and the second exponential term:

$$p(S) = \frac{\overline{\phi^2}}{2(\overline{\phi^2} + S^2)^{3/2}} \cdot \exp\left(-\frac{a^2}{2}\right) \cdot \left\{1 + \frac{3a^2\overline{\phi^2}}{4(\overline{\phi^2} + S^2)}\right\} \cdot dS$$

For large a, using the approximations $I_0(z) = I_1(z) = \{\exp(z)\}\sqrt{(2\pi z)}$

$$p(S) = \frac{a\overline{\phi^2}^{3/2}}{2(\overline{\phi^2} + S^2)^2} \cdot \exp\left\{-\frac{a^2S^2}{2(\overline{\phi^2} + S^2)}\right\} \cdot dS$$

5. Two Main Groups in the Incoming Wave Directions

It is often found, especially in cases where two transmission paths differing only in the number of ionospheric reflections are simultaneously possible, that the incoming waves are grouped about two main directions differing by a few degrees of bearing (this arising from effective tilts of the ionosphere).

If there are two main directions of incoming waves separated by some angle ζ large compared with the spread of directions about each main direction we may replace each group of waves by a plane wave with the known distribution of amplitude. If there are no specular components these two equivalent waves will then have probability distributions given by:

$$p(X_1) = X_1 \cdot \exp(-X_1^2/2) \cdot dX_1$$
$$p(X_2) = \alpha^2 X_2 \cdot \exp(-\alpha^2 X_2^2/2) \cdot dX_2$$

These two waves have the same form of distribution but the power in the X_1-wave is α^2 times the power in the X_2-wave.

Let the phase difference at a point midway between the two aerials be ξ so that the joint probability distribution of amplitudes and phases is then:

$$p(X_1, X_2, \xi) = \frac{\alpha^2 X_1 X_2}{2\pi} \cdot \exp\left\{-\left(\frac{X_1^2}{2} + \frac{\alpha^2 X_2^2}{2}\right)\right\} \cdot dX_1 \cdot dX_2 : d\xi \qquad (13)$$

The resultant amplitude X measured at a point midway between the two aerials is given by:

$$X^2 = X_1^2 + X_2^2 + 2X_1X_2\cos\xi \qquad (14)$$

and the apparent bearing θ is found to be given by:

$$\sin\theta = \sin\zeta \frac{X_1^2 - X_2^2}{X^2} \quad \text{when the aerial spacing is small}$$

therefore

$$S = \sin\theta/\sin\zeta = \frac{X_1^2 - X_2^2}{X^2} \qquad (15)$$

With the aid of equations (14) and (15) the variables in (13) may be changed and the integration carried out to give:

$$p(S, X) = \frac{4\alpha^2}{\sqrt{(1+\alpha^2)}} \cdot \frac{X^2}{\sqrt{2\pi}} \cdot \exp\left[-\frac{X^2}{2}\left\{(1+S^2)(1+\alpha^2) + 2S^2(1-\alpha^2)\right\}\right] . dX . dS \tag{16}$$

A sample probability contour diagram (for $\alpha^2 = 0{\cdot}5$) is drawn in Fig. 3a.

This distribution, like the previous ones, is symmetrical in the S-direction whatever the relative amplitudes of the two constituent waves. Although it has

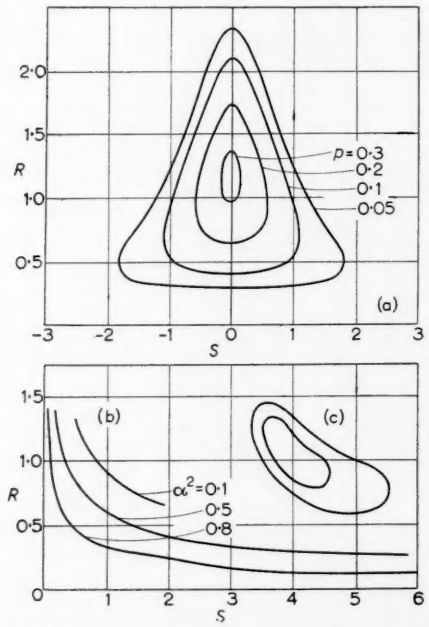

Fig. 3(a). Probability contour diagram for two groups of incoming waves (no specular components.) (b) Relation between R and S for two steady waves arriving from directions differing by ζ(ζS = sine instantaneous bearing). (c) Loci in B broadened by the addition of random components.

been found that many of the amplitude-bearing distributions obtained experimentally are asymmetrical, it appears that such distributions cannot arise from two incoming groups of waves as above except as indicated below, when both groups contain a specular component.

The calculation of the distribution of bearing and amplitude is difficult in this case and only qualitative results have been obtained.

In the simplest case where two steady waves of amplitudes 1, α, with directions differing by ζ and phase difference ξ (measured at a point midway between the two aerials) are being received.

$$S = \frac{1-\alpha^2}{1+\alpha^2+2\alpha\cos\xi}$$

VOL.
13
1958/5

where $S = \sin\theta/\sin\zeta$

θ = measured bearing angle

$$S_{\min} = \frac{1-\alpha}{1+\alpha} \quad \text{(obtained when } \xi = 0\text{)}$$

$$S_{\max} = \frac{1+\alpha}{1-\alpha} \quad \text{(obtained when } \xi = \pi\text{)}$$

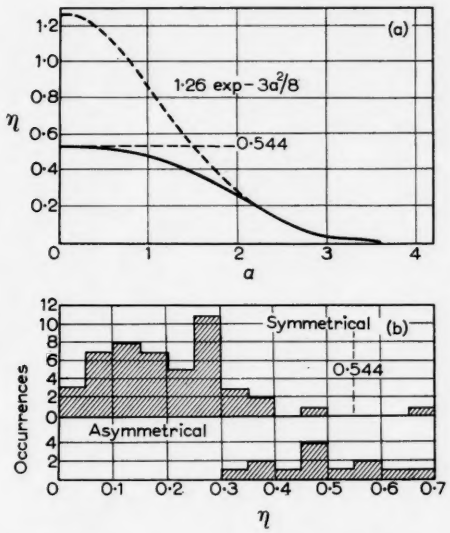

Fig. 4. (a) Variation of η with a for wave groups containing a specular component.
(b) Observed distribution of η for symmetrical and asymmetrical scatter diagrams.

The amplitude, X, is given by

$$X^2 = 1 + \alpha^2 + 2\alpha\cos\xi,$$

which yields, using a normalized amplitude R

$$(R^2 = X^2/1 + \alpha^2)$$

$$SR^2 = \frac{1-\alpha^2}{1+\alpha^2}$$

with S in the range $(1-\alpha)/(1+\alpha)$ to $(1+\alpha)/(1-\alpha)$. Some loci of S, R are plotted in Fig. 3b for various values of α. It will be noticed that these are asymmetrical. If we can now regard any random signals which are also present as leading to a general broadening of these loci the equiprobability contours will be of the form sketched in Fig. 3c. In this case, where the main changes in S or R are caused by variations in the phase difference between two relatively stable components, the correlation ratio will be high, agreeing with the experimental values shown in the bottom histogram in Fig. 4b.

6. MEASUREMENTS

A series of experimental distributions have been obtained using the small-aperture automatic direction finder described previously by WHALE and ROSS (1956). In these measurements, which included frequencies from 6 to 21 Mc/s and distances from 600 to 20,000 km, continuous chart records of bearing and relative intensity were obtained. As well as these, scatter diagrams displaying the statistical relation between bearing and amplitude were obtained on a two-dimensional pen recorder in which a pen (making dots at a constant rate) moved horizontally with bearing and vertically with amplitude. The dotting rate employed varied

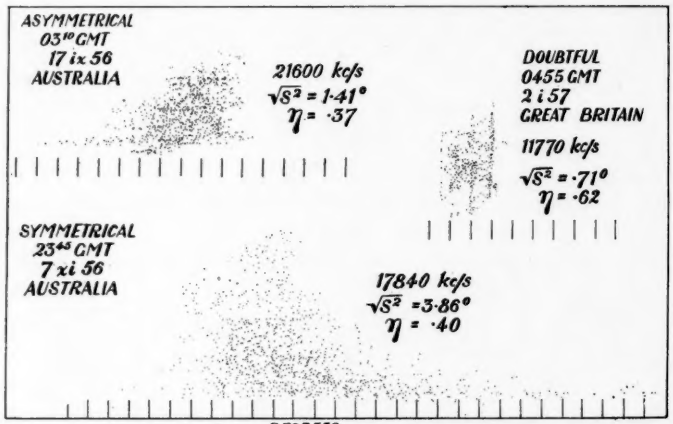

Fig. 5. Typical experimental scatter diagrams illustrating asymmetrical, symmetrical and anomalous (doubtful) cases. The vertical scale is relative amplitude.

from about 1 dot/sec under conditions of slow fading to about 4 dots/sec under conditions of fast fading. The time taken to produce a usable scatter diagram varied from about 2 min to about 12 min, depending on the dotting rate and on the spread in bearing and amplitude. Three sample scatter diagrams are reproduced in Fig. 5.

The continuous chart type of record of bearing and amplitude has been studied previously [for example ROSS (1954)] confirming the RAYLEIGH type distribution of amplitude [equation (8)] and the STUDENT's type distribution of bearing [equation (7)]. The main purpose of the continuous records in the measurements described here is to reveal any large slow variations, particularly in bearing; these may invalidate the analysis since, as in most statistical analyses, the distributions studied should be statistically stationary.

7. ANALYSIS

A total of 136 scatter diagrams were analysed by the standard statistical methods (WEATHERBURN, 1946) and the values of η_{RS} (the correlation ratio) and $\overline{S^2}$ (the bearing variance) obtained. The diagrams were divided into three groups: (i) symmetrical with bearing (42 per cent); (ii) asymmetrical (17 per cent); (iii) those obtained during changing conditions and a few inexplicable records (41 per

VOL
13
1958/

cent). The records were obtained during November, December and January, 1956–57, transmissions being chosen to give a range of frequencies and distances.

The distribution of η_{RS} is shown in the histograms in Fig. 4b. The two distributions drawn refer to the symmetrical scatter diagrams and to the asymmetrical scatter diagrams.

For the symmetrical patterns, most of the values of η_{RS} fall below the value of 0·54 which is derived in equation (10) as a maximum for a group of waves with no

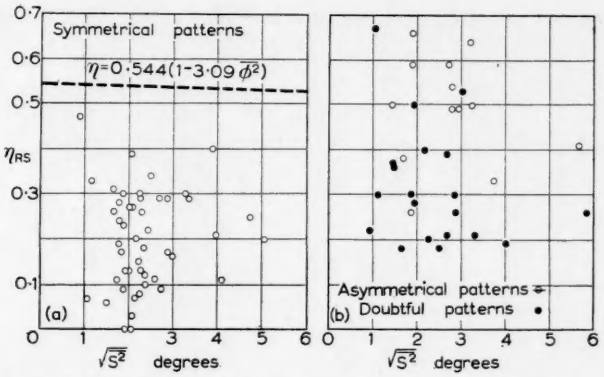

Fig. 6. Relation between the correlation ratio η_{RS} and the r.m.s. spread in instantaneous bearing for the symmetrical, asymmetrical and doubtful scatter diagrams.

specular component. From equation (10) we have, for the group of waves with no specular component that:

$$\eta_{RS} = 0{\cdot}544\,(1 - 3{\cdot}09\,\overline{\phi^2})$$

Also

$$\overline{S^2} = \frac{\overline{\phi^2}}{2} \,.\, \ln \frac{4}{\overline{\phi^2}}$$

$$\simeq \overline{\phi^2} \,.\, \log \frac{1}{\overline{\phi^2}}$$

In practice, values of $\overline{S^2}$ are less than 0·01 rad², giving $\overline{\phi^2}$ less than 0·01 rad², so that η_{RS} should not fall to less than about 70 per cent of its maximum value of 0·544. The measured variation of η_{RS} with $\sqrt{\overline{S^2}}$ is plotted in Fig. 6a.

It is difficult to calculate η_{RS} including the specular component. However, if a (the ratio of the specular to the random components) is large enough, then approximately:

$$\eta_{RS} = 1{\cdot}26 \exp(-3a^2/8)$$

The complete curve showing the variation of η_{RS} with a is thus probably similar to the one obtained by using this expression for large a and joining it to the point $\eta_{RS} = 0{\cdot}54$ when $a = 0$ as in Fig. 4a. η_{RS} certainly decreases with increasing a as can be seen by comparing Figs. 1 and 2. The more rounded form of

VOL. 13 58/59

Fig. 2 indicates a lower correlation ratio. It would appear, then, that the low values of η_{RS} for the symmetrical patterns could arise from the presence of a specular component. The "signal to noise" ratio a was not measured in these experiments as it was unnecessary in the calculation of correlation ratios.

The correlation ratio for the type (ii) (asymmetrical) scatter diagrams is consistently high, as is shown in Figs. 4b and 6b. These records probably arise from the interference of two main groups of waves arriving on slightly different bearings, each group containing an appreciable specular component.

The variation of η_{RS} with $\sqrt{\overline{S^2}}$ for the doubtful types of pattern is also shown

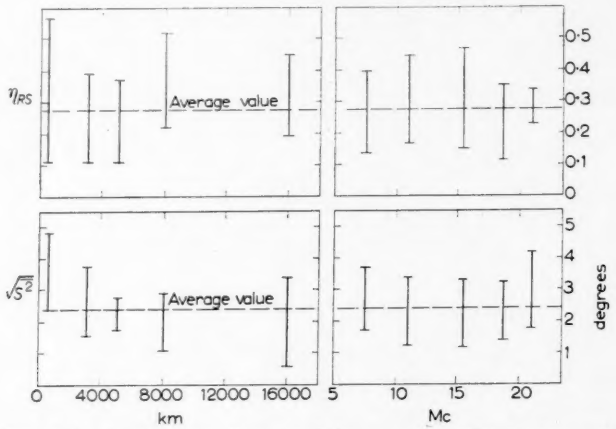

Fig. 7. Variation of the correlation ratio η_{RS} and the r.m.s. spread in bearing with distance and frequency of the transmitter.

in Fig. 6b. The fact that the values of η are generally less than for the asymmetrical case probably has little significance.

Both η_{RS} and $\overline{S^2}$ have been investigated for variations with frequency and distance. The results are indicated graphically in Fig. 7 where the standard deviation of each group of values is also shown. The observed values have been collected into groups centred on the distances and frequencies shown. The only significant tendency found is for $\sqrt{\overline{S^2}}$ to decrease with increasing distance.

It should be pointed out that this investigation of variations of correlation ratio and bearing spread is not very comprehensive. Many more measurements would be required before values could be predicted for any given combination of frequency, distance and location of path for a given set of ionospheric conditions.

Conclusion

Some fundamental relations between the bearing and the amplitude of a fading radio wave have been presented and some representative experimental measurements made on short waves reflected from the ionosphere. In these cases, the experimental measurements, while not disagreeing with the theory, indicate that it could with advantage be extended to cover those cases in which appreciable specular components are present.

VOL
13
1958/

Acknowledgements—This work was carried out at the Seagrove Radio Research Station, a section of the Physics Department, Auckland University. The station is largely financed by grants from the N.Z. Department of Scientific and Industrial Research, the Post and Telegraph Department and the Broadcasting Service.

References

Bramley N.	1951	*Proc. Instn. Elect. Engrs.* III, **98,** 19.
Cramér H.	1945	*Mathematical Methods of Statistics.* Princeton University Press.
Macnicol R. W. E.	1949	*Proc. Instn. Elect. Engrs.* III, **96,** 517.
Rice S. O.	1945	*Bell. Syst. Tech. J.* **24,** 46.
Ross W. J.	1955	Ph.D. Thesis, Auckland University.
Weatherburn C. E.	1946	*Mathematical Statistics.* Cambridge University Press.
Wooding R. A.	1955	*N.Z. J. Sci. Tech.* B **36,** 537.
Whale H. A. and Ross W. J.	1956	*Proc. Phys. Soc. Lond.* B **69,** 311.

VOL. 13 58/59

Journal of Atmospheric and Terrestrial Physics, 1958, Vol. 13, pp. 86 to 89. Pergamon Press Ltd., London

On the approximate daytime constancy of the absorption of radio waves in the lower ionosphere

S. CHAPMAN and K. DAVIES
Geophysical Institute, College, Alaska* and Brown University, Providence, Rhode Island†

(*Received* 8 *March* 1958)

Abstract—By day, the absorption of very long radio waves is nearly constant, and decidedly greater than at night; it originates in the lower ionosphere. It is here explained as due to electrons generated mainly by photodetachment from negative ions, supposed to be much greater in number, and nearly constant by day and night. The optical depth of the level concerned must be small for the photodetaching radiation, but large for the radiations able to ionize neutral particles.

EXPERIMENTAL EVIDENCE

THERE is now a considerable body of evidence which indicates that part of the total ionospheric absorption suffered by a radio wave during the process of reflection is almost independent of the solar zenith angle χ (BEYNON and DAVIES, 1955; WHITEHEAD, 1957), whereas the remaining part varies during the day. Further evidence that part of the total absorption is constant during the day is provided by observations on the reflection of radio waves of very low frequencies (BRACEWELL *et al.*, 1951), which show that on 16 kc the reflection coefficient falls suddenly before ground sunrise and remains sensibly constant until near sunset, when it rises suddenly again.

Measurements on the heights of vertical reflection of 16 kc radio waves (BRACEWELL *et al.*, 1951) show that these waves are reflected from a level of about 73 km. Hence it is reasonable to assume that the absorbing layer, which shows little dependence on cos χ, lies at or below the 73 km level.

For 16 kc waves incident obliquely on the ionosphere it may also be noted (BRACEWELL and BAIN, 1952) that the height of reflection appears to fall suddenly near local sunrise, then remains fixed until near local sunset, when it rises to the nighttime level. On higher frequencies the heights of reflection are somewhat higher and exhibit a more gradual daily variation.

THEORETICAL CONSIDERATIONS

The ionospheric absorption suffered by a radio beam of given frequency, incident normally (or at any fixed angle) on the ionosphere, is proportional to the integral $\int N\nu\, ds$ taken along the path(s) of the beam: here N is the electron density and ν is the collisional frequency of the electrons. Assuming that at each level ν is constant, then the changes of absorption, at a given level, will be governed by those of N. The simplest hypothesis is that over the height range where the absorption is important, N at each level, like the ionospheric absorption, increases

* And at the High Altitude Observatory, Boulder, there engaged in a programme of research supported by the National Bureau of Standards and the Sacramento Peak Observatory of the Air Force Cambridge Research Center.
† Working under contract AF 19(604)-2066.

VOL.
13
1958/5

near sunrise (at that level), remains almost constant throughout the daytime, and decreases near sunset.

Such behaviour of N, at low levels in the D-layer, can be explained by supposing the electron production to arise mainly by photodetachment of electrons from negative ions, whose density (n_-) is nearly constant throughout the day. The negative ions are likely to be mainly O_2^-, the ionization potential of which is about 1 eV . Consequently photons of any wavelength less than about 12,000 Å would have sufficient energy to detach the excess electron from the negative ion. Most of this ionizing radiation is only very slightly absorbed in traversing the D-layer—in other words, the optical depth of this layer is small for such radiation.

Consider any narrow band of such radiation, of intensity $S_\infty d\lambda$ outside the atmosphere. If it is absorbed (only) by a constituent of number density N, with absorption coefficient A, then the absorption in a stratum between heights h and $h - dh$, when the solar zenith angle is χ, is given by:

$$dS\, d\lambda = ASn\, (\sec \chi)\, dh\, d\lambda \tag{1}$$

Here A and S will be functions of the wavelength; S is also a function of h. Hence

$$S = S_\infty \exp\, (-A \sec \chi \int n\, dh) \tag{2}$$

OL.
13
8/59

The absorption of this band of radiation per unit volume of atmosphere is:

$$\frac{dS\, d\lambda}{\sec \chi\, dh}$$

If the absorbed radiation produces electrons at the rate β per unit of energy absorbed, then the rate of production of electrons is $(\beta \cos \chi)\ (dS/dh)\ d\lambda/\text{cm}^3$ per sec; β may be a function of λ. Denoting this rate of production of electrons by $I(\chi, h)$,

$$I(\chi, h) = \beta A(S_\infty\, d\lambda) n \exp\, (-A \sec \chi \int_h^\infty n\, dh) \tag{3}$$

So long as the absorption is small, so that $A \sec \chi \int_h^\infty n\, dh$ is small, the last factor in $I(\chi, h)$ may be taken as unity. But however small may be the absorption when the sun is overhead (that is however small the value of $A \int_h^\infty n\, dh$), for sufficiently large values of sec χ the absorption must be taken into account. Of course, for values of $\chi > 85°$, sec χ should be replaced by the Chapman function $\{\text{Ch}(R, \chi)\}$ (Chapman, 1931b; Wilkes, 1954); this function also becomes very large shortly after sunset, and shortly before sunrise.

This insensitivity to solar position is illustrated by the $I(\chi, h)$ curves given by Chapman for an isothermal atmosphere (Chapman, 1931a; see his Figs. 2–5). Two curves for an isothermal atmosphere are shown in Fig. 1; one is appropriate to low levels and the other to high levels. It is seen that for high levels ($z = 6$) the curve is nearly square shouldered, rising steeply after sunrise and remaining nearly level until near sunset when it falls steeply; z denotes the height above or below the level of peak absorption, reckoned in scale-height units. This characteristic

depends little on the assumption that the atmosphere is isothermal; the essential point is that the optical thickness be small.

For a wide band of visible and infrared radiation, for which the optical depth of the D-layer is small, the same considerations apply. Taking the exponential term in equation (3) to be sensibly unity (except when sec χ is large), the rate of electron production is given by $n \int \beta(\lambda) A(\lambda)\ S_\infty(\lambda)\ d\lambda$, where β, A and S_∞ are shown as functions of the wavelength λ. So long as n is sensibly constant throughout the day, and substantially all the electron-producing radiation is but slightly absorbed

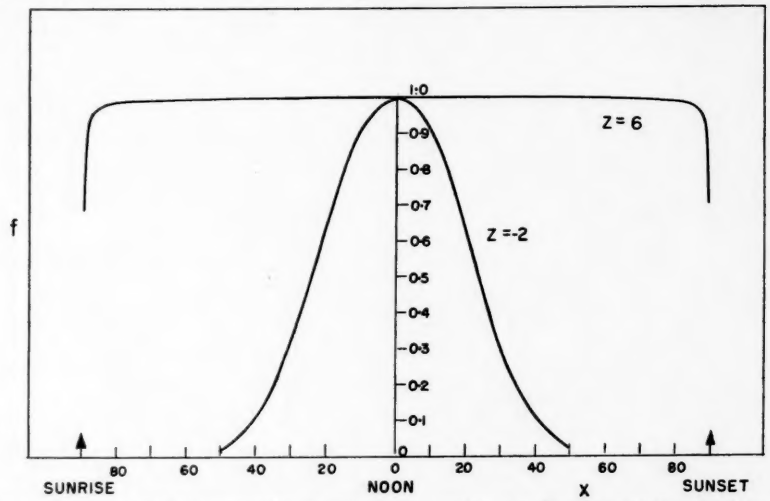

Fig. 1. Ion production as a function of solar zenith angle. f is the ratio of the rate when the zenith angle is χ to that at noon ($\chi = 0$), at the equator at the equinoxes. The curve for $z = 6$ refers to a level six scale heights above the level ($z = 0$) of peak absorption. The curve for $z = -2$ refers to a level two scale heights *below* the peak level.

in the region concerned, then the electron-production, and consequently also the electron density N, will remain nearly constant during the daytime.

The above conditions are likely to be nearly satisfied in the lower part of the D-region, as we suppose that the electrons are produced mainly from negative ions (so that we take n to be n_-). At these levels N/n_- will be small even during the daytime, owing to the rapidity of electron attachment. This implies that the negative ions destroyed by photodetachment are only a small fraction of the whole, so that n_- may be nearly constant at each level.

It is also necessary to suppose that the electron-production otherwise than by photodetachment (namely by photo-ionization of neutral particles) is relatively small. Cosmic rays will produce an almost constant small number of electrons by day and by night. Ionization by solar wave radiation will be small in the lower D-layer, and confined to a brief period around noon, because at those levels the major part of such radiation has been greatly weakened by absorption at higher levels (see the curve for $z = -2$ in Fig. 1, i.e. for levels well below the level of level of maximum absorption). As no pronounced hump occurs near noon in the diurnal curve of non-deviative radio wave absorption (e.g. that on very low frequencies), the corresponding electron production must be small.

VOL.
13
1958/5

During solar flares affairs are different. The directly ionizing radiation can penetrate to low levels, and the electron production can then exceed that arising from photodetachment. According to BRACEWELL *et al.* (1951), at such times there is little or no absorption on 16 kc, whereas on 70 kc and on 113 kc there is a fade out. This suggests that the extra ionization is produced at or above the level of reflection of 16 kc waves.

In a later paper the above qualitative explanation of the near constancy of lower *D*-region radio absorption will be examined in quantitative detail.

REFERENCES

BEYNON W. J. G. and DAVIES K.	1955	*The Physics of the Ionosphere*. Physical Society, London.
BRACEWELL R. N. and BAIN W. C.	1952	*J. Atmosph. Terr. Phys.* **2,** 216.
BRACEWELL R. N., BUDDEN K. G., RATCLIFFE J. A., STRAKER T. W. and WEEKES K.	1951	*Proc. I.E.E.* **98,** 221.
CHAPMAN S.	1931a	*Proc. Phys. Soc. Lond.* **43,** 26.
CHAPMAN S.	1931b	*Proc. Phys. Soc. Lond.* **43,** 483.
WHITEHEAD J. D.	1957	*J. Atmosph. Terr. Phys.* **10,** 12.
WILKES M. V.	1954	*Proc. Phys. Soc.* B **67,** 304

OL.
13
8/59

Journal of Atmospheric and Terrestrial Physics, 1958, Vol. 13, pp. 90 to 99. Pergamon Press Ltd., London

Resonance scattering by atmospheric sodium—V

Theory of the day airglow

J. C. Brandt and J. W. Chamberlain
Yerkes Observatory, University of Chicago

(*Received* 14 *January*, 1958)

Abstract—Chandrasekhar's theory of radiative transfer is applied to the day airglow to obtain the D_2 and D_1 brightness as a function of the sodium abundance and ground albedo. An analytic method of integrating monochromatic intensities over a Doppler profile has been developed, eliminating the necessity for numerical quadratures. This method is general and could be used to simplify calculations in the twilight and night airglow sodium problems as well. A high ground albedo can nearly double the radiation incident on the sodium "layer", compared with direct sunlight alone.

A general derivation is given of Hunten's (Part III) approximation for an effective optical thickness. In Appendix A the twilight problem is treated from the standpoint of the analytic method of line integrations and equations are given that may be used to extend the accuracy of the solutions; in Appendix B some X- and Y-functions for small optical thicknesses are tabulated; Appendix C gives basic formulae for extending the accuracy of analytic solutions to transfer problems in line radiation.

1. Introduction

The day airglow or dayglow has probably not yet been observed (Bates and Dalgarno, 1954; Morozov and Shklovsky, 1956), but its detection should be possible from the ground during a solar eclipse or from rockets and balloons above the troposphere (where Rayleigh scattering of sunlight becomes unimportant). Indeed, it appears almost inevitable that the dayglow will be measured in the near future, so we have considered it appropriate to extend this series of papers to a theoretical prediction of the D-line intensity in daytime.

As a first approximation one would expect the intensity from resonance scattering to be about the same as in twilight. There are, however, two effects that tend to change the daytime intensity, even if the sodium abundance remains constant. Firstly, the solar flux need not enter the atmosphere at a large grazing angle and (for high altitude observations, at least) the observer need not look close to the horizon to increase the D-lines relative to the background Fraunhofer spectrum. The absorption of D-line radiation by the sodium layer itself is thus much less than in twilight. Secondly, the ground albedo plays a more important role in the day. In twilight, reflection of scattered D-line radiation between the ground and the sodium layer may have a small effect on the observed intensity (Chamberlain, 1956, Part I). But in daytime the incident solar flux, as well as the scattered radiation, may be reflected. In winter or in event of a large cloud cover, ground reflection could be quite important.

The computations of this paper may thus provide observers with a realistic estimate of the intensity to be expected in the dayglow. But in the larger sense, one would like to translate observed intensities into sodium abundances. It is not likely that there is a large systematic change in the abundance between day and night, as evidenced by morning/evening ratios of intensity only slightly greater than unity (Swings and Nicolet, 1949; Cronin and Noelke, 1955; Blamont,

1956). HUNTEN (1954) has concluded that ionization during the day will not seriously decrease the abundance of neutral sodium in lower latitudes, as complete ionization equilibrium is probably not closely approached.

A direct comparison between twilight (morning and evening) and daytime abundances is, of course, desirable. But we suspect that dayglow observations will soon prove most valuable (1) in providing information on time fluctuations in the abundance during the course of one or several days and (2) in measurements of the geographical irregularities, through mapping of the dayglow from balloons. Concentrated investigations of these problems should not only help elucidate day-to-day fluctuations found in twilight, where one can observe only a few minutes a day, but they may, indeed, provide the clues necessary for a deductive solution to the problem of the origin of atmospheric sodium.

The solutions given here, based on CHANDRASEKHAR's (1950) theory of radiative transfer in finite atmospheres, are exact to all orders of scattering, and are expressed in terms of certain X- and Y-functions already tabulated by CHANDRASEKHAR and ELBERT (1952). For the dayglow problem additional values of X- and Y- functions for small optical thickness are required, and a supplementary tabulation is given in Appendix B of this paper.

CHANDRASEKHAR formulates the problem for a plane parallel atmosphere. This places some restrictions on the theory, but these limitations need be of no significance unless nearly horizontal observing angles are used. Further, the slight polarization of the D_2-line is neglected (D_1 is completely unpolarized).

An awkward problem is the integration of the monochromatic intensities (as computed with the transfer theory) over a Doppler line-profile for an assumed temperature. Previous investigations of airglow problems in this series have adopted numerical methods at this point in the development, and Part III (HUNTEN, 1956) was largely devoted to finding a means of avoiding the integration over the profile by evaluating the monochromatic solution at a single, "effective" wavelength in the line. In this paper we will develop rapidly converging series for the line intensities in terms of the X- and Y-functions, from which HUNTEN's approximation can be derived as a special case. Thus, it is hoped that accurate intensities of airglow lines as given by the theory of radiative transfer can be made available without the necessity of months of numerical work. The procedure for applying the general method to the theory of the intensity plateau in the twilight airglow is also developed in an appendix.

Finally, there remain the effects of the ground albedo on the observed intensities; with a high albedo, multiple reflections between the ground and sodium layer may even double the total intensity. The terminology of Part I (CHAMBERLAIN, 1956) will be followed throughout this paper.

2. The Dayglow Problem

The dayglow problem consists of two parts, depending on whether the observer is below or above the sodium layer. Since the sodium layer is at a height of about 85 km, observations both from below and above are feasible by rockets. The scattered intensity below the layer constitutes the first part of the problem and the scattered intensity as seen from above, the second. The geometry of the

situation is shown in Fig. 1. Let us assume for the present that the ground behaves as a Lambert's law reflector with albedo λ_0. We shall take the scattering in the sodium layer to be conservative and isotropic. Then the monochromatic intensity for the two parts of the problem is (CHANDRASEKHAR, 1950, p. 273)†

$$I_1^*(\tau_\nu - \mu_1) = \frac{F_\nu}{4\mu_1}\left\{T(\tau_\nu \mid \mu_1,\mu_0) + \frac{4\lambda_0}{(1 - \lambda_0\bar{s})}\,\mu_0\gamma_1(\mu_0)s(\mu_1)\right\} \tag{1}$$

and

$$I_2^*(0,\mu_2) = \frac{F_\nu}{4\mu_2}\left\{S(\tau_\nu \mid \mu_2,\mu_0) + \frac{4\lambda_0}{(1 - \lambda_0\bar{s})}\,\mu_0\gamma_1(\mu_0)t(\mu_2)\right\}, \tag{2}$$

where the incident solar flux in the centre of the line (or hyper-fine component),

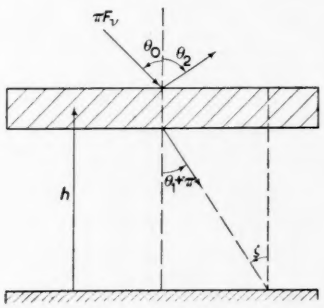

Fig. 1. Idealized plane–parallel atmosphere for dayglow problem.

perpendicular to the beam and just outside the earth's atmosphere, is πF_ν. Here $S(\tau_\nu \mid \mu,\mu_0)$ and $T(\tau_\nu \mid \mu,\mu_0)$ are CHANDRASEKHAR's scattering and transmission functions respectively. For isotropic scattering they are azimuth independent:

$$S(\tau_\nu \mid \mu,\mu_0) = \frac{\mu\mu_0}{(\mu + \mu_0)}\,[X^*(\mu)X^*(\mu_0) - Y^*(\mu)Y^*(\mu_0)] \tag{3}$$

and

$$T(\tau_\nu \mid \mu,\mu_0) = \frac{\mu\mu_0}{(\mu - \mu_0)}\,[Y^*(\mu)X^*(\mu_0) - X^*(\mu)Y^*(\mu_0)] \tag{4}$$

Also, in equations (1) and (2)

$$\gamma_1(\mu) = -\tfrac{1}{2}Q(\alpha_1 + \beta_1)[X^*(\mu) + Y^*(\mu)] \tag{5}$$

and

$$s(\mu) = \mu[1 - \gamma_1(\mu)] \tag{6a}$$

and

$$t(\mu) = \mu[\gamma_1(\mu) - e^{-\tau_\nu/\mu}], \tag{6b}$$

where the functions X^*, Y^*, α_1, β_1, Q, and $\bar{s}$ are all tabulated by CHANDRASEKHAR

† Whereas CHANDRASEKHAR's equation for the intensity above the atmosphere refers to the total monochromatic intensity, our equation (2) refers only to that portion which is scattered upward by the sodium layer. Radiation reflected by the ground and then transmitted, *without scattering*, by the sodium layer has been subtracted out. It is necessary to eliminate this nonscattered component, as it is effectively continuous radiation and cannot be integrated over the Doppler line-profile. If I_g is the upward directed intensity at the ground, then $I_g \exp(-\tau_\nu/\mu_2)$ is the intensity omitted from equation (2).

VOL
13
1958/

and ELBERT (1952). For small τ_ν and zero ground albedo ($\lambda_0 = 0$) the equations yield the formula for single scattering [Part I, equation (5)], as $X^* \to 1$ and $Y^* \to \exp(-\tau_\nu/\mu)$.

To obtain the integrated intensity of a single component in the hyperfine structure (CHAMBERLAIN, HUNTEN and MACK, 1958, Part IV) the monochromatic intensities must be integrated over a Doppler profile. Here we utilize the relations (Part I),

$$\tau_\nu = \tau_0 \exp(-x^2); \quad x = c(\nu - \nu_0)/\nu_0 U; \quad U = (2kT/M)^{1/2} \tag{7}$$

to perform the following integrals:

$$\mathscr{I}_1(\tau_0 \mid -\mu_1,\mu_0) = \frac{F_\nu}{4\mu_1}\int_0^\infty \left\{T(\tau_\nu \mid \mu_1,\mu_0) + \frac{4\lambda_0}{(1-\lambda_0\bar{s})}\,\mu_0\gamma_1(\mu_0)s(\mu_1)\right\} d\nu \tag{8}$$

$$\mathscr{I}_2(\tau_0 \mid +\mu_2,\mu_0) = \frac{F_\nu}{4\mu_2}\int_0^\infty \left\{S(\tau_\nu \mid \mu_2,\mu_0) + \frac{4\lambda_0}{(1-\lambda_0\bar{s})}\,\mu_0\gamma_1(\mu_0)t(\mu_2)\right\} d\nu \tag{9}$$

In the next section we shall consider an analytic method for evaluating integrals of this type. Specifically, we shall treat the integral of the scattering function, $S(\tau_\nu \mid \mu,\mu_0)$ which is appropriate to the dayglow as viewed from above the sodium layer for zero ground albedo.

VOL. 13 58/59

3. THE INTENSITY INTEGRAL

Equation (9) for $\lambda_0 = 0$ may be written, where x is defined by equation (7), as

$$\mathscr{I}_2(\tau_0 \mid \mu_2,\mu_0) = \frac{F_\nu U\nu_0}{4\mu_2 c}\int_{-\infty}^{+\infty} S(\tau_\nu \mid \mu_2,\mu_0)\,dx. \tag{10}$$

Expanding $S(\tau_\nu \mid \mu_2,\mu_0)$ in a Taylor's series in τ_ν about an arbitrary point a we obtain (suppressing μ and μ_0 in the functional notation), where primes denote derivatives with respect to τ_ν,

$$S(\tau_\nu) = S(a) + (\tau_\nu - a)S'(a) + \frac{(\tau_\nu - a)^2}{2}S''(a) + \frac{(\tau_\nu - a)^3}{6}S'''(a) + \ldots \tag{11}$$

Clearly, as $\tau_\nu \to 0$, the scattered intensity vanishes. This condition is equivalent to,

$$S(0) = S(a) - aS'(a) + \frac{a^2}{2}S''(a) - \frac{a^3}{6}S'''(a) + \ldots = 0 \tag{12}$$

and

$$S(\tau_\nu) = \tau_\nu S'(a) + \frac{(\tau_\nu^2 - 2a\tau_\nu)}{2}S''(a) + \frac{(\tau_\nu^3 - 3a\tau_\nu^2 + 3a^2\tau_\nu)}{6}S'''(a) + \ldots \tag{13}$$

When the series (13) is written in terms of τ_0 and x by equation (7) and substituted in the integral (10), we obtain

$$\mathscr{I}_2(\tau_0 \mid \mu_2,\mu_0) = \frac{F_\nu U\nu_0}{4\mu_2 c}\left[\sqrt{\pi}\tau_0 S'(a) + \frac{(\tau_0^2\sqrt{\pi/2} - 2a\tau_0\sqrt{\pi})}{2}S''(a) + \frac{(\tau_0^3\sqrt{\pi/3} - 3a\tau_0^2\sqrt{\pi/2} + 3a^2\tau_0\sqrt{\pi})}{6}S'''(a) + \ldots\right] \tag{14}$$

One point of immediate interest is a comparison with HUNTEN's (1956, Part III) approximation† for an effective optical thickness, $\tau_{\text{eff}} = \tau_0/\sqrt{2}$. HUNTEN's approximation in the problem under consideration gives

$$\mathscr{I}_2(\tau_0 \mid \mu_2,\mu_0) = \frac{F_\nu U_{\nu_0}}{4\mu_2 c}\sqrt{2\pi}S(\tau_0/\sqrt{2}) \tag{15}$$

Equation (15) may be derived from the general expansion by neglecting $S'''(a)$ and higher-order terms in equations (14) and (12); then to eliminate both the $S'(a)$ and $S''(a)$ terms from $\mathscr{I}$, we must have $a = \tau_0/\sqrt{2}$. Thus HUNTEN's approximation is equivalent to a polynomial expansion of S to the second degree in τ_0. This approximation is an extremely useful tool, which is often sufficiently accurate. However, the general series retains the advantage that an accurate estimate of the error committed in terminating the series at a finite number of terms is available. Further, of course, we have the machinery for extending the accuracy of the results, which may be necessary, for example, when the D_2/D_1 ratio is computed. In the case of the twilight airglow, HUNTEN's approximation breaks down quickly and is not especially suitable for evaluation of the intensity integral in that problem. We will deal with the twilight problem in Appendix A.

If we choose $a = \tau_0/2\sqrt{2}$, the coefficient of S'' vanishes in equation (14), giving

$$\mathscr{I}_2(\tau_0 \mid \mu_2,\mu_0) = \frac{F_\nu U_{\nu_0}}{4\mu_2 c}\left[\tau_0\sqrt{\pi}S'\left(\frac{\tau_0}{2\sqrt{2}}\right) + \frac{\tau_0{}^3\sqrt{\pi}[8\sqrt{3}-9]}{144}S'''\left(\frac{\tau_0}{2\sqrt{2}}\right) + \ldots\right] \tag{16}$$

Any suitable radiative transfer function could have been used in the intensity integral in place of $S(\tau_\nu \mid \mu_2,\mu_0)$, and an entirely analogous expression would have been obtained. Therefore, the accurate evaluation of these integrals has been reduced to finding the analytic expressions for the various derivatives. One can difference the radiative-transfer functions involved in the dayglow problem, for the range of parameters in question, and show that the second term in the series (16) is smaller than the first by a factor of 10^{-4}. Clearly this term is negligible for the accuracy required.‡ The problem is now very simple, as we need only the first derivatives of the transfer functions. These derivatives are among the basic equations of the problem of diffuse reflection and transmission by an atmosphere scattering radiation in the conservative, isotropic case, and are (CHANDRASEKHAR, 1950, p. 209)

$$S' = \frac{\partial S}{\partial \tau_\nu} = Y^*(\mu_2)Y^*(\mu_0) \tag{17}$$

and

$$T' = \frac{\partial T}{\partial \tau_\nu} = \frac{1}{(\mu_1 - \mu_0)}[\mu_1 X^*(\mu_1)Y^*(\mu_0) - \mu_0 X^*(\mu_0)Y^*(\mu_1)] \tag{18}$$

† HUNTEN sought to eliminate the necessity for integrating over frequency by expressing the integrated intensity, $\mathscr{I}$, in the form of the monochromatic solution (I_ν), which was evaluated with the effective optical thickness. This expression was normalized by means of the simple equations for the scattered intensity that are applicable for $\tau_\nu \to 0$.

‡ This approximation of neglecting S'' in equation (16) is roughly equivalent to HUNTEN's approximation of equation (15) and the numerical results from the two equations are nearly identical. If more terms in the expansion were to be retained, it would probably be advisable to choose a so that the coefficient of the last such term vanishes in equation (14), as the higher derivatives are cumbersome to work with (cf. Appendix C).

VOL
13
1958/

The derivatives for the ground albedo terms are not in a suitable form for the computing work, so we use HUNTEN's approximation for this term. In Appendix C, the basic formula and procedures for evaluating more derivatives will be given. With equations (16) and (17) for $\mathscr{I}_2$ and the analogous expressions for $\mathscr{I}_1$, the integrals (8) and (9) in the previous section give the solution for the dayglow problem in an accurate, concise form. Thus

$$\mathscr{I}_1(\tau_0 \mid -\mu_1,\mu_0) = \frac{F_\nu U \nu_0}{4\mu_1 c}\left\{\frac{\tau_0\sqrt{\pi}}{(\mu_1-\mu_0)}\left[\mu_1 X^*(\mu_1)Y^*(\mu_0) - \mu_0 X^*(\mu_0)Y^*(\mu_1)\right]_{\tau=\frac{\tau_0}{2\sqrt{2}}}\right.$$
$$\left. + \sqrt{2\pi}\left[\frac{4\lambda_0}{(1-\bar{s}\lambda_0)}\mu_0\gamma_1(\mu_0)s(\mu_1)\right]_{\tau=\frac{\tau_0}{\sqrt{2}}}\right\} \quad (19)$$

and

$$\mathscr{I}_2(\tau_0 \mid \mu_2,\mu_0) = \frac{F_\nu U \nu_0}{4\mu_2 c}\left\{\tau_0\sqrt{\pi}\left[Y^*(\mu_2)Y^*(\mu_0)\right]_{\tau=\frac{\tau_0}{2\sqrt{2}}}\right.$$
$$\left. + \sqrt{2\pi}\left[\frac{4\lambda_0}{(1-\bar{s}\lambda_0}\mu_0\gamma_1(\mu_0)t(\mu_2)\right]_{\tau=\frac{\tau_0}{\sqrt{2}}}\right\} \quad (20)$$

In these formulae, we have included no correction factors for absorption and scattering of the emergent beam by ozone or the troposphere. Unless observations are made from above the ozone layer, observers must reduce their measured intensities to an equivalent intensity for a point in proximity to the sodium layer. The numerical results are given for $\mathscr{I}_1(\tau_0 \mid -\mu_1,\mu_0)$ only since $\mathscr{I}_1$ and $\mathscr{I}_2$ are approximately equal for the ranges of parameters considered here. The solutions as a function of τ_0 are shown in Figs. 2 and 3. The intensities of $D_1 + D_2$ as a function of abundance of sodium based on the corrections for hyperfine structure as developed by CHAMBERLAIN, HUNTEN and MACK (1958, Part IV) are given in Fig. 4. The adopted solar flux and central intensities of the Fraunhofer lines are the same as in Part IV.

In the event of rocket or balloon observations, it would be advisable to make direct measurements of the brightness of the ground to evaluate the albedo, λ_0. If observations are made from above the sodium layer, supplementary measurements of the ground from below the layer will be necessary to eliminate the background, reflected Fraunhofer spectrum, as well as to evaluate the effect of the albedo in increasing the diffusely scattered radiation.

APPENDIX A

Analytic integration for the twilight problem

In twilight the albedo of the ground is unimportant, as shown by Table 1 of Part I. The integrated intensity of a single Doppler-broadened line in early twilight is [Part I, equation (11)].

$$\mathscr{I}_{\text{twi}}(\tau_0 \mid +\mu) = \frac{F_\nu U \nu_0}{4\mu c}\int_{-\infty}^{+\infty} \exp\left[-\frac{\tau_0}{\mu_0}e^{-x^2}\right] S(\tau_\nu \mid \mu,\mu_0)\,dx. \quad (A1)$$

VOL. 13 58/59

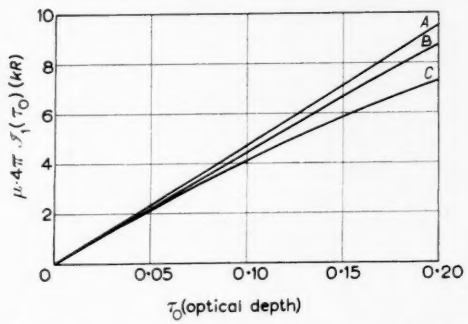

Fig. 2. Integrated intensity when $\lambda_0 = 0$ for a single Doppler line component, with optical thickness τ_0 at the centre of the component. Excitation is by the residual intensity in the Fraunhofer D_1 line for $T = 200°K$. A refers to ($\mu = 1{\cdot}0$; $\mu_0 = 0{\cdot}9$), B to ($\mu = 0{\cdot}5$; $\mu_0 = 0{\cdot}8$) and C to ($\mu = 0{\cdot}3$; $\mu_0 = 0{\cdot}4$).

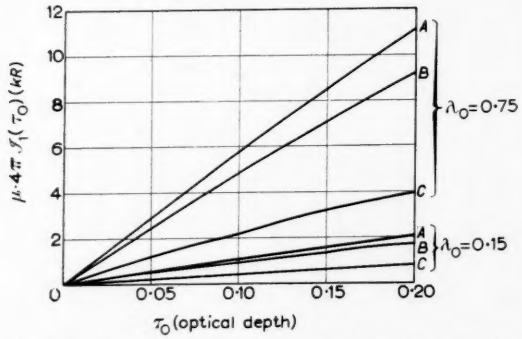

Fig. 3. Additional integrated intensity due to ground reflection for a single Doppler component. For the total intensity of a single component, the value from Fig. 3 must be added to the zero albedo value obtained from Fig. 2. A refers to ($\mu = 1{\cdot}0$; $\mu_0 = 0{\cdot}9$), B, to ($\mu = 0{\cdot}5$; $\mu_0 = 0{\cdot}8$), and C to ($\mu = 0{\cdot}3$; $\mu_0 = 0{\cdot}4$).

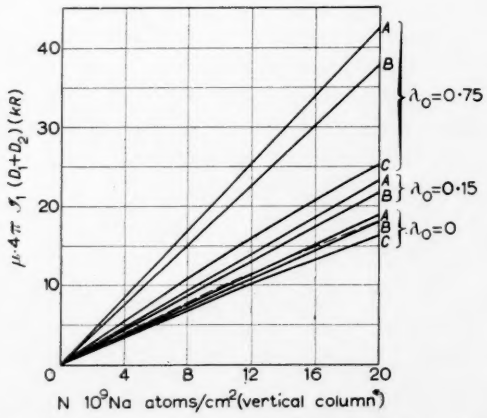

Fig. 4. Absolute intensity of $D_1 + D_2$ as a function of sodium abundance including the effects of ground reflection. A refers to ($\mu = 1{\cdot}0$; $\mu_0 = 0{\cdot}9$), B to ($\mu = 0{\cdot}5$; $\mu_0 = 0{\cdot}8$), and C to ($\mu = 0{\cdot}3$; $\mu_0 = 0{\cdot}4$). (The broken line is curve C for $\lambda_0 = 0{\cdot}15$.)

VOL.
13
1958/5

Expanding $S(\tau_\nu \mid \mu,\mu_0)$ by equation (12) and setting $S(0) = 0$, we obtain

$$\mathscr{I}_{\text{twi}}(\tau_0 \mid +\mu) = \frac{F_\nu U \nu_0 \sqrt{\pi}}{4\mu c}\left\{S'(a)\tau_0 \mathscr{B}_1\left(\frac{\tau_0}{\mu_0}\right) + \frac{S''(a)}{2}\left[\tau_0{}^2 \mathscr{B}_2\left(\frac{\tau_0}{\mu_0}\right) - 2a\tau_0 \mathscr{B}_1\left(\frac{\tau_0}{\mu_0}\right)\right] + \frac{S'''(a)}{6}\left[\tau_0{}^3 \mathscr{B}_3\left(\frac{\tau_0}{\mu_0}\right) - 3a\tau_0{}^2 \mathscr{B}_2\left(\frac{\tau_0}{\mu_0}\right) + 3a^2\tau_0 \mathscr{B}_1\left(\frac{\tau_0}{\mu_0}\right)\right] + \ldots\right\}, \quad \text{(A2)}$$

where a should be chosen judiciously to make the series converge with as few terms as possible, and where

$$\mathscr{B}_n(y) \equiv \frac{2}{\sqrt{\pi}}\int_0^\infty \exp\left[-ye^{-x^2}\right]e^{-nx^2}\,dx. \quad \text{(A3)}$$

For the case $n = 1$, these $\mathscr{B}$-functions reduce to HOLSTEIN's (1947) fractional-transmission function. Following the procedure used by DONAHUE and FODERARO (1955) and HUNTEN (1956, Part III) in treating HOLSTEIN's function, we may expand the integral of equation (A3) and integrate term by term:

$$\mathscr{B}_n(y) = \sum_{p=0}^{\infty} \frac{(-y)^p}{p!\sqrt{n+p}}. \quad \text{(A4)}$$

Evaluation of this series would allow compact and economical solutions to the twilight problem, but the $\mathscr{B}_n$-functions are not tabulated. Again an accurate estimate of the error committed in terminating the series is available; since the series alternates in sign, the error committed is less than the last term omitted.

The formal analytic integration of the twilight problem could have been done as in Section 3. If one sets $G(\tau_\nu \mid \mu,\mu_0) = \exp\left[(-\tau_0 \mid \mu_0)e^{-x^2}\right]S(\tau_\nu \mid \mu,\mu_0)$, then one would again obtain equation (14) with $G'(a)$ written for $S'(a)$, etc. However, while performing the numerical integrations for Part IV, it was learned that many terms of a Taylor's expansion would be required to represent $G(\tau_\nu \mid \mu,\mu_0)$ accurately. Thus it would be necessary to work with a large number of terms in (14) which would require that the higher order derivatives of $S(\tau_\nu \mid \mu,\mu_0)$ were accurately known. But, this would necessitate the tabulation of additional integrals (cf. Appendix C). Therefore, practical considerations dictate that the $\mathscr{B}_n$-functions be used to obtain a rapidly converging series solution to the twilight problem.

Finally, one word about the nightglow problem. If the nightglow functions introduced by CHAMBERLAIN and NEGAARD (1956, Part II) can be expressed accurately by a second-order Taylor expansion, HUNTEN's method is applicable. However, the general series is not convenient to use as it utilizes an integral function that is not tabulated.

APPENDIX B

Tabulations of X- and Y-functions

For the dayglow problem, a supplementary tabulation of the X^* and Y^* functions was necessary. The method of calculation is given by CHANDRASEKHAR (1948, 1950, pp. 202–207) and VAN DE HULST (1947). For $\tau_\nu \leqslant 0{\cdot}05$ the accuracy

should be ± 1 in the fourth decimal place and ± 2 in the fourth place for $\tau_\nu = 0{\cdot}07$. The results are given in Table B1.

Table B1. X and Y functions for conservative isotropic scattering

τ_ν	0·003		0·005		0·010		0·020		0·030		0·040		0·050		0·070	
μ	X^*	Y^*	X^*	Y^*	X^*	Y^*	X^*	Y^*	X^*	Y^*	X^*	Y^*	X^*	Y^*	X^*	Y^*
0·1	1·0092	0·9797	1·0142	0·9654	1·0247	0·9293	1·0418	0·8597	1·0557	0·7946	1·0675	0·7345	1·0776	0·6793	1·0943	0·5821
0·2	1·0093	0·9944	1·0144	0·9897	1·0253	0·9764	1·0437	0·9480	1·0594	0·9190	1·0733	0·8902	1·0858	0·8619	1·1079	0·8074
0·3	1·0093	0·9994	1·0144	0·9979	1·0255	0·9926	1·0443	0·9795	1·0607	0·9648	1·0754	0·9493	1·0888	0·9334	1·1131	0·9014
0·4	1·0093	1·0018	1·0145	1·0020	1·0256	1·0008	1·0446	0·9956	1·0613	0·9885	1·0764	0·9803	1·0904	0·9715	1·1158	0·9525
0·5	1·0093	1·0033	1·0145	1·0045	1·0256	1·0058	1·0448	1·0054	1·0617	1·0031	1·0771	0·9995	1·0914	0·9951	1·1176	0·9847
0·6	1·0093	1·0043	1·0145	1·0062	1·0257	1·0091	1·0450	1·0120	1·0620	1·0129	1·0776	1·0124	1·0921	1·0111	1·1187	1·0067
0·7	1·0093	1·0050	1·0145	1·0074	1·0257	1·0115	1·0451	1·0168	1·0622	1·0199	1·0779	1·0218	1·0925	1·0227	1·1195	1·0228
0·8	1·0093	1·0056	1·0145	1·0083	1·0257	1·0133	1·0451	1·0203	1·0623	1·0253	1·0781	1·0289	1·0929	1·0315	1·1202	1·0350
0·9	1·0093	1·0060	1·0145	1·0090	1·0257	1·0147	1·0452	1·0231	1·0624	1·0294	1·0783	1·0344	1·0932	1·0385	1·1206	1·0446
1·0	1·0093	1·0063	1·0145	1·0095	1·0258	1·0158	1·0452	1·0253	1·0625	1·0328	1·0785	1·0389	1·0934	1·0440	1·1210	1·0523

APPENDIX C

Formulae for the extension of dayglow solutions

To extend the accuracy of the solutions, further information about the various functions of radiative transfer are needed. The basis for the necessary formulae, which are particularly the derivatives, is to be found in Chapters VIII and IX of *Radiative Transfer* (CHANDRASEKHAR, 1950). Briefly we have the following:

$$\frac{\partial X^*}{\partial \tau_\nu} = y^*_{-1}(\tau_\nu) Y^*(\tau_\nu \mid \mu) \tag{C1}$$

$$\frac{\partial Y^*}{\partial \tau_\nu} = y^*_{-1}(\tau_\nu) X^*(\tau_\nu \mid \mu) - \frac{Y^*(\tau_\nu \mid \mu)}{\mu} \tag{C2}$$

$$\frac{dQ}{d\tau_\nu} = Q^2 - 2y^{(s)}_{-1}(\tau_\nu) Q \tag{C3}$$

$$\frac{d}{d\tau_\nu}(\alpha_1 + \beta_1) = y^{(s)}_{-1}(\tau_\nu)(\alpha_1 + \beta_1) \tag{C4}$$

$$\frac{d\bar{s}}{d\tau_\nu} = Q^2(\alpha_1 + \beta_1)^2 \tag{C5}$$

The moments of the Y-functions which appear above are defined by

$$y^*_{-1}(\tau_\nu) = \tfrac{1}{2}\int_0^1 \frac{Y^*(\tau_\nu \mid \mu)}{\mu}\, d\mu \quad \text{and} \quad y^{(s)}_{-1}(\tau_\nu) = \tfrac{1}{2}\int_0^1 \frac{Y^{(s)}(\tau_\nu \mid \mu)}{\mu}\, d\mu \tag{C6}$$

where $Y^{(s)}(\tau_\nu \mid \mu)$ is the standard solution tabulated by CHANDRASEKHAR and ELBERT (1952). As is explained with the tabulations, the sum of the moments $(\alpha_n + \beta_n)$ is invariant as to solution. Therefore, the only tabulations needed for the extension of the dayglow problem are those of $y_{-1}{}^*(\tau_\nu)$, $y^{(s)}_{-1}(\tau_\nu)$, and then derivatives. As a check on the computed moments, the following relation follows directly from the defining equations:

$$y_{-1}{}^*(\tau_\nu) = y^{(s)}_{-1}(\tau_\nu) + 2Q \tag{C7}$$

VOL. 13 1958/5

The first derivatives of S and T, as given by equations (17) and (18) may be derived from equations (3), (4), (C1) and (C2).

References

Bates D. R. and Dalgarno A.	1954	*J. Atmosph. Terr. Phys.* **5,** 329.
Blamont J. E.	1956	*The Airglow and the Aurorae* (Edited by E. B. Armstrong and A. Dalgarno) p. 99. Pergamon Press, London.
Chamberlain J. W.	1956	*J. Atmosph. Terr. Phys.* **9,** 73.
Chamberlain J. W. and Negaard B. J.	1956	*J. Atmosph. Terr. Phys.* **9,** 169.
Chamberlain J. W. Hunten D. M. and Mack J. E.	1958	*J. Atmosph. Terr. Phys.* In press.
Chandrasekhar S.	1948	*Astrophys. J.* **108,** 92.
Chandrasekhar S.	1950	*Radiative Transfer*, Clarendon Press, Oxford.
Chandrasekhar S. and Elbert D.	1952	*Astrophys. J.* **115,** 269.
Donahue T. M. and Foderaro A.	1955	*J. Geophys. Res.* **60,** 75.
Cronin H. E. and Noelke C. L.	1955	Final Report, Contract AF 19(604)–640 with A.F. Cambridge Research Center, Geo-Science Inc., Washington Grove, Md., U. S. A.
Holstein T.	1947	*Phys. Rev.* **72,** 1212.
Hunten D. M.	1954	*J. Atmosph. Terr. Phys.* **5,** 44.
Hunten D. M.	1956	*J. Atmosph. Terr. Phys.* **9,** 179.
Morozov V. M. and Shklovzky I. S.	1956	*The Airglow and the Aurorae* (Edited by E. B. Armstrong and A. Dalgarno) p. 201. Pergamon Press, London.
Swings P. and Nicolet M.	1949	*Astrophys. J.* **109,** 327.
van de Hulst H. C.	1947	*Astrophys. J.* **107,** 220.

OL.
13
8/59

Journal of Atmospheric and Terrestrial Physics, 1958, Vol. 13, pp. 100 to 106. Pergamon Press Ltd., London

Resonance scattering by atmospheric sodium—VI

The analytic solution for the twilight intensity*

J. C. BRANDT
Yerkes Observatory, University of Chicago, Williams Bay, Wisconsin

(*Received* 8 *March* 1958)

Abstract—With the method outlined by BRANDT and CHAMBERLAIN (1958) in Part V of this series, the analytic solution for the twilight intensity is obtained in terms of rapidly converging series expressions. All of the necessary functions for the solution are tabulated, and it is found that three terms of the series give an error less than 0·5 per cent for the range $0 \leqslant \tau_0 \leqslant 0{\cdot}20$. A sample computation is made for a angle of solar depression, β, of 6°·5 and the values are in excellent agreement with the numerical work published previously.

1. INTRODUCTION

IN Part I of this series, CHAMBERLAIN (1956) applied CHANDRASEKHAR'S (1950) theory of radiative transfer to the problem of the intensity plateau in the twilight airglow and obtained the following expression for the intensity of a single hyperfine component valid for zero ground reflection:

$$\mathscr{I}(\tau_0 \mid +\mu) = \frac{F_\nu U \nu_0}{4\mu c} \int_{-\infty}^{+\infty} \exp\left[-\frac{\tau_0}{\mu_0} e^{-x^2}\right] S(\tau_\nu \mid \mu, \mu_0)\, dx \qquad (1)$$

Here, πF_ν is the incident solar flux perpendicular to the beam and just outside the earth's atmosphere in the centre of the hyperfine component; $\tau_\nu = \tau_0 e^{-x^2}$; and $U = (2kT/M)^{1/2}$. Also, $S(\tau_\nu \mid \mu, \mu_0)$ is CHANDRASEKHAR'S scattering function, which, for conservative isotropic scattering is

$$S(\tau_\nu \mid \mu, \mu_0) = \frac{\mu\mu_0}{(\mu + \mu_0)} \left[X^*(\mu)X^*(\mu_0) - Y^*(\mu)Y^*(\mu_0)\right] \qquad (2)$$

where the functions X^* and Y^* are tabulated by CHANDRASEKHAR and ELBERT (1952). Equation (1) is valid for angles of solar depression, β, of from 4 to 7° and includes no corrections for tropospheric scattering. For ground albedo corrections, see Part I, Table 1 and for the geometry of the twilight problem see Part I, Fig. 1.

In Part IV (CHAMBERLAIN, HUNTEN and MACK, 1958), the integral in equation (1) was evaluated for a range of parameters by laborious numerical techniques. The purpose of this paper is to apply the analytic method outlined by BRANDT and CHAMBERLAIN in Part V, Appendix A to evaluate the integral and to reduce to a minimum the amount of numerical work needed to obtain the accurate radiative transfer solution to the twilight problem. Using equation (11), Part V

* The research reported in this paper was supported in part by the Geophysics Research Directorate of the Air Force Cambridge Research Center under Contract AF 19(604)-3044.

VOL
13
1958/

we expand $S(\tau_\nu \mid \mu, \mu_0)$ in series and, setting $S(0) = 0$, we obtain:

$$\mathcal{I}(\tau_0 \mid +\mu) = \frac{F_\nu U \nu_0 \sqrt{\pi}}{4\mu c}\left\{S'(a)\tau_0 \mathscr{B}_1\left(\frac{\tau_0}{\mu_0}\right) + \frac{S''(a)}{2}\left[\tau_0{}^2 \mathscr{B}_2\left(\frac{\tau_0}{\mu_0}\right) - 2a\tau_0 \mathscr{B}_1\left(\frac{\tau_0}{\mu_0}\right)\right]\right.$$
$$+ \frac{S'''(a)}{3!}\left[\tau_0{}^3 \mathscr{B}_3\left(\frac{\tau_0}{\mu_0}\right) - 3a\tau_0{}^2 \mathscr{B}_2\left(\frac{\tau_0}{\mu_0}\right) + 3a^2\tau_0 \mathscr{B}_1\left(\frac{\tau_0}{\mu_0}\right)\right]$$
$$\left. + \frac{S^{\mathrm{IV}}(a)}{4!}\left[\tau_0{}^4 \mathscr{B}_4\left(\frac{\tau_0}{\mu_0}\right) - 4a\tau_0{}^3 \mathscr{B}_3\left(\frac{\tau_0}{\mu_0}\right) + 6a^2\tau_0{}^2 \mathscr{B}_2\left(\frac{\tau_0}{\mu_0}\right) - 4a^3\tau_0 \mathscr{B}_1\left(\frac{\tau_0}{\mu_0}\right)\right] + \ldots\right\} \quad (3)$$

where

$$\mathscr{B}_n(w) \equiv \frac{2}{\sqrt{\pi}}\int_0^\infty \exp[-we^{-x^2}]e^{-nx^2}\,dx \quad (4)$$

and S', S'', etc., are the derivatives of the scattering function. Our procedure will be to tabulate all of the functions necessary for the accurate evaluation of the twilight intensity. It is found that the first three terms of the series give an accurate solution to the problem with an error below 0·5 per cent for the range $0 \leqslant \tau_0 \leqslant 0{\cdot}20$.

2. Evaluation of the Functions

The functions $\mathscr{B}_n(w)$ have the following series expansion [Part V, equation (A4)]:

$$\mathscr{B}_n(w) = \sum_{p=0}^{\infty} \frac{(-w)^p}{p!\sqrt{(n+p)}} \quad (5)$$

This series has been evaluated for $n = 1$ to 5 for the range $0 < w \leqslant 2{\cdot}0$ in steps of 0·1. The value for $w = 0$ can be evaluated directly from the integral. These calculations are simplified by existing tables of $w^p/p!$ prepared by the National Bureau of Standards (1954). The results are given in Table 1. Empirically, we find that $a = \tau_0/3$ gives small coefficients in equation (3). Then we have,

$$\mathcal{I}(\tau_0 \mid +\mu) = \frac{F_\nu U \nu_0 \sqrt{\pi}}{4\mu c}\left\{S'(\tau_0/3)\,\tau_0 \mathsf{B}_1\left(\frac{\tau_0}{\mu_0}\right) + \frac{S''(\tau_0/3)}{2}\,\tau_0{}^2 \mathsf{B}_2\left(\frac{\tau_0}{\mu_0}\right)\right.$$
$$\left. + \frac{S'''(\tau_0/3)}{3!}\,\tau_0{}^3 \mathsf{B}_3\left(\frac{\tau_0}{\mu_0}\right) + \frac{S^{\mathrm{IV}}(\tau_0/3)}{4!}\,\tau_0{}^4 \mathsf{B}_4\left(\frac{\tau_0}{\mu_0}\right) + \ldots\right\} \quad (6)$$

where

$$\mathsf{B}_1\left(\frac{\tau_0}{\mu_0}\right) = \mathscr{B}_1\left(\frac{\tau_0}{\mu_0}\right)$$
$$\mathsf{B}_2\left(\frac{\tau_0}{\mu_0}\right) = \mathscr{B}_2\left(\frac{\tau_0}{\mu_0}\right) - \frac{2}{3}\,\mathscr{B}_1\left(\frac{\tau_0}{\mu_0}\right)$$
$$\mathsf{B}_3\left(\frac{\tau_0}{\mu_0}\right) = \mathscr{B}_3\left(\frac{\tau_0}{\mu_0}\right) - \mathscr{B}_2\left(\frac{\tau_0}{\mu_0}\right) + \frac{1}{3}\,\mathscr{B}_1\left(\frac{\tau_0}{\mu_0}\right)$$
$$\mathsf{B}_4\left(\frac{\tau_0}{\mu_0}\right) = \mathscr{B}_4\left(\frac{\tau_0}{\mu_0}\right) - \frac{4}{3}\,\mathscr{B}_3\left(\frac{\tau_0}{\mu_0}\right) + \frac{2}{3}\,\mathscr{B}_2\left(\frac{\tau_0}{\mu_0}\right) - \frac{4}{27}\,\mathscr{B}_1\left(\frac{\tau_0}{\mu_0}\right) \quad (7)$$

The functions $\mathsf{B}_n(w)$ are evaluated for $n = 1$ to 4 for the range $0{\cdot}0 \leqslant w \leqslant 2{\cdot}0$ and are shown in Table 2.

Table 1. The functions $\mathscr{B}_n(w)$

w	$\mathscr{B}_1(w)$	$\mathscr{B}_2(w)$	$\mathscr{B}_3(w)$	$\mathscr{B}_4(w)$	$\mathscr{B}_5(w)$
0·0	1·0000	0·7071	0·5774	0·5000	0·4472
0·1	0·9321	0·6518	0·5295	0·4573	0·4082
0·2	0·8695	0·6011	0·4858	0·4182	0·3727
0·3	0·8117	0·5545	0·4458	0·3826	0·3403
0·4	0·7585	0·5118	0·4091	0·3501	0·3107
0·5	0·7093	0·4726	0·3756	0·3204	0·2838
0·6	0·6638	0·4366	0·3450	0·2933	0·2592
0·7	0·6218	0·4035	0·3169	0·2685	0·2368
0·8	0·5830	0·3731	0·2912	0·2458	0·2163
0·9	0·5471	0·3452	0·2677	0·2252	0·1977
1·0	0·5139	0·3195	0·2461	0·2063	0·1806
1·1	0·4832	0·2959	0·2264	0·1890	0·1651
1·2	0·4547	0·2742	0·2083	0·1732	0·1509
1·3	0·4283	0·2542	0·1917	0·1588	0·1380
1·4	0·4038	0·2358	0·1765	0·1455	0·1262
1·5	0·3811	0·2189	0·1625	0·1335	0·1154
1·6	0·3600	0·2033	0·1498	0·1224	0·1056
1·7	0·3404	0·1889	0·1380	0·1123	0·0966
1·8	0·3222	0·1756	0·1273	0·1031	0·0884
1·9	0·3052	0·1634	0·1174	0·0946	0·0809
2·0	0·2895	0·1521	0·1083	0·0869	0·0741

Table 2. The functions $\mathsf{B}_n(w)$, defined for $a = \tau_0/3$.

w	$\mathsf{B}_1(w)$	$\mathsf{B}_2(w)$	$\mathsf{B}_3(w)$	$\mathsf{B}_4(w)$
0·0	+1·0000	+0·0404	+0·2036	+0·0535
0·1	0·9321	+0·0304	0·1884	0·0477
0·2	0·8695	+0·0214	0·1745	0·0424
0·3	0·8117	+0·0134	0·1618	0·0377
0·4	0·7585	+0·0062	0·1502	0·0334
0·5	0·7093	−0·0003	0·1395	0·0295
0·6	0·6638	−0·0060	0·1297	0·0260
0·7	0·6218	−0·0111	0·1207	0·0228
0·8	0·5830	−0·0156	0·1124	0·0199
0·9	0·5471	−0·0196	0·1049	0·0173
1·0	+0·5139	−0·0231	+0·0979	+0·0150
1·1	0·4832	−0·0262	0·0915	0·0128
1·2	0·4547	−0·0289	0·0857	0·0109
1·3	0·4283	−0·0313	0·0803	0·0092
1·4	0·4038	−0·0334	0·0753	0·0076
1·5	0·3811	−0·0352	0·0707	0·0062
1·6	0·3600	−0·0367	0·0665	0·0049
1·7	0·3404	−0·0381	0·0626	0·0038
1·8	0·3222	−0·0392	0·0590	0·0027
1·9	0·3052	−0·0401	0·0557	0·0018
2·0	+0·2895	−0·0409	+0·0527	+0·0010

VOL
13
1958/

VOL. 13 58/59

Table 3. X- and Y-functions for isotropic scattering

τ	0·003		0·005		0·010		0·020		0·030		0·040		0·050		0·070	
μ	X^*	Y^*	X^*	Y^*	X^*	Y^*	X^*	Y^*	X^*	Y^*	X^*	Y^*	X^*	Y^*	X^*	Y^*
0·06	1·0091	0·9604	1·0140	0·9339	1·0240	0·8701	1·0397	0·7548	1·0515	0·6552	1·0609	0·5695	1·0685	0·4962	1·0800	0·3796
0·08	1·0092	0·9724	1·0141	0·9534	1·0245	0·9066	1·0410	0·8187	1·0541	0·7391	1·0649	0·6676	1·0740	0·6036	1·0884	0·4954
0·10	1·0092	0·9797	1·0142	0·9654	1·0247	0·9293	1·0418	0·8597	1·0557	0·7946	1·0675	0·7345	1·0776	0·6793	1·0943	0·5821
0·12	1·0092	0·9846	1·0142	0·9734	1·0248	0·9448	1·0425	0·8882	1·0570	0·8338	1·0695	0·7828	1·0804	0·7350	1·0988	0·6484
0·15	1·0093	0·9895	1·0143	0·9815	1·0250	0·9605	1·0432	0·9176	1·0583	0·8752	1·0714	0·8344	1·0832	0·7959	1·1033	0·7232
0·30	1·0093	0·9994	1·0144	0·9979	1·0255	0·9926	1·0443	0·9795	1·0607	0·9648	1·0754	0·9493	1·0888	0·9334	1·1131	0·9014
1·00	1·0093	1·0063	1·0145	1·0095	1·0258	1·0158	1·0452	1·0253	1·0625	1·0328	1·0785	1·0389	1·0934	1·0440	1·1210	1·0523

The scattering function $S(\tau_v \mid \mu, \mu_0)$ has the following derivatives:

$$\frac{\partial S}{\partial \tau_v} = S'(\tau_v) = Y^*(\mu) Y^*(\mu_0) \tag{8}$$

$$S''(\tau_v) = y_{-1}{}^*(\tau_v)[Y^*(\mu)X^*(\mu_0) + Y^*(\mu_0)X^*(\mu)] - S'(\tau_v)\left[\frac{1}{\mu_0} + \frac{1}{\mu}\right] \tag{9}$$

The values of the X^* and Y^* functions convenient for the twilight problem are given in Table 3. For $S''(\tau_v)$ we need the function $y_{-1}{}^*(\tau_v)$, which is defined in Part V, equation (C6) as:

$$y_{-1}{}^*(\tau_v) = \frac{1}{2}\int_0^1 \frac{Y^*(\tau_v \mid \mu)d\mu}{\mu} \tag{10}$$

For small τ_v, $Y^*(\mu) \to \exp(-\tau_v/\mu)$. Therefore we have:

$$\lim_{\tau_v \to 0}[y_{-1}{}^*(\tau_v)] = \frac{1}{2}\int_0^1 \frac{\exp(-\tau_v/\mu)}{\mu}\, d\mu = \frac{1}{2} E_1(\tau_v) \tag{11}$$

where $E_1(\tau_v)$ is the exponential integral. Our procedure is to evaluate $y_{-1}{}^*(\tau_v)$ numerically from the tables of CHANDRASEKHAR and ELBERT (1952) for the values $\tau_v = 0{\cdot}05$, $0{\cdot}10$ and $0{\cdot}15$, and use these results to interpolate the difference between $y_{-1}{}^*(\tau_v)$ and $\frac{1}{2}E_1(\tau_v)$ for the other needed values.

To evaluate the integrals, we need the value of the ratio $Y^*(\mu)/\mu$ as $\mu \to 0$. From the defining equation for $Y^*(\mu)$ (CHANDRASEKHAR, 1950, p. 183) we have:

$$Y^*(\mu) = \exp(-\tau_v/\mu) + \frac{\mu}{2}\int_0^1 \frac{[Y^*(\mu)X^*(\mu') - X^*(\mu)Y^*(\mu')]}{[\mu - \mu']}\, d\mu' \tag{12}$$

Since $X^*(\mu) \to 1$ and $Y^*(\mu) \to 0$ as $\mu \to 0$, we have:

$$\lim_{\mu \to 0} \frac{Y^*(\mu)}{\mu} = \frac{1}{2}\int_0^1 \frac{Y^*(\mu')}{\mu'}\, d\mu' = y_{-1}{}^*(\tau_v) \tag{13}$$

Hence, one must use an iteration procedure to obtain the values of $y_{-1}{}^*(\tau_v)$. The results are shown in Table 4. The values of $y_{-1}{}^*(\tau_v)$ may be used to extend

Table 4. The function $y_{-1}{}^*(\tau_v)$

τ_v	$y_{-1}{}^*(\tau_v)$
0·01	2·06
0·02	1·76
0·03	1·59
0·04	1·48
0·05	1·39
0·06	1·32
0·07	1·26
0·08	1·21
0 09	1·16
0 10	1·12

the accuracy of the dayglow solution or to use the series expansion method of evaluating the intensity integral in the nightglow problem. To find $S'''(\tau_\nu)$ for a given set of parameters one numerically differentiates the tabular values of $S''(\tau_\nu)$ using any of the standard formulae (e.g. HARTREE, 1955, p. 118).

3. RESULTS

Using the first three terms of equation (6) the twilight intensity of a single hyperfine component of D_1 has been computed for a horizon observation ($\mu = 0{\cdot}3$) and for a β of $6°{\cdot}5$ ($\mu_0 = 0{\cdot}113$). The values of the solar flux and the Fraunhofer

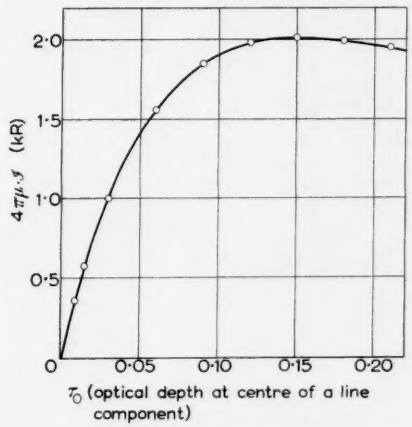

Fig. 1. Absolute horizon intensity of a single hyperfine component of the Fraunhofer D_1 line vs. the optical depth at the centre of the component for $\beta = 6°{\cdot}5$. See the text for discussion.

D_1 residual intensity, r_1, are the same as in Part IV. The results of this calculation are shown in Fig. 1. For the calculations, the temperature was taken as 200°K, but applying the correction factor of $(T/200)^{1/2}$ converts the intensity to any desired temperature of the sodium layers for the same τ_0. To change to the D_2 line, simply multiply by $r_2/r_1 = 0{\cdot}858$. This curve is in excellent agreement with the curve computed by numerical techniques in Part IV. However, our curve should be considered a replacement to Part IV results since, over the range of τ_0 under consideration, we have twice as many points to obtain a better determination of the curve. This fact could be of some importance in the bend of the curve around $\tau_0 \simeq 0{\cdot}08$, and at smaller τ_0, where the slope is relatively steep.

Since all of the functions necessary for the evaluation of the analytic formula are tabulated in this paper, it is now only a matter of minutes for the construction of additional curves for other desired values of the parameters.

Acknowledgement—Thanks are due to Dr. J. W. CHAMBERLAIN for suggestions throughout the investigation and for critically reading the manuscript.

REFERENCES

BRANDT J. C. and CHAMBERLAIN J. W.	1958	Part V. *J. Atmosph. Terr. Phys.* This issue, p. 90.
CHAMBERLAIN J. W.	1956	Part I. *J. Atmosph. Terr. Phys.* **9,** 73.
CHAMBERLAIN J. W., HUNTEN D. M. and MACK J. E.	1958	Part IV. *J. Atmosph. Terr. Phys.* **12,** 153.
CHANDRASEKHAR S.	1950	*Radiative Transfer.* Clarendon Press, Oxford.
CHANDRASEKHAR S. and ELBERT D.	1952	*Astrophys. J.* **115,** 269.
HARTREE D. R.	1955	*Numerical Analysis.* Clarendon Press, Oxford.
National Bureau of Standards	1954	*Tables of Functions and of Zeros of Functions.* NBS Applied Mathematics Series, No. 37, 145.

VOL.
13
1958/5

Journal of Atmospheric and Terrestrial Physics, 1958, Vol. 13, pp. 107 to 112. Pergamon Press Ltd., London

Height-gradient of electron-loss in the *F*-region

V. MARASIGAN, S.J.
Manila Observatory, Baguio City, Philippines

(*Received* 19 *March* 1958)

Abstract—A theoretical expression is derived for the exponential height-gradient of the coefficient of electron-loss in the *F*-region, on the assumption that this gradient completely accounts for the initial process of bifurcation. Five models are proposed: parabolic, linear, second-power, cosine and quasi-parabolic.

INTRODUCTION

WITH the rapid accumulation of data on the upper atmosphere now being obtained by many independent methods, especially by means of rockets and satellites, there arises a corresponding need to establish the mathematical relations between all these data, with the ultimate view of constructing a comprehensive theory of the upper atmosphere. The purpose of this present study is to see whether the shape of the *F*-trace as obtained by ionospheric soundings can be made to yield additional information on loss processes in that region. The actual values of the loss coefficient at various heights can best be obtained by rocket exploration. But as pointed out by BATES (1954), independent confirmation is needed, on account of certain difficulties raised by the rocket model of the atmosphere. One such difficulty may well be the extrapolations often resorted to as regards the ionospheric *F*-region.

As a first approximation, an exponential decrease of the loss coefficient with height is assumed, e.g. by MARTYN (1955) thus:

$$\alpha = \alpha_0 e^{-bz} \tag{1}$$

where b is found to be unity or more, by analysing observed lunar variations.

A second approximation is obtained from NICOLET (1954) by showing that b in (1) is related to a varying scale-height thus:

$$b = \eta\left(\frac{dH}{dz} + 1\right) \tag{2}$$

where H is the scale-height, assumed to vary linearly within each layer, and η is a constant dependent on the type of electron loss.

A further modification has been suggested by RATCLIFFE *et al.* (1956) who divide the *F*-region into three levels, of which only the intermediate level is assigned an exponential decrease of the loss-coefficient, the other two levels having a constant loss-coefficient, on the basis of empirical findings.

In this present study, attention is limited to $a(= 1/b)$, to see if its value may be calculated from the shape of the *F*-trace. With this value, it is hoped that a simple expression for the height-gradient of loss-coefficient in the *F*-region may be deduced.

DERIVATION OF THE HEIGHT-GRADIENT OF α

Let α vary with height thus:

$$\alpha = \alpha_0 e^{-z/a} \tag{3}$$

where z is the true height as measured from the bottom of the F-region, and a is a quantity to be evaluated.

Two simplifying assumptions are necessary. In the first place, it is assumed that the height-gradient of α *by itself* is sufficient to split the F-region into *F1*- and *F2*-layers (MARTYN, 1955). Secondly, it is assumed that at the beginning of the

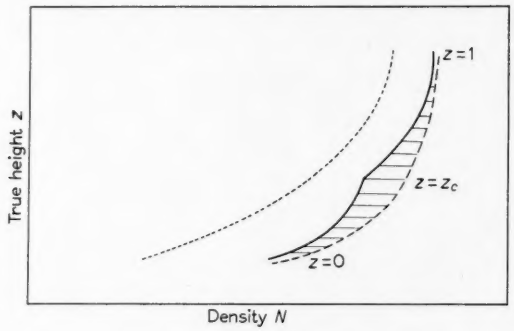

Fig. 1. Dotted curve: density distribution at time t. Dashed curve: density distribution at time $t + \Delta t$ with loss term excluded. Solid curves: density distribution at time $t + \Delta t$ with loss term included. Each horizontal line in the shaded portion of the diagram represents the magnitude of the loss term αN^m at each level. At $z = z_c$, αN^m has a maximum value.

bifurcation process, say, at 0800 hours, the increase of electron-density due to production and to movements is a continuous function of height everywhere in the F-region below the peak level. Thus, any departure from a smooth spatial distribution of electron-density must be assumed to be due solely to the loss term αN^m. (The exponent m of N in the loss term may be either 1 or 2 or in-between, depending upon the type of electron-decay.) Such a departure is the point of inflection, or cusp, on the true-height/density curve when this is starting to split into two distinct curves.

In the diagram (Fig. 1), the dotted lines represent the spatial distribution at time t; at time $t + \Delta t$, if the loss term is excluded, the resulting distribution (or "lossless distribution") is still monotonic and is represented by the dashed lines; if the loss term is included, and α decreases with height, then the product αN^m can have a turning point, say, at z_c, simply because α and N^m are hypothetically monotonic in opposite senses. The magnitude of αN^m varies with height and is represented by the length of each horizontal line in the shaded portion of the diagram. The solid line represents the resulting departure from the lossless distribution. From this, it can be deduced that when $z = z_c$,

$$\frac{d}{dz}(\alpha N^m) = 0$$

VOL. 13 1958/5

and therefore

$$\frac{d\alpha}{dz} = -\frac{\alpha}{N^m}\frac{d}{dz}(N^m) \tag{4}$$

From (3)

$$\frac{d\alpha}{dz} = -\frac{\alpha}{a} \tag{5}$$

Combining (4) and (5)

$$a = \frac{N}{m(dN/dz)} \tag{6}$$

where N and dN/dz are values on the (imaginary) lossless distribution at $z = z_c$. By substituting the numerical value of (6) in (3), we have the expression for a loss-coefficient decreasing exponentially with height.

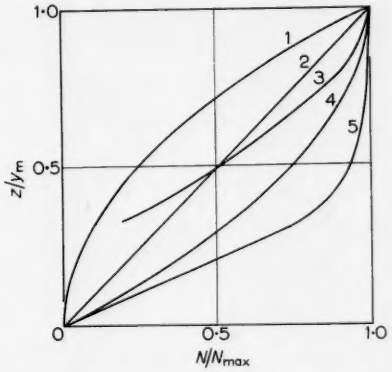

Fig. 2. Five models of density distribution: (1) second-power, (2) linear, (3) cosine, (4) parabolic, and (5) quasi-parabolic.

Five Models of the Height-Gradient of α

The behaviour of equation (6) will now be examined with the aid of five models of the lossless distribution: parabolic, linear, second-power, cosine and quasi-parabolic models. For simplicity, loss by attachment is assumed and therefore $m = 1$.

The following definitions are given:

(1) parabolic distribution: $N = N_{\max}\left[1 - \left(1 - \frac{z}{y_m}\right)^2\right]$

(2) linear distribution: $N = kz$

(3) second-power distribution: $N = \beta z^2$

(4) cosine distribution: $N = \frac{N_{\max}}{2}\left[1 + \cos\pi\left(1 - \frac{z}{y_m}\right)\right]$

(5) quasi-parabolic distribution: $N = N_{\max}\left[1 - \left(1 - \frac{z}{y_m}\right)^4\right]$

where y_m is the distance from the upper peak to the lower boundary of the F-region. The first three of these have already been found useful in the study of actual situations by RATCLIFFE (1951). The cosine model follows the suggestion of KELSO (1954) and lies in between the parabolic and linear models. The quasi-parabolic model is demanded by theoretical needs arising from the view of BRADBURY (1938) and MOHLER (1940) that the spatial maximum of electron production occurs well below the peak level of the F-region. This view seems to demand higher densities at lower levels than are given by the other four models (see Fig. 2).

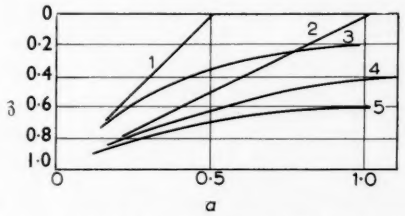

Fig. 3. Five models of $(a, \mathfrak{z})$ variations: (1) second-power, (2) linear, (3) cosine, (4) parabolic, and (5) quasi-parabolic. The parameter $\mathfrak{z}$ measures the vertical distance from the *F2* peak level to the inflection level in decimals of a unit distance. Unit distance is from the *F2* peak to the lower boundary of the F-region. The scale of the abscissa is also in decimals of this unit distance.

For convenience, let $y_m = 1$ and $\mathfrak{z} = 1 - z_c$, so that $\mathfrak{z}$ indicates how far the inflection level is from the *F2*-peak level, taking unity for the distance from this peak to the bottom of the F-region.

Solving (6) with each distribution:

parabolic model	$a = \frac{1}{2}\left(\frac{1}{\mathfrak{z}} - \mathfrak{z}\right)$
linear model	$a = 1 - \mathfrak{z}$
second-power model	$a = \frac{1}{2}(1 - \mathfrak{z})$
cosine model	$a = \frac{1}{\pi}(\operatorname{cosec} \pi\mathfrak{z} + \cot \pi\mathfrak{z})$
quasi-parabolic model	$a = \frac{1}{4}\left(\frac{1}{\mathfrak{z}^3} - \mathfrak{z}\right)$

These five models are plotted in Fig. 3.

Thus, the height-gradient of loss in the F-region can be calculated from the height of the inflection on the true-height/density curve, if the correct model can be singled out.

As an example, consider a parabolic F-region, say at 0800 hours, with $m = 1$. Let the bottom of the region be at 250 km and the upper peak at 350 km. Therefore, $y_m = 100$ km. From RATCLIFFE *et al.* (1956), $\alpha_{250} = 3 \times 10^{-4}$ sec^{-1}. Adopt the value of 0·2 for dH/dz for the entire region. Therefore, $a \simeq 0{\cdot}8$. The corresponding height of inflection is then found to be 298 km. The retarding influences for each frequency may now be applied, and the resulting trace will be somewhat

VOL
13
1958/

as represented in Fig. 4. A quasi-parabolic model would lower the whole trace. A cosine or a linear model would elevate it. A second-power model would show no inflection.

In actual analysis, the procedure is reversed to yield an empirical value of a.

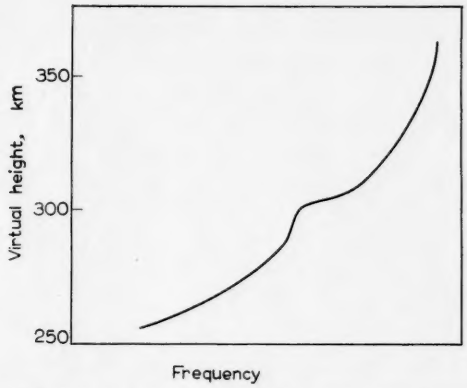

Fig. 4. Hypothetical F-trace deduced from the following assumptions: $m = 1$, $h_0F = 250$ km, $h_mF2 = 350$ km, $\alpha_{250} = 3 \times 10^{-4}$ sec^{-1}, $a \simeq 80$ km, and parabolic model.

Discussion

It would be highly desirable to search for the hidden assumptions and logical consequences of each of these models and to connect them with the theories of photochemistry of the atmospheric constituents as given by Bates (1954), and, by a judicious process of rejection, selection and composition, to work out a more accurate model. Unfortunately, this is far beyond the scope of this study. However it may be said that the choice of models depends largely on the magnitude and height-gradient of three terms: ion-production, diffusion and drift (Martyn, 1955).

Taking only the first of these, and following the view of Bradbury (1938) and Mohler (1940) that the level of maximum ion-production is far below the $F2$-peak, then it seems that the lossless distribution curve will depart from the parabolic towards higher densities at lower levels, i.e. towards the quasi-parabolic. Conversely, if this level of maximum production comes up closer to the $F2$-peak, the departure from the parabolic model will be towards the cosine, linear or second-power models, in that order. It seems, then, that the choice of models depends upon the magnitude of the height-lag between production-peak and $F2$-peak. Appleton (1955) has already worked out the parametric relations of height-lag in the E-region. Undoubtedly, their application to the F-region will afford a deeper insight into the dynamics of this region.

It is interesting to speculate on the possibility of finding two values for z_c by applying equation (6) to an appropriate model. For example, this may occur if, for a given numerical value of a, $_3$ has two roots within the range $0 < {}_3 < 1$, as when the true model happens to be a composite of two or more models at different heights; or if m varies with height. When there are two maximal turning points on the height-variation of αN^m, the region splits into three layers. Such

triple stratification is an unusual occurrence. It has been observed in connexion with a solar eclipse in the Philippines by HENNESSEY and TORRES (1956).

Likewise, the "spur", often observed at Huancayo (RATCLIFFE, 1951) and occasionally at Baguio, may conceivably be explained by a large value of a and/or a distribution about as steep as the linear model.

The value of a in equation (6) was calculated for a few representative ionograms at Baguio for different seasons and solar-cycle epochs. The parabolic model was used. The values obtained correspond to equivalent scale-height values ranging from 25 to 95 km—in fair agreement with the views of BATES (1954b) and of RATCLIFFE (1956). However, the scatter was too large to reveal any recognizable trend with season or with solar-cycle. This may be largely due to the difficulty of obtaining accurate values of true heights. BATES (1954a) has already called attention to the serious inaccuracy of $F1$-layer heights obtained by radio methods, and cites NICOLET and MANGE's (1952) suggestion and PIGGOTT's (1953) work as urgently demanding a reliable determination. Indeed, near a critical frequency, any method of true-height analysis that depends on the ray treatment is bound to be inaccurate for a study of this kind. Further investigation is needed on this point.

Acknowledgement—The author is grateful to the Rev. J. J. HENNESSEY, S.J., Director of the Manila Observatory, for his encouragement and help.

VOL
13
1958/

REFERENCES

APPLETON E. V.	1955	*The Physics of the Ionosphere* p. 20. Physical Society, London.
BATES D. R.	1954a	*Rocket Exploration of the Upper Ionosphere* (Edited by BOYD R. L. F. and SEATON M. J.) p. 347. Pergamon Press, London.
BATES D. R.	1954b	*The Earth as a Planet* (Edited by KUIPER G. P.) p. 576. Chicago University Press.
BRADBURY N. E.	1938	*Terr. Magn. Atmos. Elect.* **43,** 55.
HENNESSEY J. J. and TORRES J.	1956	*Solar Eclipses and the Ionosphere* (Edited by BEYNON W. J. G. and BROWN G. J.) p. 65. Pergamon Press, London.
KELSO J. M.	1954	*J. Atmosph. Terr. Phys.* **5,** 117.
MARTYN D. F.	1955	*The Physics of the Ionosphere* p. 212. Physical Society, London.
MOHLER F. L.	1940	*J. Res. Nat. Bur. Stand.* **25,** 507.
NICOLET M.	1954	*The Earth as a Planet* (Edited by KUIPER G. P.) p. 644. Chicago University Press.
NICOLET M. and MANGE P.	1952	*Scientific Report* No. 35. Ionospheric Research Laboratory of Pennsylvania State College
PIGGOTT W. R.	1953	Unpublished. (Quotation from BATES 1954a.)
RATCLIFFE J. A.	1951	*J. Geophys. Res.* **56,** 487.
	1956	*J. Atmosph. Terr. Phys.* **8,** 260.
RATCLIFFE *et al.*	1956	*Phil. Trans.* A **248,** 621.

Journal of Atmospheric and Terrestrial Physics, 1958, Vol. 13, pp. 113 to 121. Pergamon Press Ltd., London

The characteristic size of airglow cells

F. E. Roach, E. Tandberg-Hanssen and L. R. Megill
Boulder Laboratories, National Bureau of Standards, and
The High Altitude Observatory of the University of Colorado

(*Received* 10 *April* 1958)

Abstract—Evidence is presented for the existence of discrete 5577 airglow cells in the upper atmosphere. Independent analyses are based on (a) the comparison of diurnal intensity variations in different parts of the sky and (b) the measurement of intensity gradients on airglow isophote maps. The numerical estimation of cell size is complicated by the fact that a single cell is, in general, larger than the region observable at a given location. The typical airglow cell for the 12 nights of the study has a diameter of approximately 2500 km.

1. Introduction

Progress in the interpretation of a physical phenomenon is accelerated by quantitative information on its size. In many cases even an order of magnitude estimate is helpful to indicate the general direction in which theoretical investigations will be fruitful. The purpose of this paper is to inquire into the size of night airglow concentrations, or cells, in the upper atmosphere.

It has been known for some time that the [0I] 5577 nightglow is not uniformly bright over the sky. Thus, as illustrated in Fig. 1, a sweep around an almucantar may indicate a wide variation in brightness. It is not easy to infer sizes from these intensity changes since in general they are gradual, often appearing roughly sinusoidal when plotted in Cartesian co-ordinates. There is also a systematic change of intensity with zenith angle (Fig. 2) due to the increased path length as the horizon is approached. We have frequently made maps of the entire sky visible to a single observer by correcting for the systematic increase toward the horizon and referring the intensities to their projected values outside the troposphere. Examples are shown in Fig. 3.

An inspection of many such isophote maps suggests the existence of discrete airglow cells. The general impression is that the cells are larger than the field of view included in the circular maps (930 km in diameter if the emission height is 100 km). On rare occasions smaller airglow features have been noted (Fig. 2) at which times it is possible to detect them visually if they are of the order of 1000 R* in brightness, that is near the visual threshold for extended objects.

We shall here attempt a general approach to the problem of the scale size of nightglow patterns or cells, following two independent procedures: (1) a comparison of the diurnal changes of intensity in various parts of the sky, and (2) a measure of intensity gradients over the sky.

2. Cell Size by Comparison of Diurnal Changes

One of the early discoveries in connexion with the 5577 nightglow was the fact that it goes through significant changes of intensity during the night. Frequently

* If the airglow brightness, B, is measured in units of 10^6 quanta/cm^2 second steradian, then the brightness in rayleighs (R) is $4\pi B$.

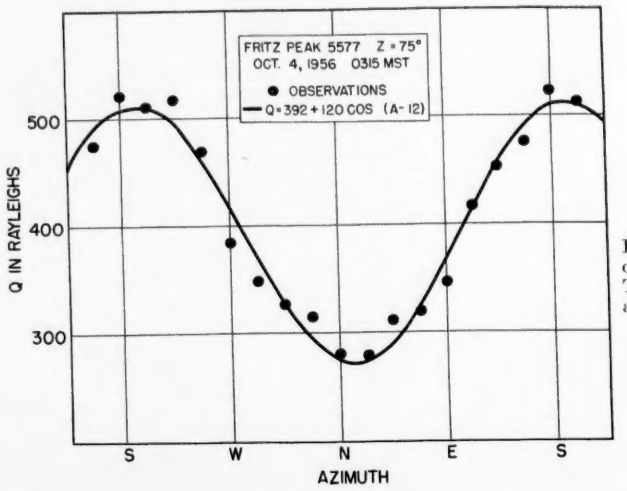

Fig. 1. Typical azimuthal change of 5577 nightglow. The smooth curve is for an assumed sinusoidal variation.

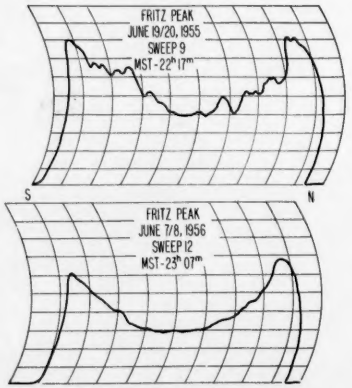

Fig. 2. Variation of 5577 nightglow brightness from the south to the north horizons. Usually there is a smooth increase of intensity from zenith to the horizon as in the lower case. Occasionally, as in the upper plot, local irregularities appear which can be detected visually.

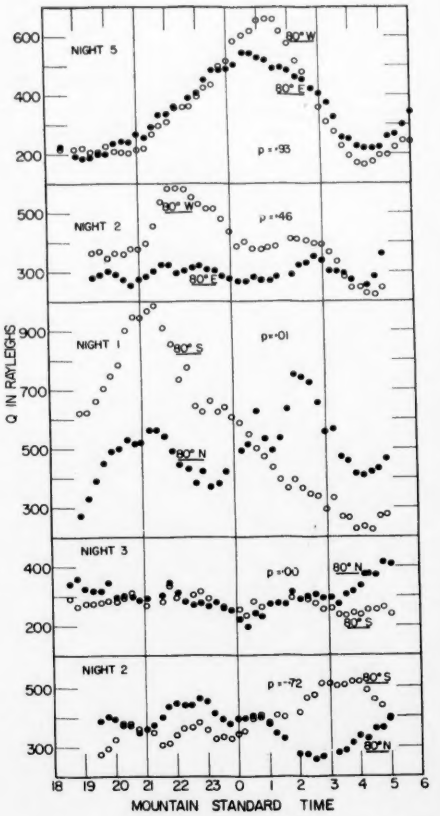

Fig. 4. Examples of diurnal variations of night-glow 5577.

VOL. 13
1958/59

VOL.
13
8/59

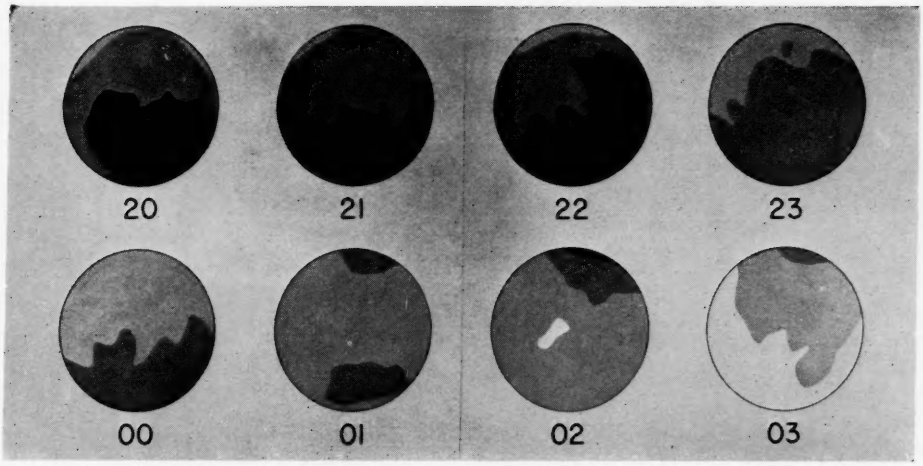

Fig. 3. Isophote maps of 5577 nightglow for each hour of the night of 1–2 October 1956.

VOL.
13
1958/5

observers have referred to a characteristic "midnight maximum" but this is by no means a universal occurrence. It is probably nearer the truth to say that there are usually (though not always) one or two definite maxima sometime during the night.

The physical basis for our analysis lies in the assumption that regions associated with the same airglow cell tend to go through similar diurnal changes. The counter assumption is that dissimilar diurnal changes of two regions imply a lack of association in a given pattern. Each type of occurrence is shown in Fig. 4. The uppermost plot in Fig. 4 shows an example in which two regions of the sky corresponding to portions of the atmosphere separated by more than 900 km (measured along the earth's surface) go through similar intensity changes with time during 1 night. We assume that these two regions are part of a single airglow cell. The other plots in Fig. 4 illustrate cases in which the diurnal variations of pairs of points in the sky go through relatively dissimilar diurnal changes.

In order to put the study into quantitative terms we shall use a correlation coefficient to express the degree of concordance of two diurnal curves. For convenience we have adopted the rank difference correlation coefficient, p, defined by:

$$p = 1 - \frac{6 \sum d^2}{n(n^2 - 1)} \tag{1}$$

where d is the difference of rank between points on the two curves at a given time and n is the total number of times of simultaneous readings.

The observational material in the present study is for 12 nights during the last quarter of the calendar year 1956. A report on deduced heights for these same nights has been given in an earlier paper (ROACH, MEGILL, REES and MAROVICH, 1958). The original records were in the form of complete sky surveys (zenith angles 0°, 40°, 60°, 70°, 75° and 80°) every 15 min. Measurements were made at sixteen equally spaced azimuths for each zenith angle (a single reading for the zenith), thus there are eighty-one readings for each survey.

We have obtained the coefficient, p, along two orthogonal paths: (1) south 80° versus all the measured regions along the meridian to north 80° and (2) east 80° versus all the measured regions along the prime vertical to west 80°. The geographical separation of the various combinations is shown in Table 1. In Tables 1 and 2 we give a summary of the numerical values of the correlation coefficients for each night and for each combination of regions.

In Fig. 5 we show for the night 30–31 October 1956, plots of p against the separation (km) along both the north–south and the east–west circles. It is noted that the correlation steadily decreases with separation. As an empirical index of cell size, L_1, we use the separation in kilometers for which the correlation coefficient is reduced to 0·31*. For this example L_1(N–S) = 900 km and L_1(E–W) = 1030 km. The same procedure was followed for the other nights of this study and the resulting measurements of L_1 are summarized in Table 3.

---

* $\pm \frac{2}{\sqrt{(n-3)}} = \pm 0{\cdot}32$ are approximately 95 per cent confidence bounds on $z = \tan h^{-1} p$ when the population correlation is zero. Hence $\pm 0{\cdot}31$ are the corresponding confidence bounds on p. See: KENDALL M. G. 1947 *The Advanced Theory of Statistics* Vol. I, p. 346. London.

Table 1. Correlation coefficients along the N–S meridian reference region 80°S

Night		Comparison region	75° S	70° S	60° S	40° S	Zenith	40° N	60° N	70° N	75° N	80° N
No.	Date (1956)	S*	128 km	208	299	383	466	549	633	724	804	932
1	1 and 2 October		0·98	0·94	0·88	0·87	0·86	0·79	0·77	0·83	0·79	0·01
2	3 and 4 October		0·73	0·49	−0·18	−0·38	−0·52	−0·49	−0·54	−0·68	−0·74	−0·72
3	6 and 7 October		0·34	0·32	0·12	0·00	0·13	0·10	−0·04	0·17	0·07	−0·03
4	30 and 31 October		0·89	0·83	0·76	0·67	0·63	0·52	0·56	0·53	0·51	0·26
5	29 and 30 November		0·95	0·88	0·85	0·80	0·72	0·72	0·71	0·64	0·63	0·55
6	30 November and 1 December		0·95	0·91	0·88	0·79	0·69	0·62	0·58	0·64	0·66	0·58
7	1 and 2 December		0·94	0·97	0·93	0·95	0·93	0·93	0·95	0·87	0·86	0·75
8	3 and 4 December		0·95	0·91	0·90	0·82	0·81	0·81	0·78	0·66	0·66	0·66
9	8 and 9 December		0·84	0·86	0·80	0·75	0·72	0·80	0·77	0·76	0·82	0·73
10	28 and 29 December		0·90	0·80	0·76	0·60	0·44	0·42	0·33	0·21	0·15	−0·03
11	29 and 30 December		0·90	0·82	0·77	0·69	0·65	0·44	0·33	0·29	0·38	0·41
12	31 December and 1 January		0·75	0·70	0·56	0·34	0·26	−0·15	−0·03	−0·24	−0·46	−0·49

* S = separation (km) of the comparison region and the reference region for an assumed emission height of 100 km.

VOL
13
1958/

PROC. ROY. SOC. A. VOL. 253, 1959, 113–128/59

Table 2. Correlation coefficients along the E–W vertical circle reference region 80° E

Night	Comparison region	75° E	70° E	60° E	40° E	Zenith	40° W	60° W	70° W	75° W	80° W
	S	128 km	208	299	383	466	549	633	724	804	932
1		0·79	0·75	0·70	0·68	0·70	0·72	0·70	0·68	0·74	0·81
2		0·66	0·34	0·10	0·01	−0·12	−0·06	0·04	0·13	0·30	0·46
3		0·78	0·74	0·61	0·34	0·32	0·35	0·25	0·30	0·30	0·45
4		0·95	0·85	0·78	0·70	0·79	0·59	0·58	0·57	0·59	0·43
5		0·97	0·94	0·94	0·93	0·93	0·95	0·93	0·94	0·93	0·93
6		0·79	0·69	0·70	0·67	0·63	0·60	0·51	0·66	0·57	0·64
7		0·95	0·90	0·88	0·79	0·76	0·76	0·68	0·59	0·65	0·46
8		0·91	0·88	0·88	0·82	0·74	0·76	0·71	0·71	0·71	0·66
9		0·82	0·81	0·53	0·52	0·59	0·59	0·62	0·53	0·62	0·62
10		0·88	0·72	0·75	0·67	0·64	0·65	0·66	0·71	0·57	0·60
11		0·83	0·75	0·71	0·53	0·55	0·53	0·48	0·42	0·21	0·32
12		0·62	0·62	0·44	0·28	0·21	0·08	0·10	0·05	0·11	0·30

Table 3. Mean nightly cell sizes (km)

Night	$\bar{Q}$ (R)	L_1		L_2	L_3
		N–S	E–W		
1	511	2100	—	1020	1350
2	395	250	230	1080	1400
3	297	200	260	1580	2710
4	423	900	1030	1210	1970
5	335	1400	—	1280	1700
6	342	1700	1700	1220	2000
7	289	—	1200	1750	2130
8	264	2000	2000	1120	2030
9	140	—	—	1220	1700
10	129	660	1500	940	1150
11	113	650	850	1080	1620
12	104	400	400	810	1040
Mean		1030	1020	1190	1730

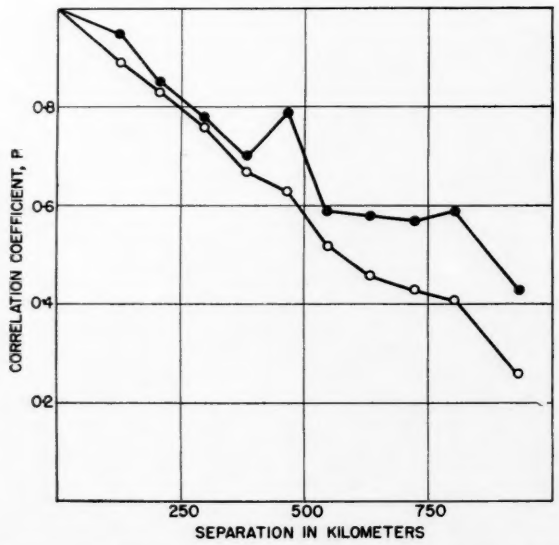

Fig. 5. Variation of the correlation coefficient, p, with separation of the regions for the night of 30–31 October 1956.

3. Cell Size by Study of Gradients

In the gradient approach to the problem of airglow cell size we shall illustrate the method first by a simple procedure that we used in our early studies. In the preparation of the isophote maps such as those shown in Fig. 3, working maps are made from circular plots of the individual readings. We refer the original

VOL
13
1958/

readings to their values outside the troposphere by (1) allowing for the scattering and extinction of the lower atmosphere, and (2) taking out the systematic increase of intensity toward the horizon. Finally the results are put into absolute intensities (rayleighs). The resulting numbers have been called the "local zenith intensity" (LZI) because, to a first approximation, they correspond to the overhead intensities in the geographical region within the circle included by the observer's photometer.

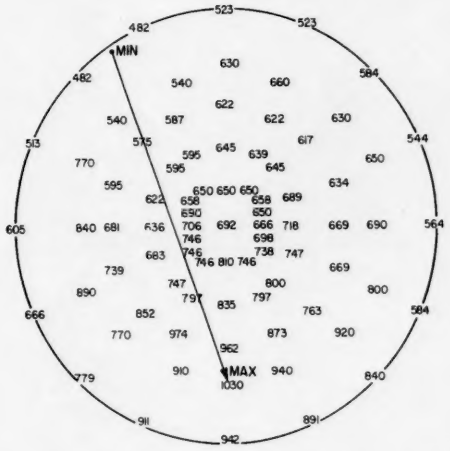

Fig. 6. Typical working chart from which isophote maps are made. The numbers represent the absolute intensities (LZI) in their proper geographical positions.

An example of a working print of such a circle plot is shown in Fig. 6. We locate the minimum and maximum readings on each plot and draw a straight line between them. We then scale the geographical separation, s, of the two points, and record the difference of absolute intensity ($\Delta Q = Q_{\max} - Q_{\min}$). As an index of the dimensions of the airglow we now introduce the quantity L_2 defined by:

$$L_2 = \frac{S}{\Delta Q/\bar{Q}} = S\,\frac{\bar{Q}}{\Delta Q} \tag{2}$$

L_2 represents the distance (km) over which the intensity changes from $\bar{Q} - \frac{1}{2}\bar{Q}$ to $\bar{Q} + \frac{1}{2}\bar{Q}$, where $\bar{Q}$ is the mean intensity $(Q_{\max} + Q_{\min})/2$. Although this is a formal numerical approach to a physical problem we shall tentatively use L_2 as an index of airglow cell size. The mean values of L_2 for each of the nights are shown in the fifth column of Table 3.

A criticism of L_2 is that it depends entirely on only two observational points for each survey. A more general procedure which gives equal weight to all sixteen readings of a given almucantar sweep is an adaptation of a technique introduced by MANRING and PETTIT (1955). Their procedure depends on the empirical fact that the variation of intensity with azimuth (for a given almucantar) is often

VOL. 13 58/59

approximately sinusoidal (see Fig. 1). The best fit for the data may be obtained in terms of a sinusoidal curve

$$Q = \bar{Q} + B \cos (A - A_m) \tag{3}$$

where $\bar{Q}$ is the mean intensity of the sixteen readings, B is the amplitude, A is the azimuth, and A_m is a phase angle (the azimuth of the maximum intensity). Equation (3) has been solved for $\bar{Q}$, B and A_m for each almucantar sweep of the

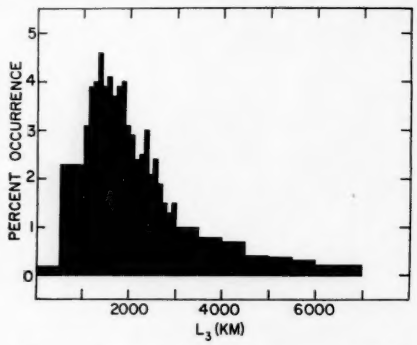

Fig. 7. Histogram of the occurrence of L_3.

12 nights under study. We shall reserve discussion of A_m for a later report and here use only the results for B and $\bar{Q}$.

We now define the quantity, L_3, by

$$L_3 = \frac{2r}{2B/\bar{Q}} = \frac{r}{B/\bar{Q}} = r\,\frac{\bar{Q}}{B} \tag{4}$$

where r is the radius (km) of the circle corresponding to the particular almucantar sweep. We note that L_3 does not depend on the accuracy of the absolute calibration of the photometer, nor on the fact that we use the LZI values of intensity rather than the directly observed slant intensities which some observers prefer. This independence is due to the fact that $B/\bar{Q}$ is dimensionless*. In Fig. 7 we show a histogram of the occurrence of L_3 for all the data of the present study (about 2600 individual determinations over the 12 nights). The maximum occurrence is for $L_3 = 1350$ km.

4. Discussion of the Results

In the last column of Table 3 we present the nightly mean values of L_3. For each night we have averaged (a) the most probable value from a histogram similar to Fig. 7 and (b) the mean from:

$$L_3 = r\,\frac{\bar{Q}}{\bar{B}}$$

* Any correction to the original readings that amounts to a multiplication does not affect the numerical value of L_3. However there is one correction, namely that for scattered light, which is subtracted from the original readings and will thus affect the evaluation of L_3. This argument does not apply to L_2 since in general the minimum and maximum points are at different zenith distances to which different multiplying constants have been applied.

VOL
13
1958/

where $\bar{Q}$ and $\bar{B}$ are means for the night. A summary of the results by all the procedures presented in this paper is given in Table 4. We interpret the present results as an indication that the existence of finite cells in the 5577 airglow is supported by the data and that, in agreement with the impression gained from an inspection of isophote maps such as those in Fig. 3, the cells are in general larger than the field of view of a given observer.

Actually L_2 and L_3 are indices of only one-half of a given cell. The complete cell will include, in addition to the gradient measured by ΔQ or B, a companion

Table 4

Quantity	Mean value
L_1	1025
L_2	1190
L_3 (from Fig. 7)	1350
L_3 (from Table 3)	1730
Mean	1325

VOL. 13 58/59

gradient in the opposite sense on the other side of the maximum region. It is not clear whether L_1 similarly is an index of only one-half of the total cell since we do not have any physical basis for the correlation or lack of correlation of the diurnal variations of the night airglow.

In conclusion we propose a doubling of the mean value of L given in Table 4 rounded to the nearest 500 km as an indication of the approximate size of airglow 5577 cells in the upper atmosphere:

2500 km

Acknowledgements—We are especially indebted to our colleagues, Mr. E. MAROVICH and Miss PAULINE JAMNICK for their assistance in the preparation of this paper. Most of the routine calculations were done with the electronic computer of the Boulder Laboratories, National Bureau of Standards.

REFERENCES

MANRING E. R. and PETTIT H. B. 1955 *The Airglow and the Aurorae* (Edited by DALGARNO A. and ARMSTRONG E.) p. 29. Published as supplement No. 5 to *J. Atmosph. Terr. Phys.* Pergamon Press, London.

ROACH F. E., MEGILL L. R., REES M. H. and MAROVICH E. 1958 *J. Atmosph. Terr. Phys.* **12,** 171.

Journal of Atmospheric and Terrestrial Physics, 1958, Vol. 13, pp. 122 to 130. Pergamon Press Ltd., London

Movements of airglow cells

F. E. Roach, E. Tandberg-Hanssen and L. R. Megill
Boulder Laboratories, National Bureau of Standards and
The High Altitude Observatory, University of Colorado

(*Received* 10 *April* 1958)

Abstract—The possibility of translatory and rotatory motions of airglow cells is examined. Evidence is presented for translatory motions in the 100 km region with speeds of the order of 100 m/sec. Rotatory motions are indicated corresponding to a mean period of 5 hr. A broad similarity seems to exist between airglow cell motions in the 100 km region and vortex cells near sea level. The problem of the mechanism responsible for the excitation of the oxygen atom to the ^1S state is discussed with particular reference to (a) photochemical reactions and (b) environmental effects.

1. Introduction

In two preceding papers it has been shown (a) that a 5577 emission height of 100 km as measured by rocket ascents is consistent with the ground observations at Fritz Peak (Roach, Megill, Rees and Marovich, 1958) and (b) that the characteristic size (diameter) of discrete airglow cells is approximately 2500 km (Roach, Tandberg-Hanssen and Megill, 1958). These papers will be referred to as Papers I and II respectively.

In the present study, Paper III of the series, we wish to depart from a static concept and present evidence leading to a dynamic interpretation of the nightglow cells discussed in Paper II.

A variable brightness of an upper atmosphere phenomenon is subject to at least three different interpretations (not mutually exclusive):

(1) There may be an *in situ* change of brightness with time as, for example, in the case of the zenith intensity of the sky during twilight as the sun successively illuminates higher and higher regions of the upper atmosphere.

(2) There may be a space movement of an excitation wave (analogous to the motion of a wave in the ocean) the individual particles not participating in the general macroscopic motion.

(3) There may be a wind motion with the individual particles more or less carried along by the large scale movements.

In this paper we shall present evidence which suggests that the 5577 airglow participates in a wind motion of the third type.

2. The Periodicity of the Diurnal Variation

In Fig. 4 of Paper II we showed some examples of the diurnal variation of intensity of the 5577 nightglow. There is no single way to describe the many types of variation which have been observed. On some nights a smoothly changing intensity results in a plot against time of a sinusoidal nature. On other nights the variation is less regular. It is an empirical fact that sometimes regions of the sky corresponding to large geographical separations have similar diurnal changes

VOL.
13
1958/5

and sometimes dissimilar ones. Thus it is possible to generalize that there is no specific periodicity of diurnal change that can be definitely assigned to all the observations at a given station.

We have examined our records systematically for individual diurnal changes that can be interpreted as periodic. By inspection of the time-intensity plots of a number of regions of the sky during the 12 nights we have estimated the time, t, corresponding to one complete cycle. The results are shown in Table 1. Values

Table 1. Period of time variation, t (hr)

Regions \ Night	1	2	3	4	5	6	7	8	9	10	11	12	
Zenith	16	(9)	>10	11	9	(10)	10	10	(6)	(3) (12)	(5)	(7)	
60° E	13	8	>10	(11)	9	(10)	7	9	10	—	(12)	—	
60° S	14	—	>10	(11)	9	12	7	9	10	—	(12)	7	
80° N	5	12	>10	8	(9)	12	8	9	11	(11)	(12)	7	
80° E	9	—	>10	(11)	(10)	(8)	10	11	12	—	(13)	—	
80° S	14	(13)	>10	10	10	(10)	8	9	9	9	12	—	
80° W	12	(12)	>10	10	9	11	9	9	(11)	(12)	9	—	
Mean	12	10	>10	9	9	11	9	9	10	9	11	7	9·7

in parentheses are less certain than the others. For the definitely determined values the range is from 5 to 16 hr. The mean of all the entries is close to 10 hr, a value which we propose to use in the following discussion.

It should be mentioned that the lack of repetition of the diurnal variation from night to night indicates that any periodicity of 24 hr or simple fraction thereof is not occurring in any regular fashion. The observed periodicity of 10 hr is approximately equal to the length of the observing night. We do not believe that this fact has prejudiced the results.

3. The Ratio: $2L/t$

We now propose as a working hypothesis that the general physical cause of the diurnal variation of intensity of the 5577 nightglow is the movement of the cells past the observer. As a first test of the hypothesis we wish to compare the speed from the ratio, $2L/t$, with directly measured movements of airglow features. In Paper II we found $2L \simeq 2500$ km which, combined with the value of t in section (2), gives

$$2L/t = \frac{2{\cdot}5 \times 10^6}{3{\cdot}6 \times 10^4} = 70 \text{ m/sec}$$

4. Measurement of Apparent Movement of Airglow Features

Since the airglow cell in most cases seems to be more than twice as large as the field of the observer it is in general not possible to follow entire cells from observations at a single station. Attempts to follow discrete *closed* features have been made in the past. For example, Roach, Pettit and Williams (1953)

Table 2.

Night	Time (MST)	Isophote	Speed of motion, W (m/sec)	Direction of motion
1	1930–2215	800R	62	N → S
1	2300–0015	600	78	NE → SW
2	0245–0415	500	51	S → N → S
2	0330–0445	250	57	NE → SW
3	1830–1945	400	94	SW → NE
4	0130–0215	600	87	NE → SW
4	0145–0300	500	80	NE → SW
4	1830–2045	400	44	NW → SE
4	0115–0400	400	84	N → S
5	2000–2200	250	147	N → S
5	2100–2245	300	137	N → S
5	2130–2315	350	161	N → S
6	1815–1945	250	70	N → S
6	2000–2100	300	240	E → W
6	0230–0415	300	33	N → S → N
6	0100–0245	400	71	NE → SW
7	2200–2345	350	102	NW → SE
7	2230–0045	400	46	NW → SE
8	2045–2200	250	110	W → E
8	0200–0245	300	97	SE → NW
Mean			92	

found a mean velocity of 250 km/hr* or 70 m/sec for a moving airglow region at Cactus Peak, California. In the present study we have measured the movement of individual isophote *lines* across the circular isophote plots (Fig. 1). This procedure permits the accumulation of a larger quantity of data than if we had used closed features since the occurrence of closed features on the maps is rare.

In Table 2 we show the results of our measurement of twenty individual cases for which movements of individual isophote lines could be followed for a sufficient length of time to yield values of the speed, W. The mean value, 92 m/sec, is close enough to the value of $2L/t$ found in the preceding section to support our working hypothesis that the diurnal variation of intensity occurs as an airglow cell passes an observer.

In the last column of Table 2 we have indicated the direction of motion of the isophote lines. It is seen that in general there is a trend for a southward direction (approximately 75 per cent of the cases). In two instances (on night 2 and night 6) the motion reversed direction during the observation period; from

* In the paper quoted the mean value was given as 500 km/hr but this was based on an assumed emission height of 200 km. For an emission height of 100 km the published value should be proportionally reduced to 250 km/hr.

VOL. 13 1958/5

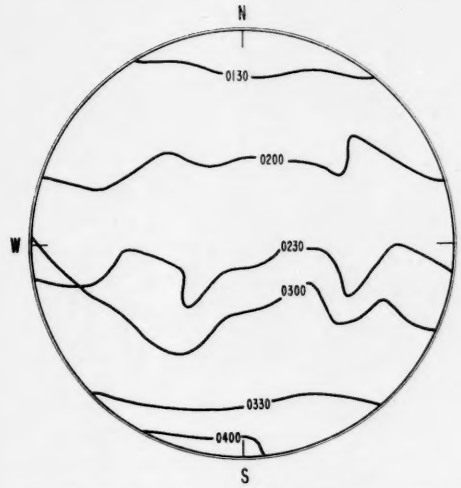

Fig. 1. Movement of 300R isophote (5577) at Fritz Peak on 31 October 1956. Between 0130 and 0400 the motion was from north to south.

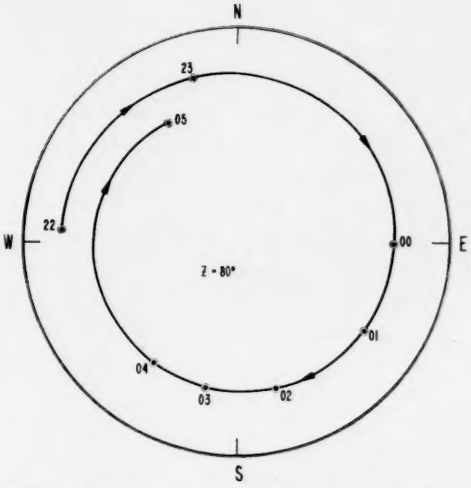

Fig. 2. Clockwise circulatory motion of the locus of A_m during a part of the night of 30–31 October 1956.

OL.
13
8/59

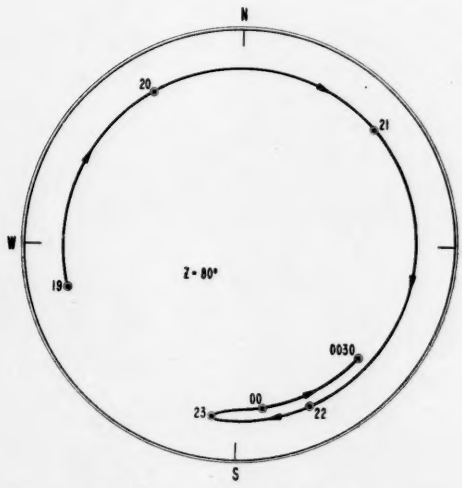

Fig. 3. Circulatory motion of the locus of A_m during the night of 4–5 December 1956. From 1900 to 2300 the motion was clock-wise. From 2300 to 0030 it was counter-clockwise.

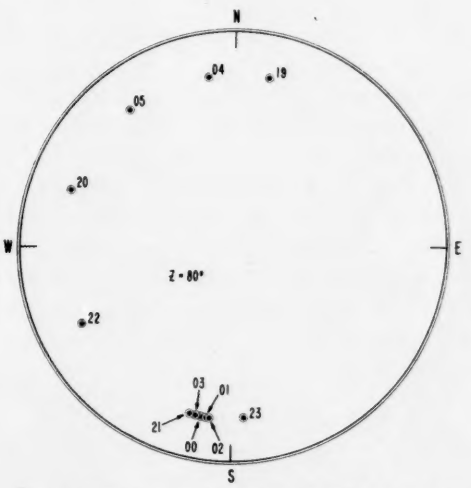

Fig. 4. The locus of A_m during the night of 28–29 December 1956. The distribution of the points seems to be random with no well defined circulatory motion.

northward to southward (on night 2) and from southward to northward (on night 6). Whether this north to south movement is a general tendency or a seasonal one can be known only when a larger sample is analysed over at least one full year.

5. Evidence for Cellular Rotation

In Paper II we used a Fourier analysis of Q versus azimuth to deduce numerical values of L_3 from the amplitude, B, of the variation. The azimuth, A_m, of maximum intensity is included in the analysis. For each night of the present study we have plotted A_m on a polar diagram for each $\frac{1}{4}$ hr of the night. During 9 of the 12 nights regular rotations were noted for several hours. Only rarely (Fig. 2) was there evidence for a complete rotation of the locus through 360° or more. More frequently, (Fig. 3) partial rotations were noted for a time with sudden reversals in direction which persisted over another interval. On three nights (example in Fig. 4) there seemed to be no systematic movement that we could interpret as a rotation.

Table 3. Period of rotatory motion (hr)

Night	Period (hrs)
1	5
2	12
3	4, 4
4	$3\frac{1}{2}$, $5\frac{1}{2}$
5	6
6	6, 3, $4\frac{1}{2}$
7	4
8	5, 4, 9
11	6, $3\frac{1}{2}$, 6
Mean	5·4

For each identifiable rotational segment we have found the mean angular velocity, ω (rad/sec). In Table 3 we record the values of P, the period for a complete rotation, from:

$$P = \frac{2\pi}{\omega}$$

The mean period of rotation is 5·4 hr from seventeen separate measurements.

6. Airglow Cells as Upper Atmosphere Cyclones

The composite picture of airglow cells presented to this point bears a general similarity to the vortex cells of the troposphere. In Table 4 we compare a tropical hurricane, an extra-tropical cyclone and an "average" airglow cell as deduced in the present study.

We note that, in spite of the ratio of 1 : 1,000,000 in the densities at 100 km and at sea-level, the total energy of an airglow cell is about 1/400 of a tropical

VOL
13
1958/

Table 4. Cell characteristics (approx.)

	Tropical hurricane	Cyclone	(Airglow) upper atmosphere
L (km)	240	1100	1200
W (m/sec)	7	11	100
P (hr)	8	170	5
ρ (g/cm^3)	10^{-3}	10^{-3}	10^{-9}
m (g)	6×10^{17}	10^{19}	2×10^{13}
E (rot) (ergs)	8×10^{24}	8×10^{24}	2×10^{22}
E (trans) (ergs)	2×10^{23}	8×10^{24}	1×10^{21}

hurricane with a similar distribution between rotational and translational energy.* The relatively high energy of the airglow cell is due to the high linear and rotational velocities indicated by our measurements.

7. The Total 5577 Light Flux in an Airglow Cell

The airglow unit, the rayleigh, represents the total (in all directions) energy per sec from a 1 cm^2 column (10^6 quanta/cm^2 sec or $3{\cdot}55 \times 10^{-6}$ erg/cm^2 sec). The total ergal flux in 5577 from an airglow cell can be easily calculated from:

$$E = 3{\cdot}55 \times 10^{-6} Q \pi L^2 \text{ ergs/sec}$$

where L is the radius (cm) of the cell. In Table 5 we list the values of E for each

Table 5. Total 5577 flux from airglow cells

Night	L (km)	$\bar{Q}$ (R)	E (ergs/sec)	Night	L (km)	$\bar{Q}$ (R)	E (ergs/sec)
1	1135	511	$7{\cdot}3 \times 10^{13}$	7	1940	289	$12{\cdot}2 \times 10^{13}$
2	1240	395	6·8	8	1575	264	7·3
3	2145	297	15·3	9	1460	140	3·3
4	1590	423	11·9	10	1045	129	1·6
5	1490	335	8·3	11	1350	113	2·3
6	1610	342	$9{\cdot}9 \times 10^{13}$	12	925	104	$1{\cdot}0 \times 10^{13}$

of the 12 nights of this study. The range is from 1×10^{13} to 15×10^{13} ergs/sec. This corresponds to a power of 1000 to 15,000 kW. During a 10 hr night an airglow cell delivers in 5577 radiation alone 10,000 to 150,000 kWh of energy.

8. Comparison of Movements of Airglow and of Auroral Features

In a recent paper Kim and Currie (1958) have reported on movements of auroral features at a height of 100 km. Rapid transient changes are lost on their all-sky photographs because of the relatively long exposures (20 sec). The pictures

* It is of interest to note that the kinetic energy in the 100 km region is comparable to the kinetic energy of the oceans. According to Deacon (1957) the total kinetic energy in the ocean is "not more than 2% of the kinetic energy of the atmosphere".

show the limiting edges of the auroral display and the authors suggest that an observer looking directly at an auroral display would seldom recognize the motions measured on the film because the "persistent features that serve as indicators of the motions are confused with the more transient features of the display".

Along the geomagnetic meridian (north–south) they were able to measure the movement of arcs and bands at times of relatively low magnetic activity. As the magnetic activity increased, rapidly moving rayed structures predominated and

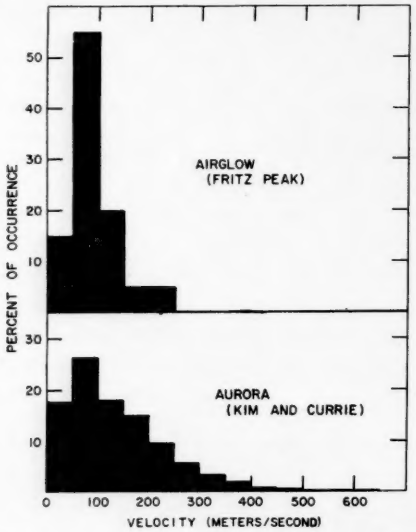

Fig. 5. Distribution of velocities for movement of airglow cells (this paper) and auroral bands and arcs (Kim and Currie, 1958).

measurements were possible only at right angles to the geomagnetic meridian (east–west). In Fig. 5 we show histograms of the distribution of measured speeds of airglow features from this paper and of auroral features (arcs and bands) moving in the north–south sense from Kim and Currie. The comparison is thus between the movements of airglow features at Fritz Peak ($\Phi = 49°$ N) and movements of auroral arcs and bands at relatively low magnetic activity at three Canadian stations.* Both phenomena show a maximum occurrence for a speed of 50 to 100 m/sec. In general the two distributions are similar although there is a significant percentage of auroral velocities greater than 250 m/sec for which we have no airglow cases.

9. Discussion and Conclusions

Many lines of evidence indicate that there are movements in the upper atmosphere. For example ionospheric drift movements have been extensively studied (Briggs and Spencer, 1954). Of particular interest are the measurements of movements of meteor trains (Liller and Whipple, 1954) since their interpretation as real winds is quite unambiguous. The wind speeds obtained by Liller and

* Saskatoon ($\Phi = 60°{\cdot}5$ N), Flin Flon ($\Phi = 63°{\cdot}8$ N) and Uranium City ($\Phi = 67°{\cdot}7$ N)

VOL
13
1958/

WHIPPLE in the 100 km region are similar to the speeds deduced from the movements of airglow isophote features in this paper. This strengthens the interpretation of the apparent airglow movements as true winds and we shall not consider further the alternative possibility that they are due to the movement of excitation waves. A basic problem of the 5577 airglow is: what is the nature of its association with the winds? The answer in terms of the empirical observations is clear: the *luminosity* of the airglow is associated with the winds, which is obvious from the fact that it is by measurement of isophote features that we deduce the speeds.

To probe into a possible relationship between 5577 airglow luminosity and wind movements is to inquire into the fundamental mechanism of the excitation of the oxygen atom to its ^1S state, the excitation potential of which is 4·2 eV. The thermal kinetic energy from the motions of the individual particles is too small to be considered seriously since the mean thermal motions correspond to a very small fraction of an electron volt.* The wind speeds are also much too small in terms of kinetic energy per oxygen atom to contribute directly to the excitation to the ^1S state. We are thus led to a search for a mechanism which utilizes the thermal or wind energies but does not depend on them directly for the excitation of the oxygen atom. Two general approaches to the problem have been suggested, namely: (*a*) photochemical reactions in which the atomic collisions serve as a means of bringing atoms together, the excitation resulting not from the kinetic energy of the collision but from the exothermic nature of the reaction; (*b*) processes which permit the concentration into individual particles of large quantities of energy by a coupling of the bulk energy of the gas with the environment.

The generally accepted photochemical reaction is the one suggested by CHAPMAN (1930) which utilizes the energy of dissociation of the oxygen molecule (5·1 eV) in the reaction

$$O + O + O \rightarrow O_2 + O\ (^1S)$$

This reaction provides a reservoir of energy, the ultimate source of which is the sun which dissociates the molecular oxygen during daylight hours. An energy cycle which depends on the sun in this way would be expected to show a systematic diurnal pattern in local time. If the 5577 nightglow is significantly due to this reaction then, under static conditions, there should be a steady decline in its intensity during the night which is definitely contrary to observation.

A photochemical reaction can vary throughout cells of a meteorological nature if there are significant changes of physical pressure and temperature throughout the cell. Thus, if there are cyclones with central lows and anticyclones with central highs in the 100 km region, this might lead to somewhat localized low and high excitation regions similar to those observed in the airglow. Whether or not the density variations can account for the observed airglow patterns is a matter of detailed calculation and is not settled.

One environmental approach to the problem involves the effect of a magnetic field on a moving, slightly ionized, gas. In the 100 km region there are about 10^{13}

* In principle one might consider the possibility of direct excitation by collision between atoms having very high velocities corresponding to the "tail" of the Boltzmann distribution curve. In practice this would apply to an extremely small fraction of the atoms.

molecules/cm^3 and about 10^4 to 10^5 ions/cm^3. Although the ions can have no significant influence on the ponderous mass motions, they are by virtue of their participation as charged particles in these wind movements, subject to the forces exerted by a magnetic field. The net result of the two forces acting on the ions is to set up conditions conducive to large scale polarizations. In a treatment of this problem, WULF (1953) has called attention to the polarization of a geostrophic wind in the upper atmosphere and the possibility that this could lead to large scale discharges with accompanying luminosity of an airglow or auroral nature.

The problem of obtaining a discharge in apparent opposition to the polarization forces is one of considerable difficulty but the existence of vortex motions introduces interesting possibilities for setting up polarization patterns. One of the striking results of the study of meteor train motions is the indication of pronounced shears in the 100 km region. At levels separated by only a few kilometres large differential wind motions have been observed which might lead to opposite polarizations and vertical discharges in adjacent regions.

This general approach is attractive in that the association between the movements and the airglow is the direct one of cause and effect.

Acknowledgements—In the preparation of this paper we have profited by stimulating conversations with our colleague, Dr. R. N. THOMAS. We also wish to thank Mr. E. MAROVICH for extensive help with the computations.

VOL
13
1958/

REFERENCES

BRIGGS B. H. and SPENCER M.	1954	*Rep. Progr. Phys.* **27,** 254.
CHAPMAN S.	1930	*Mem. R. Met. Soc.* **3,** 103.
DEACON G. E. R.	1957	*The Planet Earth* (Edited by D. R. BATES) p. 75. Pergamon Press, London.
KIM J. S. and CURRIE B. W.	1958	*Canad. J. Phys.* **36,** 160.
LILLER W. and WHIPPLE F. L.	1954	*Rocket Exploration of the Upper Atmosphere* (Edited by BOYD R. L. F. and SEATON M. J.) p. 112. Pergamon Press, London.
ROACH F. E., MEGILL L. R., REES M. H. and MAROVICH E.	1958	*J. Atmosph. Terr. Phys.* **12,** 171.
ROACH F. E., PETTIT H. B. and WILLIAMS D. R.	1953	*Astrophys. J.* **117,** 456.
ROACH F. E., TANDBERG-HANSSEN E. and MEGILL L. R.	1958	*J. Atmosph. Terr. Phys.* Preceding paper, this issue.
WULF O. R.	1953	*J. Geophys. Res.* **58,** 531.

Journal of Atmospheric and Terrestrial Physics, 1958, Vol. 13, pp. 131 to 139. Pergamon Press, Ltd., London

The electron distribution in the ionosphere over Slough—II

Disturbed days

J. O. Thomas and Audrey Robbins
Cavendish Laboratory, Cambridge

(*Received* 17 *April* 1958)

Abstract—An account is given of how the heights of maximum electron density of the *F1* and *F2* layers and the sub-peak electron content vary over Slough (England) during magnetic storms. The parameters have been taken from detailed true-height electron density distributions calculated from observed $h'(f)$ curves in 6 months representing three seasons in a year of low, and a year of high sunspot number.

Attention is drawn to the fact that variations of $h'F2$ during a storm should not be taken to represent changes of height of the *F2* layer. The height of maximum electron density in the *F2* layer is found to increase in storms, particularly at night. The height of maximum electron density in the *F1* layer also increases. Comparison with the magnetograms recorded at Abinger during individual storms shows that ionospheric storm effects occur almost immediately after the magnetic changes.

Some important changes have been noticed in the ionosphere at the time of a world-wide sudden impulse.

1. Introduction

In a companion paper, Thomas, Haselgrove and Robbins (1958) described a method of calculating the height distribution of electrons in the ionosphere from experimental records showing the virtual height (h') as a function of frequency (f). Values of the electron density (N) were deduced at a series of heights (h) for the International Quiet Days, (I.Q.D.s) for 6 months at Slough (lat. 51·5°N, long. 0·5°W). In the present paper a preliminary account is given of some of the results obtained, during the same 6 months, on ionospherically and magnetically disturbed days.*

The records analysed were made during January, September and July 1950 (high sunspot number) and December, September and June 1953 (low sunspot number). The calculation made allowance for the effect of the earth's magnetic field and made no assumptions about the shape of the layers other than that the electron density increased monotonically with height. It had the particular advantage that it could be used to obtain reliable $N(h)$ curves from the distorted $h'(f)$ traces often recorded during ionospheric disturbances. In the previous paper it was estimated that the calculated height at which a given electron density occurs is correct to within ± 10 km in the *F2* and upper *F1* layers, but may be less accurate in the lower part of the *F1* layer.

A full understanding of the nature of an ionospheric storm is not likely to be arrived at until the detailed distribution of electrons has been studied at different places. As a first step towards this understanding, it is however convenient to consider the heights (h_mF1, h_mF2) of the peaks of the layers, the maximum electron densities (N_mF1, N_mF2) and the sub-peak electron content (n_T) defined as the total number of electrons in a column of unit area below the peak of the

* The hourly $N(h)$ data for all the days in the 6 months are available in the form of tables (Thomas, Haselgrove and Robbins, 1957) and may be obtained from the Radio Group, Cavendish Laboratory, Cambridge.

F2 layer. These quantities as observed at Slough are discussed in detail for the disturbed days of the 6 months. Their relation to other quantities which have sometimes been used to describe the behaviour of the ionosphere during storms is discussed.

2. Average Results

2·1 *Heights of the peaks of the* F1 *and* F2 *layers*

The average values of the heights of the peaks of the layers for the 5 International Magnetically Disturbed Days (I.D.D.s) in each of the 6 months are

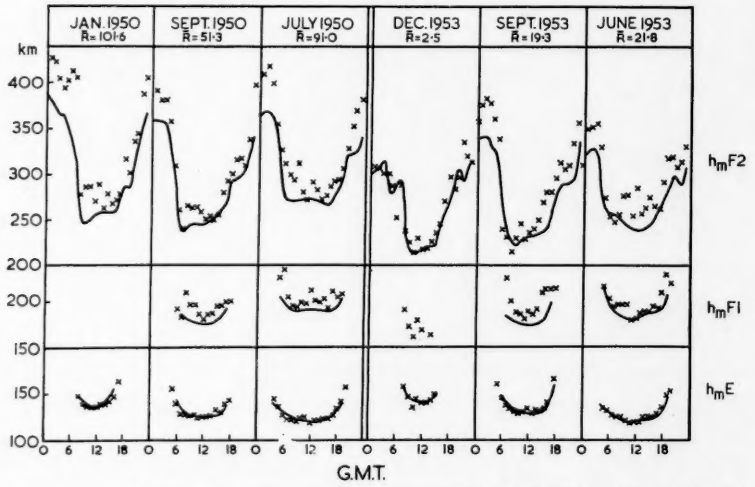

Fig. 1. The crosses show the average for 5 International Disturbed Days (I.D.D.s) of h_mF2, h_mF1 and h_mE. The lines are the corresponding quantities for the 10 International Quiet Days (I.Q.D.s) from Thomas, Haselgrove and Robbins (1958). $\overline{R}$ is the monthly average relative Zürich sunspot number.

plotted as crosses in Fig. 1. The lines in the figure show the corresponding quantities averaged for the 10 I.Q.D.s as plotted by Thomas, Haselgrove and Robbins (1958). The following points are worth noting:

(i) The value of h_mF2 for the I.D.D.s is greater than that for the I.Q.D.s.

(ii) The amount by which h_mF2 on I.D.D.s exceeds that on I.Q.D.s is greater by night than by day.

(iii) h_mF1 for the disturbed days is about 15 km greater than for the quiet days.

(iv) Although in winter the *F1* layer is not usually observable on quiet days, it is often present on disturbed days, and then h_mF1 is smaller than it is on disturbed (or quiet) days in summer and equinox.

(v) The variation of h_mE (if any) during storms is small and greater height accuracy is required to detect any effect with certainty.

In the past, because figures for the heights of the peaks of the layers have not been easily available, the behaviour of the disturbed ionosphere has sometimes been described in terms of the observed minimum virtual heights of the

VOL. 13 1958/5

layers (*h'F1*, *h'F2*). Fig. 2 shows how the average values of the minimum virtual heights of the layers vary with time of day for quiet and disturbed conditions. A comparison with Fig. 1 shows the kind of error which will be made if changes in *h'F1* and *h'F2* are taken to represent changes in the heights of the peaks of the layers. In particular it is noticeable that the difference between

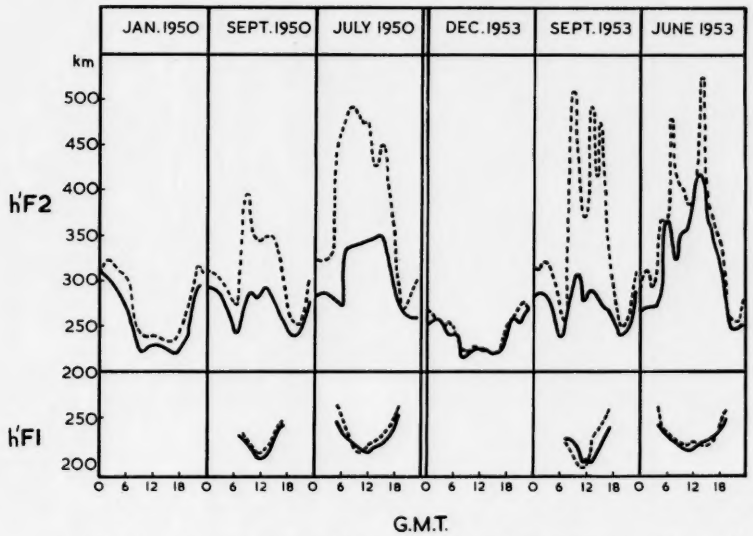

Fig. 2. Average values of *h'F2* and *h'F1* for the I.Q.D.s (continuous line) and the I.D.D.s (broken line).

h'F2 on disturbed and quiet days is greater by day than by night, whereas the opposite is true for h_mF2. The difference between the *h'F2* values may be caused by group retardation below the level of reflection, and, under certain circumstances, changes of the group height *h'F2* represent the effects of the changes in this retardation much more than the real change of the height of the *F2* layer. Much care is needed if any useful deductions are to be made about ionospheric storms from observations of *h'F2*.

2.2. *The average peak electron density* (N_m) *and the average sub-peak electron content* (n_T)

To show how the peak electron density and the sub-peak electron content alter on disturbed days, the ratio of the averages of these quantities on disturbed days to their averages on quiet days is plotted in Fig. 3. The following points are noticeable:

(i) On disturbed days both N_m and n_T tend to decrease, except possibly in winter.

(ii) Both decrease in the same ratio in months of low sunspot number, but, when the sunspot number is high, the proportional decrease in N_m is greater than that in n_T.

The average diurnal variation of N_mF1 for the five I.D.D.s and ten I.Q.D.s is

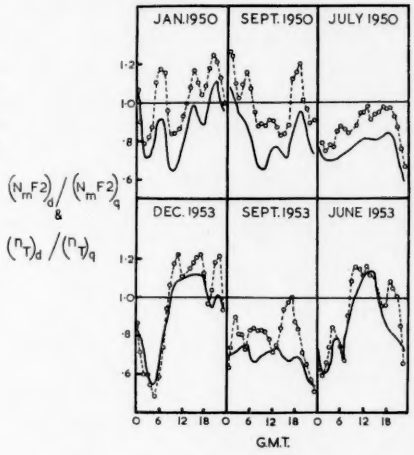

Fig. 3. The ratio of the diurnal average of N_mF2 for the I.D.D.s, $(N_mF2)_D$ to the average on the I.Q.D.s $(N_mF2)_Q$ (continuous line). The circles show the same ratio for n_T.

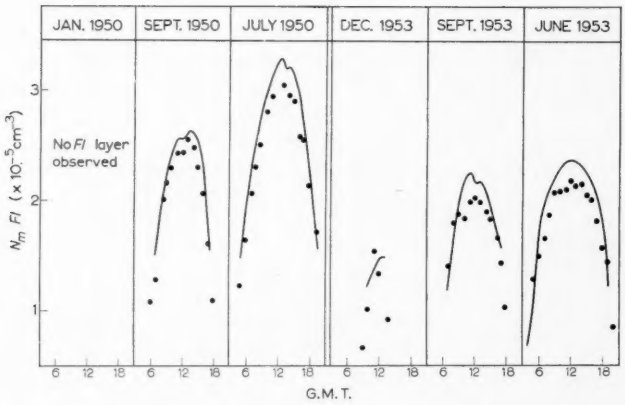

Fig. 4. The points show the average diurnal variation of N_mF1 for the 5 I.D.D.s in each month, and the continuous lines show the average variation for the 10 I.Q.D.s.

shown in Fig. 4, from which it can be seen that it is less on disturbed days than on quiet days. This phenomenon has previously been noticed by Appleton and Ingram (1935) and Berkner, Wells and Seaton (1939).

3. Studies of Individual Storms

The parameters N_mF2 and n_T show a marked dependence on storm-time, so that it is not very satisfactory to make deductions about their mean variations with solar time unless the number of days considered has been sufficient to average out the effects of storms starting at different times. It is better to consider individual storms in detail and that is what we shall do in this section.

The method is to compare the change which the storm produces in the horizontal component (H) of the magnetic field with the change which it produces in the ionospheric parameters. The undisturbed magnitude of H is taken to be that on the nearest magnetically quiet day before the disturbance, and the undisturbed magnitudes of the ionospheric parameters are taken to be those for the mean of the I.Q.D.s in the month. The difference between the "disturbed"

VOL. 13 1958/5

and "undisturbed" value of a parameter x is denoted by Δx. Magnitudes for H were read from magnetograms recorded at Abinger.

The results for five individual storms occurring during the 6 months referred to earlier are shown in Fig. 5(a). Fig. 5(b) shows the average storm-time behaviour of $\Delta N_m F2$ and $\Delta h_m F2$ for all the disturbances occurring in this period

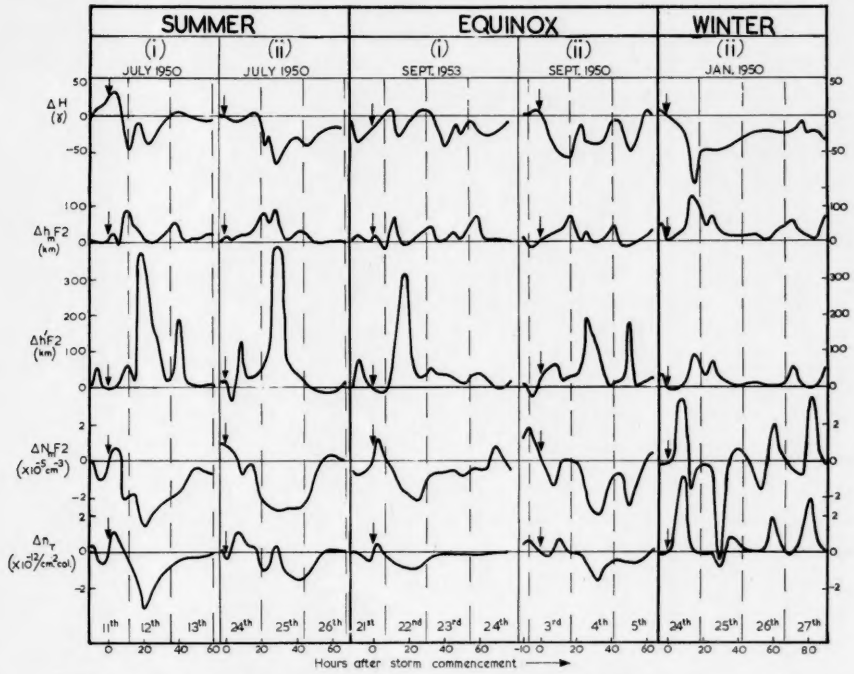

Fig. 5(a). Variation of ionospheric and magnetic parameters during five storms in summer, equinox and winter. The storms labelled (i) started during the day and those labelled (ii) started during the night. The arrows indicate the start of the disturbance and the broken lines indicate midnight.

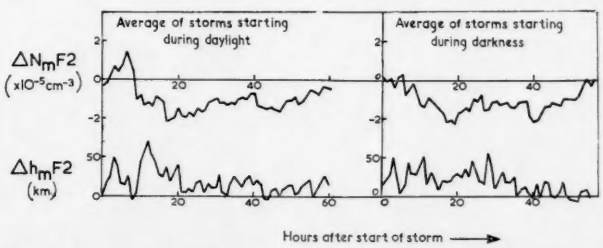
Average of storms starting during daylight
Average of storms starting during darkness
ΔN_mF2 (x10^-5 cm^-3)
Δh_mF2 (km)
Hours after start of storm

Fig. 5(b). Average storm-time variation of $\Delta N_m F2$ and $\Delta h_m F2$ for eight storms starting during the day and six storms starting at night.

together with four additional ones. While it must be emphasized that many more such storms must be studied before general conclusions are drawn, it appears that the following phenomena are always noticeable. In considering these it must be realized that the records were made only at hourly intervals.

(i) The ionospheric disturbance follows the magnetic disturbance immediately. There was no more than 1 hour's delay between the initial change of H and the initial change of N_mF2 and h_mF2.

(ii) After the initial change Δh_mF2 and ΔH reached their turning points almost simultaneously, within 1 hr of each other.

(iii) The minimum of ΔN_mF2 was, however, reached some hours later.

(iv) The strong diurnal component in Δh_mF2 is obvious; even when a disturbance started at such a time that Δh_mF2 reached a maximum during daylight hours, a subsidiary maximum was repeated again the following night.

(v) The behaviour of Δn_T is similar to that of ΔN_mF2.

(vi) The curves of $\Delta h'F2$ show that whereas it is obviously a useful parameter for detecting a disturbance, it must not be taken to indicate a corresponding movement in the peak of the layer.

The results mentioned so far in this section have been mainly for summer and equinox months. Only one appreciable disturbance occurred in the two winter months studied [see Fig. 5(a)]. An examination of some other winter disturbances seems to indicate that their storm-time behaviour is sometimes different from that for the summer and equinox months, as has already been suggested by other workers, for example Appleton and Piggott (1954).

3.1. *Ionospheric phenomena associated with a magnetic sudden impulse*

Two types of world-wide sudden changes in the magnetic field have been described. One, a sudden commencement (SC) is followed by a magnetic storm. The other, called by Ferraro *et al.* (1951) a sudden impulse (SI) is not followed by a storm.

During the months analysed three SCs and one SI occurred at Abinger. For the three SCs it was not possible to separate ionospheric effects possibly associated with the SC from those associated with the subsequent magnetic storm. The SI, however, which occurred at 1645 GMT on 1 January 1950 and was recorded at nineteen observatories reporting to the *Journal of Geophysical Research* was not followed by any noticeable magnetic disturbance; indeed, of fifteen observatories sending in data to the *Journal of Geophysical Research*, none reported a major magnetic storm about this time. It is therefore interesting to examine the ionospheric parameters associated with the magnetic changes.

The variation of H at Abinger is shown in Fig. 6 curve (a). In curve (b) ΔH is plotted for each hour. The quiet reference period was taken to be 1100 GMT on 2 January 1950 to 1000 GMT on 3 January 1950. The SI represented an increase in H of about 15γ. The ionospheric parameters are plotted in curves (c) and (d) and show that the ionosphere was severely affected only 1 hr after the SI; h_mF2, curve (c), increased rapidly and reached a height more than 125 km greater than normal about 2 hr after the SI. This height was indeed greater than any observed during the month, being 465 km instead of the quiet day average of 340 km, and was comparable with the heights observed later in the month during large storms. The large increase in $h'F2$ at this time, shown in curve (d), suggests either a real height increase of the whole layer or an increase of ionization low down.

VOL
13
1958/

The maximum electron density in the *F2* layer was decreasing before the SI, continued to fall sharply after the SI and remained depressed for about 9 hr. Large fluctuations in N_mF2 are, however, common in winter and it is not possible to state with certainty that a significant decrease in N_mF2 occurred. The sub-peak electron content showed no significant change following the SI.

At the time of an SC, APPLETON and PIGGOTT (1950) have detected a quick decrease of f_0F2 followed immediately by an increase, the whole change lasting about $\frac{1}{2}$ hr. This phenomenon seems to be different from the one discussed here.

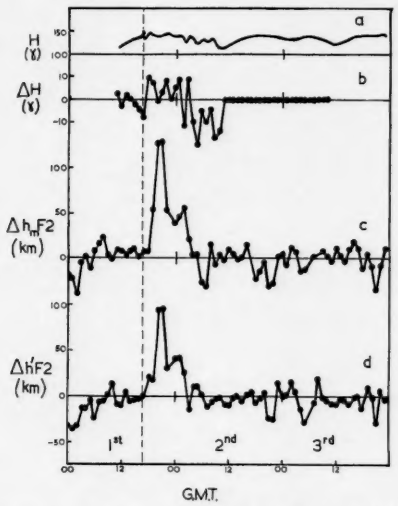

Fig. 6. The magnetic sudden impulse of 1 January 1950 and the associated ionospheric height changes. The broken line shows the time of occurrence of the SI.

HARDWICK (1953) has described two occasions on which similar marked ionospheric changes occurred during magnetically quiet periods as indicated by the geomagnetic planetary K figures; it may well be that those disturbances were associated with sudden impulses of the same type as that described in this paper.

3.2. *Summary of results*

In summarizing our results it is desirable, for reasons given previously, to concentrate attention on the phenomena during individual storms. The following phenomena then appear to characterize the ionosphere over Slough during magnetic storms.

(i) In summer and equinox the peak electron densities in the *F1* and *F2* layers are less during the main phase of a storm than at corresponding times on quiet days.

(ii) The total sub-peak electron content, the *F2* layer electron content and the peak electron density of the *F2* layer vary in a similar way during a storm.

(iii) The heights of the peaks of the *F1* and *F2* layers both increase during a storm. In moderately large storms, the increase in h_mF2 may be up to about

150 km at night and up to about 75 km in the day. In summer and equinox the daytime increase of h_mF2 is much smaller than that of $h'F2$ which is often 600 km or more.

(iv) The increase of the height of the *F2* peak is greater by night than by day. $h'F2$ also increases at night but not by as much as h_mF2.

(v) The height, and the magnitude, of the peak electron density in the *F2* layer begin to change almost as soon as a change is observable in the magnetic field. The height reaches its extreme value within 1 hr of the time when the field reaches its extreme, but the peak electron density does not reach its minimum value until several hours later.

(vi) An increase in the height of the *F2* peak may be associated either with an increase or a decrease of the magnetic field during an ordinary storm, or with the sudden increase in an SI.

4. Discussion of Results

It has been suggested by Martyn (1953) that changes in the ionosphere during a magnetic storm might be caused by vertical movements of the electrons, with velocity v, resulting from the additional current system responsible for the storm. It is interesting to enquire what deductions could be made about these movements from the facts discussed in this paper.

First we consider the peak of the *F1* layer which is supposed to be situated at a height where the electrons disappear by a recombination process in which the recombination coefficient (α) is independent of height. According to the well known theory we may write:

$$\frac{dN}{dt} = q - \alpha N^2 - \text{div}\,(Nv)$$

where q is the rate of production of electrons and div (Nv) is the electron transport term.

Since the difference in the height of the *F1* peak on a storm and on a quiet day is small compared with the scale height, it seems reasonable to suppose that q and α are approximately the same on these days and that the difference in the peak electron density N_m is caused by a change of the transport term. Then using suffixes Q and D to denote values on quiet and disturbed days respectively and assuming that the movement term on quiet days is zero at the peak of the *F1* layer

$$[\text{div}\,(Nv)]_D \simeq \alpha({N_{m_Q}}^2 - {N_{m_D}}^2)$$

Thus for example using the values of the average N_mF1 on the 10 I.Q.D.s and 5 I.D.D.s for July 1950 and putting $\alpha = 5 \times 10^{-9}\,\text{cm}^3\,\text{sec}^{-1}$, we find that the transport term due to the storm is $104\,\text{cm}^{-3}\,\text{sec}^{-1}$.

At the maximum of *F1* in summer, $\frac{dN}{dh} \simeq 0$ so that:

$$\left(\frac{dv}{dh}\right)_D = \frac{104}{N_D} \simeq +3{\cdot}5 \times 10^{-4}\,\text{sec}^{-1} \qquad \text{i.e. } +0{\cdot}35\ \text{(m/s) per km}$$

where v is the vertical drift velocity.

VOL
13
1958/

The difference between the transport term on disturbed and quiet days can also be determined by studying the average electron densities at a fixed height in the *F1* layer. This has been done at two heights in the *F1* layer and as can be seen from the table the transport term due to the storm is of the same order as the figure above from the peak electron density results.

Month	$[\text{div } (Nv)]_D - [\text{div } (Nv)]_Q$ cm^{-3} sec^{-1}	
	180 km	160 km
Sept. 1950	89	41
July 1950	90	61
Sept. 1953	79	33
June 1953	36	22

These calculations indicate that the additional transport term due to the storm was always positive at the levels considered for the storms analysed.

Similar calculations for the *F2* layer require a knowledge of both the mechanisms of electron production and loss in this region, and at the present time these are not known with certainty.

VOL. 13 58/59

Acknowledgements—This work was carried out as part of a programme of research supported by a grant from the Department of Scientific and Industrial Research. We are much indebted to Mr. H. F. Finch of the Royal Greenwich Observatory, Herstmonceux, for the loan of magnetograms from Abinger. We wish to thank again those whose assistance we acknowledged gratefully in Part I of this work, particularly Dr. K. Weekes.

References

Appleton E. V. and Ingram L. J. 1935 *Nature, Lond.* **136,** 548.

Appleton E. V. and Piggott W. R. 1950 *Nature, Lond.* **165,** 130.

Appleton E. V. and Piggott W. R. 1954 *The Physics of the Ionosphere* (Camb. Ionosph. Conf.) p. 219. Physical Society, London.

Berkner L. V., Wells H. W. and Seaton S. L. 1939 *Terr. Magn. Atmos. Elect.* **44,** 283.

Ferraro V. C. A., Parkinson W. C. and Unthank H. W. 1951 *J. Geophys. Res.* **56,** 177.

Hardwick B. 1953 *J. Atmosph. Terr. Phys.* **3,** 347.

Martyn D. F. 1953 *Proc. Roy. Soc.* A **218,** 1.

Thomas J. O., Haselgrove J. and Robbins A. R. 1957 *Tables of Ionospheric Electron Density, Slough (England)* (*Ser. B No. 1.*) Cavendish Laboratory, Cambridge.

Thomas J. O., Haselgrove J. and Robbins A. R. 1958 *J. Atmosph. Terr. Phys.* **12,** 46.

Journal of Atmospheric and Terrestrial Physics, 1958, Vol. 13, pp. 140 to 154. Pergamon Press Ltd., London

The relationship between atmospheric radio noise and lightning

F. HORNER
(Official communication from D.S.I.R. Radio Research Station, Slough)

(*Received* 20 *April* 1958)

Abstract—Examination of atmospherics in a bandwidth of 300 c/s at 10 kc/s from storms of known location in Europe has shown that in median amplitude, amplitude range and frequency of occurrence, they corresponded with what would be expected from lightning discharges to ground. Other experiments in Australia showed that atmospherics from tropical storms had overall durations similar to those of lightning discharges, and consisted of a series of pulses. From their amplitudes it seemed reasonable to suppose that the largest pulses originated in ground strokes but the number of pulses was much greater than would have been expected from ground strokes alone. The smaller recorded pulses were mainly associated with the larger ones, but it is not clear in what part of the lightning discharge they originated.

High frequency atmospherics had similar durations to those recorded at very low frequencies, but were more continuous. The start and finish of HF atmospherics tended to coincide with large V.L.F. pulses. The atmospherics were much longer than would have been expected if stepped leader discharges had been the main source.

1. INTRODUCTION

ATTEMPTS have been made at various times to relate the characteristics of atmospheric radio noise from distant thunderstorms to their electrical characteristics as deduced from measurements at close range. In the study of noise it is useful to know the nature of the radiation from a typical flash; some of the apparently random features of the noise may then appear somewhat less random and more predictable. Conversely the examination of the noise structure may lead to new information on the properties of the lightning flashes.

The object of this paper is to present some preliminary results of experiments designed to relate quantitatively the detailed features of narrow-band noise to the known characteristics of lightning flashes. Emphasis is on the V.L.F. band but some comments on H.F. noise are made.

2. THE SIGNIFICANT FEATURES OF LIGHTNING DISCHARGES AS NOISE GENERATORS

Information on the mechanism of the lightning discharge has been derived largely from direct measurements of currents in strokes to ground, from photographs of flashes, and from so-called "waveform records". This term has been used to describe records of the time-variation of the field strength obtained with wideband receivers covering a large part of the frequency range up to 100 kc/s. Limitation of the range has been necessary to avoid interference from the large number of transmitters at higher frequencies.

These studies have revealed a number of complex discharge processes which have been adequately reviewed elsewhere (THOMAS and BURGESS, 1947; WORMELL, 1953; PIERCE, 1953, 1955b). Here it is necessary only to summarize the main features of the discharges as sources of noise.

VOL.
13
1958/5

Discussions on flashes which reach the ground are based on the assumption that they have the following characteristics:

(a) A leader discharge with a current less than 1000 A, proceeds downwards and occupies a total time of up to several hundred milliseconds (THOMAS and BURGESS, 1947; WORMELL, 1953; CLARENCE and MALAN, 1957; PIERCE, 1955a). Part of this discharge, lasting 1–10 msec, often takes place in steps, of length 50 m at intervals of 70 μsec on the average (THOMAS and BURGESS, 1947, PIERCE, 1953). The precise form of the rest of the leader discharge is not so well understood.

(b) When the leader reaches the ground it is followed by a return stroke proceeding upwards along the ionized channel. The characteristics of this discharge are assumed to conform to the expressions given by BRUCE and GOLDE (1941) in which the current at the ground is given by:

$$I = 20{,}000\,[\exp(-4{\cdot}4 \times 10^4 t) - \exp(-4{\cdot}6 \times 10^5 t)] \quad \text{A} \qquad (1)$$

and the length of the discharge channel carrying this current increases upwards at a speed:

$$v = 8 \times 10^7 \exp(-3 \times 10^4 t) \quad \text{m/sec} \qquad (2)$$

(c) After the initiation of the return stroke the ionization in the channel may continue at a high density for several milliseconds and during this time there may be sudden increases in the current, giving rise to what have been called M–components of field (MALAN and COLLENS, 1937; MALAN and SCHONLAND 1947). These may be expected to appear sometimes as separate events in a tuned receiver, since they will contain frequency components which are not present in the intervals between them.

(d) Further return strokes may occur up the same channel, preceded by a dart leader, which is a low-current discharge proceeding down to ground in a single step. Flashes with two or more return strokes are called "multiple flashes," and the statistical distributions of peak currents, numbers of strokes per flash, etc., are taken from BRUCE and GOLDE (1941).

(e) Field changes occur in the intervals between the return strokes of a multiple flash (WORMELL, 1953; PIERCE, 1955a), but there are apparently no discharges of the stepped-leader type (MALAN and SCHONLAND, 1947). The field changes may possibly be the result of some form of corona-discharge (MALAN and SCHONLAND, 1947, 1953). Field-changes may continue after the final return stroke of a multiple flash (WORMELL, 1953; PIERCE, 1955a).

(f) Thunderstorm cells, which have a recognizable and self-contained structure (1949a) have a life of the order of 1 hr in temperate regions, and produce flashes to ground at an average rate of about 1/min (1949b).

Not all the above characteristics of discharges are established beyond doubt. For example NORINDER (1947) has suggested that some return strokes have much slower current variations than are given by equation (1). BARLOW, FREY and NEWMAN (1954) have proposed the addition of a third exponential term in this equation to represent a slow decay of current, and have also indicated that the numbers in equation (2) need revision. These changes have little effect on the predicted energy at 10 kc/s, which is the main subject of this paper, so the Bruce and Golde equations have been used without modification.

The mechanism of those discharges which do not reach the ground is not so well-understood. PIERCE (1955b) has stated that they are entirely of the leader type, without rapid transfer of charge analogous to the return stroke. ISHIKAWA (1956) has observed rapid field changes which he attributed to cloud discharges of a dart-leader type.

In temperate regions about 40 per cent of flashes are to ground (PIERCE, 1955a), but the proportion appears to be much smaller, perhaps 10 per cent, in tropical regions (WORMELL, 1953).

3. THE AMPLITUDE OF THE V.L.F. FIELD FROM A RETURN STROKE

3.1. *The amplitude as deduced from the current variation*

Several workers have deduced the V.L.F. amplitude spectrum of the field from a return stroke, using empirical data on the discharge currents or movements of charge (BARLOW *et al.*, 1954; EDWARDS, 1956; WATT and MAXWELL, 1957; HILL, 1957a,b). Attention here will be focused on the field in a selected narrow band. The disturbance at the aerial is generally of sufficiently short duration for the shape of the output pulse from a narrow-band receiver to be determined almost entirely by the receiver frequency-response curve. The discussion will be in terms of the peak amplitudes of the pulses, expressed as an equivalent vertical component of electric field at the aerial.

VOL.
13
1958/5

The peak amplitude from a typical return stroke is derived in an Appendix. The stroke is assumed to have the characteristics defined in Section (2) and the amplifier to have at least two tuned circuits of equal selectivity. The field-strength is assumed to vary inversely with the distance from the source; the actual relationship is more complex and has been the subject of considerable investigation in recent years (WAIT, 1957; CHAPMAN and MACARIO, 1956) but it will not be considered here because only approximate field-strengths are discussed and the inverse distance law appears to be a reasonable approximation at 10 kc/s up to a range of 5000 km.

At 10 kc/s the peak envelope field strength at distance r km is estimated in the Appendix to be $10\,B/r$ mV/m in a bandwidth B c/s. If $B = 300$, a value commonly used in the experiments (between points giving response 3 dB below maximum), the peak field is approximately $3000/r$ mV/m.

This formula is for what has been called a "typical" return stroke. It would be desirable to be more specific, mathematically and to quote a median or average value, but this cannot be done unless the whole range of amplitudes is known. Peak currents in return strokes vary over a wide range and while 20,000 A is about the median value of the recorded peak currents in typical experiments, these have in general been subject to a lower observational limit in the range 1000–5000 A. If many return strokes occurred with smaller currents, the median value might be considerably less than 20,000 A. For the moment, the significance attached to the formula is that any atmospheric greater than a quarter of the derived value for a particular distance is almost certainly from a return stroke, while the origin of any smaller ones is open to question. The statistics of the amplitude distributions will be discussed later in more detail.

3.2. *Data on amplitudes of atmospherics received in southern England*

Experimental evidence on amplitudes is not easily collected, owing to the difficulty of recording a representative sample of atmospherics from a particular storm of known position, and to the wide range of amplitudes from one storm.

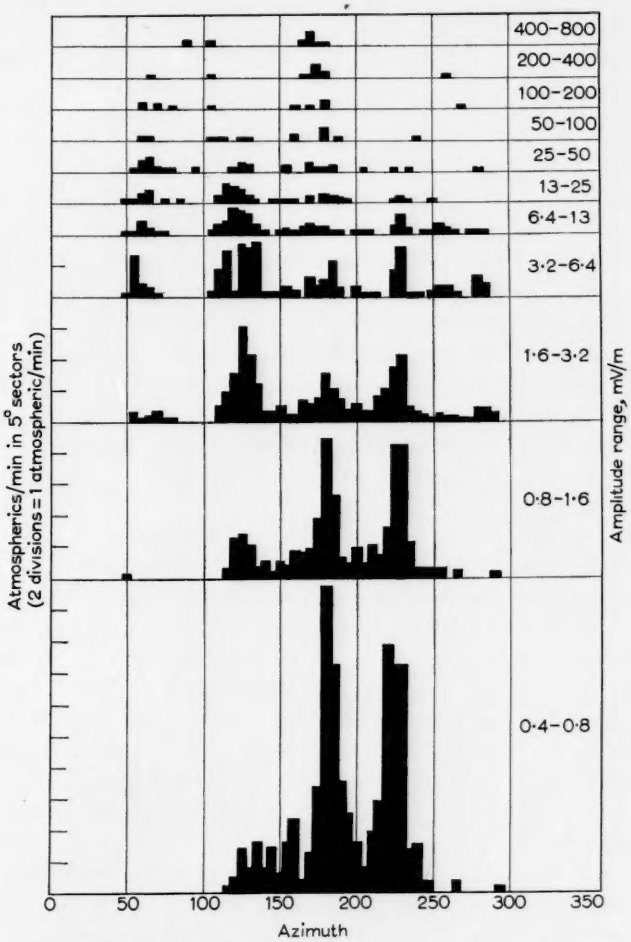

Fig. 1. Histogram of atmospherics received 1700–1800 local time 5 Oct. 1956.

General agreement with the estimated amplitudes at 10 kc/s is obtained in routine observations with cathode-ray direction-finders with a bandwidth of 300 c/s. For example it is known that for observing storms at a distance of 1000 km, a suitable amplifier gain is that for which a full-scale trace corresponds to a peak field-strength of 4 mV/m. Also in observations on more local storms a sensitivity of 100 mV/m full-scale is needed to record storms at 50 km. Both these figures conform to the estimated values of return stroke fields.

Edwards (1956) has presented the spectra of atmospherics from two storms,

at ranges of 250 and 1600 km. From his curves the median values of the amplitudes of atmospherics in a bandwidth of 300 c/s at 10 kc/s are found to be 50 mV/m and 3 mV/m respectively. These values are both larger than would be expected, particularly that for the shorter range, but there is evidence that only the larger atmospherics were recorded.

Further evidence has been obtained from observations taken at Slough on the afternoon of 5 October 1956 when there were several storm areas in Northern Europe. Continuous film records of the bearings on a cathode-ray direction-finder with a bandwidth of 300 c/s at 10 kc/s were taken for about 1 hr. The gain was changed at intervals of a few minutes to record atmospherics having a total amplitude range of 60 dB.

Figure 1 shows the rate at which atmospherics were received, as a function of bearing, in each 2 : 1 amplitude range. Small-amplitude traces (below 1 mV/m) from east and west directions were recorded along the line of travel of the film and were difficult to see, but otherwise the plot is considered to show a representative sample of the atmospherics received in the hour.

The records were interpreted in terms of the positions of storms derived from meteorological records. In the following discussion the field strength in brackets after each quoted distance is the peak value to be expected from the typical return stroke at that distance. The bearings may in general be assumed to be correct to within 5°.

The group at 65° was identified with a small storm area at 500 km (6 mV/m). A significant feature of this group is a well-defined lower limit to the amplitudes, at 1·6 mV/m. The few scattered atmospherics of high amplitude between 90° and 110° were attributed to the remains of local storms which had been occurring throughout the afternoon in southern England. There were no small atmospherics from these directions. The group centred at 120° was thought to have originated in storms in northern Italy at a distance of 1000 km (3 mV/m). The large atmospherics at 160°–180° came from storms in the English Channel and northern France at 170–400 km (7–18 mV/m). There is some indication that the atmospherics from these sources were mainly in amplitude ranges greater than 1mV/m but the prominent source centred on 180°, believed to be in West Africa at 5000 km, (0·6 mV/m) may have obscured some small atmospherics from the nearer sources. The group at 225° was probably from storms in South America at 8000 km (0·4 mV/m). Both this and the West African source undoubtedly produced many atmospherics below the lower amplitude limit recorded. The few large atmospherics at about 260°–280° were probably from storms in the west of England at 200 km (15 mV/m); these were evidently not accompanied by many atmospherics below 1·6 mV/m.

The atmospherics from the North Sea (bearings near 65°) and from Italy (bearings near 120°) are sufficiently well-identified for a study to be made of their amplitude distributions. It was found that the peak amplitudes, expressed in logarithmic units, could be represented approximately by a normal distribution according to which the probability of a given peak exceeding E dB is:

$$Q(E) = \frac{1}{\sigma\sqrt{(2\pi)}} \int_E^\infty \exp\left[-\frac{(e - E_m)^2}{2\sigma^2}\right] d$$

VOL.
13
1958/5

where E_m is the median value of the peak amplitudes (dB)
σ is the standard deviation of E

The parameters E_m and σ are used to define the distribution. In a true normal distribution 16 per cent of the amplitudes exceed the median by more than the standard deviation.

The distribution for the sector 60°–70° is shown in curve *A* of Fig. 2, in which the co-ordinate system is such that a normal distribution is a straight line. The median value is 24 dB, or about 16 mV/m, which is reasonable, considering that a typical return stroke would be expected to give a component pulse of 6 mV/m and

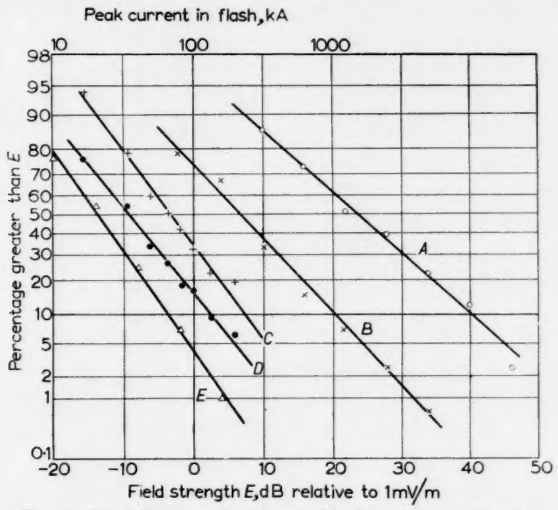

Fig. 2. Distribution of peak amplitudes of atmospherics.
(A) ○ Atmospherics received in southern England from the sector 60–70°, 5 Oct. 1956.
(B) × The same from the sector 105–135°.
(C) + Atmospherics received in west Australia from the sector 7–13°, 24 Oct. 1953.
(D) ● Constituent pulses in the atmospherics recorded in (C).
(E) △ Data on peak currents in lightning flashes (from BRUCE and GOLDE).

each atmospheric is represented by its largest component. The standard deviation is 12 dB.

In the data from storms in Italy (bearings 105–135°) the lower limit of amplitudes is indefinite, owing to possible confusion with small amplitude atmospherics from other sources. However, if the most frequent amplitude (2·2 mV/m) is assumed to be the median value, the distribution shown in plot *B* is obtained. This is similar to plot *A* with a slightly smaller range (standard deviation 10 dB) and the assumed median value, although somewhat low, approximates to what would be expected.

The distribution of peak currents in lightning flashes, derived from the mean of data quoted by BRUCE and GOLDE (1941), is shown in plot *E*. As mentioned previously this plot should be viewed with some caution because of the lower amplitude limit imposed by the recording techniques. The slope is greater than those of the distributions of atmospherics, the standard deviation corresponding to 8 dB. The atmospherics would be expected to have a greater amplitude range

than the peak currents, because they depend on other variable factors such as the current waveforms, the orientation of the flashes and the propagation conditions. In general, therefore, both the median amplitudes and the amplitude ranges suggest that return strokes were the predominant source of the peak amplitudes of the atmospherics. Some of the smaller atmospherics may have been from cloud strokes, but the amplitude distributions showed no evidence of two distinct amplitude ranges, corresponding to return and cloud strokes respectively.

Consider now the rates at which atmospherics were received from the various centres. On the assumption of 1 ground-flash/min from a storm cell it could be deduced that there were about four cells in the North Sea storm, ten in the English Channel and Northern France, twenty in Northern Italy and at least twenty, and probably many more, in each of the African and South American centres. The figures for European storms seem reasonable in relation to the thunderstorm activity indicated by meteorological records. The figures for the tropical thunderstorms seem very low, which may indicate that only a few of the strongest atmospherics were received or may be confirmation of the smaller proportion of ground strokes in tropical storms. However, reviewing all these results, there is obviously no difficulty in postulating a sufficient number of sources for all the received atmospherics to be identified with return strokes.

4. The Detailed Structure of Noise at V.L.F.

The conclusion that noise at V.L.F. originates mainly in return strokes has been reached by considering the amplitudes of traces on a cathode-ray direction-finder as recorded on film moving at slow speed. These records do not show the fine structure of the atmospherics, which is often quite complex, and the amplitudes recorded are those of the largest components in each atmospheric. It is these which apparently originate in return strokes, but the possibility is not excluded that a number of smaller components from other parts of a flash are associated with the larger ones. A study of the detailed structure of the atmospherics is required to determine whether these are present.

Some film records of bearings on a V.L.F. cathode-ray direction-finder were examined by Kamada (1953) and repeated traces from the same direction were attributed to the successive return strokes of a multiple flash. No analysis of the amplitudes of the components was presented, however, and, moreover, the film speed used was insufficient to resolve those closer than 10 msec. In the next section data from records taken at much higher film speed are discussed, but it is first necessary to define more precisely some of the terms used.

Meteorologists distinguish between a "stroke" which is a single discharge, and a flash, which comprises the whole of the discharge process which would appear as a single event to the eye, but which might be a multiple flash consisting of a large number of strokes.

Similar distinctions are required in discussing the components of atmospheric noise, and the following definitions will be used.

(a) A "pulse" will refer to a single pulse from a narrow-band receiver. With a bandwidth of 300 c/s, a pulse might result from several discharges, provided that their overall duration is less than 1 msec. Most pulses at V.L.F. have a shape

VOL
13
1958/

determined by the bandwidth (when this is 300 c/s or less) indicating that the disturbance at the aerial lasts for a time much shorter than 1 msec.

(b) A "group" of pulses will refer in a general way to a sequence occurring at a rate higher than the average rate in the noise as a whole, irrespective of whether they are known to originate in the same lightning flash.

When the noise is related to particular phenomena in the thunderstorm the following definitions will be used.

(c) An "atmospheric" is the noise event arising from a complete lightning flash.

(d) A "multiple atmospheric" is one consisting of more than one pulse and is analogous to a "multiple flash", except that it will not be assumed that all the pulses necessarily originate in return strokes.

Evidence from experiments such as that described in Section (3.2) indicates that atmospherics generally have many more constituent pulses than would correspond with data on strokes in multiple flashes. For example the rate of arrival of atmospherics on 5 October, derived from Fig. 1, can be compared with the counts of individual pulses for that time of the year, which have been studied extensively (HORNER and HARWOOD, 1956). The number of atmospherics exceeding 1 mV/m on this day was only one-tenth of the number of individual pulses exceeding this value in average October conditions, despite the fact that the day was particularly stormy. As an average figure of three is usually quoted for the number of return strokes per flash, it seems that either this figure is incorrect, or the atmospherics contained many pulses which did not originate in return strokes.

VOL. 13 58/59

4.1. *Data from high-speed film records*

Film records of the directions of atmospherics have been obtained by CLARKE C. (unpublished) on a cathode-ray direction-finder at Perth, Australia. The absence of man-made interference enabled a high gain to be used and in the records to be discussed a full scale deflexion corresponded to 2 mV/m peak. The film speed was 30 cm/sec which was sufficient to resolve pulses separated in time by 1 msec. Those at shorter intervals would overlap in any case owing to the small bandwidth of the receiver (450 c/s at 10 kc/s).

From a cursory examination of films taken at 1600 hours local time on 24 October 1953 it was evident that the pulses were occurring in groups and the subsequent analysis was designed to show whether the groups could be identified with multiple lightning flashes. All the atmospherics were received from northerly directions, and since storms were entirely northerly, as far as was known, there were no atmospherics which could be interpreted as having arrived by the longer great circle path.

The main difficulty was to select a group which could be reasonably assumed to have originated in a single flash. On a $\frac{1}{2}$ min sample of the film a selection was made of atmospherics arriving from a particular direction. There was a prominent source on bearing 10° and all atmospherics between 7° and 13° were assumed to originate in this storm area, probably in the East Indian archipelago about 3000 km away. A typical return stroke at this distance would be expected to give a half-scale deflexion, and there were in fact seventy-six traces greater than half-scale in the half-minute.

A plot of the selected atmospherics was made in the form shown in Fig. 3, which is a sample 600 msec long. It was necessary to decide which of the groups were likely to be multiple atmospherics rather than a chance association of a number of pulses from different sources.

From previous work on multiple flashes it was known that intervals between return strokes are usually less than 100 msec, so as a working basis it was assumed that any longer interval was a break between two groups which might, on other evidence, be identified as different atmospherics. This procedure yielded sixteen single isolated pulses and forty-nine groups of two or more pulses. Most of the

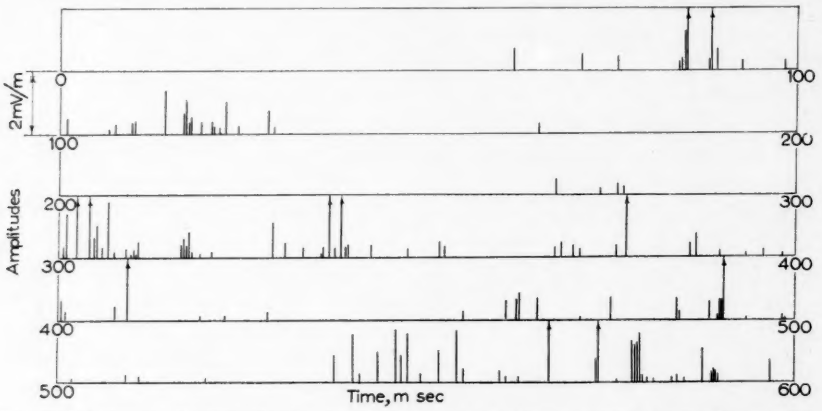

Fig. 3. Incidence of atmospherics from the sector 7°–13° at Perth, Australia, 24 Oct. 1953, 1600 local time. Frequency, 10 kc/s; bandwidth, 450 c/s; the record is continuous, each horizontal strip representing 100 msec; arrow heads indicate traces larger than full scale (2 mV/m).

groups were thought to be multiple atmospherics because there were several periods of 2 or 3 sec with no pulses, which would have been statistically unlikely if most of the pulses had been unrelated.

For further evidence the statistical distributions of the overall durations of the groups, the number of pulses in them and the intervals between the pulses were compared with the corresponding data for lightning flashes quoted by BRUCE and GOLDE (1941). The durations were taken from original records of the Radio Research Station and the numbers and intervals from those of SCHONLAND. These comparisons, shown in Fig. 4, indicated that the overall durations were similar, but that the noise groups tended to contain more pulses, at shorter intervals, than the strokes of a multiple flash.

If only the larger noise pulses are considered, much better agreement can be obtained. Curves are shown which were derived by using the same grouping as before (based on consideration of all the pulses) but plotting only the data for pulses greater than $\frac{1}{2}$ mV/m. The new curve for durations has not been plotted, because the change was inappreciable. The other two distribution curves show that by suitable choice of threshold the characteristics of the noise groups have been made to correspond with those of multiple flashes. This may mean that the lightning data, obtained from photographs of the flashes and measurements of

VOL
13
1958/

near field, relate only to the larger strokes, and possibly that the smaller pulses in the C.R.D.F. record did not originate in return strokes. Simultaneous records of noise and lightning discharges at close range are required to resolve this uncertainty.

KAMADA's (1953) results indicated fewer pulses per atmospheric than the present data, in fact the percentage of multiple atmospherics (15 per cent) was

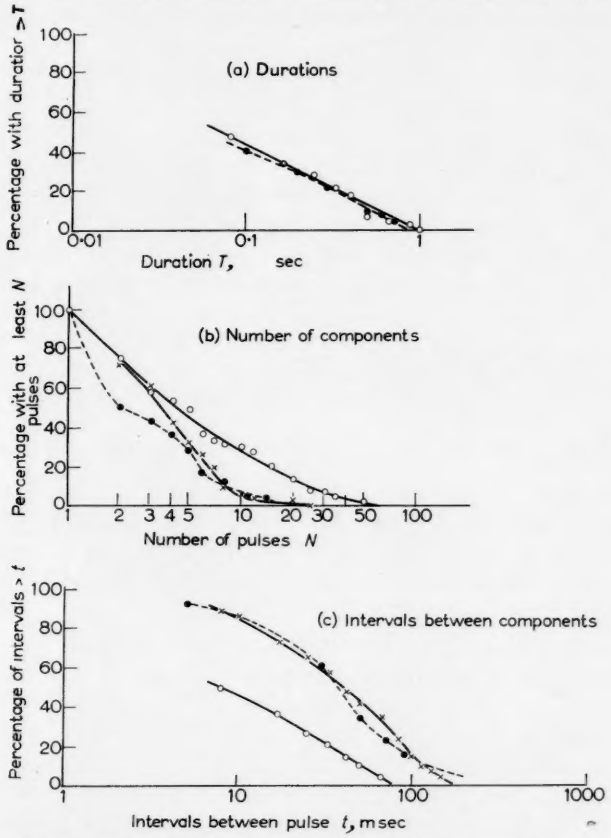
Percentage with duration > T
(a) Durations
Duration T, sec
Percentage with at least N pulses
(b) Number of components
Number of pulses N
Percentage of intervals > t
(c) Intervals between components
Intervals between pulse t, msec

Fig. 4. Characteristics of atmospherics. ○ all atmospherics; × atmospherics > ½ mV/m; ——●— lightning data from BRUCE and GOLDE.

much lower even than the usual corresponding figure for multiple lightning flashes. It is likely that many pulses in his records were not resolved at the film speed used and if a triggered display was used, as seems probable from the records shown, many of the smaller pulses may have been eliminated.

Whether or not the small pulses originated in return strokes, the Australian records strongly suggested that the large and small pulses in a group were part of the same atmospheric. This was demonstrated by dividing the record into intervals of about ½ sec and counting the number of large and small pulses in each interval. The distributions followed each other very closely; in fact with the division at ½ mV/m the numbers of large and small pulses in most intervals were

nearly equal. Furthermore there were sixteen intervals with no large pulses and sixteen with no small ones, and fourteen of these coincided. It was therefore concluded that all the pulses in a selected group were from a common source.

The evidence from these film records suggests that in a typical multiple atmospheric there are a number of relatively large pulses with amplitudes, spacings and overall duration corresponding to the return strokes of multiple flashes, but that there are, interspersed, smaller pulses which are not accounted for in lightning flash data.

The amplitude distributions of the atmospherics are plotted in Fig. 2 for comparison with the data from southern England. Plot *D* shows the distribution of the individual pulses and plot *C* the atmospherics (i.e. the largest pulses in the groups defined above). The median value of the pulse amplitudes (9 dB, or 0·35 mV/m) is less than would be expected from a return stroke at 3000 km (1 mV/m) but 16 per cent of the pulses exceeded this expected value. The distribution, had similar slope to that of the plot of peak currents (plot *E*); the standard deviation was 9 dB. The distribution in each of the seventeen atmospherics with more than ten pulses had also similar general slope. The median value of the peak amplitudes of the atmospherics (plot *C*) was 6 dB higher than that of the constituent pulses, and the plot had similar slope (standard deviation 8 dB).

5. Some Features of Noise at High Frequencies

Noise in the H.F. band originates mainly in parts of the lightning discharge other than the return stroke. Where the change takes place from the V.L.F. type of noise to the H.F. type is not known precisely but there is probably a transition in the L.F. band. Noise at 500 kc/s recorded by NORINDER (1947) was found to be more akin to H.F. than to V.L.F. noise.

THOMAS and BURGESS (1947) attempted to derive the amplitude of H.F. noise from consideration of the return strokes alone, and found it necessary to assume that they were more numerous than they were thought to be from other evidence. Moreover they used the model of the return stroke described in Section (2), with smooth current variation, and H.F. noise would be expected to arise in small irregularities in the waveform. Furthermore, NORINDER's records show that atmospherics at 500 kc/s have long durations—up to several hundred milliseconds and are more continuous than the series of pulses which are typical of a V.L.F. atmospheric.

AIYA (1955) recently estimated the intensity of H.F. noise on the assumption that it originates in the stepped leader discharge. The model he adopted for the stepped leader was a series of current pulses separated by 74 μsec, each with a maximum rate of change of current of 10^{10} A/sec, the overall duration of the series being about 1 msec. Agreement was said to have been obtained between the noise predicted in this way and measured values, but the method of measurement used appears to depend more on the number and amplitude of the noise bursts than on their duration.

Preliminary records of the detailed structure of high frequency noise in England show that the noise occurs in bursts, with amplitudes in reasonable agreement with

VOL.
13
1958/5

VOL.
13
8/59

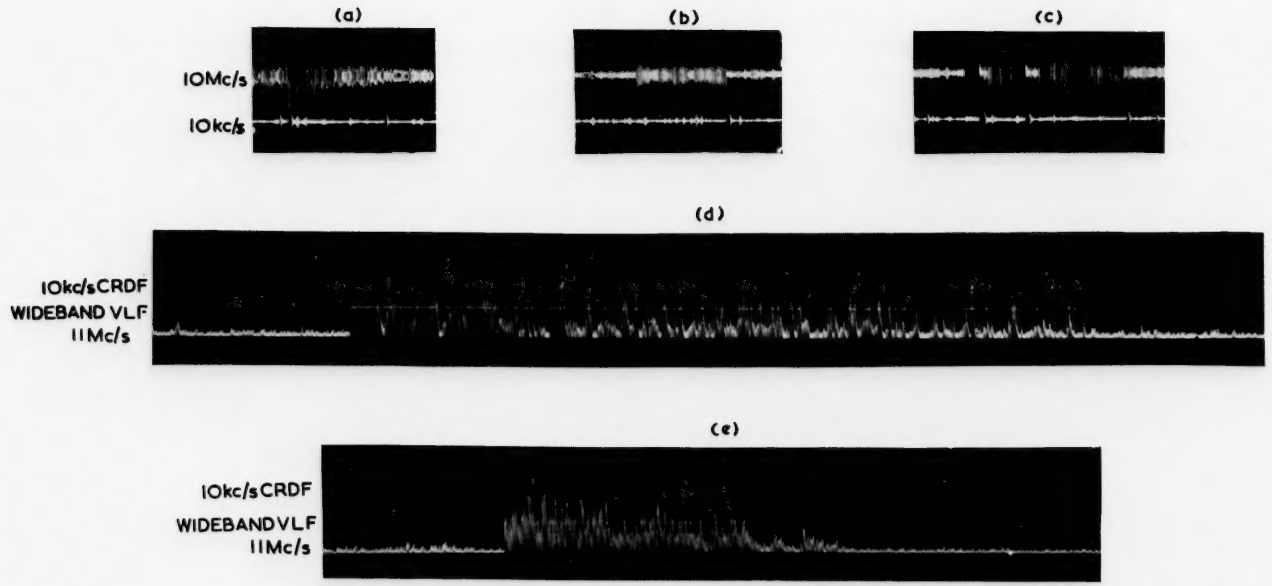

Fig. 5. Comparison of H.F. and V.L.F. noise.

VOL.
13
1958/5

those measured in India, when allowance has been made for differences in frequency and bandwidth. The durations of the bursts, however, are of the order of 100 m sec or more, which are in general agreement with NORINDER's 500 kc/s results. This suggests that stepped leaders of the type described are not the sole, or even the main, source of the noise in temperate regions.

Table 1. Data for records shown in Fig. 5

Record	(a)	(b)	(c)	(d)	(e)
Date	25.8.52	25.8.52	25.8.52	18.7.56	19.7.56
Time (GMT)	1500	1500	1500	1400	1800
Duration (msec)	150	180	220	1000	650
H.F. bandwidth (kc/s)	5	13	5	0·5	0·5
H.F. peak field (μV/m)	1	$\frac{1}{2}$	1	3*	not known
V.L.F. bandwidth (c/s)	300	300	300	300	300
V.L.F. peak field (mV/m)	3	4	4	5*	10*

* Full scale trace—field actually exceeded this value.

When noise is recorded simultaneously at H.F. and V.L.F. it is found that V.L.F. pulses often occur throughout the H.F. burst (Fig. 5). V.L.F. pulses coincide with either the start [Fig. 5(a)] or the end [Fig. 5(b)] of an H.F. burst more frequently than would be expected by chance. Also there is a tendency for a V.L.F. pulse to be followed by a brief lull in the H.F. noise [Fig. 5(c)]. On many occasions, however, there is no obvious correlation between the occurrences in the two frequency bands. These atmospherics probably originated in storms several hundred kilometres away.

In these examples there is no evidence, other than the statistics of the distributions in time, that the H.F. and V.L.F. noise had a common origin, or indeed that all the H.F. noise burst was from a single source. Further evidence has been obtained by recording the V.L.F. noise as a directional trace. Figs. 5(d) and 5(e) are records of this type in which there are three traces. The top trace on each record is from a 10 kc/s direction finder; the broken nature of the upper trace on Fig. 5(d) was due to a spurious brilliance modulation at 50 c/s and may be disregarded, while the upper baseline cannot be seen in Fig. 5(e). The bottom trace on each record is noise at 11 Mc/s (the lower half of the trace has been blanked out) and the trace in the middle is the output from a wideband V.L.F. receiver (waveform recorder). Figure 5(d) shows an example in which the long H.F. burst is accompanied by a series of V.L.F. pulses from one direction. This is further evidence for a common source for all the recorded noise. Figure 5(e)

shows a continuous burst of H.F. noise accompanied at the beginning by a few V.L.F. pulses. Examination of the centre trace on the original record showed that there was appreciable V.L.F. energy received during the whole of the H.F. burst, although the 10 kc/s directional traces were confined to the early part. Records 5(d) and 5(e) were obtained during periods with local storms.

The general impression gained from records of this type is that H.F. noise is radiated during the whole of a lightning flash. There is a tendency for the noise level to be high just before a V.L.F. pulse and lower just after it, as would be expected from a stepped leader mechanism, but the preceding noise bursts are of much longer duration than the commonly-accepted duration of a stepped leader. It appears, therefore, that any analysis based entirely on the characteristics of stepped-leaders is likely to lead to erroneous results. It is more probable that the noise is associated with the so-called "slow" changes of electrostatic field and may be from the corona-type of discharge suggested by MALAN and SCHONLAND (1953).

6. CONCLUSIONS AND DISCUSSION OF OUTSTANDING PROBLEMS

A typical atmospheric at very low frequencies has been shown to consist of a number of pulses. There is evidence that the largest pulses in most of the atmospherics originate in return strokes, in temperate regions at least, and the overall durations of the atmospherics agree closely with those of multiple lightning flashes. Fifty per cent were longer than 70 msec and 10 per cent longer than 600 msec. However the total number of pulses is much greater than the number of return strokes which a multiple flash is commonly supposed to contain. In the Australian data, for example, 75 per cent of the atmospherics had two or more pulses, 50 per cent had ten or more and 10 per cent had twenty-five or more. Whether the smaller pulses are from return strokes or from some other part of the lightning discharge is yet to be determined. No evidence has so far been found to suggest that they arise in the stepped-leader mechanism or in the *M*-components in the continuing ionization following a return stroke.

From previous data on the currents in lightning flashes, the peak field from a typical return stroke has been estimated to be $10\ B/r$ mV/m at a distance r km when measured in a bandwidth B c/s at 10 kc/s, provided that $r < 5000$ km. Median amplitudes of atmospherics in the European data are in fair agreement with this formula. Median amplitudes in tropical storms are somewhat lower than the estimated values, but this may be only an indication of the smaller percentage of return strokes in tropical storms. If this is the explanation, it must be concluded that much of the V.L.F. noise from tropical storms originates in parts of the discharge other than the return strokes. More measurements of peak fields of atmospherics from storms at known distances are required, particularly in tropical regions and preferably by methods in which the component pulses can be distinguished.

The distribution of the peak amplitudes of either atmospherics or their constituent pulses from limited storm areas can be represented by a log-normal distribution. The standard deviations have been found to be between 8 and 12 dB and this may be compared with the variability in the peak currents in

VOL
13
1958/

return strokes, which has a standard deviation of 8 dB. These conclusions are based on only a few measurements and require confirmation.

Preliminary observations of atmospherics at high frequencies indicate that they have overall durations similar to those of V.L.F. atmospherics but that they are more continuous. There is a tendency for either the start or the finish of the H.F. atmospheric to coincide with a V.L.F. pulse and for other V.L.F. pulses during the atmospheric to be followed by brief periods of relatively low H.F. noise. The form of the H.F. noise suggests that the stepped-leader part of the discharge is not the main source, and more experimental work is required both to establish the statistical properties of the noise bursts and to determine their origin.

Acknowledgements—The work described above was carried out as part of the programme of the Radio Research Board and is published by permission of the Director of Radio Research of the Department of Scientific and Industrial Research.

The assistance of the Meteorological Office in providing information on the locations of thunderstorms is acknowledged.

References

Aiya S. V. C.	1955	*Proc. Inst. Radio Engrs., N.Y.* **43,** 966.
Barlow J. S., Frey G. W. and Newman J. B.	1954	*J. Franklin Inst.* **258,** 187.
Bruce C. E. R. and Golde R. H.	1941	*J. Instn. Elect. Engrs.* **88,** 487.
Chapman F. W. and Macario R. C. V.	1956	*Nature, Lond.* **177,** 930.
Clarence N. D. and Malan D. J.	1957	*Quart. J. R. Met. Soc.* **83,** 161.
Edwards A. G.	1956	*J. Brit. Instn. Radio Engrs.* **16,** 31.
Horner F. and Harwood J.	1956	*Proc. Instn. Elect. Engrs.* B **103,** 743.
Hill E. L.	1957a	*Proc. Inst. Radio Engrs., N.Y.* **45,** 775.
Hill E. L.	1957b	*J. Franklin Inst.* **263,** 107.
Ishikawa H.	1956	*J. Geomagn. Geoelect., Kyoto* **8,** 136.
Kamada T.	1953	*Proc. Res. Inst. Atmosph., Nagoya Univ.* **1,** 90.
Malan D. J. and Collens H.	1937	*Proc. Roy Soc.* A **162,** 175.
Malan D. J. and Schonland B. F. J.	1947	*Proc. Roy. Soc.* A **191,** 485.
Malan D. J. and Schonland B. F. J.	1953	In *Thunderstorm Electricity* (Edited by Byers H. R.). pp 238. University of Chicago Press.
Norinder H.	1947	*J. Franklin Inst.* **244,** 109 and 167.
Pierce E. T.	1955a	*Quart. J. R. Met. Soc.* **81,** 211.
Pierce E. T.	1955b	*Quart. J. R. Met. Soc.* **81,** 229.
Thomas H. A. and Burgess R. E.	1947	*Survey of Existing Information and Data on Radio Noise over the Frequency Range* 1–30 *Mc/s.* Radio Research Special Report No. 15, H.M.S.O., London, Code No. 47–29–15.
Wait J. R.	1957	*Proc. Inst. Radio Engrs., N.Y.* **45,** 760.
Watt A. D. and Maxwell E. L.	1957	*Proc. Inst. Radio Engrs., N.Y.* **45,** 787.
Wormell T. W.	1953	*Quart. J. R. Met. Soc.* **79,** 3.
	1949a,b	*The Thunderstorm* Chaps. I & IV. U.S. Dept. of Commerce.
	1953	*Thunderstorm Electricity* (Edited by Byers H. R.). University of Chicago Press.

APPENDIX

The V.L.F. field from a return stroke

The waveform of the current in the return stroke, at the ground, is assumed to be given by:

$$I = I_0 [\exp(-\alpha t) - \exp(-\beta t)] \quad \text{A}$$

and the channel carrying this current is assumed to increase in length at a speed

$$v = v_0 \exp(-\gamma t) \quad \text{m/sec}$$

With a narrow band receiver at V.L.F. the form of the output pulse due to a stroke is known and it is required to determine the peak amplitude of the pulse.

The frequency spectrum of the field is first derived by Fourier analysis of the time-variation of the moment of the discharge. The vertical electric radiation field strength E at a large distance r from the stroke, at the surface of a perfectly conducting earth is:

$$E = \frac{2}{10^7 r} \frac{dM}{dt} \quad \text{V/m}$$

where $M = \int i \, dl$

and i is the instantaneous current in the element of length dl. The frequency spectrum of dM/dt is given by:

$$f(\omega) = jI_0 v_0 \omega \frac{(\beta - \alpha)(\alpha + \beta + \gamma + 2j\omega)}{(\alpha + j\omega)(\beta + j\omega)(\alpha + \gamma + j\omega)(\beta + \gamma + j\omega)}$$

where ω is the angular frequency.

With the values of the parameters given in Section (2), $f(\omega) = 14 \times 10^6$ at 10 kc/s and the corresponding field strength is $E(\omega) = 2{\cdot}8/r$ V/m, where r is in metres.

To determine the amplitude of the pulse which corresponds to this frequency spectrum, integrated over a bandwidth B c/s, the pulse shape is assumed to be determined by the bandwidth, and the peak amplitude can be shown, by Fourier analysis to be:

$$e_m = \frac{2\pi B}{\exp(n-1)} \frac{(n-1)^{n-1}}{(n-1)!} \frac{1}{\sqrt{(2^{1/n} - 1)}} E(\omega)$$

where B is measured between 3 dB points and n is the number of tuned circuits.

For $n \geqslant 2$, $e_m = 3{\cdot}4\, BE(\omega)$ approximately. Substituting the value for $E(\omega)$ at 10 kc/s and changing r to kilometres

$$e_m = \frac{10B}{r} \quad \text{mV/m}$$

VOL
13
1958/

Journal of Atmospheric and Terrestrial Physics, 1958, Vol. 13, pp. 155 to 164. Pergamon Press Ltd., London

Satellite tracking by H.F. direction finder

J. L. WOLFE
National Research Council, Radio and Electrical Engineering Division, Ottawa, 2, Canada

(*Received* 14 *April* 1958)

Abstract—A method of satellite tracking using an H.F. direction finder is outlined and commented on. The results of tracking *Sputniks I* and *II* are given, along with an approximation of the size of error to be expected.

INTRODUCTION

RADIO direction finders have been used successfully to track surface objects having low velocities. The height and speed of the first earth satellite, launched on 4 October 1957, created new problems and exposed limitations in H.F. D.F. tracking when the azimuth only can be measured. This report shows the method used in tracking *Sputnik I* by H.F. D.F. and gives the results that were obtained.

DATA COLLECTION

The equipment consisted of a twin-channel C.R. D.F. with an Adcock antenna (WATSON-WATT and KEEN, 1922). All observations were made on the 20·005

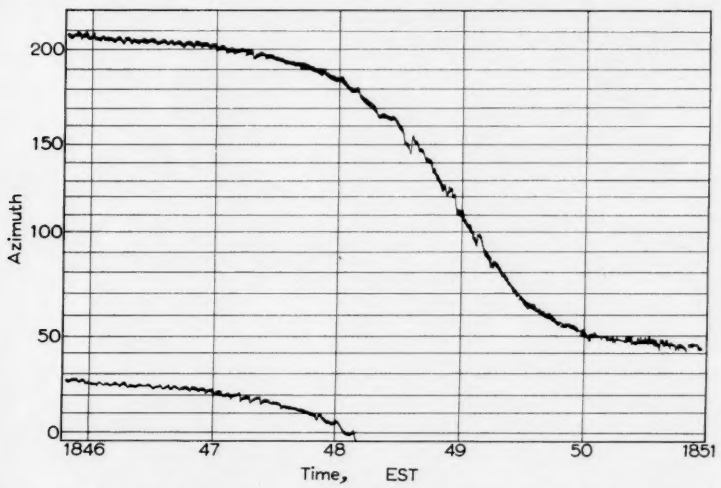

Fig. 1. An example of a paper record showing the bearing of *Sputnik I* as a function of time.

Mc/s signal. The data was collected in two periods. On 7 and 8 October bearings were taken on the satellite over ground ranges up to 6500 miles. On 15 October tracking was again resumed, but the signals were much weaker than before.

For close crossings, bearing changes up to 5°/sec were measured. Since it was impossible for an operator to get accurate bearing information quickly enough, the azimuth was recorded on paper at the rate of five readings/sec (MCLEISH, 1957). An example of a paper record is shown in Fig. 1. For distant crossings, the rate of

azimuth change was slow enough to allow an operator to take the bearings. The data for Fig. 2 was taken in this way.

Method of Tracking

Bearing plotted against time yields an S-curve as shown in Figs. 1 and 2. The time and bearing at nearest approach (t_0 and B_0 respectively) can be determined from the point of inflexion on the curve. Since the velocity of the observer

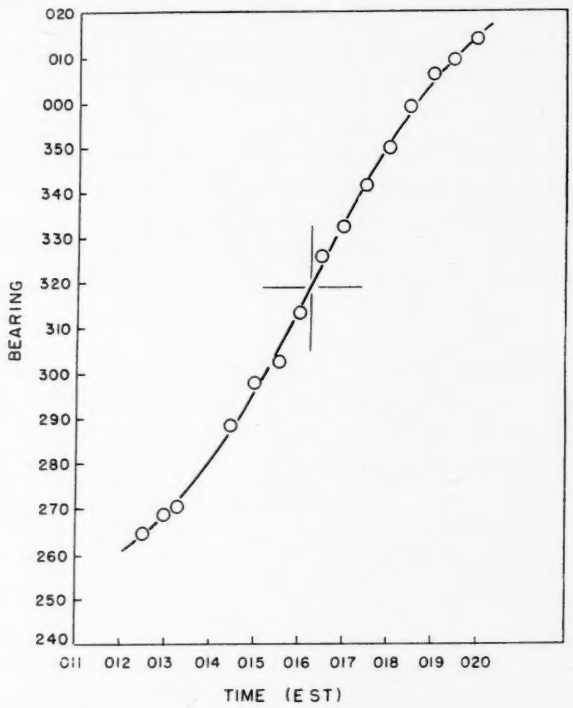

Fig. 2. An S-curve obtained from bearing information taken by an operator.

is much less than that of the satellite, the observer was assumed to be stationary. This means the S-curve should be symmetrical about the point of inflexion. The first problem was to determine this point as accurately as possible. The S-curve was plotted twice, then one plot was turned through 180° so that the bearing scales and time scales were parallel but increasing in opposite directions. The curves were matched as closely as possible and the values of t_0 and B_0 were taken as the points where the values of the time scales and bearing scales coincided. From the value of B_0 the satellite's direction of travel can be determined and from the values of t_0, B_0 and the satellite's speed, the distance of nearest approach can be determined.

A second method of determining the inflexion point was also used. A family of S-curves was drawn for a constant period $T = 96{\cdot}0$ min and a variable distance of nearest approach, from $\delta = 1°$ to $\delta = 15°$ where δ is the angle at the centre

VOL
13
1958/

of the earth subtended by radii passing through the observer and through the point of nearest approach. The curves were drawn from the relation derived in Appendix I, which also assumes a stationary observer and a circular orbit. The inflexion point was taken as the position on the observed S-curve which coincided

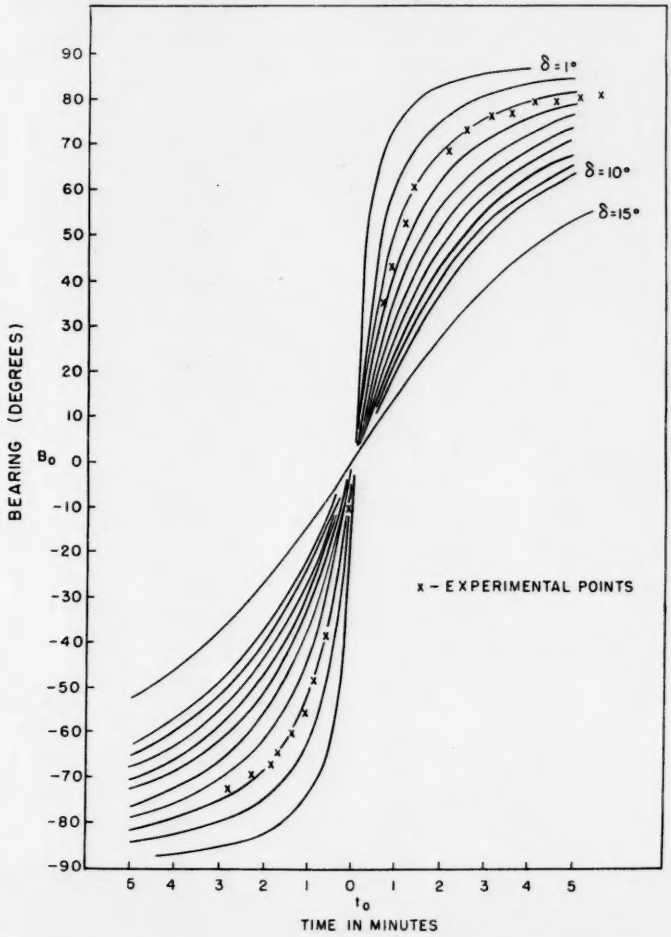

Fig. 3. The family of lines are the theoretical S-curves that were obtained for a circular orbit and a stationary observer (Appendix I). The values of bearing and time for one crossing are shown as experimental points.

with the known inflexion point of the family of curves when the two plots were matched. Fig. 3 shows the experimental points taken on 20 October 1957 at 2000 hours EST compared with the family of curves that was drawn. This method can also be used to estimate d_0, the distance of nearest approach. In Fig. 3 the observed curve matches the theoretical curve for $\delta = 3°$ quite closely. This would indicate a ground range at the point of nearest approach of about 200 miles.

In order to get the distance of nearest approach more accurately, d_0 was

calculated, using every experimental point of the curve, by the equation derived in Appendix I, substituting the values of B_0 and t_0 that were previously found for the same crossing. Inspection of the equation will show that errors in d_0 become extremely large for small errors in the bearing or in the time of points near the inflexion point. Thus values of the distance of nearest approach for these points were not used in finding the mean value of d_0.

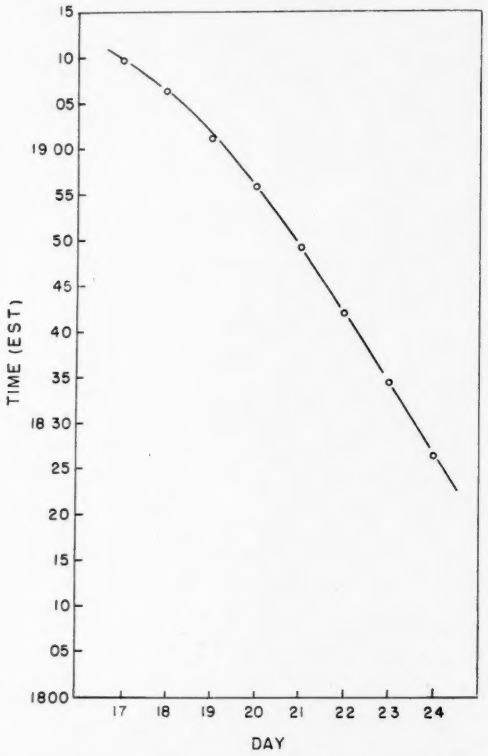

Fig. 5. Times of crossing the forty-fourth parallel for successive fifteenth passes.

A correction can be made in the apparent direction of travel of the satellite due to the motion of the observer. If d_0 is small it is shown in Appendix II that:

$$\sin \beta = \frac{0{\cdot}047 + \sin \rho}{1 + 0{\cdot}047 \sin \rho}$$

where β = the true direction of travel at $t = t_0$

ρ = the apparent direction of travel at $t = t_0$ and is equal to $B_0 \pm 90°$.

In the case of *Sputnik I* this correction was $+2{\cdot}1°$ for all south to north crossings observed from Ottawa.

The tracks that were determined are plotted for the period of observation on the map shown in Fig. 4, using the values of B_0, d_0 and β that were obtained. The crossing shown on 8 October was the only one taken during the first observational

VOL.
13
1958/5

OL.
13
8/59

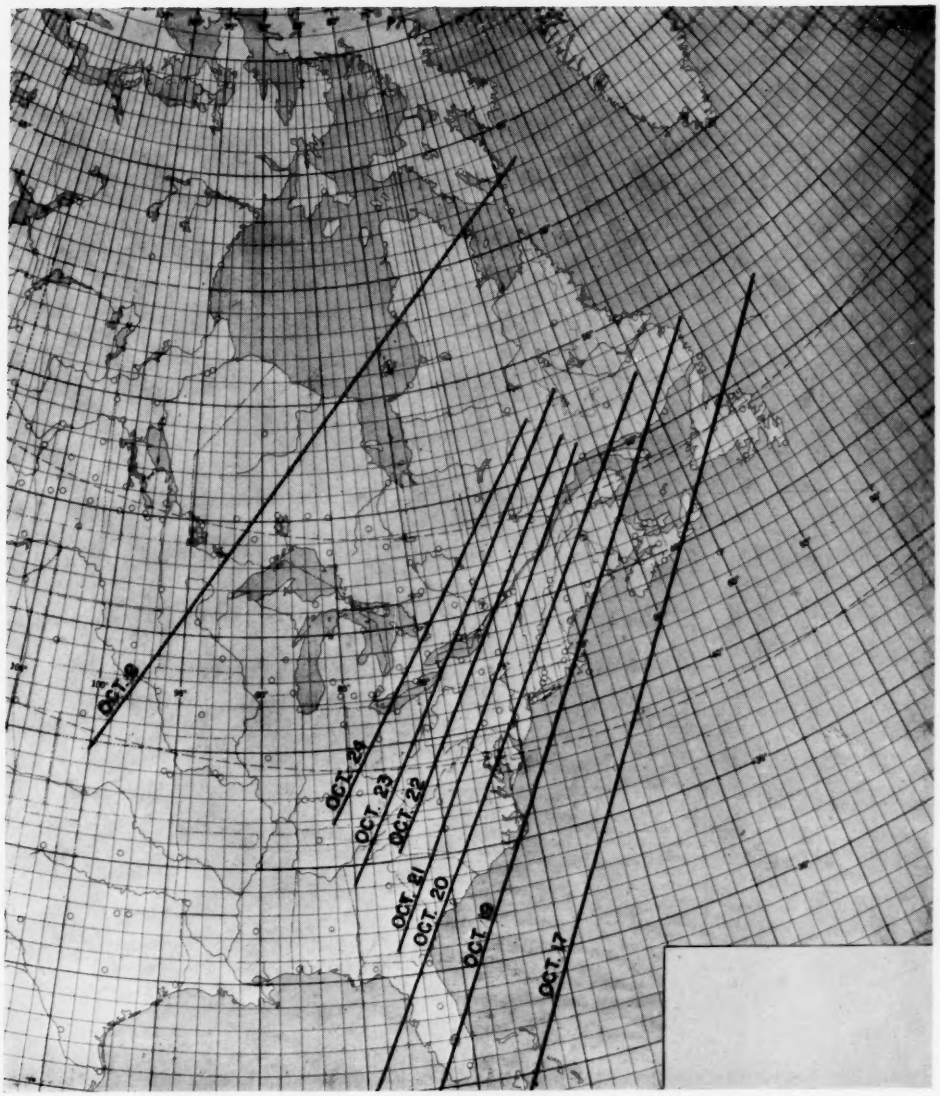

Fig. 4.

VOL.
13
1958/5

period, which was close enough to give a good S-curve. A record of the crossing on 18 October was obtained, but only the time and distance of nearest approach could be determined due to the failure of the equipment to print the bearing scale.

Results

Three quantities were determined from successive fifteenth crossings. These are:

(1) The mean period and the rate of decrease of the mean period;

(2) The inclination of the orbit;

(3) The daily shift in longitude and hence the precession.

Figure 5 shows the times of crossing the forty-fourth parallel on consecutive days as determined by scaling along the tracks shown in Fig. 4. The mean period is obtained by dividing the time elapsed between consecutive crossings by the known

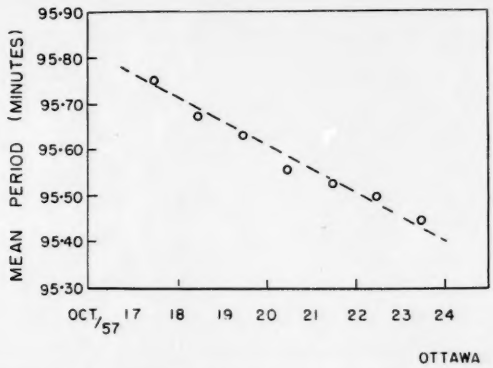

Fig. 6. The mean period for fifteen trips around the orbit is shown for 8 consecutive days.

number of revolutions per day (15). The mean periods obtained were found to decrease at the rate of 3 sec/day or about 0·2 sec/rev as shown in Fig. 6.

The inclination ($\gamma°$) can be found by spherical trigonometry from the latitude and direction of travel at time $t = t_0$.

$$\cos \gamma = \sin \beta \cos l$$

where l is the latitude associated with the direction of travel when $t = t_0$. The values of γ that were found are:

Date	γ
Oct. 17	69°16′
19	68°26′
20	66°33′
21	67°21′
22	66°18′
23	65°57′
24	62°19′

The average of these values is 66°36′

The precession can be determined from the daily drift in longitude and the period. The drift per day and the precession were found to be:

Date	Drift (deg. of long.)	Prec. (deg.)
Oct 17	5·6	2·9
19	2·8	3·2
20	2·4	3·1
21	1·8	2·6
22	2·1	3·0
23	2·1	3·2
24		

The average precession is 3·0° per day

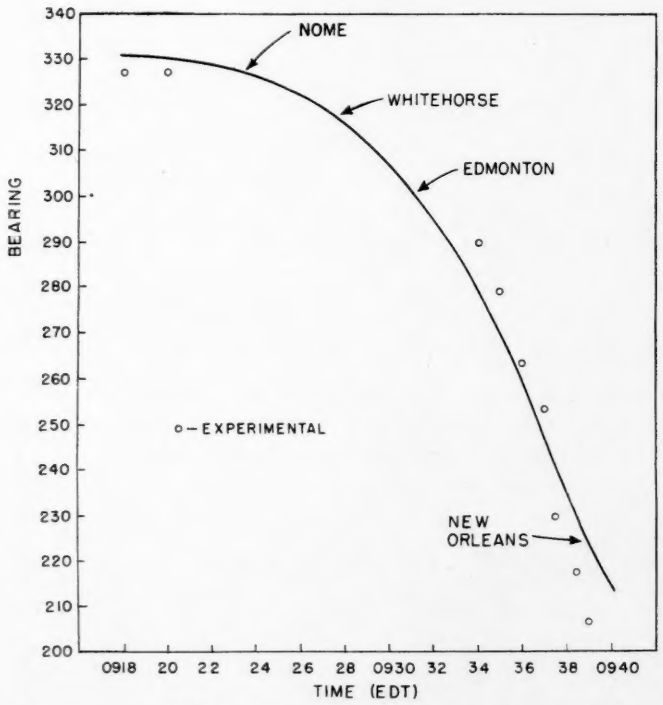

Fig. 7. A comparison of the bearing that was observed, shown as circles, and the bearing that would be expected for a period $\tau = 96{\cdot}0$ min and an inclination $\gamma = 65°$.

Accuracy

The assumption of a circular orbit could be the source of large errors, depending on the eccentricity. In the case of *Sputnik I*, an eccentricity of 0·05 would give a fluctuation in angular velocity of ± 10 per cent about the mean angular velocity. Thus the maximum expected error in the distance d_0 should be ± 10 per cent for the close crossings observed between 17 and 24 October. The eccentricity will

cause the S-curve to be unsymmetrical about the inflexion point, unless the point of nearest approach corresponds to the apogee or perigee. If, however, the observations are taken while the satellite travels through a small portion of its orbit, the angular velocity will not change appreciably and the errors in B_0 and t_0 due to the eccentricity will be small.

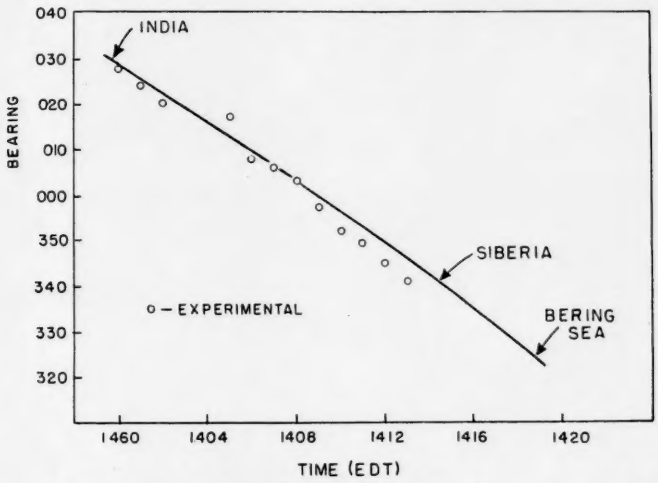

Fig. 8. A comparison of the bearing that was observed, shown as circles, and the bearing that would be expected for a period $\tau = 96{\cdot}0$ min and an inclination $\gamma = 65°$.

With so few observations and so many possible sources of error, it is difficult to estimate the accuracy of the bearing and time values for the point of nearest approach. From previous propagation experiments it is felt that the errors will not be likely to exceed 3° in B_0 and 6 sec in t_0.

Discussion

Little has been said about the data collected on 7 and 8 October. Some examples of these observations are shown in Figs. 7, 8, 9 and 10. The solid line indicates the bearing that would be expected for a period $\tau = 96{\cdot}0$ min and an inclination $\gamma = 65°$, as found by other observers (*Nature*, 1957). (See fourth entry in reference list.) It was impossible to determine the time and bearing at nearest approach because the S-curves were nearly straight lines. It was possible, however, to get a fair estimate of the range from the rate of bearing change and the period.

During most of the observations after 17 October, periodic fading of 13 c/min was noticed. It usually occurred as the satellite was approaching and about to change bearing quite rapidly. When paper records were taken a bearing wobble of 13 c/min was found on the approach side of the S-curves as shown in Fig. 2. This appeared to be polarization error due to the rotation of the transmitted field pattern and is therefore a measure of the satellite spin. In general the signal was received for a longer period on the approach for south to north crossings and

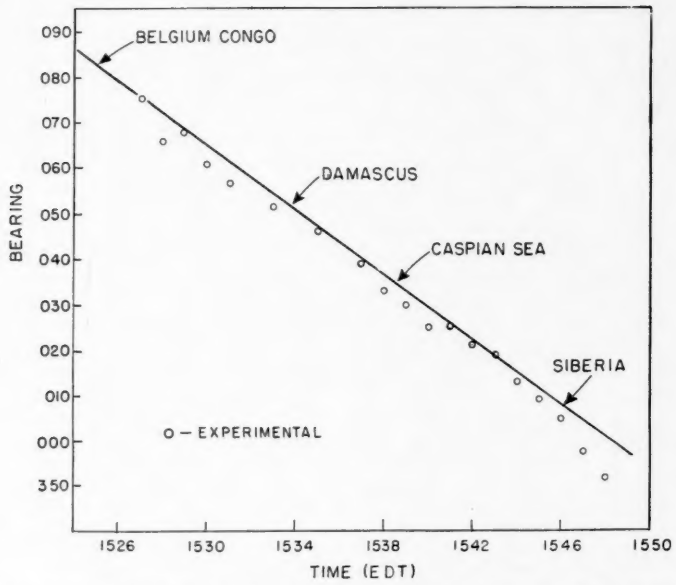

Fig. 9. A comparison of the bearing that was observed, shown as circles, and the bearing that would be expected for a period $\tau = 96{\cdot}0$ min and an inclination $\gamma = 65°$.

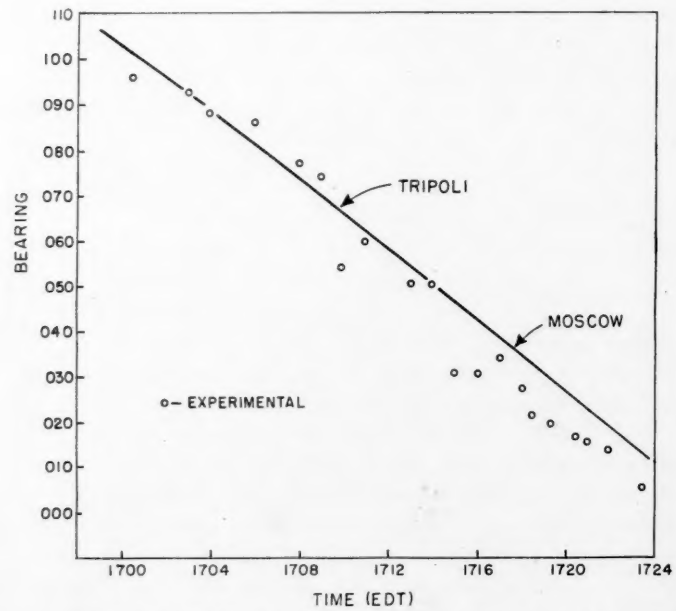

Fig. 10. A comparison of the bearing that was observed, shown as circles, and the bearing that would be expected for a period $\tau = 96{\cdot}0$ min and an inclination $\gamma = 65°$.

VOL
13
1958/

faded out quite rapidly when receding from the receiver due to greater ionospheric attenuation north of Ottawa.

It has been suggested that the anomalies which occurred in Doppler measurements (STANESBY, 1958) may be explained by comparison with bearing data. For example, if the phenomenon was caused by a lateral deviation of the transmission path the bearing would also be affected. If the doppler anomalies were caused by changes in the path length due to a vertical motion of the ionosphere, no corresponding effect would be found in the bearing records.

CONCLUSIONS

The results of tracking *Sputnik I* are:

(1) The period was originally about 96·0 min and by 20 October was decreasing by 3 sec/day.

(2) The inclination of the orbital plane was $66\frac{1}{2}°$.

(3) The precession was westward at 3·0°/day.

The scanty data obtained on *Sputnik II* yields the following estimates:

(1) The period was 104·5 min.

(2) The inclination of the orbital plane was 66°.

It appears that under certain conditions satellites can be tracked quite well using this method. These conditions are:

(1) The distance of nearest approach is less than 1000 miles.

(2) The eccentricity of the orbit is small.

(3) The signal strength must be large enough to obtain steady bearings for several minutes about the time of nearest approach.

VOL. 13 58/59

APPENDIX I

Assume a stationary observer. The track of the satellite will be a great circle. At the point of nearest approach let the angle at the centre of the earth subtended by the observer and the satellite be $\delta°$ (Fig. 11).

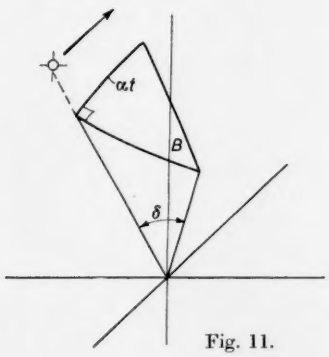

Fig. 11.

Let the angular velocity of the satellite about the earth be $\alpha°$/min.

If we measure time and bearing from the point of nearest approach the spherical triangle can be solved.

$$\tan B = \frac{\tan \alpha t}{\sin \delta}$$

For *Sputnik I* a value of 3·75°/min was used.

APPENDIX II

Let us consider the situation at $t = t_0$. For all calculated values, d_0 was less than 10° and so we may approximate by using two dimensions.

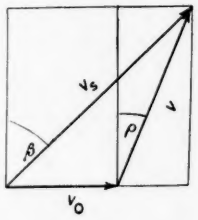

Fig. 12.

Let the satellite have a velocity v_s in the direction β. The observer has a velocity v_0 moving west to east.

v is the apparent velocity in the direction ρ, which the observer will measure (Fig. 12).

From the geometry:

$$\sin\beta = \frac{v_0 + v\sin\rho}{v_s}$$

$$= \frac{v_0}{v_s} + \frac{(v_s^2 + v_0^2 - 2\,v_s v_0 \sin\beta)^{1/2}\sin\rho}{v_s}$$

$$= \frac{v_0}{v_s} + \left[1 + \left(\frac{v_0}{v_s}\right)^2 - \frac{2v_0}{v_s}\sin\beta\right]^{1/2}\sin\rho$$

if $v_0 \gg v_s$

$$\sin\beta = \frac{v_0}{v_s} + \left(1 - \frac{2v_0}{v_s}\sin\beta\right)^{1/2}\sin\rho$$

$$= \frac{v_0}{v_s} + \left(1 - \frac{v_0}{v_s}\sin\beta\right)\sin\rho$$

Rearranging we get:

$$\sin\beta = \frac{\frac{v_0}{v_s} + \sin\rho}{1 + \frac{v_0}{v_s}\sin\rho}$$

For an observer at Ottawa and for *Sputnik I*:

$$\frac{v_0}{v_s} = 0{\cdot}047$$

Acknowledgements—I would like to thank Mr. C. W. MCLEISH for his assistance in all phases of the report and Mr. G. EVANS and Mr. L. COX for their ideas and helpful criticism. I am also indebted to the Russian scientists who made this report possible.

REFERENCES

KEEN R.	1922	*Wireless Direction Finding.*
MCLEISH C. W.	1957	Not yet published.
Staff of Mullard Radio Astronomy Observatory, Cambridge	1957	*Nature, Lond.* **180,** 879.
Staff of Royal Aircraft Establishment, Farnborough	1957	*Nature, Lond.* **180,** 937.
STANESBY H.	1958	*J. Instn. Elect. Engrs.* **105,** 96.
WATSON-WATT R. A. and HERD J. F.	1926	*J. Instn. Elect. Engrs.* **64,** 611.

VOL 13 1958/5

Journal of Atmospheric and Terrestrial Physics, 1958, Vol. 13, pp. 165 to 197. Pergamon Press Ltd., London

RESEARCH NOTES

The correction of sodium twilight glow observations*

(*Received* 27 *January* 1958)

RECENT communications by DONAHUE (1956) and HUNTEN (1957) have treated the problem of correcting observations of the sodium twilight glow for white light by the lower atmosphere. Correspondence between us has shown that there still existed some misunderstandings which confused the matter considerably. This note attempts to clear up the confusion.

The difficulty arises chiefly because DONAHUE had in mind a sodium-vapour detector for use in early twilight (solar depression between 0 and 5°); HUNTEN on the other hand was most interested in a grating spectrometer useful in late twilight (depression greater than 5°). For the latter instrument only, it is possible to determine the correction by an approximate method which is much easier to apply.

VOL.
13
8/59

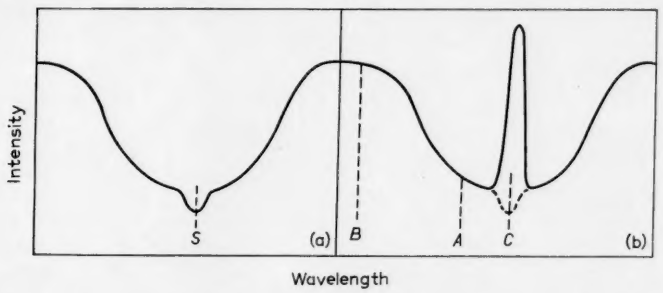

Fig. 1
(a) Schematic representation of the spectral profile of the white light scattered by this lower atmosphere.
(b) The same including the sodium emission line.

Let us consider for simplicity that there is only one *D*-line instead of two; this will not affect the following argument at all. The white light scattered by the lower atmosphere has the spectral profile shown schematically in Fig. 1(a). There is a wide absorption line produced in the solar atmosphere, and a narrow one produced in the earth's atmosphere. DONAHUE's paper was concerned with the latter, since the former is not overwhelmingly important with a sodium-vapour detector.

The fact that the telluric absorption and emission lines are the same shape would greatly complicate the correction procedure if it were not for one fortunate fact. This is that the spectral profile of the white-light component remains the same all through twilight and can be observed by itself in the setting sun.

As a result there is the possibility of applying a direct method of obtaining a correction

* The research reported in this paper has been sponsored in part by the Geophysics Research Directorate of the Air Force Cambridge Research Center, Air Research and Development Command, under Contract AF 19(604)-1831 and in part by the National Science Foundation under Grant NSF-G4531.

for the photometer which HUNTEN has proposed. This avoids the need to apply a theoretical correction following the lines of the calculation presented by DONAHUE.

The instrument used must take two measurements, one at the wavelength of the line and one at a nearby wavelength. Let these readings be called S and C; C is measured at wavelength A by the sodium-vapour detector and at B by the spectrometer (Fig. 1). The true intensity of the line will be called I and that of the continuum R (for Rayleigh). During twilight,

$$S = g_1 aR + cI$$

$$C = g_2 bR + dI$$

in practice one or more of the constants may be zero. The factors g_1 and g_2 are introduced to account for the possibility of different scattering coefficients in the lower atmosphere at the wavelength of the line and the comparison wavelength. For the measurement on the setting sun an attenuation factor k will be introduced and I is zero; then

$$S_0 = kaR, \qquad C_0 = kbR,$$

$$a/b \equiv f = S_0/R_0$$

Now eliminate R from the first expression:

$$I = h(S - fC)$$

$$= H(S - C) + (1 - f)C$$

where $$h = b/(bc - ad)$$

and it is assumed that

$$g_1 = g_2$$

If the absolute value of I is required, then h will be measured with the aid of a suitable standard. The second form of the equation represents the common procedure of measuring the line above the continuum and adding a fraction of the latter.

If the instrument has relatively low resolution it can only be used in late twilight because the effect of the solar absorption line is very large. It is thus permissible to observe the sky just after sunset instead of the sun just before; this presents much less of a problem. But if the observations of the emission are to be made in early twilight this simplified procedure is obviously incorrect.

Caution must be observed in applying this correction particularly with regard to the possibility of variations in sodium distribution in space and time. Strictly the method only applies to the case in which twilight observations are made on the zenith sky. It then allows automatically for the possibility that the solar beam may pass through a region where the sodium abundance differs significantly from that in the region under observation. In other cases, particularly where the direction of observation is out of the plane of the sun's rays, this correction is applicable only when no serious geographical variation in sodium abundance occurs.

The University of Pittsburgh
Pittsburgh, Pennsylvania
T. M. DONAHUE

University of Saskatchewan
Saskatoon, Canada
D. M. HUNTEN

References

DONAHUE T. M. 1956 *J. Atmosph. Terr. Phys.* **9**, 262.
HUNTEN D. M. 1957 *J. Atmosph. Terr. Phys.* **11**, 67.

VOL.
13
1958/5

Radio reflections on low frequencies from 75–90 km height during intense aurora activity

(*Received* 23 *December* 1957)

THE ionosphere at high latitudes is largely influenced by auroral activity. To study the various phenomena such as sporadic layers formed during aurora, oblique auroral reflections and absorption in the lower part of the ionosphere associated with aurora, a number of all-sky cameras are now operating in the north of Sweden and ionosphere recorders, using high speed PPI recording system make simultaneous records of the ionosphere each minute.

The new type of ionosphere recorder constructed at the Uppsala Ionospheric Observatory is now installed at Uppsala and at the new ionospheric station at Lycksele, latitude 64° 37′N and longitude 18° 45′E. The recorder has the following specification:

Frequency range = 0·33–20 Mc/s
Pulse power = 20–50 kW
Recording speed = one 16 mm film picture/min
Recording speed = paper record/3 min

The recorder is operated on a vertical delta-antenna on the range 1·5–20 Mc/s and on a large specially designed low-frequency antenna on frequencies 0·33–1·5 Mc/s.

An all-sky aurora camera is installed at Lycksele and during recent observations a photoelectric cell of multiplier type records the aurora zenith activity.

The study of low frequency reflections down to 0·33 Mc/s was of special interest during the first observations. Generally, reflections from the lower *E*-layer and the *D*-region have been observed by a number of investigators, LINDQUIST (1951) in Sweden, DIEMINGER (1952) in Germany, GARDNER and PAWSEY (1953) in Australia and GREGORY (1956) in New Zealand and others. LINDQUIST has observed reflections associated with aurora from low heights on frequencies somewhat higher than 1 Mc/s.

The inefficiency of equipment and antennae on low frequencies however has made regular observations difficult. Reflections from low layers <100 km have mostly been studied during undisturbed conditions, at lower latitudes but the type of low frequency reflections reported in this note may be of interest, since they only occur when auroral activity is present.

The *first* phase of an auroral situation in the ionosphere is usually characterized by increasing height of the *F2*-layer. In about 100–110 km height an auroral *E*-layer is formed, which is quite similar to the daytime *E*-layer but has greater vertical extension. The critical frequency of this layer may rise up to 7–8 Mc/s and has usually well pronounced ordinary and extraordinary components. Multiple reflections are quite common, thus little absorption below this layer is often observed.

In the *second* phase more absorption takes place, the minimum frequency of the *E*-layer increases and less multiples are recorded. The ionizing corpuscles penetrate to lower regions and auroral forms with ray-structures are often seen at this time.

The *third* phase is characterized by high absorption of radio-waves often resulting in polar black-out and strong, usually red coloured aurorae with ray-structure.

During the second and third phase the low frequency low-height reflections are observed on heights varying between 75–90 km. Figures 1 and 2 give an example of such a situation studied at Lycksele, 25 November 1957. The upper curve in Fig. 1 is the zenith intensity record made with photoelectric cell recorder. The ionospheric data are plotted as a modified *f*-plot so that both the minimum frequency of the auroral *E*-layer, *f*-min *NE* and the

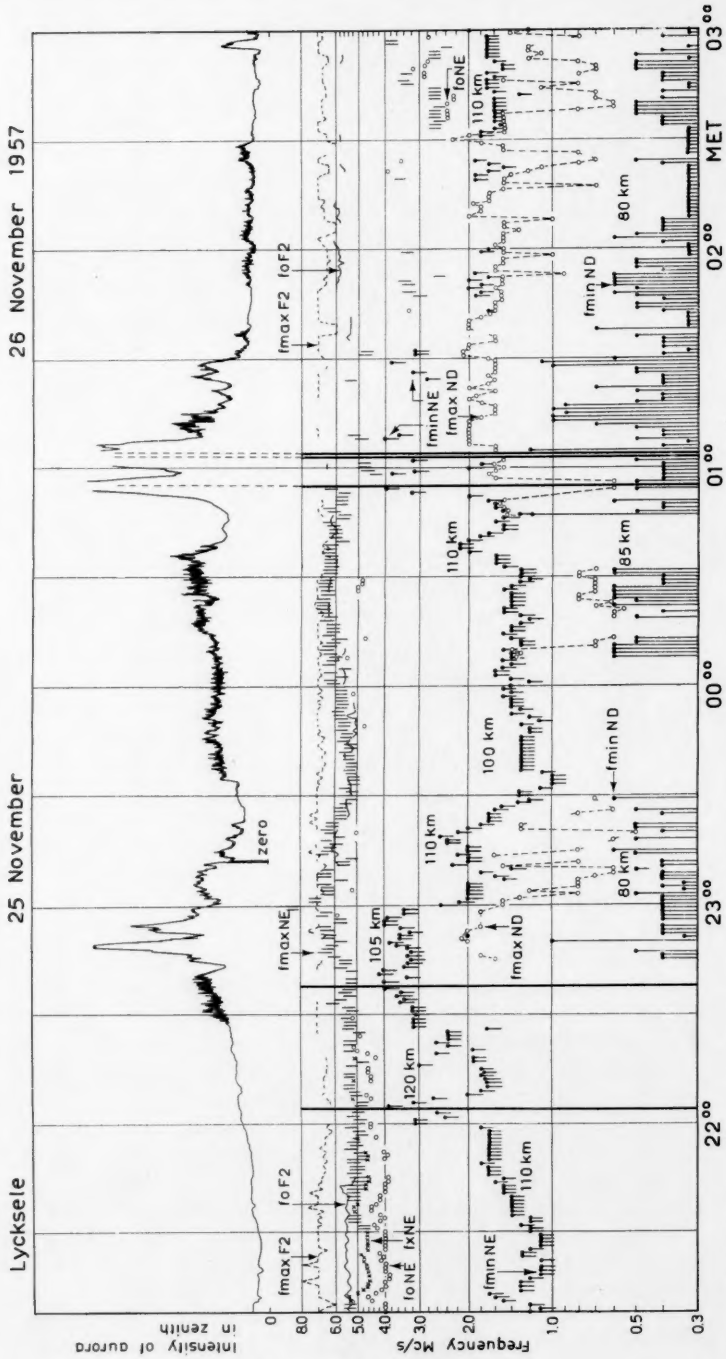

Fig. 1. Diagram showing the occurrence of low frequency reflections *ND* from about 80 km level during strong auroral activity.

VOL.
13
1958/5

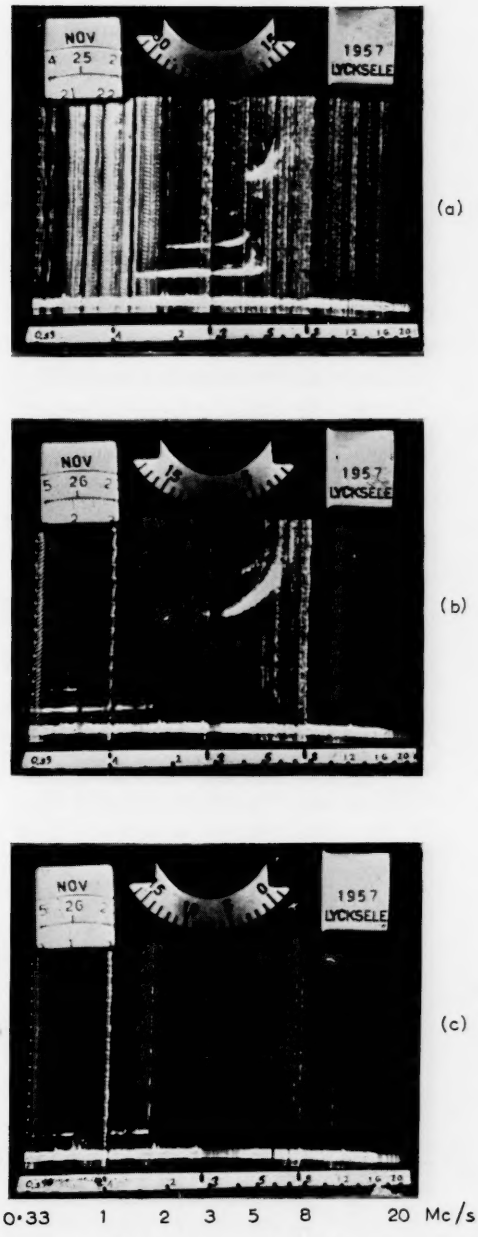

Fig. 2. Ionosphere records showing A: aurora *E*-reflections, B and C: reflections from about 80 km level on frequencies down to 0·33 Mc/s.

VOL
13
1958/

lowest frequency of D-region reflections, f-min ND may be seen. From the diagram it can be seen that the aurora D-reflections from about 80–85 km height, ND appear just when the aurora flames up and when f-min NE shows high values. After this intense phase the ND-reflections continue some time after the decrease of the auroral activity. This tendency is seen after both tops of the zenith intensity curve. It is further observed that the ND-reflections even disappear again when the auroral activity reaches very high values. In Fig. 1 this situation is marked at 0055 and 0103 hours, just at the maximum phase of the aurora.

In Fig. 2 the type NE-reflections are seen on picture A at 2122 hours. The type ND-reflections are seen on picture B at 0209 hours and on picture C at 0107 hours. On picture B the ND-reflections show distinct multiple-reflection and on picture C the NE- and $F2$-reflections are totally absorbed.

This type of low frequency reflections may be explained as coming from a low sharp border of ionization established by particles of high penetration energy. The electron density curve from the NE-layer and down to about 75 km height may be of varying shape. Reflections from the types NE and ND mostly occur in quite separated levels but it happens that ND-reflections merge into the NE-reflections. The maximum electron density in 100 km height during a strong aurora is of the order 10^6 electron/cm^3. For reflections of the actual low frequencies 10^3–10^4 electron/cm^3 are sufficient. The low frequencies therefore penetrate a very small part into the region, thus these reflections can be observed when the higher frequencies are totally absorbed.

Results from a longer series of these observations will be communicated later.

Uppsala Ionospheric Observatory, section of Research Institute of National Defence, Sweden

W. Stoffregen

VOL. 13 58/59

References

Lindquist R.	1951	*Chalmers Tek. Högsk. Handl.* No. 103.
Dieminger W.	1952	*J. Atmosph. Terr. Phys.* **2,** 340.
Gardner F. F. and Pawsey I. L.	1953	*J. Atmosph. Terr. Phys.* **3,** 321.
Gregory J. B.	1956	*Austr. J. Phys.* **9,** 324.

Very long distance ionospheric propagation

(*Received* 10 *February* 1958)

The purpose of this note is to indicate one possible ionospheric refraction condition which allows reception of radio wave energy at considerable distances from the transmitter. This type of propagation, acting in conjunction with the whistler (or magnetic) propagation mode, may permit the detection of identical low frequency radio signals at several "conjugate pairs".

As a model for the subsequent discussion, the earth and its ionosphere may be represented by two concentric, non-magnetic spheres whose radii are r_2 and r_1 respectively (see Fig. 1). The inner surface of the outer sphere, and the outer surface of the inner sphere are reflective. In general, the behaviour of an electromagnetic wave propagating within the spherical shell of thickness $z = r_2 - r_1$, depends upon whether $\lambda \gg z$; $\lambda \simeq z$ or $\lambda \ll z$, where λ = wavelength. For the purpose of this discussion, only the latter condition is of interest.

When $\lambda \ll z$, geometrical ray treatment may be employed for a wave originating at or close to the surface of the inner sphere. With perfect specular reflectors, electromagnetic energy introduced between the spheres is reflected indefinitely. However, there will be some rays, which, because of their angle of incidence upon the outer sphere, pass through the original source, P, after one transit around the shell. For these rays the energy density at any point along the path is the sum of that contained in the forward and backward rays. In essence, a series of multiple images is formed within the shell.

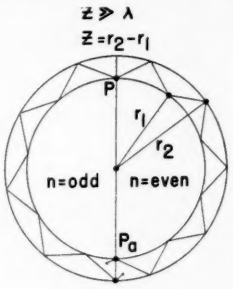

Fig. 1.

Let α = central angle subtended at the centre of the spheres between two successive reflection points. The multiple images formed during one circumferential transit of the ray occur when:

$$n\alpha = \pi \tag{1}$$

is satisfied, where n = integer. An illustration of this condition for a longitudinal section through the source, P, is given in Fig. 1 for n = odd and n = even.

Of particular interest are the rays which leave the source P and impinge on the antipodal point P_a, i.e. those rays for which n is even. With spherical specular reflectors, the rays originating at P remain in the meridional plane containing P_a and the centre of the sphere. The antipodal signal strength depends upon the integrated intensity of all waves passing through P_a, i.e. upon the integrated value of those waves satisfying equation (1) when n is an even integer. Rays whose central angle does not satisfy equation (1) are propagated indefinitely, and intersect P every x transits around the shell, where $2\pi x = m\alpha$, x and m being mutually prime.

The minimum value of n in equation (1) is easily determined for the earth's atmosphere. Considering $z = 100$ km for the E-ionic layer, the tangent ray from the earth subtends a central angle $\alpha = 10°{\cdot}1$, whence, from equation (1), $n = 18$. The maximum value of n for the actual ionosphere is limited by the skip distance and determined by the electron concentration, height of the layer, angle of incidence of the radio ray, etc.

The effect of multiple reflections on the signal intensity at P_a may be easily determined. Neglecting losses other than those arising from incomplete reflection, the final amplitude, I, and initial amplitude I_0 are related by:

$$I = I_0(R)^n = I_0\, R_{\text{eff}} \tag{2}$$

where R = reflection coefficient. The signal attenuation at great distances may be considered to vary as $(1/l)\varepsilon^{-bl}$ where l = path length. The effective reflectivity of the path $R_{\text{eff}} = (R)^n$ is given in Table 1. It is clear that the signal intensity after several transits around the earth may be quite small. The reflectivity of the ionosphere varies considerably but a value of 0·9 or higher may be considered representative for long waves under normal conditions.

VOL
13
1958/

The actual ionosphere and earth depart considerably from the idealized model discussed above. They are neither concentric nor spherical. The ionic layers act at times as diffuse, and on other occasions as specular, imperfect reflectors whose reflectivity varies with space and time. Not only are they spatially heterogeneous, but their condition is a function of time (diurnal, seasonal, period of solar cycle and transient effects arising from solar

Table 1. Effective coefficient of reflectivity after n reflections

n	R_{eff}
1	0·9
5	0·59
10	0·35
15	0·21
20	0·12
25	0·07

$R_{ett} = (0{\cdot}9)^n = R^n$

activity). In addition to regular diurnal and seasonal variations, the layers are subject to strong, short-lived disturbances. Reflection characteristics over the sunlit and dark ionospheres may differ markedly. However, in spite of the numerous defections from the idealized model, it is believed that a sufficient number of low frequency rays may be expected to arrive at P_a to insure reception of the antipodal signal. That such signals propagate around the world has been verified on many occasions.* Some studies have also been made on antipodal signals.†

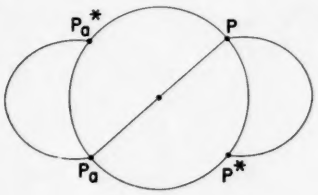

Fig. 2.

It is interesting to determine the antipodal reception possibilities for a frequency of 15 kc/s where $\lambda/z = \frac{1}{5}$. Experience has shown that these reflections are noticeably constant during both day and night, indicating the presence of a stable reflecting layer most of the time. Under these conditions, radiated energy should be detectable at the antipodes. As recent results have shown, the signal also may be received at the magnetic conjugate point P^* via the magnetic mode.‡ Propagation conditions then become similar to those shown in Fig. 2, where P^* and $P_a{}^*$ are the conjugate points of P and P_a, respectively. (Conjugate points are defined as those points on the surface of the earth joined by the same magnetic line of force).

If radio wave energy at a frequency of 15 kc/s is radiated at P by a lightning discharge, some of the energy would be magnetically channelled to P^*, and some focused to P_a.

* (Brown, 1949; Eckersley, 1927; Griffiths, 1947; Hamburger and Rawer, 1947; Hess, 1947, 1948, 1949; Howe, 1927; Hulburt, 1928; Lassen 1948; Quaek, 1927; Quaek and Moegel, 1926, 1927, 1929; Taylor and Young, 1928; von Schmidt, 1934, 1936).

† (Berkner, 1932; CCIR, 1937; Guierre, 1920; Namba, 1931; Round, 1925; Whale, 1956).

‡ (Helliwell, 1956; Morgan, 1956; Storey, 1953).

Under certain conditions, conjugate reception seems to be exceptionally enhanced; it would be interesting to determine the signal strengths observable at the antipodal foci on these occasions.

Propagation between the two modes, of course, may be easily distinguished. The time of arrival for the antipodally focused wave would be of the order of 0·01 sec whereas that arriving by magnetic channelling would be about several seconds. The relative intensity of the antipodal and whistler signals will depend upon the ionospheric conditions existing during the time of propagation. In general, however, the antipodal mode probably has its maximum efficiency when the source is located at low and middle latitudes whereas the whistler mode is most efficient at the higher latitudes. With the antipodal mode, diurnal variations may be rather small except near sunset because of the relative stability of the region reflecting waves at 15 kc/s. Although somewhat high for whistler propagation, this frequency, nevertheless, has been channelled magnetically.

It should be noted that with the actual earth, P_a* and P* would not be antipodal because of the existence of quadrapole moments in the terrestrial magnetic field. However, because of the frequent behaviour of the ionosphere as a diffuse reflector, antipodal signals between P* and P_a* (considered as areas rather than points) may be possible. In the latter case (Whales, 1956) lateral deflexions out of any given meridional P–P_a plane occur.

Vice Chairman, Arctic Committee,
U.S. National Committee for IGY

N. C. Gerson

References

Berkner L. V.	1932	*J. Res. Nat. Bur. Stand.* **8,** 265.
Brown J.	1949	*J. Geophys. Res.* **54,** 367.
CCIR	1937	Document No. 25.
Eckersley T. L.	1927	*J. Instn. Elect. Engrs.* **65,** 600.
Griffiths H. V.	1947	*Wireless Engr.* **24,** 162.
Guierre M.	1920	*C. R. Soc. Fr. Elect.* Ser. 3. **10,** 247.
Hamburger L. and Rawer K.	1947	*Z. Naturf.* **2a,** 521.
Helliwell R. E.	1956	*L. F. Propagation Studies.* Stanford University Rept. TR 56–189.
Hess H. A.	1947	*Z. Naturf.* **1,** 499.
Hess H. A.	1948	*Proc. Inst. Radio Engrs., N.Y.* **36,** 981.
Hess H. A.	1949	*Proc. Inst. Radio Engrs., N.Y.* **37,** 986.
Howe G. W. O.	1927	*Jb. Drahtl. Telegr.* **30,** 42.
Hulburt E. O.	1928	*Proc. Inst. Radio Engrs., N.Y.* **16,** 287.
Lassen H.	1948	*Funk u. Ton* **49,** 420.
Morgan M. G., Dinger H. E. and Allcock G. M.	1956	*Nature, Lond.* **177,** 29.
Namba S., Iso E. and Ueno S.	1931	*Proc. Inst. Radio Engrs., N.Y.* **19,** 2000.
Quaek E.	1927	*Proc. Inst. Radio Engrs., N.Y.* **15,** 341.
Quaek E. and Moegel J.	1926	*Jb. Drahtl. Telegr.* **28,** 177.
Quaek E. and Moegel J.	1927	*Jb. Drahtl. Telegr.* **30,** 41.
Quaek E. and Moegel J.	1929	*Elektrotech. Nachr.* **6,** 45.
Round H. J., Eckersley T. L., Tremellen K. and Lunnon F. C.	1925	*J. Instn. Elect. Engrs.* **63,** 933.
Storey L. R. O.	1953	*Phil. Trans.* **A246,** 113.
Taylor A. H. and Young L. C.	1928	*Proc. Inst. Radio Engrs., N.Y.* **16,** 561.
von Schmidt O.	1934	*Ann. Phys., Paris* **19,** 891
von Schmidt O.	1936	*Z. Tech. Phys.* **17,** 443.
Whales H. A.	1956	*J. Atmosph. Terr. Phys.* **9,** 159.

VOL.
13
1958/5

OL.
13
8/59

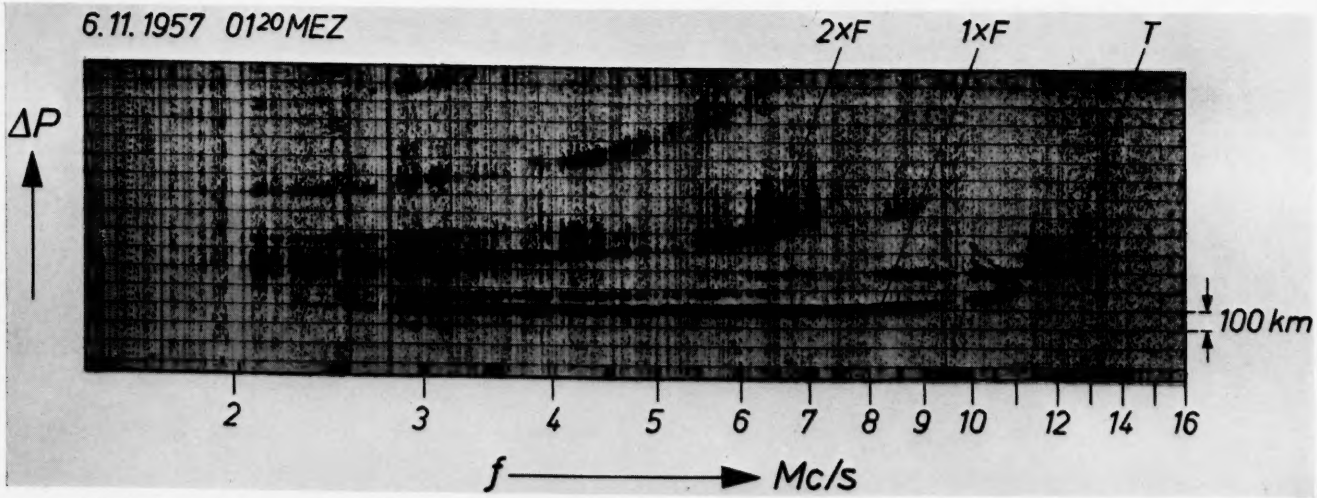

Fig. 1. Sweep frequency record Sondankylä–Lindau (1965 km). 1 × *F* one hop *F*-reflection; 2 × *F* two hop *F*-reflection; *T* trace of unknown origin. [MÖLLER, p. 173.]

VOL.
13
1958/5

Further results of sweep frequency oblique incidence experiments

(*Received* 21 *February* 1958)

SINCE September 1957 sweep frequency measurements are being carried out between Sodankylä 67°22′ N, 26°39′ E (transmitter) and Lindau 51°39′ N, 10°7·5′ E (receiver) over a distance of 1965 km. In a previous research note (MÖLLER, 1956) it was mentioned that over a shorter path of 1320 km echoes extending from the junction point of the high angle and the low angle ray to higher frequencies were observed on 10 per cent of the records at night-time. Over the greater distance of nearly 2000 km these "whiskers" were recorded even more frequently.

In addition records were obtained with a separate trace extending to a frequency 25 per cent higher than the classical MUF. This isolated trace crossing the high angle ray of the $1 \times F$-reflection is marked T in Fig. 1. The traces corresponding to the classical theory are marked $1 \times F$ and $2 \times F$ respectively. These traces are in good agreement with the theory. The vertical critical frequency calculated by the method of the "inverted transmission curve" fits well to the critical frequency f_0F2 observed at the Swedish station Uppsala in the midpoint of the trajectory.

Whilst the "whiskers" (MÖLLER, 1956) were changing in shape from one $\frac{1}{2}$ hr record to the other, the isolated trace seems to be very stable during 2 or 3 hr. It is assumed that it is due to reflections at auroral layers.

Another interesting result of the experiments is that single hop E-reflection is present under normal conditions during daylight. Usually it is thought that the limiting distance for single hop E is approximately 1800 km corresponding to an angle of elevation of 3°, and that the radiation of operational antennae is negligible for smaller angles. It results however from our experiments that even over a distance of 1965 km single hop E gives a distinct trace on the record. That would correspond to an angle of elevation of 2° for the observed height of 110 km. It is not unlikely that some additional atmospheric refraction producing a downward bending of the waves is responsible for the observed effect.

This work was carried out by the Max-Planck-Institut für Aeronomie, Institut für Ionosphärenphysik at Lindau/Harz, in co-operation with the Finnish Academy of Science.

Max-Planck-Institut für Aeronomie H. G. MÖLLER
Institut für Ionosphärenphysik,
Lindau, Germany

REFERENCE

MÖLLER H. G. 1956 *J. Atmosph. Terr. Phys.* **9**, 155.

On instrument effects in ionosphere data

(*Received* 21 *February* 1958)

WHILE variable-frequency measurements of regular ionospheric layers, such as E, F_1 and F_2, are reliable under normal conditions, things are different with the sporadic E-layer. During the last decade, an appreciable amount of observational data of the Es-top-frequency (fEs) has been published by a large number of stations. As is well-known, however, the

usefulness of such data is restricted due to this quantity also being a function of the electric characteristics of the equipment.

From engineering practice it is possible to define three sensitivity curves with respect to frequency for transmitter, receiver and antenna, respectively. ⌜They display more or less abrupt changes and, for the antenna, apparent resonance points and effects on the radiation pattern which may vary from the desired vertical transmission. The pattern may also be affected by variations in the ground-reflection coefficient, caused by the water contents of the ground. The entire frequency range having been subdivided into overlapping ranges each 1 Mc wide, say, sectional integrals indicate the behaviour of the equipment.

The sensitivity characteristics "S" being a function of frequency "f", we have:

$$S = \varphi(f) \tag{1}$$

and integrals:

$$\int_{f_n}^{f_{n+1\cdot0}} \varphi(f)\, df; \qquad \int_{f_{n+0\cdot5}}^{f_{n+1\cdot5}} \varphi(f)\, df$$

where "n" means the lower limiting frequency of the range under consideration, e.g. if $n = 5$, $f_n = 5$ Mc/s, $f_{n+0\cdot5} = 5{\cdot}5$ Mc/s, $f_{n+1\cdot0} = 6{\cdot}0$ Mc/s, etc.

Allowing for discrepancies in the tuning synchronization, the curves or sectional integrals could be combined to one curve, which may be called the "effective ionospheric sensitivity characteristics S_{eff}". This quantity shows a negative deviation where the measurement is adversely affected by non-ionospheric effects. For instance, frequencies measured as being just below such a "dip" may actually be higher.

Technical characteristics required for this method being very rarely made available by ionospheric stations, the author has developed a theoretical adaptation method and checked it during his large-scale propagation investigations (ALBRECHT, 1956; ALBRECHT, 1957), particularly for its applicability to E_s-measurements. The method aims at obtaining the S_{eff}-characteristics from published single values of critical or top frequency. Occurrence sums for single frequencies with respect to frequency show a normal statistical distribution, provided the numbers are statistically sufficient, and dips in the S_{eff}-characteristics appear as deviations from this normal distribution. An adaptation term A indicates the probable amount in megacycles by which a single frequency measurement f_j is too low due to non-ionospheric effects. Thus the frequency measured as f_j may actually be f_j' and

$$f_j' = f_j + A \tag{2}$$

Due to recent calculations:

$$A = \frac{1}{4{\cdot}8}\left[\frac{\exp 2\left(\dfrac{\sigma_1 + \sigma_5 - 2\sigma_3}{3\sigma_1}\right)}{\sqrt{\{\cosh 3{\cdot}2\,(f_{n+1\cdot0} - f_j)\}}} + \frac{\exp 2\left(\dfrac{\sigma_2 + \sigma_6 - 2\sigma_4}{3\sigma_2}\right)}{\sqrt{\{\cosh 3{\cdot}2\,(f_{n+1\cdot5} - f_j)\}}}\right] \tag{3}$$

$f_{n+1\cdot0} > f_j$

where σ_1 = monthly occurrence sum between f_n and $f_{n+1\cdot0}$
σ_2 = monthly occurrence sum between $f_{n+0\cdot5}$ and $f_{n+1\cdot5}$
σ_3 = monthly occurrence sum between $f_{n+1\cdot0}$ and $f_{n+2\cdot0}$
σ_4 = monthly occurrence sum between $f_{n+1\cdot5}$ and $f_{n+2\cdot5}$
σ_5 = monthly occurrence sum between $f_{n+2\cdot0}$ and $f_{n+3\cdot0}$
σ_6 = monthly occurrence sum between $f_{n+2\cdot5}$ and $f_{n+3\cdot5}$

Numerical constants are fundamentally based on experience in communication engineering. In certain cases, monthly occurrence sums may have to be replaced by those during longer periods.

VOL
13
1958/

By this method, published data of several stations have now been investigated, and the majority of their *fEs*-values was thus changed to mutually comparable data.

This new approach will be discussed in detail in a future paper.

H. J. ALBRECHT

Haldenhof 7,
Schramberg-Sulgen,
West Germany

REFERENCES

ALBRECHT H. J. 1956 *J. Wireless Inst. Austr.* **24,** No. 10.
ALBRECHT H. J. 1957 *Geofis. pur. appl.* **38,** 169–180.

The Faraday—rotation rate of a satellite radio signal*

(*Received* 17 *March* 1958)

THE rate of Faraday rotation of a plane-polarized wave transmitted by a satellite is easily measured by recording the amplitude of the signal received with a plane-polarized antenna on the ground. This note describes a simple but surprising property of this rotation rate, for the approximation of a flat earth.

The satellite is assumed to travel at a constant height h and with a constant velocity V. Co-ordinate axes are taken as shown in Fig. 1, with the z-axis vertical, and the x-axis parallel to the satellite path PQ. The receiver O is taken as the origin of co-ordinates, and the ray path OP makes an angle i with the z-axis.

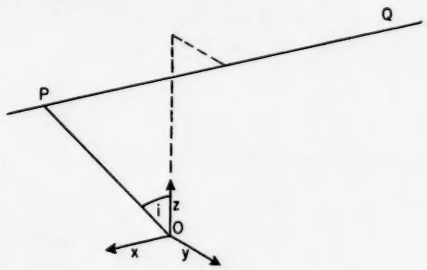

Fig. 1.

The rotation angle α is given by the formula (BROWNE *et al.*, 1956)

$$\alpha = K \int_0^h B_L N(z) \sec \theta \, dz$$

in rationalized MKS units, where

B_L = component of the earth's field along the ray path
θ = angle between the ray path and the vertical
$N(z)$ = electron density at height z
$K = \eta e^3/4\pi^2 m^2 f^2 = 4{\cdot}055 \times 10^{-12}$ MKS units for 108 Mc/s

* The work described in this note was supported by the Research Projects Office of the Army Ballistic Missile Agency under Contract DA-36-061-ORD-577.

and e is the charge on the electron, m its mass, η the intrinsic impedance of free space, and f is the wave frequency. For a flat earth, this formula reduces to:

$$\alpha = KB_L N_T \sec i$$

where N_T = electron density/area column below height h.

The direction cosines of OP are $(x/OP, y/OP, h/OP)$. If the magnetic field vector has components (B_x, B_y, B_z);

$$B_L = (xB_x + yB_y + hB_z)/OP$$

and $\sec i = OP/h$

therefore $\alpha = (KN_T/h)(xB_x + yB_y + hB_z)$

and $\delta\alpha/\delta t = V\,\delta\alpha/\delta x = KN_T B_x V/h$

The rate of rotation is, therefore, constant for a given direction of satellite motion for *any* receiving site, and is proportional to the component of the earth's magnetic field resolved along the satellite path. This holds provided the quasi-longitudinal condition is fulfilled: i.e. provided the ray path is not within 2° of perpendicularity to the magnetic field, for 108 Mc/s frequency.

S. A. Bowhill

Ionosphere Research Laboratory
The Pennsylvania State University
University Park, Pennsylvania

VOL
13
1958/

Reference

Browne I. C., Evans J. V., Hargreaves J. K. and Murray W. A. S. 1956 *Proc. Phys. Soc. Lond.* B **69**, 901.

Solar radiation on decimeter waves as an index for ionospheric studies

(*Received* 17 *March* 1958)

The only index of solar activity usually considered for ionospheric studies is the Wolf sunspot number R. Although the defects of this index have been known for a long time, it is widely used because of its simplicity and the fact that it is available for several solar cycles. Its definition is rather arbitrary and its value depends strongly on the conditions of observation. According to Kiepenheuer (1953) the probable error for a daily value is of the order of 15 per cent and is naturally less (a few per cent) for the monthly mean values.

As a matter of fact the index R has proved to be very useful for solar terrestrial relationship studies considered on a monthly or annual basis, but it has not given very satisfactory results for comparisons made on a daily basis.

Up to now the other solar indices (sunspot areas, corona, plages . . .) which have been proposed and require a more complex work of elaboration, have not brought any better results than the Wolf number.

The aim of this note is to show that the intensity of solar radiation on decimeter waves can probably supply an index of solar activity useful for ionospheric studies on a time scale shorter than the month.

Several daily measurements of solar radiation are now available in the decimetric range, but only the 10·7 cm data of COVINGTON cover a complete solar cycle and are suitable for comparison with the Wolf number.

The mean flux density F radiated daily by the sun on the wavelength 10·7 cm is of course a quantity perfectly defined. The Covington measurements have been very care-

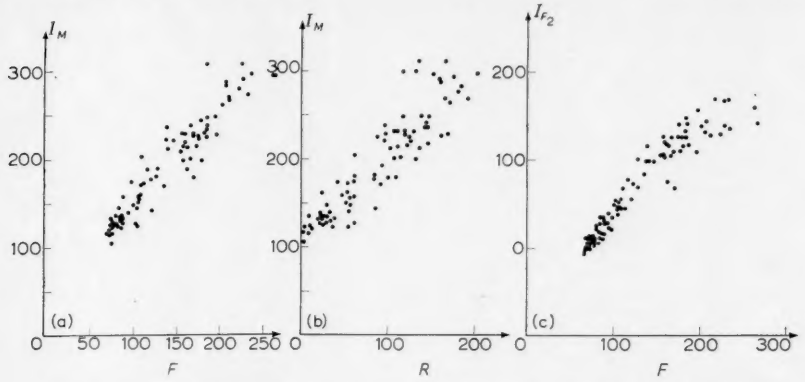

Fig. 1. Correlation diagrams of monthly mean values of solar and ionospheric indices:
(a) E-layer ionization index (I_M) versus 10·7 cm solar radiation expressed in $10^{-22} W/m^2$ c/s (F).
(b) I_M versus Zurich sunspot number (R).
(c) MINNIS's index (IF_2) versus F.

fully calibrated and are probably comparable among themselves with a relative accuracy of the order of a few per cent (MEDD and COVINGTON, 1958). This internal consistency is quite satisfactory for any work of correlation and is much better for F than for R.

In order to check the relative merits of the indices F and R it is necessary to compare their variations with those of ionospheric characteristics related, for instance, to the ionizing flux which produces the ionospheric layers. Unfortunately, there exists no published list of ionospheric indices, either monthly or daily. The amount of work necessary to compute an index related to the F_2-layer ionization being very great, we have limited our comparisons to the ionization index of the E-layer (MITRA, 1952):

$$I = \frac{(f_0 E)^4}{\cos Z}$$

where f_0E is the noon critical frequency of the E-layer measured at Fribourg and Z the zenith angle of the sun.

The comparisons of the indices F and R have first been done on a monthly basis, by taking the monthly mean value of F and R [Figs. 1(a) (b)] and a monthly index I_M calculated according to the above formula, where f_0E is the monthly median of the noon critical frequencies and cos Z is a mean value for the month.

The diagrams of Fig. 1 show that on the monthly basis both indices give comparable results; however they are both better than the sunspot area (DENISSE and KUNDU, 1951).

The comparison of daily values is more difficult because the measurements of f_0E and solar radiation are not done at the same hour UT, and because most of the f_0E values are measured with an accuracy of $\frac{1}{10}$Mc/s which gives for the daily values of I an uncertainty about four times greater than for F. We obviate these two difficulties by comparing the 5-day mean values of these indices.

To get rid, as much as possible, of the errors that might come from the occurrence of

sporadic E-layer we have restricted for each year (1947–1956) our comparison to the 5-day mean values centred on the days 3, 8, 13, 18, 23 and 28 February and March.

The correlation diagrams of Figs. 2(a), 2(b) and 2(c) show clearly that the variations of the E-layer ionization is more closely related to the radio solar index F than to the Wolf number R or to the sunspot area A when the 5 day means are considered.

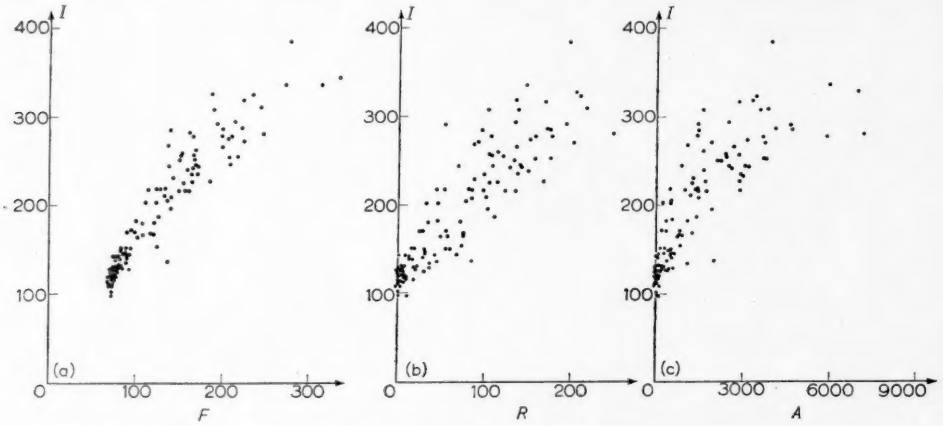

Fig. 2. Correlation diagrams of 5 day mean values of solar and ionospheric indices:
(a) E-layer ionization index I versus 10·7 cm solar radiation (F).
(b) I versus Zurich sunspot number (R).
(c) I versus sunspot area (A).

VOL
13
1958/

Similar comparisons made with an E-layer index (Porto Rico) supplied by the National Bureau of Standards have given identical results.

The correlation diagram between the monthly mean values of F and the monthly mean values of the Solar index IF_2 computed by Minnis (1955) [Fig. 1(c)] shows that both indices have probably the same value as far as F_2-layer studies are concerned.

It can be concluded that the 10·7 cm flux density of the solar radiation is a solar index as good as any for ionospheric studies on a time scale of the order of the month or larger; it is better than the others for comparisons made on a shorter time scale.

There is of course no reason to think that the 10·7 cm solar radiation is the best choice that can be made as a solar index, but the fact that it is simple and well defined, already known for about one solar cycle, and furthermore closely related with ionospheric phenomena claims for its adoption in the place of the Wolf number for most ionospheric studies.

We would like to thank Dr. K. Rawer for supplying the Friebourg data, and the Director of the National Bureau of Standards (Boulder) for giving the opportunity to one of us (J. F. D) to stay at the Bureau, and making available ionospheric indices.

Observatoire de Meudon
Seine et Oise
France

M. R. Kundu
J. F. Denisse

References

Kiepenheuer K. O. 1953 *The Sun* pp. 323–324. University of Chicago Press.
Medd W. J. and Covington A. E. 1958 *Proc. Inst. Radio Engrs. N.Y.* **46,** 112–118.
Mitra S. K. 1952 *The Upper Atmosphere* (2nd Ed.) p. 300. The Asiatic Society.
Denisse J. F. and Kundu M. R. 1957 *C. R. Acad. Sci. Paris* **244,** 45–47.
Minnis C. M. 1955 *J. Atmosph. Terr. Phys.* **7,** 301–321.

Note on short range echoes on ionospheric recorders

(*Received* 25 *March* 1958)

SHORT range echoes of minimum virtual height 40–50 km have been reported from ionospheric recorders for many years, the most recent being by OKAMOTA *et al.* (1957). A summary of these reports was prepared by ELLYETT (1947). MAJOR (1955) pointed out that all stations reporting these echoes were near the sea and that they might be an island phenomena. More recently DOWDEN (1957) investigated these echoes and found that their direction of arrival was near horizontal. He also showed that back scattering from sea waves was the only feasible mechanism which could give echoes of comparable strength to those received.

DOWDEN's suggestion that absence of echoes at night might be an instrumental effect, was examined and found to be correct. Using manual instead of automatic receiver gain control, the echoes appeared at night with, on the average, the same intensity as during the day. Apparently then the absence of these echoes at night is due to the A.V.C. action on the receiver of the considerably stronger incoming radio signals.

Further, when the dead time of the receiver due to the transmitter pulse was altered, the minimum range at which these echoes appeared altered correspondingly. Echoes down to 23 km range were obtained.

Decreased *E*- and *F*-echo strength corresponding to increased sea echo strength has been reported as blanketing. In times of ionospheric disturbance, the lower integrated noise level gives, due once again to A.V.C. action, increased receiver sensitivity so that sea echoes are apparently stronger when ionospheric echoes are weakened.

This work was carried out during the 1957 expedition to Macquarie Island under the auspices of Antarctic Division, Department of External Affairs. Acknowledgement is due to the Ionospheric Prediction Service, Department of the Interior, for the loan of the equipment, a Radio Research Board type J28 ionospheric recorder, and to Professor WEBSTER, University of Queensland, for helpful advice.

N. M. BRICE

University of Queensland,
St. Lucia, Brisbane

REFERENCES

OKAMOTA H., OSE M., AIDA K.	1957	*Rep. Ionos. Res., Japan* **11,** 50.
ELLYETT C. D.	1947	*Terr. Magn. Atmos. Elec.* **52,** 1.
MAJOR G.	1955	*Nature, Lond.* **175,** 862.
DOWDEN R. L.	1957	*J. Atmosph. Terr. Phys.* **11,** 111.

* Formerly Ionospheric Prediction Service, Sydney.

Horizontal drifts and temperature in the lower part of region *E*

(*Received* 10 *April* 1958)

Two main methods have been used to study horizontal movement in region *E*. In the closely spaced receiver "fading method" the velocity of movement of ionospheric irregularities is calculated from the time delays between corresponding maxima and minima in the fading patterns recorded at three receiving sites. In general, vertically incident pulse transmissions at a frequency of about 2 Mc/s have been used. In the meteor method, horizontal movements in the 80–100 km height range have been studied using radar reflections from ionized meteor trails.

The use of CW type signals for investigating the ionosphere is usually limited by the uncertainty concerning the mode of reflection which is being observed and by the possible influence of multiple signals. However, under certain conditions, this uncertainty is practically eliminated and useful measurements can then be made using signals from short or medium wave broadcast transmitters.

Recently at the Department of Physics, University College of Swansea, we have studied movement in the ionosphere using CW signals from a distant powerful broadcasting transmitter which have been reflected at considerable obliquity from the lower part of region *E*. Details of these experiments will be given elsewhere but it may be stated here that apart from the fact that CW signals at oblique incidence are used (in place of pulse signals at vertical incidence), the technique is practically identical with that used in the normal fading method. One of the uncertainties inherent in the fading method concerns the precise level in the ionosphere at which the irregularities responsible for the fading are located since irregularities at any level below that of reflection are possible contributors to the observed fading. This uncertainty is, of course, lessened at lower frequencies, since the degree of penetration of the ionized layer is then correspondingly smaller. In the present experiments the fading of the received signal was characterized by two fairly distinct fading rates. These we term the "slow" and "fast" fading rates and they correspond to about 0·7 fades and 9 fades/min respectively. Horizontal drift velocities have been estimated from both the slow and the fast fading and it is probable that the values obtained will generally refer to two distinct levels in the ionosphere. We now consider some results obtained over the noon period in the summer and winter of 1957 and 1957–8 using this method, in relation to other measurements of *E*-layer movements made in Great Britain.

The results of a long series of measurements at Cambridge using the pulse fading method on 2 Mc/s have been published by Briggs and Spencer (1954). These show that near noon, the mean values of the velocity magnitude (v) and direction (ϕ) are:

$$\text{summer } v = 58 \text{ m/s} \qquad \phi = 87^\circ \text{ E of N}$$
$$\text{winter } v = 71 \text{ m/s} \qquad \phi = 293^\circ \text{ E of N}$$

Recent work (Jones, 1958), indicates that in the case of vertically incident signals at frequencies between 2 and 2·6 Mc/s the ionospheric irregularities responsible for the fading are near the level of reflection. We shall therefore assume that these Cambridge results refer to a level of about 105 km in winter and of about 100 km in summer. These are, of course, only approximate figures but are adequate for the present purposes. Results obtained at Manchester by the meteor method have been published by Greenhow and Neufeld (1955). These workers have shown that the total wind in the meteor region consists of 12-hr, 24-hr and prevailing components and from their results we can estimate the mean total magnitude of the velocity and it's direction at noon. These results show

VOL.
13
1958/5

that for measurements made over the twelve month period September 1954–August 1955, the mean values of v and ϕ at noon are:

summer $v = 11$ m/s $\quad \phi = 145°$ E of N

winter $v = 38$ m/s $\quad \phi = 150°$ E of N

Since these average figures refer to meteors at all levels within the meteor region (80–100 km) we shall assume that they refer to a mean level of about 90 km.

The recent Swansea results, again for the noon period, are:

summer: (i) $v = 19$ m/s $\quad \phi = 191°$ E of N

(ii) $v = 44$ m/s $\quad \phi = 324°$ E of N

winter: (i) $v = 46$ m/s $\quad \phi = 43°$ E of N

(ii) $v = 80$ m/s $\quad \phi = 42°$ E of N

The two sets of results (i) and (ii) refer respectively to the "slow" and "fast" fading mentioned above. In attempting to fix the level to which the Swansea results refer we may be guided by the fact that for the conditions of the experiment, the "equivalent vertical incidence frequency" (MARTYN, 1935) was about 200 kc/s. At noon the level of reflection might thus be expected to be about 90 km so that this will certainly be the upper height limit for the drift results given above and it is to be added that there is evidence that for these low frequency signals the fading level concerned is in fact rather below the level of reflection. We shall tentatively assume that the measurements refer to a height of 80 km. A more precise indication of this level is obtained by considering these results in relation to those of other workers. Figure 1 shows a plot of direction of

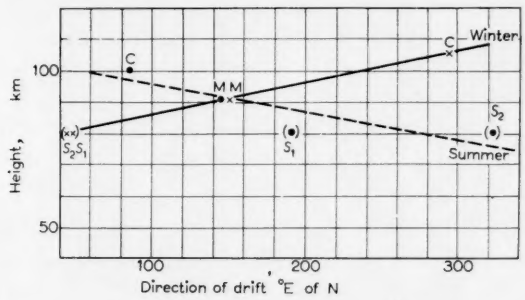

Fig. 1.

drift against height, at noon for the summer and winter seasons. It will be seen that the Cambridge and Manchester results indicate a rotation in the direction of drift with height which is in opposite senses in the two seasons, and that the directions found in the Swansea experiments fit well with this rotation if it be assumed that at winter noon both the slow and fast fading are due to irregularities near the 80 km level, and that at summer noon, the slow component refers to the 85 km level but the fast component to a level of about 75 km. It is to be emphasized that no great accuracy is claimed for these estimates of height but it is relevant to note that recently BANERJI (1955) concluded that the fading of 150 kc/s signals arises from the influence of random *absorption* rather than random scattering by irregularities and at noon, for latitude 40° N, he estimated the level of these irregularities as about 77 km. It would thus appear that in this matter the present experiments are consistent with the results of these long-wave studies in locating the fading centres at a level below the reflection level.

If now we accept the approximate estimates for the levels of the slow and fast fading

given above, and consider the height gradient in the magnitudes of the observed drift velocities, we get the curve shown in Fig. 2. It will be seen that in both seasons the results indicate a distinct minimum in velocity magnitude in the 80–90 km region.

There is now a large body of evidence for a marked temperature minimum near the 80 km level and it seems probable that this minimum in temperature and that in velocity,

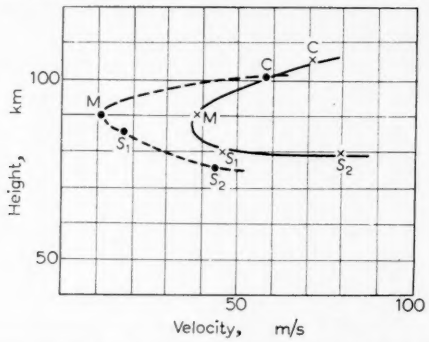

Fig. 2.

indicated by the present work, are not unrelated. In this connexion it is relevant to note that rocket grenade experiments at latitude 30° N have shown that lower down in the atmosphere, a maximum in wind velocity occurs between 50 and 60 km which is also near a level of maximum temperature (Brasefield, 1954). A survey of all available data on temperature has been made recently by Murgatroyd (1957) and from this one finds that, at temperate latitude stations, the winter temperature in the height range 50–80 km is larger than that in summer (in contrast to the seasonal variation at lower heights). It will be seen from Fig. 2 that, in the height range considered (75–100 km), drift velocities in winter are also larger than those in summer. An important factor in determining the magnitude of the horizontal wind velocity in the atmosphere is the horizontal temperature gradient. The fact that the present results indicate that in the high atmosphere there is a correlation between the magnitude of the drift velocity and temperature suggests that, at any particular level, the horizontal temperature gradient is itself related to the actual magnitude of the temperature at that level, larger gradients being associated with higher temperatures. If subsequent work confirms the suggested link between drift velocity and temperature, then the investigation of the vertical structure of ionospheric drifts may prove fruitful in the study of the temperature of the upper atmosphere.

Acknowledgement—This work was carried out as part of the programme of the Radio Research Board of the Department of Scientific and Industrial Research and this note is published by permission of the Director of Radio Research.

W. J. G. Beynon
G. L. Goodwin

Department of Physics
University College, Swansea

References

Banerji R. B.	1955	*J. Geophys. Res.* **60,** 431.
Brasefield C. J.	1954	*J. Geophys. Res.* **59,** 234.
Briggs B. H. and Spencer M.	1954	*Rep. Progr. Phys.* **17,** 245.
Greenhow J. S. and Neufeld E. L.	1955	*Phil. Mag.* **46,** 549.
Jones I. L.	1958	*J. Atmosph. Terr. Phys.* **12,** 68.
Martyn D. F.	1935	*Proc. Phys. Soc. Lond.* **47,** 323.
Murgatroyd R. J.	1957	*Quart. J. R. Met. Soc.* **83,** 417.

VOL.
13
1958/5

A new antenna to eliminate ground wave interference in ionospheric sounding experiments*

(*Received* 13 *April* 1958)

THE radiation fields of a half-wave, horizontal linear antenna, located at the surface of an imperfect earth, have been calculated. These calculations reveal that:

(1) A horizontally polarized field is radiated in the plane normal to the centre of the antenna. This field is maximum in the vertical direction, and consequently is ideally suited for experiments requiring upward radiation. This horizontally polarized field is given by the expression

$$E_{\text{hor}} = \frac{-iI_0}{2\pi}\sqrt{\left(\frac{\mu_v}{\epsilon_v}\right)}\frac{2\cos\theta}{\sqrt{(1/u^2 - \sin^2\theta) + \cos\theta}}\frac{\exp\{i(kR - \omega t)\}}{R}$$

θ is the colatitude angle measured from the vertical and

$$1/u^2 = \frac{\omega^2\mu\epsilon + i\omega\mu\sigma}{\omega^2\mu_v\epsilon_v}$$

This field has been plotted in Fig. 1 for a large value of σ.

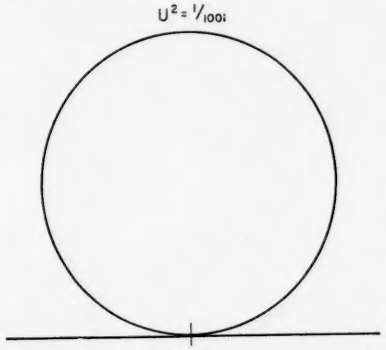

Fig. 1. Radiation pattern of the horizontally polarized field in the plane normal to the centre of the antenna.

(2) A vertically polarized ground wave field is radiated along the axis of the antenna. This ground wave field, plotted in Fig. 2, is zero in the plane normal to the centre of the antenna. This vertically polarized field is given by the expression

$$E_{\text{vert}} = \frac{-iuI_0}{2\pi}\sqrt{\left(\frac{\mu_v}{\epsilon_v}\right)}\left[\frac{2\cos\phi\cos\left(\frac{\pi}{2}\cos\phi\right)}{\sin^2\phi}\right]\left[\frac{\exp\{i(kR - \omega t)\}}{R}\right]$$
$$\left[1 + i\pi w\exp(-\omega) + \begin{matrix}\text{higher}\\ \text{order}\\ \text{terms}\end{matrix}\right]$$

* This research was supported by the U.S. Air Force through the Air Force Office of Scientific Research of the Air Research and Development Command under contract No. AF 18(600)-1552, with the exception of the experimental data, which were obtained in doing research supported by the Office of Naval Research under contract Nonr-220(07).

where w is the "numerical distance" in SOMMERFELD's notation and ϕ is the longitude angle measured about the vertical.*

The radiation pattern of this antenna makes it extremely well suited for ionospheric soundings, since a receiver located in the ground wave null receives only the reflected sky wave signal. Thus complicated electronic circuits to separate the ground wave and sky wave signals are eliminated.

Three antennae have been constructed in order to investigate further the properties of this type of antenna.

(1) The first antenna was a half-wavelength long at 197 Mc/s and was located above dry rocky soil. The radiation pattern of the horizontally polarized field in the mid-plane of the antenna was measured and found to agree closely with Fig. 1. This experiment

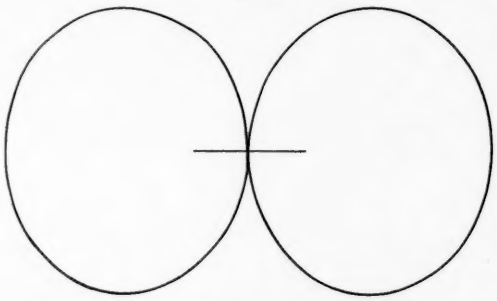

Fig. 2. Radiation pattern of the vertically polarized ground wave at the surface of the earth.

VOL
13
1958/

also provided a measurement of input resistance as a function of height. These data show fluctuations of resistance about 70 Ω for h greater than $\lambda/4$, and as h approaches zero the input resistance increases rapidly. This rise is attributed to increased ground losses.

(2) A second antenna, resonant at 60 kc/s, was approximately 2000 m long and had an average height of 1 m. The current distribution on the antenna was found to be nearly cosinusoidal. The input resistance of the antenna was 127 Ω, 24 of which are attributed to copper losses. By increasing the average height of the antenna to 3·4 m, the resistance representing radiation and earth absorption losses was reduced from 103 to 55 Ω. This change may be attributed entirely to a reduction in the ground losses.

(3) A third antenna was erected at approximately the same site as that of the 60 kc/s antenna. It consisted of a wire 8000 m long, supported about 3·4 m above the ground. Switches were located along the wire so that the antenna could be tuned to different frequencies by opening the appropriate switches. The antenna could be operated at half-wave resonance in the frequency range of 18 to 250 kc/s. The radiation pattern of the vertically polarized ground wave field was measured at the surface of the ground and found to be in excellent agreement with Fig. 2. In the midplane, no fields were found to exist at the surface of the ground. At a frequency of 18 kc/s, the radiation and ground losses were 62 Ω. The measured quality factor Q of the antenna was 12.

The third antenna was used in CW, vertical incidence ionospheric sounding experiments by BERGMAN *et al.* Since the receiver was located in the ground wave null, it received only the reflected sky wave signal. The transmitter was an 800 W, CW generator,

* It is interesting to note that this is a superposition of a wave of the form of the conventional space-wave, which predominates for small values of w, a wave of the form of SOMMERFELD's "surface wave", and the higher order terms which represent corrections for larger w. The "surface wave" component represents essentially two-dimensional energy flow over the surface of the ground with exponential decay with increasing distance due to ground absorption losses.

tunable over a frequency range from 14 to 70 kc/s. The receiving site was located about 64 km from the transmitter, at a point approximately on the perpendicular bisector of the transmitting antenna. The receiving antennae were crossed dipoles about 100 ft long orientated parallel and normal to the line of the transmitting antenna. Since only the downcoming, low-frequency, sky wave was present, these two antennae gave directly the relative amplitudes and phases of the sky-wave components polarized parallel to and normal to the plane of incidence. The geometry of the sites is shown in Fig. 3. The particular spacing and orientation was governed by the geography of the area.

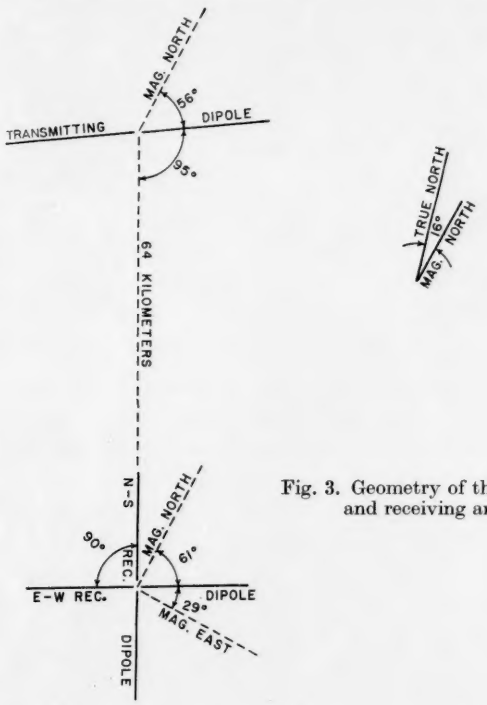

Fig. 3. Geometry of the transmitting and receiving antennae.

In order to obtain data on the reflecting height of the ionosphere, and of changes in this height, a CW signal was transmitted. At the receiving site the phase angle between this received signal and a reference signal of constant phase relationship to the transmitted signal was measured. In order to obtain the reference phase, the two sites were chosen to be within an optical line of site, so that the reference phase could be transmitted between them by a V.H.F. communication channel.

The actual mechanization of the system started from a 50 kc/s crystal oscillator as standard. The oscillator drove the transmitter amplifier directly. At the transmitting site the oscillator frequency was divided down to 1612 c/s and this signal was sent over the V.H.F. link to the receiver. At the receiving site the 1612 c/s signal was multiplied by 27 and 5 to generate two frequencies for the two local oscillators of a double-conversion, superheterodyne, receiver. The receiver output, when receiving the sky-wave signal, was also 1612 c/s. A phase angle measurement between the two 1612 c/s signals then gave directly the desired angle data.

A block diagram of the complete system is shown in Fig. 4. The V.H.F. transmitter operated on a frequency of 30 Mc/s.

VOL. 13 58/59

The receiving site was also equipped with a standard field strength meter to measure the amplitude of the received sky wave. The measured values agree closely with the above equation for E_{hor}.

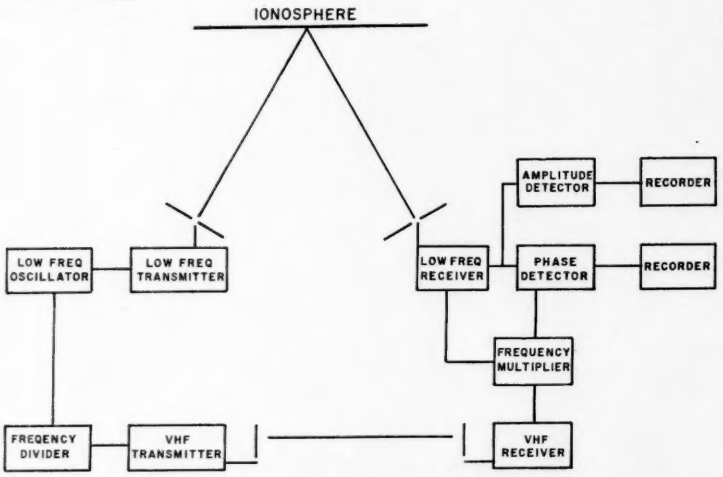

Fig. 4. Block diagram of the transmitting and receiving system.

The magnitude of the ratio of the total field directly above the antenna to the free space field for a relative capacitivity of 6, is plotted in Fig. 5 as a function of the product of frequency and resistivity. This figure is derived from the equation for E_{hor}. Hence for maximum upward radiation at a given frequency, the resistivity of the underlying earth must be as large as possible. The authors intend to construct an 8·4 kc/s antenna

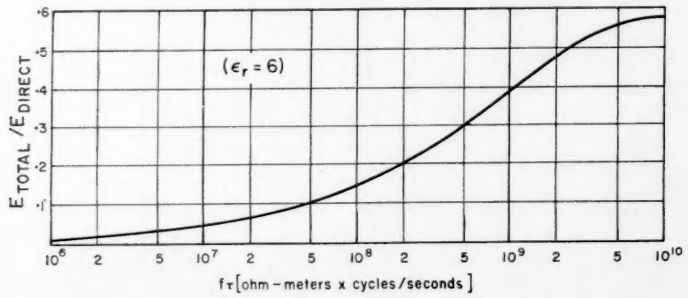

Fig. 5. Magnitude of ratio of total field directly above the antenna to free space field.

for use in V.L.F. propagation experiments. In order to find a site with extremely high ground resistivity, extensive measurements were made throughout Central and Southern California. The areas covered included such extremes in climate as the Mojave Desert and high mountainous terrain. Highest values of ground resistivity were found in geological areas with little faulting in the underlying substructure, while the amount of annual rainfall and other climatic conditions were of little significance. Consequently, a site was selected in the Sierra Nevada Mountains where large areas of relatively unfractured granite were found to exist.

R. S. Macmillan
W. V. T. Rusch
R. M. Golden

California Institute of Technology
Pasadena, California

VOL
13
1958/

The diurnal variation of f_0F2 near the auroral zone during magnetic disturbances

(*Received* 23 *April* 1958)

Introduction

During magnetic storms the critical frequency of the *F2*-layer, f_0F2, usually decreases and this well known effect (Appleton and Ingram, 1935) has been the subject of numerous statistical studies. Separating between disturbed and quiet days, the departure in the critical frequency, Δf_0F2, due to magnetic storms can be studied more closely. It has been shown that the variation in Δf_0F2 can be separated into two components, a S_D-component which depends on local time and a D_{st}-component which depends on storm time (Fukushima, 1949; Martyn, 1951).

The aim of this note is to study the S_D-component for some stations in Scandinavia and Great Britain. It will be shown that the S_D-variation observed at Longyearbyen (80° N) is similar to that observed at middle latitude stations, but the S_D-variation at Tromsö (70° N) is reversed. There is thus an analogy with the latitude effect of the geomagnetic storms, where the S_D-current systems are reversed within the auroral zone (Fukushima, 1953).

Solar Diurnal Variation of the Ionospheric Storm in the *F2*-Layer

Waldo Lewis and McIntosh (1953) have made a statistical study of the S_D-component of Δf_0F2 at Slough. Two conclusions may at once be drawn from their diagrams:

(a) The diurnal mean of f_0F2 decreases with increasing geomagnetic storminess;

(b) During the daytime, Δf_0F2 shows almost sinusoidal variation with approximately one wavelength from sunrise to sunset, and with maximum depression in f_0F2 *before* noon. This means that the difference between the afternoon- and the morning-values of f_0F2 is greater during magnetic storms than during quiet conditions. The amplitude (A) of this "sinus curve" increases with the magnetic activity.

In our study we find that even for single stormdays at a middle latitude station, the mean *afternoon-values* of Δf_0F2, which we shall denote as $\overline{(\Delta f_0F2)}_A$, are usually greater than the corresponding mean *morning-values* $\overline{(\Delta f_0F2)}_M$. In order to treat separate stormdays we define a quantity $\delta \equiv \overline{(\Delta f_0F2)}_A - \overline{(\Delta f_0F2)}_M$ to replace the amplitude A of the "sinus-curve".

The S_D-Component of Δf_0F2 Near the Auroral Zone

The mean diurnal variation of f_0F2 for two disturbed days in October 1956 is shown in Fig. 1 together with the S_Q-values for the same month. It may be seen that f_0F2 is more depressed in the morning than in the afternoon at Slough (55° geom. lat.), Upsala (58° geom. lat.) and Kjeller (60° geom. lat.). At Kiruna (64° geom. lat.) and Tromsö (67° geom. lat.), on the other hand, the depression is greatest in the afternoon.

In order to study this latitude variation of $S_D(\Delta f_0F2)$ more closely, we have computed the mean diurnal variation of Δf_0F2 for geomagnetic stormdays ($\bar{K} \geqslant 4{\cdot}5$) for each season during the period 1951–1957 for Kjeller and Tromsö, and during the period June 1956–August 1957 for Longyearbyen, Spitzbergen (74° geom. lat.). The results are given in Fig. 2 together with the corresponding values for Slough during the period 1947–1951 for days when $\bar{K} \geqslant 3{\cdot}8$ (after Waldo Lewis and McIntosh, 1953). The smoothed curves show that the quasi-sinusoidal variation found at Kjeller is similar to that at Slough, most clearly seen in the summer and the autumn.* At Tromsö the Δf_0F2-curves are also

* The frequently occurring "sporadic *F*"-trace in the night is easily misinterpreted as an *F2*-trace. This may be the reason for the high morning values at Kjeller in the autumn and the winter.

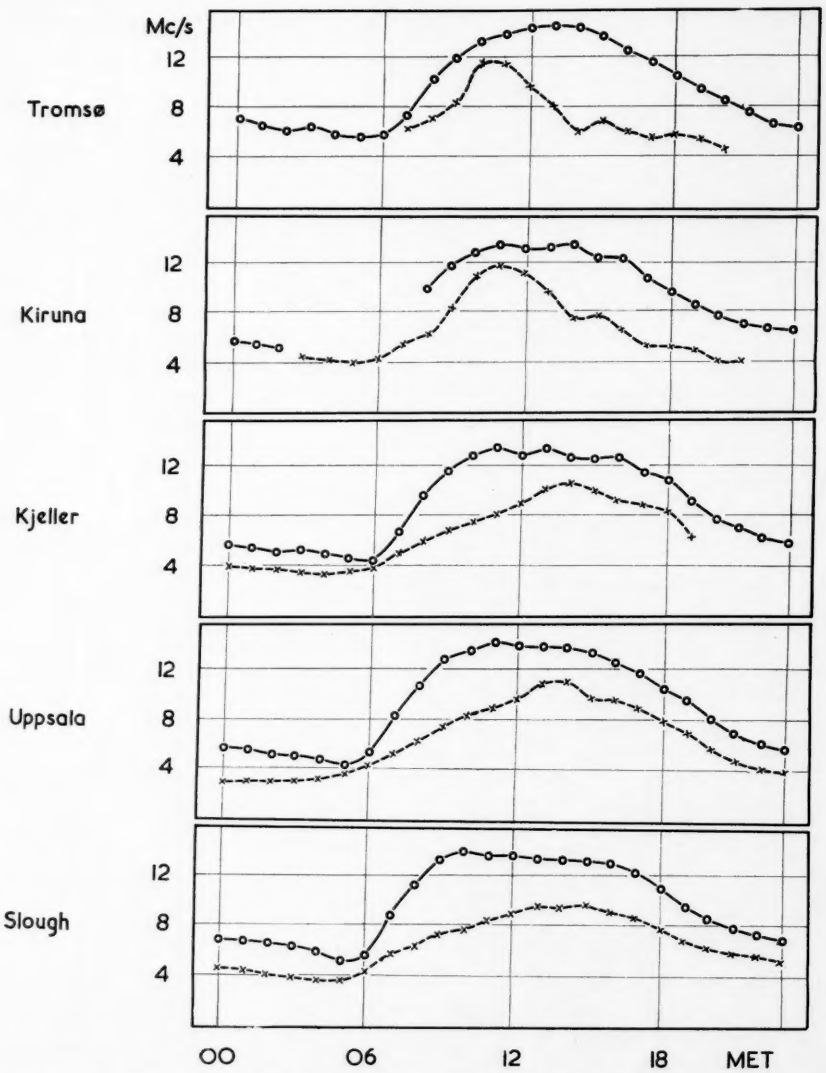

Fig. 1. Mean diurnal variation of f_0F2 in October 1956 during quiet conditions (continuous curves) and during disturbed conditions (broken curves).

"sinusoidal", but the diurnal trends of these curves have been reversed. This effect is most clearly seen during the winter, spring and autumn. Furthermore, we see from Fig. 2 that at Longyearbyen, lying north of the auroral zone, the phase is almost the same as at Slough.

NAGATA and OGUTI (1953) have studied the S_D-component of Δf_0F2 for College, Alaska. This station is lying on the same auroral isochasm as Tromsö. The maximum depression of f_0F2 during magnetic storms was found to occur just *before* local noon. The apparent discrepancy between their results and our results is difficult to explain without making similar investigations for the neighbouring stations in Alaska and Canada.

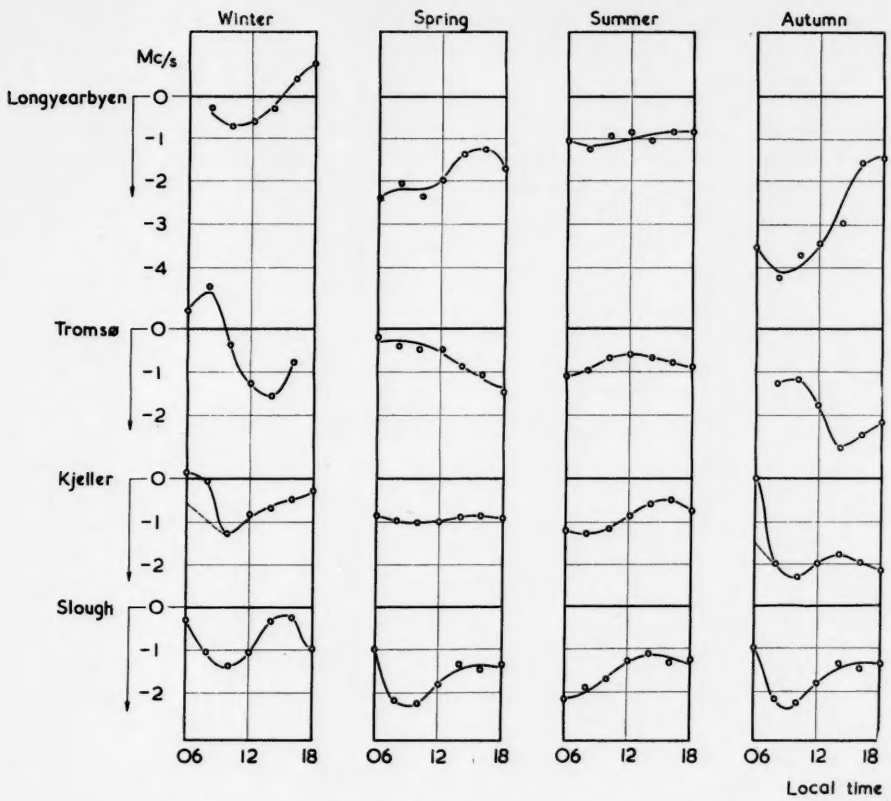

Fig. 2. Mean diurnal variation of $\Delta f_0 F2$ during disturbed days.

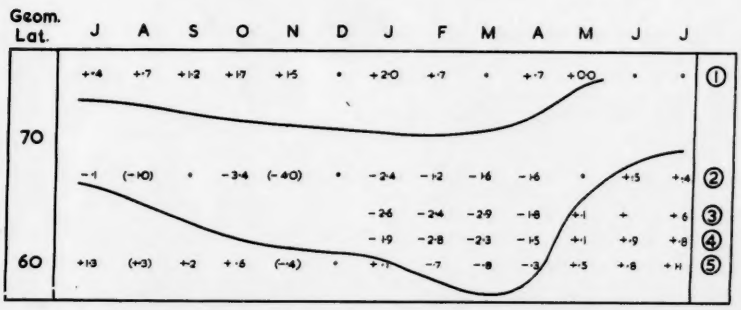

Fig. 3. Seasonal- and latitude-variation of δ during the period July 1956–July 1957. (1: Longyearbyen, 2: Tromsö, 3: Kiruna, 4: Lycksele, 5: Kjeller.)

Figure 2 shows that the phase of the S_D-component of the ionospheric storm is reversed somewhere between Kjeller and Tromsö and somewhere between Tromsö and Longyearbyen. In order to study qualitatively the seasonal variation of the positions of these phase shifts, we have calculated the mentioned parameter δ for each day when $\bar{K} \geqslant 4{\cdot}5$ during the period July 1956–July 1957 for some stations in Scandinavia. The mean monthly values of this parameter are indicated in Fig. 3, and lines are drawn for $\delta = 0$. The phase

shifts ($\delta = 0$) appear to be situated most northerly in the summer and is moving southward in the autumn and the winter. Longyearbyen remains north of the northern phase shift all the year.

In accordance with the results of WALDO LEWIS and MCINTOSH we should expect δ to be correlated with magnetic activity. In our study we found that this was the case only in those months when the station was not near the zones where the phase was shifting. Within the phase-shifted zone the correlation was negative, and outside the zone the correlation was positive.

CONCLUSION

The observed S_D-variations of f_0F2 at Kjeller and at Longyearbyen in daytime are in fair agreement with the variations obtained at Slough, the depression being greater in the morning than in the afternoon during magnetic storms. At Tromsö, on the other hand, the greatest depression occurs in the afternoon. The phase-shifted zone is moving southward in the winter and northward in ths summer.

Acknowledgements—The above work is part of a research project sponsored by the Air Research and Development Command, United States Air Force, under contract AF 61(514)–937.

BERNT MAEHLUM

Norwegian Defence Research Establishment,
Kjeller, Norway

REFERENCES

APPLETON E. V. and INGRAM L. T.	1935	*Nature, Lond.* **136**.
FUKUSHIMA N.	1949	*Rep. Ionos. Res. Japan* **3**.
	1953	*J. Fac. Sci., Tokyo Univ.* Sec. 2, **8**.
MARTYN D. F.	1951	*Proceedings of Second Meeting, Mixed Commission on the Ionosphere*
	1953	*Proc. Roy. Soc.* A **218**.
NAGATA T. and OGUTI T.	1953	*Rep. Ionos. Res. Japan* **7**.
WALDO LEWIS R. P. and MCINTOSH D. H.	1953	*J. Atmosph. Terr. Phys.* **3**, 186.

VOL.
13
1958/5

A peculiar type of periodic fading

(*Received* 24 *June* 1958)

DURING the course of observations on fading patterns of short-wave radio signals transmitted from Delhi on 25·62 m on the 22 March 1958 a peculiar type of pattern was recorded. This commenced from about 0115 hours (I.S.T.) and lasted for nearly an hour. A few of the patterns recorded during this period are shown in Figs. 1–3. The following features of the pattern may be noted.

Shortly before 0115 hours the pattern looked like a slow random type which gradually changed into a rhythmic one at about 0118 hours when the frequency was found to be 16 c/min. Very soon the beat nature of the periodic pattern appeared and at about 0125 hours while the frequency of the periodic pattern was about 17·5 c/min, the beat frequency was 1·28 c/min. The presence of beat indicates the existence of two periodicities of close frequencies. The beat frequency as well as the frequency of the periodic pattern fluctuated, but the beat nature of the pattern continued up to about 0155 hours. At about 0138 hours

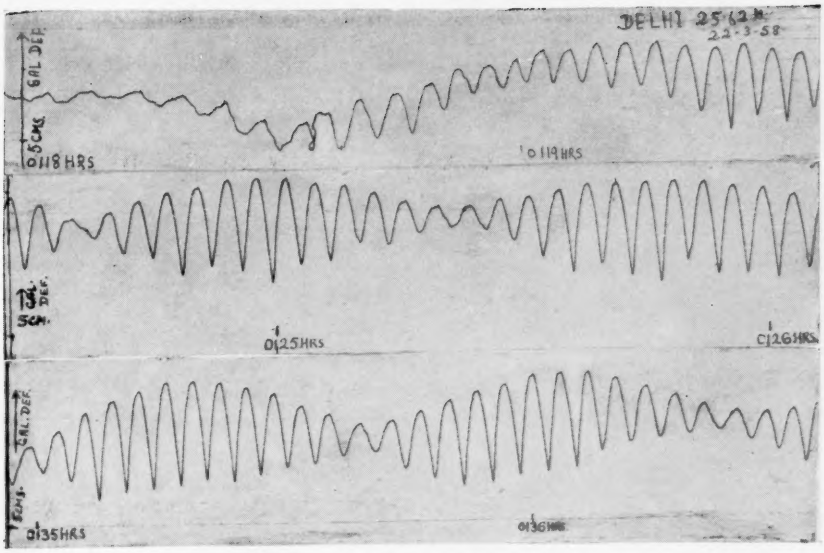
DELHI 25·62 M.
22-3-58
CAL. DEF.
0·5 CMS.
0118 HRS
0119 HRS
1 CM.
SCM.
0125 HRS
0126 HRS
CAL. DEF.
0135 HRS
0136 HRS

Fig. 1.

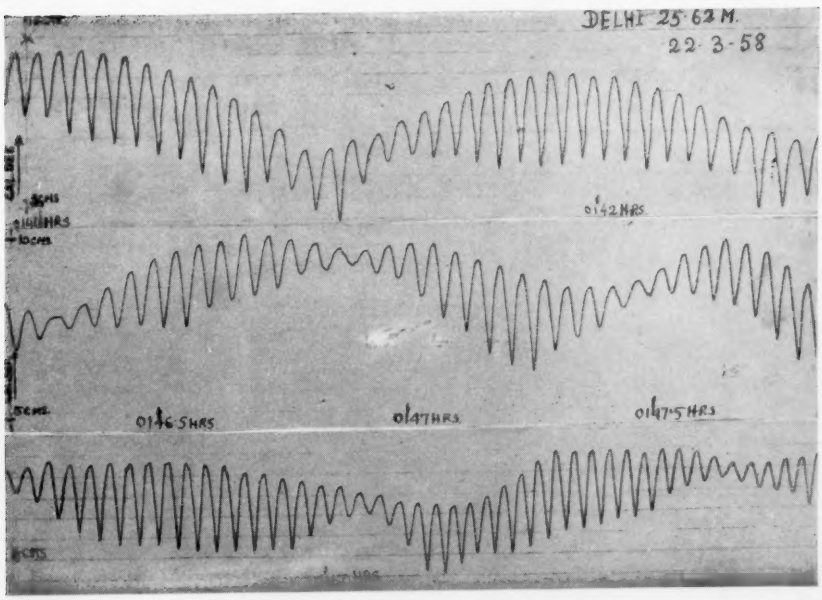
DELHI 25·62 M.
22·3·58
CAL DEF.
0142 HRS
0146 5 HRS
0147 HRS
0147·5 HRS

Fig. 2.

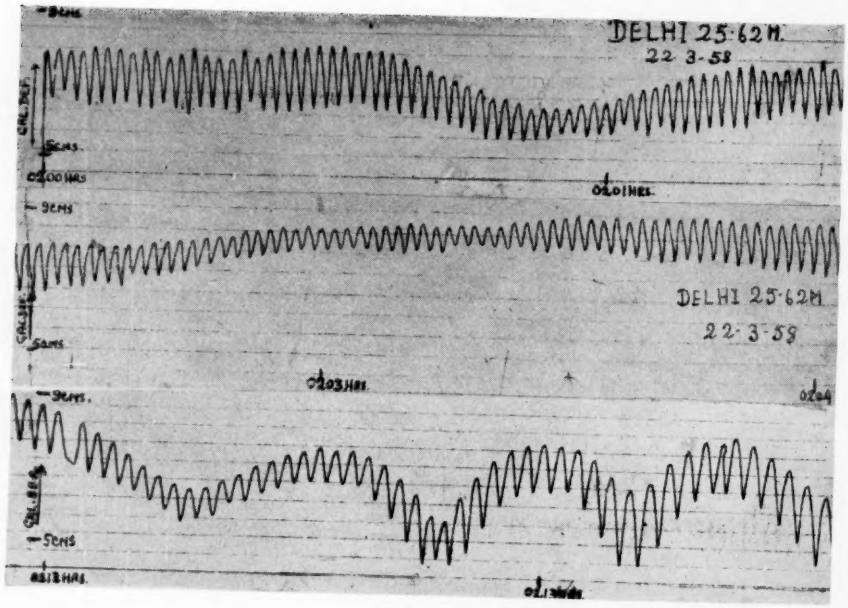

Fig. 3.

VOL.
13
1958/5

an additional periodic undulation appeared, superimposed upon the beat pattern. The former became more prominent at about 0212 hours while the beat feature practically disappeared.

From the available ionospheric data for the date and time concerned, the possibility of interference between singly and doubly reflected rays from the *F2*-layer was examined and found to be small. There was also no possibility of reflections from either the *E*-layer or the abnormal *E*-layer. Under such circumstances, the periodic pattern observed may be considered to be of APPLETON–BEYNON (1947) type, as the frequency of the radio signal for which the fading pattern was recorded was apparently close to the m.u.f. An attempt to receive transmission on 19 m band from Delhi was not successful during the period of observation.

The beat nature of the fading pattern conclusively indicate the existence of two periodicities of close frequencies and hence the presence of three reflected rays. If we consider the additional periodic undulation, we have to assume the presence of a fourth reflected ray. APPLETON and BEYNON (1947) have suggested the possibility of four reflections in case an oblique-ray suffers reflection from *F2*-layer near m.u.f. conditions. The four reflected rays in such a case would correspond to the upper and lower trajectory rays of the ordinary and extraordinary components. It is true that the chances of simultaneous reflections of these four types of rays would be small, but, is possible under favourable conditions. What is, however, more surprising is the long duration of the periodic patterns. The periodic patterns observed by APPLETON and BEYNON (1947) lasted for only 14 min and the time during which two periodicities occurred simultaneously was even less. Some workers, e.g. BANERJEE and SINGH (1948), have no doubt reported the existence of magneto–ionic periodicity for a much longer time, but it was of a very small frequency and of a simple type.

APPLETON–BEYNON type of periodic patterns are usually obtained during morning and evening hours when the electronic-density of the reflecting layer is changing. This explains why they do not last for a long time. It may be suggested, however, that a similar periodic pattern may be obtained if the incident wave has a frequency very close to the m.u.f. of the *F2* layer, and this layer is moving vertically without any appreciable variation in its electronic-density. Under such condition the periodic patterns may last much longer. Further investigations are in progress.

B. N. SINGH
R. L. RAM

Physics Laboratory,
Patna University, Patna, India

REFERENCES

APPLETON E. V. and BEYNON W. F. G. 1947 *Proc. Phys. Soc. Lond.* **59,** 58.
BANERJEE S. S. and SINGH R. N. 1948 *Indian J. Phys.* **22,** 413.

Long-distance single *F*-hop transmission

(*Received 5 July* 1958)

IN 1955 it was predicted by two of the authors (DIEMINGER, 1955; DIEMINGER and MÖLLER, 1956) that the high-angle ray of single *F*-hop propagation should be observable even at distances greater than the limiting distance of the ray radiated tangentially from

the earth. That prediction was based on the relative strongness of the high-angle ray as observed in oblique incidence sweep frequency pulse experiments over a distance of 1300 km. Recently that hypothesis has been confirmed by observations between England and Canada (WARREN and HOGG, 1958), and it has been shown (KIFT, 1958) that the observed traces fit well to the calculated ones. The relatively high field strength of the high-angle ray is clearly demonstrated by sweep frequency pulse transmissions over a path of 2000 km. Series of records taken with different sensitivities of the receiver reveal that during daylight the high-angle ray of the *F1*-path is even stronger than the low-angle ray. Decreasing the sensitivity by 20, 40 and 60 dB respectively (Fig. 1) the "nose" and the high-angle ray is affected least. It has been shown (RAWER, 1956) that under special conditions the attenuation of the high-angle ray caused by spatial divergence is compensated by smaller losses on the shorter way through the *D*-layer. In addition the low-angle ray may suffer more selective absorption on its way through the *E*-layer than the high-angle ray. Apparently these special conditions are prevalent for a time on certain circuits. The difference of attenuation for the high- and low-angle ray in the *D*-layer is demonstrated clearly by records taken during a S.F.E. over a distance of 2000 km (Fig. 2). During the main phase starting at 1333 hours the low-angle ray of the *F1*-path is completely absent owing to the high attenuation on its long way through the enhanced *D*-layer whereas the high-angle ray of *F1*- and the *F2*-path piercing the *D*-layer at steeper angles are much less affected. Full details will be given in a later communication.

Max-Planck-Institut fur Aeronomie,
Institut für Ionosphären-Physik,
(206) *Lindau über Northeim (Hann.), Germany*

W. DIEMINGER
H. G. MÖLLER
G. ROSE

VOL
13
1958/

REFERENCES

DIEMINGER W.	1955	*Colloquium on Radio Propagation, Venice.*
DIEMINGER W. and MÖLLER H. G.	1956	*Nuovo Cim.* N. 4 del Supplemento al Vol. 4, Serie X.
WARREN E. and HAGG E. L.	1958	*Nature, Lond.* **181,** 34.
KIFT F.	1958	*Nature, Lond.* **181,** 1459.
RAWER K.	1956	*C. R. Acad. Sci., Paris,* **243,** 797.

Sudden cosmic noise absorption associated with the solar event of 23 March 1958

(*Received* 15 *August* 1958)

AN unusually large absorption effect (SCA) was observed in our records of cosmic radio noise at 30 Mc/s on 23 March 1958. The effect started at 0955 UT and ended at about 1245 UT as shown in Fig. 1. Several observatories reported solar flares occurring around the time. These are summarized in Table 1.

There are certain unusual features in this SCA effect that encouraged us to examine it in detail. First, the effect was the largest observed in this laboratory and far exceeded 13 dB at the time of maximum corresponding to about $1{\cdot}4 \times 10^4$ dB for $(f + fL) = 1$ Mc/s, and

VOL. 13 58/59

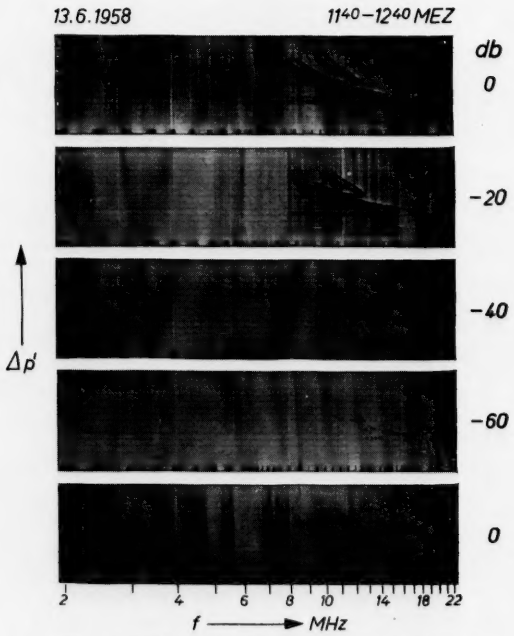

Fig. 1. Oblique incidence ionograms with different sensitivity of the receiver (−0, −20, −40, −60, −0 dB). Distance 2000 km (Sodankylä–Lindau).

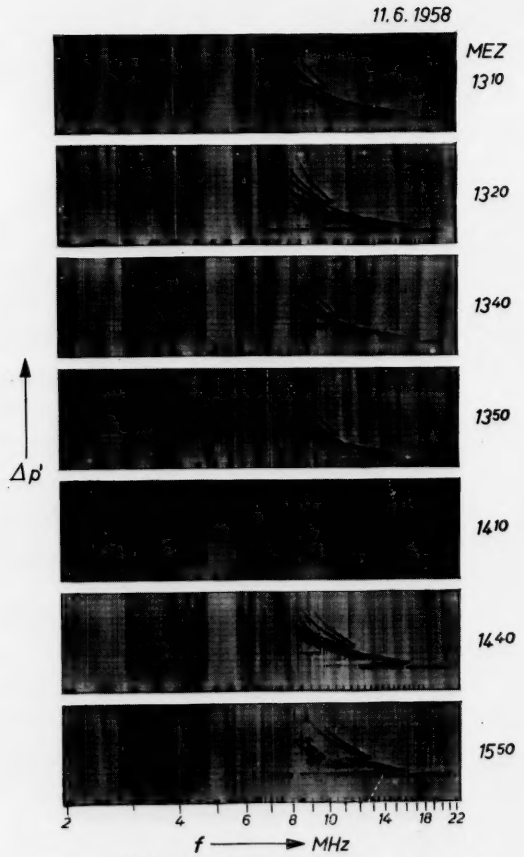

Fig. 2. Oblique incidence ionograms during a Mögel–Dellinger-effect (S.F.E.). Start of S.F.E. at 1333 hours MEZ. Distance 2000 km (Sodankylä–Lindau).

[Dieminger, Möller and Rose, pp. 191–2]

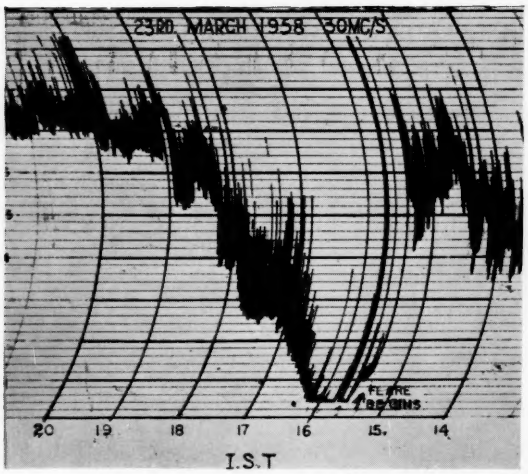

Fig. 1. The record of 30 Mc/s, SCA observed on 23 March 1958 at New Delhi. The constant minimum level between 1010 and 1045 UT is attributed to residual thermal radiation from the lower ionosphere.
[SARADA, pp. 192–4.]

VOL
13
1958/

Table 1. Optical observations of the flare of 23 March 1958

Locality	Class	Time in GMT			Line width of H_α at maximum
		Beg.	Max	End	
Nizamiah	2	1016	1018	1027	3·6
Boulder	3+	b0958	—	1210	—
Wendelstein	3+	0950	1010	1308	—

would therefore indicate an excess absorption some thirty-five times the normal value. Secondly, it was observed that for about $\frac{3}{4}$ hr the recorded aerial temperature was constant at a temperature of about 300°K. This residual radiation we attribute to the thermal radiation from the lower ionosphere such as that reported earlier by PAWSEY and GARDNER

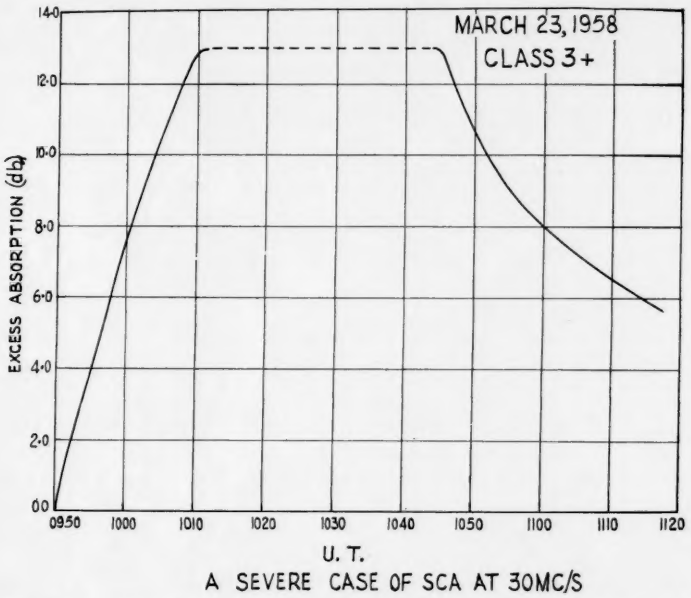

Fig. 2. Excess ionospheric absorption caused by the flare of 23 March 1958 as a function of time obtained from Fig. 1. A correction has been made to eliminate the effect of the thermal radiation from the lower ionosphere.

(1951). Such radiation will remain unaffected while the galactic radiation is blacked out. If T_s be the sky temperature and T_i the temperature of the ionospheric region responsible for this radiation, the observed aerial temperature T_{ob} is given by:

$$T_{ob} = T_s e^{-\tau} + T_i(i - e^{-\tau}) \qquad (1)$$

where τ is the optical depth and is proportional to absorption.

In determining the real variation in absorption, one must therefore deduct the contribution due to T_i from the curve in Fig. 1 in accordance with equation (1). The resulting absorption curve is shown in Fig. 2.

The decay curve was then analysed according to the following equations (APPLETON and PIGGOT, 1954):

$$\frac{dA/dt}{A} = -\alpha(N_f + N_0) \tag{2}$$

$$\frac{1}{A} = \frac{1}{A_0} + \frac{\alpha}{G}t \tag{3}$$

where A is the excess absorption, α the effective recombination coefficient, N_f, and N_0 the value of the electron density during flare and during normal times, and G is the constant of proportionality relating A and N.

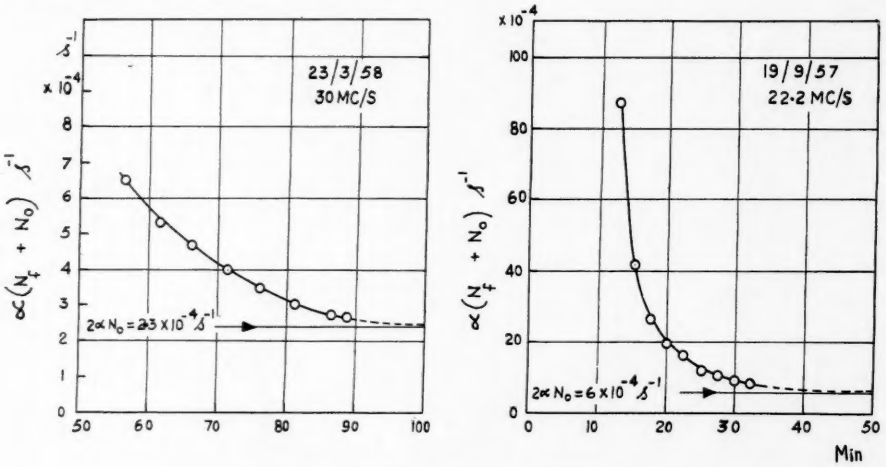

Fig. 3. Values of $\alpha(N_f + N_0)$ for the flare of 23 March 1958.

Values of $\alpha(N_f + N_0)$ so derived are given in Fig. 3. The following points may be noted:

(1) First, the values are abnormally low: being only about 7×10^{-4} sec^{-1} near the peak of the flare and about $2{\cdot}3 \times 10^{-4}$ sec^{-1} at the end. Values normally encountered are shown in the right hand curve of Fig. 3 in which the results of analysis for a flare on 19 September 1957 are shown. In this $\alpha(N_f + N_0)$ falls from a value of about 90×10^{-4} sec^{-1} to about 6×10^{-4} sec^{-1} at the end of the flare.

(2) Secondly, although values of $\alpha(N_f + N_0)$ plotted against $\Delta \log \rho$ give a straight line for an appreciable range, there is some discrepancy between N_f/N_0 (as obtained from Fig. 3) and $(\log \rho)_f/(\log \rho)_0$. The latter value is around 35, while the former has a value between 3 and 4.

It seems possible that a substantial portion of the observed attenuation was due to processes other than collisional absorption.

I wish to thank Mr. R. PARTHASARATHY for his help during the course of the experiments and for valuable suggestions.

National Physical Laboratory, New Delhi-12, India (Miss) K. A. SARADA

REFERENCES

PAWSEY J. L., MCCREADY L. L. and GARDNER F. F. 1951 *J. Atmosph. Terr. Phys.* **1**, 261.

APPLETON E. V. and PIGGOT W. R. 1954 *J. Atmosph. Terr. Phys.* **5**, 141.

VOL. 13 1958/5

Electron density profiles in the ionosphere during the I.G.Y.

(Official communication from the DSIR Radio Research Station, Slough, England)

(*Received* 2 *May* 1958)

In many parts of the world during the last 20 years, regular measurements have been made of the maximum electron density (N_m) and the approximate true height (h_m) of the various layers in the ionosphere. Both these parameters can be obtained fairly easily from the $h'(f)$ curves (ionograms) which are produced by automatic pulse-sounding equipment and tabulated values of N_m and h_m are generally available. On the other hand, only an extremely small amount of accurate information is available on $N(h)$ profiles, the distribution of electron density with height in the ionosphere, and how these profiles vary with time, season and geographical location. It follows that very little is known about the variation of N with time at a constant true height (the $N(t)$ curve). The ionograms contain all this information but the mathematical procedure for deriving an $N(h)$ profile from an $h'(f)$ curve is very laborious, especially if the effect of the geomagnetic field is taken into account. Fortunately electronic computers are now available and they have opened up a new era in this field since they can readily be used to compute $N(h)$ profiles from ionograms.

Table 1.

Observatory	Location	
Slough	51°29′N;	00°34′W
Ibadan	07°26′N;	03°54′E
Singapore	01°19′N;	103°49′E
Port Stanley	51°42′S;	57°51′W

The purpose of this note is to outline the scope of a programme of such computations which has been organized by the Radio Research Station of the Department of Scientific and Industrial Research, at Slough, and which forms part of the United Kingdom programme of observations during the International Geophysical Year. The $N(h)$ profiles are being produced by Ferranti Ltd. on a "Pegasus" automatic digital computer using $h'(f)$ data obtained at the four observatories listed in Table 1.

For each observatory, profiles are being calculated for each hour of the day for about 4 days/month beginning in July 1957. When the ionograms are suitable, Regular World Days are selected for analysis; when this is not practicable, other days are substituted. This programme will be continued until December 1958 when the possibility of extending the work will be considered.

The analysis is carried out according to a method which has recently been described (Thomas *et al.*, 1958) and which makes no *a priori* assumptions about the variation of electron density with height except that it increases monotonically.

Table 2. $N(h)$ profiles (unit of electron density 10^5 cm^{-3})

Port Stanley (*Falkland Islands*) — 27 *July* 1957

h (km)	*Local Mean Time* 0000	0100	0200	0300	0400	0500	0600	0700
420	1·57							
410	1·53	1·68	1·76	1·65	1·78			
400	1·44	1·65	1·73	1·58	1·74			
390	1·28	1·61	1·70	1·46	1·69			
380	1·10	1·50	1·62	1·29	1·60			
370	0·85	1·36	1·50	1·10	1·45			
360	0·40	1·17	1·34	0·81	1·25	1·85		
350		0·82	1·13	0·28	1·03	1·80		
340			0·80		0·50	1·70		
330						1·56		
320						1·36		
310						1·11		
300						0·59	2·07	
290							2·01	
280							1·93	
270							1·77	
260							1·57	3·31
250							1·16	3·14
.								.
200								0·79
.								.
160								0·21
h_mF2	429	415	418	419	412	366	302	263
N_mF2	1·61	1·70	1·79	1·70	1·79	1·89	2·09	3·35
h_0	360	345	335	350	340	295	245	160
N_0	0·40	0·28	0·36	0·28	0·50	0·12	0·28	0·21

Microfilm copies of the tables will be sent to the four I.G.Y. World Data Centres which collect ionospheric data at Boulder, Moscow, Slough and Tokyo. A limited number of booklets containing the tables will also be available.

It can be applied to $h'(f)$ curves from any observatory merely by changing the geomagnetic dip angle and the gyro-frequency, both of which are taken into account in the calculations. A fuller account of the use of a digital computer to carry out the calculations is in preparation and will be available later (Thomas and Vickers, in press).

The production of $N(h)$ profiles is now proceeding on a routine basis and the computer has been programmed to print out the data in the form shown in Table 2 from which either the $N(h)$ or $N(t)$ variations can easily be extracted. It has also been found convenient to have the values of h_mF2 and N_mF2 computed and printed out at the bottom of the tables together with h_0 and N_0, the height and electron density at the base of the E or F layer as appropriate.

VOL. 13 1958/5

References

Thomas J. O., Haselgrove J. and Robbins A. R.	1958	*J. Atmosph. Terr. Phys.* **13,** 46.
Thomas J. O. and Vickers M. D.	1959	The reduction of $h'(f)$ records to $N(h)$ profiles using an electronic digital computer. In press.

Indices of geomagnetic activity

of the Observatories Hartland (*Ha*), Eskdalemuir (*Es*) and Lerwick (*Le*) March to June 1958

The figures given on pages 197 to 199 represent the K-indices for three-hour intervals, beginning with 00–03 hrs for the first and ending with 21–24 hrs for the eighth figure.

March 1958

Day	*Ha* Range for $K = 9 : 500\gamma$		*Sum*	*Es* Range for $K = 9 : 750\gamma$		*Sum*	*Le* Range for $K = 9 : 1000\gamma$		*Sum*	*Day*
	K-Indices			*K-Indices*			*K-Indices*			
1	4101	2112	12	4112	2112	14	3111	2112	12	1
2	1222	2002	11	1122	1112	11	1122	2112	12	2
3	0123	3354	21	1113	3444	21	1112	3465	23	3
4	4443	3343	28	4332	3343	25	6433	3343	29	4
5	3353	3334	27	3353	3334	27	3354	3335	29	5
6	4433	3345	29	4433	3334	27	6532	4434	31	6
7	3433	3333	25	3433	3333	25	3533	2433	26	7
8	4332	3132	21	4333	3233	24	4432	3233	24	8
9	4333	3332	24	4233	3232	22	4333	3332	24	9
10	4322	3333	23	4322	3333	23	4322	3433	24	10
11	4123	3355	26	4102	3354	22	4112	2466	26	11
12	5553	3433	31	6543	3433	31	7854	4444	40	12
13	4443	3342	27	4443	4452	30	6554	5473	39	13
14	3102	5422	19	3111	5522	20	3111	4422	18	14
15	1344	2322	21	2344	2322	22	1333	4342	23	15
16	4323	2223	21	4323	2323	22	5432	2223	23	16
17	3234	4352	26	2234	3441	23	2233	3462	25	17
18	2342	4443	26	2332	4543	26	3433	3665	33	18
19	3344	4455	32	4333	4555	32	4542	5566	37	19
20	5433	3455	32	4443	3455	32	5533	3456	34	20
21	4432	4435	29	4432	4534	29	5431	4455	31	21
22	6322	3224	24	5422	3224	24	7522	3225	28	22
23	4324	3352	26	4324	2352	25	4333	2362	26	23
24	3322	3554	27	2332	3554	27	3433	3576	34	24
25	4333	3544	29	4232	3544	27	6422	4544	31	25
26	2223	4533	24	3223	4533	25	3323	5534	28	26
27	3222	2324	20	3232	2324	21	5232	2324	23	27
28	2232	3433	22	2232	2433	21	2321	1432	18	28
29	3223	3332	21	2222	3332	19	4211	2322	17	29
30	1034	4534	24	1133	5633	25	1133	5644	27	30
31	3333	3332	23	2322	3333	21	3333	3333	24	31

April 1958

Day	*Ha* Range for $K = 9 : 500\gamma$			*Es* Range for $K = 9 : 750\gamma$			*Le* Range for $K = 9 : 1000\gamma$			*Day*
	K-Indices		*Sum*	*K-Indices*		*Sum*	*K-Indices*		*Sum*	
1	3323	3343	24	3322	3343	23	4322	4343	25	1
2	3344	4543	30	3344	4533	29	3333	4434	27	2
3	4332	2344	25	3322	2344	23	5432	2344	27	3
4	3333	4355	29	3333	4465	31	4323	5576	35	4
5	4433	2333	25	3432	3333	24	5433	3334	28	5
6	4223	3334	24	3223	3334	23	5223	4436	29	6
7	2322	3333	10	3322	3333	22	4332	3343	25	7
8	2222	3323	19	2222	2233	18	2322	2333	20	8
9	2311	2222	15	2212	2323	17	2322	2333	20	9
10	1012	1122	10	2122	2222	15	1111	2222	12	10
11	2213	2123	16	2202	2223	15	1202	1212	11	11
12	0012	1222	10	0112	2322	13	0112	1322	12	12
13	1121	1211	10	1212	1222	13	1221	1212	12	13
14	2133	4433	23	2123	4432	21	2113	4434	22	14
15	4442	2343	26	5432	2333	25	5432	2344	27	15
16	3333	3444	27	3233	4444	27	4433	3465	32	16
17	5333	4455	32	5333	4556	34	6543	4667	41	17
18	4543	3445	32	4433	4454	31	5633	4556	37	18
19	3223	3344	24	3333	4444	28	4323	3444	27	19
20	3332	2324	22	2333	3343	24	3331	3334	23	20
21	1322	2324	19	2322	3324	21	2322	3334	22	21
22	2121	2110	10	2222	1210	12	3221	1211	13	22
23	0012	2433	15	0012	2323	13	1112	2433	17	23
24	3341	2322	20	3332	2322	20	3432	3333	24	24
25	4321	3210	16	3322	3210	16	3322	3210	16	25
26	0011	2542	15	0012	2542	16	1112	3442	18	26
27	0121	2343	16	0113	2433	17	1212	2443	19	27
28	3333	3334	25	3323	3334	24	3323	4444	27	28
29	4433	3434	28	4433	3433	27	4443	3443	29	29
30	4343	3334	27	4333	3444	28	4333	3445	29	30

May 1958

1	3233	2444	25	3223	2444	24	5333	3445	30	1
2	3323	2231	19	2322	2232	18	4322	1232	19	2
3	1212	2223	15	1212	2223	15	1212	2223	15	3
4	3222	2123	17	3222	3213	18	3222	2113	16	4
5	2211	1434	18	2211	2434	19	3312	2334	21	5
6	3322	1311	16	3122	2221	15	3322	2221	17	6
7	1221	1123	13	1122	1123	13	1112	1123	12	7
8	2221	3323	18	1112	3333	17	1122	3233	17	8
9	2143	2221	17	2133	3222	18	2133	2121	15	9
10	3224	3443	25	3324	3443	26	3223	3433	23	10
11	0023	3330	14	1133	3331	18	1033	2331	16	11
12	0022	2444	18	1121	2443	18	1022	2435	19	12
13	3233	4434	26	3232	4444	26	4223	4557	32	13
14	5342	3344	28	4343	4343	28	6443	5445	35	14
15	3432	2453	26	3433	3453	28	4532	3444	29	15

VOL.
13
1958/5

May 1958 (*contd.*)

Day	*Ha* Range for $K = 9 : 500\gamma$			*Es* Range for $K = 9 : 750\gamma$			*Le* Range for $K = 9 : 1000\gamma$			*Day*
	K-Indices		*Sum*	*K-Indices*		*Sum*	*K-Indices*		*Sum*	
16	3321	3422	20	3222	3422	20	4422	3431	23	16
17	3423	3343	25	2323	3343	23	3322	4344	25	17
18	4233	3433	25	3222	3433	22	3323	3443	25	18
19	1342	2233	20	2332	3232	20	3332	3232	21	19
20	2111	2122	12	2111	2223	14	3212	2222	16	20
21	3320	1121	13	3222	3221	17	3322	2211	16	21
22	1111	3201	10	1122	3311	14	1122	2211	12	22
23	2100	0120	6	3111	1221	12	2112	1121	11	23
24	0001	2100	4	0112	2211	10	1112	2211	11	24
25	0222	1444	19	1111	2444	18	1112	1334	16	25
26	4333	5424	28	4323	6524	29	4434	7644	36	26
27	3323	4434	26	2223	4434	24	3323	4345	27	27
28	4332	3333	24	4222	3333	22	5431	3333	25	28
29	5444	4542	32	4444	5442	31	5546	5454	38	29
30	3322	2313	19	3322	2313	19	4322	2424	23	30
31	3312	3667	31	2313	4677	33	3433	4678	38	31

June 1958

1	6543	3443	32	8643	3443	35	8753	3455	40	1
2	4334	4430	25	3334	4431	25	5333	5442	29	2
3	0111	2311	10	1121	2321	13	1222	2331	16	3
4	1312	1210	11	1212	1221	12	1212	1221	12	4
5	0122	3411	14	1122	3421	16	1112	3331	15	5
6	0232	2434	20	1233	2434	22	1232	1325	19	6
7	5555	3343	33	7655	4343	37	9955	4333	41	7
8	1112	2443	18	1112	2443	18	2112	1335	18	8
9	4233	3455	29	4233	3445	28	5333	3447	32	9
10	4333	3334	26	4433	4335	29	6633	4435	34	10
11	3333	3333	24	3323	3333	23	4523	3333	26	11
12	1433	3422	22	1323	3422	20	1433	3333	23	12
13	2321	2332	18	2222	2332	18	2221	1332	16	13
14	2122	3154	20	2122	3153	19	2122	2144	18	14
15	2443	3320	21	2344	3221	21	3343	2221	20	15
16	3132	3321	18	3233	3221	19	3223	3321	19	16
17	1211	1111	9	1222	1221	13	1212	1121	11	17
18	0011	3332	13	1012	3332	15	1112	3323	16	18
19	1121	2432	16	1212	3432	18	1112	3332	16	19
20	2001	2223	12	2011	3223	14	2111	2213	13	20
21	3445	5654	36	3435	6654	36	4444	6665	39	21
22	5444	3244	30	5444	4344	32	6554	4234	33	22
23	3321	2331	18	3322	3332	21	3332	2331	20	23
24	3333	2333	23	3333	3334	25	3333	3334	25	24
25	3224	4433	25	3223	4443	25	3323	2443	24	25
26	2222	2322	17	2222	3322	18	3322	3322	20	26
27	2122	1223	15	2222	2223	17	2122	2223	16	27
28	2343	3566	32	2243	3566	31	2333	3458	31	28
29	6653	5432	34	6753	6452	38	8864	7653	47	29
30	2221	1332	16	2222	2332	18	2221	2332	17	30

OL.
13
8/59

Papers to be published in future issues

R. SATYANARAYANA *et al.*: Triple-splitting of the *F*-echoes

E. B. ARMSTRONG: The temperature in the atmospheric region emitting the nightglow OI 5577 line and in regions above faint auroral arcs

R. W. WRIGHT and N. J. SKINNER: Lunar tides in the sporadic *E* layer at Ibadan

C. A. ONWUMECHILLI: A study of the equatorial electrojet—I. An experimental study

C. A. ONWAMECHILLI: A study of the equatorial electrojet—II. A model electrojet that fits *H* observations

H. HELM *et al.*: Measurements of magnetic declination during the solar eclipse of October 23rd 1957

H. A. WHALE: The effects of ionspheric irregularities and the auroral zone on the bearings of short-wave radio signals

M. N. RAO and A. P. MITRA: Effect of vertical drifts on the nocturnal ionization of the lower ionosphere

A. W. HARRISON and A. V. JONES: Observations of Meinel N_2 bands near $1{\cdot}5\mu$ in the auroral spectrum

J. A. THOMAS and E. K. SMITH: A survey of the present knowledge of sporadic *E* ionization

W. R. FRENCH, Jr. and R. L. CHASSON: Atmospheric effects on the hard componeat of cosmic radiation near sea level

C. COLLINS and P. A. FORSYTH: A bistatic investigation of radio-aurora

C. M. MINNIS: Ionospheric changes at Singapore during the solar eclipse of 14th December 1955

A. A. WEISS: The limitations of narrow-beam radio equipments in the detection of weak meteor showers

B. PETERS: Cosmic ray produced radioactive isotopes as tracers for studying large scale atmospheric circulation

R. G. RASTOGI: Geomagnetic influence on the *F1* and *F2* regions of the ionosphere—effect of solar activity

J. W. KING: Ionospheric self-demodulation and self-distortion of radio waves

J. E. TITHERIDGE: Ray paths in the ionosphere. Approximate calculations in the presence of the earth's magnetic field

G. C. REID and C. COLLINS: Observations of abnormal VHF radio wave absorption at medium and high latitudes

L. A. MANNING: Oblique echoes from over-dense meteor trails

B. RAMACHANDRA RAO *et al.*: Study of horizontal drifts in the *F1* and *F2* regions of the ionosphere at Waltair

L. HARANG and J. TRÖIM: Determination of the angle of arrival of auroral echoes

W. N. ABBOT and S. CHAPMAN: On the aurora of 19 August 1950, photographed from Greece

L. THOMAS: Some measurements of horizontal movements in region *F2* using widely spaced observing stations

G. McK. ALLCOCK: The electron density distribution in the outer ionosphere derived from whistler data

R. MONTALBETTI: Photoelectric measurements of hydrogen emissions in aurorae and airglow

C. M. MINNIS and G. H. BAZZARD: Some indices of solar activity based on ionospheric and radio noise measurements

C. H. CUMMACK: Chapman behaviour in the lower ionosphere

G. S. KENT: High frequency fading observed on the 40 Mc/s wave radiated from artificial satellite 1957α

G. S. AITCHISON and K. WEEKES: Some deductions of ionospheric information from the observations of emissions from satellite 1957α2—I. The theory of the analysis

G. S. AITCHISON *et al.*: Some deductions of ionospheric information from the observations of emissions from satellite 1957α2—II. Experimental procedure and results

C. A. VENTRICE and E. R. SCHMERLING: Coefficients for the rapid reduction of *L'–F* records to *N–h* profiles without computing aids

E. L. HAGG *et al.*: Spiral occurrence of sporadic *E*

F. HEPBURN: Interpretation of smooth type atmospheric wave forms

M. W. McELHINNY: Some further analyses of *E* layer measurements in South Africa during the solar eclipse of 25 December 1954

C. S. WARWICK and R. T. HANSEN: Geomagnetic activity following large solar flares

W. H. WARD: On the origin of terrestrial particles from solar flares

V. A. BAILEY: Some possible effects caused by strong gyro waves in the ionosphere—I

M. H. REES: Absolute photometry of the aurora—I

M. H. REES: Absolute photometry of the aurora—II

P. C. CLEMMOW and M. A. JOHNSON: A contribution to the theory of the motion of weak irregularities in the ionosphere

W. J. G. BEYNON and G. M. BROWN: Geomagnetic distortion of region *E*

G. F. WALTON: Calculation of the vertical distribution of atmospheric ozone

N. F. BARBER and D. D. CROMBIE: VIF reflections from the ionosphere in the presence of a transverse magnetic field

L. G. H. HUXLEY: A discussion of the motion in nitrogen of free electrons with small energies with reference to the ionosphere

J. M. MALVILLE: Type *B* aurorae in the Antarctic

W. BECKER: New methods and some results concerning true ionospheric height calculation

B. BANDYOPADHYAY: The early morning *E2*-layer and some evidence of pre-sunrise *F*-layer splitting

W. L. PRICE: Anomalous ionospheric reflection during solar eclipses

J. D. WHITEHEAD: Sudden changes in the virtual height of radio waves reflected from the *E*-region of the ionosphere

M. D. VICKERS: The effect of the *F1*-layer on the calculation of the height of the *F2*-layer

F. MARIANI: A new theoretical model of the composite *F* layer

C. A. ONWUMECHILLI and N. S. ALEXANDER: Variations in the geomagnetic field at Ibadan, Nigeria—I. Solar variations

C. A. ONWUMECHILLI and N. S. ALEXANDER: Variations in the geomegnetic field at Ibadan, Nigeria—II. Lunar and luni-solar variations in *H* and *Z*

VOL
13
1958/

Journa lof Atmospheric and Terrestrial Physics, 1959, Vol. 13, pp. 201 to 204. Pergamon Press Ltd. Printed in Northern Ireland

Triple-splitting of the *F*-echoes

R. Satyanarayana, K. Bakhru and S. R. Khastgir
Banaras Hindu University, Banaras 5, U.P., India

(*Received* 5 *September* 1957)

Abstract—An account is given of the polarization studies made on the triple *F*-echoes, obtained by employing pulses of waves of frequency, 3 Mc/s, at vertical incidence. The polarization studies revealed that the first component after the ground-pulse was the normal extraordinary component having a right-handed sense of rotation, the second component was the normal ordinary component having a left-handed sense of rotation and the third component was the *Z*-component having a left-handed sense of rotation.

In addition to the coupling process suggested by Eckersley and Rydbeck between the ordinary and extraordinary waves, and operative only in high geomagnetic latitudes, the partial reflection and transmission at the level of ionospheric reflection for the ordinary component have been considered as a plausible process for getting the *Z*-component. Since the coupling process is not likely to produce a detectable *Z*-component at low geomagnetic latitudes, the occasional presence of the *Z*-component at low latitudes has been attributed to the partial reflection and transmission process which may take place at all latitudes. The view that the *Z*-component really corresponds to the left-handed ordinary component suffering reflection at the level corresponding to $p_0^2 = p^2 + p \cdot p_H$ has been supported.

1. Introduction

Triple-splitting of the *F*-echoes, which is of a common occurrence in high geomagnetic latitudes, was first observed by Eckersley in 1933. Subsequently triple-splitting was reported by Harang (1936) from Tromso, by Newstead (1948) from Hobart, by Scott (1950) from Clyde River, by Rydbeck (1950) from Kiruna, by Hogarth (1951) from Fort Chimo, and by Landmark (1952) from Oslo. Triple-splitting of the *F*-echoes in low geomagnetic latitudes was first reported by Toshniwal (1935) from Allahabad in India, and recently by Mitra (1955) from Delhi. The polarization measurements of Hogarth (1951) and Landmark (1952) revealed that of the three split components, the first component after the ground-pulse was the normal extraordinary component polarized with a right-handed sense of rotation, the second component was the normal ordinary component with a left-handed sense of rotation and the third component, the so-called *Z*-component, was polarized with a left-handed sense of rotation. These results have been supported in our present experimental studies of polarization of the three split components observed at Banaras (25° 18′ 25″N, 83° 0′ 46″E).

2. Experimental Arrangements

The pulse-transmitter used in these experiments was of a self-excited Hartley-type oscillator, employing an oscillatory valve, Philips Type 2·5/300, capable of generating an output of 135 W under Class C operation. The radio-frequency pulses of short duration were produced by the conventional grid-blocking action. The duration of the pulse was about 150 μsec and the pulse repetition frequency was about 130 pulses/sec. A centre-fed dipole aerial of suitable length with a properly matched transmission line was used with the pulse-transmitter. The echoes were received by a Hallicrafter's Communication Receiver having two *R*/*F* and two *I*/*F* stages and delineated on a Du Mont cathode-ray oscillograph.

For the study of polarization of the echoes, the circularly polarized receiving aerial system of Ratcliffe and White (1933) was employed. This aerial system consisted of a pair of similar "crossed" loop-aerials, 1 m^2, capable of rotation, as a whole, about a common vertical axis. The two loops, which were tuned by means of a pair of two-ganged condensers, were coupled by two pairs of inductance coils placed symmetrically in the two aerial circuits. A commutator was inserted in one of the two loop-aerial circuits to reverse the direction of current flowing in the loop which was connected to the communication receiver. Employing the ground-pulse from the pulse-transmitter, the mutual inductance between the two pairs of coils was adjusted so that the height of the ground-pulse was independent of the orientation of the loop-aerial system. The aerial system then responded selectively *either* to the right-handed component *or* to the left handed component depending upon the position of the commutator.

3. Experimental Results

After the adjustment of the aerial system for the selective reception of either of the two magneto–ionic components, the left-handed or the right-handed echo was received for the "direct" or the "reverse" position of the commutator. When it was necessary to examine both the ordinary and the extraordinary components simultaneously on the oscillograph, the echoes were received on a single loop-aerial only by disconnecting the other loop circuit.

The triple-splitting of the F-echoes observed in these experiments is shown in Figs. 1 and 2. The oscillograms obtained with a single loop-aerial (unpolarized receiver) and with the left-handed and the right-handed polarized aerial system corresponding to the two positions of the commutator are shown one after another in these figures. It can be seen that in addition to the triple F-echoes in the first-order reflection in Fig. 1 and second-order in Fig. 2, the echoes from the sporadic E-region and also a new type of M-echo, shown at the position marked "M," are present. The *left-handed* sense of rotation shown by the M-echo,* which was different from the *right-handed* polarized M-echo of Ratcliffe and White (1933) and the *predominantly* left-handed polarization revealed by the E_s-echo have already been discussed (Satyanarayana, Bakhru and Khastgir, 1956). Besides the usual right-handed extraordinary and the left-handed ordinary components, a third component (the so-called Z-component), showing left-handed polarization, was observed. The component showing the shortest delay and the component in the intermediate position corresponded to the usual extraordinary and the ordinary components.

3. Interpretations of the Observed Triple-splitting of the F-Echoes

In explaining triple-splitting of the F-echoes, Eckersley (1950) and Rydbeck (1950) suggested that at the stage of transition from one mode of propagation to the other there would be a "coupling" between the ordinary and the extraordinary waves. At low geomagnetic latitudes, however, such coupling would be too weak

* The left-handed M-echo observed by us has been called M-ordinary or M_0-echo.

VOL
13
1958/

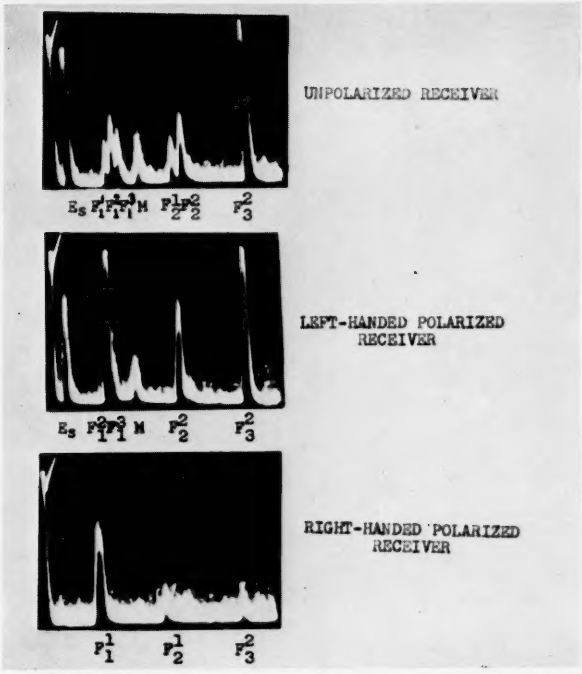

Fig. 1. Echoes from the E_s- and F-regions observed with unpolarized and polarized aerial systems. The oscillogram taken with the unpolarized receiver shows the presence of E_s- and M_0-echoes with evidence of triple-splitting of F-echoes in the first-order of reflection.

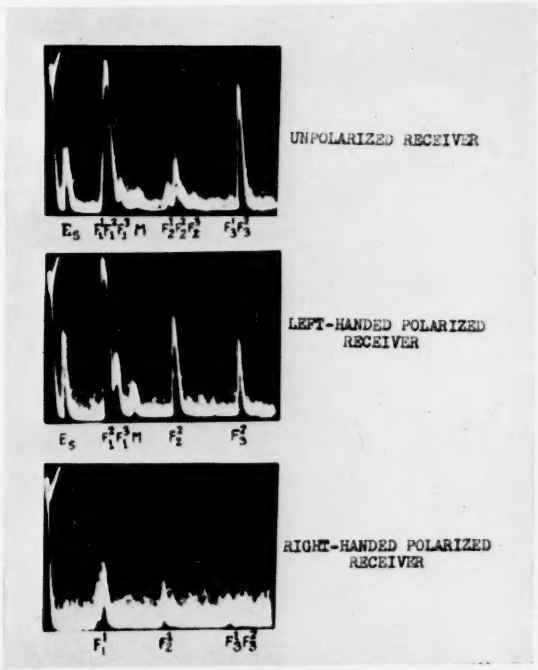

Fig. 2. Echoes from the E_s- and F-regions observed with unpolarized and polarized aerial systems. In the oscillogram taken with the unpolarized receiver there is evidence of triple-splitting of F-echoes in the first- and second-orders of reflection. The oscillograms taken with the left-handed and the right-handed polarized receiver are similar to those in Fig. 1.

VOL.
13
1958/5

to produce triple-splitting. In order to explain the rare occurrence of triple-splitting of F-echoes at low geomagnetic latitudes, RYDBECK indicated that a strong step-like increase in the electron-density could produce a Z-component of recordable strength, although nothing is known as to how such a step-like increase in electron-density could take place.

SCOTT (1950) gave an alternative explanation of the triple-splitting of the F-echoes. According to SCOTT, the triple-splitting would be due to the longitudinal propagation of the part of the incident wave scattered from the layer, as the wave from the transmitting aerial would be incident over a wide angle. This explanation is evidently based on the supposition of scattering centres in the F-region, which finds support from the observations of RIVAULT (1950) and others. According to SEATON (1948) the Z-component was due to the longitudinal propagation of the ordinary wave of APPLETON and BUILDER (1933) in a region of high geomagnetic field. It can be seen that for such explanation, as given by SCOTT and SEATON, to hold there should be a high geomagnetic field.

Recently MITRA (1955) attempted to explain the occurrence of the Z-component in low geomagnetic latitudes. According to him the Z-component is due to the longitudinal ordinary component and he postulates arbitrarily the existence of a very high electron collisional frequency in the F-region for such a longitudinal mode of propagation to take place. In view of the absence of any physical basis for taking a very high value of the electron collisional frequency in the F-region, MITRA'S explanation of the Z-component does not appear to be tenable.

BANERJI (1952) considered the triple-splitting as due to the partial reflection and transmission of the ordinary component. According to him the ordinary component which partially penetrates at its first reflection level, corresponding to $p_0^2 = p^2$, would go up and get reflected at a higher level, corresponding to $p_0^2 = p^2 + p \cdot p_H$. By means of elaborate calculations BANERJI showed that the absorption of the extraordinary component would be extremely large above its reflection level, given by $p_0^2 = p^2 - p \cdot p_H$, thereby ruling out any possibility of the partially penetrated extraordinary component getting reflected from the "fourth condition" level corresponding to $p_0^2 = p^2(p^2 - p \cdot p_H/p^2 - p_L^2)$, or the higher level $p_0^2 = p^2 + p \cdot p_H$. Thus according to this view of partial reflection and transmission, three components are expected, the first two being the usual extraordinary and the ordinary and the third, the Z-component having polarization corresponding to the ordinary.

That the Z-component getting reflected from the level given by $p_0^2 = p^2 + p \cdot p_H$ corresponds to the ordinary wave can be easily understood from the dispersion curves showing μ^2 against the electron-density, N, of the ionospheric layer in the case $y = (p_H/p) < 1$, for the transverse mode of propagation (see BHAR, 1936).

Judging from the above considerations, we are inclined to think that the echo farthest from the ground-pulse is due to the Z-component suffering reflection at the point, given by $p_0^2 = p^2 + p \cdot p_H$, and showing left-handed sense of polarization, when examined with the polarized receiver. The other two echoes are the normal extraordinary and the ordinary components getting reflected from the levels, $p_0^2 = p^2 - p \cdot p_H$ and $p_0^2 = p^2$ respectively. There is therefore no

necessity of assuming a longitudinal mode of propagation in the F-region where the electron collisional frequency ν is usually very much less than the critical collisional frequency ν_c.

It is evident that according to this view the observation of an *ordinary* left-handed echo in addition to the usual ordinary left-handed and extraordinary right-handed echoes is dependent on the condition of partial reflection and transmission at the ordinary level of reflection. Since in partial reflection the intensity is reduced, there is less chance of observing the echoes due to the Z-component along with the two usual magneto–ionic components. In high geomagnetic latitudes, besides this partial reflection process which may occur at all latitudes and which may give rise to an occasional Z-component, the coupling-process, as suggested by Eckersley (1950) and Rydbeck (1950), between the ordinary and the extraordinary waves must be operative, so that the triple-splitting should be more frequently observed in high geomagnetic latitudes than in low latitudes.

Acknowledgements—We wish to thank the Council of Scientific and Industrial Research for grants which have enabled us to carry out this investigation.

References

Appleton E. V. and Builder G.	1933	*Proc. Phys. Soc. Lond.* **45,** 208.
Banerji R. B.	1952	*Indian J. Phys.* **26,** 28.
Bhar J. N.	1936–37	*Sci. & Cult.* **2,** 322.
Eckersley T. L.	1950	*Proc. Phys. Soc. Lond.* B **63,** 49.
Harang L.	1936	*Terr. Magn. Atmos. Elect.* **41,** 143.
Hogarth J. E.	1951	*Nature, Lond.* **161,** 597.
Landmark B.	1952	*J. Atmosph. Terr. Phys.* **2,** 254.
Mitra S. N.	1955	*J. Tele. Comm. Eng.* **1,** 35.
Newstead G.	1948	*Nature, Lond.* **161,** 312.
Ratcliffe J. A. and White E. L. C.	1933	*Phil. Mag.* **16,** 125.
Rivault E.	1950	*Proc. Phys. Soc. Lond.* B **163,** 126.
Rydbeck O. E. H.	1950	*J. Appl. Phys.* **21,** 1205.
Satyanarayana R., Bakhru K. and Khastgir S. R.	1956	*J. Sci. Industr. Res.* B **15,** No. 7, 331.
Scott J. C. W.	1950	*J. Geophys. Res.* **55,** 64.
Seaton S. L.	1948	*Proc. Inst. Radio Engrs., N.Y.* **36,** 450.
Toshniwal G. R.	1935	*Nature, Lond.* **135,** 471.

VOL.
13
1958/5

Journal of Atmospheric and Terrestrial Physics, 1959, Vol. 13, pp. 205 to 216. Pergamon Press Ltd. Printed in Northern Ireland

The temperature in the atmospheric region emitting the nightglow OI 5577 line and in regions above faint auroral arcs

E. B. ARMSTRONG
Department of Applied Mathematics, The Queen's University of Belfast

(*Received* 22 *March* 1958)

Abstract—A number of observations of nightglow and auroral temperatures made with a photoelectric scanning Fabry–Perot interferometer are presented and discussed. The results suggest that the temperature of the region emitting the nightglow λ5577 radiation lies within the range 180° to 220°K, with a most likely value of 190°K. Temperatures measured above faint auroral arcs ranged from 310° to 540°K. The published temperatures of the upper atmosphere obtained spectroscopically are surveyed.

INTRODUCTION

A SERIES of measurements of the width of the OI λ5577 line in the nightglow and above faint auroral arcs was made near Ballyclare, Co. Antrim (lat. 54°47′), during the early part of 1956, using a photoelectric pressure-scanning Fabry–Perot interferometer. The apparatus has been described elsewhere (ARMSTRONG, 1956), and was subsequently improved by replacing the aluminium films on the interferometer plates by three-layer (ZnS—cryolite—ZnS) dielectric reflecting coats. Five-layer coats were not used, because the coating-plant employed at the time was in an experimental state, and the keeping-quality of the five-layer samples which it produced was uncertain. It was, however, realized that at the orders of interference intended for the observations, three-layer coats deposited for the yellow-green would be capable of yielding useful preliminary results. Full details of the performance of the instrument, its calibration and the method of obtaining line width from fringes observed in the presence of background light were presented at the Colloque International de Spectroscopie Interférentielle organized by the Centre National de la Recherche Scientifique, Bellevue, Paris, in September 1957, and are to be published. A summary of the results is given below with the best examples of the observations, and some aspects of the results are discussed in conjunction with results obtained by other investigators using spectroscopic methods.

OBSERVATIONS

Figure 1 shows the arrangement of the apparatus schematically, the design being based on the system originated by JACQUINOT and DUFOUR (1949). Two orders of interference were used, 45,500 and 150,600, the spacers consisting of three steel balls for the former and a Hilger quartz spacer-ring for the latter. A mercury manometer indicated the chamber pressure in the case of the low order, and a water manometer in the case of the high order. The chamber pressure was raised with a hand pump, and the observing procedure generally consisted in allowing the pressure to fall in steps, a reading of the photon count on the rate-meter being taken at each pressure value. The scanning speed was limited by the

integrating time necessary for suitably accurate photon counting in the case of the nightglow, two fringes being recorded in about 30 min, and by the time required to change the pressure and read the manometer and ratemeter in the case of aurorae. Only steady aurorae, such as faint green arcs or glows could be observed successfully in this way. The instrument was checked after each observing run either visually or by a run using a G.E.C. water-cooled mercury-198 lamp as source.

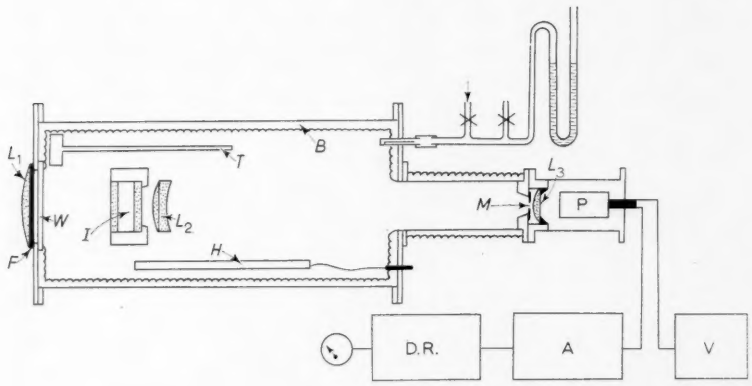

Fig. 1. Schematic arrangement of the pressure-scanning Fabry–Perot interferometer. L_1: Simple lens for de-focusing stars; F: Ilford 110 gelatine filter; W: glass window; I: etalon; L_2: telescope objective; T: thermostat: H: heater; B: heat-insulating lining; M: scanning mask; L_3: field lens; P: photomultiplier; V: high-voltage pack; A: simple pulse amplifier; D and R: Ekco Ratemeter Type 1037 A_2 with discriminator.

In all observations the instrument pointed NNW at a zenith distance of about 70°. The diameter of the field was about 5°, a value set by the focal length of the lens L_1, Fig. 1, whose purpose was to prevent the focusing of the stars on the scanning aperture and to widen the field. In the auroral observations the green arcs were always low in the northern sky, below the level of the centre of the field, so that the region under observation was taken to be just above the arc in each case. The glow observations were made when the arcs were below the horizon.

Figures 2(a), 2(b) and 2(c) show examples of a nightglow, an auroral and a checking run respectively. The fringes from the sky were subsequently re-plotted to eliminate the effect of changing background light intensity and, where necessary, fringe intensity during the run, provided that the changes were continuous. The resulting fringe profiles between maximum and minimum intensity were matched to corresponding calculated fringe profiles for various line widths and the instrumental parameters of the apparatus. The latter included the effective reflecting power of the etalon coats, and this was determined by observation of the fringes from the ^{198}Hg λ5461 line of the isotope lamp at both the orders used.

Table 1 shows the results, the temperature obtained from each fringe in a run being given, thus illustrating the magnitude of the errors arising in the apparatus and the drawing of the fringes.

VOL
13
1958/

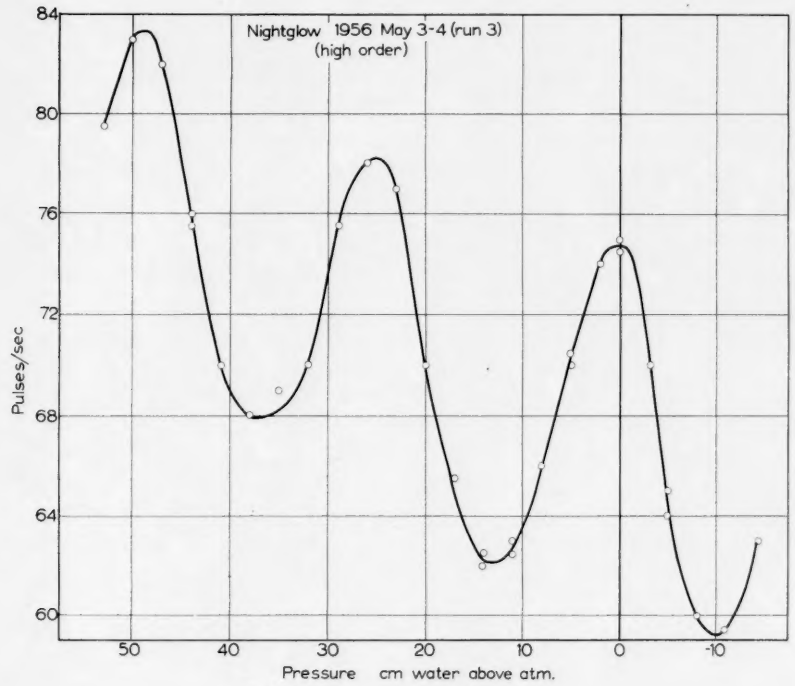

Fig. 2. (a) Nightglow 5577 fringes.

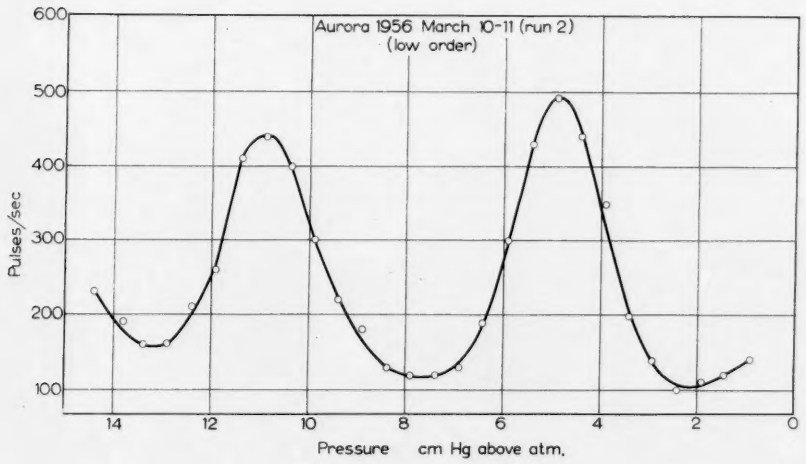

Fig. 2 (b) Aurora 5577 fringes.

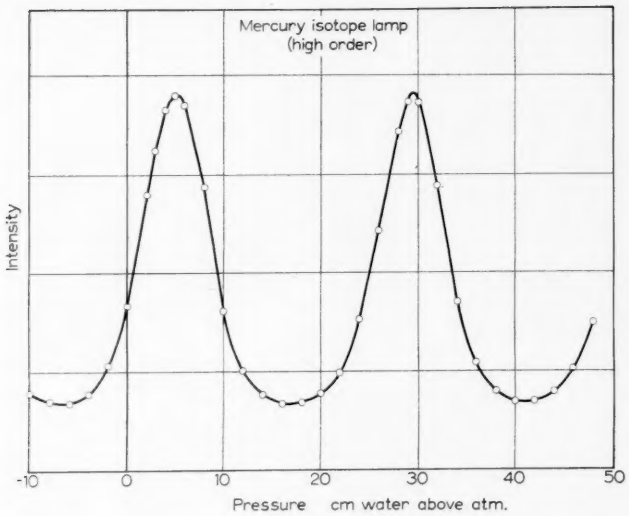

Fig. 2 (c) ^{198}Hg 5461 fringes.

Table 1. Nightglow OI λ5577

Low order		
1956 14–15 Feb.	Run 1 (01·14–02·00 UT)	Fringe 1: 210°K Fringe 2: 235°K
	Run 2 (03·55–04·36 UT)	Fringe 1: Incomplete Fringe 2: 150°K (distorted)
1956 5–6 March	Run 1 (00·15–00·25 UT)	Fringe 1: Incomplete Fringe 2: 235°K
	Run 2 (00·50–01·30 UT)	Fringe 1: Incomplete Fringe 2: 180°K
High order		
1956 13–14 April	Run 1	Unsuccessful
	Run 2 (02·35–03·00 UT)	Fringe 1: 180°K Fringe 2: 180°K
1956 15–16 April	Run 1 (02·00–02·45 UT)	Fringe 1: 220°K Fringe 2: 190°K
1956 3–4 May	Run 1 (00·31–00·50 UT)	Fringe 1: 210°K Fringe 2: 180°K (distorted)
	Run 2 (00·54–01·13 UT)	Fringe 1: 190°K Fringe 2: 210°K
	Run 3 (01·18–01·45 UT)	Fringe 1: Incomplete Fringe 2: 190°K Fringe 3: 190°K

Table 1. (*contd.*) OI λ5577 in faint aurorae

Low order		
1956 16–17 Feb.	Run 1	Unsuccessful
	Run 2	Unsuccessful
		Glow
	Run 3 (02·25–02·58 UT)	Fringe 1: Disturbed
		Fringe 2: 385°K
		Fringe 3: 385°K
1956 10–11 March	Run 1	Unsuccessful
		Diffuse arc
	Run 2 (23·28–23·48 UT)	Fringe 1: Disturbed
		Fringe 2: 440°K
		Fringe 3: 510°K
		Glow
	Run 3 (02·34–02·52 UT)	Fringe 1: Disturbed
		Fringe 2: 540°K
High order		
		Arc
1956 16–17 April	Run 1 (23·44–00·05 UT)	Fringe 1: Incomplete
		Fringe 2: 310°K
	Run 2	Unsuccessful
		Arc
	Run 3 (00·27–00·42 UT)	Fringe 1: Incomplete
		Fringe 2: 345°K
		Glow
	Run 4 (01·00–01·12 UT)	Fringe 1: Incomplete
		Fringe 2: 255°K (distorted)

VOL. 13 58/59

Discussion

In considering the nightglow observations, it would seem desirable to treat the low-order and high-order results separately, since the latter are undoubtedly more accurate. The low-order temperatures range from 150°K to 235°K. Leaving out the lower value (150°K) of this range, which is of doubtful significance because of the distorted fringe, the range becomes 180°K to 235°K. The high-order range may be given as 180°K to 220°K. The mean of the high-order fringes is 194°K and since run 3, 3–4 May, giving 190°K for both fringes was perhaps the most reliable of the series, having three fringe peaks and two well-recorded complete fringes, it would appear that at latitude 54°47′ in the springtime, the temperature of the region emitting the nightglow OI λ5577 radiation lies between 180°K and 220°K, with a most likely value of 190°K. The less accurate low-order results are in keeping with this value.

The range of temperature observed in aurorae of the type mentioned above was 310°K to 540°K, neglecting the distorted fringe giving 225°K, and considering the results for both orders together. The observations were unsupported by simultaneous height measurements, so that to obtain an idea of the altitudes involved, arc heights were assumed to lie within the range given by HARANG (1951) for the lower borders of weak auroral arcs. HARANG's height distribution

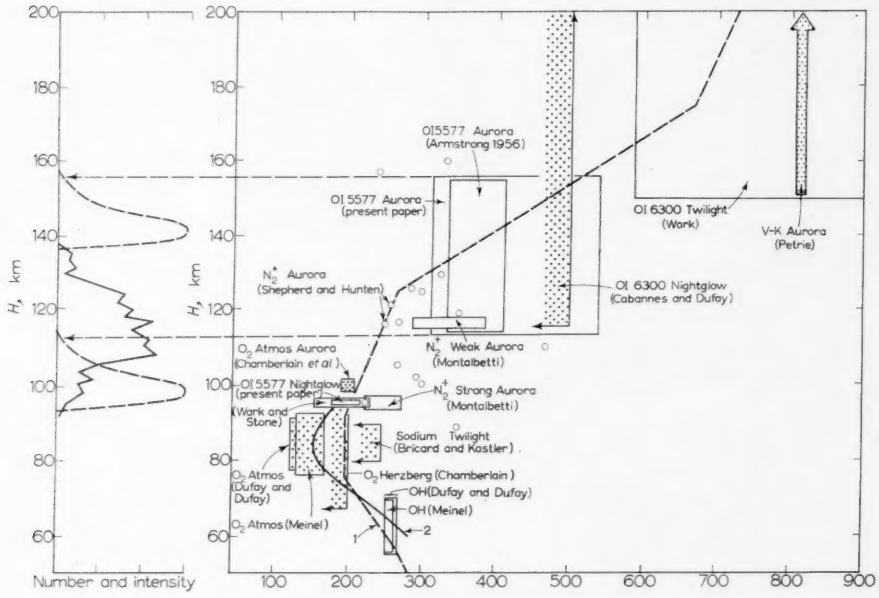

Fig. 3. Left:———height distribution diagram for the lower borders of weak auroral arcs (HARANG).
– – – –vertical intensity distribution curves for an auroral arc.
Right: temperature–altitude diagram.
(1) The A.R.D.C. (U.S.A.) model atmosphere, 1956.
(2) The I.P.G. (U.S.S.R.) rocket data.
Unshaded: emissions for which altitude measurements are reasonably certain.
Shaded: emissions for which altitude measurements are lacking or uncertain.

diagram is reproduced at the left of Fig. 3. The two broken-line curves superimposed upon it are vertical intensity distribution curves for an auroral arc (HARANG, 1946), placed at the lower and upper limits. The regions under observation, above the arcs as described, were thus likely to be within the altitude range determined by the two arrows in the figure. This range is used in conjunction with the temperatures obtained in the above auroral runs for the placing of the results on the temperature–altitude diagram at the right of Fig. 3.

This diagram is constructed for the purpose of comparing the present results with those obtained spectroscopically by other investigators, for the comparison of spectroscopic and photometric data with two temperature–altitude curves that have been given recently, and for the tentative location of emitting regions

VOL 13 1958/

for which temperatures have been measured but whose altitudes are unknown. The two curves are:

(1) The A.R.D.C. (U.S.A.) model atmosphere, 1956 (MINZNER and RIPLEY, 1956).

(2) The I.P.G. (U.S.S.R.) rocket data (MICHNEVICH, 1957). The presentation of the spectroscopic temperatures on the figure is similar to that adopted by KUIPER (1952). In the present case, however, temperatures and altitudes for the various emissions are shown by *unshaded* rectangles where sufficient consistent data are available, the extent of each rectangle giving an indication of the degree of accuracy to which the parameters are known. In cases where altitudes have not been measured, or where measured altitudes and temperatures are in serious conflict with each other or with theory, the rectangles are shown *shaded*, possible height ranges having been assigned to the emissions by considerations discussed below in each specific case. One set of auroral observations is shown as circular points for convenience, as will be explained.

The spectroscopic temperatures and altitude measurements used in the diagram are as follows:

Nightglow Emissions

(1) OI λ5577

Temperature: (a) 155–231°K (WARK and STONE, 1954). Method: Fabry–Perot interferometer (photographic) (b) 180–220°K (present paper). Method: Fabry–Perot interferometer (photoelectric).

Altitude: In view of the uncertain results given by both the van Rhijn and triangulation methods of determining the height of the layer, the value of 95 km, obtained with a rocket-borne photometer for the region of maximum intensity (KOOMEN, SCOLNIK and TOUSEY, 1956) has been adopted in Fig. 3. (The slight spread in altitude shown is purely for the sake of clarity.) Further rocket measurements by HEPPNER, STOLARIK and MEREDITH (1957) are in agreement with this value, and show that the green-line emission lies entirely between 90 and 120 km, with a very sharp lower boundary.

(2) OI λ6300–λ6364.

Temperature: Not above 400–500°K (CABANNES and DUFAY, 1956). Method: Fabry–Perot interferometer (photographic).

Altitude: ROACH and MEINEL (1955), using the van Rhijn technique, estimated that the layer altitude lay within the range 116–143 km, but pointed out that this value depended upon the assumptions made regarding the extinction coefficient. It would thus appear that this method is as uncertain in the case of the red lines as in that of the green. HEPPNER, STOLARIK and MEREDITH (1957) state that their rocket-borne photometer, flown to a height of 163 km, failed to reach the layer, and recent observations by BARBIER (1957) of the variations of intensity of the red lines at an altitude of 15° around the horizon in the course of a night strongly suggest a height of 300 km for the emission. As a consequence of BARBIER's measurement a theoretical study by CHAMBERLAIN (1958), in which it is assumed that the emission arises from the dissociative recombination of O_2^+, places the layer

between 250 and 300 km, so that the evidence against the van Rhijn altitude is very considerable. Figure 3 nevertheless combines the Cabannes–Dufay temperature measurement with a possible altitude range of 116–300 km, the matter being discussed further under Conclusions.

(3) OH *emission*

Temperature: (a) 260 ± 5°K (MEINEL, 1950). Method: from the distribution of rotational energy in the resolved *P*-branches of the bands, and from the ratio of the total intensities of the *P*, *Q* and *R* branches. (b) 255–270°K (DUFAY and DUFAY, 1951). Method: from the distribution of rotational energy in four of the bands.

Altitude: ROACH, PETTIT and WILLIAMS (1950) placed the emission at 70 km by using the van Rhijn method, which is in better agreement with theory (BATES and NICOLET, 1950), than the much greater altitudes obtained by some other investigators. [See table by CHAMBERLAIN and MEINEL (1954) for a summary of experimentally determined altitudes.] In the case of OH the van Rhijn results also agree with the rocket measurements by HEPPNER, STOLARIK and MEREDITH, who found the emission to be below 90 km, and at least as low as 56 km. In view of this indefinite upper limit and the observed value of the temperature, the maximum altitude chosen for Fig. 3 is the van Rhijn 70 km result.

(4) O_2 *Atmospheric emission;* (0,1) *band*

Temperature: (a) 150 ± 20°K (normal intensity): 200 ± 10°K (enhanced) (MEINEL, 1950). Method: from a study of the band profile. (b) About 130°K (DUFAY and DUFAY, 1951). Method: from the rotational line intensity distribution (although the particular spectrogram did not permit great accuracy). The reality of the temperature measured in this way is held in some doubt by CHAMBERLAIN (1954), on the grounds that fluorescent scattering from the (0,0) band, which adds to the (0,1) band emission, may also modify the profile, but there are also grounds for believing that this is not the case. The (0,0) band itself is not detected at ground level.

Altitude: MEINEL (1950) and BERTHIER (1956) judged the altitude to be the same as that of the OH emission, and without making an actual determination, suggested 80 km, the region of the temperature minimum. DUFAY and DUFAY (1951) pointed out that if 70 km is to be accepted for the height of the OH emission, as measured by ROACH, PETTIT and WILLIAMS, and if the two emissions are in fact at the same altitude, then in one of the two cases the distribution of the molecules in the rotational states does not correspond to thermal equilibrium. MEINEL's common altitude for the OH and O_2 emission was obtained by a van Rhijn technique with a series of spectrograms (rather than with filter photometry) which is probably too insensitive a method to differentiate between 70 and 80 km, so that it is thus uncertain which of the two parameters is to be accepted. In Fig. 3 it is tentatively assumed that the O_2 temperature is in fact lower than that given by OH, and the altitude is taken to be at the temperature minimum as shown. It is not possible to state whether the layer was higher or lower during the period of enhancement which was not a normal polar

VOL. 13 1958/5

auroral phenomenon, as no polar auroral emissions were observed at the same time.

(5) *Herzberg* O_2 *emission*

Temperature: 200°K or less (CHAMBERLAIN, 1955). Method: from the position of the rotational line of maximum intensity in a band. This estimate was made from an ultraviolet spectrum obtained with a 75 hr exposure. Because of the calibration difficulties associated with such long exposures, and the fact that the rotational line intensities are not known, the temperature could be found to the above degree of accuracy only by assuming that the rotational line of maximum intensity lay within the unresolved band head.

Altitude: A height of 200 km for the region emitting these bands was obtained by BARBIER (1953), which agrees neither with the above temperature nor with theory (BATES and DALGARNO, 1953). It would appear from the temperature that the region is again in the neighbourhood of the minimum, and theory in fact places it near the OI λ5577 layer. A wide range of altitude is nevertheless depicted in Fig. 3, since the temperature was not obtainable to an accuracy sufficiently high to localize the emission more closely.

Twilight Emissions

(1) NaD-*lines*

Temperature: About 240°K (BRICARD and KASTLER, 1944). Method: by a study of the transmission of the twilight Na *D*-lines through a vessel containing sodium vapour at various temperatures. The lines were found to be narrow, the width indicating the above temperature, presumably as an upper limit.

Altitude: Studies of the emission by HUNTEN (1956) with a photoelectric spectrometer gave a height of 84 $\pm$ 5 km for the layer, which is adopted in Fig. 3 since there are no conflicting data.

(2) OI λ6300 *emission*

Temperature: 790 $\pm$ 120°K and 710 $\pm$ 130°K (WARK, 1956). Method: Fabry–Perot interferometer (photographic). These results were obtained from two photographs made at latitude 64°52′, at a time when there was all-night twilight, the solar depression remaining almost constant throughout the exposure-times of 1–2 hr. The temperature range shown on Fig. 3 is 580–910°K, thus including the lowest and highest possible values.

Altitude: WARK estimated the height of the emitting region to be between 150 and 200 km from the fact that the height of the earth's shadow during the exposures was about 70 km and by assuming an additional screening layer 100 km high. This is supported by a theoretical study of the twilight emission by CHAMBERLAIN (1957).

Auroral Emissions

(1) OI λ5577 *emission*

Temperature: (a) 330–410°K (ARMSTRONG, 1956). Method: Fabry–Perot interferometer (photoelectric).

(b) 310–540°K for various arcs (present paper). Method: Fabry–Perot interferometer (photoelectric).

Altitude: All these observations refer to the regions above faint green arcs, the possible range of altitudes concerned having been discussed already.

(2) N_2^+ *emissions*

Temperature: There have been many temperature measurements made from the distribution in intensity of the rotational lines of the *R*-branch of the (0,0) and (0,1) bands of the negative system, a summary of the earlier work being given by Vegard and Tonsberg (1935). Two more recent series of observations are given here.

(a) 275–465°K for high altitude aurorae, 222–274°K for medium altitude aurorae, 150–220°K for low altitude aurorae (Shepherd and Hunten, 1955). Method: from the profiles of the unresolved bands recorded with a photoelectric scanning spectrometer.

Altitude: For many of their spectra, Shepherd and Hunten measured the corresponding heights by parallax photography. They remark, however, upon the difficulty of obtaining true temperatures for high aurorae owing to radiation from lower features being received at the same time, thus modifying the band profiles. Figure 3 includes some of the simultaneous temperature and height measurements, taken from their published diagram, and shown as circular points.

Temperature: (b) 335 ± 52°K for the mean temperature of weak aurorae: 250 ± 23°K for the mean temperature of strong aurorae (Montalbetti, 1957). Method: from the well resolved rotational structure of the (0,0) band in photographic spectra of various types of aurorae.

Altitude: No altitude measurements were made, but from the difference in height between strong and weak aurorae, determined by the Norwegian workers, Montalbetti deduced a temperature gradient of 6°/km in the auroral region. In Fig. 3 the above temperatures are related to Harang's (1944) mean altitudes for the lower borders of weak and strong aurorae, 114·3 km and 94·7 km respectively.

(3) *Vegard–Kaplan bands of* N_2

Temperature: 815°K for the mean temperature from five *V–K* bands (Petrie, 1952). Method: from the rotational structure of the bands on spectrograms.

Altitude: Petrie assumed that his observations were of the tops of the auroral features, since the temperature appeared to be so high. Stormer's height distribution diagrams (see Harang, 1951) show that aurorae (in shadow, as distinct from sunlit) above 200 km are by no means uncommon, and Petrie's high temperature is thus associated with altitudes above 150 km in Fig. 3.

(4) O_2 *Atmospheric emission:* (0,1) *band*

Temperature: About 200°K (Chamberlain, Fan and Meinel, 1954). Method: from the band profile. The band on the spectrum used was insufficiently strong and unblended for an accurate determination.

VOL. 13 1958/5

Altitude: No simultaneous height measurement could be made, and the authors associate the temperature with the lower auroral region at about 100 km, although they remark that the fluorescent scattering of the (0,0) band radiation might give rise in this case also to a modification of the profile of the (0,1) band, and therefore a misinterpretation of the true temperature of the emitting region. Figure 3 tentatively associates the above temperature value with an altitude of 100 km.

Conclusions

Some conclusions which may be drawn from the results reviewed in Fig. 3 are as follows:

(a) The temperature of 190°K at 95 km for the region emitting the OI λ5577 radiation, determined by the method outlined in this paper, supports previous spectroscopic observations which indicate that the temperature in the minimum at 80–85 km is much less than 200°K, and may be as low as 130°K. A rather more probable minimum temperature, however, would appear to be 150°K, when weight is given to curve 2 (Michnevich).

(b) Unless the profile of the (0,1) band of the nightglow O_2 atmospheric infrared emission is in fact modified by fluorescent scattering from the (0,0) band, as suggested by Chamberlain, the emitting region is above that of the OH emission rather than at the same level, and is probably located at the temperature minimum. The cause of the non-auroral enhancement of the O_2 emission, and the consequent rise in observed temperature with an implied change in altitude is apparently still unknown.

(c) There is very serious conflict between the twilight OI λ6300 temperature (Wark) and Cabannes and Dufay's nightglow value, when Chamberlain's theoretical study, which places the nightglow emitting region above the twilight emission, is taken into account. The altitude given by Chamberlain for the nightglow emission is between 250 and 300 km, and above 150 km for the twilight emission. The twilight temperature is in agreement with this and with all other results shown in Fig. 3, but the low temperature for the nightglow is difficult to explain unless combined with Roach and Meinel's (1955) van Rhijn altitude (116–143 km). Since van Rhijn measurements are now questioned, and since Barbier's recent measurement of the layer altitude by another method giving 300 km, is in agreement with theory, it would seem necessary to await further observations of temperature before the discrepancy can be resolved.

(d) The temperatures determined by the writer for the region immediately above auroral arcs are not inconsistent with the weak aurora values found by Montalbetti, especially those associated with faint arcs and clouds. Taking into consideration the results and conclusions of Shepherd and Hunten, it would seem that auroral temperatures determined from any but the simplest and most well-defined auroral forms would be subject to misinterpretation due to the influence of radiation from a diversity of heights on band or fringe profiles.

(e) There is clearly insufficient data to extend the temperature–height relation above 200 km. Interferometer studies of high red auroral rays, supported by

parallax measurements might be one possible method of carrying investigations to greater altitudes.

Acknowledgements—The writer is indebted to Professor D. R. BATES, F.R.S., for his support of this work, and to both him and Dr. A. DALGARNO for discussions. The interferometer was obtained with a grant from the Gassiot Committee of the Royal Society, and thanks are due to Mrs. E. B. ARMSTRONG for her assistance with the observations.

REFERENCES

ARMSTRONG E. B.	1956	*The Airglow and the Aurorae* (Edited by ARMSTRONG E. B. and DALGARNO A.) p. 366. Pergamon Press, London and New York.
BARBIER D.	1953	*Ann. Astrophys.* **16,** 96.
BARBIER D.	1957	*C.R. Acad. Sci., Paris* **244,** 1809.
BATES D. R. and DALGARNO A.	1953	*J. Atmosph. Terr. Phys.* **4,** 112.
BATES D. R. and NICOLET M.	1950	*J. Geophys. Res.* **55,** 301.
BERTHIER P.	1956	*Ann. Geophys.* **12,** 113.
BRICARD J. and KASTLER A.	1944	*Ann. Geophys.* **1,** 53.
CABANNES J. and DUFAY J.	1956	*The Airglow and the Aurorae* (Edited by ARMSTRONG E. B. and DALGARNO A.) p. 73. Pergamon Press, London and New York.
CHAMBERLAIN J. W.	1954	*Astrophys. J.* **119,** 328.
CHAMBERLAIN J. W.	1955	*Astrophys. J.* **121,** 277.
CHAMBERLAIN J. W.	1958	*Astrophys. J.* **127,** 54
CHAMBERLAIN J. W. and MEINEL A. B.	1954	*The Earth as a Planet* (Edited by KUIPER, G. P.) p. 561. Chicago University Press.
CHAMBERLAIN J. W., FAN C. Y. and MEINEL A. B.	1954	*Astrophys. J.* **120,** 560.
DUFAY J. and DUFAY M.	1951	*C.R. Acad. Sci., Paris* **232,** 426.
HARANG L.	1946	*Terr. Magn. Atmos. Elect.* **51,** 381.
HARANG L.	1951	*The Aurorae* p. 42. Chapman and Hall, London.
HEPPNER J. P., STOLARIK J. D. and MEREDITH H. L.	1957	*Trans. Amer. Geophys. Un.* **38,** 394.
JACQUINOT P. and DUFOUR C.	1949	*J. Rech.* **6,** 91.
KOOMEN M. J., SCOLNIK R. and TOUSEY E.	1956	*Trans. Amer. Geophys. Un.* **37,** 351.
KUIPER G. P.	1952	*The Atmosphere of the Earth and Planets* (2nd Ed.) p. 417. Chicago University Press.
MEINEL A. B.	1950	*Astrophys. J.* **112,** 120.
MEINEL A. B.	1950	*Astrophys. J.* **112,** 464.
MICHNEVICH B. B.	1957	*Usp. Fiz. Nauk, Mosk.* **63,** 197.
MINZNER R. A. and RIPLEY W. S.	1956	*Air Force Surveys in Geophys.* No. 86, Cambridge Research Center, Bedford, Mass.
MONTALBETTI R.	1957	*Canad. J. Phys.* **35,** 831.
PETRIE W.	1952	*Phys. Rev.* **86,** 790.
ROACH F. E., PETTIT H. and WILLIAMS D. R.	1950	*J. Geophys. Res.* **55,** 183.
ROACH F. E. and MEINEL A. B.	1955	*Astrophys. J.* **122,** 530.
SHEPHERD G. G. and HUNTEN D. M.	1955	*J. Atmosph. Terr. Phys.* **6,** 328.
VEGARD L. and TONSBERG E.	1935	*Geofys. Publ.* **11,** No. 2.
WARK D. Q.	1956	*Nature, Lond.* **178,** 689.
WARK D. Q. and STONE J. M.	1955	*Nature, Lond.* **157,** 254.

VOL
13
1958/

Journal of Atmospheric and Terrestrial Physics, 1959, Vol. 13, pp. 217 to 221. Pergamon Press Ltd. Printed in Northern Ireland

Lunar tides in the sporadic *E*-layer at Ibadan

R. W. WRIGHT* and N. J. SKINNER
University College, Ibadan, Nigeria

(*Received* 15 *March* 1958)

Abstract—An analysis of the lunar semi-diurnal tides in *fEs* and *h'Es* is made for Ibadan. The results are presented in the form of harmonic dials. Comparisons are made between these results and those of other stations.

1. INTRODUCTION

IN recent years, considerable information has been accumulated concerning the amplitudes and phases of the lunar semi-diurnal variations in the different ionospheric regions. An interesting feature of this work is that a lunar variation of fairly large amplitude has been reported (MATSUSHITA, 1952, 1953) for the parameter *fEs*, the "top frequency" of reflection from the sporadic *E*-layer. This is especially noteworthy since no comparable tidal oscillation in f_0E, the critical frequency of the normal *E*-layer, has yet been reported. It is the purpose of this communication to provide some additional information from results obtained at Ibadan, Nigeria.

VOL. 13 58/59

2. LUNAR TIDES IN *fEs*

At Ibadan, typical "equatorial type" *Es* is normally present during the daylight hours and *fEs* follows a smooth diurnal variation with a maximum at noon. Very little *Es* is present at night. For the purposes of this lunar tidal investigation, only measurements made on equatorial type *Es* have been considered and data is thus restricted to the hours between 0700 and 1700 GMT inclusive. Each month during the period November 1953 to October 1956 has been treated separately. In each case the normal diurnal variation was removed from the data by subtracting the individual hourly values from the corresponding monthly mean values. These differences were then arranged in lunar time and the amplitudes and phases of the second harmonic components were calculated in the normal manner. The results are plotted in the harmonic dial of Fig. 1. The probable error ellipse is shown by the broken line and it contains about half the points, indicating a relatively normal distribution. The small ellipse provides an estimate of the probable error of the mean value for all the points. The harmonic dial shows that a highly significant lunar semi-diurnal variation exists of mean amplitude 0·41 Mc/s with the maximum occurring 7·5 hr after lunar transit.

The parameter *fEs* is often considered an unsatisfactory measure of *Es* ionization on account of its dependence upon equipment sensitivity and upon absorption in the lower ionosphere. From routine absorption measurements made using a frequency of 5·8 Mc/s, we have calculated the apparent partial

* Now at University College of Ghana.

reflection coefficient, *R'Es*, of the sporadic *E*-layer. This parameter is free from the afore mentioned objections since the effect of absorption is largely eliminated by comparing the amplitudes of the *Es* and *F2* reflected echoes and the equipment sensitivity is monitored daily. Noon values of *R'Es* covering a 2 year period

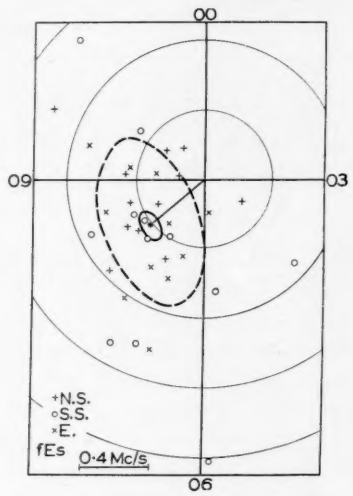

Fig. 1. Harmonic dial showing the amplitudes and phases of the lunar semi-diurnal tides in the parameter *fEs*. Each point represents 1 month's data.

were available for Ibadan and these have been examined for a semi-diurnal lunar tide. For comparison purposes, noon values of *fEs* for a 5 year period have been similarly analysed and the results are shown below in Table 1.

Table 1

Es parameter	Amplitude *P2*	Time of maximum after lunar transit (hr)
Noon *R'Es*	0·003	8·5
Noon *fEs*	0·3 Mc/s	9·0
fEs (0700–1700)	0·41 Mc/s	7·5

Whilst little can be said about the relative amplitudes of these tides, the agreement in phase is sufficiently good to suggest that *fEs* is a reliable indicator of *Es* ionization density.

The *fEs* data has also been separated into seasons. Fig. 2(a) is a harmonic dial showing the mean tidal components for northern solstice (N.S.), equinoxes (E) and southern solstice (S.S.) together with the corresponding probable error ellipses.

3. Lunar Tides in *h'Es*

The only other *Es* parameter commonly scaled is the virtual height *h'Es*. An analysis has been made of values of *h'Es* measured between 0800 and 1600

VOL
13
1958/5

hours GMT for a period of 1 year. These values were the result of a special scaling of routine ionograms in which the heights were measured to the nearest 1 km at the highest frequency recorded, i.e. where the trace was thinnest. By measuring the heights in this way the effect of echo amplitude on the virtual height (LYON

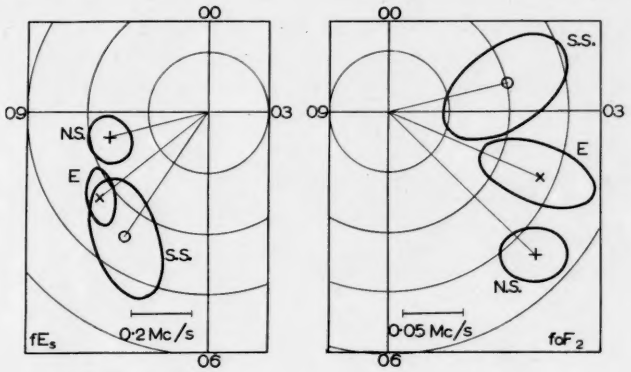

Fig. 2. (a) Harmonic dial showing the seasonal variation of the tide in *fEs* at Ibadan. (b) Harmonic dial showing the seasonal variation of the tide in f_0F2 at Ibadan (after BROWN, 1956).

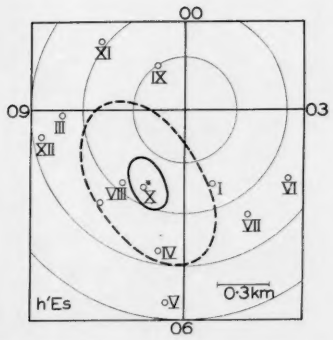

Fig. 3. Harmonic dial showing the monthly values of the semi-diurnal tidal components in *h'Es*. The points are numbered I–XII according to the month.

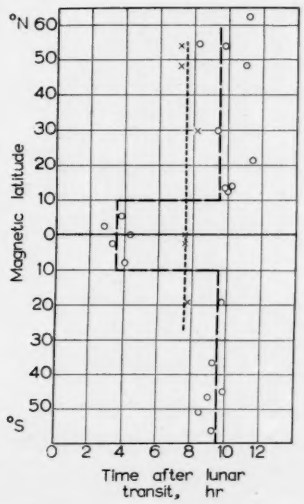

Fig. 4. Showing the variation with magnetic latitude of the time after lunar transit of maximum tidal amplitude. Crosses refer to tides in *fEs* and circles to tides in f_0F2.

and MOORAT, 1956) was minimized. The harmonic dial showing the lunar semi-diurnal components for each month is given in Fig. 3 together with the probable error ellipses. It is seen that the mean tidal variation is of amplitude 0·22 km with the maximum occurring 7·0 hr after lunar transit.

4. DISCUSSION OF RESULTS

Lunar tidal variations in *fEs* and *h'Es* have been investigated by MATSUSHITA (1952, 1953) using routine published *Es* data for five widely spread stations. THOMAS and SVENSON (1955) have examined the lunar tide in *h'Es* for Brisbane using special night-time measurements only. The results of all known tidal measurements in the sporadic *E*-layer are summarized in Table 2.

One striking feature that emerges from this table is that the time of maximum amplitude of *fEs* is about the same for all stations irrespective of their latitudes.

Table 2

Station	Observer	*fEs*		*h'Es*		Remarks
		P2 (Mc/s)	*t2* (hr)	*P2* (km)	*t2* (hr)	
Slough	MATSUSHITA	0·17	7·2	—	—	Used routine published values
Washington		0·17	7·2	0·46	5·8	
Kokobunji		0·35	8·2	—	—	
Huancayo		0·33	7·5	0·17	1·2	
Brisbane		0·34	7·7	0·70	5·7	
Brisbane	THOMAS and SVENSON	—	—	0·69	6·7	Used night-time values only
Ibadan	SKINNER and WRIGHT	0·41	7·5	0·22	7·0	Used daytime values only

In contrast to this, as is well known, the phase of the lunar tide in f_0F2, the critical frequency of the *F2* layer, reverses suddenly at magnetic latitudes 10°N and 10°S. This difference in behaviour is well illustrated by Fig. 4 in which the times after lunar transit for maximum tidal amplitude are plotted against the magnetic latitude for as many stations as possible. Points referring to f_0F2 tides and *fEs* tides are plotted as circles and crosses respectively. The explanation of this difference may lie in the fact that *Es* in moderate latitudes is of a different type and origin to that in low latitudes where its presence is known to be intimately connected with the equatorial "electrojet" current system (SKINNER and WRIGHT, 1957). The apparent agreement in phase may thus be merely fortuitous. The variation with season of the phases at Ibadan is similar to that observed in f_0F2 by BROWN (1956) [see Fig. 2(b)]. This similarity lends additional support to the theory (SKINNER and WRIGHT, 1957) that the *Es* and *F2* layers are linked by the same electrodynamical forces near the magnetic equator.

In Table 2 it is seen that the *h'Es* tides are all approximately in phase with the exception of that for Huancayo. Further observations of such tides are clearly necessary before a definite conclusion can be drawn. It is our experience that routine *h'f* ionograms can only be used as a source of data provided that a separate careful scaling of the records is made. It seems a dubious procedure to use the

VOL 13 1958/5

routine scalings (measured only to the nearest 10 km) unless a very long sequence of data is studied. It is also important that measurements should be considered for only one type of *Es* at any one station.

References

Brown R. A.	1956	*J. Atmosph. Terr. Phys.* **9,** 144.
Lyon A. J. and Moorat A. J. G.	1956	*J. Atmosph. Terr. Phys.* **8,** 309.
Matsushita S.	1952	*J. Geomagn. Geoelect., Kyoto* **4,** 40.
Matsushita S.	1953	*Rep. Ionos. Res. Japan* **7,** 45.
Skinner N. J. and Wright R. W.	1957	*Proc. Phys. Soc. Lond.* B **70,** 833.
Thomas J. A. and Svenson A. C.	1955	*Austr. J. Phys.* **8,** 554.

OL.
13
8/59

Journal of Atmospheric and Terrestrial Physics, 1959, Vol. 13, pp. 222 to 234. Pergamon Press Ltd. Printed in Northern Ireland

A study of the equatorial electrojet—I

An experimental study

C. A. ONWUMECHILLI
Physics Department, University College, Ibadan, Nigeria

(*Received* 14 *April* 1958)

Abstract—An account is given of the photographic registration of the variation of the earth's horizontal magnetic force (H) across the magnetic equator in Nigeria from November 1956 to January 1957. As the period was magnetically quiet and the records were good, it has been possible to make a detailed study of the quiet day variation. The latitude of the maximum range of H was found to be about 0·5° from the magnetic towards the geographic equator. The daily variation curve of H is found to change its form as the magnetic equator is crossed from south to north and a method is introduced for the study of this change. It is shown that the fluctuations in H-variation curve characteristic of equatorial stations occur at the same time and in the same form at equatorial stations that may be distant from one another. The magnitudes of the same fluctuation at two stations are in about the same ratio as the daily ranges at the stations. It is thus likely that the indentations in the H-variation curve arise from fluctuations in the ionizing agent from the sun.

1. INTRODUCTION

EGEDAL (1947, 1948) pointed out that abnormally large daily ranges of H-variation may be expected close to the magnetic equator in any continent and suggested that this may be due to a narrow band of electric current flowing in the ionosphere near that equator. On the contrary, the spherical harmonic analysis of the data collected during the International Polar Year 1932–1933, showed (HASEGAWA and OTA, 1948, PRICE and WILKINS, 1951) that the line of the maximum daily range of H should be between the magnetic and geomagnetic equators in South America and Africa but to the south of these equators in the far east. It became necessary to make measurements of H-ranges near the magnetic, geomagnetic and geographic equators in order to (a) determine the line of maximum range of H and (b) study the characteristics of the ionospheric current (the equatorial electrojet) which causes the large H-ranges.

The measurements of H daily range near the equators in South America by GIESECKE, in Togoland by PONTIER (1950), in Sudan by MADWAR (1953) and all but one of the Indian measurements (PRAMANIK and HARIHARAN, 1953) were made with the Quartz Horizontal Force Magnetometer (QHM). The series of spot values obtainable from the QHM may not give the full daily range especially near the magnetic equator where fluctuations often occur in the daily variation of H even on very quiet days (CHAPMAN and BARTELS, 1940 p. 242). This and magnetic disturbance might have contributed largely to the lack of smoothness in the graph of H daily range against latitude obtained by the investigators. Most of their measurements were also confined to one side of the magnetic equator. The need therefore arises for the continuous photographic registration of H-variation under quiet condition at a series of stations on both sides of the magnetic equator. The work described here was designed to answer that need.

Preliminary measurements were made at Ilorin (8–14 Sept. 1956) and later records of H-variation were obtained at Ikeja (6–13 Oct. 1956). During the main

VOL.
13
1958/5

tour centred on the December solstice (25 November 1956 to 21 January 1957) continuous photographic registration of H-variation was made for about 6 days at each of the eight stations (in Fig. 1): Ilorin, Bida, Minna, Tegina, Kaduna, Zaria, Kano and Katsina. The stations are evenly distributed and they stretch to about

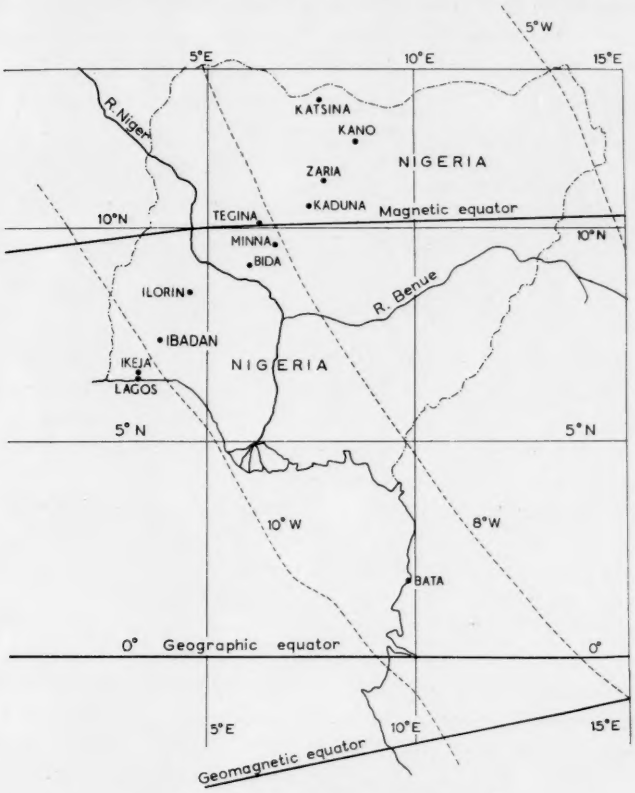

Fig. 1. Map of Nigeria showing field stations and equators.

a distance of 3° latitude on either side of the magnetic equator. The period was mostly magnetically quiet and only 3 days fell outside BARTELS' limit ($C_p < 1{\cdot}2$) for undisturbed days. Ibadan magnetic observatory (7° 26·6′ N, 3° 54′ E) was used as a base station.

2. EQUIPMENT

The simple, portable variometer was designed and built by Prof. N. S. ALEXANDER, University College, Ibadan. It is the usual La Cour type of H-variometer in which a magnet is suspended on a fused silica fibre perpendicular to the magnetic meridian. The effect of temperature is compensated by means of a variable magnetic shunt. On the magnet is attached a small piece of an alloy, "mutemp", (manufactured by Richard Thomas & Baldwins Ltd., Birmingham) the induction and therefore permeability of which in a fixed field varies very considerably and linearly with temperature in the range of 0° to 40°C. Temperature compensation is

obtained by changing the length of the strip of "mutemp". The temperature coefficients of the four suspension systems used on the tour were: +0·15; −0·01; negligible; +0·20 gamma/°C. (The positive indicates overcompensation.) During the tour, actual temperatures were also recorded with a bimetallic thermograph so that corrections could be made where necessary.

A plywood box 141·5 cm × 33 cm × 39 cm high provides the darkroom necessary for photographic recording. In the diagrams of the box [Figs. 2(a) and 2(b)]

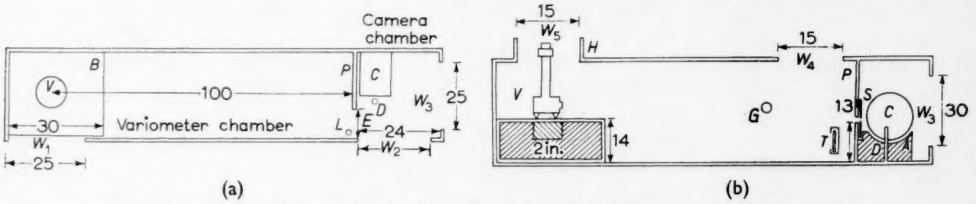

Fig. 2. Showing details of the box housing the variometer. (a) Plan; (b) elevation.

the dimensions are in centimetres except where otherwise indicated. W_1, W_2 to W_5 are windows which give access to the pieces of apparatus inside the box. A is a block of wood and B is a raised platform. C is the camera (clock, drum and case). P is a partition wall on which an adjustable slit S is attached. On the variometer V is a converging lens of focal length 100 cm. The retort stand L holds the recording lamp T of long straight filament. G is a miniature lamp which when switched on illuminates the variometer chamber and makes time-marks on the photographic records. All materials used in the box are wood and tested brass and aluminium.

When in use the box is sheltered by a tent designed to reduce temperature range and fluctuations. It is a double tent with a separation (air space) of about 7 in. all the way round. The box is thus sheltered from both the direct rays of the sun and direct radiation from the outer tent exposed to it. In the daytime the ends of the tent are opened to allow for free circulation of air and at night they are closed to hinder cooling of the inside of the tent. Two thermometers one inside and the other outside the tent indicate when the opening and closing should be done to minimize temperature gradient.

The small lamps used require very little electric power. The mains, transformed down to 5 V, was often used but where this was not possible, a 6 V car battery was substituted.

3. CALIBRATION

Hourly time-marks are put on the records for most hours during the daytime, allowance being made for "parallax error".

At about hourly intervals, absolute measurements of H are made with a QHM stationed at about 25–50 m from the variometer. On a day's record, the ordinate (from a fixed base line to the H-variation curve) is determined for the time the absolute observation is made. A graph of these ordinates against the corresponding absolute values of H gives the scale value in gammas/mm. The graphs are linear even for days of large daily ranges (the line for Tegina in Fig. 3 is for the second largest quiet day range, 197 gammas, recorded on the tour).

VOL 13 1958/5

Before setting out for the field work, the recordings of the portable variometer were compared with those of the standard variometer at the Ibadan observatory. The pair of simultaneous records is given in Fig. 4 and the calibration graph for the portable variometer record is in Fig. 3. Table 1 shows the good agreement between the ranges from the two records.

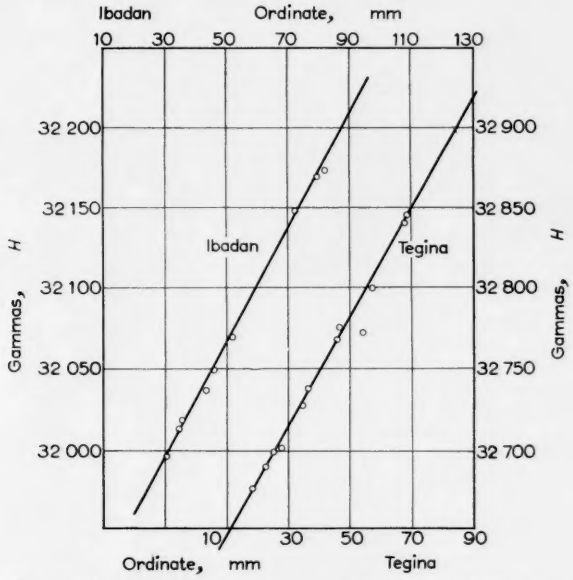

Fig. 3. Showing calibration curves for Ibadan and Tegina.

Table 1. Comparison of the portable and observatory variometer records

Date	Hour of minimum	Hour of maximum	Observatory range (gamma)	Portable range (gamma)
8.11.56	0520–0620	1120–1220	178	180
8.11.56	1800–1900	1120–1220	143	145
9.11.56	0500–0600	1030–1130	153	154

4. Experimental Results

4.1. *Daily ranges*

Placing a translucent sheet of paper with millimetre squares on a day's photographic record of H-variation, the mean ordinate (from a fixed base line) of the variation curve may be determined for any hour interval.

The hour intervals whose mean ordinates are minimum and maximum respectively are easily selected. The difference between these mean ordinates is the daily range in (mm) and is converted to gammas with the scale value. Table 2 shows the mean daily ranges for the stations and their ratios to the corresponding Ibadan

Table 2. Showing H mean daily range at stations and their ratios to Ibadan

Station	Station range		Ibadan range		Ratios	
	quiet (1)	all (2)	quiet (3)	all (4)	quiet (5)	all (6)
Ikeja	105	109	122	122	0·86	0·89
Ilorin	134	137	107	109	1·26	1·27
Bida	145	>151	97	97	1·49	>1·67
Minna	118	136	83	77	1·56	1·90
Tegina	208	165	141	109	1·47	1·58
Kaduna	133	133	107	107	1·14	1·14
Zaria	87	118	82	103	1·00	1·11
Kano	99	>120	110	129	0·91	>0·93
Katsina	79	>86	89	87	0·86	>0·97
Ilorin (Sept.)	190	182	147	140	1·30	1·30

ranges. Two types of ranges are given, one under quiet condition and the other for all days quiet or disturbed. No part of a record with K_p index greater than 3 is included under quiet conditions. Those with 3 may or may not be included depending on the strength of the local effects. Where more than one continuous half of a day is quiet (the maximum is therefore quiet) and the other part is disturbed, two ranges are taken: one from the quiet part and another from the whole day.

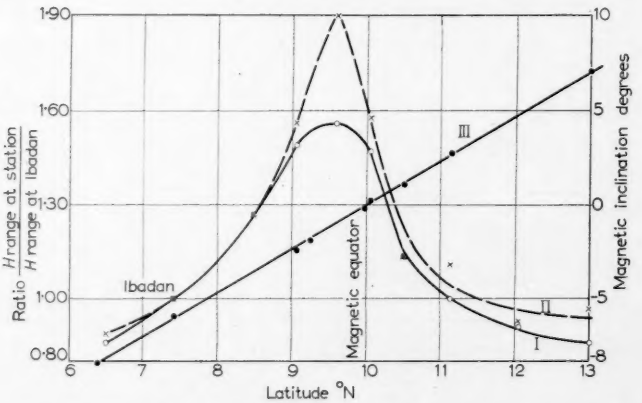

Fig. 5. Showing ratios of H daily range against latitude: ○ under quiet condition; × under all conditions; ● dip.

ALEXANDER (1955) determined magnetic inclination with the earth inductor of the Department of Terrestrial Magnetism (D.T.M) of the Carnegie Institution of Washington (C.I.W.). These are shown in Table 3 along with the co-ordinates of the stations. The dip against latitude, gives a good straight line Fig. 5, curve III from which the other values in Table 3 have been interpolated. The line also establishes

VOL.
13
58/59

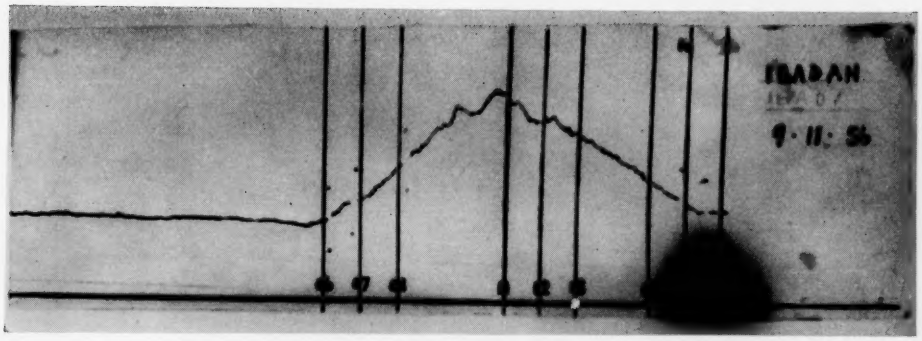

(a)

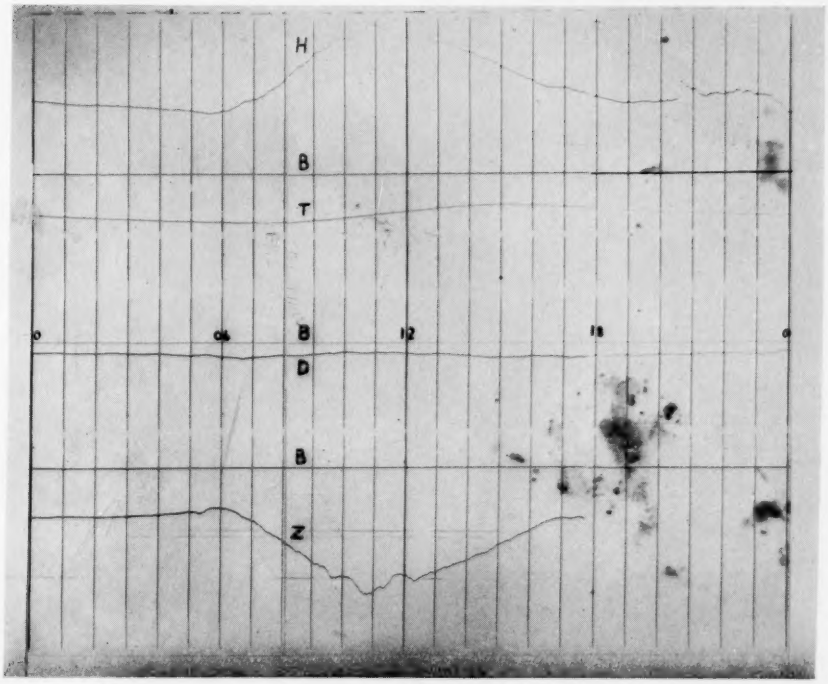

(b)

Fig. 4. Showing the simultaneous records made with the portable and the observatory variometers. (a) Recorded with the portable variometer; (b) recorded with the observatory variometer.

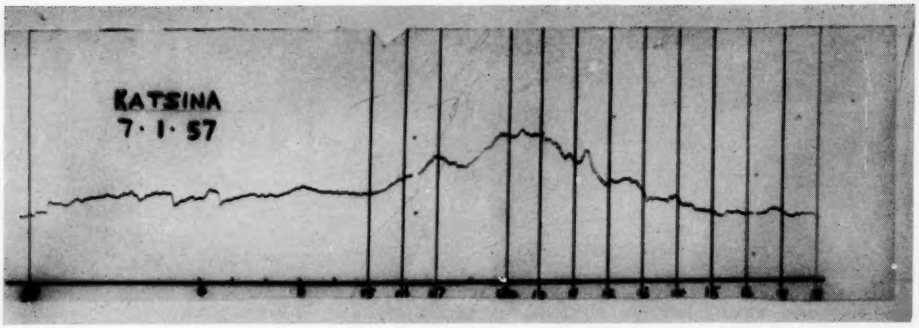

(a)

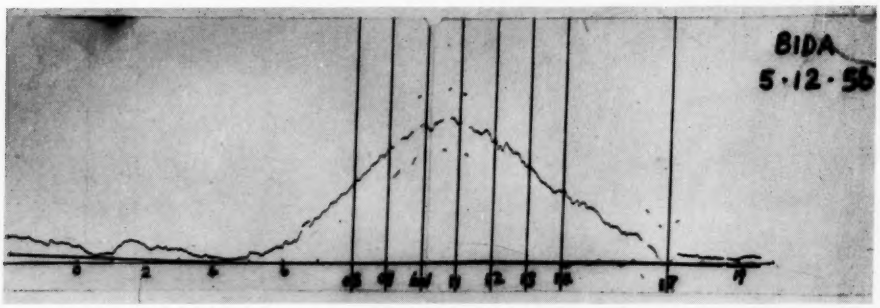

(b)

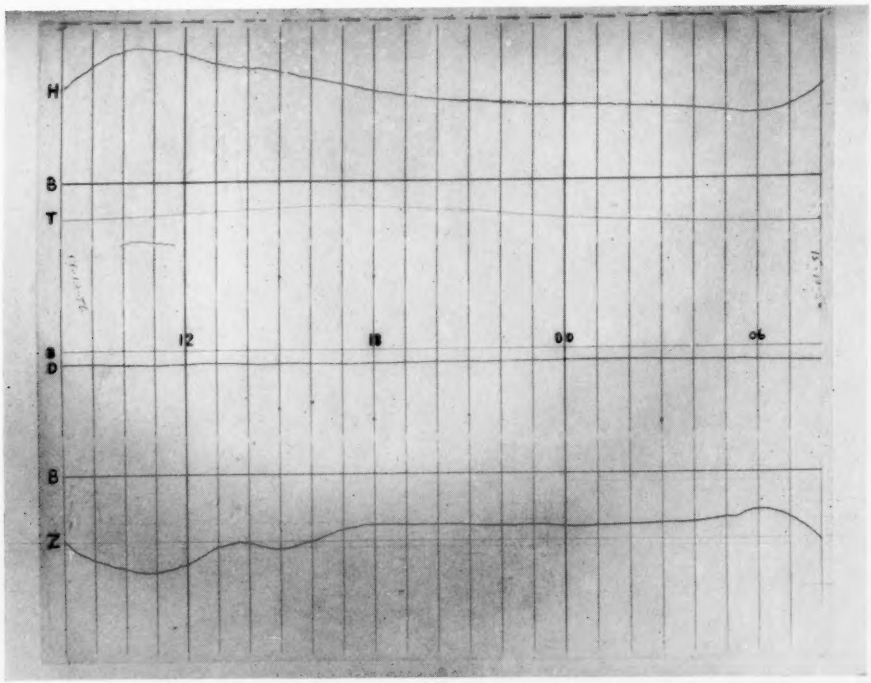

(c)

Fig. 7. Photographic records showing types of daily variation of H around the magnetic equator. (a) N-type, north of the equator; (b) E-type, at the equator; (c) S-type, south of the equator. Ibadan record of 14–15 October 1956.

VOL.
13
1958/5

that around longitude 6° E, the dip is zero at latitude 10° N in agreement with the isoclinic map of 1945 by VESTINE *et al.* (1948, p. 524).

Fig. 5 shows the variation of the range ratios with latitude and a similar variation will be expected with dip. Curve I gives the variation for quiet days only, and Curve II for all days. Curve I is smooth and the following conclusions may be

Table 3. Showing co-ordinates of the stations

Station	Lat. N	Long. E	Inclination	Geomag. lat.
1. Ikeja	6° 36′	3° 21′	−8° 10′	9·9°
2. Ibadan	7° 26′	3° 55′	−5° 50′*	10·7°
3. Ilorin	8° 29′	4° 34′	−3° 23′	11·6°
4. Bida	9° 04′	6° 01′	−2° 27′*	11·8°
5. Minna	9° 36′	6° 34′	−00° 58′	12·3°
6. Tegina	10° 04′	6° 12′	+00° 18′*	12·8°
7. Kaduna	10° 31′	7° 26′	+1° 05′*	12·1
8. Zaria	11° 08′	7° 14′	+2° 44′*	12·9°
9. Kano	12° 03′	8° 32′	+4° 50′	14·3°
10. Katsina	13° 00′	7° 37′	+7° 06′*	15·5°
	9° 59′	6° 12′	−00° 11′*	
	9° 15′	6° 02′	−1° 54′*	
	10° 24′	6° 23′	+00° 55′*	

* As determined by ALEXANDER.

drawn from it. (i) A maximum is clearly indicated about 0·5° south of the magnetic equator in a locality where the dip is about −1°. (ii) At the region of maximum, the range is about 1·80 times that at stations only 3° to the north or south. (iii) The curve shows some asymmetry about the maximum. Curve II is similar to I and indicates a higher maximum in the same place as I. Here the range at the region of the maximum is about 2·20 times that at 3° away. The points are scattered especially as we get farther from the base station. Since this curve depends on more days than curve I, the scatter shows the adverse effect of disturbance on the smoothness of the curve.

As is already known (CHAPMAN and BARTELS, 1940, p. 234), the daily ranges of H varied greatly in the same station from day to day. But a relatively high range in the station always meant a relatively high range at Ibadan. It is worthy of note that the ratios also varied considerably. The range of variation in each station is shown in Table 4, but this reveals no definite pattern.

4.2. *Forms of equatorial* H*-variation*

It is easily noticeable from the records that H-diurnal variation reaches a maximum much earlier north of the magnetic equator than at Ibadan. In general, the difference is of the order of 1 hr but there are one or two cases of about 2 hr. In fact the shape of H-variation curve changes as the magnetic equator is crossed from south to north. The quiet day variation is of three main types which may conveniently be denoted by S, E and N. The S-type is predominant south of the

Table 4. Showing the variation of H-range ratios at field stations

Station	Ratio limits	Station	Ratio limits
Ikeja	0·76–0·99	Kaduna	0·90–1·32
Ilorin	1·21–1·30	Zaria	0·77–1·20
Bida	1·38–1·78	Kano	0·79–1·04
Minna	1·31–2·00	Katsina	0·59–1·02
Tegina	1·41–1·53	Ilorin (Sept.)	1·27–1·33

equator, the E-type around the equator and the N-type north of the equator. The equatorial type, E, is symmetrical about a maximum around 1100 hours local time and often has equal minima about 0500 and 1800 local time. The southern type, S, rises from a minimum about 0500 to a maximum about noon and then falls slowly until the next minimum the following day. The northern type, N, rises steadily from midnight to a maximum about 1000 and then falls to a minimum around 1800 hours local time. Typical records of the forms are shown in Fig. 7. Six records of each type were selected and their hourly values were averaged and plotted in Fig. 6. The northern type was selected from Zaria, Kano and Katsina records,

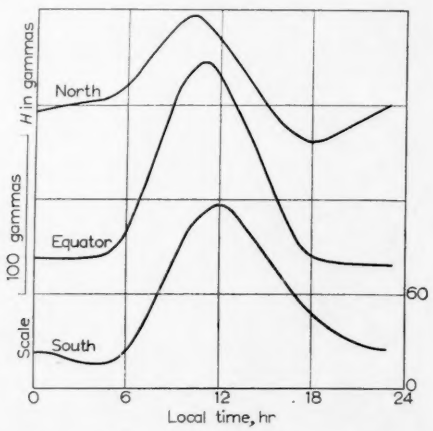

Fig. 6. Showing types of daily variation of H around the magnetic equator.

the equatorial type from Bida, Minna and Kaduna, and the southern type from Ibadan and Ilorin. The 4 days selected from Ibadan (S-type) were also included in the E- and N-types (two in each) as a check.

Besides the shift in the time of maximum, the great difference between these types is that unlike E, the S- and N-types are not symmetrical. A quantitative estimation of this asymmetry has been made as follows. We define the sunrise value of H denoted by H_r as its mean value in 1 hr interval centred on any minimum between 0400 and 0600 hours local time. If no minimum occurs in this interval, H_r is the mean from 0430–0530 local time. Likewise, the sunset value H_s is

VOL. 13 1958/5

centred on either a minimum between 1700 and 1900 or on 1800 local time. Then the measure of asymmetry (A_s) is defined as the sunset minus the sunrise value divided by the daily range R.

$$A_s = \frac{H_s - H_r}{R} \qquad (1)$$

Only quiet days were used in the computation of the asymmetry.

Considering equation (1) in the light of the above, we expect A_s to be positive south of the equator (S-type), zero at the equator (E-type), and negative north of the equator (N-type). These are borne out by the measurements in Table 5.

Table 5. Showing the mean values of the measure of asymmetry (A_s)

Station	Asymmetry (A_s)		Station	Asymmetry (A_s)	
	at station	at Ibadan		at station	at Ibadan
Ikeja	0·300	0·349	Kaduna	−0·096	—
Ilorin	0·229	0·333	Zaria	−0·236	0·456
Bida	0·022	0·363	Kano	−0·008	0·326
Minna	0·008	0·319	Katsina	−0·503	0·349
Tegina	0·055	0·315	Ibadan (mean)	—	0·352

Mean of A_s at Ibadan for the whole period 0·352 ± 0·036

The measure of asymmetry A_s has been plotted against both latitude and longitude. Whereas it shows no recognizable connexion with longitude, it is reasonably linear with latitude (Fig. 8). This indicates that the change of form occurs progressively across the equator.

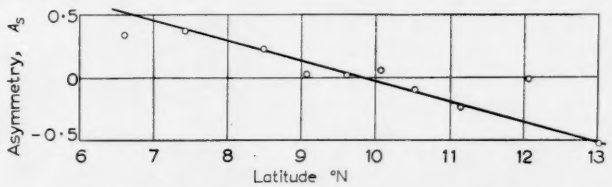

Fig. 8. The variation of asymmetry (A_s) with latitude.

4.3. *Equatorial indentations*

Chapman and Bartels (1940) p. 242 have mentioned that even on quiet days, the H-variation at Huancayo has fluctuations peculiar to the equator. These fluctuations also exist at Ibadan and at the field stations where records were made. Every indentation on Ibadan record is in fact reproduced at the field stations.

This characteristic of equatorial variation has not been studied before. In an attempt to study it, it would be desirable to have a simultaneous recording from outside the immediate equatorial zone in order to be sure what is peculiar to the

equator. This was not possible. It was therefore necessary to use only obviously quiet days and any part of a record with K_p index greater than 3 was rejected.

A comparison of magnetograms shows that within the limit of our stations, the equatorial indentations occur simultaneously in spite of the difference between the times the variation reaches a maximum. From the magnetograms of 31 December ($C_p = 0{\cdot}3$); 4 January ($C_p = 0{\cdot}2$) and 5 January ($C_p = 0{\cdot}2$), the times of occurrence of 106 indentations at Ibadan and Kano have been measured. Sixty-eight were coincident in time and the remaining thirty-eight, as the distribution curve Fig. 9(a) shows, have indicated no significant tendency to occur earlier in either of the stations.

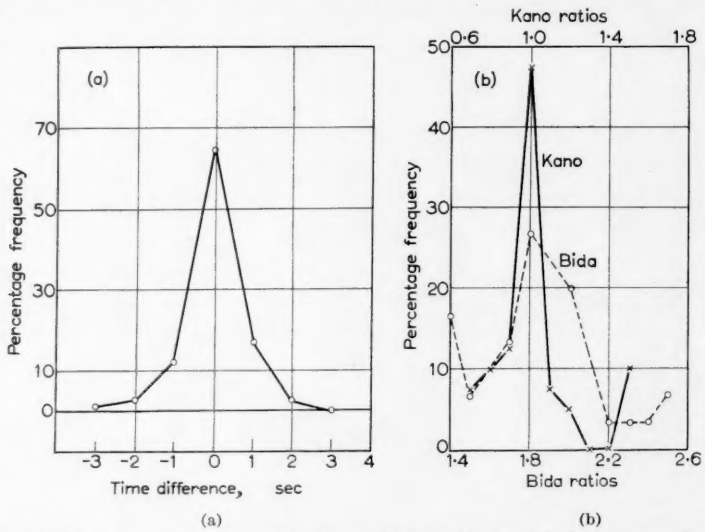

(a) (b)

Fig. 9. (a) Histogram of difference in time of fluctuations. (b) Histogram of ratios of fluctuation magnitudes.

The magnitudes of these indentations have also been measured. The difficulty in obtaining accurate values lies in the choice of a baseline. The fluctuations are superimposed on the diurnal variation. When the latter is changing rapidly, the fluctuations are elongated—at the beginning if the diurnal variation is increasing and at the end if it is decreasing. On account of this it is even more difficult to compare measurements at two stations where the diurnal variation is not changing in the same way at the same time. The difference of about 1 hr in the time of maximum mentioned above, means that an indentation will be measured at Ibadan and any northerly station, say Kano, under two different conditions of the general rate of change. These considerations were borne in mind in making the measurements.

Some forty comparisons of the magnitudes of the indentations at Ibadan and Kano gave a mean ratio (Kano to Ibadan) of $1{\cdot}00 \pm 0{\cdot}21$. Also thirty comparisons of their magnitudes at Ibadan and Bida were made from the days 5 December ($C_p = 0{\cdot}5$); 6 December ($C_p = 0{\cdot}7$); 7 December ($C_p = 0{\cdot}5$). The mean ratio was (Bida to Ibadan) $1{\cdot}79 \pm 0{\cdot}29$. The histograms of these measurements are shown in Fig. 9(b).

VOL. 13 1958/5

5. Discussion of Results

5.1. *Variation of ratios of daily ranges*

When only the strength of a current system changes, it is not expected that the ratio of the magnetic fields it produces at any two points will change. The considerable changes (Table 4) found in the ratios of the daily ranges at one particular field station to the corresponding ranges at Ibadan cannot therefore be explained by uniform changes in the strength of the S_q-current system. Perhaps a general change in the strength of the S_q-current system may have local variations, but this alone may not explain these large changes in the ratios. If the electrojet is between two stations that receive its effect, a shift of the electrojet towards one of the stations will relatively increase the range of H at that station and decrease it at the other, with a consequently enhanced effect on the ratio. With this interpretation, the changes in the ratios suggest that the region of maximum influence of the electrojet is not static but shifts northwards on certain days and southwards on others.

5.2. *Position of maximum ratio of ranges*

In south India, Pramanik and Yegnanarayanan (1952) measured H with the QHM at three stations whose dips are about $-1{\cdot}9°$, $-0{\cdot}1°$ and $+0{\cdot}8°$. The ratio of the daily range of H to the corresponding range at Kodaikanal was highest at the dip of $-1{\cdot}9°$ between the geographic and magnetic equators. It is obviously not possible to determine the maximum from these. Madwar (1953) has suggested a probable displacement of the maximum towards the geographic equator but it is difficult to justify any statement on the matter from the scattered points of his plot. Pontier (1950) and Giesecke in 1951 did not find any clear displacement of the maximum from the magnetic equator. This is not surprising if the displacement is always as small as found here, for Pontier took measurements at intervals of 1° latitude and Giesecke at intervals of 150 km (1·35° latitude). However, Chapman (1951) later estimated that Giesecke's results indicated a maximum about 1° south of Huancayo. This would mean a displacement of 0·3° from the magnetic towards the geographic equator. The present measurements have definitely established a slight displacement of the position of the maximum from the magnetic towards the geographic equator.

Some suggestions as to the position of the line of maximum range of H have already been mentioned in Section (1). Martyn (1949) also suggested that the range is a maximum at a "mean magnetic equator", midway between the magnetic and geomagnetic equators. The finding here is nearest to the suggestion of Egedal (1947) who favours the magnetic equator. The mean longitude of these measurements would be crossed at about 5° N latitude by the line of maximum range determined by Hasegawa and Ota (1948), and Price and Wilkins (1951) and at about 3·5° N latitude by the "mean equator" of Martyn (1949), whereas a marked maximum occurs at about 9°36′N latitude. The difference between these and the finding here is so large that in our longitude, it may definitely be concluded that they have not been confirmed by experiment.

Price and Wilkins (1951) also found that the line of maximum range would move opposite to the movement of the sun. These measurements were centred

almost exactly at the December solstice, so, we may for all practical purposes take the sun to be on the average at the tropic of Capricorn. If the maximum moved from 5° N to 9° 36′ N as the sun moved from the geographic equator to Capricorn, it would be expected to move down to 0° 24′ N when the sun moves to the tropic of Cancer—a total movement of 9° 12′. This is absurdly large, for one thing it would have been easy to detect it even from one observatory like Huancayo. We may conclude that in the longitude of the present measurements, if the line of maximum range is to move according to Price and Wilkins its movement will not be compatible with its mean position they found.

Three suggestions may be given to explain this slight displacement of the maximum. The studies of the influence of Hall polarization field on ionospheric conductivity (Hirono, 1950a, 1950b and 1952, Baker and Martyn, 1953) appear to have clearly established that the east–west S_q-current will be greatly increased where the dip is zero in the ionosphere. The magnetic field on the surface of the earth is influenced by local peculiarities. It is possible that at the height of the ionosphere where the effect of these peculiarities should be reduced, the distribution of the magnetic field is different. If anything, it should tend towards a simplification, that is, nearer the dipole field, in which case the magnetic equator there will be nearer the geomagnetic. These considerations will lead to a displacement of the region of maximum H-range from the magnetic towards the geomagnetic equator. This is not necessarily in disagreement with the finding here but it is not supported by the Indian measurements where larger range ratios were found on the side of the magnetic equator remote from the geomagnetic.

Secondly, it may be suggested that the magnetic and geographic equators have influences of their own, the former being the more powerful. This is quite conceivable since the two important elements of the dynamo theory—conductivity and tidal air velocities—are respectively controlled by these equators. This means a maximum always between the magnetic and geographic equators but nearer the magnetic. This is in agreement with all indications of displacement so far found.

It may however be observed that if it were certain that the maximum should occur at the magnetic equator, then the present results show that in the December solstice, in our longitude, the maximum has moved in the same direction as the sun. The shift would then be attributed to the effect of sun's declination on ionospheric conductivity.

5.3. *Magnitude of the maximum range*

The measurements of Giesecke in South America show that the daily range of H at its maximum is double that at about 5° south of it. Pramanik and Hariharan (1953) concluded from all the Indian measurements that the range near the magnetic equator is about double that outside the narrow belt of high ranges. It is not safe to make estimates from the results of Pontier (1950) and Madwar (1953) in view of their doubtful correction of the ranges. Here, the range at the maximum is found to be 1·8 to 2·2 times that at about 3° away from it. All agree among themselves. They also agree with Baker and Martyn (1953), who, putting typical values of ionospheric parameters into their equation found that the equatorial current is enhanced by a factor of 1·87 over that outside the equator. All these

VOL
13
1958/

indicate that as EGEDAL (1948) concluded, the maximum is sharply peaked and the effect of the electrojet is limited to a very narrow zone.

5.4. *The asymmetry of the curve of range ratios*

Curve I, Fig. 5 is not symmetrical even when judged not from the magnetic equator but from the position of maximum range. For equal distances on opposite sides of the maximum, a higher ratio tends to occur between the magnetic and geographic equators. This is not so apparent in the less satisfactory curve II. The Indian results seem to indicate it but the scarcity of measurements to the south of the magnetic equator makes a definite conclusion unsafe. The existence of this asymmetry if finally established, will support the second explanation [Section (5.2)] for the displacement of the position of maximum range.

5.5. *Forms of equatorial* H*-variation*

North of the magnetic equator, H reaches a maximum in its diurnal variation at a time that would be expected from the records of older observatories in similar situations; but south of the equator this maximum is delayed (there it comes nearer noon than 1100 hours, local time). That the delayed maximum south of the equator is not a peculiarity of the period of the tour is shown by the analysis of Ibadan observatory records (soon to be published).

BARTELS and JOHNSTON (1940) have studied the influence of the lunar upon the solar daily variation of H at Huancayo. They concluded that the diurnal variation curve of H is often modified by the lunar variation. This does not explain the types of equatorial H-variation found here since Ibadan maintains its form at the time other forms are recorded near or north of the equator. In this connexion it is worthy of note that the mean value of A_s (the measure of asymmetry) for Ibadan in each period at a field station is positive whereas A_s for that station may be negative. This means that the forms are not due to a day-to-day change of type of S_q but to a definite geographical distribution of S_q-form. The same idea is emphasized by the linear relationship of A_s with latitude (Fig. 8). Moreover, the mean value of A_s for Ibadan in each of the periods at field stations is fairly constant. Since the mean ($0{\cdot}352 \pm 0{\cdot}036$) is ten times the standard deviation, there is little doubt as to its constancy in those two months; but the lunar variation changes with the age of the moon. We therefore conclude that the influence of L on S_q is at best only a small contributory factor to the forms of equatorial H-variation found here. The constancy of A_s for Ibadan also suggests that A_s is a reliable measure of the asymmetry which may, for each station, have a value possibly varying only with season.

5.6. *Equatorial indentations*

The fluctuations in the diurnal variation curve of equatorial H have been shown to occur simultaneously at widely separated equatorial stations [Fig. 9(a)]. Ratios of the magnitudes of the fluctuations to the corresponding fluctuations at Ibadan have been determined for Kano ($1{\cdot}00 \pm 0{\cdot}21$) and Bida ($1{\cdot}79 \pm 0{\cdot}29$). In the light of these ratios, two suggestions may be made as to the origin of the equatorial indentations. The ratios are somewhat higher than the corresponding ratios of the ranges (0·91 for Kano and 1·49 for Bida). If significant differences in the ratios

were established, an origin in the electrojet would suggest itself; for, in that case, it would be expected that the ratios of the fluctuations would be greater than those of the ranges because the latter include a part arising from the "normal" variation (without the electrojet) and this normal variation should not be much different at the station and at Ibadan.

The differences between the ratios of the ranges and those of the indentations are however within the error limits. The origin should therefore be such that it affects both ranges and magnitudes of the fluctuations through the same media and in about the same proportions. It is more likely that these indentations are reflections of fluctuations in the ionizing agent from the sun, perhaps, ultraviolet radiation. The phenomenon is to be likened to solar flare effect and both have the common property of occurring in the daytime. It may be that the reason why it has been observed only near the magnetic equator is that it is greatest there. Even if the effect is world-wide but proportional to the diurnal ranges (as measurements here suggest), it will hardly be detectable at stations far from the magnetic equator. Because of the small value of the zenith angle of the sun and the great enhancement of ionospheric conductivity, fluctuations in the ionizing agent will affect magnetic changes most effectively near the magnetic equator. The preponderance of indentations around noon strongly supports this view. Solar flare effects are abnormally large at Huancayo, near the magnetic equator (MCNISH, 1937). It is suggested that the indentation is another widely distributed phenomenon with abnormally large amplitude near the magnetic equator.

VOL
13
1958/

Acknowledgements—I owe immense gratitude to the following: Prof. N. S. ALEXANDER for building the variometer used for the field work and for many helpful discussions; Prof. R. W. WRIGHT for constant encouragement and many useful discussions; Dr. J. EGEDAL and Dr. A. J. LYON for very helpful discussions.

REFERENCES

ALEXANDER N. S.	1955	Private communication.
BAKER W. G. and MARTYN D. F.	1953	*Phil. Trans.* A **246,** 281.
BARTELS J. and JOHNSTON H. F.	1940	*Terr. Magn. Atmos. Elect.* **45,** 269.
CHAPMAN S.	1951	*Arch. Met., Wien* A **4,** 368.
CHAPMAN S. and BARTELS J.	1940	*Geomagnetism* (1st. Ed.) Oxford University Press.
EGEDAL J.	1947	*Terr. Magn. Atmos. Elect.* **52,** 449.
EGEDAL J.	1948	*Nature, Lond.* **161,** 443.
HASEGAWA M. and OTA M.	1948	*Trans. Ass. Mag. Elec. Bull.* **13,** 426.
HIRONO M.	1950a	*J. Geomagn. Geoelect., Kyoto* **2,** 1.
HIRONO M.	1950b	*J. Geomagn. Geoelect., Kyoto* **2,** 113.
HIRONO M.	1952	*J. Geomagn. Geoelect., Kyoto* **4,** 7.
MADWAR M. R.	1953	*Bull. Inst. Égypt.* **36,** 5.
MARTYN D. F.	1949	*Nature, Lond.* **163,** 685.
MCNISH A. G.	1937	*Terr. Magn. Atmos. Elect.*, **42,** 109
PONTIER L.	1950	*Ann. Gèophys.* **6,** 238.
PRAMANIK S. K. and HARIHARAN P. S.	1953	*Indian J. Met. Geophys.* **4,** 353.
PRAMANIK S. K. and YEGNANARAYANAN S.	1952	*Indian J. Met. Geophys.* **3,** 212.
PRICE A. T. and WILKINS G. A.	1951	*J. Geophys. Res.* **56,** 259.
VESTINE *et al.*	1948	C.I.W. Publication No. 578, Washington.

Journal of Atmospheric and Terrestrial Physics, 1959, Vol. 13, pp. 235 to 257. Pergamon Press Ltd. Printed in Northern Ireland

A study of the equatorial electrojet—II

A model electrojet that fits H-observations

C. A. Onwumechilli
Physics Department, University College, Ibadan, Nigeria

(*Received* 14 *April* 1958)

Abstract—Methods are developed for separating the observed variation of the horizontal magnetic force (H) into its two component parts—the effect of the equatorial electrojet and the "normal variation" without the electrojet. It is shown that in such a separation, it is necessary to allow for the possible phase difference between the two component parts. Theoretical curves from the electrojet regarded as a horizontal current band of uniform intensity are found to fit the experimental points reasonably well. The electrojet is found to have a height of from 100 to 125 km, a width of 4° latitude and the current intensity at the height of 100 km is 6700 A/degree latitude. The effect of the electrojet on the vertical component (Z) of the earth's magnetic field is found to have a maximum value at about 250 km from the jet.

It is shown that after 600 km from the electrojet, the H-effect of the jet becomes very small whereas the Z-effect is large enough to explain the large Z-ranges observed in such regions. The geographical distribution of the forms of H-variation curve across the magnetic equator is explained as a result of the superposition of the "normal" variation and the electrojet effect. It is pointed out that Z-ranges observed at various parts of the world near the magnetic equator indicate a lack of symmetry about that equator and this is explained with a theory developed in this paper. Some suggestions are given about the relative importance of the geographic, magnetic, and geomagnetic equators in geomagnetic variation.

VOL. 13 58/59

1. Introduction

The object of this paper is to study the characteristics of a particular model of the electrojet which fits the variation of H as recorded and described in Part I.

The magnetic variation measured at any station near the electrojet may be regarded as made up of two parts—the "normal variation" and the electrojet effect. The "normal variation" is the variation which would be expected at the station if there were no equatorial anomaly in ionospheric conductivity. The whole earth would then conform to the pattern of variations measured at places outside the influence of the electrojet. The first step in the study of the electrojet is an attempt to separate these two parts.

Chapman (1951b) worked out the mathematical equations for various models of the electrojet. His idea of the jet current at the time appears to have been, a current system entirely separable from the "normal" but merely having a similar direction with it near the magnetic equator. Thus a consideration of the return path of the jet was paramount. Since then the study of ionospheric conductivity (Hirono, 1950a,b, 1952; Maeda, 1952; Baker and Martyn, 1953) has shown that the abnormally large ranges of equatorial H result from the intensification of S_q-current system around the line of zero dip in the ionosphere. It will therefore appear that we do not need a return path for the jet separate from that of the S_q current. The effect of the return currents would therefore have been included in the "normal" part of the variation field and we only need consider the direct effect of the great enhancement of S_q-current around the line of zero dip.

2. First Method of Investigation

One method of investigation is to assume that the parts N and J contributed to the daily range R by the normal variation and the jet effect respectively are numerically additive.

Then we have $$R = N + J \tag{1}$$

Fig. 1 shows a symmetrical curve giving the variation of the daily range

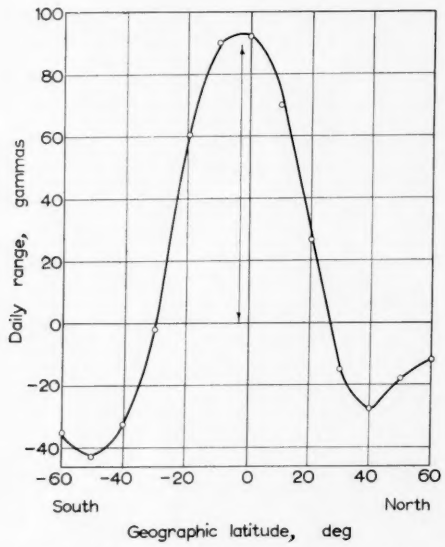

Fig. 1. Showing how the daily range of the geomagnetic north component of the earth's magnetic field varies with geographic latitude in the months around December solstice.

of the geomagnetic north component (X) with geographic latitude. The points are the means of ranges for December solstice (November to February) taken from the tabulations of Vestine *et al.* (1948) pp. 75–83. They are based on 11 years data (1922–33), collected from 100 observatories all over the world (five from Africa).

The main features of the curve are the shift of the maximum range from the geographic equator to 3° south of it (a seasonal effect), and the phase reversal of X at 27°N (also a seasonal effect). At the equinox the maximum range is expected at the geographic equator and the phase reversal at about $\pm 30°$ latitude. These features are expected to apply to the H-variation recorded in Nigeria.

The main part of the curve, from zero range to the maximum, may be represented by a parabola with the equation:

$$L^2 = \frac{1}{a}(N_0 - N) \tag{2}$$

VOL
13
1958/5

or by a cosine curve with the equation:

$$N = N_0 \cos 3L \tag{3}$$

where L is the latitude measured from 3°S, N is the normal range at latitude L, N_0 is the normal range at 3°S, and a is a constant.

There is little difference between the results but on the whole the parabolic relation was found to be more satisfactory, so we proceed with equation (2). Since $N = 0$ at $L = 30°$, we have:

$$N = a(900 - L^2) \tag{4}$$

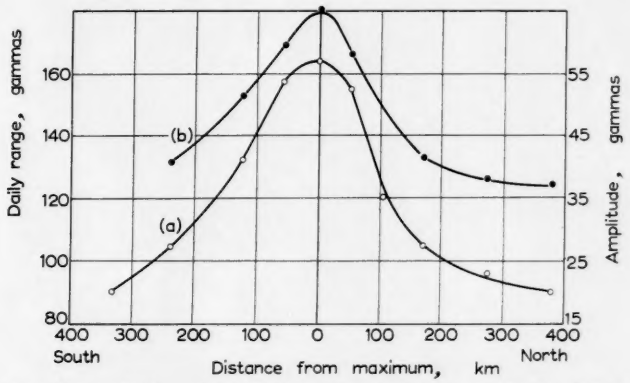

Fig. 2. Showing the variation of (a) daily range of H, (b) amplitude of first harmonic component of H, with distance from the latitude of maximum range of H.

If on the days on which records are taken simultaneously at two stations, the position of the electrojet is on the average midway between them, the jet effect J at the two stations will be almost the same. If the ranges R_1 and R_2 at the stations on the same day are known, equation (1) gives the difference $(N_1 - N_2)$ between their normal ranges and since the latitudes are known, this difference leads to the value of a. But no two stations at which measurements were made are exactly equally distant from and on opposite sides of the electrojet. The following procedure was therefore adopted. The observed ranges at the field stations are reduced to 105 gamma range at Ibadan (mean of Ibadan range during the tour) using the ratios plotted in Fig. 5, curve I of Part I. These reduced ranges are plotted in Fig. 2(a). From it the range at the "image" of Ibadan (240 km north of the electrojet, Ibadan being 240 km south) is taken as R_2. The difference $R_1 - R_2$ (7·5 gammas) is adjusted to 7·85 gamma to conform with actual conditions at the field station (Kano) nearest to the "image". During the period at Kano the range at Ibadan was 110 gamma.

Putting the latitudes of the stations in equation (4) we get from equation (1)

$$R_1 - R_2 = N_1 - N_2 = 109{\cdot}1a = 7{\cdot}85 \text{ gamma}$$

Hence $a = 0{\cdot}072$ gamma.

Knowing a, the normal ranges for all field stations are obtained using equation (4); in particular $N = 64$ gamma at the geographic equator. The values of J for each field station are then obtained from (1) using the mean ranges under quiet conditions (Table 2 of Part I). The ratio of each J to J_i found for Ibadan based on the same days are shown in Table 1. We could now proceed to estimate the height and width of the electrojet from these ratios, but first let us examine another viewpoint.

3. Second Method of Investigation

One assumption of the above method that is hard to justify is that the jet effect in every station is in phase with the normal variation thus making their ranges numerically additive. In such a method the jet effect can be over- or underestimated depending on its phase difference with the "normal". The forms of H-variation curve discussed in Part I Section (4.2) strongly suggest that in fact this error has been incurred. Here a method is outlined which with sufficient data may be used to remedy the situation.

3.1. *Theory of the method*

At any time t, the observed variation H_0 at a station is the vector sum of the normal variation H_s and the electrojet effect H_e at that station. So that vectorially we have:

$$\bar{H}_0 = \bar{H}_s + \bar{H}_e \tag{5}$$

These may be analysed into their Fourier components. The following symbols are used:

B_n is the observed amplitude of the nth harmonic;

E_n is the amplitude of the nth harmonic of the jet effect;

S_n is the amplitude of the nth harmonic of the normal variation;

ϕ_n is the observed phase angle of the nth harmonic;

α_{ne} is the phase angle of the nth harmonic of the jet effect;

α_{ns} is the phase angle of the nth harmonic of the normal variation;

s, e as subscripts refer to normal and electrojet effect at station;

1, 2 as subscripts refer to any two stations.

Then we write:

$$H_s = \Sigma S_n \sin (nt + \alpha_{ns}) \tag{6}$$

$$H_e = \Sigma E_n \sin (nt + \alpha_{ne}) \tag{7}$$

$$H_0 = \Sigma B_n \sin (nt + \phi_n) \tag{8}$$

$$= \Sigma S_n \sin (nt + \alpha_{ns}) + \Sigma E_n \sin (nt + \alpha_{ne}) \tag{9}$$

The components for any value of n in equations (8) and (9) may now be compared.

VOL. 13 1958/5

Here we are mainly concerned with the strongest component (the diurnal, $n = 1$). So dropping the subscript we have for the diurnal component:

$$B \sin \phi = \mathrm{E} \sin \alpha_e + S \sin \alpha_s \tag{10}$$

$$B \cos \phi = E \cos \alpha_e + S \cos \alpha_s \tag{11}$$

From (10) and (11) several equations can be derived expressing any one of the six symbols in terms of any four others. Those used here are:

$$B \sin (\phi - \alpha_e) = S \sin (\alpha_s - \alpha_e) \tag{12}$$

$$B \sin (\phi - \alpha_s) = E \sin (\alpha_e - \alpha_s) \tag{13}$$

$$S^2 = B^2 + E^2 - 2BE \cos (\phi - \alpha_e) \tag{14}$$

3.2. *Practical application of the method*

From the analysis of the observed records we get B and ϕ. Any of the equations (13) and (14) may be used to calculate E but each contains two of the three unknowns S, α_s, and α_e.

Since there is no intention to reconstruct the daily variation of the jet, only the first harmonic is necessary for the investigation of its latitude distribution. It is thought (CHAPMAN, 1951a, b) that the jet reaches its maximum about 1100 hours LT. The major component (the first) should reach a maximum at this time, and thus α_e may be taken as 285°. However, we are now in a position to make an experimental determination of this angle. It is almost certain that the symmetrical form of H-variation curve (Part I, Fig. 6) found in the immediate neighbourhood of the magnetic equator indicates that the electrojet effect on the days considered greatly overshadowed the normal variation. The 6 days typical of this form have been analysed harmonically and the phase angle of the first component was 283°56′. This confirms expectation and throughout we shall take α_e as 284°. To what extent this may vary from day to day and with season is not known. It was found from December records and when applied to the mean of a group of days it will probably be a fair approximation for November, December and January, and perhaps for most parts of the year, since solar daily variation at Ibadan shows no significant seasonal variation of phase. There is no way of ascertaining as yet the phase of the jet for each day.

Then we still need to know either S or α_s. A standard value of S may be interpolated from any suitable tabulation of its variation with latitude and longitude. Otherwise it may be determined by the same method used for N in Section (2). If the parabolic relation (2) is true for N it should equally apply to S (the major component of N).

So we write $$L^2 = \frac{1}{b}(S_0 - S) \tag{15}$$

and as before $$S = b(900 - L^2) \tag{16}$$

All complete records obtained on quiet days during the tour have been analysed. (The analysis was not possible for Ikeja because at that station there was no complete record under quiet conditions, and the analysis for Kaduna cannot be

used because during the period of observations at Kaduna, no complete record was obtained at Ibadan observatory.)

Since measurements were not actually made at the "image" of Ibadan, B_2 and ϕ_2 for the image have been obtained as follows. The observed amplitudes B were reduced to 40·48 gamma amplitude at Ibadan (the mean of Ibadan amplitudes for the tour), and plotted against distance from Minna (the station with a maximum). From this curve [Fig. 2(b)], the amplitude B_2 at the image of Ibadan

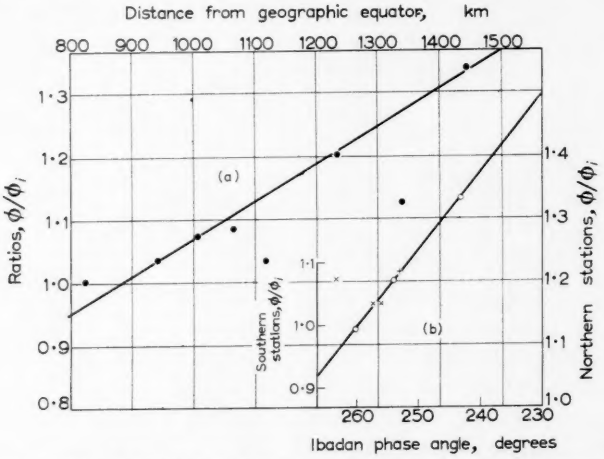

Fig. 3. Showing (a) The variation of phase ratios with distance from geographic equator. (b) The variation of phase ratios with observed phase angle at Ibadan. *Key to (b):* × southern stations; ○ northern stations.

was interpolated. Its value, 38·70 gamma was reduced to 37·6 gammas to conform with actual conditions at the nearest field station (Kano) when Ibadan amplitude was 39·33 gamma.

The observed phase angles at the stations were divided by the corresponding phase angles at Ibadan (Table 4). In Fig. 3(a) the ratios are plotted against distance of the station from the geographic equator. It does not appear safe to interpolate from this graph although it is reasonably linear. Another plot of the same phase ratios with the observed phase angles at Ibadan [Fig. 3(b)] is more satisfactorily linear. The graph is however not straightforward.

If we express this linear relation between the ratio of phases r and the observed phase angle at Ibadan ϕ_1 by the equation:

$$r = d - c(\phi_1 - 260) \tag{17}$$

we find that whereas the gradient c has the same value (0·0123) for all latitudes, the constant d is 1·00 for southern stations but 1·13 for northern stations. The significance of this difference between north and south is not very clear but there is no doubt that an interpolation made from it will conform with the trend of observations during the tour. While observations were being made at Kano (the nearest station to Ibadan "image"), the mean phase angle at Ibadan was 260°. Putting this in equation (17) we obtain 294° as ϕ_2 the corresponding phase angle at Ibadan "image".

VOL. 13 1958/5

Substituting equation (16) in equation (14) we get

$$b^2(900 - L^2)^2 = B^2 + E^2 - 2BE \cos(\phi - \alpha_e) \tag{18}$$

And since we now know L_1, B_1, ϕ_1 for Ibadan and L_2, B_2, ϕ_2 for Ibadan image, they may be put in equation (18) obtaining two equations quadratic in E and linear in b^2. Since Ibadan and its "image" are equally distant from the jet, E will be the same at the two stations, so eliminating b we solve the quadratic for E and later obtain b. The following solutions were obtained:

$$E = 15{\cdot}7 \text{ or } 64{\cdot}7 \text{ gamma}; \quad b = 0{\cdot}033 \text{ gamma} \tag{19}$$

The higher solution for E is too high. It is found that under any reasonable assumptions of the width and height of the electrojet, its effect on H will not disappear until after 22·5° latitude from the jet. We have to reject the higher solution because this invalidates the very basis of the solution for in that case, even values so far from the jet that they are regarded as normal would contain considerable jet effect.

S is calculated for all the stations from equation (16), in particular, $S = 29{\cdot}4$ gamma at the geographic equator. These values of S (Table 1) are then used to

Table 1. Showing the separation of the "normal" and the electrojet variations

Station	$L°$ N	Distance from 0° lat. (km)	Distance from max. H (km)	Normal range N (gamma)	Ratio J/J_i	Normal amplitude S (gamma)	Ratio E/E_i
(1)	(2)	(3)	(4)	(5)	(6)	(7)	(8)
Ikeja	9·600	733	333	58	0·71	26·7	—
Ibadan	10·433	826	240	57	1·00	26·1	1·00
Ilorin	11·483	942	124	55	1·58	25·3	1·67
Bida	12·067	1007	59	54	2·28	24·9	1·82
Minna	12·600	1066	0	53	2·50	24·5	2·47
Tegina	13·067	1117	51	52	1·86	24·1	1·84
Kaduna	13·517	1170	104	51	1·40	23·7	—
Zaria	14·133	1235	169	50	1·48	23·1	1·27
Kano	15·050	1339	273	49	0·94	22·3	0·91
Katsina	16·000	1444	378	46	1·03	21·3	0·10
"Image"	14·767	1306	240	49	1·00	22·5	1·00

obtain $(\alpha_s - \alpha_e)$, $(\phi - \alpha_s)$ and E from equations (12) and (13). The values of α_s using the higher solution for E also furnish another reason why that solution should be rejected. They indicate that the normal variation would reach its maximum at an absurdly early time (e.g. at 0030 and 2015 hours LT for Zaria and Ibadan respectively).

Having calculated E for all stations and computed their ratios to E_i at Ibadan, we are in a position to estimate the height and width of the electrojet from them [Section (5)].

4. JET EFFECTS ON Z AND H AT IBADAN

If a theoretical model of the electrojet which fits the experimental observations on H can at the same time satisfy a condition derived from Z-variation, the conclusions drawn from it will have a greater measure of certainty. Therefore the ratio of Z to H at Ibadan has been determined which a model will be required to satisfy in addition to fitting the H-measurements.

The "normal" range at Ibadan (57 gamma) found from the parabolic relation (4) is taken to correspond to the VESTINE *et al.* (1948) mean of X (75 gamma) in the months around December solstice. Using the proportional relation between the monthly ranges of X and their mean, the corresponding monthly ranges of H are worked out for Ibadan. These monthly normal ranges of H are then subtracted

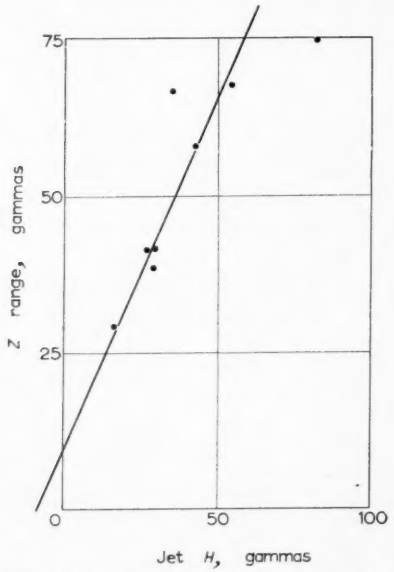

Fig. 4. Showing the relation between jet H and observed Z ranges at Ibadan on international quiet days in December solstice.

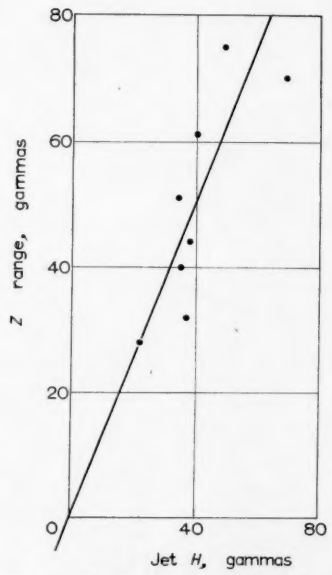

Fig. 5. Showing the relation between jet H and observed Z ranges at Ibadan on undisturbed days in December solstice.

from the corresponding observed monthly ranges of H at Ibadan observatory. The differences representing the jet effect J have been plotted against the corresponding observed monthly ranges of Z from Ibadan observatory. Two kinds of ranges have been used for the plot—ranges on international quiet days and ranges on undisturbed days ($C_p < 1{\cdot}2$). These graphs show some scatter which is not altogether surprising; for one thing, the Z-ranges have not been corrected for seasonal variation and secondly, the ratios used to correct for seasonal variation in X may not apply to Ibadan longitude. It is however the best that can be done in the circumstances. The line of Fig. 4 has a gradient $Z/H = 1{\cdot}11$ and an intercept of 10 gammas whereas the line of Fig. 5 has a gradient of $Z/H = 1{\cdot}23$ and an intercept of 1 gamma.

VOL
13
1958/

5. Comparing Observations with Models of Electrojet

5. *The electrojet as a linear current*

A current of i e.m.u. flowing in an infinite straight line produces at a perpendicular distance r cm, a magnetic field of $2i/r$ Oe, normal to both the line and the perpendicular distance. So, if we neglect the sphericity of the earth, and regard the electrojet as an infinite linear (or cylindrical) current of strength I e.m.u., flowing perpendicular to the magnetic meridian at a height of h cm above the line of maximum H-range, it can easily be shown that at a distance x cm along the meridian, it produces a magnetic field whose horizontal (H) and vertical (Z) components are given by:

$$H = \frac{2Ih}{h^2 + x^2} = H_0 \cdot \frac{h^2}{h^2 + x^2} \tag{20}$$

$$Z = \frac{2Ix}{h^2 + x^2} = H_0 \cdot \frac{x \,.\, h}{h^2 + x^2} \tag{21}$$

and

$$\frac{Z}{H} = \frac{x}{h} \tag{22}$$

where H_0 is the value of H directly under the current. Between the limits of our stations, the declination changes from 8·45° W at Ibadan to 5·8° W at Katsina, with about 7·0° W at Minna (Alexander, 1955). Since also in this area, the magnetic equator runs nearly parallel to the parallels of geographic latitude the error in regarding the magnetic latitudes of the stations as measures of the distance x is therefore only about 0·75 per cent and the angle between the jet effect on H and the local meridian does not at any station exceed about 1·5°. Hence no corrections need be applied to the above equations or any others based on them.

For Ibadan $x = 240$ km, therefore $h = 216$ or 195 km according as $Z/H = 1{\cdot}11$ or 1·23 [equation (22)]. However, the jet ought to have a width.

5.2. *The electrojet as a current band of uniform intensity*

The next stage is to regard the jet as a horizontal band of current of width $2w$ cm and uniform intensity C e.m.u./cm. The band is considered to be made up of elementary currents placed side by side; and suitably integrating the results for a linear current we get:

$$H = 2C \tan^{-1} \frac{2 \,.\, v}{1 + u^2 - v^2} \tag{23}$$

$$Z = C \ln \frac{1 + (u + v)^2}{1 + (u - v)^2} \tag{24}$$

$$2(\tan^{-1} v) \cdot \frac{H}{H_0} = \tan^{-1} \frac{2 \,.\, v}{1 + u^2 - v^2} \tag{25}$$

$$2\left(\tan^{-1} \frac{2 \,.\, v}{1 + u^2 - v^2}\right) \cdot \frac{Z}{H} = \ln \frac{1 + (u + v)^2}{1 + (u - v)^2} \tag{26}$$

where, for convenience, $u = x/h$, and $v = w/h$.

In Fig. 6 is shown the variation of v with Z/H for fixed values of u [equation (26)]. From each curve the values of u and v may be found for which Z/H equals any predetermined value (e.g. 1·23). These values of u and v determine h and w that will give the desired value of Z/H (1·23 for Ibadan) but it is further required that equations (23) or (25) should fit the H-observations when these values (of u and v) are put into it. In view, however, of the difference between the values of Z/H found from Figs. 4 and 5, it was not considered advisable to apply the above

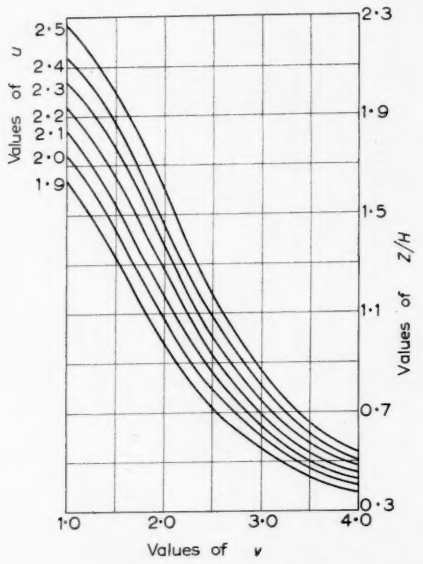

Fig. 6. Showing the variation of Z/H with v at constant u.

method strictly since it would limit the investigation to a single value of Z/H. Instead, values of u and v that fit the H-observations have been found for values of Z/H between 0·95 and 1·33 (Table 3). Only two cases for E/E_i (Fig. 8 from second method) and two cases for J/J_i (Fig. 7 from first method) have been drawn out. In each of these figures, the curve is drawn from equation (25) putting in the values of h and v indicated, and the points are from observations of H at the field stations. The values of u and v in Table 3 will fit the experimental points as well as those drawn out.

6. Discussions

6.1. H-*ranges from the parabolic relation*

In Nigeria, little error is incurred by identifying the geomagnetic north component X with the horizontal force H. Changes in the horizontal force H, the geomagnetic north force X and east force Y are connected by the equation:

$$\Delta H = \cos (D - \psi) \, . \, \Delta X + \sin (D - \psi) \, . \, \Delta Y \qquad (27)$$

Since in Nigeria D, the declination is negative (Part I, Fig. 1) and ψ, the angle

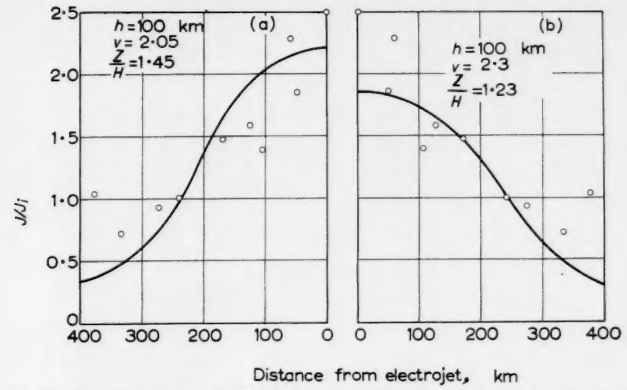

Fig. 7. Showing the variation of J/J_i with distance from the electrojet.

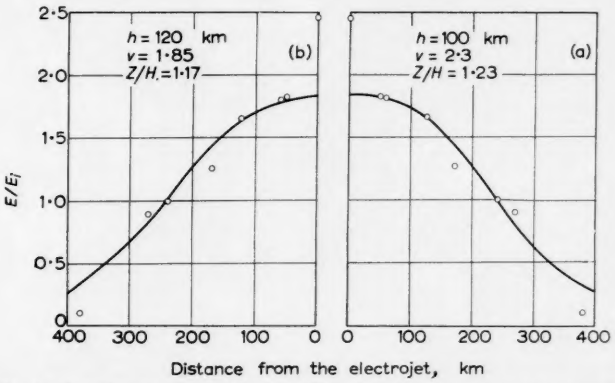

Fig. 8. Showing the variation of E/E_i with distance from the electrojet.

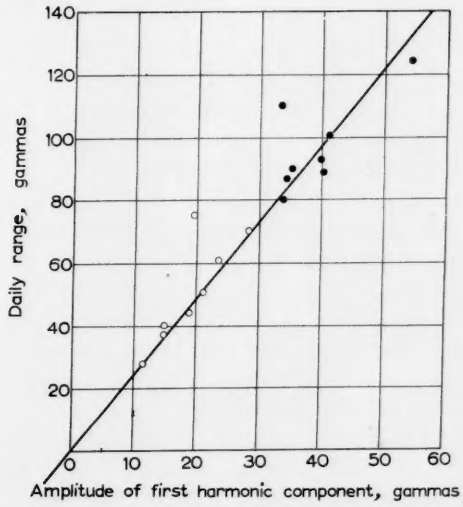

Fig. 9. Showing the relation between the daily range of force (H or Z) with the amplitude of its first harmonic component. ● Horizontal force; ○ Vertical force.

VOL. 13 58/59

between the geographic and geomagnetic meridians, is also negative and of the same order as D (McNISH, 1936), the cosine factor is high and the sine factor small. Taking secular changes into account, it can be shown that the error in identifying X with H is less than 0·9 per cent.

The normal ranges resulting from the parabolic relation (4) are now compared with observations. First, a in equation (4) came out about double b in equation (16) as might be expected; in particular, for Ibadan $N/S = 2{\cdot}18$ in good agreement with $R/B = 2{\cdot}44$ (Fig. 9) at Ibadan observatory. Observations of H near the geographic equator in Africa near the longitude of Ibadan are compared in Table 2 with VESTINE's mean ranges for December solstice and the ranges from the parabolic relation. The measurements at Moka, Bata, Niefang and Fernando Po are given by ROMANA and CARDUS (1955). In Table 2 the ranges in brackets are

Table 2. Comparing observed H-ranges with ranges from the parabolic relation

Observers	Year	Bata 1·80° N 9·80° E (gamma)	Niefang 1·85° N 10·30° E (gamma)	Moka 3·30° N 8·70° E (gamma)	Fernando Po 3·80° N 8·80° E (gamma)
VESTINE *et al.* X	1922–33	91	91	89	88
Parabolic N	1956–57	63	63	62	62
MARTINEZ and CAPUZ	1949–50	70 (56)			
CARDUS	1951	65 (62)			
ROMANA and CARDUS	1952		55 (62)		
NAVARO	1933			(67)	
ROMANA and CARDUS	1950				64

the results of correcting the observed ranges for solar activity. Whereas the observed ranges are significantly lower than the ranges from VESTINE *et al.* (1948), they are in excellent agreement with ranges from the parabolic relation. We therefore conclude that the "normal" ranges used in the theoretical investigation are appropriate. It is suggested that since VESTINE *et al.* (1948) did not correct for longitude effect, their tabulations might have been affected by the high ranges of observatories like Huancayo near the magnetic equator.

Since the intensity of S_q changes from day to day (CHAPMAN and BARTELS, 1940, p. 234), the values of N and S found from the parabolic relation should be regarded as standard values which should be corrected for use on any particular day. They could be corrected as follows. Suppose a station near the electrojet has a standard amplitude of the first harmonic S_1 and a second station in the same longitude but outside the jet effect has a corresponding value of standard amplitude of the *first* harmonic S_2. The actual value S'_2 observed on any day at this second station is different from S_2. If S_1' is the actual value (of the normal) that occurred at the first station near the jet on the same day, it is reasonable to say that:

$$S_1'/S_1 = S_2'/S_2$$

This gives the corrected value S_1' for the purpose of calculating E from the equations any day. In the present investigation, it was not possible to obtain S_1'.

6.2. *The two methods of investigation*

A closer examination of Fig. 2 shows that maximum H-range probably occurred about 5 km south of Minna but since the position of the electrojet is not known to an accuracy of better than 5 km, Minna has been taken as the position of the electrojet.

The experimental points of Fig. 8 fit the theoretical curves fairly well. This is surprising when it is remembered that the jet will not have exactly the form assumed for mathematical convenience. Fig. 7 is not as satisfactory as Fig. 8 and it is worse when the ratios J/J_i are worked out from ranges reduced to a mean (105 gammas) at Ibadan. This shows that in separating the normal and the electrojet effect it is necessary to allow for the possible phase difference between them.

6.3. *The height of the electrojet*

In the range of Z/H between 0·95 and 1·33 at Ibadan, the fitting height of the electrojet is between 89 and 240 km (Table 3). For $Z/H = 1{\cdot}11$ (Fig. 4), the resulting height is between 125 and 140 km; for $Z/H = 1{\cdot}23$ (Fig. 5), the height is between 95 and 115 km; and for $Z/H = 1{\cdot}17$ (the mean), the height is between 100 and 125 km. We may therefore conclude from these measurements that if the form of the electrojet is similar to that assumed, its height is between 95 and 140 km but most probably between 100 and 125 km.

Generally the height of the electrojet is expected to be about 100 km but there are really very few determinations of it. The only positive evidence in fact is the current encountered by a rocket from 93 km until it stopped rising at 105 km height (Singer *et al.*, 1951). This, however, must be regarded with care since strong magnetic disturbance (possibly associated with ionospheric disturbance) was in progress at the time of observation. (For the Greenwich day K_p-index sum was 47+ and C_p-character figure was 1·8.) Moreover, neither the altitude limit nor the direction of the current was determinable.

Calculations of ionospheric conductivity depend on conditions assumed to prevail there. Baker and Martyn (1953) for their conditions found maximum conductivity at a height of about 104 km. For two models of the ionosphere differing mainly in the depth of the trough between E and F_1 regions, Hirono (1953) found maximum conductivity at about 125 km for one case and for the other at 105 or 100 km depending on whether the maximum electron density is at a height of 110 or 100 km. These are in agreement with the estimate of a height of 100 to 125 km given here.

6.4. *The width of the electrojet*

Whichever of the values of Z/H at Ibadan is accepted, it makes little difference to the fitting width of the electrojet. In Table 3 it is seen that for Z/H between 1·10 and 1·23 and h between 100 and 140 km, the width of the electrojet only

varies between 420 and 460 km. The mean (440 km or 4° latitude) is therefore a more accurate determination than the estimation of the height. There is no other determination to compare with this—the theoretical investigators of ionospheric conductivity merely assumed working widths.

6.5. *The intensity of the electrojet*

Ibadan observatory records on all undisturbed days in December 1956 and January 1957 were analysed into harmonic components. From the first harmonic component and allowing for the phase difference between the jet and the normal, the jet effect E_i at Ibadan was found to be 15·1 gammas. From the theoretical values of E_0/E_1 for the fitting models of the jet given in Table 3 as H_0/H_i, it is

Table 3. Showing the characteristics of the electrojet that fits the observations of H

u_i	v	h (km)	width $2w$ (km)	H_0/H_i	$(Z/H)_i$	C (A/° lat.)	$1+\frac{C}{3500}$	x for Z_{max} (km)
2·7	2·61	89	464	1·85	1·30	6460	2·85	249
2·6	2·5	92	462	1·86	1·33	6560	2·87	249
2·5	2·4	96	470	1·85	1·25	6600	2·89	250
2·4	2·3	100	460	1·84	1·23	6670	2·90	251
2·3	2·17	104	447	1·86	1·23	6820	2·95	249
2·2	2·1	109	458	1·83	1·20	6920	2·96	256
2·1	1·95	114	446	1·86	1·20	7120	3·04	250
2·0	1·85	120	444	1·84	1·17	7180	3·05	252
1·9	1·73	126	437	1·84	1·13	7380	3·11	252
1·8	1·6	133	427	1·86	1·12	7730	3·21	250
1·7	1·5	141	423	1·84	1·10	7880	3·24	254
1·6	1·38	150	415	1·84	1·09	8200	3·34	256
1·5	1·25	160	400	1·84	1·07	8650	3·47	256
1·4	1·10	172	378	1·85	1·05	9320	3·66	255
1·3	0·95	185	351	1·85	1·03	10,209	3·92	254
1·2	0·80	200	320	1·86	1·01	11,600	4·30	256
1·1	0·65	218	284	1·84	0·97	13,400	4·84	260
1·0	0·40	240	192	1·84	0·95	20,600	6·88	259

easy to work out the value of E_0 at $u = 0$. Then from equation (23), the maximum value of the current about noon is easily calculated. This represents the jet current superposed on the normal during December 1956 and January 1957. Naturally, the intensity of the current increases with the height (Table 3). There are no determinations with which these may be directly compared.

On very broad bases, CHAPMAN (1951b) estimated the normal current intensity in the low latitudes as 3500 A/° lat. Using this uncertain value, the factors by which the jet current is intensified over the normal are given in column 8 of Table 3. The factor 1·87 found by BAKER and MARTYN (1953) is to be compared with 2·90 for the height they used (100 km). They considered their value an underestimation.

VOL. 13 1958/5

6.6 *The electrojet effect on* Z

It is easily shown from equation (24) that the electrojet effect on Z is a maximum (on one side and a minimum on the other) where

$$u^2 = 1 + v^2 \tag{28}$$

Thus if w (the half width) is very small compared with h, the distance of the maximum is of the same order as the height but if very large the distance is of the same order as the half width. The very high Z-ranges at Ibadan therefore suggest a large width and a position of maximum not far from Ibadan. Both are borne out by the determination here according to which the latitude of the maximum is extremely close to Ibadan observatory. The distances of the maximum for the various heights are given in Table 3 from which it is seen that the distance varies little, in fact it hardly varies at all. For the heights of between 100 and 140 km it lies between 249 and 256 km and there is no definite trend in the variation. We may therefore say with greater accuracy than in the determination of either the height or the width that the distance of maximum-Z is about 250 km from the position of maximum-H (only 10 km south of Ibadan observatory).

It may be noted that the magnetic latitude of the maximum-Z effect is $-2{\cdot}7°$ showing that if conditions everywhere are the same as here, both Huancayo (mag. lat. $+1{\cdot}3°$) and Kodaikanal (mag. lat. $+1{\cdot}7°$) are not close to the maximum-Z. About longitude 77·5° E in South India, Pramanik and Hariharan (1953) observed H- and Z-ranges between magnetic latitudes $+1{\cdot}3°$ and $+2{\cdot}8°$. The maximum ratio of their observed Z- to observed H-range was about 0·52 at about mag. lat. $+2{\cdot}2°$, which is in fair agreement with the corresponding ratio of 0·55 at Ibadan.

The mean amplitude and phase of the first component of observed Z during December 1956 and January 1957 at Ibadan were obtained. During the same period the jet effect E on H at Ibadan was 15·1 gamma. The jet effect on Z at Ibadan was therefore 16·8 or 18·6 gamma according as Z/H was 1·11 or 1·23. Putting these in equation (14) we obtain 4·4 and 3·5 gamma respectively as the amplitudes of the first component of the "normal" variation. These compare well with values from tropical observatories.

Fig. 9 shows that at least in the months of December solstice used in the plot, there is a good linear relationship between the daily range and the amplitude of the first harmonic component of both H and Z at Ibadan, and that the constant of proportionality (2·44) is the same for both. The amplitudes of normal Z above therefore imply "normal" Z-ranges of 11 and 9 gamma respectively. First, we note the little difference between the results obtained with the gradients of Figs. 4 and 5 whose intercepts differ so much. Secondly, the mean range of 10 gamma is considered a satisfactory determination of normal Z at Ibadan. McNish (1949 p. 338) suggested a maximum normal Z-range of from 12 to 18 gamma at about latitude $\pm 40°$. The value 17 gamma given by Vestine *et al.*, 1948, pp. 81–83) for Ibadan latitude is probably too high for the same reason that their H-ranges are high.

6.7. *Reconstruction of the variations of magnetic effects of the electrojet during December* 1956 *and January* 1957

When the jet effect on H at Ibadan during December 1956 and January 1957 is put in equation (23), C is found to be 6 gamma in force units, for the case of 100 km height. (The height of 100 km is chosen for easy computation. The use of other fitting h and v in Table 3 will scarcely make any difference in the results).

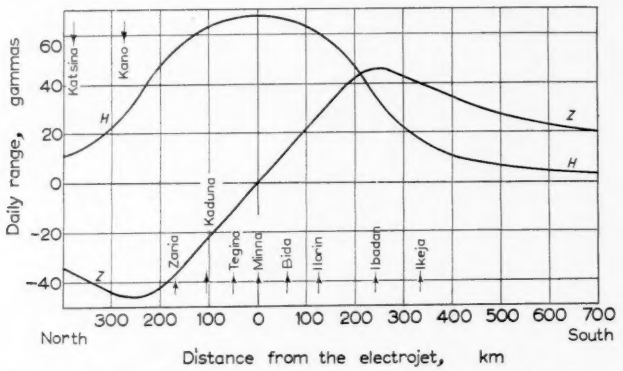

Fig. 10. Showing a reconstruction of the variations of electrojet effects on H and Z (December–January 1956–57) with distance from the electrojet.

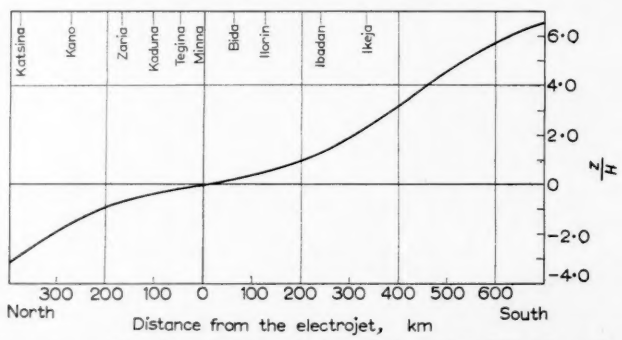

Fig. 11. Showing a reconstruction of the variation of electrojet Z/H (December 1956–January 1957) with distance from the electrojet.

Since Z at Ibadan is predominantly an electrojet effect, the relationship between Z-range and amplitude of the first harmonic (Fig. 9) should hold good for the magnetic effects of the electrojet. Thus if the right-hand side of equation (23) is multiplied by 2·44 the values of H from that equation would be daily ranges. The same applies to equation (24). From these the daily ranges of H and Z and from equation (26) the Z/H resulting from the electrojet during December–January 1956–1957 are calculated for various distances from the jet (Figs. 10 and 11).

From Fig. 10 it is seen that the electrojet effect on H varies but little in a narrow belt of about half the total width; then it declines and from the edge of the jet, it begins to decrease rapidly outwards. In the short distance of 400 km,

H-range has decreased from its maximum of 68 gammas to only 11. At 600 km H-range is 4 gamma and thence it becomes almost negligible.

In Fig. 10 upward Z is regarded as positive to conform with the practice at Ibadan observatory. Within the electrojet, Z increases almost linearly with latitude and reaches a maximum just outside the edge of the jet. From a maximum of 46 gamma, Z declines slowly and at 600 km from the jet, its daily range is still 23 gamma (half the maximum). The table below extends the daily ranges of Z plotted.

x (km)	700	800	900	1000	1100	1200	1300	1400
Z-range (gamma)	19·5	17·0	15·1	13·5	12·3	11·3	10·4	9·7

The figure and the table show that for the jet model that fits the H-observations, the jet effect on Z is quite considerable a long way from the jet, even in regions where the corresponding effect on H has become vanishingly small.

The high value of Z-range (39 gamma) observed by ROMANA and CARDUS (1955) in 1952 at Niefang (roughly 860 km from the jet) can therefore be explained at least partly as jet effect. However, in view of the uncertainty of the scale value with which the above was obtained, a better estimate may be 22 gamma obtained from direct measurement with B.M.Z. With a jet strength equal to that of December–January we are considering, jet Z at Niefang would be about 16 gamma leaving a reasonable value of 6 gamma as "normal" range of Z close to the geographic equator.

From the latitude distribution of Z-ranges found here, it appears that CHAPMAN (1951b) was right in interpreting Z-ranges of from 30 to 40 gamma at places like Alibag and Manila as having been influenced by the electrojet, even though H-ranges in those places were not particularly high.

Just outside the edge of the electrojet, Z is about maximum and H is decreasing rapidly, so the rate of change of Z/H is greatest. This is exemplified by the large change in a distance of 40 km in the table.

Distance x (km)	220	230	240	250	260
Z/H	1·035	1·136	1·230	1·354	1·460

Ibadan is in this range and obviously this rapid change makes it difficult to obtain a good value of Z/H at Ibadan and might be a major cause of the scatter in Figs. 4 and 5. Some evidence has been given [Part I, Section (5.1)] that the jet might be shifting northwards or southwards on certain days and it is likely that the jet being part and parcel of the S_q current will have some seasonal movement between December and February. Any such shifts of the electrojet, alter Z/H at Ibadan. It is interesting to note that a shift of only 10 km will cause the difference between 1·11 and 1·23 found for Z/H at Ibadan from Figs. 4 and 5, and the position of the jet is not known to an accuracy of better than 10 km.

Table 4. Showing the phase relation of the "normal" variation and electrojet effect

Station	Observed amplitude (gamma)		Observed phase (°)		Ratio	Phase of "normal" (°)		Ratio	Difference in phase of normal and jet		$\frac{\alpha_s - \alpha_e}{\alpha_i - \alpha_e}$
	B_s	B_i	ϕ_s	ϕ_i	ϕ_s/ϕ_i	α_s	α_i	α_s/α_i	$\alpha_s - \alpha_e$	$\alpha_i - \alpha_e$	
Ibadan (mean)	—	40·48	—	255·3	1·000	—	233·3	1·000	—	−49·9	+1·000
Ilorin	51·13	40·25	266·7	257·2	1·035	247·15	240·0	1·030	−36·85	−44·0	+0·838
Bida	64·05	44·55	282·7	263·4	1·075	280·65	246·4	1·140	− 3·35	−37·6	+0·090
Minna	60·58	37·96	274·5	253·1	1·085	259·9	235·6	1·215	−24·1	−48·4	+0·498
Tegina	72·63	51·41	264·9	255·9	1·035	202·1	216·0	0·935	−81·9	−68·0	+1·210
Kaduna	39·53	—	266·5	—	—	254·0	—	—	−30·0	—	—
Zaria	35·81	35·07	303·6	254·1	1·195	315·35	241·95	1·303	+31·35	−42·05	−0·750
Kano	36·02	39·33	292·6	260·0	1·125	297·95	246·25	1·210	+14·0	−37·75	−0·370
Katsina	31·42	34·77	323·9	243·3	1·334	327·4	206·55	1·587	+43·4	−71·45	−0·610

VOL
13
1958/

Here, it may be mentioned in passing that a cursory examination of Z/H at Ibadan for the other seasons reveals a similar scatter in the plots and indicates lower values of Z/H. If the lower values are confirmed and they are wholly explained by movement of the electrojet it will mean that the jet moves opposite to the movement of the sun in agreement with PRICE and WILKINS (1951).

6.8. *The influence of earth currents*

Very little is certain about the induction effects of restricted current systems like the electrojet. The small width of the jet keeps its area much below the limit (0·1 of the earth's area) given by CHAPMAN (1935) for which induction may be considered to contribute about 0·4 of the total variation. CHAPMAN (1951b) thought that the method of representing the induction effect of a linear current by the field of its image leads to overestimation of the effect. However, MCNISH (1938) developed a method which he believed could lead to a separation of the external and internal fields. The method is applicable only when both H and Z are measured at a number of suitably placed stations. He concluded that the current he was studying had an appreciable width. His ratio of the induced to the inducing field does not therefore apply to the narrow electrojet. His method implies, however, that in the range of influence of such current bands, the induced field bears a constant ratio to the inducing field. In that case, our method which depends on ratios will not be much affected even if the induced field is not negligible. The value of the jet current would however have been overestimated.

VOL. 13 58/59

7. INTERPRETATION OF SOME RESULTS

7.1. *Phase variation across the magnetic equator*

In Part I Section (4.2) evidence was produced that the type of H-variation curve changes as the magnetic equator is crossed from south to north. Here the phenomenon is shown to result from the superposition of the electrojet effect on the "normal" variation the phase of which varies with latitude. Fig. 3(a) shows that the observed phase of the first harmonic component of H increases fairly linearly with latitude. This is just another way of showing that H reaches its maximum progressively earlier as the latitude increases to the north.

Using methods developed in Section (3.1) the phase of the "normal" variation and its difference from the phase of the electrojet variation have been determined (Table 4). In the table, B is the observed amplitude; ϕ is the observed phase; α_s is the normal phase at a field station; α_e is the electrojet phase. Subscript i refers to Ibadan, s refers to a field station.

In Fig. 12(a) the ratios α_s/α_i are plotted against distance from the geographic equator (latitude). A good linear relationship is obtained showing that the phase of the normal variation increases progressively with latitude. The ratio $(\alpha_s - \alpha_e)/(\alpha_i - \alpha_e)$ plotted in Fig. 3(b) decreases linearly with latitude, but the points are a bit scattered around the magnetic equator.

The forms of variation curve and the time of maximum may be explained in this simple way. Well south of the magnetic equator, the normal phase is behind the electrojet phase. The jet effect and the normal are both small about sunrise but soon after the jet effect increases rapidly to a maximum about 1100 hours LT.

After 1100 hours the jet effect begins to decline but as the normal is larger and still increasing, the aggregate is still a rise. The late maximum of the normal (the larger) delays the observed maximum and gives the observed curve the effect of a slow decline after noon. Near the jet, its effect is so large that the daily variation curve almost takes the form symmetrical about 1100 hours expected of the jet. Well north of the jet, its effect again becomes rather small and the normal phase is in advance of the jet. Although the jet effect is small in the morning the more important normal variation is already increasing to its maximum before

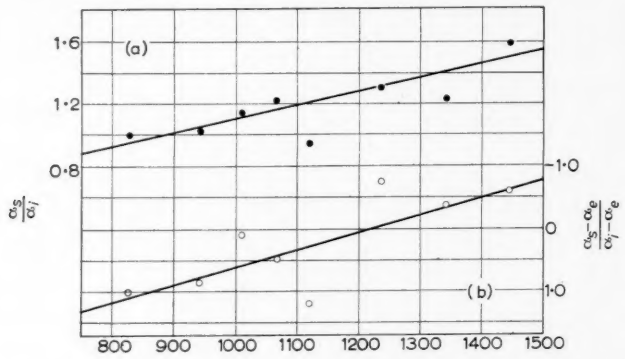

Fig. 12. Showing the variation of the ratios α_s/α_i and $(\alpha_s - \alpha_e)/(\alpha_i - \alpha_e)$ with latitude.

1100 hours. The jet effect continues to increase till 1100 hours but being small it does not prevent the occurrence of a maximum before 1100 hours and a rapid decrease after the maximum.

It is to be realized that the explanations given in this section are merely general pictures. It is not possible to explain the variation curve fully from the phase relations of only one of the components that make it up. However, the first component being the most important, it can give the general kind of idea expressed above. It has to be pointed out also that since the normal amplitude used for each station is not necessarily the normal amplitude occurring on the days in question, the resulting phases are affected and may be larger or smaller than the actual phase.

7.2. *The asymmetry of* Z*-ranges*

A general remark may be made here about the magnitude of Z-ranges so far observed north and south of the magnetic equator. The variation of Z seems to show lack of symmetry about this equator. Very high Z-ranges (50 to 80 gamma) so far observed (at Ibadan and in India) have all been south of the magnetic equator (where the dip is negative).

Although Pramanik and Hariharan (1953) in India along longitude 77·5° E measured Z-variation from magnetic latitude $+1{\cdot}3°$ to $+2{\cdot}8°$, they obtained Z-ranges of only 20 to 40 gamma. Even if allowance is made for a possible shift of the jet to the north or south of the magnetic equator, it would be expected that

VOL
13
1958/

in the extent of their stations, they would have observed Z-ranges as high as those at Ibadan (the magnetic latitude of Ibadan is $-2{\cdot}57°$). Along the same longitude in the same area in India, PRAMANIK and YEGNANARAYANAN (1952) obtained the results below.

Dip	$+0{\cdot}8°$	$-0{\cdot}1°$	$-1{\cdot}9°$
Mean Z-range (gamma)	43	56	76
Z-range limits (gamma)	36–48	50–69	49–112
Mean H-range (gamma)	159	138	153

Putting their results together with those of PRAMANIK and HARIHARAN (1953), it is seen that from about $0{\cdot}4°$ to $2{\cdot}8°$ north magnetic latitude, the observed range of Z was 20 to 48 gamma, but immediately the magnetic equator was crossed to the south, the range increased to magnitudes similar to those observed at Ibadan. This suggests an asymmetry about the magnetic equator which is not easily explained.

If the electrojet is a horizontal current band, the asymmetry of Z-ranges will not result from the effect of the jet which is undoubtedly more important than normal Z in those areas. The structure of the jet is not expected to be as simple as the idealized case treated in Section (5.2) and the asymmetry may well result from its structure.

VOL. 13 58/59

However, a more obvious explanation of the asymmetry is the interaction between the electrojet effect and the normal variation in Z. If the two vectors have about the same phase as at Ibadan, the observed amplitude would be almost the scalar sum of their amplitudes but if they are about 180° out of phase, it would be almost the scalar difference of their amplitudes. The idealized Z-variation based on CHAPMAN's (1919) analysis is symmetrical about the geographic equator. North of the equator, the variation is of the same form for all latitudes up to 60°N. It follows that if the electrojet is interposed between two northern stations, the normal variation will at one station aid the jet effect and at the other oppose it.

The idealized curves (CHAPMAN and BARTELS, 1940, p. 215) show that at all northern stations like Ibadan and all the Indian stations under discussion, normal Z (positive upwards) is a maximum about 1100 hours LT. If the electrojet is an east–west current as is generally supposed, it would also produce about 1100 hours LT a maximum upward (Z) field to the south and a maximum downward (Z) field to the north of it. Thus at Ibadan and the two Indian stations with negative dip, the jet effect and the normal are fairly in phase agreement whereas at the other Indian stations with positive dip, they are in phase opposition. This explains the observations so far made.

On the assumption that the idealized curves of CHAPMAN represent normal Z-variation fairly well, the explanation above may be generalized as follows. Where the electrojet is not along the geographic equator, the Z-component of the magnetic variation produced by it is roughly in phase agreement with and aids the normal Z-variation in the region between the jet and the geographic

equator but elsewhere, they are in phase opposition and the normal variation reduces the Z-effect of the electrojet.

7.3. *A suggestion about the equators*

We now examine an overall picture of the suggestion, that the equators considerably influencing magnetic variations are the magnetic and the geographic.

From a model electrojet that fits the observations the latitude variation of the electrojet effect on H during December–January 1956–57 has been reconstructed. The table below extends the variation shown in Fig. 10.

Dist. x (km)	400	500	600	700	800	900	1000
H-range (gamma)	11	6	4	3	2·3	1·8	1·5

That the magnetic equator greatly influences magnetic variations is no longer in doubt, but this table and the discussion in Section (5.3) of Part I show that the electrojet effect on H is small after 400 km and is very likely negligible after 600 km even if its strength in another season were to be double what is found for December–January. To explain the large ranges of H found near the equators, it is therefore suggested that besides the magnetic, the geographic equator plays a great part through its control of the tidal motion and ionization density in the ionosphere. The large ranges of from 55 to 67 gammas (Table 2) observed near the geographic equator near the longitude of Ibadan cannot be ascribed to the jet (a distance of 860 km from it). On the other hand it has been shown that they are in excellent agreement with the "normal" ranges found from the parabolic relation. Their magnitude has to be associated with the geographic equator. From this suggestion, the following may be expected.

(a) The latitude distribution of H-ranges near the magnetic equator should be slightly asymmetrical. On the side of the geographic equator, the declining jet effect is slightly offset by increasing geographic effect and the resulting ranges are higher than on the other side where both effects are declining. The cases of asymmetry so far reported are in agreement.

(b) The position of maximum H-ranges should be slightly displaced as found towards the geographic equator. The displacement is expected to be small since the jet is by far the more important influence.

(c) The largest ranges of H on the whole earth should occur where the geographic and magnetic equators are coincident. This cannot be tested with observations so far made. It is in fact being suggested that the magnitude of H-ranges observed depend (among other things) on the nearness of the jet to the geographic equator.

(d) If a homogeneous set of H-ranges is plotted in the plane of two co-ordinate axes—the magnetic and geographic latitudes—the lines of equal ranges should demonstrate the relative influence of the equators.

The geomagnetic equator has not been mentioned. After all, it merely results

VOL.
13
1958/5

from a useful and convenient mathematical approximation of the earth's field. It is, however, a good approximation to the magnetic equator when dealing with phenomena at great distance from the earth's surface.

Acknowledgements—I owe immense gratitude to the following: Prof. N. S. ALEXANDER for building the variometer used for the field work and for many helpful discussions; Prof. R. W. WRIGHT for constant encouragement and many useful discussions; Dr. J. EGEDAL and Dr. A. J. LYON for very helpful discussions.

REFERENCES

CHAPMAN S.	1919	*Phil. Trans.* A **218,** 1.
CHAPMAN S.	1935	*Terr. Magn. Atmos. Elect.* **40,** 349.
CHAPMAN S.	1951a	*Proc. Roy. Soc.* B **64,** 833.
CHAPMAN S.	1951b	*Arch Met., Wien,* A **4,** 368.
HIRONO M.	1953	*J. Geomagn. Geoelect., Kyoto* **5,** 22.
MAEDA K.	1952	*J. Geomagn. Geoelect., Kyoto* **4,** 63.
MCNISH A. G.	1936	*Terr. Magn. Atmos. Elect.* **41,** 37.
MCNISH A. G.	1938	*Terr. Magn. Atmos. Elect.* **43,** 67.
MCNISH A. G.	1949	*Terrestrial Magnetism and Electricity* (Edited by FLEMING J. A. New York.
ROMANA A. and CARDUS J. O.	1955	*Publ. Oss. del Ebro* No. 14.
SINGER *et al.*	1951	*J. Geophys. Res.* **56,** 265.

OL.
13
8/59

Journal of Atmospheric and Terrestrial Physics, 1959, Vol. 13, pp. 258 to 270. Pergamon Press Ltd. Printed in Northern Ireland

The effects of ionospheric irregularities and the auroral zone on the bearings of short-wave radio signals

H. A. WHALE
Seagrove Radio Research Station, Auckland, New Zealand

(*Received* 6 *May* 1958)

Abstract—The nature of the observed variations in the received bearing of the signals from short-wave radio stations at various distances is discussed and the origins of some of the effects are suggested. The major part of the daily variation of bearing of stations up to about 15,000 km distant arises from the refraction of the ray in the *F1*-region when it is reflected from the *F2*-region. A discussion of the curving of the ray path by successive small changes of direction at each reflection point leads to the concept of an antipodal area replacing the geometrical antipodal point. The large changes in direction associated with the passage of a ray through the auroral regions suggest a method of plotting the shape of the absorbing parts of the auroral zone by observations at a place remote from this zone. A sample plot obtained by this method is presented.

INTRODUCTION

THE bearing of a short radio wave that has been reflected from the ionosphere is known to deviate from the great circle drawn through the transmitting and the receiving sites. This effect has been reported by many workers (BUDDE, 1950; BRAMLEY and ROSS, 1951; ECKERSLEY and FARMER, 1945; WHALE and ROSS, 1956, etc.) over a range of transmission distances varying from zero (vertical incidence measurements) to somewhat greater than 20,000 km (the long-path great circle distance from England to New Zealand).

It is necessary, in this work, to distinguish between the rapid fluctuations of bearing which arise from interference between the various components in the incoming group of waves (a fairly comprehensive study has been presented by WHALE and DELVES, 1958) and the relatively slow variations which arise from changes in propagation conditions. While these latter changes have long been recognized as indicating effective tilts in the ionosphere, the fact that it is a refraction process on which many of them depend has not previously been demonstrated.

In this paper an attempt is made to describe the nature of the deviations observed at the various distances and to ascribe causes to some of the observed effects. A distinction is made between the phenomena observed at distances less than about 15,000 km and those at distances greater than 15,000 km since the large slow variations of bearing occur only at the greater distances, i.e. when the transmitting and receiving stations are approaching the antipodal condition.

EQUIPMENT

These bearing measurements have been made on various direction-finders, but mostly on the rotating interferometer at Seagrove (WHALE, 1954). This is essentially a recording direction-finder which requires about 3–4 min to make one measurement of bearing and elevation angle. Although it can be used for obtaining information on the statistics of the rapid fluctuations of bearing and elevation

VOL.
13
1958/5

angle, the records used in this paper have been averaged over some fairly long interval, usually 1 hr or $\frac{1}{2}$ hr. In this way the rapid fluctuations occurring in less than $\frac{1}{2}$ hr are suppressed. These rapid fluctuations are still important in determining the sharpness of the records obtained on the interferometer since, if the fluctuations are too large (indicating a large spread in the incoming wave directions), the signals at the two aerials may become uncorrelated and it is then necessary to reduce the distance between the aerials until some correlation is restored. The normal spacing used for the interferometer aerials is about 60 m but in view of the very disturbed ionospheric conditions prevailing in 1957 this has lately been reduced to 25 m for measurements on signals from stations in Europe.

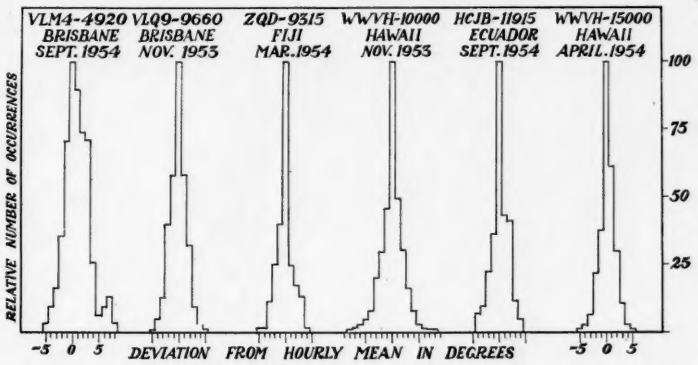

Fig. 1. Histograms of the bearing deviations from the mean for each hour for the months shown.

Short distance measurements

A large number of measurements have been made on a few stations which transmitted for sufficiently long periods to enable the diurnal variations to be obtained accurately. The stations which were found most useful in this work were:

VLQ9,	Brisbane	on 9660 kc	at 2250 km distance,	291° great circle bearing,
VLM4,	Brisbane	4920 kc	2250 km	291°
ZQD,	Fiji	9315 kc	2000 km	9°
WWVH,	Hawaii	10,000 kc	7000 km	32°
WWVH,	Hawaii	15,000 kc	7000 km	32°
HCJB,	Equador	11,915 kc	9450 km	100°

The day-to-day variation of the bearing (averaged over 1 hr) at any particular time may be up to about 5°. Although the shape of the curve for the average diurnal variation (obtained by averaging over 1 month, for example) is different for different frequencies, distances and directions of the stations observed, the day-to-day variations for stations at relatively short distances are usually of the same order of magnitude. This is shown in Fig. 1 where some typical histograms are plotted. The way in which the standard deviation of the day-to-day variations changes with distance is plotted in Fig. 2. In order to obtain a simple measure of the spread of the histograms in Fig. 1, these have been assumed to be normally

distributed. It is known that since the short-term (rapid) bearing fluctuations are interference effects they must have a distribution that is more sharply peaked than a normal curve (ROSS, 1955; WHALE and DELVES, 1958). From the cumulative distribution curves, it appears that the day-to-day variations may also be slightly peaked but this probably arises from the relatively small number of observations used in obtaining some of the distributions. This "peakiness" has been ignored in obtaining the values of the standard deviation plotted in Fig. 2. Each point on this graph represents about 100 hr or more observations obtained during some 1 month in the period 1953–1956. It is seen that the standard deviation remains almost constant up to about 135° angular distance (15,000 km). The full line curve labelled $\sin\theta = (\tan\frac{1}{2}\Lambda_0)/36$ is discussed below in connexion with small circle propagation.

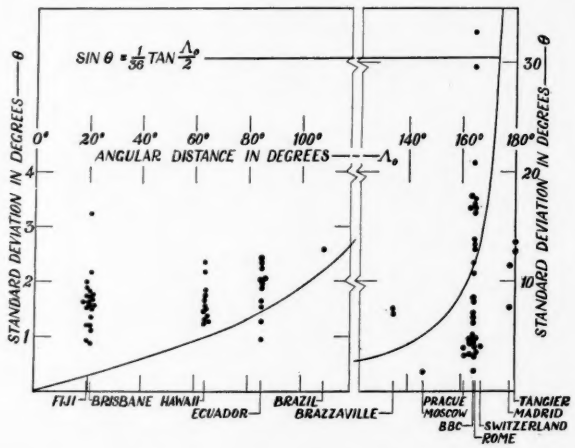

Fig. 2. Standard deviations obtained from observations similar to those plotted in Fig. 1 as a function of the path-length. The full line curve represents the limit of the expected deviations allowing 0·5° change of direction per 18° hop.

Short distance diurnal bearing changes

When the observed bearing angles are averaged over a month and then plotted as a function of time, it is found that most stations show a decrease of bearing (measured east of north) with time while the path is in daylight. This decrease is almost linear as is seen, for example, by comparing the full line measured curve in Fig. 3D with the straight dotted line, and is the most significant part of the daily variation curve (these measurements are on WWVH, Hawaii, true bearing 32° E). Another typical set of results for station ZQD, Fiji, is presented in Fig. 3E. In this curve, the measured bearings are drawn as open dots. Tilting of the reflecting layer is not sufficient to account for the observed deviations from the great circle bearing in these cases. It has been shown (TITHERIDGE, 1956) that the linear portions of these curves arise from refraction in the *F1*-layer of waves that are reflected at the *F2*-layer.

A diagrammatic representation of the refraction of a wave in an underlying layer is given in Figs. 3A and 3B showing how this "prism" effect operates in

VOL
13
1958/

changing the bearing angle (in Fig. 3A, which is an end-on view of the path) and the elevation angle (in Fig. 3B, which is a side view of the path) of the received ray. The case of refraction through a uniform layer is illustrated in Fig. 3C; in this case it is well known that there is no resultant change in direction apart from that arising from a slight increase in the apparent height of the reflecting layer. The consistency between the deviations in bearing and elevation angle on two paths almost at right-angles has been demonstrated previously in connexion with the measured effective tilts of the ionosphere (WHALE, 1956a).

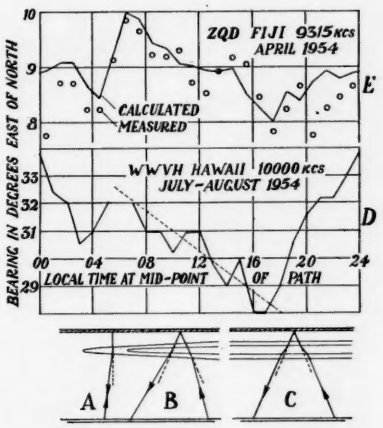

Fig. 3.
A. End-on view of "prism" effect in a refracting layer.
B. Side view of "prism" effect.
C. Refraction in a uniform layer.
D. Observed average diurnal bearing curve (full-line) with linear decrease (dotted line) for comparison.
E. Observed average diurnal bearing change (circles) with the bearing calculated from the monthly median values of the ionosphere characteristics (full-line).

From a well-known result in the theory of propagation through an ionized medium for the phase-path of a wave transmitted through a parabolic layer, it can be shown that the horizontal angle $\Delta\theta$ through which the wave is deviated is given by:

$$\Delta\theta = (2H/f_c)\{1 - (z + 1/z) \,.\, \tanh^{-1} z\}(df_c/dp) \cot i \qquad (1)$$

where fc = critical frequency of the layer
$z = f \cos i/f_c$
i = angle of incidence of the wave on the ionospheric layer
df_c/dp = gradient of critical frequency perpendicular to the path
H = semi-thickness of the parabolic layer.

The angle through which the wave is deviated can be calculated from contours of the critical frequency of the *F1*-region of the ionosphere since it is known that for this region of the ionosphere the variation of the electron density with height is nearly parabolic and that the semi-thickness is nearly always about 40 km.

The *F1* critical frequencies are not usually published in the ionosphere prediction bulletins but may be derived from the *E*-region critical frequencies to a fair accuracy by multiplying these by a factor of 1·4.

The total calculated deviations arising from *F1*-refraction plus a small amount of *F2*-tilting are drawn as the full line in Fig. 3E. The values of the ionosphere characteristics were not available for the mid-point of this path, as would have been desirable, but were obtained by interpolation from those measured at Brisbane and at Rarotonga.

The night-time variations do not seem to arise in any such simple manner; there is very little *F1*-region at night so that it seems that the night-time fluctuations are possibly caused by patches of *E*-region ionization obstructing some of the possible ray-paths.

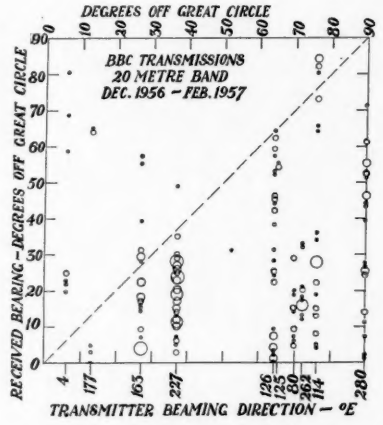
DEGREES OFF GREAT CIRCLE
BBC TRANSMISSIONS
20 METRE BAND
DEC. 1956 – FEB. 1957
RECEIVED BEARING – DEGREES OFF GREAT CIRCLE
TRANSMITTER BEAMING DIRECTION – °E

Fig. 4. Received bearing (difference between received bearing and great circle bearing) as a function of transmitter beaming direction (difference between nominal transmitter beaming direction and great circle direction).

Long-distance transmissions

The distinguishing characteristic of the long-distance transmissions is that the observed bearings are no longer nearly always close to the great circle bearing of the transmitter from the receiver. The experimental observations are difficult since it is seldom possible to receive the same frequency transmitted on the same aerial for very long periods of time.

Transmitting beaming direction

While a change in the transmitter beaming direction in the case of a short path transmission will have little effect on the received signal other than to change its strength, it seems possible that, over the longer paths, such a change could give rise to changes in the direction of the incoming signal. In general, it may be said that, if there is only one possible path then change in transmitter direction will alter only the signal strength, but that if several paths are simultaneously possible a change in the transmitter directivity may result in a change in the received direction. The difficulty lies in deciding what paths are possible.

VOL
13
1958/

Some typical results of an extensive investigation into the effect of the transmitter beaming direction on the bearing of the received signal are plotted in Fig. 4 which is representative of the measured values of the bearing angle of BBC short-wave broadcasts on frequencies between 9 Mc and 21 Mc. Each circle represents the received bearing averaged over about 1 hr, the size of the circle being proportional to the number of times a particular bearing was observed during the period of the investigation. The plot shows the departure of the received bearing from the great circle bearing (taken as 170/350° E), without regard to the sign of the departure so that the scale vertically is 0–90°, as a function of the difference between the nominal transmitter beaming direction and the great circle bearing of the receiver from the transmitter (taken as 190/10° E), again without regard to the sign of the difference, so that the horizontal scale is also 0–90°. The diagonal dashed line is the locus of bearings which are the complement of the transmitter beaming directions; in the idealized case of a transmitter situated antipodally to the receiver on a smooth spherical earth surrounded by a smooth spherical ionosphere concentric with the earth, this line would give the received bearing for any transmitter beaming direction. The horizontal line forming the base of the diagram is the locus of bearings which lie along the great circle direction. In general, it has been found that most of the points like in the bottom right-hand half of the diagram, i.e. most of the signals arrive from some direction between the great circle direction and the complement of the transmitter beaming direction. A difficulty in this type of investigation is that, even with sharply beamed aerials, the direction in which the received ray left the transmitter is not known with much accuracy. It is important that, since all frequencies in all beaming directions cannot always be received, there is some unavoidable bias in the results in Fig. 4. Many of these signals have travelled through or near to the auroral regions and, as is shown in a later section, must be considered in relation to those regions.

A further series of experiments which throw some light on the effect of a change in the transmitter beaming direction was made possible when the British Post Office arranged for the transmission from Slough of a fixed frequency first on one aerial and then on another. The measurements covered seven days between 24 October and 11 November 1955. Some of the results have been presented previously in a New Zealand Post Office report (NZPO, 1956). In these experiments the two aerials employed were first an almost omni-directional aerial (horizontal dipole) and secondly a rhombic aerial beamed in the direction 310° E. This is 60° off the great-circle direction and should thus be effective in demonstrating any change of the received direction with change of the transmitting direction. The average over the 7 days of the value of the quantity (bearing for rhombic transmitting aerial)—(bearing for dipole transmitting aerial) is plotted as a function of time in Fig. 6A for receiving stations both at Seagrove (Auckland) and at Awarua (Invercargill). The measurements at the latter station were made by NZPO personnel using an Adcock type direction-finder. There is a small effect on the received bearing (consistent between the two stations) arising from the change in aerial directivity but as this is only of the order of a few degrees it would be insignificant when considered in relation to the usual large spread of these bearings.

Some further results obtained on BPO transmissions, this time made on the automatic direction-finder at Seagrove (WHALE and ROSS, 1956), in which the bearing at the time of changeover of the aerials was observed very closely, also showed negligible change of the received bearing, even when the transmitter beaming direction was changed by 180°. A sample record obtained during such a changeover is plotted in Fig. 6B. It is interesting that some measurements made at Awarua on a similar direction-finder on these same transmissions (February 1958) occasionally showed very large changes of bearing when the transmitter

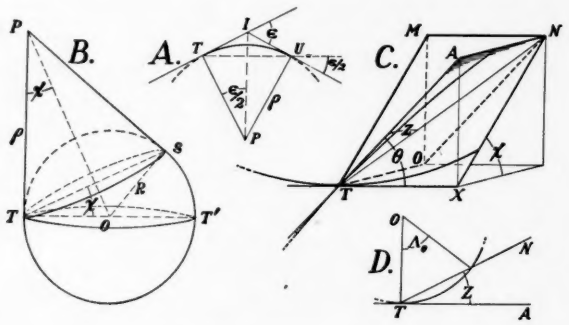

Fig. 5. Small circle propagation.

beaming direction was changed. This is connected with the fact that Awarua is only 9° angular distance away from being antipodal to the transmitting station while Seagrove is $15\frac{1}{2}°$ away from antipodal.

The antipodal area and small circle propagation

Since the beaming direction of the transmitter may be relatively unimportant in determining the incoming bearing there must be some restraining effect by the optimum path on the use of other paths by the ray. In this connexion, the problem of small circle propagation and the concept of an antipodal area replacing the geometrical antipodal point are useful and are discussed below. A note introducing these two aspects has appeared previously (WHALE, 1956b); the theoretical basis of that note is given here.

In the idealized picture of a smooth spherical earth surrounded by a smooth spherical ionosphere concentric with the earth, the path followed by a radio wave has, as its trace on the surface of the earth, the great circle connecting the transmitter to the receiver. As the ionosphere is not perfectly smooth and as the ground at which the wave is reflected between each ionospheric reflection is similarly not a specular reflector, there will be a spreading of the wave at each reflection so that a small bending of the wave-normal direction may occur at each.

In Fig. 5A, which represents a projection on the earth's surface of a single hop ionospheric path, a change of direction of ϵ at the ionospheric reflection point I results in an apparent change in bearing at the receiver of $\epsilon/2$. The radius of curvature ρ of an equivalent continuous curve connecting T (transmitter) and

U (receiver) and passing through these points with the correct azimuth is thus given by:

$$\rho = (TU/2) \operatorname{cosec} (\epsilon/2) \tag{2}$$

$$\simeq \Lambda R/\epsilon, \text{ since } \epsilon \text{ is small,}$$

where Λ = angular distance between T and U
R = radius of the earth

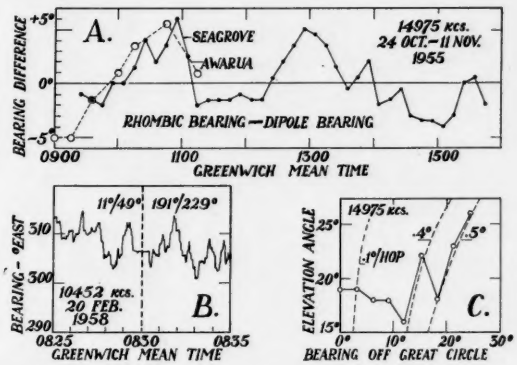

Fig. 6. A. Difference in observed bearing as transmitter beaming direction is changed.
B. Detail of a changeover as beaming direction is changed from 11°/49° to 191°/229° using split-beam aerials.
C. Increase of elevation angle with deviation from the great circle under quiet conditions.

The path followed by this equivalent ray is a line of constant radius of curvature ρ, the curvature at any point being measured in the plane tangential to the earth's surface at that point. Such a curve is formed where a cone touches the surface of the earth, the constant radius of curvature being the length of the side of the cone, PT in Fig. 5B. The ray path traced on the surface of the earth is thus a small circle. The angular distance SOT' by which this small circle avoids the point T', antipodal to T, is then given by

$$\tan (SOT'/2) = \tan \chi = R/\rho = \epsilon/\Lambda \tag{3}$$

where χ = angle STT' in Fig. 5B:

This relation is of value in determining the size of the antipodal area when the allowable curvature of the paths is known. For example, if 10 hops are required between the transmitter and its antipodal point, and if ϵ is 0·5°/hop, so that ϵ/Λ is 1/36, the radius r of the circular antipodal area is given by:

$$r = R \angle SOT' = 400 \text{ km}$$

This means that a receiving station situated within 400 km of the antipodal point of the transmitter could, in the absence of restrictions on paths imposed by ionospheric conditions, expect to receive the signals along any bearing at all.

Since, for a given roughness of the ionosphere, the allowable change in direction

per hop increases rapidly with the elevation angle, the higher angle rays would be expected to show greater range of bearings than those arriving at a low angle of elevation. This effect has been observed experimentally in the series of measurements from which Fig. 6A was derived. The average elevation angle is plotted as a function of the departure of the received bearing angle from the great circle direction in Fig. 6C; this curve has been published previously (WHALE, 1956b). The sudden increase in the elevation angle at about 15° off the great circle bearing is taken as an indication that the limit of the bending allowed at the normal elevation angle has been reached and that any further bending requires more hops and thus that the wave will arrive from a higher elevation angle. The measurements indicate, in this case, that the normal maximum bending was about 0·5°/hop. This is the figure that has been used elsewhere in this paper as being representative of fairly quiet conditions.

When the two stations are not, as in the above case, nearly antipodal, the curvature required by a small circle path so that it may arrive at the receiver at an angle θ to the great circle path may also be calculated. Both the great circle path and the small circle path in Fig. 5B leave the transmitter T along the same bearing, i.e. the two paths if projected on to the tangent plane at T touch there. These paths do not meet elsewhere. If, now, the plane containing the great circle path is rotated by an angle θ about the line TOT', the two paths will intersect at T and V, say, and these angles of intersection are both equal to θ. The plane containing the great circle ($TANO$ in Fig. 5C) and the plane containing the small circle ($TXNM$ in Fig. 5C) intersect along the line TN. The angle ATN is given by:

$$\tan ATN = \sin\theta \cot\chi \tag{4}$$

Angle ATN is half the angular distance Λ_0 from T to the second intersection between the two circles (Fig. 5D) so that:

$$\sin\theta = \tan\chi \tan\frac{\Lambda_0}{2} = \frac{\epsilon}{\Lambda}\tan\frac{\Lambda_0}{2} \text{ from (3)} \tag{5}$$

This relation is plotted in Fig. 2 assuming that $\epsilon/\Lambda = 1/36$ and thus shows the range of the expected bearing variations under these conditions. This value of θ represents a limit to the wanderings of the bearing about the mean bearing determined by the effective tilts of the ionosphere. An approximation to its value can be obtained in practice by measuring the day-to-day deviations of the bearing from the mean bearing for a particular hour of the day. In this measurement the rapid fluctuations arising from interference between the various incoming rays are removed by first averaging the bearings over each hourly period. It is seen from Fig. 2 that the standard deviation of the observed fluctuations is consistently greater than the value given by equation 5 for the very short paths (up to about 60° angular distance). This probably arises from the fact that higher elevation angles and thus shorter hops (leading to more bending of the ray per hop) are generally observed for these shorter paths.

VOL. 13 1958/5

Diurnal variations on long distance transmissions

In Fig. 7 is drawn a selection of plots of the bearing of stations in Great Britain as measured in Auckland. It will be noticed from these plots that changes of 40° or more in bearing are observed, these changes sometimes occurring as steady drifts and sometimes including rapid jumps of 20° or more. They are considerably greater than the variations of up to about 4 or 5° that occur on the short distance transmissions and are also much larger than the changes considered above in the discussion on small circle propagation. Some more effective bending

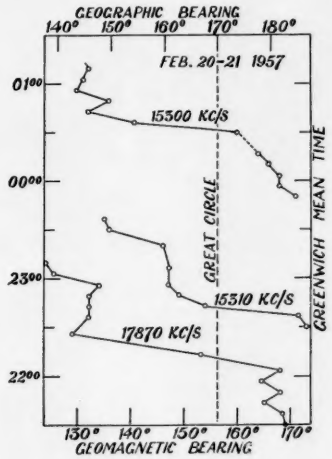

Fig. 7. Observed bearings of BBC signals at Auckland.

mechanism than the normal roughness of the ionosphere is needed to explain such large deviations from the great circle path. The waves which show this large bending are those which have passed near to the auroral regions and since these regions are very disturbed and would behave as very rough surfaces a considerable change in direction could occur there. The parts of the auroral zone which are absorbing to radio waves can be regarded as being similar to an optical stop, i.e. we can picture the auroral zone as being illuminated from behind by the waves from the transmitter, those waves which encounter the absorbing regions being stopped while those which reach the outer scattering regions may bend round and thus arrive at the receiver.

Once these waves have left the vicinity of the very rough auroral regions, their curvature will be limited to that allowed by the normal roughness of the ionosphere. From the measurements on the shorter distance transmissions it has been found that under normal fairly quiet conditions this will allow a further change of bearing of about 2° in covering the 60° angular distance from the southern auroral zone to the receiver and about 4° in covering the 120° distance from the northern auroral zone to the receiver. This suggests that the boundaries of the absorbing parts of the auroral regions could be located with reasonable accuracy from direction-finding measurements made in Auckland. The slow changes in bearing

in Fig. 7 may be ascribed to slow changes in the size, position and shape of the auroral regions. The sudden jumps in bearing, however, must arise from a switching of the main ray from one possible path to another more favourable path and thus depend on the structure of the absorbing regions within the roughly circular overall shape. Before the bearing of a wave that has passed through the auroral zone may be predicted, a knowledge of the extent and location of the absorbing regions of the auroral zone is required. This information, usually

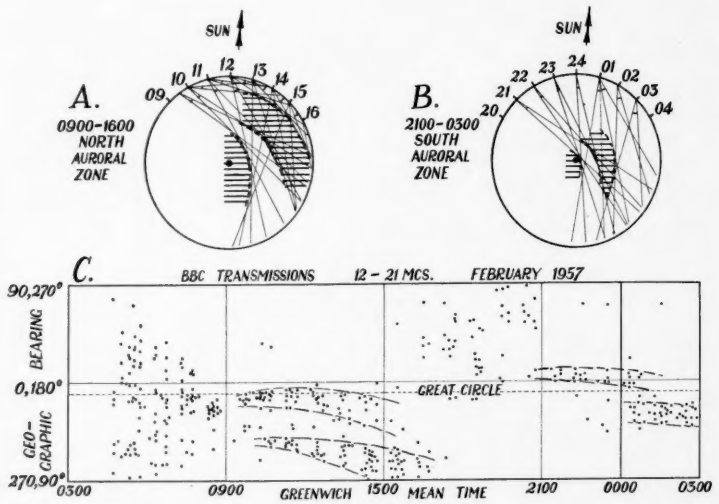

Fig. 8. A,B. Derived plots of the absorbing regions of the auroral zones.
C. Observed bearings of BBC signals during February 1957.

obtained by direct measurement by stations situated in or near to the auroral regions, is not available for all times of the day and for all seasons of the year. It seems that this direction-finding technique at a more accessible site for obtaining this information may be rather promising. The results obtained for one sample month are presented in the next section.

Location of the absorbing parts of the auroral regions

The average auroral zones, as found from measurements on the visible aurora, are rings centred on the geomagnetic axis poles. The position of the line of maximum aurora, when measured at a fixed location, appears to move N and S during a 24 hr period, being furthest from the equator at midday. From these well-known observations, it seems probable that the auroral region, of some relatively stable shape, pivots around the geomagnetic pole retaining a fixed aspect to the sun.

In order that the shape of the auroral zone may be found from the measured bearings, these must first be converted into actual ray-paths near the magnetic poles. A suitable projection for this is the polar gnomonic projection which is tangential to the earth's surface at the geomagnetic poles. This projection has the

VOL.
13
1958/5

additional advantage that all great circles become straight lines and hence the plotting of ray-paths is greatly simplified. To find the shape of the zone we must assume that it remains constant for the period of the observations and that it remains fixed in position with the receiving point moving round it once in 24 hr.

During the daytime at the receiver, most of the rays from European stations received in Auckland pass close to the south auroral zone while during the night most of them pass close to the north auroral zone. All great circles through the receiving point pass through its antipode so that the pattern may equally well be referred to this antipodal point, the bearings of rays arriving from near to the north auroral zone being plotted on the same projection as those from the south. A 12 hr adjustment in the time is necessary, however, if the orientation to the sun is to be preserved. It has been suggested that the auroral effects arising from positive particles may be different from and occur at different places from those arising from negative particles (MEEK, 1956) so that it is possible that the auroral zone is asymmetrical about a line joining the sun to the earth. However, the time adjustment of 12 hr ensures that the orientation of the pattern is preserved, the plotted shape being a satellite's view of the southern auroral zone and a seal's view of the northern auroral zone.

All the measured bearings of BBC short-wave broadcasts received at Seagrove during February 1957 are plotted in Fig. 8C, each dot on the diagram being the average value of the bearing during the hour centred on the dot. The diagram has been compressed vertically, bearings and their reciprocals being plotted on the same vertical scale; the signals in the period 0900–1500 GMT arrived from the north while those in the period 2100–0300 GMT arrived from the south. The dashed lines which have been drawn to enclose the most common bearings found during these two periods have been used to construct Figs. 8A and 8B. The measured bearings have been converted to geomagnetic bearings, taking the geomagnetic poles as being at (78·5°N, 78°W) and (78·5°S, 102°E), and plotted on the gnomonic projection. The radius of the boundary circle represents the distance of the receiving point or its antipode from the nearer geomagnetic pole and is 50·3° of angular distance in each case.

From previous measurements made by workers in Canada and elsewhere it seems that the auroral absorbing regions may occur as relatively narrow bands. The signals could thus cross them at right angles fairly easily, the ionosphere reflection points occurring on each side of the absorbing band so that the wave effectively straddles the zone, pointing to the shaded portions in Figs. 8A and 8B as the measured absorbing regions. It is immediately obvious that, while of similar shape, the two diagrams are very different in size indicating that during this period the north and south auroral zones were of different size or were not similarly situated with respect to the geomagnetic poles. This investigation refers to the average shape of the auroral zone during the month of February 1957. The variation of shape, size and location with the season, magnetic activity, etc., requires further investigation. Figure 8C is typical of the other months for which a sufficient number of bearings to produce a pattern has been obtained in that the distributions for the two most clearly defined periods, viz. 0900–1500 GMT and 2100–0300 GMT, are often of different shapes.

CONCLUSION

From a discussion of the bearing changes over relatively short distance transmission paths it is concluded that the normal amount of scattering by rough reflecting surfaces is inadequate to explain the very large bearing changes that are observed on waves that have passed near to the auroral regions. It is thought that these changes arise from absorbing and scattering processes occurring in or near to these regions and it is concluded that the measurement of the bearings of signals that have passed through the auroral zones lead to a method of plotting the shape of the absorbing part of these zones.

Acknowledgements—Apart from some of the results obtained at Awarua by the New Zealand Post Office, the work described above was carried out at the Seagrove Radio Research Station, Auckland. This Station is operated by the University of Auckland with grants from the N.Z. Department of Scientific and Industrial Research, the N.Z. Post Office and the N.Z. Broadcasting Service.

REFERENCES

BRAMLEY E. N. and ROSS W.	1951	*Proc. Roy. Soc.* A **207,** p. 251.
BUDDE W.	1950	*Z. Naturf.* **5a,** 683.
ECKERSLEY T. L. and FARMER F. T.	1945	*Proc. Roy. Soc.* A **184,** 196.
MEEK J. H.	1955	*J. Atmosph. Terr. Phys.* **6,** 313.
N.Z.P.O.	1956	N.Z. Post Office Research Report No. 12.
ROSS W. J.	1955	Thesis for Ph.D., Auckland University.
TITHERIDGE J. E.	1956	Thesis for M.Sc., Auckland University.
WHALE H. A.	1954	*Proc. Phys. Soc. Lond.* B **67,** 553.
WHALE H. A.	1956a	*Proc. Phys. Soc. Lond.* B **69,** 301.
WHALE H. A.	1956b	*J. Atmosph. Terr. Phys.* **9,** 159.
WHALE H. A. and ROSS W. J.	1956	*Proc. Phys. Soc. Lond.* B **69,** 311.
WHALE H. A. and DELVES L. M.	1958	*J. Atmosph. Terr. Phys.* **13,** 72.

VOL
13
1958/

Journal of Atmospheric and Terrestrial Physics, 1959, Vol. 13, pp. 271 to 290. Pergamon Press Ltd. Printed in Northern Ireland

Effect of vertical drifts on the nocturnal ionization of the lower ionosphere

M. N. Rao and A. P. Mitra
Radio Propagation Unit, NPL, New Delhi–12

(*Received* 2 *May* 1958)

Abstract—Effect of vertical ionic drift velocities on the night-time ionization density in the lower ionosphere for heights ranging between 80 km to 130 km is studied by a method of successive approximation. Values are also given of the effective recombination coefficient as a function of height and time for these drift velocities. Velocities ranging from 1 to 20 km/hr are used. The resultant ionization profiles for velocities 1–5 km/hr represent magnetically quiet conditions, while those for higher velocities would represent disturbed conditions of increasing severity. It will be noted that the ionization density decreases for upward drift and increases for downward drift.

The present work provides a quantitative explanation of the sudden cessation of night-time echoes of low-frequency radio waves at times of magnetic disturbances, such as those observed at the Pennsylvania State University (Lindquist, 1953).

VOL. 13 58/59

1. Introduction

Virtual height of reflection as a function of time and frequency for the lower ionosphere at night is not normally available since the ionization in this region falls below the limit of detection of routine ionospheric recorders. However, individual attempts have been made to study the night-time ionization of the lower ionosphere using specially constructed low frequency transmitters and sometimes extending the low frequency limit of P'–f recorders (Nertney, 1951; 1952; Passow, 1952; Watts and Brown, 1950). Ionization profiles and the recombination processes that govern the temporal variations of these profiles at night have also been studied by Parkinson (1955) and A. P. Mitra (1957a, b). Mitra, in particular, has given a recombination coefficient model as a function of height (from 80 to 115 km) and time (up to 8 hr after sunset) using observations on critical frequency of the E-region at Watheroo and low frequency measurements on ionospheric absorption and virtual height under normal conditions and have estimated the effects of such recombination on assumed sunset models of ionization.

All these studies refer to quiet conditions for which the dynamic effect is small. Peiffer and Mitra (1954) have estimated that for quiet conditions vertical drift velocity at E-region heights vary between 1–5 km/hr. It is believed that during (magnetically) disturbed times this drift velocity is enhanced (Martyn, 1953). The mechanism involved assumes that the electrostatic field developed in the auroral zone during storms spreads over the earth through the ionosphere in such a way as to produce a current whose interaction with the earth's magnetic field produces drift in the ionospheric regions. Such drifts will affect the night-time ionization profiles. It is the purpose of this paper to study such effects. Using drift velocities ranging from 1 to 20 km/hr we have calculated the effective recombination coefficient and ionization density by a method of successive approximation over a

range of heights from 80 km to 130 km and covering the whole night after sunset for different vertical drift velocities.

The resulting ionization profiles provide us with a quantitative explanation of the phenomenon of sudden cessation of night-time echoes of low frequency radio waves such as those observed at the Pennsylvania State College under magnetically disturbed conditions (Lindquist, 1953).

2. Lower Ionospheric Ionization for Quiet Conditions

Night-time ionization in the lower ionosphere consists mainly of electrons, positive molecular ions (YZ^+), positive atomic ions (X^+) and negative ions, the distribution of which for quiet nights have been discussed by Mitra (1957b).

Variations of these quantities over the night depend primarily on the electron densities we start with, which is normally that corresponding to sunset condition, and to the nature of the recombination processes occurring at that height and time. Reasonable models of the sunset electron density have been given by Mitra (1957a, b) and Parkinson (1955), based partially on experimental results and partially on theory. Even though these models cannot be accepted as final, we will use them in our work as the best models available to date, keeping in mind the uncertainties that must exist in these models. Variation of the electrondensity profiles over the night hours is then dependent on the recombination processes which consist principally of dissociative recombination of daytime molecular ions, of radiative recombination of atomic ions of presumably meteoric origin (Nicolet, 1954) and recombination proceeding through negative ions. The height distribution of various positive and negative ions have been obtained emperically by Mitra leading to effective recombination coefficient models for quiet times.

Under disturbed conditions associated with enhanced vertical drifts, we will deal with essentially the same system of ionization, and therefore we shall in this work use the models given by Mitra, specifically those of height distribution of the sunset electron density and the atomic ions (X^+) and negative ions. It is also important to draw attention to the fact that both X^+ and λ, the ratio of the negative ions to electrons, vary but little over a 10 hr night (Mitra, 1957a, b).

3. Some Relevant Theoretical Relationships

We shall now develop a mathematical expression for the night-time electron density as a function of time and height, including the effects of vertical drifts. Mitra (1957) has shown that at night the electrons disappear by recombination with positive molecular ions (YZ^+) and positive atomic ions (X^+), whose ionization potential is too low to allow transfer of charge to the molecule. The relevant reactions are:

$$YZ^+ + e \rightarrow Y' + Z' \ (\alpha_D)$$

$$X^+ + e \rightarrow X + h\nu \ (\alpha_e)$$

In addition recombination occurs through processes involving negative ions. Hence for the E-region and below one can write:

$$n(X^+) + n(YZ^+) = N + \bar{n} = N(1 + \lambda) \qquad (1)$$

VOL
13
1958/

where

N = concentration of electrons
$\bar{n}$ = concentration of negative ions
$n(X^+)$ = concentration of atomic ions X^+
$n(YZ^+)$ = concentration of the molecular ions YZ^+
α_D = coefficient of dissociative recombination for YZ^+
α_e = coefficient of radiative recombination
λ = ratio of the concentrations of negative ions and electrons

We can now write

$$\frac{\partial}{\partial t}[N(1+\lambda)] = -\alpha_D n(YZ^+)\, N - \alpha_i n(YZ^+)\bar{n} - \alpha_e n(X^+)N \tag{2}$$

where α_i is the coefficient of recombination between YZ^+ and negative ions.

It will be noted in equation (2) that we have not accounted for the ionic recombination process involving (X^+) and negative ions since it is known that such reactions are very slow and consequently negligible (MITRA, 1957).

Now $\alpha_e \simeq 10^{-12}$ cm^3/sec, so that it can be neglected in comparison with α_D and α_i which are of the order of 10^{-8} cm^3/sec. Moreover, λ may be supposed to be approximately constant with time (MITRA, 1957), such that:

$$\frac{\partial N}{\partial t} = -(\alpha_D + \lambda\alpha_i)N^2 + (\alpha_D + \lambda\alpha_i)\frac{n(X^+)N}{(1+\lambda)} \tag{3}$$

If we now include the effect of vertical drifts, the above equation becomes:

$$\frac{\partial N}{\partial t} = -(\alpha_D + \lambda\alpha_i)N^2 + (\alpha_D + \lambda\alpha_i)\frac{n(X^+)N}{(1+\lambda)} - \frac{\partial}{\partial z}(Nv) \tag{4}$$

where

v = vertical ionic drift velocity (measured positively upwards)
z = reduced height $= (h - h_0)/H$
h = height corresponding to electron density N
h_0 = height of the reference level
H = scale height of the region

3.1. *Time variation of the maximum electron density*

It is difficult to obtain an analytical solution of equation (4) for conditions appropriate to the region under consideration at night. However, it is sometimes sufficient to consider only the variation of maximum electron density in which case the problem is considerably simplified. In this case:

$$\frac{\partial N}{\partial z} = 0$$

and so

$$\left[\frac{dN}{dt}\right]_{z_m} = \left[\frac{\partial N}{\partial t}\right]_{z_m}$$

Hence, equation (4) becomes, at the peak of the layer:

$$\frac{dN_m}{dt} = -(\alpha_D + \lambda\alpha_i)N_m{}^2 + (\alpha_D + \lambda\alpha_i)\frac{n(\mathrm{X}^+)N_m}{(1+\lambda)} - v'N_m \tag{5}$$

where N_m is the maximum electron density and all other terms in equation (5), namely λ, $n(\mathrm{X}^+)$, v and z correspond to z_m.

The corresponding equation for height (z_m) is obtained by differentiating equation (4) with respect to z and putting $\partial N/\partial z = 0$ We then have

$$\frac{\partial^2 N_m}{\partial z \partial t} = -N_m{}^2\alpha_i \frac{\partial \lambda}{\partial z} + N_m \frac{\partial}{\partial z}\left[(\alpha_D + \lambda\alpha_i)\frac{n(\mathrm{X}^+)}{(1+\lambda)}\right] - N_m \frac{\partial^2 v}{\partial z^2} - v\frac{\partial^2 N_m}{\partial z^2} \tag{6}$$

We now assume that the excursion of z over a night is not large and can be neglected. This assumption appears to be justified for normal conditions, for the total variation in height over a night does not appear to exceed 10 km.*

In this section we shall treat this simple case first by solving equation (5) as a Bernaulli equation.

We take 115 km level as the height of maximum ionization at sunset. This is also our reference level h_0, so that z_m is zero at sunset and by our assumption continues to be zero all throughout the night. Also λ at 115 km is very nearly equal to zero (Mitra, 1957).

Hence, equation (5) may now be written as:

$$\frac{dN_m}{dt} = -\alpha_D N_m{}^2 + \alpha_D n(\mathrm{X}^+)N_m - N_m v' \tag{7}$$

The solution of which for $t = 0$ at sunset is:

$$N_m = \frac{N_{sm}\exp\left(\int \psi\, dt\right)}{1 + N_{sm}\,\alpha_D \int \exp\left(\int \psi\, dt\right) dt} \tag{8}$$

where $\psi = \alpha_D n(\mathrm{X}^+) - v'$

and N_{sm} = sunset maximum electron density.

In order to determine N_m from equation (8), one must have a picture of the vertical drift velocity as a function of height and time suitable for the E-layer.

The velocity appearing in this equation may be caused by horizontal (or vertical drifts) which are periodic in nature or thermodynamic drifts of less regular nature. The periodic velocity would be predominantly semi-diurnal. For this drift, various functions have been reported in literature. For example, for the F-region Martyn (1947) used:

$$v = v_0 \exp(pz)$$

and also

$$v = v_0 \sin(\omega t + \sigma z)$$

For the E-region, Kirkpatrick (1949) used:

$$v = v_0 \sin(\omega t + \sigma z)$$

* This result has been obtained from an examination of the $h'E$ observations made at Watheroo, 1938–39, which are obtained from the Carnegie Institute of Washington.

VOL. 13 1958/5

whereas PEIFFER and MITRA (1955) used

$$v = v_0[1 - c \exp(-pZ)] \sin(\omega t + \phi)$$

and

$$v = v_0\left(\frac{a}{z^2} + \frac{b}{z} + c\right) \sin(\omega t + \phi)$$

It may be noted that these equations, although specifically formulated for tidal drifts, may also apply approximately for other drifts with appropriate changes in ω and ϕ.

In this work we use a velocity function of the form

$$v = v_0 \exp(pz) \sin(\omega t + \theta)$$

where v_0 is the amplitude of the drift, θ the phase angle assumed to be constant with height, p a constant and ω is 30°/hr.

Taking this velocity function and integrating between the limits 0 to t, equation (8) becomes:

$$N_m = \frac{N_{sm} \exp(\phi - \phi_0)}{1 + N_{sm}\alpha_D \int_0^t \exp(\phi - \phi_0)\, dt} \tag{9}$$

Where

$$\phi = \alpha_D n(\mathrm{X}^+)t + \frac{pv_0 \exp(pz)}{\omega} \cos(\omega t + \theta)$$

$$\phi_0 = \frac{pv_0 \exp(pz)}{\omega} \cos\theta$$

3.2. *General case*

Even though the analytical solution of equation (4) is not known at present, we can get N by the method of successive approximation.

Now equation (4) can be written as:

$$\frac{dN}{dt} = -\alpha_{\mathrm{eff}} N^2 \tag{10}$$

where α_{eff}, the effective recombination coefficient is given by:

$$\alpha_{\mathrm{eff}} = (\alpha_D + \lambda\alpha_i)\left[1 - \frac{n(\mathrm{X}^+)}{N(1+\lambda)}\right] + \left[\frac{1}{N}\frac{\partial v}{\partial z} + \frac{v}{N^2}\frac{\partial N}{\partial z}\right] = \alpha(\lambda, \mathrm{X}^+) + \alpha(v) \tag{11}$$

Solving equation (10) with respect to time over a small interval of time and treating α_{eff} as a constant during that small period, we get:

$$N = \frac{N_0}{1 + \alpha_{\mathrm{eff}} N_0 t} \tag{12}$$

where t is the time interval, and N_0 and N are the electron densities at the beginning and the end of the interval respectively.

Using this equation and starting with a known sunset electron density distribution one can calculate N for various hours of the night by successive

steps of one hour intervals or even less. The accuracy of the results depends, of course, on how small the time interval is.

4. Distortion of Night-time Ionization Profiles for Various Vertical Drifts

4.1. *Characteristics of the drifts*

The unknown parameters associated with the vertical drift velocity v are p, θ and v_0. These can be estimated as follows.

The gradient p has been estimated from the velocity functions given by Martyn (1954) from electrodynamical considerations. From the curves given by Martyn we have obtained a value of 0·85 for p for high latitudes and approximately unity for low latitudes.

The phase θ has been chosen such that the maximum upward velocity occurs at 0300 hours for high latitudes and 2100 hours for low latitudes (Peiffer and Mitra, 1955). This gives $\theta = -\pi$ for high latitudes and $\theta = 0$ for low latitudes with $t = 0$ chosen at 1800 hours.

The drift velocity v_0 has been empirically estimated by Peiffer and Mitra to have an amplitude in the range of 1–5 km/hr for normal conditions in the E-region. This value is also consistent with theoretical values estimated from observed variations of the terrestrial magnetic field (Fejer, 1953; Martyn 1953–54; Chapman and Bartels, 1940) and from the observed horizontal drift velocities (nearly 100 km/hr) in the E-region. The latter give a range 1–20 km/hr. In addition to the vertical drifts caused by atmospheric motions, there may exist vertical atmospheric winds, which, in the E-region and below, will drag ions and electrons along with neutral molecules. Manning *et al.* (1954) have shown that these vertical winds have a velocity of the order of 5 km/hr.

From this it can be concluded that under normal conditions v_0 is around 1–5 km/hr. But under magnetically disturbed conditions one would expect the vertical drift amplitude to increase by an amount depending upon the degree of disturbance (Martyn, 1953).

In view of the above, velocity amplitudes ranging from 1–20 km/hr are used in the present work. Since we have considered only drifts of semi-diurnal periodicity, $\omega = 30°$/hr.

4.2. *Ionization parameters*

The ionization parameters involved are the distributions of sunset electron concentration, of the atomic ion concentration and of the negative ion to electron ratio. Values for these quantities have been given recently by A. P. Mitra (1957) for heights 80–130 km and for normal conditions. These are reproduced in Table 1.

For α_D and α_i values of 10^{-8} cm^3/sec and 5×10^{-8} cm^3/sec have been assumed.

4.3. *Ionization profiles*

We will now obtain α_{eff}, the effective recombination coefficient, and N, the electron density from equations (11) and (12) for various heights of the ionosphere ranging from 80 km to 130 km (at intervals of 5 km) for various hours of the

VOL. 13 1958/5

Table 1. Values of N_s, $n(X^+)$, λ and α_{eff} at sunset for different heights (figures in parentheses indicate the power of ten)

Height (km)	N_s	$n(X^+)$	λ	Sunset α_{eff}
80	2·4 (1)	0	5·2 (1)	2·6 (−6)
85	2·7 (2)	0	3·2 (0)	1·7 (−7)
90	7·0 (2)	0	9·4 (−1)	6·0 (−8)
95	1·5 (3)	1·6 (3)	1·3 (0)	2·3 (−8)
100	1·0 (4)	3·1 (3)	2·2 (−1)	1·6 (−8)
105	2·4 (4)	4·7 (3)	8·0 (−2)	1·2 (−8)
110	4·0 (4)	6·2 (3)	4·0 (−2)	1·0 (−8)
115	4·4 (4)	7·0 (3)	0	8·4 (−9)
120	4·2 (4)	7·0 (3)	0	8·3 (−9)
125	3·5 (4)	7·0 (3)	0	8·0 (−9)
130	3·2 (4)	7·0 (3)	0	7·8 (−9)

night (namely 1800 hr to 0600 hr) and for different vertical drift velocities (namely 1, 5, 10, 15 and 20 km/hr). These calculations have been done for low latitudes only (less than 35°) in which case the phase of the drift velocity θ becomes zero. Similar calculations can be carried out for high latitudes (greater than 35°) using the appropriate value for θ.

At some time t_c, the value of which depends on the amplitude of the drift velocity, N will become equal to $n(X^+)/(1+\lambda)$, thus making $\alpha(\lambda, X^+) = 0$. It is important to remember that the contribution of this term after this time t_c ceases to exist. The term t_c will, in general, fall between the times t_r and t_r+1 where $(t_{r+1} - t_r)$ is the interval chosen for the particular calculation. It is therefore necessary to determine in advance the value of t_c, which is given approximately by the following formula:

$$(t_c - t_r)\sin\{\omega(t_c - t_r) + \theta\} = \frac{1 - \dfrac{n(X^+)}{N_r(1+\lambda)}}{v_0 \exp(pz)\left[1 + \dfrac{(1+\lambda)}{n(X^+)}\dfrac{\partial}{\partial z}\left\{\dfrac{n(X^+)}{(1+\lambda)}\right\}\right]}$$

where N_r is the electron density corresponding to the time t_r.

It may be noted that this approximate formula ceases to be valid for very large drift velocities such as 20 km/hr. For such velocities calculation of N should be made at more frequent intervals.

Values of the effective recombination coefficient thus obtained are given in Table 2. In addition, normalized values of α_{eff} for three different arbitrarily chosen heights, namely 80 km, 90 km and 110 km are plotted in Figs. 1, 2 and 3 respectively. Electron density profiles for different vertical drift velocities computed with these values are represented in Figs. 4 to 8.

Ionization profiles for $v_0 = 1$–5 km/hr may be supposed to represent the normal conditions while those for higher velocities represent conditions of magnetic

Table 2. Values of effective recombination coefficient for various times and heights for different drift velocities (figures in parentheses indicate power of ten)

v_0 = 1 km/hr

h (km)	$t = 0$	$t = 1$	$t = 2$	$t = 3$	$t = 4$	$t = 5$	$t = 6$	$t = 7$	$t = 8$	$t = 9$	$t = 10$
80	2·6 (−6)	3·1 (−6)	3·4 (−6)	3·6 (−6)	3·3 (−6)	2·7 (−6)	2·5 (−6)	2·2 (−6)	3·2 (−6)	2·0 (−6)	2·1 (−6)
85	1·7 (−7)	1·8 (−7)	1·8 (−7)	1·9 (−7)	1·8 (−7)	1·8 (−7)	1·6 (−6)	1·5 (−7)	1·4 (−7)	1·4 (−7)	1·5 (−7)
90	6·0 (−8)	6·3 (−8)	6·6 (−8)	6·6 (−8)	6·5 (−8)	6·0 (−8)	5·6 (−8)	5·2 (−8)	4·8 (−8)	5·0 (−8)	5·3 (−8)
95	2·3 (−8)	2·6 (−8)	2·4 (−8)	2·0 (−8)	1·5 (−8)	9·0 (−9)	2·3 (−9)	−4·1 (−9)	−6·9 (−9)	−4·6 (−9)	−9·2 (−10)
100	1·6 (−8)	2·2 (−8)	1·5 (−8)	1·2 (−8)	9·6 (−9)	6·6 (−9)	3·4 (−9)	8·0 (−10)	−6·4 (−10)	−6·4 (−10)	6·4 (−10)
105	1·2 (−8)	1·2 (−8)	1·0 (−8)	8·6 (−9)	6·7 (−9)	4·6 (−9)	2·4 (−9)	4·3 (−10)	−7·2 (−10)	−5·4 (−10)	4·8 (−10)
110	1·0 (−8)	1·1 (−8)	9·0 (−9)	7·6 (−9)	5·6 (−9)	3·3 (−9)	1·0 (−9)	−7·0 (−10)	−1·3 (−9)	−1·0 (−9)	1·2 (−10)
115	8·4 (−9)	1·2 (−8)	7·6 (−9)	6·1 (−9)	4·1 (−9)	1·7 (−9)	−1·1 (−9)	−2·9 (−9)	−3·7 (−9)	−3·4 (−9)	−2·4 (−9)
120	8·3 (−9)	8·7 (−9)	8·2 (−9)	7·1 (−9)	5·1 (−9)	2·1 (−9)	−1·5 (−9)	−4·1 (−9)	−5·3 (−9)	−5·0 (−9)	−3·5 (−9)
125	8·0 (−9)	9·3 (−9)	9·6 (−9)	8·8 (−9)	6·3 (−9)	2·3 (−9)	−3·2 (−9)	−8·5 (−9)	−1·1 (−8)	−1·0 (−8)	−5·9 (−9)
130	7·8 (−9)	1·1 (−8)	1·4 (−8)	1·4 (−8)	1·1 (−8)	4·4 (−9)	−6·0 (−9)	−1·6 (−8)	−2·0 (−8)	−1·6 (−8)	−8·7 (−9)

v_0 = 5 km/hr

h (km)	$t = 0$	$t = 1$	$t = 2$	$t = 3$	$t = 4$	$t = 5$	$t = 6$	$t = 7$	$t = 8$	$t = 9$	$t = 10$
80	2·6 (−6)	3·4 (−6)	4·3 (−6)	4·9 (−6)	4·9 (−6)	3·4 (−6)	1·8 (−6)	−4·7 (−7)	−1·5 (−6)	−1·3 (−6)	0·0
85	1·7 (−7)	2·2 (−7)	2·5 (−7)	2·7 (−7)	2·5 (−7)	2·0 (−7)	1·3 (−7)	5·8 (−8)	0·0	0·0	6·1 (−8)
90	6·0 (−8)	8·1 (−8)	9·3 (−8)	9·7 (−8)	9·5 (−8)	7·7 (−8)	4·7 (−8)	1·3 (−8)	−9·6 (−9)	−1·1 (−8)	4·8 (−9)
95	2·3 (−8)	4·3 (−8)	5·7 (−8)	5·6 (−8)	3·8 (−8)	1·3 (−8)	−1·3 (−8)	−4·0 (−8)	−5·5 (−8)	−4·4 (−8)	−2·7 (−8)
100	1·6 (−8)	2·1 (−8)	2·4 (−8)	2·3 (−8)	1·9 (−8)	8·5 (−9)	−6·4 (−9)	−1·7 (−8)	−2·3 (−8)	−2·2 (−8)	−1·5 (−8)
105	1·2 (−8)	1·5 (−8)	1·7 (−8)	1·7 (−8)	1·4 (−8)	7·2 (−9)	−5·8 (−9)	−1·4 (−8)	−1·7 (−8)	−1·5 (−8)	−9·0 (−9)
110	1·0 (−8)	1·3 (−8)	1·6 (−8)	1·8 (−8)	1·5 (−8)	7·3 (−9)	−4·9 (−9)	−1·7 (−8)	−1·9 (−8)	−1·3 (−8)	−7·0 (−9)
115	8·4 (−9)	1·2 (−8)	1·5 (−8)	1·7 (−8)	1·5 (−8)	8·0 (−9)	−8·0 (−9)	−2·0 (−8)	−2·0 (−8)	−1·1 (−8)	−4·4 (−9)
120	8·3 (−9)	1·7 (−8)	2·6 (−8)	2·7 (−8)	2·0 (−8)	8·0 (−9)	−1·1 (−8)	−2·9 (−8)	−2·6 (−8)	−4·0 (−9)	1·1 (−8)
125	8·0 (−9)	3·5 (−8)	6·2 (−8)	5·0 (−8)	3·2 (−8)	7·5 (−9)	−2·2 (−8)	−3·4 (−8)	1·5 (−9)	6·1 (−8)	2·9 (−7)
130	7·8 (−9)	6·5 (−8)	9·6 (−8)	1·0 (−7)	9·8 (−8)	6·0 (−8)	−3·2 (−8)	−1·8 (−8)	2·2 (−7)	1·6 (−6)	9·2 (−6)

VOL 13 1958/9

VOL. 13
8/59

Table 2.—(*continued*)

v_0 = 10 km/hr

h (km)	$t = 0$	$t = 1$	$t = 2$	$t = 3$	$t = 4$	$t = 5$	$t = 6$	$t = 7$	$t = 8$	$t = 9$	$t = 10$
80	2·6 (−6)	4·7 (−6)	6·2 (−6)	7·3 (−6)	7·3 (−6)	4·9 (−6)	2·6 (−7)	−3·5 (−6)	−4·7 (−6)	−4·5 (−6)	−2·4 (−6)
85	1·7 (−7)	2·7 (−7)	3·4 (−7)	3·8 (−7)	3·7 (−7)	2·7 (−7)	7·5 (−8)	−9·4 (−8)	−1·8 (−7)	−1·4 (−7)	−4·3 (−8)
90	6·0 (−8)	1·0 (−7)	1·3 (−7)	1·3 (−7)	1·2 (−7)	9·0 (−8)	3·0 (−8)	−3·0 (−8)	−6·6 (−8)	−6·5 (−8)	−4·2 (−8)
95	2·3 (−8)	9·0 (−8)	1·2 (−7)	1·2 (−7)	9·9 (−8)	4·0 (−8)	−4·9 (−8)	−1·3 (−7)	−1·6 (−7)	−1·2 (−7)	−5·8 (−8)
100	1·6 (−8)	2·8 (−8)	3·8 (−8)	4·5 (−8)	4·1 (−8)	1·8 (−8)	−2·5 (−8)	−5·8 (−8)	−5·6 (−8)	−3·5 (−8)	−1·6 (−8)
105	1·2 (−8)	2·2 (−8)	3·3 (−8)	3·8 (−8)	3·0 (−8)	1·2 (−8)	−1·6 (−8)	−4·0 (−8)	−4·0 (−8)	−1·9 (−8)	−6·3 (−9)
110	1·0 (−8)	1·7 (−8)	2·8 (−8)	2·6 (−8)	3·1 (−8)	1·4 (−8)	−1·9 (−8)	−4·0 (−8)	−3·5 (−8)	−1·5 (−8)	−4·0 (−9)
115	8·4 (−9)	2·4 (−8)	3·8 (−8)	4·6 (−8)	3·8 (−8)	1·5 (−8)	−2·3 (−8)	−5·0 (−8)	−3·3 (−8)	−1·1 (−8)	5·0 (−9)
120	8·3 (−9)	2·7 (−8)	5·7 (−8)	1·0 (−7)	9·0 (−8)	3·0 (−8)	−3·4 (−8)	−8·1 (−8)	−6·1 (−8)	−4·4 (−8)	1·8 (−7)
125	8·0 (−9)	3·1 (−8)	7·8 (−8)	2·1 (−7)	2·3 (−7)	1·1 (−7)	−1·0 (−7)	−1·2 (−7)	8·0 (−8)	9·6 (−7)	5·0 (−6)
130	7·8 (−9)	6·3 (−8)	1·4 (−7)	1·5 (−7)	1·1 (−7)	3·1 (−8)	−6·2 (−8)	2·8 (−7)	2·7 (−6)	4·2 (−5)	4·6 (−4)

v_0 = 15 km/hr

h (km)	$t = 0$	$t = 1$	$t = 2$	$t = 3$	$t = 4$	$t = 5$	$t = 6$	$t = 7$	$t = 8$	$t = 9$	$t = 10$
80	2·6 (−6)	5·7 (−6)	9·1 (−6)	1·3 (−5)	1·3 (−5)	6·0 (−6)	−1·8 (−6)	−9·6 (−6)	−1·2 (−5)	−7·5 (−6)	−3·1 (−6)
85	1·7 (−7)	3·0 (−7)	4·3 (−7)	5·1 (−7)	4·7 (−7)	3·0 (−7)	0·0	−2·1 (−7)	−2·8 (−7)	−2·4 (−7)	−1·1 (−7)
90	6·0 (−8)	1·2 (−7)	1·7 (−7)	2·2 (−7)	2·0 (−7)	1·1 (−7)	0·0	−1·0 (−7)	−1·7 (−7)	−1·6 (−7)	−8·4 (−8)
95	2·3 (−8)	8·4 (−7)	1·4 (−7)	1·8 (−7)	1·5 (−7)	6·6 (−8)	−9·0 (−8)	−2·0 (−7)	−2·1 (−7)	−1·6 (−7)	−7·6 (−8)
100	1·6 (−8)	3·3 (−8)	5·8 (−8)	9·3 (−8)	9·6 (−8)	4·3 (−8)	−4·2 (−8)	−8·9 (−8)	−9·3 (−8)	−5·6 (−8)	−2·1 (−8)
105	1·2 (−8)	2·4 (−8)	4·3 (−8)	6·5 (−8)	6·2 (−8)	2·9 (−8)	−4·3 (−8)	−7·6 (−8)	−6·4 (−8)	−3·1 (−8)	−1·1 (−8)
110	1·0 (−8)	2·0 (−8)	4·2 (−8)	7·4 (−8)	7·9 (−8)	4·2 (−8)	−7·5 (−8)	−9·2 (−8)	−6·3 (−8)	−3·0 (−8)	−9·0 (−9)
115	8·4 (−9)	2·1 (−8)	5·5 (−8)	1·1 (−7)	1·2 (−7)	4·5 (−8)	−9·5 (−8)	−1·2 (−7)	−8·4 (−8)	−2·7 (−8)	−2·5 (−9)
120	8·3 (−9)	2·6 (−8)	8·5 (−8)	1·9 (−7)	2·4 (−7)	1·1 (−7)	−1·4 (−7)	−2·2 (−7)	−1·1 (−7)	2·5 (−7)	9·0 (−7)
125	8·0 (−9)	4·1 (−8)	1·3 (−7)	3·2 (−7)	5·6 (−7)	3·7 (−7)	−2·5 (−7)	−4·6 (−7)	1·5 (−7)	6·0 (−6)	1·2 (−5)
130	7·8 (−9)	7·3 (−8)	2·6 (−7)	7·0 (−7)	1·5 (−6)	4·0 (−7)	−6·4 (−7)	−9·9 (−7)	1·6 (−5)	1·4 (−4)	8·0 (−4)

Table 2.—(*continued*)

v_0 = 20 km/hr

h (km)	$t = 0$	$t = 1$	$t = 2$	$t = 3$	$t = 4$	$t = 5$	$t = 6$	$t = 7$	$t = 8$	$t = 9$	$t = 10$
80	2·6 (−6)	7·0 (−6)	1·6 (−5)	3·8 (−5)	7·4 (−5)	3·9 (−5)	−7·3 (−6)	−4·1 (−5)	−5·9 (−5)	−3·0 (−5)	−8·3 (−6)
85	1·7 (−7)	3·6 (−6)	5·4 (−7)	6·9 (−7)	7·7 (−7)	6·5 (−7)	−7·0 (−8)	−8·1 (−7)	−8·6 (−7)	−6·3 (−7)	−3·6 (−7)
90	6·0 (−8)	1·4 (−7)	2·2 (−7)	3·0 (−7)	3·0 (−7)	2·0 (−7)	1·2 (−7)	−1·9 (−7)	−2·9 (−7)	−2·5 (−7)	−1·2 (−7)
95	2·3 (−8)	1·1 (−7)	1·7 (−7)	2·5 (−7)	2·7 (−7)	1·4 (−7)	−6·8 (−7)	−2·4 (−7)	−3·2 (−7)	−2·7 (−7)	−1·1 (−7)
100	1·6 (−8)	4·2 (−8)	9·3 (−8)	1·7 (−7)	2·6 (−7)	2·9 (−7)	−1·1 (−7)	−3·5 (−7)	−2·6 (−7)	−1·2 (−7)	−3·3 (−8)
105	1·2 (−8)	2·5 (−8)	6·6 (−8)	1·4 (−7)	2·3 (−7)	1·6 (−7)	−7·0 (−8)	−1·9 (−7)	−2·0 (−7)	−4·3 (−8)	2·0 (−9)
110	1·0 (−8)	2·4 (−8)	5·3 (−8)	1·2 (−7)	2·5 (−7)	2·1 (−7)	−1·0 (−7)	−3·5 (−7)	−1·9 (−7)	5·0 (−8)	2·0 (−7)
115	8·4 (−9)	2·5 (−8)	7·2 (−8)	1·5 (−7)	3·2 (−7)	2·8 (−7)	−1·5 (−7)	−4·0 (−7)	−1·3 (−7)	6·8 (−7)	3·7 (−6)
120	8·3 (−9)	3·2 (−8)	1·2 (−7)	2·5 (−7)	4·9 (−7)	4·7 (−7)	−2·3 (−7)	−4·8 (−7)	4·2 (−7)	5·5 (−6)	6·0 (−5)
125	8·0 (−9)	5·6 (−8)	2·4 (−7)	5·3 (−7)	1·2 (−6)	1·1 (−6)	−5·5 (−7)	−5·0 (−7)	3·4 (−6)	4·5 (−5)	1·1 (−3)
130	7·8 (−9)	1·1 (−7)	4·4 (−7)	1·3 (−6)	2·7 (−6)	1·6 (−6)	−1·2 (−6)	1·6 (−6)	1·9 (−5)	5·7 (−4)	3·2 (−2)

VOL
13
1958/

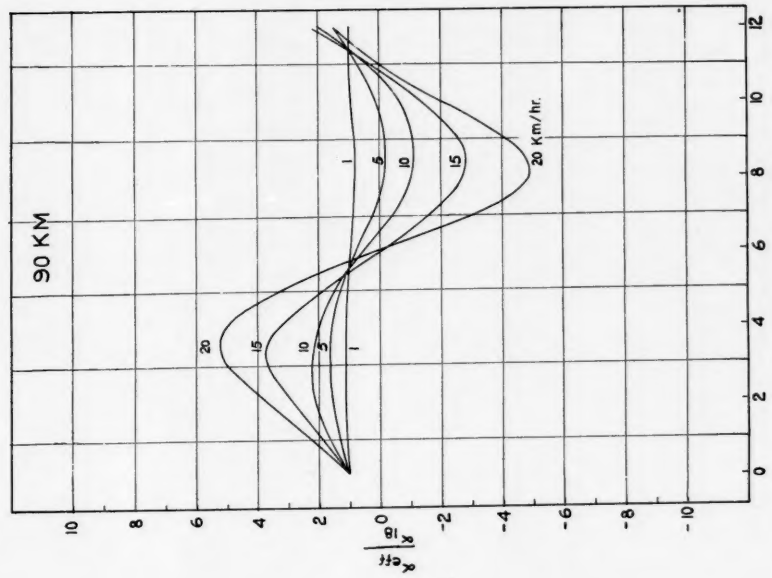

Fig. 2. Theoretical plot of normalized values of effective recombination coefficient versus time after sunset at 90 km.

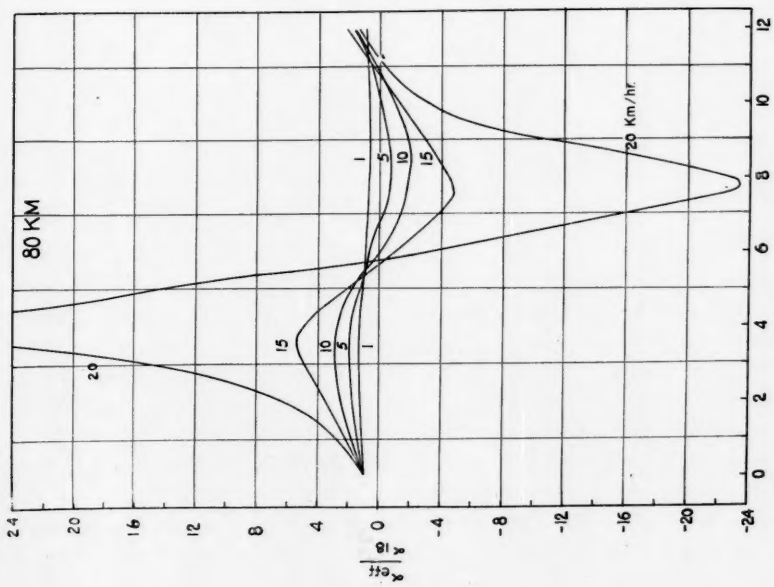

Fig. 1. Theoretical plot of normalized values of effective recombination coefficient versus time after sunset at 80 km.

VOL. 13 58/59

disturbance of increasing severity. It will be noted that N decreases when the drift is upwards and increases when the drift changes its phase at 0000 hours.

Maximum electron density throughout the night for different drift conditions (extracted from the general profiles of electron density) is plotted in Fig. 9.

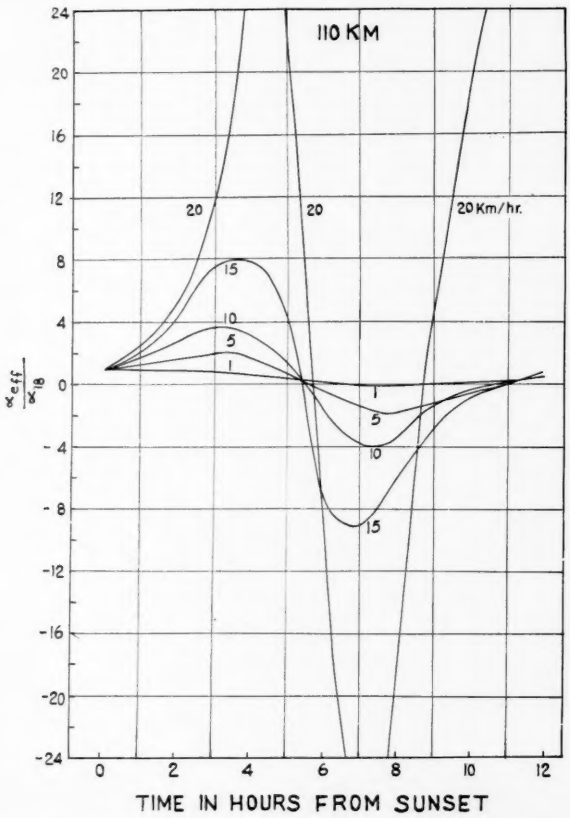

Fig. 3. Theoretical plot of normalized values of effective recombination coefficient versus time after sunset at 110 km.

Variation obtained from the approximate analytical equation (9) is also given for comparison—this is shown by dotted curves. The difference indicates the effect introduced by the change in height of maximum ionization. While the two sets of curves agree fairly well for small values of v, differences become important for large velocities.

The abnormally large values of α_{eff} and consequent low values of electron density for heights above 120 km in the early morning hours is probably not genuine and may have arisen from the neglect of higher overlapping layers.

It is of interest to see how the reflection height of different low frequency radio waves such as 16, 50, 75 and 150 kc/s vary with the time of the night under different drift conditions These are plotted in Fig. 10. It may be remembered

VOL.
13
1958/5

that for the phase assumed ($\theta = 0$) the drift velocity is upwards for the first 6 hr after sunset and downwards for the next 6 hr. The height of reflection thus increases for all these frequencies when the drift is upwards and decreases when it

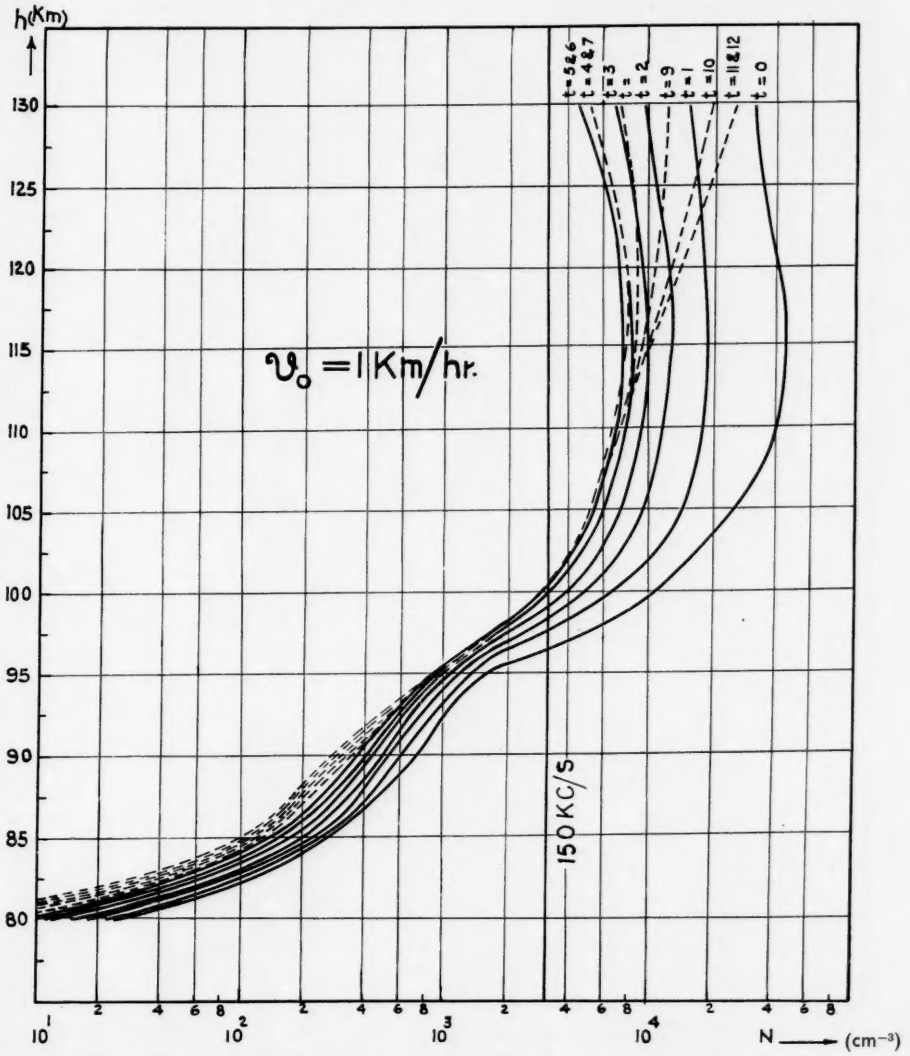

Fig. 4. Theoretical plot of the electron density versus height for various hours of the night when $v_0 = 1$ km/hr.

is downwards and also there are discontinuities in all these curves for large drift velocities (except in the case of 16 kc/s which requires drift amplitudes of more than 20 km/hr to produce such a discontinuity). This discontinuity is due to the lowering of N_m below that required for reflection, which causes the phenomenon of "breaking" of the E-layer. This we now proceed to discuss in detail.

5. "Breaking" of Region E for Large Drift Velocities

It has been observed in the Pennsylvania State College (Lindquist 1953) that the (night-time) virtual height of reflections of 150 kc/s wave which is originally around 100 km jumps up to a height of nearly 150 km on certain occasions

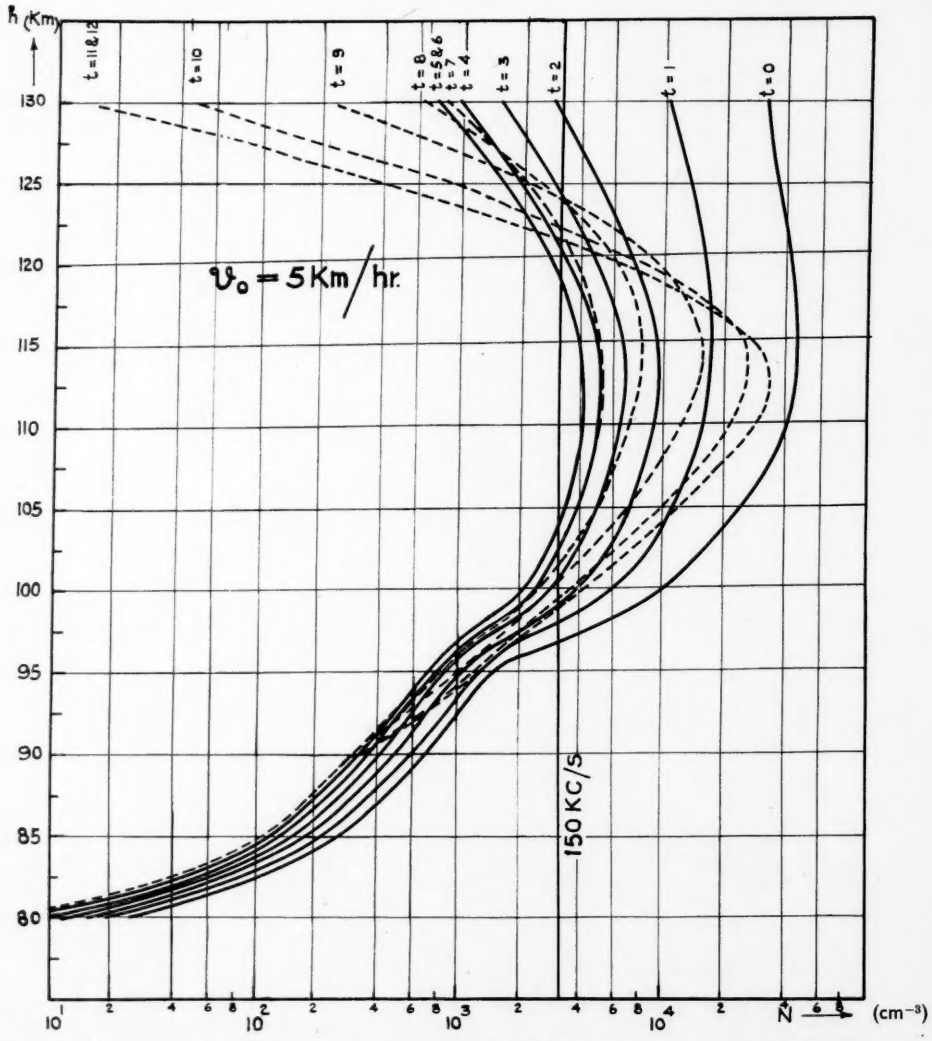

Fig. 5. Theoretical plot at the electron density versus height for various hours of the night when $v_0 = 5$ km/hr.

associated with large K-indices, remains there for some period and again suddenly drops down to the normal level.

Peiffer and Mitra (1955) advanced a suggestion that these echoes (which are sometimes called "150 km echoes") are caused by the lowering of the E-region

VOL.
13
1958/5

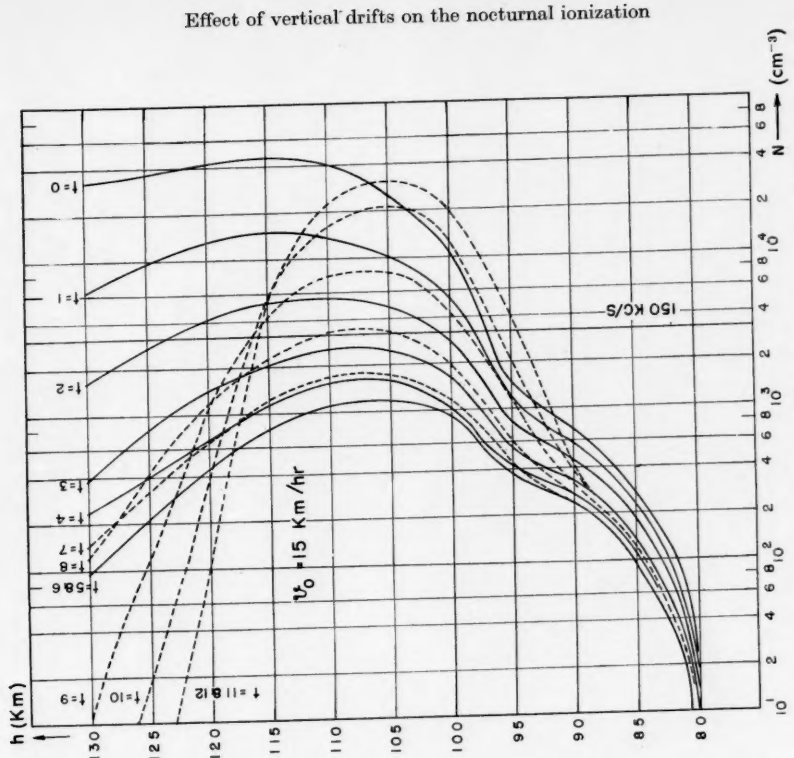

Fig. 7. Theoretical plot of the electron density versus height for various hours of the night when $v_0 = 15$ km/hr.

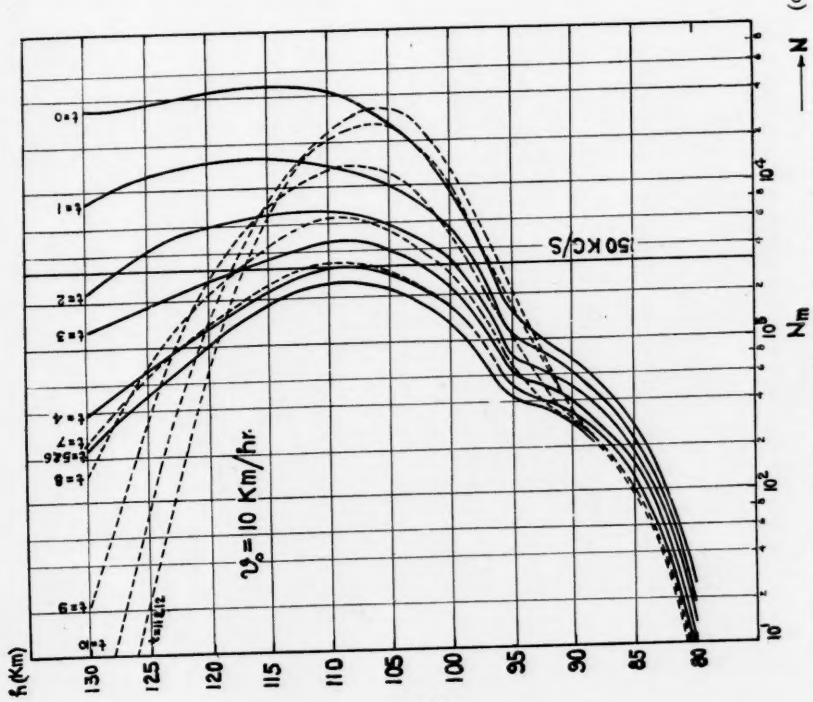

Fig. 6. Theoretical plot of the electron density versus height for various hours of the night when $v_0 = 10$ km/hr.

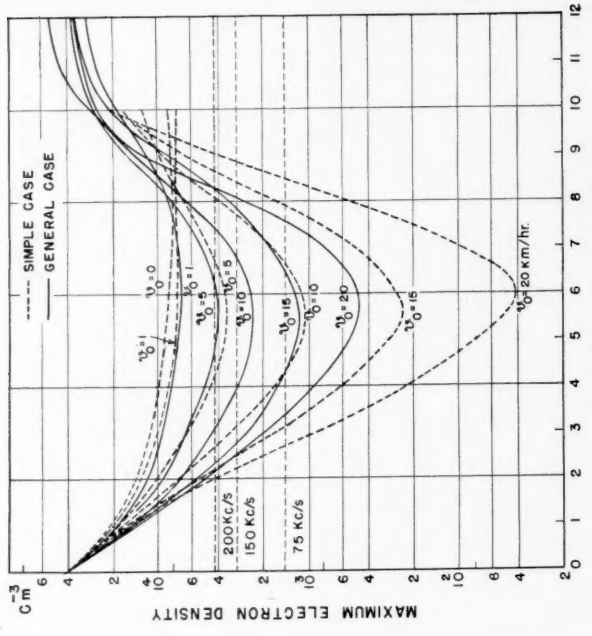

Fig. 9. Theoretical plot of maximum electron density versus time in hours after sunset for different vertical drift velocities. (a) Dotted lines represent the simple case of constant height of maximum ionization. (b) Continuous lines represent the general case.

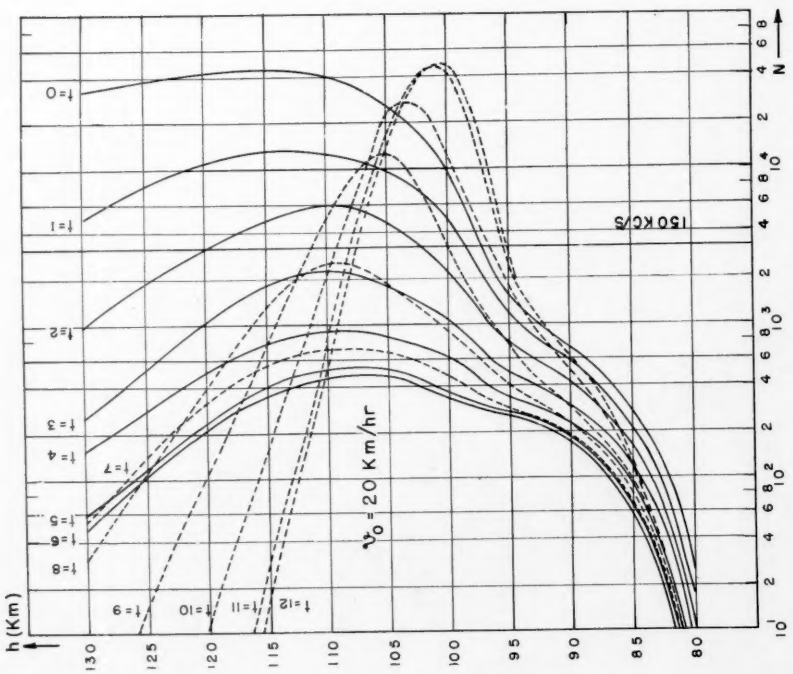

Fig. 8. Theoretical plot of the electron density versus height for various hours of the night when $v_0 = 20$ km/hr.

VOL.
13
1958/5

electron density due to enhanced vertical ion transports at that time. They found that under normal conditions the vertical drift velocity ($\simeq$1 km/hr) is not sufficient to affect the E-region excepting at late night hours, but the layer would be considerably distorted for large vertical drifts which one would associate with magnetic disturbances. Indeed, the layer density would sometimes fall sufficiently low to allow even low frequencies to penetrate the layer completely and be reflected from a higher layer. They were not, however, able to obtain the reappearance of the echo, and suggested that such reappearance may be explained if one takes account of the additional nocturnal ionization that undoubtedly exists in this layer.

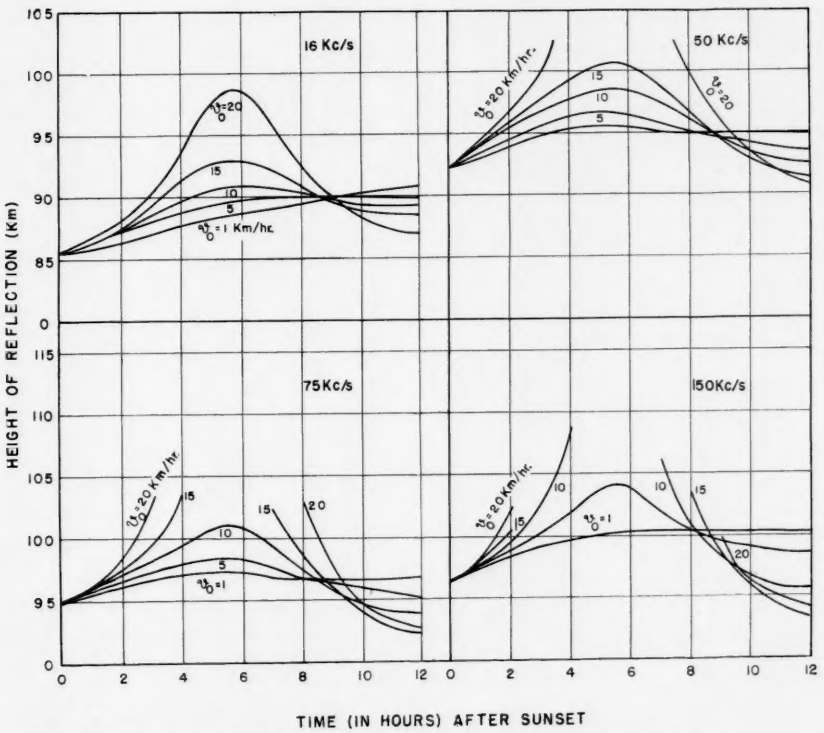

Fig. 10. Theoretical plot of the height of reflection of 16, 50, 75 and 150 kc/s waves versus time in hours after sunset for different vertical drift velocities.

In view of the results reported in the earlier sections, we are now in a position to examine this hypothesis afresh.

On turning to the profiles (Figs. 4 to 8) one finds that the electron density decreases rapidly after sunset and for large velocities the decrease is so large that the maximum electron density becomes insufficient to reflect most of the low frequency radio waves. The minimum frequency for which the layer would "break" for a particular drift velocity is given in Fig. 11. It will be observed that, under normal conditions, this frequency is as high as 300 kc/s; for drifts of 10 and 20 km/hr they are as low as 115 kc/s and 24 kc/s respectively. Detailed

characteristics of breaking and reformation for some specific low frequencies (e.g. 75, 150 and 200 kc/s) are given in Fig. 9. Figure 12 gives a plot of the variation of the times of "breaking" and "reformation" of the layer for these specific frequencies as a function of the drift velocity and Fig. 13 gives a similar plot of the duration of breaking. It will be noted that drift velocities needed to just "break" the layer for 75, 150 and 200 kc/s are of the order of 13·5, 8 and 4·5 km/hr

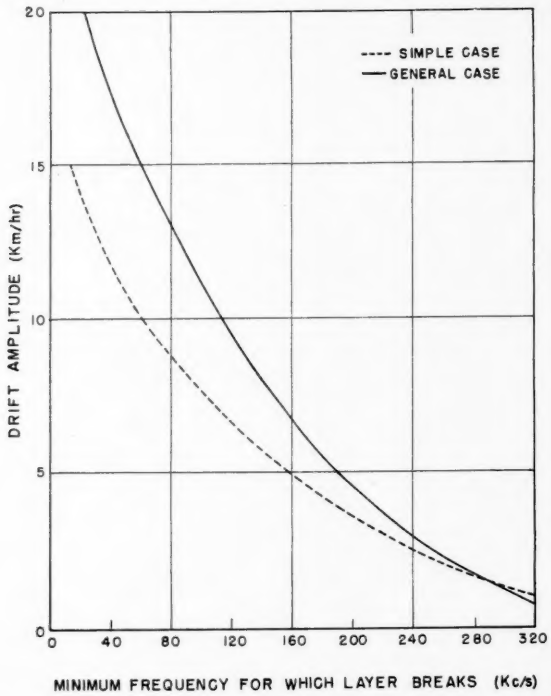

Fig. 11. Theoretical relationship between the vertical drift velocity and the minimum frequency for which the layer breaks. (a) Dotted line represents the simple case of constant height of maximum ionization. (b) Continuous line represents the general case.

respectively. In other words, the disturbed conditions should be such as to enhance the vertical drifts to these values in order that breaking can just occur. Larger drift velocities would be required to cause any prolonged breaking. For 75 kc/s, for example, a 3 hr breaking of the layer would need a drift amplitude of 16·5 km/hr whereas the same drift would produce breaking with 150 and 200 kc/s which would last for about 5 and 6 hr respectively.

Now, analysis of the "150 km echoes" (Lindquist, 1953; Chaffee, 1954) has shown that the occurrence and disappearance of these echoes are intimately connected with conditions of high magnetic activity. Lindquist, for example, has shown that for 150 kc/s breaking can only occur if the K-index exceeds a certain minimum value, this minimum value being greater, the longer the 150 km echo lasts. Chaffee (1954) has demonstrated a 27-day recurrence tendency in the curcorence of this echo. This would appear to confirm our initial hypothesis in

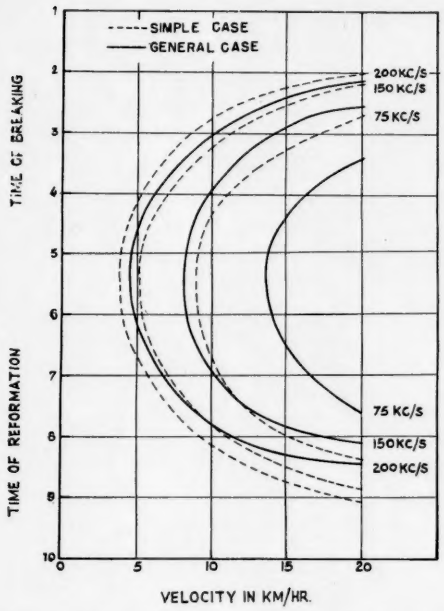

Fig. 12. Theoretical plot of the times of breaking and reformations in hours after sunset versus vertical drift velocity for 75, 150 and 200 kc/s waves. (a) Dotted lines represent the simple case of constant height of maximum ionization. (b) Continuous lines represent the general case.

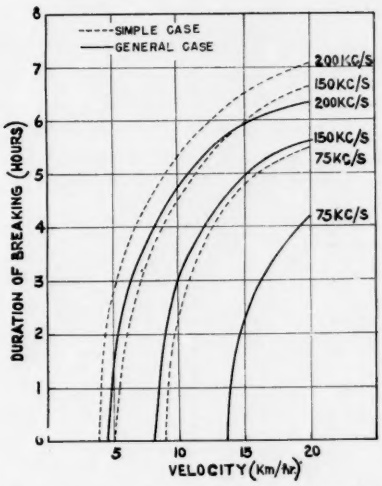

Fig. 13. Theoretical plot of the duration of breaking versus vertical drift velocity for 75, 150 and 200 kc/s waves. (a) Dotted lines represent the simple case of constant height of maximum ionization. (b) Continuous lines represent the general case.

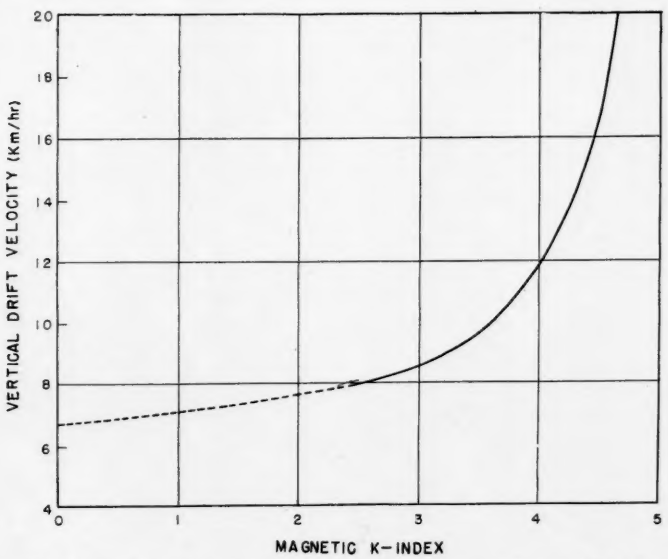

Fig. 14. Relation between vertical drift velocity and magnetic k-index.

which we assume the ionospheric effects of magnetic disturbances to occur through vertical drifts which are enhanced during such disturbances. From the data given by Lindquist, it is then possible to obtain an approximate relationship between K-index and vertical drift velocity in the E-region. Such a relationship is portrayed in Fig. 14. This relationship is, of course, highly approximate, since the data are not sufficiently large in number, and are at present available only for one frequency, viz. 150 kc/s. However, using this as a very rough guide, we would infer that for 75 kc/s breaking will occur only if K-index exceeds the value 4. Under magnetically quiet conditions it would appear from Fig. 14 that the vertical drift velocity is around 7 km/hr.

References

Chaffee D. D.	1954	*J. Geophys. Res.* **59,** 549.
Chapman S. and Bartels J.	1940	*Geomagnetism* **1,** 531.
Fejer J. A.	1953	*J. Atmosph. Terr. Phys.* **4,** 184.
Kirkpatrick C. B.	1949	*Aust. J. Sci. Res.* A **1,** 423.
Lindquist R.	1953	*J. Atmosph. Terr. Phys.* **4,** 10.
Manning L. A., Peterson A. M. and Villard O. G.	1954	*J. Geophys. Res.* **59,** 47.
Martyn D. F.	1947a	*Proc. Roy. Soc.* A **189,** 241.
	1947b	*Proc. Roy. Soc.* A **190,** 273.
	1953–54	*Phil. Trans.* A **246.**
	1953	*Proc. Roy. Soc.* A **218,** 1.
Mitra A. P.	1957a	*J. Atmosph. Terr. Phys.* **10,** 140.
	1957b	*J. Atmosph. Terr. Phys.* **10,** 153.
Nertney R. J.	1951–52	Scientific Report, No. 28 and 39. Ionospheric Research Laboratory, Pennsylvania State College.
Nicolet M.	1954	Scientific Report No. 72. Ionospheric Research Laboratory, Pennsylvania State College.
Parkinson R. W.	1955	*J. Atmosph. Terr. Phys.* **7,** 203.
Passow R. L.	1952	Scientific Report No. 40. Ionospheric Research Laboratory, Pennsylvania State College.
Peiffer H. R. and Mitra A. P.	1955	*J. Atmosph. Terr. Phys.* **6,** 291.
Watts J. M. and Brown J. N.	1950	*J. Geophys. Res.* **56,** 179.

VOL
13
1958/

Journal of Atmospheric and Terrestrial Physics, 1959, Vol. 13, pp. 291 to 294. Pergamon Press Ltd. Printed in Northern Ireland

Observations of Meinel N_2^+ bands near 1·5 μ in the auroral spectrum*

A. W. HARRISON† and A. VALLANCE JONES
Physics Dept., University of Saskatchewan, Saskatoon, Saskatchewan, Canada

(*Received* 5 *May* 1958)

Abstract—The 0,1 and 1,2 Meinel bands have been observed in the auroral spectrum at 1·46 μ and 1·53 μ. The maximum observed absolute brightnesses of these bands were found to be 148 and 426 kilorayleighs (kR) respectively. The brightness of the 1,2 band appears to be anomalously high and this may be a result of preferential excitation by collision with $O^+(^2D)$ ions. A feature of high but fluctuating brightness at 1·59 μ agrees in wavelength with the 2,3 N_2^+ band but appears to be somewhat brighter than is consistent with this identification. It is possible that the latter emission may arise from the excitation in aurora of the 0,1 $^1\Delta_g - ^3\Sigma_g^-$ O_2 band. An unidentified emission has been observed at 1·61 μ on some of the auroral spectra obtained.

INTRODUCTION

THE band system arising from transitions between the $A^2\pi$ and $X^2\Sigma$ states of N_2^+ was discovered in the photographic region of the auroral spectrum by MEINEL (1951). Further bands of this system have been observed between 0·9 and 1·0 μ by BAGARIAÇKI and FEDOROVA (1955) with the help of an infrared image converter and by HUNTEN and LYTLE (see HUNTEN, 1957) using an infrared photomultiplier in a spectrometer. HARRISON and VALLANCE JONES (1957) have reported observations of the 1,0 and 0,0 N_2^+ bands at 0·92 μ and 1·105 μ respectively. The PbS spectrometer used in this work has been described by GUSH and VALLANCE JONES (1955). Since the work reported in our earlier paper was completed further bands of the Meinel system have been discovered in the neighbourhood of 1·5 μ.

OBSERVATIONS

The results to be described were obtained during the intense aurora of 4–5 February, 1957. Six typical recorder traces over the spectral range 1·40 to 1·67 μ are reproduced in Figs. 1 and 2. These traces are representative of a set of fourteen spectra obtained during the display. The spectral slit width was 200 Å. Throughout the series of spectra, the features at 1·46 μ and 1·53 μ recurred persistently. These wavelengths agree to within 0·1 μ with the wavelengths predicted for the origins of the 0,1 and 1,2 Meinel bands as set out in Table 1 below. These two observed features may therefore be tentatively assigned to these bands.

A further strong emission feature was observed to occur on four spectra at 1·59 μ. The tracing of Fig. 1(c) is typical of these. This feature may be the 2,3 N_2^+ band which should occur at 1·59 μ. The predicted relative intensity of this band (Table 1) is an order of magnitude smaller than that of the 0,1 band at 1·46 μ. The mean brightness observed for the 1·59 μ features was nearly equal to the mean brightness of the 1·46 μ band. Therefore, it is possible that at least some of the

* The research reported in this paper has been sponsored by the Geophysics Research Directorate of the Air Force Cambridge Research Center, Air Research and Development Command, under Contract AF 19(604)–1831.

† Now at Canadian Armament Research and Development Establishment, Valcartier, P.Q., Canada.

Table 1. Wavelengths, calculated intensities and observed intensities of of N_2^+ Meinel bands

Band	Wavelength (μ)	Calculated relative brightness	Observed maximum brightness (kR)	Observed mean brightness* (kR)
0,1	1·465	100	148	100
1,2	1·524	43	426	320
2,3	1·587	7	200	98

* The mean brightness is the average for the three brightest spectra obtained for each feature.

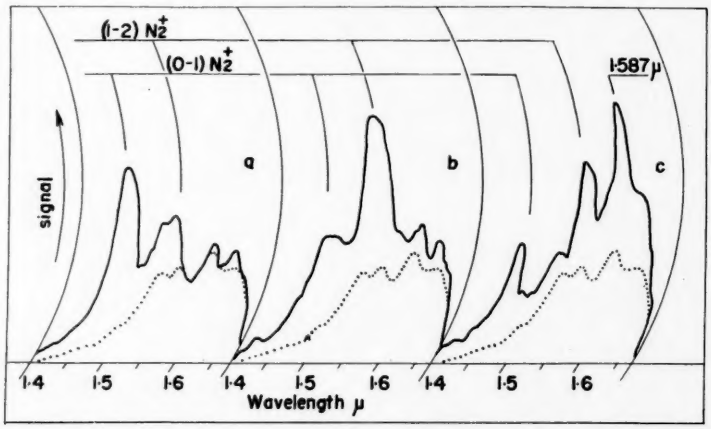

Fig. 1. Auroral spectra obtained on the night of 4–5 February, 1957. The wavelengths and proposed identifications of the principal emission features are indicated. These are consecutive spectra obtained in a total time of 3 min.

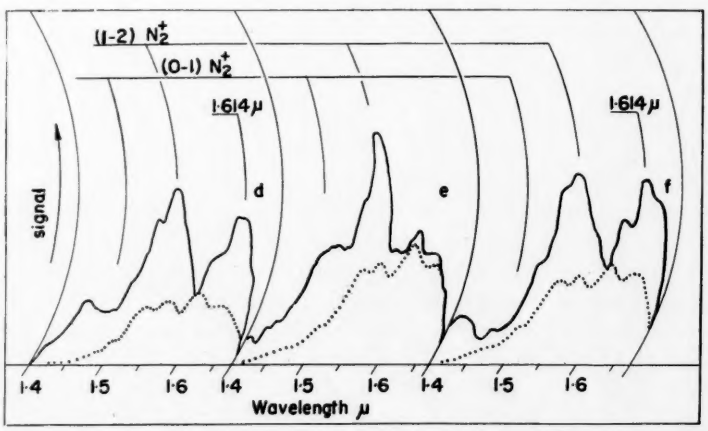

Fig. 2. Further auroral spectra as described for Fig. 1 except that these were not obtained in consecutive scans.

emission at 1·59 μ should be ascribed to an auroral excitation of the $^1\Delta_g$–$^3\Sigma_g^-$ O_2 band which has also been observed recently in the evening twilight airglow by VALLANCE JONES and HARRISON (1958). Further work now in progress is directed toward the solution of this problem. Four of the spectra (for example, (d) and (f), Fig. 2) show a feature at 1·61 μ. An identification of this feature has still to be made. Its maximum observed brightness was 110 kR* (kilorayleighs).

BRIGHTNESS MEASUREMENTS

The absolute brightness of the spectral features were derived from the records by the procedure described by HARRISON and VALLANCE JONES (1957). The results were corrected for the background emission arising from the nightglow OH bands. The line of sight of the spectrometer was kept pointing towards the brightest part of the aurora so that the zenith distance (upon which the brightness of the night glow radiations depends) was not constant during the time taken for the spectrometer to record a spectrum (60 sec). An approximate correction for the nightglow emission was made by fitting the nightglow emission curve to the auroral spectrum in a region where the auroral emission appeared to be negligible. In view of the fluctuations in intensity during the scanning period, the relative brightnesses of the emission features as given by single spectra such as appear in Figs. 1 and 2 have little significance.

The results of the measurements are set out in Table 1. The second column gives the predicted band origins calculated from the data of DOUGLAS (1953) and COSTER and BRONS (1932). The third column gives the calculated brightnesses of the bands relative to a value of 100 kR for the 0,1 band. These values are corrected roughly for atmospheric absorptions. In carrying out the calculation which is the same as that referred to by HARRISON and VALLANCE JONES (1957), the populations of the $v' = 0, 1, 2, 3$ and 4 levels were taken to be in the ratio 400 : 200 : 100 : 49 : 22. Since the relative populations of the $v' = 0$ and $v' = 1$ levels were obtained by extrapolation from the relative intensities given by MEINEL (1951), the calculated intensities can have a qualitative significance only. The fourth column of Table 1 gives the maximum observed brightness of the bands. The brightnesses given in column 5 are mean values for the three brightest spectra observed for each feature. Such mean values should be somewhat less subject to statistical errors and give a more reliable indication of the observed relative brightness than the result in column 4.

The values in Table 1 suggest that the band originating in the $v' = 1$ vibrational level is abnormally strong compared with that originating from the $v' = 0$ level. This peculiarity in our results was pointed out to us by Dr. D. M. HUNTEN and noted by him in a general survey of spectroscopic work on aurora carried out at Saskatoon (HUNTEN, 1957). As pointed out by OMHOLT (1957) such an enhancement of the $v' = 1$ level of the $^2\Pi$ state of N_2^+ could arise from the reaction:

$$O^+(^2D) + N_2(X^1\Sigma g) \rightarrow O(^3P) + N_2^+(A^2\pi_u\, v' = 1)$$

which is in exact resonance to within 0·01 eV.

* The brightness in rayleighs (HUNTEN, ROACH and CHAMBERLAIN, 1956) equals $4\pi B$, where B is the angular surface brightness of the emitting layer in units of 10^6 photon/cm^2 steradian sec.

References

Bagariaçki B. A. and Fedorova N. I.	1955	*Dokl. Akad. Nauk SSSR* **103,**1009.
Coster D. and Brons H. H.	1932	*Z. Phys.* **73,** 747.
Douglas A. E.	1953	*Astrophys. J.* **117,** 380.
Gush H. P. and Vallance Jones A.	1955	*J. Atmosph. Terr. Phys.* **7,** 285.
Harrison A. W. and Vallance Jones A.	1957	*J. Atmosph. Terr. Phys.* **11,** 192.
Hunten D. M.	1957	*Ann. Géophys.* **14,** 167 (1958).
Hunten D. M., Roach F. E. and Chamberlain J. W.	1956	*J. Atmosph. Terr. Phys.* **8,** 345.
Meinel A. B.	1951	*Astrophys. J.* **114,** 431.
Omholt A.	1957	*J. Atmosph. Terr. Phys.* **10,** 324.
Vallance Jones A. and Harrison A. W.	1958	*J. Atmosph. Terr. Phys.* **13,** 45.

VOL.
13
1958/5

Journal of Atmospheric and Terrestrial Physics, 1959, Vol. 13, pp. 295 to 314. Pergamon Press Ltd. Printed in Northern Ireland

A survey of the present knowledge of sporadic-E ionization

J. A. THOMAS* and E. K. SMITH†

(*Received* 9 *May* 1958)

1. INTRODUCTION

THIS survey paper is an attempt to fill the need for a general summary of the present state of our knowledge of the sporadic-E (E_s) layer of the ionosphere. At the present moment a large amount of scattered data concerning sporadic-E reflections is available, but there is, as yet, no theory which completely explains any one of the variety of types of E_s reflections found in different parts of the world. We aim to present a summary in which the gaps in our information may easily be seen, and which will be of use for further theoretical studies of the problems associated with E_s.

In making such a survey we must, of course, draw heavily on the work of other authors, and we wish, therefore, to make a general acknowledgement to all those who have contributed to our knowledge of this subject.

OL.
13
8/59

Definition

For the purposes of this survey we will adopt the IGY definition of sporadic-E reflections (*Annals of the IGY*, 1957). Thus we consider as an E_s-reflection any abnormal E-region reflection which is characterized by one or more of the following:

(1) Random time of occurrence;

(2) Partial transparency;

(3) Variation of penetration frequency with transmitter power as deduced from F-region reflections;

(4) Uniform apparent reflection height, regardless of frequency.

Further, in accordance with IGY scaling practice, we will not consider very weak echoes such as are returned by the meteoric-E layer described by NAISMITH and other workers (DIEMINGER, 1957; ELLYETT *et al.*, 1952; NAISMITH, 1954, 1956).

Outline

In the following sections we discuss briefly the various techniques available and what information can be gained from their use. This is followed by the classification of E_s into various zones and types, and the next section contains the main bulk of the known information in tabular form. The final section deals briefly with some general theoretical considerations and makes some tentative recommendations. A bibliography is included.

* Department of Physics, University of Queensland, Brisbane, Australia.
† Ionospheric Research Section, National Bureau of Standards, Boulder, Colorado.

2. Techniques

Ionosondes at vertical incidence

The continued use and analysis of routine $h'f$ soundings has provided (and will undoubtedly continue to provide) data concerning the regularities of sporadic-E on a world-wide basis. In particular, the occurrence, form, height, maximum (or top) and blanketing frequencies, reflection coefficient, and the geographical, seasonal and diurnal variations of these properties, may be obtained. The use of known changes in the system gain of the ionosonde is of importance in discriminating among various types of E_s, even at one station.

Oblique-incidence ionosphere sounders

Experiments designed to test the validity of the secant law as applied to the critical frequencies of the regular ionospheric layers yield information of the same sort for sporadic-E. Typically an experiment of this type involves three ionosphere sounders. Two are modified and carefully synchronized so that each records the transmissions of the other. These two are separated some desired distance, say 1000 km. The third ionosonde operates in normal fashion and is placed at the midpoint of the path. The $P'f$ records then show, among other things, to what extent reciprocity holds for the two directions of transmission and whether the MUF's observed over the oblique-incidence path are those which would have been predicted from the $h'f$ records of midpoint sounder (Wright).

Fixed-frequency vertical-incidence observing

A number of fixed-frequency methods of observing (all mainly continuous in time) are available. The straightforward $h't$ type of observation (particularly with expanded range scale) is the most common method used. Measurements of the virtual height, the relative strength, and changes in phase path of the echoes are all comparatively easy to make, and lead to estimates of horizontal and vertical movements, scattering polar diagrams, fine structure of the layer, and possible electron content changes due to E_s-patches. Measurements of the drift may be made using closely-spaced receivers, widely-spaced receivers, and direction-finding systems.

Back-scatter sounding methods

There are two general types of ionospheric back-scatter equipments in use today: "fixed-frequency, swept-azimuth", and "swept-frequency, fixed-azimuth". Both of these make use of the fact that for a one-hop ionospheric propagation path, a small amount of energy is returned to the transmitter through ground back-scatter by way of ionosphere reflections; and the returned signal is enhanced at the skip distance. Occasionally back-scatter takes place directly from ionospheric irregularities. In sporadic-E research, the fixed-frequency swept-azimuth method is particularly suitable for studying the location and movement of E_s clouds.

Other oblique-incidence sounding methods

Several other types of oblique-incidence data have been utilized in the study of E_s. Special circuits have been set up specifically for the determination of HF

VOL.
13
1958/5

and VHF sporadic-E field-strength levels. The carefully calibrated circuits used for ionosphere scatter transmission experiments have yielded valuable E_s field-strength data as a by-product. Reports of long distance transmission in the 50–100 Mc/s range have been analysed for their E_s information. The collection and analysis of data on amateur radio contacts (50 Mc/s) and of reports of long-distance television reception have been made. These studies lead to information concerning the geographic distribution and movements of E_s-patches, and the frequency and distance dependence of E_s-propagation at VHF.

Rocket measurements

Rocket flights through the E-region at times when E_s is observed by the normal radio (ionosonde) technique should give (in addition to data on the pressure, density, constituents, ionizing radiations, etc.) information on the ionization as a function of height. These measurements are becoming increasingly numerous and reliable, and will obviously be of considerable importance for determining the structure of the E_s-layer.

Correlations of sporadic-E

Extensive examinations have been made by various workers into the association between various features of E_s and the following:

(1) Various weather features (including thunderstorms);
(2) Meteoric activity;
(3) Aurora and airglow;
(4) Magnetic effects;
(5) Solar activity;
(6) Lunar and solar tidal effects;
(7) Other ionospheric features (e.g. forward scatter, scintillations).

3. Division Into Zones and Types

There are two points of view which may be profitably adopted in considering the world-wide distribution of sporadic-E as observed on vertical-incidence sounding equipment. The first of these is to consider all the different forms of sporadic-E found in one locality to represent manifestations of a single phenomenon known as "sporadic-E". It is then possible to chart the geographical variations of "sporadic-E" so as to arrive at geographical "zones", and to prepare a simple display of the temporal variations of the phenomenon at a given locality. This viewpoint, which might be termed the macroscopic approach, has been followed by some workers for their descriptions of the time variations of E_s, and by others for geographical variations.

A second method of attack involves first classifying the sporadic-E observed at any given locality into various sub-classes or "types". This typing may be based on the characteristics of the sporadic-E trace as observed on a single ionogram or it can be expanded to include time variations as well. If this is done carefully each

"type" of E_s now constitutes a reasonably consistent phenomenon and its morphology and geographical extent may be separately studied. In relation to the "macroscopic" approach, this method can be termed the "microscopic" approach.

The advantages of the macroscopic technique are that tabulated data scaled from ionograms in accordance with international conventions by the world-wide network of ionosphere stations may be used directly. Also, these data have about as much complexity as the communications engineer can use. The drawbacks of the macroscopic method are twofold. In the first place many diverse effects have been quite arbitrarily lumped together. Secondly the data have been obtained from many different types of equipments and considerable differences appear to exist in the interpretation of scaling instructions. The microscopic approach is scientifically preferable, but has the drawback that (at least until recently) it involves the re-scaling of film records.

E_s-zones

The time variations of sporadic-E become quite markedly different as one goes southward from the maximum of the northern auroral zone. Fig. 1 illustrates this effect with contour maps of E_s-occurrence (percentage of time that the sporadic-E critical frequency, fE_s, exceeds 5 Mc) for Narsarssuak, Greenland (maximum of the auroral zone), White Sands, N. M. (centre of the north temperate zone), Huancayo, Peru (equatorial zone), and Watheroo, Australia in the south temperate zone. It is seen that for Narsarssuak the E_s-occurrence is largely a night-time phenomenon with little seasonal variation. At Huancayo, on the magnetic equator, there is again little seasonal variation, but the E_s is almost entirely a daytime phenomenon. For White Sands and Watheroo it is seen that E_s occurs strongly in the summer with maxima falling in June–July for White Sands and December–January for Watheroo.

The striking temporal variations shown above have been utilized (SMITH, 1957) in determining the boundaries between the auroral and temperate zones, and the temperate and equatorial zones. Inside the auroral zone there is correlation between E_s-occurrence (fE_s greater than 5 Mc) and auroral percentage frequency days as given by VESTINE *et al.* (1947). The transition from auroral to temperate zone characteristics takes place on the average at about the 15 per cent auroral isochasm (maximum of the auroral zone equals 100 per cent). This is quite close to the 60° parallel of geomagnetic latitude which is commonly taken as the southern boundary of the auroral zone. MATSUSHITA (1952) showed that the equatorial zone can be considered to be bounded by the plus and minus 10° isopleths of magnetic dip. Fig. 2 shows the locations of these various zones. It also shows contours of sporadic-E occurrence during the daytime for the June solstice period. Quite a pronounced longitude variation is apparent in this map which shows a maximum near Japan and a minimum in South Africa.

E_s-types

The problem of classifying sporadic-E into sub-groups or types is very difficult. Prior to the IGY there had been no agreed-upon set of E_s types, and there was consequently some difficulty in relating one author's "types" to another's. There

VOL
13
1958/

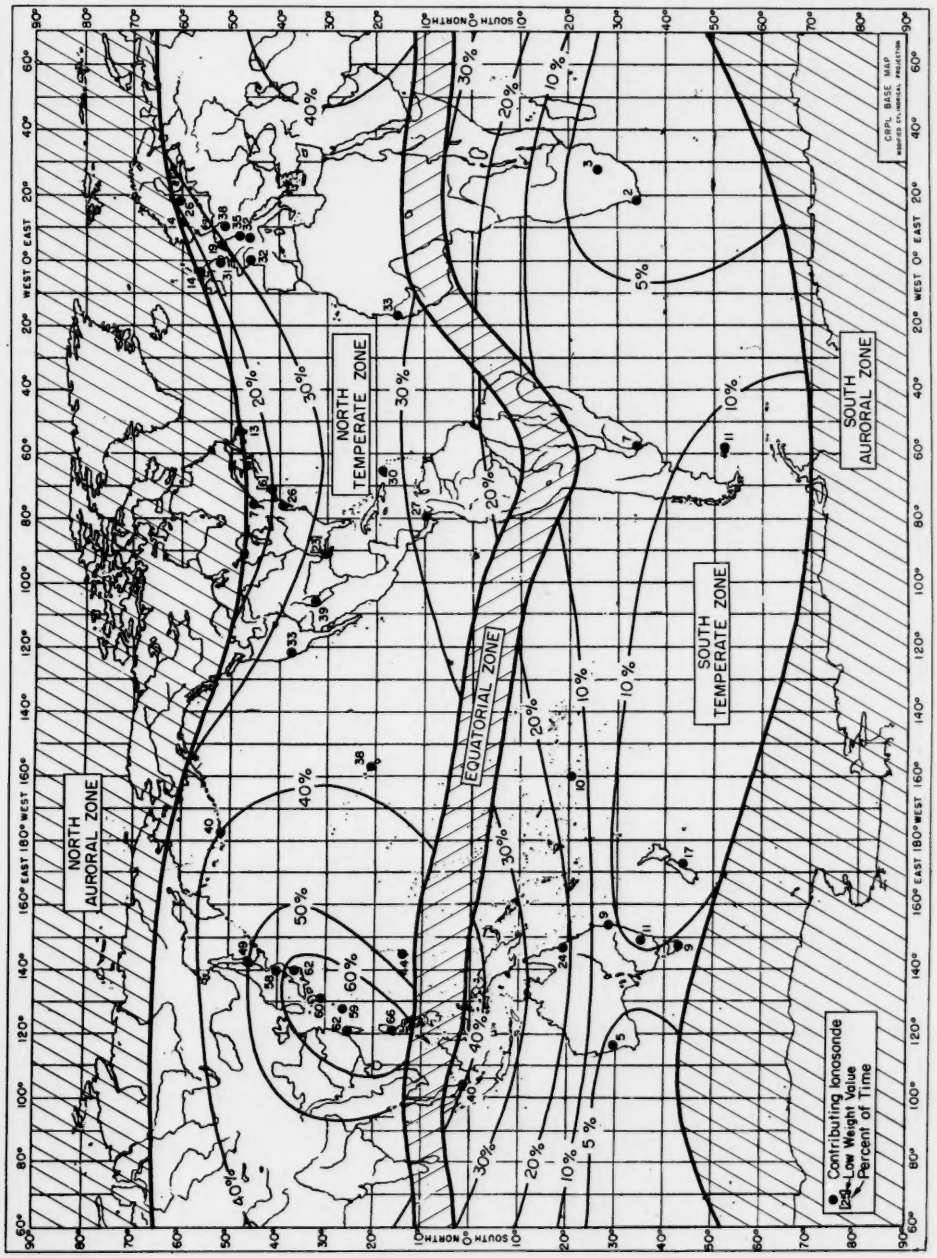

Fig. 1. Map showing boundaries of E_s zones and percent of the daytime hours during the June solstice months (0600 to 1800 local time, May through August) during which fE_s exceeded 5 Mc for the period 1948 through 1954 (after SMITH, 1957).

VOL. 13 58/59

is now available (*Annals of the IGY*, 1957) the IGY "Classification of E_s according to its appearance on the ionogram". This standard set of types is the result of extensive study by an international committee of experts, and should help to ensure that future workers are describing the same phenomena. The most recent

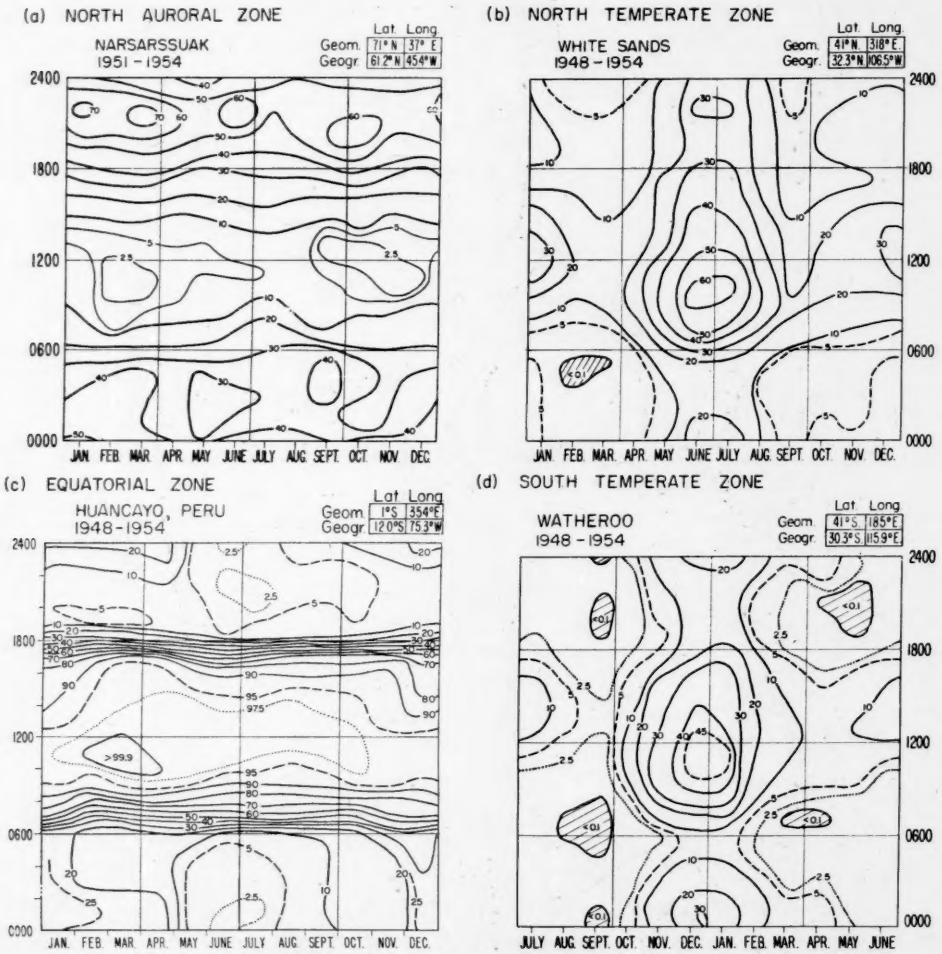

Fig. 2. Sample temporal variations in E_s in terms of percentage of time for which fE_s exceeded 5 Mc (after SMITH, 1957).

description of the E_s types by this group (SMITH, private comm.) is reproduced as Appendix I to this paper.

For temperate latitudes four predominant types exist, viz: h (high), c (cusp), l (low), and f (flat, when no regular E-layer is present). For the auroral zone it is necessary to add types a (auroral), r (retardation), and s (slant); and for the equatorial zone, types q (equatorial) and s (slant), in addition to the temperate zone types. An "unclassifiable" type (n) is added to accommodate those types of records which do not fall into any one of the above classifications.

It is useful to consider briefly the relation between IGY types and the types discussed by various authors in earlier works. The types "r", "s", "a" and "q" are the same as four types discussed by SMITH (1957). Types h and c have been described by a number of authors beginning with APPLETON and NAISMITH (1940); these two types have sometimes been grouped together and discussed under the heading of "sequential" E_s (MCNICOL and GIPPS, 1951; THOMAS, 1956a). Type "a" has its origin in a correlation study of visual aurorae and E_s by KNECHT (1956a) and has also been described by BECKER (1957). It is difficult to find a good correspondence between the IGY types and numerous other types, as the latter often cover more than one IGY type (MCNICOL and GIPPS, 1951; MEEK, 1949).

4. TABULATED DATA

1	2		3	4	5
Zone	Type		$h'f$ Example	Effect of $h'f$ system gain changes	Diurnal variation of fE_s
	IGY	Other			
Equatorial	q	Huancayo (6) Fringe (10) Equatorial (3)		Sensitive	Essentially daytime phenomenon (3, 6). Occasional night occurrence
	s	Slant (6)		Sensitive	Daytime
Temperate	h		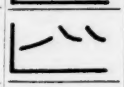	Insensitive (8, 9)	Dawn minimum in all seasons. E_{ss}: Summer max. at 1000, 1700 hours Winter max. at 1200 hours E_{sc}: Summer max. at 2300 hours Winter max. at 1500 (2300) hour (6, 7)
	c	E_{ss} (2)	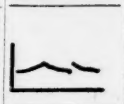	Insensitive (8, 9)	
	l	E_{sc} (2)	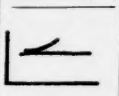	Insensitive for the most part (8, 9)	
	f		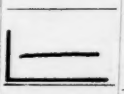	Insensitive for the most part (8, 9)	
Auroral	a			Sensitive	Night-time phenomenon (6)
	f			Usually sensitive, but sometimes not	
	r	Retardation (1, 4)		Insensitive?	Largely night-time
	s			Sensitive (5)	Daytime at Godhaven (5) Night-time at College, Ala. (6)

References in parentheses: (1) LINDQUIST, 1950; (2) MCNICOL and GIPPS, 1951; (3) MATSUSHITA, 1952; (4) MEEK, 1949; (5) OLESON, to be published; (6) SMITH, 1957; (7) THOMAS, 1956a; (8) THOMAS *et al.*, 1957; (9) THOMAS *et al.*, 1956; (10) WELLS, 1946.

2	6	7	8
Type	Seasonal variation of fE_s	Diurnal variation of f_bE_s	Seasonal variation of f_bE_s
q	Almost uniform. Slight minimum in winter–spring (1)	Non-blanketing	Non-blanketing
s		Non-blanketing	Non-blanketing
h	E_{ss}: Summer max. and gradual decay to spring equinox	Dawn minimum in all seasons	E_{ss}: Summer max. and gradual decay to spring equinox
c	Rapid rise to summer values	E_{ss}: Summer max. at 1000, 1700 hours	Rapid rise to summer values
l	E_{sc}: Winter and summer maxima Spring equinox is very low (1, 2).	Winter max. at 1200 hours E_{sc}: Blanketing frequencies generally quite low for this type—not often greater than 3 Mc/s (2)	E_{sc}: Essentially non-blanketing (2)
f			
a	No variation at auroral maximum. Equinoctial max. as depart from auroral max. (1)	Usually non-blanketing	
f			
r	Little variation	One type non-blanketing Other type blankets, but variation unknown	
s	Alaska—Winter (autumn) maximum	Non-blanketing	

References in parentheses: (1) SMITH, 1957; (2) THOMAS, 1956a.

VOL 13 1958/5

2	9	10	11
Type	Partial transmission range (fE_s–f_bE_s)	No. of multiple reflections*	Sunspot cycle correlation
q		Never > 1	
s		Never > 1	
h	E_{ss}: From 0·1 to 1·0 Mc/s	2–3 in summer morning 1 at summer midday 1–2 in winter	Strong inverse correlation of number of multiple reflections, due to sunspot-cycle changes in D-region absorption. No other changes are observed, thus confirming the lack of change of characteristics with system gain change (column 4) (1, 2)
c	E_{sc}: Generally much greater than for E_{ss} (~2–4 Mc/s) (2)	2–4 in summer 1–2 in winter	
l		1–2 summer 1–2 winter	
f		3–4 summer 1–2 winter	
a		Normally 1	Probable
f		Generally 1 Occasionally 2–4	
r	Large	Normally 1	
s		Normally 1	

* Counting first reflection.
References in parentheses: (1) Smith, 1957; (2) Thomas, 1956a.

2	12	13
Type	Diurnal and seasonal variation of $h'E_s$	Apparent vertical thickness
q	95–105 km; no seasonal change	
s	Lowest height is same as for q-type	
h	Semi-diurnal changes (± 5 km) which change phase with season. Summer maxima of $h'E_s$ at 0700, 1800 hours. Winter maxima at 0100, 1100 hours (5, 6)	E_{ss}: Initially 20 km thick, but rapidly thinning with apparent downward motion and increase in partial transmission range to a value $\sim$1 km (6)
c	Higher mean level in summer than in winter	
l		For cusp (c)-type, measurements indicate $\sim$5 km when partial transmission range is small (1)
f	Some evidence for stratification of levels (2, 3, 6) Oblique echoes often observed	M-echo measurements on this type indicate apparent thicknesses less than 0·5 km (4)
a	$h'E_s$ appear to be the slant range of the associated aurora (5)	
f		
r		
s		

References in parentheses: (1) Briggs, 1951b; (2) Gregory, 1956; (3) Helliwell, 1952; (4) Hosking, 1957; (5) Smith, 1957; (6) Thomas, 1956a.

VOL. 13 1958/5

2	14	15	16
Type	Lunar effects	*M*-echo occurrence	Range spreading and scattering polar diagram
q	Time of disappearance is partially controlled by lunar tidal currents in *E*-region (3)	Never occurs	Generally a spread echo is observed.
s		Never occurs	Generally spread
h	Summer lunar S.D. tide in fE_s, ~0·3 Mc/s at 08 hours	*M*-echoes occur in the temperate zone for about 80–90% of all E_s-occurrences	E_{ss}: Echoes are not substantially spread. Value of the half-amplitude angle of the E_s-scattering polar diagram (θ_0) is ~8° (1, 4)
c	Lunar S.D. tide in $h'E_s$, ~0·5 km at 06 hours (2)	Occasionally occurs when no E_s is observable (4)	
l			E_{sc}: Later stages of this type in winter show considerable spreading Value of θ_0 ~ 22° (1, 4)
f	Lunar S.D. tide 0·7 km at Brisbane		
a			Usually shows some spreading
f			Generally spread, but occasionally not
r			Generally spread
s			Spread echoes

References in parentheses: (1) Briggs and Phillips, 1950; (2) Matsushita, 1953b; (3) Matsushita, 1957; (4) Thomas, 1956a.

2	17	18	19
Type	Meteor correlation	Magnetic correlation	Weather and thunderstorm correlation
q		Very high correlation with equatorial electrojet within the zone $\pm 10°$ of magnetic dip (7, 15, 16)	
s		Possible correlation with bay disturbances	
h	Wind shear effects (determined from meteoric echo equipment) shows stratification levels about 6 km apart.	Slight negative correlation between 30° and 60° N geomagnetic latitude	Generally no correlation, but good evidence of strong correlation with certain types of thunderstorms in India (1, 9, 14)
c	Metallic meteoric particles may produce ionization at 100 km level after slow diffusion from higher levels	Zero correlation up to 30° N (16)	
l	No *direct* correlation with any one of the major types. Good correlation with some weak low level echoes not included in IGY classification (2, 3, 4, 4, 5, 10, 11, 12, 13)	Very small declination change associated with intense E_s ionization (6)	
f			
a		Positive correlation	
f		Positive correlation	
r		Positive correlation	
s		Correlation with bay disturbances (8, 17)	

References in parentheses: (1) BHAR, 1936; (2) DIEMINGER, 1957; (3) ELLYETT *et al.*, 1952; (4) GIPPS, 1947; (5) GREGORY, 1956; (6) HOJO and YONEZAWA, 1953; (7) MATSUSHITA, 1952; (8) MATSUSHITA, 1956; (9) MITRA and KUNDU, 1954; (10) NAISMITH, 1954; (11) NAISMITH, 1956; (12) NEUZIL, 1955; (13) NICOLET, 1955; (14) RASTOGI, 1955–1956; (15) SKINNER and WRIGHT, 1957; (16) SMITH, 1957; (17) WELLS, 1947.

VOL.
13
1958/5

2	20	21	22
Type	Scintillation correlation	Drifts and growth of E_s-patches	E_s-patch size
q			
s			
h	Good correlation between low elevation scintillations and sporadic-E	Drifts in northern hemisphere generally towards west. Evidence of some degree of preferred orientation for elongated irregularities. In southern hemisphere E_{ss} drifts generally to N or NW.	E_{ss}: May be up to several hundred kilometres in extent (5, 6, 7, 10, 11, 12, 13, 15, 18, 19, 20, 21)
c	Evidence of extension of E_s-patches along the magnetic field (1, 24)	E_{sc} drifts generally to N or NE. All drifts ~60 m/s	E_{sc}: Often 10–20 km. Larger patches made up of aggregations of these smaller clouds (21)
l		Spaced $P'f$ measurements now in progress suggest patches may sometimes grow at one point without any apparent drift in from one side (2, 3, 4, 5, 6, 7, 9, 10, 14, 15, 17, 22, 23)	
f			Some suggestion from rocket data of very small scale patches (~0·5 km) (16)
a		Evidence for elongation of patches along magnetic field (9)	
f		Extremely rapid apparent vertical and horizontal movements observed at some stations (8)	
r			
s			

References in parentheses: (1) Bolton *et al.*, 1953; (2) Briggs and Spencer, 1954; (3) Chapman, 1953; (4) Clark and Peterson, 1956; (5) Clark, 1957; (6) Davidson, 1955; (7) Gerson, 1955; (8) Hagg and Hanson, 1954; (9) Harang and Pedersen, 1957; (10) Harvey, 1955; (11) McNicol and Gipps, 1951; (12) Maeda *et al.*, 1935; (13) Matsushita, 1952; (14) Matsushita, 1953a; (15) Peterson, 1957; (16) Pfister, 1957; (17) Phillips, 1952; (18) Rawer, 1955; (19) Seddon, 1958; (20) Smith, 1957; (21) Thomas, 1956a; (22) Thomas and Burke, 1956; (23) Tilton, 1951; (24) Wild and Roberts, 1956.

1	23	24
Zone	Oblique incidence data	Rocket information
Equatorial		Current sheet detected at 100 km level (17)
Temperate	General statistical agreement with secant law but no detailed agreement for certain types of E_s (1, 2, 4, 5, 7, 10, 15, 16, 18, 19, 20, 21, 22) Some evidence for linking VHF field strength measurements with $fE_s + 4$ Mc/s rather than just fE_s (9)	Ionization contours often show only a steep gradient associated with E_s reflection. Sometimes a thin slab ($\sim$1 km) of high electron density is detected. (8, 13, 14) Some suggestion of stratification levels at intervals of 6 km (11) Night-time flux of L_y-α radiation $\sim 10^{-2}$ ergs/cm^2 per sec per ster. rad. detected (6) Number of meteor particles detected $\sim$1/min per cm^2 (3) NO released at 100 km produced ionized patch lasting several minutes (12)
Auroral		

References in parentheses: (1) Aono and Kuriki, 1957; (2) Bailey *et al.*, 1955; (3) Berg and Meredith, 1956; (4) Clark, 1957; (5) Dyce, 1955; (6) Friedmann, 1957; (7) Gerson, 1955; (8) Jackson, 1954; (9) Kono *et al.*, 1954; (10) Peterson, 1957; (11) Pfister, 1957; (12) Pressman *et al.*, 1956; (13) Seddon, 1954; (14) Seddon, 1958; (15) Shearman and Martin, 1956; (16) Silberstein, 1954; (17) Singer *et al.*, 1952; (18) Strohfeldt *et al.*, 1954; (19) Sulzer, 1955; (20) Sulzer and Ferguson, 1952; (21) Tilton, 1951; (22) Weider, private communication.

1	25	26	27	28
Zone	Focusing effects	Sequential E_s starting times	Echo amplitude distribution	Phase-path information
Equatorial				
Temperate	Very slight apparent curvature effects are found in E_s reflections. Various methods of analysis indicate tilts $\sim 2^\circ$ and radii of curvature $\sim$500 km (1, 5, 6).	The starting time of sequences is a function of latitude, and follows the seasonal changes in the position of the S_q-current foci in the northern hemisphere (4).	This analysis leads to a discrimination of various types of E_s on the basis of the type of distribution obtained (2, 3).	This gives information concerning the ionization introduced between ground and F-region when an E_s-patch moves overhead. Evidence suggests a re-arrangement of the pre-existing ionization, but is not definite as yet.
Auroral				

References in parentheses: (1) Briggs, 1951a; (2) Chatterjee, 1953; (3) McNicol, 1949; (4) Matsushita, 1955; (5) Thomas, 1956b; (6) Uyeda and Nakata, 1956.

VOL 13 1958/

1	29
Zone	Airglow measurements
Equatorial	
Temperate	Past correlations of total E_s with airglow lines has proved suggestive but not statistically significant (2). Recent information as to the heights of the principal airglow constituents gives (1): green line (λ5577, atomic oxygen) . . . . . 95–100 km yellow line (λ5890, λ5896, sodium D) . . . . . 85 km infra-red (OH vibr.-rot. spectrum) . . . . . 70 km red line (λ6300, λ6363, atomic oxygen) – – – – – – – – – – – *F*-region
Auroral	

References in parentheses: (1) ROACH *et al.*, to be published; (2) SMITH, private communication.

5. General Considerations

With the exception of the obviously related types (e.g. sequential E_s classified as *h*, *c* and *l* in turn), the production and/or maintenance of the E_s-layer must be somewhat different for each type, if only because of the differing associated temporal variations and correlations. The differing sporadic content of the various theory types must also be considered in developing any detailed theory.

Considerations of the lifetime of ionization produced by any of the mechanisms in current favour for the normal ionospheric layers, show that none of these mechanisms are suitable for the production and maintenance of E_s patches which may last throughout the night or drift considerable distances either horizontally or vertically.

Listed below are the suggestions which have been put forward over the years to explain (a) the peculiar properties exhibited by the E_s-echoes, and (b) the cause of such ionization:

(a) (1) A thin layer or slab of ionization (RAWER, 1939; RYDBECK, 1944 a, b, 1948);

(2) A steep gradient of ionization (JACKSON, 1954; SEDDON, 1954; WHALE, 1951);

(3) A cloud-like or patchy layer of ionization (RATCLIFFE and PAWSEY, 1933; RAWER, 1948; THOMAS, 1956a);

(b) (1) Particle bombardment (APPLETON and NAISMITH, 1940; SMITH, 1957; WELLS, 1947, 1948);

(2) Meteor bombardment (direct and indirect) (APPLETON and NAISMITH, 1947; DIEMINGER, 1957; ELLYETT *et al.*, 1952; GREGORY 1956, private communication; LINDQUIST, 1950; MITRA *et al.*, 1934; NAISMITH, 1954, 1956; NEUZIL, 1955; NICOLET, 1955; PIERCE, 1938; SCHAFFER and GOODALL, 1932);

(3) Thunderstorms (APPLETON and NAISMITH, 1933; APPLETON *et al.*, 1937; BEST *et al.*, 1938; BHAR, 1936; CHATTERJEE, 1953; COLWELL, 1934; ISTED, 1954; KIRBY and JUDSON, 1935; MIMNO, 1937; MITRA and KUNDU, 1954; RASTOGI, 1955–1956; RATCLIFFE and WHITE, 1933; THOMAS, 1956a; WILSON, 1925);

(4) Scattering from a turbulent medium (BEST *et al.*, 1938; BOOKER, 1950; ECKERSLEY, 1932; GALLET, 1951, 1954, 1955; VILLARS and WEISSKOPF, 1954, 1955; WATSON-WATT, 1933);

(5) Currents and associated tidal forces (MARTYN, 1953; MATSUSHITA, 1952, 1955, 1957; RAWER, 1955; SKINNER and WRIGHT, 1957; SMITH, 1957; THOMAS, 1956a);

(6) Possible re-arrangement of pre-existing ionization.

These suggestions will not be further discussed here. Our present knowledge is sufficient to enable us to say only that any one, or indeed all of these processes may be necessary to explain the types of E_s observed at a particular station. In various regions some mechanisms must obviously find more favour than others (e.g. particle bombardment in the auroral region.)

It is obvious from the Tabulated Data (No. 4) that a large number of the blank spaces, and more detailed information about other sections, will be filled in by the analysis of the IGY results. Other data can, however, be obtained only by rather more refined techniques than those in use at most IGY stations.

Subjects deserving special experimental attention are

(1) The determination of the growth and decay of E_s-patches;

(2) The ionization content changes due to E_s-patch movements;

(3) The oblique-incidence propagation effects and their relation to E_s-parameters.

On the theoretical side, a more complete analysis is necessary of the relation between suggested causes of E_s-ionization and suggested ionization structures, bearing in mind the ionization lifetime necessary to explain the observed effects.

Acknowledgement—This survey was carried out while one of us (J. A. T.) held a Nuffield Foundation Dominion Travelling Fellowship. The authors would like to express their gratitude both to the Nuffield Foundation for its support and to the Boulder Laboratories of the National Bureau of Standards and the Cavendish Laboratory of Cambridge University for the use of their facilities.

REFERENCES

AONO Y. and KURIKI I. 1957 XII URSI General Assembly Boulder No. 25/Comm III.

AONO Y. and MINAGUICHI T. 1950 *Rep. Ionos. Res. Japan* **4,** 103.

APPLETON E. V. and NAISMITH R. 1933 *Proc. Phys. Soc. Lond.* **45,** 389.

APPLETON E. V. and NAISMITH R. 1940 *Proc. Phys. Soc. Lond.* **52,** 402.

APPLETON E. V. and NAISMITH R. 1947 *Proc. Phys. Soc. Lond.* **59,** 461.

APPLETON E. V., NAISMITH R. and INGRAM L. J. 1937 *Phil. Trans.* A **236,** 191.

APPLETON E. V., NAISMITH R. and INGRAM L. J. 1939 *Proc. Phys. Soc. Lond.* **51,** 81.

VOL. 13 1958/5

Bailey D. K., Bateman R. and Kirby R. C.	1955	*Proc. Inst. Radio Engrs., N.Y.* **43,** 1181.
Becker W.	1957	*Arch. Elektr. Übertr.* **11,** 101.
Berg O. E. and Meredith L. H.	1956	*J. Geophys. Res.* **61,** 751–754.
Best J. E., Farmer F. T. and Ratcliffe J. A.	1938	*Proc. Roy. Soc.* A **164,** 96.
Bhar J. N.	1936	*Nature, Lond.* **138,** 481.
Bolton J. G., Stanley G. J. and Slee O. B.	1953	*Aust. J. Phys.* **6,** 434.
Booker H. G.	1950	Proceedings of Pennsylvania Conference on Ionospheric Physics A, p. 171.
Bray W. J., Saxton J. A. and White R. W.	1956	*Proc. Instn. Elect. Engrs.* B **103,** 236.
Briggs B. H.	1951a	*Proc. Phys. Soc. Lond.* B **64,** 255.
Briggs B. H.	1951b	*J. Atmosph. Terr. Phys.* **1,** 345.
Briggs B. H. and Phillips G. J.	1950	*Proc. Phys. Soc. Lond.* B **63,** 907.
Briggs B. H. and Spencer M.	1954	*Rep. Progr. Phys.* **17,** 245.
Chapman J. H.	1953	*Canad. J. Phys.* **31,** 120.
Chatterjee B.	1953	*J. Atmosph. Terr. Phys.* **3,** 229.
Clark C. and Peterson A. M.	1956	*Nature, Lond.* **178,** 486.
Clark C.	1957	Tech. Rep. No. 24, Radio Prop. Lab., Stanford University.
Colwell R. C.	1934	*Nature, Lond.* **133,** 948.
Davidson D.	1955	Tech. Rep. No. 230, Cruft Lab., Harvard University.
Davies K. and Hagg E. L.	1955	*J. Atmosph. Terr. Phys.* **6,** 18.
Dieminger W.	1913	*Naturwissenschaften* **1,** 29.
Dieminger W.	1951	*Proc. Phys. Soc. Lond.* B **64,** 142.
Dieminger W.	1957	Statement at XII URSI General Assembly Boulder.
Dieminger W., Geisweid K. H. and Möller H. G.	1955	*Nachrichtentech Z.* **8,** 578.
Dyce R. B.	1955	*Trans. Inst. Radio Engrs., N.Y. PGAP* **3,** 76.
Eckersley T. L.	1932	*J. Instn. Elect. Engrs.* **71,** 405.
Ellyett C. D.	1947	*Terr. Magn. Atmos. Elect.* **52.**
Ellyett C. D., Roth W. and Jackson J.	1952	URSI Doc. No. 9, Comm III.
Ferrell O. P.	1948	*Proc. Inst. Radio Engrs., N.Y.* **36,** 879.
Friedmann H.	1957	Statement at XII URSI General Assembly Boulder.
Findlay J. W.	1953	*J. Atmosph. Terr. Phys.* **3,** 73.
Gallet R. M.	1951	*C. R. Acad. Sci., Paris* **233,** 1649.
Gallet R. M.	1954	Lab. Nat. Radioelectricite, Paris, December.
Gallet R. M.	1955	*Proc. Inst. Radio Engrs., N.Y.* **43,** 120.
Gerson N. C.	1955	*J. Atmosph. Terr. Phys.* **6,** 113.
Gherzi E.	1950	*Nature, Lond.* **165,** 38.
Gipps G. de V.	1947	*J. Coun. Sci. Industr. Res. Aust.* **20,** 407.
Gregory J. B.	1956	*Aust. J. Phys.* **9,** 324.
Gregory J. B.		Private communication.
Hagg E. L. and Hanson G. H.	1954	*Canad. J. Phys.* **32,** 790.
Harang L.	1941	*Terr. Magn. Atmos. Elect.* **46,** 279.
Harang L. and Landmark B.	1954	*J. Atmosph. Terr. Phys.* **4,** 322.
Harang L. and Pedersen K.	1957	*J. Geophys. Res.* **62,** 183.

HARVEY J. A.	1955	*Aust. J. Phys.* **8,** 523.
HELLIWELL R. A.	1952	URSI Doc. A. G. No. 170, Comm III.
HOJO H. and YONEZAWA T.	1953	*Rep. Ionos. Res. Japan* **7,** 61.
HOSKING R. H.	1957	*Aust. J. Phys.* **10,** 220.
	1957	*Annals of the IGY* **3,** Part 1.
ISTED G. A.	1954	*Marconi Rev.* **17,** 37.
JACKSON J. E.	1954	*J. Geophys. Res.* **59,** 377.
KIRBY S. S. and JUDSON E. B.	1935	*Proc. Inst. Radio Engrs., N.Y.*, **23,** 733
KITCHEN F. A. and TREMELLEN K. W.	1952	*Proc. Instn. Elect. Engrs.* III A **99,** 290.
KNECHT R. W.	1956	*J. Geophys. Res.* **61,** 59.
KONO T.	1950	*Rep. Ionos. Res. Japan* **4,** 127.
KONO T., UESUGI Y., HIRAI M. and ABE G.	1954	*J. Radio Res. Lab.* **1.**
KUPPERIAN J. E., BRYAN E. T., CHUBB T. A. and FRIEDMANN N. H.		*Ann. Géophys.* To be published.
LINDQUIST R.	1950	*Ark. Geofys.* **1,** No. 11, 247.
MCNICOL R. W. E.	1949	*Proc. Instn. Elect. Engrs.* III **96,** 517.
MCNICOL R. W. E. and GIPPS G. DE V.	1951	*J. Geophys. Res.* **56,** 17.
MAEDA, KONOMI, ISAGAWA, MINOHARA and ITO	1935	*Rep. Radio Res. Japan* **5,** 151, 451.
MARTYN D. F.	1934	*Nature, Lond.* **133,** 294.
MARTYN D. F.	1953	*Phil. Trans.* A **246,** 306.
MARTYN D. F. and PULLEY O. O.	1936	*Proc. Roy. Soc.* A **154,** 455.
MATSUSHITA S.	1951a	*J. Geomagn. Geoelect., Kyoto* **3,** 44.
MATSUSHITA S.	1951b	*J. Geomagn. Geoelect., Kyoto* **3,** 119.
MATSUSHITA S.	1952	*Rep. Ionos. Res. Japan* **6,** 118.
MATSUSHITA S.	1953a	*J. Geomagn. Geoelect., Kyoto* **5,** 109.
MATSUSHITA S.	1953b	*Rep. Ionos. Res. Japan* **7,** 45.
MATSUSHITA S.	1955	*J. Geomagn. Geoelect., Kyoto* **7,** 91.
MATSUSHITA S.	1956	*J. Geomagn. Geoelect., Kyoto* **8,** 156.
MATSUSHITA S.	1957	*J. Atmosph. Terr. Phys.* **10,** 163.
MEEK J. H.	1949	*J. Geophys. Res.* **54,** 339.
MIMNO H. R.	1937	*Rev. Mod. Phys.* **9.**
MITRA S. K.	1950	Proceedings of Pennsylvania Conference on Ionospheric Physics, Volume 2.
MITRA S. K., SYAM P. and GHOSH B. N.	1934	*Nature, Lond.* **133,** 294.
MITRA S. K. and KUNDU M. R.	1954	*Nature, Lond.* **174,** 798.
	1950	Mixed Commission on Ionosphere, ICSU.
MÖLLER H. G.	1956	*J. Atmosph. Terr. Phys.* **9,** 155.
NAGAOKA H.	1929	*Proc. Imp. Acad. Japan* **5,** 233.
NAISMITH R.	1954	*J. Atmosph. Terr. Phys.* **5,** 73.
NAISMITH R.	1956	*Wireless Engr.* **33,** 159.
NELSON J. H.	1955	*Radio Electron.* **26,** 36.
NEUZIL L.	1955	*Meteors* p. 96. Pergamon Press, London.
NICOLET M.	1955	*Meteors* p. 99. Pergamon Press, London.
OLESON J.		*J. Geophys. Res.* To be published.
PETERSON A. M.	1957	*Annals of the IGY* **3,** 361.
PFISTER W.	1957	Paper presented XII URSI General Assembly Boulder, Comm III.
PHILLIPS G. J.	1952	*J. Atmosph. Terr. Phys.* **2,** 141.
PIERCE J. A.	1938	*Proc. Inst. Radio Engrs., N.Y.* **26,** 892.
PINEO V. C.	1950	*Science* **112,** 50.
PRECHNER L. J.	1955	*Marconi Rev.* **18.**
PRESSMAN J. *et al.*	1956	*J. Chem. Phys.* **25,** 187.
RANZI I.	1932	*Nature, Lond.* **130,** 368.

VOL.
13
1958/5

Rastogi R. G.	1955-56	*Indian J. Met. Geophys.* **8,** No. 1.
Ratcliffe J. A. and Pawsey J. L.	1933	*Proc. Camb. Phil. Soc.* **29,** 316.
Ratcliffe J. A. and White E. L. C.	1933	*Proc. Phys. Soc. Lond.* **45,** 399.
Rawer K.	1939	*Ann. Phys., Lpz.* **35,** 385.
Rawer K.	1948	*Nature, Lond.* **163,** 528.
Rawer K.	1953	*Die Ionosphare.* Noordhoff, Groningen-Hohland.
Rawer K.	1955	*Geofis. Pur. Appl.* **32,** 170.
Roach F. E., Megill L. R., Rees M. H. and Marovich E.		*J. Atmosph. Terr. Phys.* To be published.
Rydbeck O. E. H.	1944a	*Chalmers Tek. Högsk. Handl.* **34,** 151.
Rydbeck O. E. H.	1944b	*Chalmers Tek. Högsk. Handl.* **34,** 168.
Rydbeck O. E. H.	1948	*Chalmers Tek. Högsk. Handl.* **74.**
Schaffer J. P. and Goodall W. M.	1932	*Proc. Inst. Radio Engrs., N.Y.* **20,** 1131.
Seddon J. C.	1954	*J. Geophys. Res.* **59,** 463.
Seddon J. C.	1958	*J. Geophys. Res.* In press.
Seddon J. C., Pickar A. D. and Jackson J. E.	1954	*J. Geophys. Res.* **59,** 513.
Shapley A. H. *et al.*	1957	Second Report of the Special Committee on World-Wide Ionospheric Soundings of the URSI/AGI Committee.
Shearman E. D. R. and Martin L. T. J.	1956	*Wireless Engr.* **33,** 190.
Silberstein R.	1954	*Trans. Inst. Radio Engrs., N.Y. PGAP,* **2,** 56.
Singer S. F., Maple E. and Bowen W. A.	1952	*Nature, Lond.* **170,** 1093.
Skellet A. M.	1931	*Phys. Rev.* **37,** 1668.
Skellet A. M.	1933	*Proc. Inst. Radio Engrs., N.Y.* **20.**
Skellet A. M.	1935	*Proc. Inst. Radio Engrs., N.Y.* **23,** 132.
Skinner N. J. and Wright R. W.	1957	*Proc. Phys. Soc. Lond.* B **70,** 833.
Smith E. K.	1952	*Trans. Inst. Radio Engrs., N.Y. PGAP* **2,** 54.
Smith E. K.	1953	*Radio Electron.* **24,** 54.
Smith E. K.	1957	NBS Circular 582, U.S. Govt. Printing Office.
Smith E. K.		Private communication. Report on study performed jointly with F. E. Roach.
Strohfeldt M., McNicol R. W. E. and Gipps G. de V.	1954	*Aust. J. Sci. Res.* A **5,** 464.
Sulzer P. G.	1955	*J. Geophys. Res.* **60,** 411.
Sulzer P. G. and Ferguson E. E.	1952	*Proc. Inst. Radio Engrs., N.Y.* **40,** 1124.
Thomas J. A.	1956a	*Aust. J. Phys.* **9,** 228.
Thomas J. A.	1956b	*Aust. J. Phys.* **9,** 574.
Thomas J. A., Brown H. E. and Cairns G. G.	1957	*Aust. J. Phys.* **10,** 310.
Thomas J. A. and McNicol R. W. E.	1955	*Proc. Instn. Elect. Engrs.* B **102,** 793.
Thomas J. A. and Burke M. J.	1956	*Aust. J. Phys.* **9,** 440.
Thomas J. A. and Svenson A. C.	1955	*Aust. J. Phys.* **8,** 554.
Thomas J. A., Svenson A. C. and Brown H. E.	1956	*Aust. J. Phys.* **9,** 159.
Tilton E. P.	1951	*Radio Electron.* **22,** 28.
Uesugi Y., Kasuya I. and Orimo J.	1956	*J. Radio Res. Lab.* **3,** 265.
Uyeda H. and Nakata Y.	1956	*J. Radio Res. Lab.* **3,** 119.
Vestine E. H. *et al.*	1947	*Publ. Carneg. Instn.* 580.

VILLARS F. and WEISSKOPF V. F.	1954	*Phys. Rev.* **94,** 232.
VILLARS F. and WEISSKOPF V. F.	1955	*Proc. Inst. Radio Engrs., N.Y.* **43,** 1232.
WATSON-WATT R. A.	1933	*Proc. Roy. Soc.* A **141,** 715.
WEIDER B.		Private communication.
WELLS H. W.	1946	*Proc. Inst. Radio Engrs., N.Y.* **34,** 950.
WELLS H. W.	1947	*Terr. Magn. Atmos. Elect.* **52,** 315.
WELLS H. W.	1948	Sixth Report I.C.S.U. p. 78.
WHALE H. A.	1951	*J. Atmosph. Terr. Phys.* **1,** 233.
WILD J. P. and ROBERTS J. A.	1956	*J. Atmosph. Terr. Phys.* **8,** 55.
WILSON C. T. R.	1925	Private communication.
WRIGHT J. W.		Private communication.

APPENDIX 1

IGY E_s types

The following description of sporadic-*E* types appears on pp. 11, 12, and 13 of the Second Report of the Special Committee on World-Wide Ionospheric Soundings (SMITH, private comm.). This committee was appointed by the URSI/AGI Committee in September 1955 and this report constitutes the latest official recommendation on ionogram scaling practice for use during the International Geophysical Year.

Description of standard types

The nine standard types of E_s are identified by small (lower case) letters; ***l, c, h, q, r, a, s, f, n.*** These letters are suggestive of the names low, cusp, high, equatorial, retardation, auroral, slant, flat and unclassified, respectively; it is strongly emphasized that these names are suggestive, not restrictive. . . . The standard types are:

l: A flat E_s-trace at or below the normal *E*-layer minimum virtual height (daytime only).

c: An E_s-trace showing a relatively symmetrical cusp at or below f_0E. This is usually continuous with the normal *E*-trace though, when the deviative absorption is large, part or all of the cusp may be missing (daytime only).

h: An E_s-trace showing a discontinuity *in height* with the normal *E*-layer trace at or above f_0E. The cusp is not symmetrical, the low frequency end of the E_s-trace lying clearly above the high frequency end of the normal *E*-trace (daytime only).

q: An E_s-trace which is diffuse and non-blanketing over a wide frequency range. The spread is most pronounced at the upper edge of the trace. (This type is common in daytime in the vicinity of the magnetic equator).

r: An E_s-trace which is non-blanketing over part or all of its frequency range showing an increase in virtual height at the high frequency end similar to group retardation. This is distinguished at present from true group retardation (a blanketing thick layer included in the *E*-layer tables: f_0E, $h'E$) by the lack of group retardation in the *F*-traces at corresponding frequencies.

a: An E_s-pattern having a well defined flat or gradually rising lower edge with stratified and diffuse (spread) traces present above it. These sometimes exceed over several hundred kilometers of virtual height.

s: A diffuse E_s-trace which rises steadily with frequency. This usually emerges from another E_s-trace which should be classified separately. At high latitudes the slant trace usually starts to rise from a horizontal E_s-trace, *l*, *h*, or *f*, at frequencies which greatly exceed the *E*-layer critical frequency (e.g. about 6 Mc/s) whereas at low latitudes it usually rises from equatorial type E_s, *q*, at frequencies near the *E*-region critical frequency.

f: An E_s-trace which shows no appreciable increase of height with frequency. The trace is usually relatively solid at most latitudes. This classification is used primarily at night.

n: An E_s-trace which cannot be classified into one of the standard types. This must not be used for intermediate cases between any two classes. A choice should always be made whenever possible, even if it is doubtful.

VOL. 13 1958/5

Journal of Atmospheric and Terrestrial Physics, 1959, Vol. 13, pp. 315 to 345. Pergamon Press Ltd. Printed in Northern Ireland

A bistatic radio investigation of auroral ionization*

C. COLLINS and P. A. FORSYTH
Radio Physics Laboratory, Defence Research Board, Ottawa, Canada

(*Received* 5 *May* 1958)

Abstract—The scattering of radio waves in the upper atmosphere during auroral disturbances has been studied by means of a number of radio systems in which each transmitter was separated from its associated receiver by a distance of about 1000 km. Some twenty of these systems were used in a network covering a large area in Canada. The frequencies were in the range 30–50 Mc/s. At least four different kinds of auroral events are distinguishable. Of these, two appear to be associated separately with different phases of visible aurora, the third with a later stage in the auroral process which is not observed visually, and a fourth with the recurrent daytime absorption which often precedes an auroral disturbance. The term "radio-aurora", which applies to all of the events, is used to avoid confusion with that part of the auroral process which is observable visually. In these four events, evidence is found for three separate scattering mechanisms, each of which has been proposed previously as the principal source of radar echoes from aurora.

INTRODUCTION

THE term "radio-aurora" is used here to indicate the ionospheric ionization, associated with auroral disturbances, that gives rise to radio reflections in the very-high and ultra-high frequency ranges. There is, at the present time, very little evidence to link this ionization with visible auroral displays. It appears that very sensitive radar equipment can sometimes detect such ionization when the aurora, if present, is too weak to be visible to the naked eye. It is hoped that the wider use of the term "radio-aurora" will tend to reduce the confusion, which is apparent in the literature, between the optical and the radio phenomena. With the rapid development of radio techniques it is probable that within a few years there will exist a more detailed knowledge about the occurrence and generation of radio-aurora than now exists concerning the corresponding optical phenomenon. The differentiation which is implied by the use of a separate term may also serve to emphasize the very great need for more experimental work aimed at establishing the degree of correspondence between the optical and radio phenomena.

A large number of investigations of radio-aurora have been carried out in the last few years. An excellent summary of the work up to 1956 has been presented by LITTLE *et al.* (1956). More recently, the frequency range of successful experiments has been extended upward to the vicinity of 400 Mc/s by FRICKER *et al.* (1957). In all this work the principal tool has been the radar equipment. This method of investigation, which has also been called the "back-scatter" method, makes use of a radio transmitter and receiver located at the same station, and might be called the single-station, or monostatic, method in contrast to the two-station or bistatic method. Some progress has been made with regard to the statistical occurrence of radio-aurora for a few locations, but this work has been done using a different frequency for each location. There are a number of seeming inconsistencies between the interpretations presented by various authors. This

* Work carried out under Project No. PCC D48–28–35–05.

divergence of opinion about the physical nature of radio-aurora probably is due, at least in part, to an incomplete understanding of the mechanism (or mechanisms) by which radio waves are scattered by auroral ionization.

The use of a bistatic method for the radio investigation of auroral ionization is not new, even at very high frequencies. The method, which in its simplest form consists of the reception of radio signals from distant transmitters after reflection or scattering in the ionosphere, has been used by DYCE (1955) and others. It was pointed out earlier (LOVELL *et al.*, 1957), that the method was capable of producing quantitative local, as well as synoptic, information. The method has also been used to investigate the reflection mechanism during specific auroral displays for which the close association of the optical and radio phenomena was not in doubt (FORSYTH and VOGAN, 1957). However, the present investigation seems to be the first in which the bistatic method has been used as the principal tool in a comprehensive study of auroral ionization. The similarity of the experimental arrangement used for these studies and that used for some meteor studies has led to the term "forward scatter" to describe the auroral reflection process, and also to indicate the method of measurement. In fact, the present study suggests that scattering from radio-aurora occurs under a wide variety of geometrical conditions and for that reason the present authors prefer the name "bistatic" for the method since this refers only to the disposition of the equipment at two stations.

During the past three years, twenty experimental "circuits" have been established in eastern and central Canada. Each circuit consists of transmitting and receiving equipment operating on a single frequency and separated by a distance of several hundred kilometres. Sometimes, a single transmitter is used at a central point to serve several circuits, which operate over different paths radiating from that point. Also, two or more circuits, each of which operate at a different frequency, often are used over the same path. For example, four transmitters located at Royal Canadian Air Force Station Greenwood, in Nova Scotia, were used in conjunction with four receivers located at Ottawa in order to provide four circuits over the single (Greenwood–Ottawa) path. Some of the earlier circuits, such as those on the Greenwood–Ottawa path were installed initially for meteor studies (see, for example, VOGAN and CAMPBELL, 1957), but recently they have been used exclusively for auroral studies. As part of the Canadian programme for the International Geophysical Year ten new circuits for auroral investigations were installed during 1956 and 1957 in the west-central part of Canada. One purpose of these circuits is to provide statistical information about the occurrence of radio-aurora. In order to investigate more fully the reflection mechanism, the primary consideration in their location was a wide variation in the geometrical relationships between the path directions and the direction of the earth's magnetic field.

The principal objective of the present paper is the consideration of the physical nature of radio-aurora and of the various reflection mechanisms (since it will be evident that more than one mechanism operates). Statistical evidence on the occurrence of radio-aurora is introduced as part of the argument relating to these problems. Most of the experimental evidence was collected from the early experimental circuits which have operated for several years. More recent results from the IGY network are included because of their obvious significance.

VOL
13
1958/5

The present investigation is based principally upon data obtained from the continuous operation of experimental circuits over long periods of time. Also included are data from a number of experiments designed to elucidate specific problems. In this paper the presentation of the experimental results is preceded by a brief description of the equipment, the geographical distribution of the paths and the method of analysis of the records. The results are presented in subsequent sections, most of them in the order in which they were obtained. Some discussion is included with each set of results in order to indicate its significance and also to indicate the need for the subsidiary measurements. However, an attempt is made to reserve the principal arguments concerning the nature of radio-aurora to a separate section which follows the experimental evidence.

Experimental Arrangements

The receiving equipment was essentially the same at all stations. The amplitude of the received signal was recorded in both linear and logarithmic form. Low-noise receivers with a bandwidth of 1·3 kc/s were used with moving chart recorders having a frequency response of 2 c/s. Further details of these recording techniques have been given by Vogan and Campbell (1957). For several of the shorter experiments, which involved the simultaneous recording of four rapidly fading signals, a magnetic tape recorder was used. With this recorder it was possible to play back the redorded signal at one-tenth of the recording speed. These signals were then re-recorded on a moving chart instrument with a frequency response of 45 c/s. Most of the recordings were made on single-chart recorders with curvilinear co-ordinates. Simultaneous recordings intended for detailed comparison were made on multi-channel recorders with rectilinear co-ordinates.

All transmissions were unmodulated and were interrupted for a few minutes at regular intervals for the purpose of identification. Horizontal five-element yagi antennae were used at all the sites, with the exception of Yellowknife. Here, the antenna consisted of a pair of stacked horizontal square loops in order to provide the necessary wide angle of radiation in the horizontal plane. Antenna heights were chosen to provide maximum illumination for a point, at a height of 100 km, above the centre of the path. The somewhat different conditions which existed on the Churchill–Ottawa path are discussed separately in a later section.

The most important characteristics of the experimental circuits are given in Table 1, and their geographical distribution is shown in Fig. 1. It can be seen from the disposition of the mid-path reflecting regions that this network permits the observation of radio-aurora over an extensive area. While some of the circuits have common parameters which permit the direct comparison of data, the paths all differ in their geometrical relationship with the earth's magnetic field. The Greenwood–Ottawa and Suffield–Winnipeg paths are almost due east–west and the geomagnetic latitudes of their mid-points differ by only 2°. The eastern circuit is, however, approximately 1500 km from the zone of maximum auroral occurrence while the western circuit is 500 km nearer this region. The paths have a longitudinal separation of about 35°. This physical and temporal separation means that the paths have different propagational characteristics. Widespread ionospheric events should appear on both paths but local disturbances should affect

Table 1. VHF circuits used for studies of radio-aurora

Transmitter location	Receiver location	Path length (km)	Freq. (Mc/s)	Transmitter power (W)
Greenwood	Ottawa	860	32·22	100
			39·22	100
			48·82	100
			49·98	100
Churchill	Ottawa	1910	39·23	100
			48·83	100
Churchill	Winnipeg	1000	39·23	100
			48·83	100
Suffield	Winnipeg	1000	39·21	100
			48·81	100
Yellowknife	Baker Lake	900	38·07	700
			49·99	700
Yellowknife	Churchill	1120	38·07	700
			49·99	700
Yellowknife	The Pas	1180	38·07	700
			49·99	700
Yellowknife	Saskatoon	1200	38·07	700
			49·99	700
Yellowknife	Sulphur Mountain	1200	38·07	700
			49·99	700

VOL 13 1958/

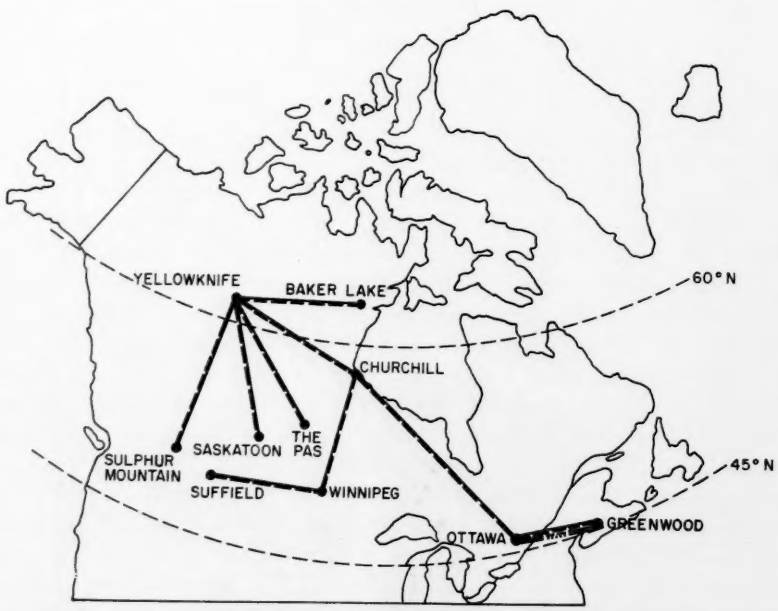

Fig. 1. Map showing VHF circuits used for the study of radio-aurora. The use of more than one circuit over each path is indicated by the addition of broken lines.

one circuit but not the other. The geometrical relationship with the magnetic field is similar for both paths and might be described as asymmetric. Propagational conditions may be quite different on the north and south sides of each of these paths. The Churchill–Winnipeg path for which the mid-point is approximately 500 km. from the zone of maximum auroral occurrence, lies almost at right angles to the Suffield–Winnipeg path. The geometry of this path possesses a degree of symmetry not found on any of the other paths, since the transmitter-receiver line lies close to the direction of the horizontal component of the magnetic field and crosses the isoclinic lines almost at right angles. The Churchill–Ottawa path has a mid-region at approximately the same geomagnetic latitude of 55° as the Churchill–Winnipeg path but lies 13° to the east. The most important parameter here is the path length of 1910 km. For reflections at a height of 100 km, radiation angles at the transmitting antennas will be about $1\frac{1}{2}°$ in the vertical plane; this is to be compared with angles of 9° and 10° at the other stations.

The mid-regions of the ten circuits in western Canada that have their transmitters at Yellowknife are disposed on an arc of approximately 1000 km in length, across the auroral zone. Since both Yellowknife and Churchill are situated close to the region of maximum auroral occurrence, the orientations of the paths permit observations in regions located to the south, to the north and within the zone of maximum activity. These path orientations also provide a set of geometrical relationships between the signal path and the direction of the earth's magnetic field which are related to each other, and are different to those mentioned in the preceding paragraph.

VOL. 13 58/59

Analysis of the Recordings

The recordings produced by the equipment described in the preceding section show many instances of disturbed propagational conditions. In most cases the disturbance is evidenced by an increase in the amplitude of the received signal. Attempts have been made previously to classify these various occurrences according to the appearance of the records. The signals received at the Radio Physics Laboratory in Ottawa from a transmitter located at Cedar Rapids, Iowa, were analysed in 1953 by Vogan (unpublished). Later, a similar investigation of the Cedar Rapids signals as received at Ithaca, New York, was carried out by Dyce (1955). The classification schemes used in these earlier attempts differed from the present one in several particulars. In addition, the use of only a single path severely handicapped each of the earlier studies.

In evolving a classification scheme for the disturbed periods, the objective is to choose each class of event in such a way that it is related to a specific propagational condition which, in turn, can be related to a specific physical state of the upper atmosphere. To this end, the present classification scheme depends not only upon the appearance of the records but also upon information about related phenomena. The most valuable subsidiary information appears to be that concerning disturbances of the magnetic field.

Naturally, the records show many events that are not related directly to the subject of this paper. The recordings, in the absence of any unusual propagational condition, show only the sharp spikes produced by the signals reflected from

individual meteor trails. The appearance of the record under such conditions is similar to the right hand (earlier) and left hand (later) portions of the record reproduced in Fig. 2. In that figure, the gaps in the trace are due to the automatic silencing arrangement which shuts the transmitter off for short periods at regular intervals. During a large meteor shower the appearance of the record changes noticeably, but the positive identification of the event as a meteor shower is not difficult (see, for example, FORSYTH and VOGAN, 1955). Occasionally the signal level is increased by interfering signals, which originate in the sun or as spurious emissions from communication systems. Since these unwanted signals continue through the silent periods of the wanted transmitter, the events are easily identified on the records. The occurrence of absorption has been described previously (FORSYTH and VOGAN, 1957) and is evidenced by a decrease in amplitude of the meteor signals and of the cosmic noise background signal that is recorded during the periods of transmitter silence.

The present study is concerned principally with three types of events which give rise to enhanced signal levels. While the classification is necessarily somewhat subjective, the descriptions that follow, together with the illustrations, will serve to indicate the general characteristics of each group. On rare occasions it is difficult to assign an individual event to a given class but this difficulty does not seem to have been a significant source of error in the present investigation:

Type-E. This event shows on the record as a sudden strong enhancement of the signal for a period that is usually about an hour but sometimes extends to as much as 3 hr. Figure 2 shows a typical example of a type-*E* enhancement that extends over a period of somewhat less than 2 hr near midnight (UT). The enormous increase in signal strength usually overloads the recording meter to an extent that precludes the observation of fading in the signal. When the signal level is less than that required for full-scale deflection of the meter it exhibits very slow deep fading. Events of this class are quite rare and, with the exception of a few high-latitude occurrences which have coincided in time with weak magnetic disturbances, they can not be associated with magnetic events. It seems reasonable to associate type-*E* events with the passage, near or across the path, of highly reflecting clouds of ionization in the *E*-region. Such clouds are known to exist and are at least one of the phenomena that are designated collectively in the ionospheric literature as sporadic-*E*.

Type-S. Another class of event is illustrated in Fig. 3. The mean signal level rises slowly and smoothly and the enhancement lasts for several hours. The meteor signals are still visible on the record but the broad area that is filled in on the record between 1500 and 2100 UT indicates that the signal was subject to much fading at a rate that was not too rapid for the recording pen to follow. Type-*S* events are not associated with magnetic disturbances.

Type-A. The principal subject of the present study is the class of signal enhancement which appears to be related to auroral ionization. In fact, there appear to be at least three kinds of type-*A* enhancement that produce quite different patterns on the record but are, nevertheless, closely associated with magnetic disturbances. These have been assigned the designations A_1, A_2 and A_3.

VOL
13
1958/5

J. ATMOS. TERR. PHYS. 1959. Vol. 13, pp. 320–8/59

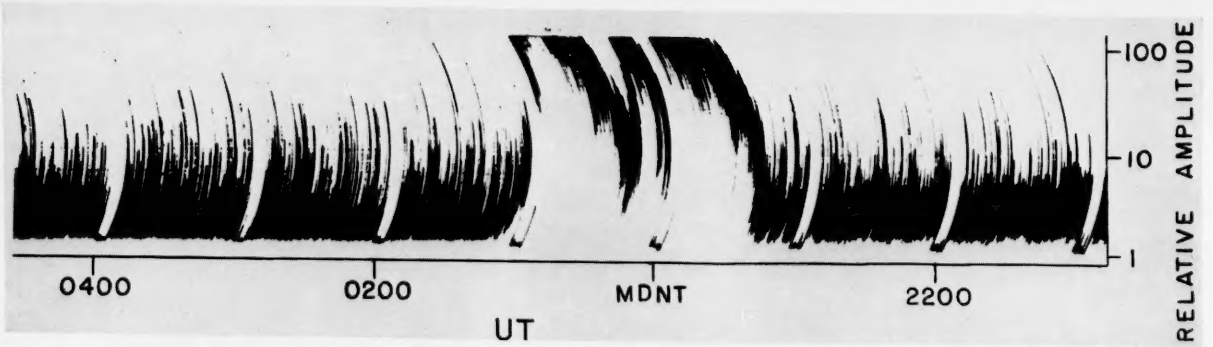

Fig. 2. Sample record obtained on the Greenwood–Ottawa path at a frequency of 39·22 Mc/s on 30 October 1957. The record shows a type-*E* event occurring near midnight UT. The remainder of the record shows the normal meteor signals received when propagational conditions are undisturbed.

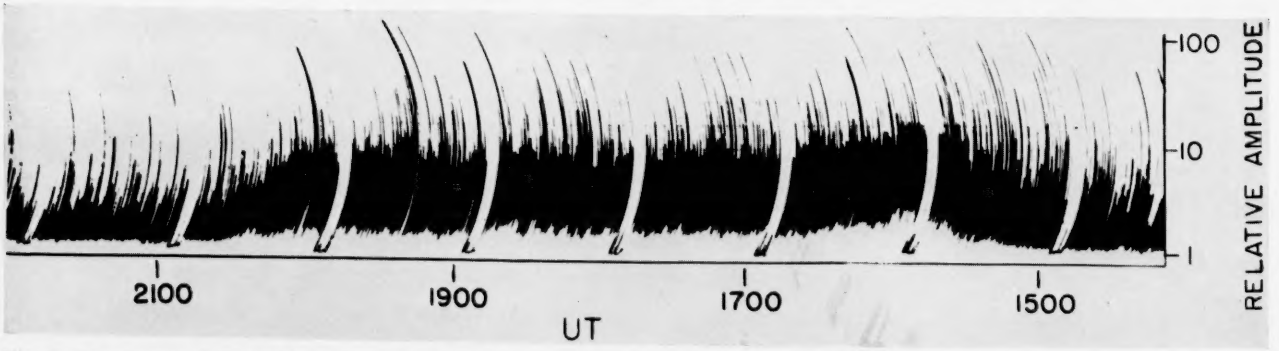

Fig. 3. Sample record obtained on the Greenwood–Ottawa path at a frequency of 39·22 Mc/s on 14 April 1957, showing a type-*S* event.

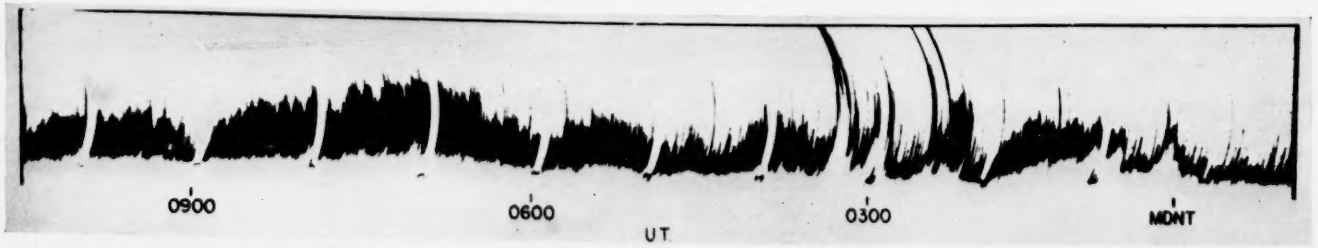

Fig. 4. Sample record obtained on the Greenwood–Ottawa path at a frequency of 39·22 Mc/s on 12 March 1958. The record shows an A_1-event which occurred just after midnight, an A_2-event which occurred between 0200 and 0400 and an A_3-event between 0500 and 1000.

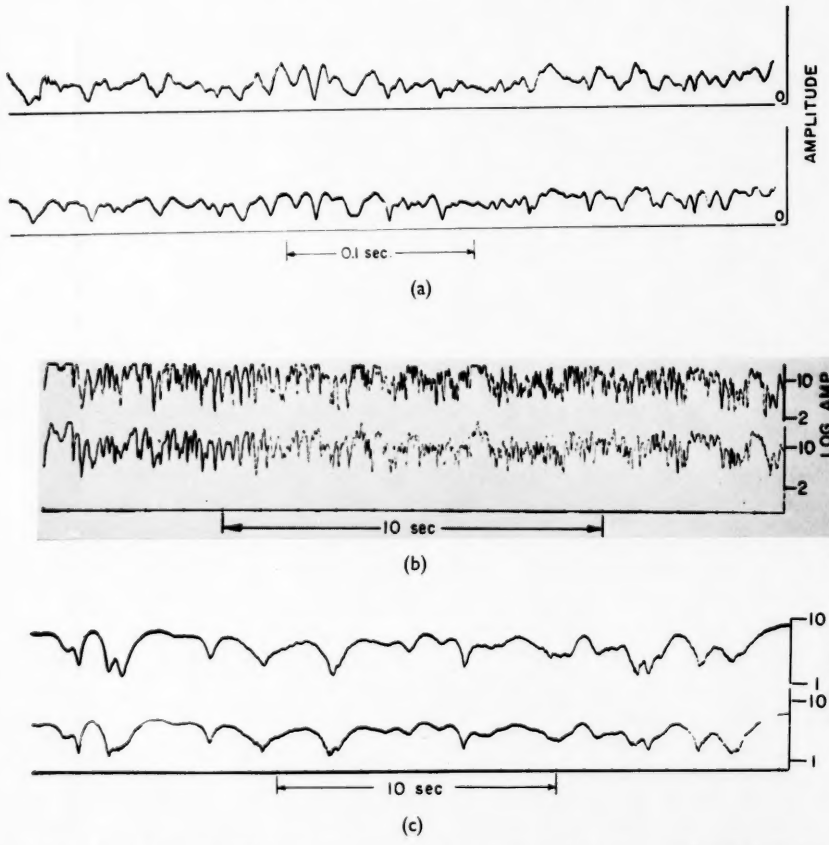

Fig. 10. Sample records obtained with spaced antennae: (a) A_1-event on Greenwood–Ottawa path with antenna spacing of two wavelengths. (b) A_2-event on Churchill–Ottawa path with antenna spacing of three wavelengths showing moderate rate of fading. (c) A_2-event on Churchill–Ottawa path with antenna spacing of three wavelengths showing slow rate of fading.

VOL.
13
1958/5

On a few occasions a positive association has been established between the occurrence of visible aurora and enhancements of the recorded signal level. In all such cases the recorded event was of the A-type. There is some indication that the two sub-classes A_1 and A_2 are associated with separate stages in the development of the visible display. The start of a type-A event is usually clearly defined and is sometimes associated with a short period of absorption. A typical occurrence is shown on the record reproduced in Fig. 4.

The A_1-signal is often quite large and its most distinctive characteristic is a high rate of fading. Since this fading is too rapid to permit the recording meter to follow the signal fluctuations, the result is a characteristic "thin trace" on the record, which shows neither deep fading nor large meteor spikes. An example of this type of signal enhancement occurred between midnight and 0100 UT in the period covered by the record of Fig. 4.

The A_2-signal is large and subject to deep irregular fading at a much slower rate than that of A_1. As a result, the fading is recorded as an irregular band on the record. The record of Fig. 4 contains an example of an A_2-event occurring between 0200 and 0400 UT.

The A_3-event is similar in appearance to the S-event and may also last for several hours. In Fig. 4 the record for the period from 0500 to 1000 UT is typical of that which is classified A_3. The principal point of distinction between the A_3- and S-events is the association of the A_3-event with a magnetic disturbance. In practice, if a doubtful event is associated with an A_1- or A_2-event then it is classified as A_3. Alternatively, the magnetic K-figure (index of disturbance) for a neighbouring observatory is consulted and if this index is greater than four in the 3 hr period near the beginning of the enhancement, the event is classified as A_3. Although this set of approximate criteria is sometimes difficult to apply unambiguously, there seems to be no need to adopt a more rigorous set. After a magnetic disturbance, the A_3-enhancement may last well into the following day when it becomes increasingly difficult to decide whether the enhancement should be classed as A_3 or whether, in fact, it has given place to an S-enhancement. Quite frequently in a type-A enhancement only the A_3-event appears. When two or more of the different events appear it is usually, but not always, in the order; A_1, A_2, A_3.

The analysis consisted, in the first instance, of an examination of records for the Greenwood–Ottawa path and the tabulation of the hours during which each of the disturbance events occurred. As soon as it seemed evident that the classification system possessed some physical significance, the analysis was extended to the two orthogonal paths, Suffield–Winnipeg and Churchill–Winnipeg, and later, for the purpose of elucidating particular questions, to other paths.

The Statistical Results

Most of the statistical results were obtained for operating frequencies close to 40 Mc/s. The relative occurrences of the different types of disturbance events for three paths are shown as percentages of the total operating period in Table 2. Two groups of results for the Greenwood–Ottawa path are shown in the table. In addition to the results of a 2 year period for this path, the results of a 1 year period are given in order to permit direct comparison with data for the other two paths.

Table 2. Relative occurrence of various events

Circuit	Mid-point geomagnetic latitude	Operating period	Hours of recording	% time of occurrence		
				E	*S*	*A*
Greenwood–Ottawa	56·7°	Oct. 1955 Oct. 1957	17001	0·25	5·6	3·7
Greenwood–Ottawa	56·7°	July 1956 June 1957	8564	0·2	5·3	3·2
Suffield–Winnipeg	58·9°	July 1956 June 1957	7968	0·2	3·6	5·9
Churchill–Winnipeg	64·0°	July 1956 June 1957	8232	1·2	12·4	8·9

The paths are listed in Table 2 in order of increasing geomagnetic latitude of the mid-points. It will be noted that for type-*A* events the occurrence increases with increasing latitude. For type-*S* events the occurrence is much greater for the Churchill–Winnipeg path than it is for the two low-latitude paths. The percentage occurrence of type-*S* events for the Churchill–Winnipeg path is significantly greater even than the occurrence of type-*A* on the same path. The percentage occurrence of type-*E* events is not large for any path, but it too is greatest for the Churchill–Winnipeg path. While there is no doubt concerning the reality of the large percentage occurrence figures for types-*A* and *S* on this path, that for type-*E* is suspect. A particularly intense type-*A* event might easily be classified as type-*E* and there is a greater likelihood of this occurring for the Churchill–Winnipeg path. In fact, the type-*E* events observed on the lower latitude paths show no significant correlation with magnetic disturbances whereas for the higher latitude there seems to be a slight tendency for these events to occur more frequently during magnetic disturbances. It may be assumed therefore that the events classified as type-*E* for the Churchill–Winnipeg path included some events which more properly could have been classified as type-*A*.

Although the occurrence or non-occurrence of a contemporaneous magnetic disturbance was sometimes used as the criterion for distinguishing between *S*- and A_3-events, no similar criterion was needed in the case of A_1- or A_2-events. It is of interest therefore to indicate the degree of correlation between magnetic events and all type-*A* events. In Fig. 5(a) the monthly occurrence (expressed as a percentage of the recording period) of *A*-events for the Greenwood–Ottawa path is plotted as a histogram for the 2 year period. For comparison the monthly mean values of A_p are plotted as the broken line. The daily planetary magnetic figure, A_p, is based on a linear scale of disturbance whereas *K*, a 3-hour index, is based on a quasi-logarithmic scale of disturbance. The close association between the periods of frequent occurrence of type-*A* disturbances and periods of frequent occurrence of magnetic disturbances is evident from the figure. The monthly occurrence of *S*-events for the same period is plotted in the histogram of Fig. 5(b) together with the same curve of monthly mean A_p values. In this case little or no correlation is

apparent. The correlation coefficient between the two sets of data of Fig. 5(a) is $+0{\cdot}8$ whereas that for Fig. 5(b) is $-0{\cdot}2$. There can be no doubt about the significance of the former figure in spite of the small number of data involved but the latter figure is of doubtful significance.

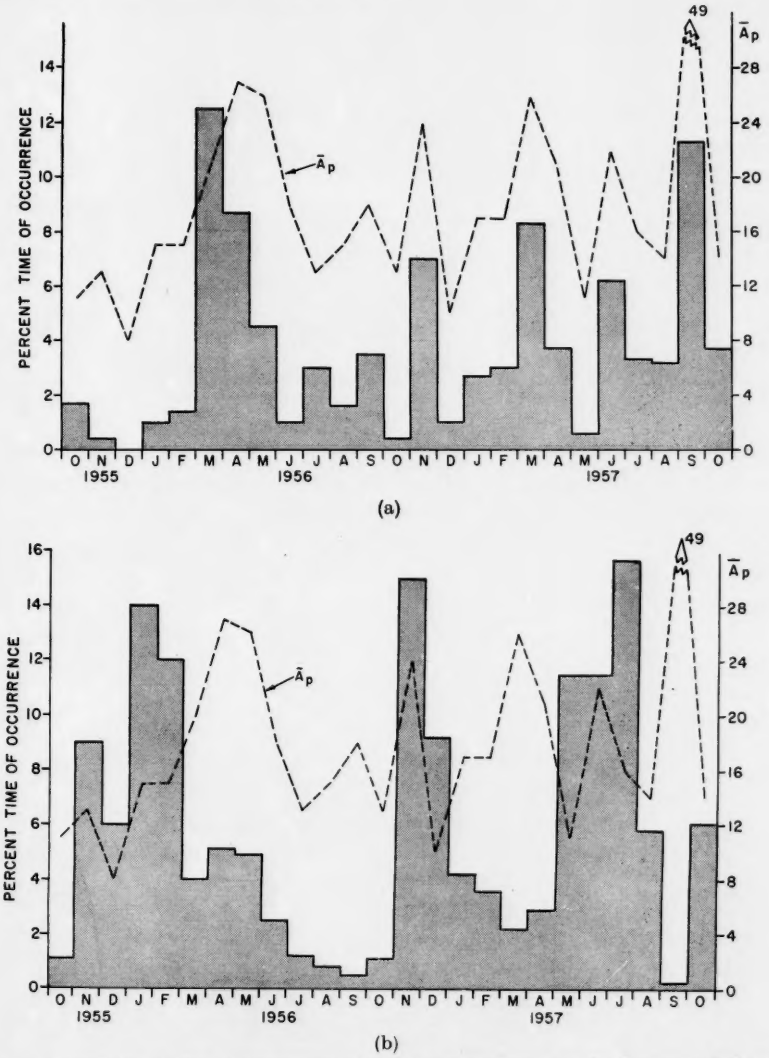

Fig. 5. Percentage of time of occurrence of signal enhancements on the Greenwood–Ottawa circuit shown by months as histograms. The broken lines show the corresponding monthly mean values of the planetary magnetic index A_p; (a) type-A events (b) type-S events.

Further evidence of the physical significance of the classification scheme is found in the diurnal variation of occurrence of A- and S-events. In Figs. 6(a), 6(b) and 6(c) the diurnal variations of percentage occurrence of S-events, are plotted

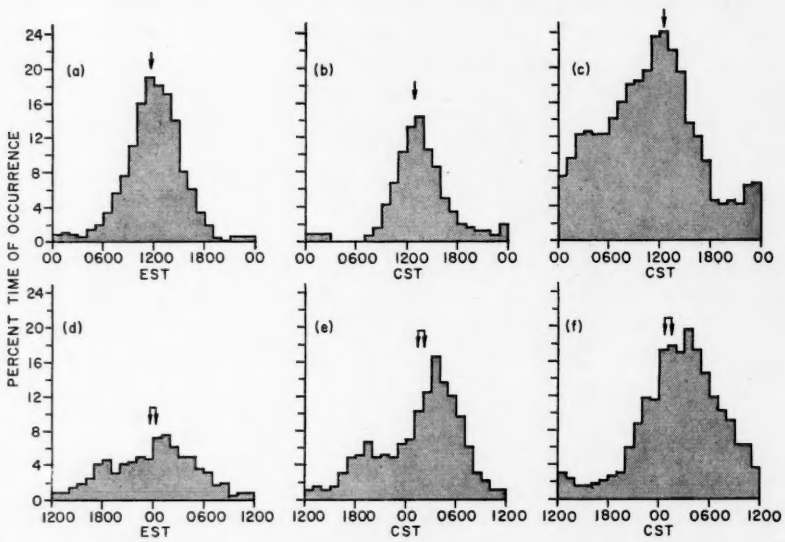

Fig. 6. The diurnal variation of occurrence of signal enhancements July 1956 to June 1957, for type-S events on (a) Greenwood–Ottawa, (b) Suffield–Winnipeg, (c) Churchill–Winnipeg, circuits and for type-A events (d) Greenwood–Ottawa, (e) Suffield–Winnipeg, (f) Churchill–Winnipeg, circuits. In (a) (b) and (c) the arrows indicate local noon at the path mid-points. In (d), (e), (f), the arrows indicate the range of time of occurrence of magnetic midnight.

VOL
13
1958/

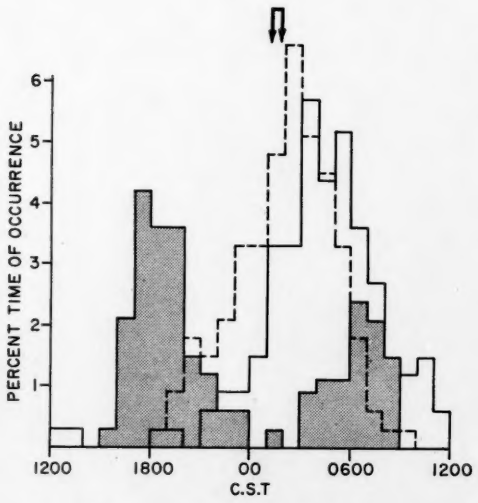

Fig. 7. The data of Fig. 6(e) replotted to show the relative contributions of A_1-events (shaded histogram), A_2-events (dashed-line histogram) and A_3-events (solid-line histogram).

respectively for the Greenwood–Ottawa, Suffield–Winnipeg and Churchill–Winnipeg paths. The vertical arrow on each graph indicates local noon at the mid-point of the path. The corresponding histograms for the A-events are shown in Figs. 6(d), 6(e) and 6(f). On these diagrams the arrows designate magnetic midnight at the mid-point of the path. The times of occurrence of magnetic midnight were calculated by a method similar to that indicated by CHAPMAN and BARTELS (1940). These times vary during the year over the range indicated. From Fig. 6 it is immediately evident that S-events are essentially a daytime effect whereas A-events occur mainly at night. There is a strong tendency for the occurrence of S-events to be disposed symmetrically about the time of local noon for the mid-point of the path, even for paths with quite different directions. As in the case of E-events, the high incidence of periods of enhanced signal on the Churchill–Winnipeg circuit may have led to some mutual contamination between A_3- and S-events. This effect may have altered the shape of the curves of Figs. 6(c) and 6(f) for the mid-morning hours but it is not likely that the other portions of the curves were affected. The diurnal variation histograms for the A-events (Figs. 6(d), 6(e) and 6(f)) show strong night-time maxima. For each path, the highest peak occurs just after local magnetic midnight although there is an indication of a secondary maximum which occurs before magnetic midnight. This secondary maximum is much less pronounced in Fig. 6(f).

In Fig. 7 the data of Fig. 6(e) are replotted to show the contributions of each of the three types of A-events to the total diurnal variation. It is seen that the evening maximum is due almost entirely to A_1-events, and that there is another group of A_1-events in the morning hours. The diurnal variation of A_1-events is strikingly similar to that found for "sputter" by BAILEY *et al.* (1955). The peak in occurrence after midnight is due to both A_2- and A_3-events which are concentrated in this period. The relative occurrence of A_1-, A_2- and A_3-events is not the same for the different paths. The A_1-events occur most frequently on the Greenwood–Ottawa and Suffield–Winnipeg paths. For the Churchill–Winnipeg path the occurrence of A_1-events is very rare and for the few examples which have been observed the classification is doubtful. It is probable that no true A_1-events have been recorded on this path. On the other hand, A_1-events are observed on the various circuits radiating from Yellowknife but much less frequently than on the two southernmost circuits. It is interesting to compare the data of Fig. 7 with the results given by BULLOUGH and KAISER (1955) who used radar equipment located near Manchester and found that diffuse echoes occurred during the earlier part of the night and discrete echoes during the later part. The diurnal variation shown in Fig. 7 for the A_3-events is in marked contrast to that shown in Fig. 6(b) for the S-events. This dissimilarity constitutes further justification for the retention of the separate classifications of A_3 and S.

The diurnal variations of Figs. 6(a), 6(b) and 6(c), suggest that the agency responsible for the S-events is itself subject to solar control. A group of data from the Greenwood–Ottawa path was used to test this suggestion. The logarithm of percentage occurrence of S-events for each hour of the day averaged over the month of July 1957, was plotted against the logarithm of the cosine of the solar zenith angle for that hour. The result is shown in Fig. 8 where it will be seen that a very

strong dependence upon solar zenith angle is indicated. The horizontal bar associated with each of the points is a measure of uncertainty and represents the square root of the number of events occurring in each hourly interval. Except at the lower values of percentage occurrence, the agreement between morning and afternoon values is excellent and leaves no doubt that the S-events are subject to solar control.

From the statistical evidence some suggestions can be made concerning the mechanisms by which the various events are generated. The S- and A_3-events seem to be similar in nature. The fact that one can progress into the other (A_3 into S) suggests that the same regions may be involved. The very strong solar control of

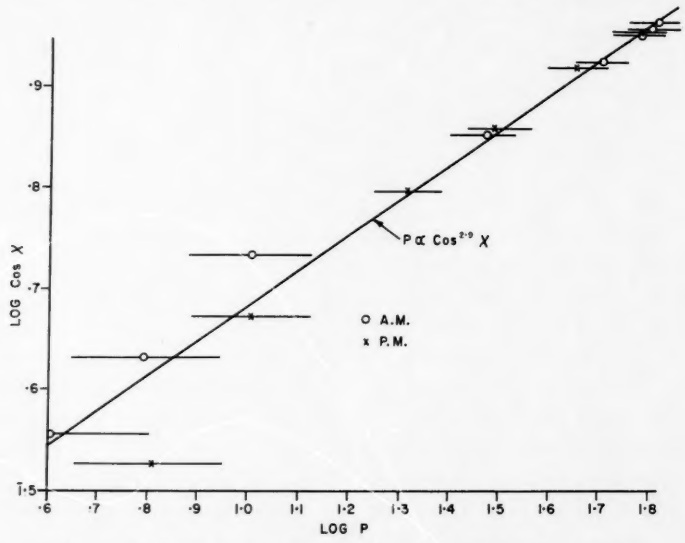

Fig. 8. The solar dependence of type-S events for July 1957 on the Greenwood–Ottawa circuit.

the S-events, together with the fact that there is no appreciable asymmetry in time about local noon at the path mid-point, suggests that the S-events, and probably the A_3-events as well, are caused by an increase in ionization near the mid-point of the path at E-region heights or below. The nature of the signal fluctuations for these events suggests that the electromagnetic energy is scattered simultaneously from a large number of inhomogeneities in the ionization. Both the S-events and the A_3-events are very stable, lasting for hours at a time. Since the A_3-events characteristically last much longer than do visible auroral displays it must be assumed that they result from a part of the auroral process that does not produce luminosity. Further, if it is confirmed that the region responsible for the A_3-events is at E-region heights or below, then the production of ionization must be continuous throughout the whole of each such event, because otherwise the ionization would disappear rapidly by recombination and attachment.

The A_1- and A_2-events differ markedly in the nature of the signal fluctuations but from the evidence so far presented it is difficult to suggest separate mechanisms.

It seems significant that they occur characteristically at different times, but perhaps the more significant observation is that A_1-events occur frequently on low-latitude paths but less frequently on those at higher latitudes. This circumstance suggests that the A_1-events are more sensitive than the A_2-events to the geometrical relationship between the path direction and the direction of the earth's magnetic field. This characteristic, often called "aspect sensitivity", will be examined more thoroughly later.

The statistical evidence is not definitive. The suggestions regarding mechanisms are mentioned at this point in order to assist the reader in evaluating the evidence presented in the following sections.

The Churchill–Ottawa Path

The very long experimental path between Churchill and Ottawa has proven to be extremely useful. Although it was operated only for a period of about 8 months, the evidence seems quite clear. The horizon for any radio antenna is not sharp and depends in part upon the height of the antenna and in part upon refraction in the atmosphere. The length of the Churchill–Ottawa path (1910 km) is such that only a small area of the E-region is illuminated by both antennae. Events that occur at heights appreciably below 100 km will not be observed, even if they occur over the mid-point. Because of the length of the path the common volume that is observable from both termini is limited also in the lateral direction.

Because of the limitation of the common volume both with regard to height and lateral extent, meteor signals are rarely seen on the Churchill–Ottawa path. In fact, of the various types of signal enhancement described previously, only the A_2-events occur with any frequency. No clear examples of A_1-, A_3- or S-events have been observed. When A_2-events are observed they seem to start very suddenly and the signal level is much more irregular than for the shorter paths (see Fig. 12). This characteristic is consistent with the known behaviour of visible aurora. Since the visible phenomenon is highly variable and patchy it might be expected to give rise to irregular signals when the area of observation is limited to a few hundred square kilometres. On the other paths, where the area of observation is much larger, the irregularities in time would tend to be smoothed out.

The Direction-finding Experiments

In an effort to determine the regions of the sky that are responsible for the various types of signal, several simple direction-finding experiments were performed. At Ottawa, in addition to the regular recording equipment, a separate receiver and recording apparatus was used in conjunction with a rotating antenna. The antenna consisted of a simple horizontal dipole, well removed from obstructions, that was rotated in the horizontal plane by a small motor at the rate of 1 rev/5 min. While the radiation pattern of a dipole is very broad, the sharp null of sensitivity in the direction of the dipole axis can be used for accurate direction finding. Thus, the recorded signal showed sharp minima at the times when the axis of the dipole passed through the direction of arrival of the radio signals. Since the signals were always subject to fading it was necessary to include some integration in the recording system and to compare in detail the direction-finding records with the

regular recordings, in order to identify the significant minima. Taken by themselves, the rotating-dipole results are subject to an ambiguity of 180°. This amgibuity was resolved by intercomparing the records from the rotating dipole with those obtained with several fixed directive antennae that had different sensitivity patterns.

The rotating-dipole equipment was in operation on the Greenwood–Ottawa path during only two type-E events. On one occasion seven good bearings were obtained, all located within a few degrees of the path-direction although one bearing of 5° to the south of the path-direction was obtained. On the other occasion some thirty bearings were obtained. All of these bearings were clustered within 10° of the path-direction while most of them were considerably closer to this direction.

For the type-S events, many good bearings were obtained. Most of the bearings were clustered around the path-direction although the spread was greater than for the E-events, and on rare occasions departures of as much as 30°–40° from the path-direction were observed. There seems to be no doubt that S-events are due to scattering of the radiation from ionic inhomogeneities near the mid-point of the path. The failure to observe S-events on the Churchill–Ottawa path, although they are observed frequently on the Churchill–Winnipeg path, can be due only to the fact that the active region is too low to be observed. While no lower limit can be established by the present measurements it is probable that the height of the active region is in the vicinity of 80 km.

VOL.
13
1958/5

The amplitude characteristics of the A_1-events made it extremely difficult to obtain accurate bearing measurements. On the few occasions when good bearings were obtained they were widely scattered in the region to the north of the path-direction. All the bearings were between 20° and 90° from this direction.

It was possible to observe the direction of arrival of A_2-signals for both the Greenwood and Churchill transmissions. For the shorter path (Greenwood–Ottawa) the bearings were located in the quadrant to the north of the path-direction and spread widely throughout this quadrant. On the longer path (Churchill–Ottawa) the bearings were much more concentrated, due, no doubt, to the very much restricted common volume of antenna illumination. Since this effect is so striking it is illustrated in Fig. 9, where the frequency of occurrence of bearings is shown as a histogram. While all the bearing observations are to the north of the path-direction, most of them are within 15° of this direction and the distribution is sharply peaked for a direction of about 7°.

The directional evidence concerning A_3-events was obtained on the Greenwood–Ottawa path and is very similar to that for the S-events. Practically all of the bearing determinations are clustered about the path-direction. On a few occasions when A_3-signals were replaced for short periods by A_2-signals, the bearings changed in a striking fashion from the path-direction to much more northerly directions. This evidence combined with that obtained on the Churchill–Ottawa path would seem to demonstrate that the active region for the A_3-events is also low in the atmosphere and may, in fact, coincide with that for the S-events. Certainly, the signals exhibit the same characteristics. It seems very probable that the same region and the same kind of ionic inhomogeneities are responsible in each case.

OL.
13
8/59

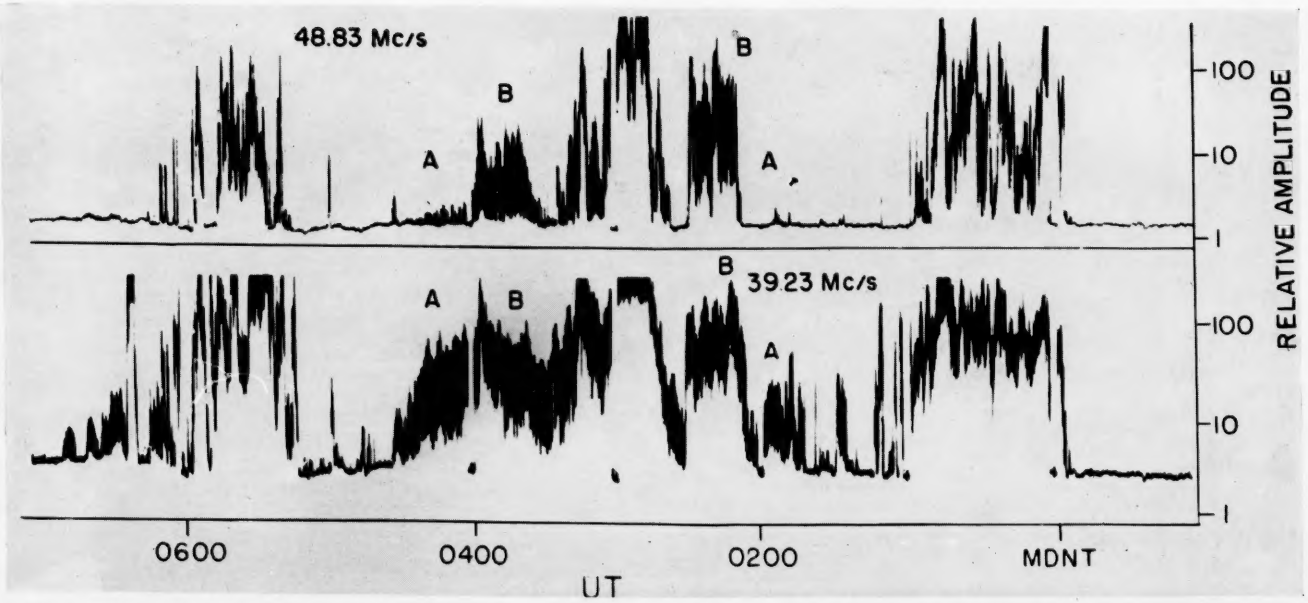

Fig. 12. Recordings obtained simultaneously at two frequencies during an A_2-event on Churchill–Ottawa path, 23 September 1957.

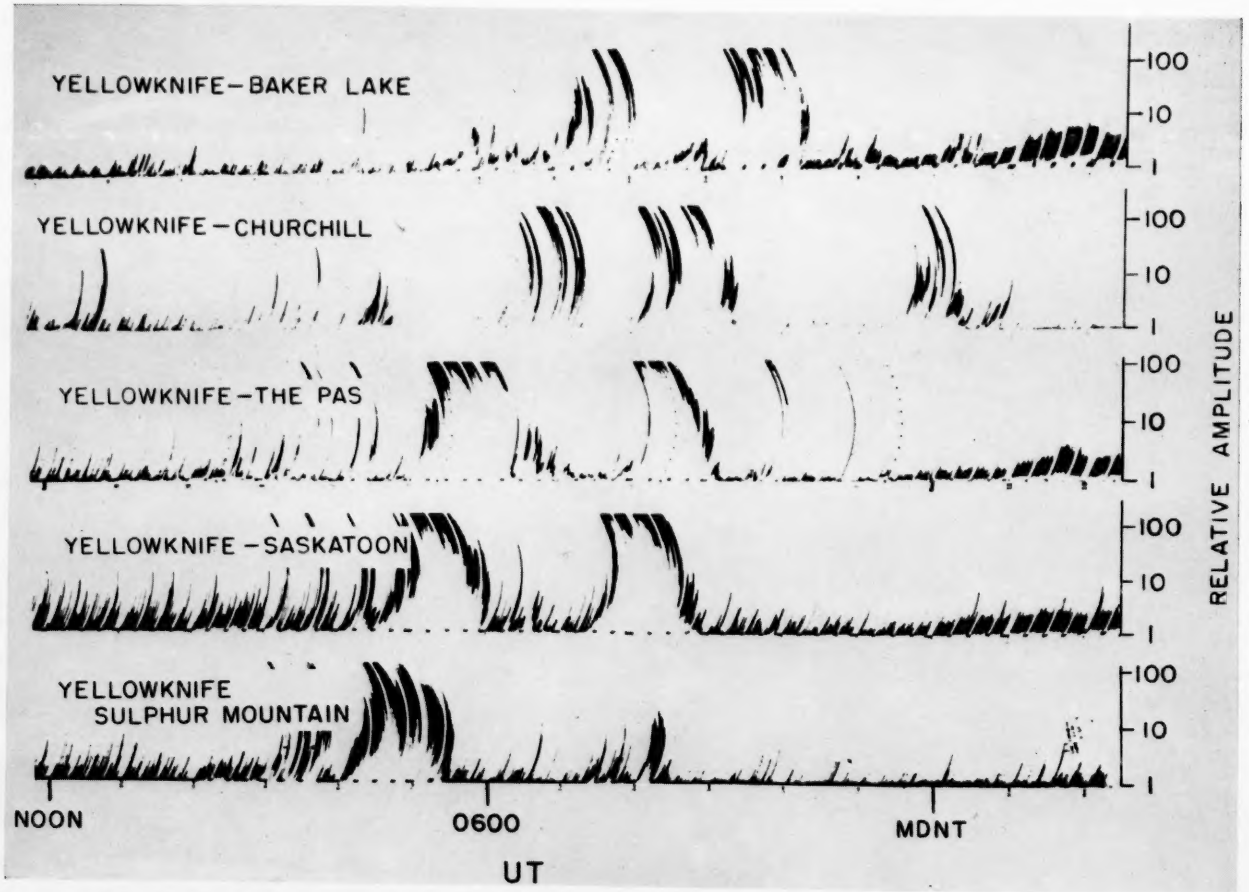

Fig. 14. Simultaneous recordings on five IGY VHF circuits obtained on 5 December 1957, showing the southerly motion of radio-aurora.

VOL. 13
1958/5

In addition to the rotating-dipole measurements, continuous directional measurements of a different kind were made for a period of 1 year on the Churchill–Winnipeg and Suffield–Winnipeg paths. For each path the antenna system consisted of two yagi antennae separated by a distance of two wavelengths along a line that was perpendicular to the path-direction. Since the two antennae were joined electrically they formed an interferometer system that gave rise to a number of lobes in the horizontal sensitivity pattern of the antenna system. By means of an automatic switching device the phase of one of the antennae was reversed with respect to the phase of the other at intervals of 15 min. For the "in-phase" condition the central sensitivity lobe of the antenna system was directed along the

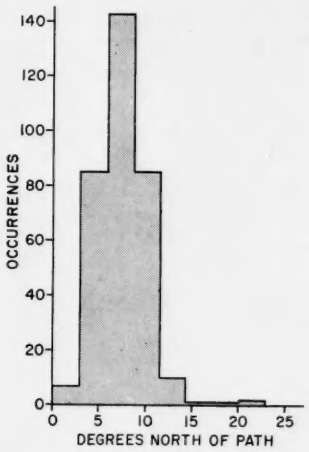

Fig. 9. The distributions of directions of arrival measured to the north of the path-direction as seen from Ottawa for A_2-events observed at a frequency of 39·23 Mc/s on the Churchill–Ottawa path.

path-direction. For the "anti-phase" condition a minimum of the sensitivity pattern was directed along the path-direction and there were two principal lobes directed at 14° on either side of the path-direction. For signals that arrived from a range of directions well off the path-direction either the "in-phase" or "anti-phase" condition might have produced temporarily the greater signal but there would have been no long-term preference for either condition. On the other hand, signals that arrived from the path-direction would have produced the greater signal consistently for the "in-phase" condition. The results obtained on both paths for the 12 month period were in agreement with those obtained for the shorter period with the rotating dipole at Ottawa. For the S- and A_3-events, the "in-phase" signal tended to be as much as from 6 to 10 dB above the "anti-phase" signal. For the A_1- and A_2-events there was no consistent preference for either condition. These results constitute further evidence that the A_1- and A_2-signals tend to arrive from directions well away from the path-direction whereas A_3- and S-signals are scattered from regions near the path mid-point.

The Size of the Auroral Scattering Centres

The fading that is always present in the signals suggests that for each class of event the scattering mechanism must involve simultaneously a large number of ionic inhomogeneities. If this is so, the wave front of the scattered radiation when it arrives at the receiving station should exhibit spatial variations in intensity. The characteristics of this kind of scattering have been studied in detail by Ratcliffe (1956). The scale size of the amplitude variations in the scattered radiation is related to the scale size of the scattering region. In particular, if the scale size in the scattered radiation is found to be significantly larger than the wavelength then it is reasonable to conclude that the scale size of the scattering region is also larger than the wavelength. The scale size of the amplitude variations in the scattered radiation is defined as the scale of the auto-correlation function taken over a significant area of the wave front. This scale size may be estimated approximately by determining the correlation coefficient of the time variations of signal amplitude observed at two antennae separated by various distances. The scale size of the scattering region is also defined in terms of the appropriate auto-correlation function. The scale size determined by radio measurements is the weighted mean size of the inhomogeneities that give rise to the scattered signal. For example, the presence of a number of ionic inhomogeneities that are much smaller than the wavelength would not be revealed if these inhomogeneities do not contribute independently to the scattered signal.

Attempts were made to estimate the size of the irregularities responsible for the scattering of signals associated with radio-aurora. For the Greenwood–Ottawa path four antennae were placed at intervals of one wavelength along a line that was perpendicular to the path-direction. Since these observations were very subject to interference from noise and from meteor signals, they could be made usefully only when the signal level was high. For the Churchill–Ottawa path only two antennae were used. As well as being displaced laterally with respect to the path-direction these two antennae were separated vertically by about one wavelength and the actual distance between the antennae was about three wavelengths. Good observations were obtained during A_1- and A_2-events for the Greenwood–Ottawa path and during a variety of A_2-events for the Churchill–Ottawa path. In all of these observations a high degree of correlation was observed between the fading of the signals received on the spaced antennae. This evidence is not conclusive in the case of the A_1-events because there is no directional evidence for these particular signals. It is possible that the signals were arriving from directions well to the north of the path-direction and that in consequence the direction of arrival made a small angle with the line along which the antennae were disposed. The direction-finding evidence indicates that such directions of arrival do occur occasionally. Since several events are involved which extended over significant periods of time it is not probable that this unfavourable direction of arrival was experienced for all the observations. No similar objection can be raised with regard to the A_2-observations since some of these were carried out on the Churchill–Ottawa path.

Typical records which illustrate the degree of correlation that was observed with the spaced antennas are shown in Fig. 10 for three widely differing fading speeds. Figure 10(a) shows a section of the record obtained during an A_1 event

VOL
13
1958/5

with antenna separation of two wavelengths and illustrates the very rapid fading which is characteristic of the A_1-signals. The records shown in Figs. 10(b) and 10(c) were obtained on the Churchill–Ottawa path (antenna spacing three wavelengths) and illustrate, respectively, medium and slow fading rates. It can be seen that there is a significant degree of correlation for each record pair.

For the A_2-events, and most probably for the A_1-events as well, it seems reasonable to conclude that the horizontal dimensions of the scattering centres are fairly large—at least as large as the wavelength that was used (7·5 m). It was concluded by BOOKER (1956) that the back-scattered radio signals observed from radio-aurora were due to ionic inhomogeneities having horizontal dimensions of the order of 20 cm. The present observations, while obviously not entirely comparable to those discussed by BOOKER, do not support his conclusion.*

ASPECT SENSITIVITY

It was first postulated by HERLOFSON (1947) that radar reflections from aurora could be observed only when the condition for specular reflection was fulfilled (i.e. when the radar waves were incident normally on the auroral structures). Since the visible auroral structures are known to lie along the lines of force of the earth's magnetic field it can be shown that the rigorous operation of this condition would severely restrict the areas of the world from which radar observations of radio-aurora could be made. In particular, radar observations could not be made in the vicinity of the auroral zone. Since that time, evidence has been accumulated by many observers to show that reflections from radio-aurora can be observed in the neighbourhood of, and even to the north of, the auroral zone where the specular reflection condition can not be closely approximated. On the other hand, the evidence does indicate that echoes are seen more often when the specular condition is approached. This characteristic has come to be known as aspect sensitivity but there is no general agreement as to the mechanism by which it arises. It was pointed out recently by FORSYTH and VOGAN (1957) that the observed degree of aspect sensitivity would result if the scattering centres were prolate spheroids with a ratio of length to diameter of three or four and both dimensions were large compared to the wavelength. Apparently, a similar estimate had been made independently by KAISER (1956) and both estimates were in press at the same time.

In the bistatic case the geometry of specular reflection is more complicated but a useful approximation can be arrived at in the following way. If the magnetic field lines are projected into the plane which bisects the transmission path, then the condition for specular reflection is that the projected magnetic lines be tangent to a circle drawn in this plane about the transmitter–receiver axis as centre. Since the lower edge of the visible auroral structures is usually above 100 km in height, it is customary to consider only heights in excess of this value. In order to discuss the degree of aspect sensitivity which obtains in any particular circumstance it is convenient to define an "aspect angle". This angle is measured in the mid-plane

* *Note added in proof*—On the other hand recent measurements of the same kind made during S- and A_3-events indicate that, at least on some occasions, the scattering centres for these events may have quite small dimensions, perhaps less than the wavelength used.

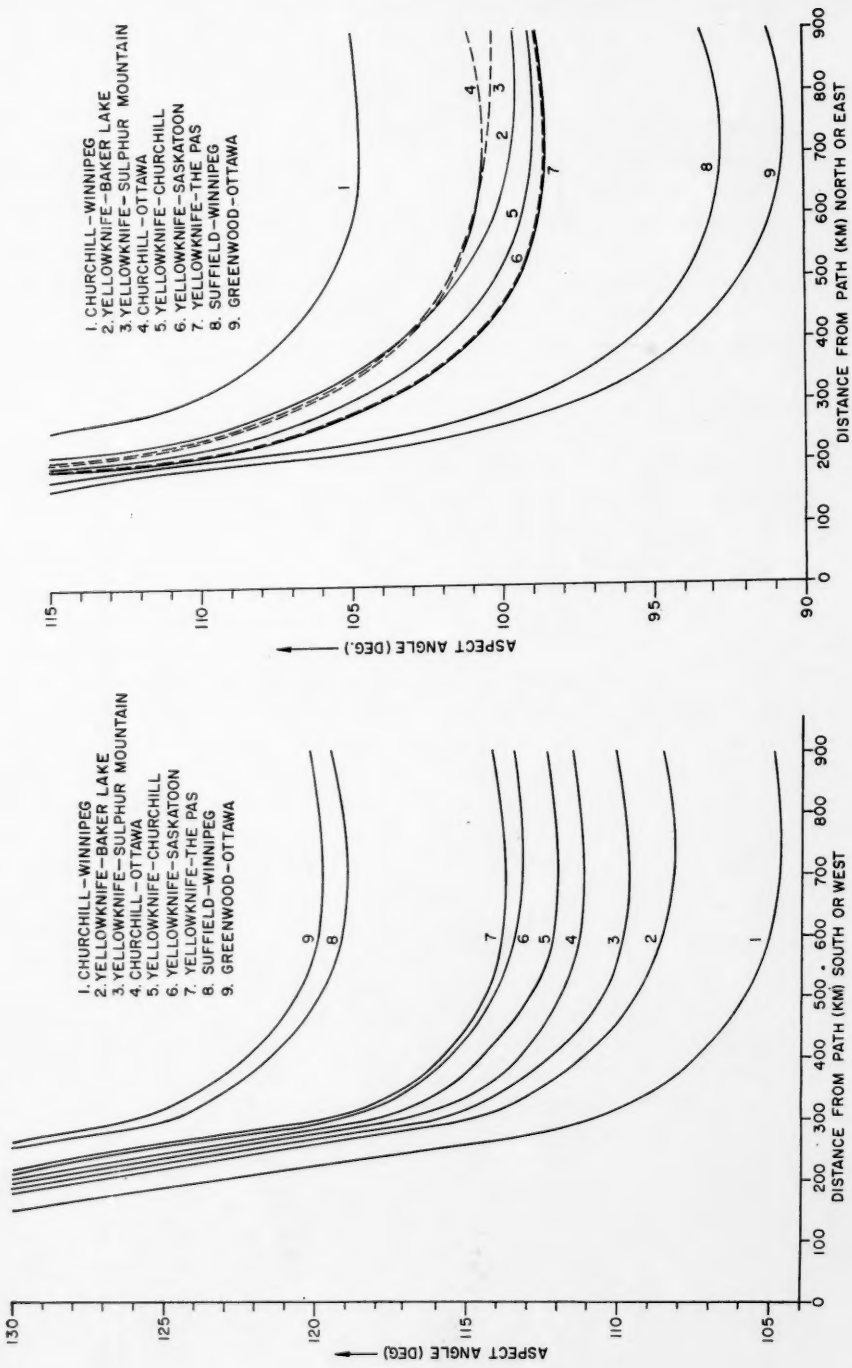

Fig. 11. Aspect angles for the nine paths as a function of distance from the path. For each path the angles for one side are shown in (a) and for the opposite side in (b).

VOL
13
1958/

described previously and is the angle between the line joining the transmitter–receiver axis to the point under investigation and the direction of the earth's magnetic field as projected into the mid-plane. This analysis, while restricted to the mid-plane, gives a very useful picture of the aspect geometry for any path. Aspect angles have been calculated for the 100 km level for each of the paths used for this investigation. These angles are shown in Fig. 11 as a function of the distances, measured along the ground, from the transmission path. The appropriate curve for one side of each path is shown in Fig. 11(a) and for the other side in Fig. 11(b). The condition for specular reflection is that the aspect angle be equal to 90°. It is apparent that this condition is not fulfilled for any of the paths. There is, however, a region on the north side of the Greenwood–Ottawa path where the aspect angle is within 1° of perpendicularity and a similar region near the Suffield–Winnipeg path where the discrepancy is less than 3°. For most of the other paths the most favourable aspect angles approach only to within about 10° of the specularity condition. The most unfavourable conditions are found on the Churchill–Winnipeg path where the aspect angle on both sides of the path approaches only to within about 15° of perpendicularity.

It will be recalled that A_1-events are observed frequently on the Greenwood–Ottawa and Suffield–Winnipeg paths but not on the Churchill–Winnipeg path. Since A_1-events are observed, though infrequently, on more northerly paths (e.g. Yellowknife–Baker Lake) this effect cannot be due simply to the latitude of the Churchill–Winnipeg path. It seems evident that the A_1-events occur most frequently on the paths having the most favourable aspect angles, and therefore that the mechanism which produces these events must be aspect sensitive. The degree of aspect sensitivity is such as to preclude the reception of the scattered signal when the aspect angle is more than 15° from specularity. There were no A_1-events observed on the Churchill–Ottawa path. Although the aspect angles are not particularly favourable for this path, the lack of A_1-events may be due to the fact that the region of most favourable aspect angle is not included in the volume of common antenna illumination.

In contrast to the A_1-events the A_2-events exhibit little aspect sensitivity. Since the A_2-events tend to occur on the side of the path having the most favourable aspect angles, some modest degree of aspect sensitivity may safely be assumed. For the Churchill–Ottawa path a comparison of Fig. 9 and Fig. 11(b) suggests that most of the A_2-signals were scattered from a region where the aspect angle was at least 30° or 40° from specularity.

The A_3-events and S-events show no aspect sensitivity. The direction-finding evidence shows that these signals tend to arrive from the path-direction rather than from regions where the aspect angle is favourable. It might be postulated that the scattering takes place from flat horizontal clouds of ionization, but the usual spread in directions of arrival is too large to support this suggestion. It seems likely that the scattering takes place from nearly isotropic clouds of ionization.

Frequency Dependence Experiments

The frequency dependence of radio reflections from auroral ionization has been investigated for a monostatic system by Forsyth (1953) and for the present

bistatic arrangement by FORSYTH and VOGAN (1957). Both these investigations were limited to occasions when the radio reflections appeared to be closely associated with visible aurora. In each case evidence was found for the existence within small regions of the aurora of electron densities of about 10^7 cm^{-3}. Such electron densities are sufficient to reflect completely radio waves that have frequencies in the lower part of the VHF band. It was pointed out that those experiments, while confirming the operation of this "critical" reflection mechanism, could not exclude the possibility that other mechanisms were operating at the same time.

The study that made use of the Greenwood–Ottawa path (that of FORSYTH and VOGAN, 1957), failed to differentiate between the different kinds of events. It is now clear that the investigation referred mainly to A_2-events although some measurements made during A_1-events were included. In order to investigate the scattering mechanism for the other classes of events a similar study has now been made of the signals received during A_1-, A_3- and S-events. The underlying principle in this study is that for all mechanisms involving only low electron densities the ratio of signal amplitudes observed on two frequencies can be specified within fairly narrow limits. However, if critical reflection is involved this ratio can vary between wide limits. If three frequencies are used the critical reflection process is more completely defined, since a large ratio of amplitudes will be observed for the pair of frequencies that bracket the critical frequency and a smaller ratio for the other pair.

The effect of critical reflection can be seen qualitatively in Fig. 12. The records shown were obtained simultaneously for frequencies of 48·83 Mc/s and 39·23 Mc/s on the Churchill–Ottawa path during an A_2-event. A casual inspection of the figure will reveal several periods (such as those marked A) when the amplitude of the signal received on the lower frequency was many times that received on the higher frequency. Also, there are other periods (such as those marked B) during which the amplitudes received on the two frequencies were nearly equal. This behaviour suggests that during the former (A) periods the electron density within the scattering centres was sufficient to reflect strongly the lower frequency but not to reflect the higher frequency, that is that the electron density was between about 2 and 3×10^7 cm^{-3}. For the latter (B) periods the electron density would appear to have been greater than the critical value for the higher frequency, 3×10^7 cm^{-3}.

Figure 13 shows the results of a more detailed examination of an A_1-event, an A_3-event and an S-event, using three-frequency recordings obtained on the Greenwood–Ottawa path. The recordings were logarithmic in amplitude and were made during 1955. These records were chosen in preference to the later, more accurately calibrated, linear records which were used for the earlier paper, because the logarithmic amplitude scale is more suited to the identification of the different events and provides a more suitable range of amplitudes for the A_3- and S-events. The results are plotted on an XY-diagram of the kind used in the earlier paper (FORSYTH and VOGAN, 1957). In this diagram X and Y represent ratios of signal amplitudes which are defined in the following way: using the subscripts 9, 8 and 6 to refer to quantities associated respectively with frequencies of 32·22, 39·22 and

VOL
13
1958/5

48·82 Mc/s; if A is the received signal amplitude and λ the wavelength, then:

$$A_9' = A_9/\lambda_9$$

and similarly for the other wavelengths (frequencies). It should be noted that these measurements were made with scaled equipments, that is, the transmitter powers

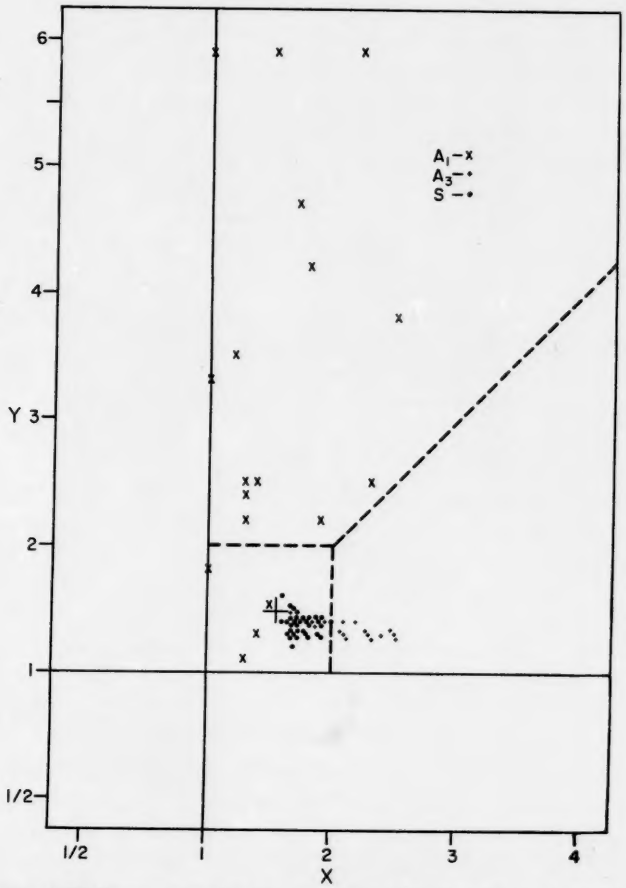

Fig. 13. The XY-diagram showing the experimental points for an A_1-event, an A_3-event and an S-event on the Greenwood–Ottawa path.

were equal and the antenna systems had similar radiation patterns and equal gains. The ratios X and Y are then:

$$X = A_8'/A_6'$$

and

$$Y = A_9'/A_8'$$

In Fig. 13 the points that represent the measurements made during the A_1-event

are widely scattered, suggesting the operation of critical reflection. In fact, for most of the points:

$$Y \gg X$$

a condition that indicates electron densities within the scattering centres ranging between $1{\cdot}3 \times 10^7$ cm^{-3} and $1{\cdot}9 \times 10^7$ cm^{-3}. In contrast, the points that represent the measurements made during the A_3-event are clustered closely together, in spite of the fact that the total variation in amplitude was considerable. The points for the S-event are clustered similarly. The concentration of points in this area of the diagram indicates that critical reflection is not involved and that in both cases the scattering takes place in regions of relatively low electron density. The large cross in Fig. 13 indicates the position on the XY-diagram that corresponds to the case of scattering from isotropic, large, ionic inhomogeneities according to the theory first presented by Booker and Gordon (1950) and extended by Bailey *et al.* (1952). The condition required for the cross to be located at the position shown rather than at the position, $X = Y = 1$, is:

$$4\pi l \sin \theta/2 \gg \lambda$$

where l is the scale size of the ionic inhomogeneity and θ is the angle between the direction of incidence of the electromagnetic radiation and the scattered ray direction. For the present circumstances this condition reduces to:

$$l \gg 2 \text{ m}$$

Unfortunately, the inaccuracies in the absolute calibrations of the particular records that were used for this analysis appear to be large enough to produce a displacement on the XY-diagram (for a particular set of measurements) of about 0·5 in X and somewhat less in Y. As a result, it is not possible to conclude positively that the scattering is of the Booker–Gordon kind but in view of the direction-of-arrival measurements, which suggest isotropic scatterers, this type of scattering seems to be the most probable for both the A_3- and S-events.

Polarization Measurements

Some further evidence concerning the scattering mechanisms was obtained from a polarization experiment. The experiment consisted of receiving the signal on the Churchill–Ottawa path simultaneously on two dipole antennae, one oriented to receive horizontally polarized radiation, the other oriented to receive vertically polarized radiation. The transmitted radiation was horizontally polarized. These observations were confined necessarily to the A_2-events. However, the use of the Churchill–Ottawa path had the advantage of ensuring that the signal directions of arrival were limited to a narrow sector. The results showed that, characteristically, the amplitude of the received signal with vertical polarization was nearly as great as that with horizontal polarization. There was some fluctuation in the ratio of the amplitudes of the signals received on the orthogonal antennae, but rarely was the vertically polarized signal very much smaller than the horizontally polarized signal.

The nearly complete depolarization of the signal during the scattering process has been observed for back-scatter from radio-aurora by Harang and Landmark

VOL.
13
1958/5

(1954), and by McNamara and Currie (1954). One possibility is that this depolarization comes about by Faraday rotation of the plane of polarization. If the dimensions of the scattering centres are large (of the order of 1 km), a significant amount of Faraday rotation might take place. The depolarization that results from this cause should decrease rapidly with increasing frequency. Another possibility is that the depolarization comes about by multiple scattering. The evidence already presented indicates that each scattering centre is nearly isotropic and tends to reflect completely the incident radiation. Multiple scattering in an assembly of such scatterers would lead to a high degree of depolarization. At frequencies above those used in the present study, a smaller number of scattering centres would be involved because of the higher electron densities required to reflect totally the incident radiation. Thus, at higher frequencies, for this mechanism also, the transmitted polarization would tend to be preserved in the scattered signal. The back-scatter observations mentioned above are in accord with either picture of the scattering process.

The Geographical Extent of Radio-aurora

Although it is not the purpose of this paper to present synoptic information, some of the early results from the IGY network reveal interesting time sequences in the occurrence of radio-aurora at different places. One such sequence is shown in Fig. 14. The records were obtained simultaneously on the five paths radiating from Yellowknife. The records refer to a frequency of 38 Mc/s and the times shown are Universal Time, between 6 and 7 hr ahead of the various local times. For these circuits, the transmitter silent periods occured at 15 min intervals. The records are shown in order of decreasing geomagnetic latitude at the path mid-points. The most striking effects are the two major enhancements (A_2-events) which occur at progressively later times with decreasing latitude. This uniform behaviour applies even to the Yellowknife–Baker Lake path, which is well north of the auroral zone, and seems to contradict the widely-held view that auroral disturbances start in the auroral zone and move both north and south from it. There is evidence of a separate earlier event within the auroral zone (Yellowknife–Churchill record). If the occurrence of this earlier event is typical, it could easily lead to the belief that the aurora does move both north and south from the auroral zone.

The right hand side of Fig. 14 represents daylight hours for all of the paths. On four of the paths the end of a widespread S-event is visible near 2200 UT, while on the fifth, the Yellowknife–Churchill path, there is evidence of daytime absorption. This association of daytime absorption within the auroral zone with an S-event on either side of the auroral zone seems to be typical and suggests a common origin for the two phenomena.

Discussion

One of the most unexpected results of the statistical analysis was the infrequent occurrence of E-events. It seems clear that these events are caused by the passage near the mid-point of the path of a cloud of intense ionization, the dimensions of which are sufficiently great to permit the specular reflection of the radio waves. Before the systematic classification of the events was undertaken it was often assumed that this particular type of sporadic-E ionization was responsible for most

of the daytime periods of enhanced signals on relatively short paths. The data of Table 2 indicate that, at least over the range of latitudes 45°N to 55°N, during years of moderate to high solar activity, the occurrence of this type of sporadic-*E* ionization is very rare.

The scattering mechanisms which give rise to the various *A*-events are not completely defined by the experiments, but the present evidence does much to resolve the controversy which has existed in the literature for the past 10 years. During this time various authors have presented evidence in support of different scattering mechanisms. The principal point of contention has been the degree to which aspect sensitivity controls the occurrence of reflections from radio-aurora (see the discussion of KAISER, 1956). One group has contended that the scattering centres are sufficiently aspect sensitive to give rise to intense reflections even when the electron density is so low within individual clouds of ionization that they are nearly transparent to the radio waves. The alternative opinion has been that although aspect sensitivity is present, it is not sufficient to give rise to reflection from regions of low ionic density.

The present study indicates that there are three distinct scattering mechanisms. The A_1-events are characterized by high aspect sensitivity. The scattering polar diagram seems to be no broader than about $\pm 15°$ in the plane containing the earth's magnetic field, and is probably much narrower than this value if measured in the usual manner to half-power points. The particular example of an A_1-event investigated in Fig. 13 involved critical reflections. The present bistatic radio systems possess a sensitivity which is comparable to that of medium-powered radar systems. It is possible that a substantial increase in sensitivity would lead to observable scattering even for electron densities below the critical value. The fact that the A_1-events are observed very rarely at high latitudes and more frequently at low latitudes may have led to some differences of interpretation among various investigators. It may be that the A_1-events predominate for latitudes below those covered in the present study, in which case it would be quite proper to emphasize the aspect sensitivity of the reflections.

The A_2-events show only slight aspect sensitivity, and also arise by critical reflection. These events are seen more frequently in higher latitudes than are the A_1-events. This fact accounts presumably for the reluctance of Canadian and British investigators to accept theories which predicate extreme aspect sensitivity. During the present bistatic investigation, A_2-scattering has been observed for aspect angles that varied from a few degrees to at least 30° or 40° from the specular condition. On the other hand, in radar investigations, echoes are observed only rarely when the aspect angle differs from the specular condition by more than 12°–15°. There is an important difference between the bistatic and monostatic systems. For the bistatic system the radio waves always follow paths which make small angles with the horizontal, even under conditions of unfavourable aspect angle. For the monostatic (radar) system unfavourable aspect angles are always associated with high elevation angles for which the radio waves follow paths that must make large angles with the horizontal. The fact that the bistatic system can observe scattering from radio-aurora for much less favourable aspect angles than can the radar system, indicates that at least in part the radar limitation is due to

VOL.
13
1958/5

the high elevation angles rather than to the unfavourable aspect angles. A different line of reasoning was used earlier (CURRIE, FORSYTH and VAWTER, 1953) to arrive at the same conclusion. As a result it was postulated that when the auroral structures were viewed at high elevation angles the scattering centres were screened from the radar by underlying local absorbing regions. The existence of strongly absorbing regions associated wih auroral structures is now well established (see for example, FORSYTH and VOGAN, 1957, REID and COLLINS, 1958). However, it is not yet proven that these regions are sufficiently localized to provide the necessary screening at high elevation angles and at the same time to provide little or no screening at low angles.

The fact that A_1- and A_2-events show aspect sensitivity and A_3-events show no aspect sensitivity is consistent with the suggestion that A_1- and A_2-events occur at heights greater than 100 km and that A_3-events occur at much lower heights. Above 100 km the magnetic field of the earth should partially control diffusion and thus tend to cause the elongation of the scattering centres in the field direction. For the lower heights the high-collision frequency renders the magnetic field ineffective and diffusion should proceed isotropically.

It appears very likely that only the A_1- and A_2-events are associated with visible auroral displays. The fact that there exists a third phase of the auroral disturbance, the A_3-event, which is probably observable only by radio means may assist in the interpretation of recent radar results. At first, radar investigations were confined to studies of ionization which could be associated directly with visible aurora, but more recently with the advent of more sensitive systems such as that described by MCNAMARA (1958), it has become evident that while not all visible aurora gives rise to radar reflections, radar reflections are observed much more frequently than can be explained by the occurrence of visible aurora. For the bistatic system the A_3-events gave rise characteristically to signals of lesser amplitude than did either the A_1- or A_2-events. Nevertheless, the A_3-events occurred most frequently. A system of substantially less sensitivity would have observed only the A_1- and A_2-events. The A_1-events were observed at large angles from the path direction. The A_2-scattering centres appear to be nearly isotropic and were frequently observed also at large angles from the path-direction. For these reasons it is not likely that the bistatic arrangement enjoys any significant amplitude advantage over the monostatic arrangements (except, of course, for the absorption effect) in the observation of A_1- and A_2-events. On the other hand, the A_3-events, which arise by scattering of the Booker-Gordon type, are observed much more readily with the bistatic arrangement. The advantage enjoyed by the bistatic system for the observation of these events is probably not less than 10 dB nor more than 25 dB. This advantage is not too great to be overcome by modern radar equipment but does increase the gap between the level of sensitivity at which only A_1- and A_2-events are observed and the level at which all three events are observed. It is interesting to note that because of the lower height at which the A_3-scattering arises, the absorption mechanism can not be invoked as a means of limiting the elevation angle to which the A_3-events could be observed by means of radar. However, if the scattering region is only a few kilometres in vertical thickness the maximum scattered signal will be observed at a relatively low elevation angle

determined by the thickness of the scattering region and, in some circumstances by the radar pulse length.

It has been indicated that at high latitudes for a radar system of low sensitivity the A_2-events would predominate. If, on the basis of Fig. 7, the A_1-events can be associated with the early stages of the visible auroral displays (the homogeneous forms), and the A_2-events can be associated with the later stages (the forms with structure), it is not surprising that the early radar investigations at high latitudes emphasized the association between the radar reflections and the auroral forms which displayed some structure.

Most of what has been said about the observation of A_3-events by means of radar could also apply to the S-events. It seems possible that S-events were actually observed by radar at Ottawa and at Saskatoon as early as 1952 (MCKINLEY and MILLMAN, 1953, FORSYTH *et al.*, 1953). The scattering region for those observations appeared to be at a height of about 85 km. There is little doubt that the S-events have been observed during investigations of the ionospheric forward-scatter phenomenon described by BAILEY *et al.* (1952). In recent years there has been a considerable amount of discussion concerning the continuous signal which is observed in these investigations. The most recent opinion seems to be that the propagation is supported at night by meteor reflections and during the day by scattering from ionic inhomogeneities in the lower ionosphere (BAILEY, 1957a). This opinion is based on the diurnal variation of signal level which follows meteor activity at night but shows a strong maximum at noon. This daytime peak is very similar to that which would be obtained by averaging the signal strength observed during a number of S-events. Presumably the observed variation of S-occurrence with latitude indicates a decrease in magnitude of the effect with decreasing geomagnetic latitude (subject also to the mitigating solar control which will be discussed later). The substantial increase in sensitivity associated with the ionospheric forward-scatter equipment used by BAILEY *et al.* would tend to offset the effect of latitude. Alternatively, it might be postulated that the basic phenomenon which gives rise to the S-events is present every day but is normally very weak and is observed irregularly in the present investigation because of the low sensitivity which has been used. This interpretation is more nearly in accord with that first proposed by BAILEY *et al.* but ignores the association of the S-events with auroral zone phenomena. If the ionospheric scattering described by BAILEY *et al.* were due only of the interaction of regular ionospheric ionization and regularly occurring atmospheric turbulence then it might be expected that the hourly signal levels would tend to recur on successive days. In fact, the day-to-day signal variation is considerable and suggestive of the sporadic-S events observed in the present study.

The recent observation of radar reflections from aurora at a frequency close to 400 Mc/s by FRICKER *et al.* (1957) is important new evidence concerning the nature of radio-aurora. Since some of the echoes were long enduring it seems likely that they may be associated with A_3-events. The positive association of reflections at so high a frequency with an A_3-event would permit the derivation of more information concerning the size of, and the electron density distribution within, the scattering centres. Most of the observations appear to be subject to aspect sensitivity and these probably refer to A_1-events. It has been suggested that aspect sensitivity

VOL
13
1958/

may increase with growing frequency. The actual contours of constant electron density within the scattering centres probably approximate prolate spheroids with major axes lying along the direction of the magnetic field. If the minor axis of the spheroid were much smaller than the wavelength and the major axis much larger than the wavelength then the scatterer would resemble a line source and the width of the scattering polar diagram, would decrease with increasing frequency. On the other hand, if both dimensions of the spheroid are large compared to the wavelength (as is suggested by the present measurements) then geometric optics can be used to derive the scattering polar diagram, which is dependent only on the curvature of the surface or to a first approximation on the ratio of major to minor axes. These latter conditions should then be constant for all higher frequencies and the degree of aspect sensitivity should then be constant with increasing frequency. As has been indicated, the degree of aspect sensitivity observed at frequencies near 50 Mc/s suggests a major-to-minor axis ratio of about 4 : 1. The observation of A_1-events at a frequency of 400 Mc/s does not imply necessarily that critical reflections are involved. With substantially increased sensitivity it should be possible to observe scattering from aspect-sensitive clouds of ionization when the electron density is appreciably below the critical value for reflection at this frequency (10^9 cm^{-3}). Only simultaneous observations on two relatively closely spaced frequencies can settle this point. It could be postulated also that the scattering centres have a dual composition, an extremely aspect-sensitive inner core that reflects the higher frequency (400 Mc/s) and an outer shell that reflects the lower frequency (50 Mc/s). It is difficult to visualize a mechanism by which this distribution of ionization would come about, but if it did exist there would be many occasions when the generating agency was less strong and when the inner core would be observable at the lower frequency. Since the observations give no indication of this effect, it seems more reasonable to ascribe any apparent increase of aspect sensitivity at the higher frequency to a relative increase in occurrence of A_1-events, in comparison with the occurrence of A_2-events, with increasing frequency.

Turning now to the possible mechanisms by which the various events are generated, it seems likely that each event owes its existence to a qualitatively different agency. In addition to the aspect sensitivity of the A_1-events there is the characteristically high fading rate. This fading suggests the random motion of the scattering surfaces and is consistent with the rates of motion to be expected from ambipolar diffusion at heights of the order of 100 km. This suggestion implies that the ionization is formed discontinuously and that each scattering centre has a relatively short life-time. On the other hand, the A_2-scattering centres that are probably located in the same general height range, appear to be much more stable and suggest a more slowly varying mechanism of generation. In this case the time scale of the major fluctuations may well be of the order of seconds, a value which is consistent with the luminosity fluctuations in the rayed forms of visible aurora. It is interesting to note that MEINEL (1954) associated the first phase of aurora (the homogeneous forms) with the influx of solar protons and the second phase (the rayed forms) with a local generating mechanism, possibly a discharge induced by local electric fields. The present knowledge of the A_1 and A_2 radio events is at

least consistent with the interpretation presented by MEINEL, although recent spectroscopic observations made at Churchill by MONTALBETTI (1958) suggest that the true picture may be more complex.

The A_3-events are probably not associated with visible aurora. This might be expected since the scattering region seems to be below 85 km in height. This height is less than those normally found in visible aurora. It is not possible to ascribe the A_3-events to residual ionization from the auroral display since any such ionization would disappear quickly, principally by electron attachment to form negative ions. It is necessary, therefore, to postulate a continuing mechanism that can operate with nearly constant intensity over periods of several hours. The spatial distribution of the ionization is probably governed by local turbulence. There is ample evidence, from visual and radio observations of meteor trails, that large scale turbulence exists in the lowest regions of the ionosphere. The similarity of the A_3- and S-events suggests that the spatial distribution of ionization is characteristic of the region rather than the generating agency. There seems to be little direct evidence concerning the nature of the generating agency, but the total amount of ionization formed per unit volume need not be large. An agency which inhibits or reverses the process of negative ion formation would be particularly effective. The low-energy part of the soft X-ray spectrum detected in auroral latitudes by VAN ALLEN (1955) seems to be a valid possibility, especially since it appears that this radiation has been detected in the absence of visible aurora.

The S-events, since they are associated geographically with the auroral zone might be considered to represent yet another part of the auroral process. The association between the recurrent daytime absorption observed at places within the auroral zone and the simultaneous occurrence of S-events at places just outside the auroral zone, needs further study. Some aspects of this problem have been examined already by REID and COLLINS (1958). Similar examples of high-latitude absorption that occurrred in association with low-level scattering regions have been presented recently by LANDMARK (1958). At the present moment there is not enough data concerning the daytime absorption to establish the connexion statistically; however, there seems to be no doubt that the association is real for a few particular cases. The occurrence of absorption within the auroral zone may indicate that the ionization is more intense there than in regions outside of the auroral zone where the phenomenon is detected as an S-event. An alternative possibility is that the auroral zone ionization extends to lower levels in the atmosphere. From the evidence presented by REID and COLLINS it seems probable that the presence of ionization at unusually low levels in the atmosphere is the correct interpretation. In any case, the occurrence of S-events raises the same difficulties concerning the generating mechanism as does the recurrent daytime absorption. In addition, for the S-events the basic phenomenon must be much more widespread and more frequently occurring. However, it need not be as intense as that required for the daytime absorption.

The geographical association of S-events with the auroral zone indicates that the basic cause of these events must be the influx of particles which are capable of being deflected by the earth's magnetic field. Since the daytime absorption, and presumably also the S-event, tends to occur within a few hours of a solar event,

VOL
13
1958/

the particles must travel with high velocity and penetrate deeply into the earth's atmosphere. The nature of the particles has been discussed at length by CHAPMAN and LITTLE (1957) and by BAILEY (1957a). BAILEY first suggested that the primary particles were calcium ions but recently he has indicated (BAILEY, 1957b) that he now considers it more likely that protons are the important particles. In support of his first suggestion it may be noted that JONES (1957), by means of spectroscopic observations made at Saskatoon, has detected calcium ions in the lower ionosphere in amounts which vary irregularly through a wide range. Whatever the basic cause of the ionization it seems likely that at these low levels the electrons will be removed rapidly by attachment to form negative ions. The strong solar dependence is then due to the action of solar radiation in recreating the ionization by photo-detachment. One difficulty with this explanation results from the very small amount of energy required for the photo-detachment process. The wavelengths involved are in the red and infra-red part of the spectrum and so will be attenuated only slightly by passage through the upper parts of the atmosphere. As a result, the photo-detachment process should proceed rapidly to saturation as soon as the appropriate layers are illuminated, whereas Fig. 8 indicates a continuous dependence upon solar zenith angle over a wide range of angles. However, this concept of the phenomenon is probably much too simplified, and should be extended to include the many competing processes that must be involved. A more accurate knowledge of the height of the scattering region and of the pertinent electron densities would be of great assistance in these studies.

VOL. 13 58/59

An illustration of the parts played by particles and by solar radiation in the occurrence of *S*-events is provided by the two most southerly paths. The Greenwood–Ottawa path is only about 2° lower in geomagnetic latitude, but a full 5° lower in geographic latitude, than the Suffield–Winnipeg path. As a result of the difference in geomagnetic latitude, it might be expected that the particle influx would be slightly greater for the Suffield–Winnipeg path. However, this small difference of particle influx seems to be more than offset by the increased values of $\cos \chi$ which occur on the Greenwood–Ottawa path. Table 2 shows that the occurrence of *S*-events on the Greenwood–Ottawa path is slightly, but significantly, greater than that on the Suffield–Winnipeg path. Over the range of latitudes investigated it appears that when comparable longitudes are involved the occurrence of *S* decreases continuously with decreasing latitude. The interaction of the two agencies may cause this trend to reverse at lower latitudes.

CONCLUDING REMARKS

The existence of at least four distinctive kinds of radio events, associated geographically with the auroral zone, appears to have been established. There is, nevertheless, still a considerable uncertainty about the method by which the ionization is generated in each case. The present evidence has made it possible to outline the characteristics of the three different scattering mechanisms involved and to give at least a qualitative physical description of each. It is particularly satisfying to note that some support has been found in one or other of these three scattering mechanisms for most of the various reflection processes which have been proposed by auroral investigators over the past 10 years.

The bistatic method seems to be particularly effective in studies of radio-aurora. It is doubtful if the four distinct auroral events would have been recognized if the present study had made use only of monostatic systems. It would seem to be desirable now to attempt the identification of these events by other techniques.

The tentative associations, which have been made in this paper between radio-aurora and visible aurora, have been made mainly on the basis of statistical evidence with the addition of a small number of direct visual observations. This situation is most unsatisfactory. It seems evident that if these associations can be established more firmly, a good deal of the present knowledge concerning the visible aurora could be carried over into the radio field where the measurements can be made more simply, more sensitively and more continuously, than by any other method. Certainly, in any comprehensive attack on the basic problem of auroral physics—the understanding of the process by which auroral phenomena are generated—all the available evidence, including the optical and radio evidence, should be combined. In any case, since the radio methods offer the advantage of continuous measurements in daylight and through overcast, it would seem worthwhile to make a particular effort to interpret each of the four classes of radio-auroral events in terms of existing auroral knowledge.

Acknowledgements—The authors are grateful to the many people who have contributed to the present study by maintaining the transmitting and receiving facilities. Particular thanks are due to those who co-operated in the installation and maintenance of the ten circuits that are in use as part of the Canadian IGY programme. These people have included Mr. J. H. CRYSDALE of the Radio Physics Laboratory, Mr. J. M. WALKER of The Pas, Manitoba, and various members of the following organizations: National Research Council of Canada, Department of Transport, University of Saskatchewan, Royal Canadian Corps of Signals and Giant Yellowknife Gold Mines Ltd.

VOL
13
1958/

REFERENCES

BAILEY D. K.	1957a	*J. Geophys. Res.* **62,** 431.
BAILEY D. K.	1957b	Private communication.
BAILEY D. K., BATEMAN R. and KIRBY R. C.	1955	*Proc. Inst. Radio Engrs,. N.Y.* **43,** 1181.
BAILEY D. K., BATEMAN R., BERKNER L. V., BOOKER H. G., MONTGOMERY G. F., PURCELL E. M., SALISBURY W. W. and WIESNER J. B.	1952	*Phys. Rev.* **86,** 141.
BOOKER H. G.	1956	*J. Atmosph. Terr. Phys.* **8,** 204.
BOOKER H. G. and GORDON W. E.	1950	*Proc. Inst. Radio Engrs., N.Y.* **38,** 401.
BULLOUGH K. and KAISER T. R.	1955	*J. Atmosph. Terr. Phys.* **6,** 198.
CHAPMAN S. and BARTELS J.	1940	*Geomagnetism.* Clarendon Press, Oxford.
CHAPMAN S. and LITTLE C. G.	1957	*J. Atmosph. Terr. Phys.* **10,** 20.
CURRIE B. W., FORSYTH P. A. and VAWTER F. E.	1953	*J. Geophys. Res.* **58,** 179.
DYCE R.	1955	*Trans. Inst. Radio Engrs., N.Y.* PGAP **3,** 76.
FORSYTH P. A.	1953	*J. Geophys. Res.* **58,** 53.

Forsyth P. A., Currie B. W. and Vawter F. E.	1953	*Nature, Lond.* **171,** 352.
Forsyth P. A. and Vogan E. L.	1955	*Canad. J. Phys.* **33,** 176.
Forsyth P. A. and Vogan E. L.	1957	*J. Atmosph. Terr. Phys.* **10,** 215.
Fricker S. J., Ingalls R. P., Stone M. L. and Wang S. C.	1957	*J. Geophys Res.* **62,** 527.
Harang L. and Landmark B.	1954	*J. Atmosph. Terr. Phys.* **4,** 322.
Herlofson N.	1947	*Nature, Lond.* **160,** 867.
Jones A. V.	1957	Private communication.
Kaiser T. R.	1956	*The Airglow and the Aurorae.* Pergamon Press, London.
Landmark B.	1958	*J. Atmosph. Terr. Phys.* **12,** 79.
Little C. G., Rayton W. M. and Roof R. B.	1956	*Proc. Inst. Radio Engrs., N.Y.* **44,** 992.
Lovell A. C. B., Forsyth P. A. and Harang L.	1957	*Annals of the IGY.* **3,** 337.
McKinley D. W. R. amd Millman P. M.	1953	*Canad. J. Phys.* **31,** 171.
McNamara A. G.	1958	*Canad. J. Phys.* **36,** 1.
McNamara A. G. and Currie B. W.	1954	*Nature, Lond.* **174,** 1153.
Meinel A. B.	1954	*Proc. Nat. Acad. Sci., Wash.* **40,** 943.
Montalbetti R.	1958	Private communication.
Ratcliffe J. A.	1956	*Rep. Prog. Phys.* **19,** 188.
Reid G. C. and Collins C.	1958	*J. Atmosph. Terr. Phys.* In press.
van Allen J. A.	1955	*Phys. Rev.* **99,** 609, A12.
Vogan E. L. and Campbell L. L.	1957	*Canad. J. Phys.* **35,** 1176.

VOL. 13 58/59

Journal of Atmospheric and Terrestrial Physics, 1959, Vol. 13, pp. 346 to 350. Pergamon Press Ltd. Printed in Northern Ireland

Ionospheric changes at Singapore during the solar eclipse of 14 December 1955

C. M. MINNIS
(Official communication from DSIR Radio Research Station, Ditton Park, Slough, Bucks)

(*Received* 14 *May* 1958)

Abstract—The *E*- and *F1*-layer data obtained at pairs of stations during the eclipses of 1952 and 1954 were consistent on each occasion with a single model for the distribution of sources of ionizing radiation on the sun. The results obtained at Singapore in December 1955 can not be explained in terms of any likely distribution. It seems possible that vertical movements, and the consequent invalidity of the Chapman theory, may have been responsible for this discrepancy. No significant change occurred in the critical frequency of the *F2*-layer but there is evidence of a complex redistribution of ionization in the lower part of the *F*-layer.

1. INTRODUCTION

The track of the annular eclipse of 14 December 1955 lay about 1400 km to the north of Singapore where the unobscured fraction of the sun's disk fell to 0·50 at the maximum phase (Table 1).

VOL.
13
1958/5

Table 1. Duration of eclipse at Singapore 14 December 1955

LMT					
Noon	Height (km)	Beginning	Middle	End	A_{min}
1159	100	1354	1534	1654	0·50
	200	1356	1536	1656	0·50

LMT = UT + 7 hr

On the day of the eclipse, $h'(f)$ records were made at intervals of about four minutes during the period 1215–1745 LMT. Control data were obtained by making records every quarter hour during the same period from 9–19 December except on 17 December. Figure 1 shows the changes which occurred in the various critical frequencies on the day of the eclipse with, for comparison, the median values for the control days.

2. *E*-LAYER

An attempt has been made to analyse the behaviour of the *E*-layer by computing the change with time of a function (J) which has been used successfully on several

previous occasions to represent variations in the intensity of the ionizing radiation during an eclipse and which is defined in equation (1):

$$\left(N^2 + \frac{1}{\alpha'}\frac{dN}{dt}\right)\sec^n \chi = A'(q_0/\alpha') = J \qquad (1)$$

A' is the unobscured fraction of the ionizing radiation and the remaining symbols have the usual meanings.

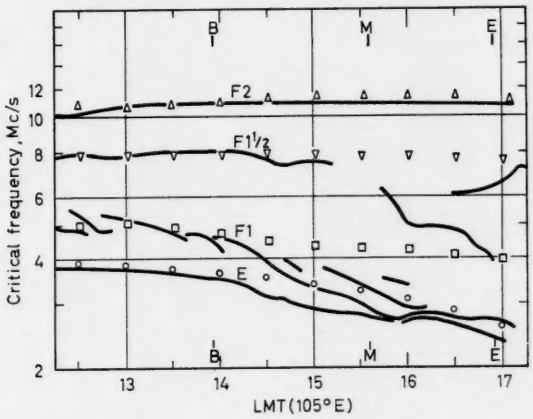

Fig. 1. Critical frequencies at Singapore during the eclipse of 14th December 1955.
——— 14 December
△ △ ▽ ▽ □ □ ○ ○ Control days (median)

The relation between $\log f_0E$ and $\log \cos \chi$ for the December control period is not linear but it can be represented empirically by the expression:

$$\log f_0E = 0{\cdot}584 + 0{\cdot}277 \log \cos \chi + 0{\cdot}028 \exp (11{\cdot}1 \log \cos \chi) \qquad (2)$$

Since f_0E cannot, in consequence, be represented as a simple power of $\cos \chi$, it has been necessary to replace the usual $\sec^n \chi$ term in equation (1) by a multiplying factor, based on equation (2), which reduces the observations to the condition $\chi = 0$.

The resulting values of J are shown in Fig. 2 for two values of the effective recombination coefficient: $\alpha' = \infty$ and 10^{-8} cm^3 sec^{-1}. This figure also shows the changes in J which have been computed assuming that the ionizing radiation was emitted uniformly from the whole of the sun's disk and it is evident that the differences between the two curves are very considerable. The main features of the curve showing the actual changes in J during the eclipse are the rapid fall soon after first contact, the very flat minimum (which implies practically no change in intensity for almost an hour), and finally the bifurcation at 1546 LMT. It would be possible to attribute the initial fall in J to a hypothetical extended bright source near the west limb of the sun; the flat minimum could then be interpreted as the

result of the gradual uncovering of this source while, at the same time, a second extended source in the north-east quadrant was being covered. This explanation seems to be an improbable one for it would require the reduction in the intensity of one source to be almost exactly balanced by the increase in the other during a period of almost 1 hr.

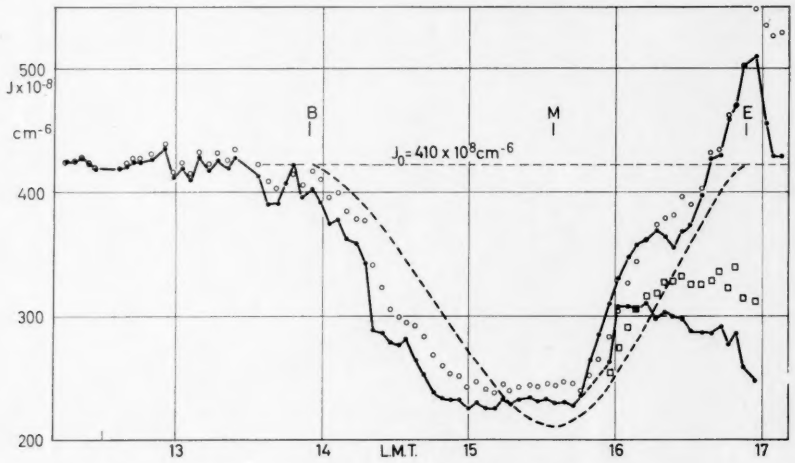

Fig. 2. Changes in $J(E$-layer) at Singapore during the solar eclipse of 14 December 1955.

●——● $\alpha'_E = 10^{-8}$ cm^3 sec^{-1}

○ ○ | □ □ | $\alpha'_E = \infty$

– – – – Uniformly bright disk.

The bifurcation in J after 1546 is due to the existence of two possible alternative values for f_0E. If continuity is used as a criterion, the lower frequency ought probably to be identified as f_0E, but the upper frequency leads to values for J which are nearer to the expected magnitudes. The upper frequency, however, seems to have originated, at about 1430, as a small ledge below the point of inflection which represents f_0F1; by about 1550 this ledge appears to have dropped down to E-layer levels. Under conditions of the kind just described, the simple Chapman-layer theory can hardly be valid and it seems unwise, therefore, to assume that J may be used as a reliable measure of radiation intensity on this occasion.

Because of these doubts concerning the significance of J, it would be unwise to use the later stages of the eclipse to provide evidence concerning the postulated bright source in the north-east quandrant. In view of the improbable assumption associated with the postulation of this source and the doubts which have been thrown on the interpretation of J during the second half of the eclipse, it seems doubtful whether, even during the first half, there is any justification for assuming that J can be regarded as an accurate indicator of the intensity of the ionizing radiation. It is concluded that, owing to difficulties in interpreting the behaviour

of the *E*-layer during this eclipse, it is not possible to use the Singapore data by themselves to provide any reliable information on the distribution of the sources of solar ionizing radiation.

3. Ionization in the *F*-region

The distribution of the ionization in the *F*-region at Singapore is often complicated by the existence of a ledge, which will be referred to as the *F1*½-layer, at a height intermediate between the *F1*- and *F2*-layers (Fig. 3). The presence of

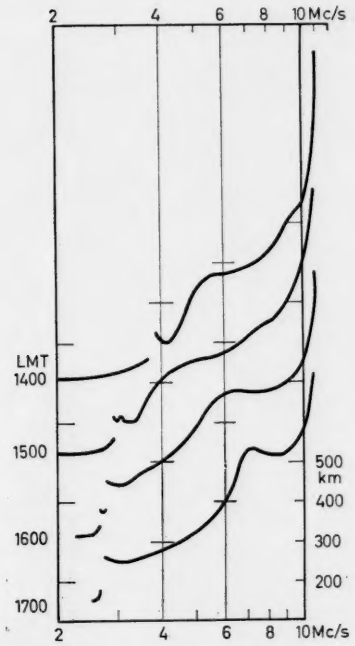

Fig. 3. *h'f* traces at Singapore, 14 December 1955.

the *F1*- and *F1*½-ledges is indicated only by an increase in group retardation extending in each case over a frequency range of a few Mc/s. For this reason accurate values representing the critical frequencies of these layers can not be given and, to minimize subjective errors, the frequencies at which the appropriate points of inflexion occur in the *h'f* trace have been quoted as f_0F1 and $f_0F1\frac{1}{2}$. This procedure results in a value of only 1·3 for the ratio f_0F1/f_0E which implies that the values of f_0F1 are roughly 10 per cent less than the "true" critical frequencies.

From 1400 to 2000 on the day of the eclipse, f_0F2 was slightly below the median value for the control days; this can not be assumed to be due to the eclipse because even lower values were recorded on three control days. Nevertheless, even though no definite eclipse effect occurred at the peak of the *F2*-layer, it is evident from the changes in f_0F1 and $f_0F1\frac{1}{2}$ that considerable changes took place in the lower levels of the *F*-layer as a whole.

In the *F1*-layer the impression gained from an inspection of the $h'(f)$ records is of a succession of ledges moving downwards through the lowest part of the *F*-layer. This effect is reflected in the discontinuous curve marked *F1* in Fig. 1 and no simple interpretation of it can be given.

The point of inflection representing $f_0F1\frac{1}{2}$ during the eclipse is quite clearly defined until about 1500 after which the $h'(f)$ trace becomes almost linear over a wide frequency range. In Fig. 3 the isolated branch between 4 and 6 Mc/s represents what appears, at first, to be a reappearance of the $F1\frac{1}{2}$-layer although at a later stage it seems to represent the *F1*-layer. Under circumstances of this kind, it is difficult to escape the conclusion that no simple scheme of labelling the different layers is applicable and that the true nature of the changes taking place could only be understood after computing a series of $N(h)$ profiles.

4. CONCLUSIONS

The use of the function J as an indicator of the variations, of the intensity of the ionizing radiation during a solar eclipse, implies that the ionospheric layer in question may be considered as a Chapman layer. During the 1952 and 1954 eclipses, the values of J observed at pairs of ionospheric observatories were found to be consistent on each occasion with a single model for the distribution of sources of ionizing radiation. (MINNIS, 1955, 1956.) These results seem to show that the layers used did, in fact, conform fairly closely to Chapman's theory.

For the eclipse of December 1955, the values of J calculated for the *E*-layer are difficult to explain in terms of any reasonably probable solar model. Moreover, there is some doubt, in the later stages of the eclipse, as to which of two cusps represents f_0E. This ambiguity arises from the existence of a cusp, at approximately *E*-layer height, which appears to have originated in a ledge at the base of the *F1*-layer. If any vertical movements actually did occur, the simple Chapman theory would no longer be valid and this may account for the peculiar behaviour of J.

Although f_0F2 did not change significantly during the eclipse, the behaviour of f_0F1 and $f_0F1\frac{1}{2}$ showed that the lower part of the *F*-layer was affected. A serious study of these changes would require an investigation of the redistribution of electron density with true height which took place during the eclipse.

Acknowledgements—The work described above was carried out as part of the programme of the Radio Research Board. The paper is published by permission of the Director of Radio Research of the Department of Scientific and Industrial Research. The operation of the ionospheric recorder at Singapore was the responsibility of the Officer-in-Charge at the time, Mr. G. H. BAZZARD.

REFERENCES

MINNIS C. M. 1955 *J. Atmosph. Terr. Phys.* **6**, 91–112.
MINNIS C. M. 1956 *J. Atmosph. Terr. Phys.* **9**, 201–209.

VOL
13
1958/

Journal of Atmospheric and Terrestrial Physics, 1959, Vol. 13, pp. 351 to 370. Pergamon Press Ltd. Printed in Northern Ireland

Cosmic-ray produced radioactive isotopes as tracers for studying large-scale atmospheric circulation

B. Peters
Tata Institute of Fundamental Research, Bombay, India

(*Received* 2 *July* 1958)

Abstract—In the interval between two consecutive condensations of moisture, atmospheric air accumulates radioactive isotopes produced by cosmic-ray particles in collisions with nitrogen, oxygen and argon. The production rates of these isotopes per gramme of air depends strongly on altitude and latitude; the rate of removal depends, between rains, essentially on the half-life of each isotope. These facts can be used to label air masses and to trace their trajectories.

The isotopes which seem to be most useful for meteorological investigations are: ^{32}P (half-life 14 days); ^{33}P (25 days); ^{7}Be (53 days); and ^{35}S (87 days).

Their concentrations have been studied in rains in India during 1956–1957 and approximate values have been obtained for the annual fall-out. These experimental fall-out values have been compared with the values which one calculates from the expected isotope production by cosmic radiation in various parts of the atmosphere.

From such a comparison one can draw the following conclusions:

(1) The fall-out based on the annual production of the isotope ^{7}Be agrees well with the measured annual fall-out. The measured fall-out of ^{32}P is somewhat higher and that of ^{33}P and ^{35}S between two and five times higher than the calculated values. The discrepancy is probably significant, although the fall-out data are not very accurate; it is presumably due to an underestimate of the contribution which neutrons with energy below $\sim$40 MeV are making to the number of nuclear disintegrations in argon.

(2) The data indicate that condensation of water vapour removes cosmic-ray induced radioactivity from the air very efficiently. One can, therefore, conclude that different isotopes appear in rain water in the same proportion in which they existed in the air before the moisture was removed.

(3) Stratosphere air differs markedly from air which has remained in the troposphere throughout the period between successive condensations and precipitations; apart from the fact that its level of activity will in general be higher, it contains a much larger proportion of long-lived compared to short-lived isotopes. Air which has descended from the stratosphere and moves into lower regions, remains clearly distinguishable for very long periods until it has been strongly diluted or else cleansed by condensation. The simultaneous determination of radioactivity due to two or more isotopes in an individual rain leads, therefore, to information on the past history of the air mass from which the water was condensed.

(4) A detailed analysis of twenty-one rain samples from various parts of India, taken between July and December 1957, showed that none of the corresponding air masses had the characteristics of air which had descended from the stratosphere.

1. Introduction

It is customary and usually convenient to divide the atmosphere of the earth into the convective region of the troposphere and the stratified stable region of the stratosphere. The tropopause which is the boundary layer between these two regions is well defined over most of the global surface and the transport of air across this boundary is very slow. In some places, however, the tropopause surface is broken; such breaks seem to be associated with the occurrence of jet streams. There exists a zonal belt, usually at a latitude of about 30°, where the high lying equatorial tropopause gives place to the much lower lying tropopause of the middle latitudes. Breaks in the tropopause also occur occasionally at higher latitudes. It is likely that most of the exchange of air between stratosphere and troposphere

* At present at the Institute for Theoretical Physics, University of Copenhagen, Denmark.

takes place through such gaps. The stratospheric air of higher latitudes thus enters the troposphere of lower latitudes. Presumably the circulation is completed by the poleward flow of air from the upper troposphere and the lower stratosphere of equatorial latitudes.

This description of general atmospheric circulation is certainly over-simplified. The zonal and meridional circulations change in intensity with longitude, also with the seasons, and possibly even from year to year. The detailed features have not yet been clarified. The important question as to how, where and at what rate the exchange of air between the troposphere and the stratosphere takes place and to what extent there is mixing between different layers within the stratosphere can also not yet be answered with confidence.

In the course of the last 30 years, important methods for studying large-scale atmospheric circulation have been developed based on measurements of atmospheric ozone and of water vapour in the upper atmosphere. Ozone is produced as a result of dissociation of oxygen molecules by solar radiation of wavelength $\lambda \leqslant 2420$ Å. Its production is confined to the stratosphere, and most of it takes place between 27 and 35 km. Since ozone production depends on the intensity of solar radiation, it is higher in summer than in winter and higher near the equator than near the poles. The ozone concentration of the atmosphere, however, varies in the opposite manner: it is much larger at high latitudes than in the tropical belt and higher in winter than in summer. This shows clearly that its distribution is determined to a large extent by meridional circulation.

Similarly, long series of measurements of water vapour in the stratosphere have clearly shown that the vapour pressure present in the lower layers of the stratosphere over England corresponds closely to the vapour pressure appropriate to the temperatures of the equatorial tropopause and not to those of the local tropopause.

While measurements of ozone and water vapour have proved very valuable in establishing some characteristics of large scale circulation, it is, nevertheless, still difficult to get a complete picture of the vertical and horizontal motion of air masses from such data, in spite of the greatly expanded scale on which measurements of ozone have been carried out in recent years. One of the most serious difficulties stems from the fact that the processes which destroy ozone in the atmosphere are very complex and probably depend on altitude, moisture content, temperature, wind speed near ground, as well as on organic material and dust contained in the aerosol.

It would, therefore, be useful to supplement the existing techniques by discovering other properties of air which are characteristic of the latitude and altitude where it circulates, properties which could serve as a label by which one can recognize an air mass when it is rapidly transported into a region where normally the characteristics are quite different. In this paper, it is shown that various radioactive isotopes produced by cosmic radiation can serve as useful labels for tracing the motion of air masses.

The isotopes in question belong to the elements beryllium, phosphorus and sulphur, and result from nuclear disruptions of atmospheric constituents by cosmic radiation. They have in common with ozone that they are produced

VOL
13
1958/

primarily, though not exclusively, in the upper layers of the atmosphere. In contrast to ozone their production does not fall during the night and has no seasonal component, it is independent of time. It also differs from ozone production in its dependence on latitude: isotope production increases as one proceeds from the equator towards the pole.

From the point of view of possible meteorological applications, however, the most important difference between cosmic-ray produced radioactivity and ozone lies in the laws which govern the removal from the atmosphere. In the case of ozone these laws are very complex; they are comparatively simple in the case of airborne radioactivity. The removal of cosmic-ray produced isotopes occurs essentially in either of two ways:* through radioactive decay or through the condensation of moisture and its subsequent precipitation as rain or snow. The simultaneous presence of several radioisotopes with very different half-lives in one and the same air sample facilitates the task of distinguishing between the effects due to the two removal mechanisms.

In Section (2) of this paper, cosmic-ray produced isotopes are discussed which may be useful for the study of air circulation. It also contains a discussion of the results of experiments carried out at our laboratory by RAMA and ZUTSHI (1958) and by GOEL *et al.* (1958), designed to measure the rate at which these isotopes are deposited on the surface of the earth.

Section (3) contains a brief discussion of an investigation carried out by LAL *et al.* (1958), in which the rate of production of the relevant isotopes is calculated as a function of altitude and latitude for the entire atmosphere. Some results of these calculations are important for the present purpose:

(1) The production of isotopes per gramme of air varies rapidly with altitude. It also increases with latitude (by about a factor 5 between the equator and the poles).

(2) Troposphere production is nearly independent of geographic location; here, the increase of cosmic ray intensity with latitude just compensates the decrease in the height of the tropopause. The increase in isotope production with latitude is entirely confined to the stratosphere.

(3) The proportions in which different isotopes are produced are nearly independent of height and of geographic location.

(4) The estimates of annual fall-out based on long-term measurements of isotope concentration in rain water are close to the calculated values for some isotopes and higher than the calculated values for others. It seems that condensation and subsequent precipitation is an efficient mechanism for removing all those radioisotopes which are of interest in this discussion.

If one now makes the plausible assumption that, after precipitation, an air mass is instantaneously free of radioactivity, then, since the production of isotopes in all parts of the atmosphere is known, the concentration of an isotope in the air will be a function only of the latitude and height in which the corresponding air mass has moved since it was last cleansed of activity. With this assumption the relation

---

* A third way, molecular exchange reactions at the surface of the earth, is important only in the case of ^{14}C, and does not concern us here.

between isotope concentration and air trajectory can be derived for each isotope; it depends strongly on its half-life.

We shall show, in Section (4), that different trajectories of air masses can lead to very different values for the concentrations and to very different values for the ratios between the concentration of two isotopes of unequal half-lives. The isotopes have, therefore, the most essential property required of useful tracers: activity measurements carried out on a single air mass can supply information on the history of its motion.*

So far, our experimental work has been confined to the analysis of rain water; this means that we have determined only the ratio between concentrations of isotopes as they existed in the air mass from which the moisture was condensed, but that, except in a few pilot experiments, we have not yet determined absolute concentrations. Nevertheless, as shown in Section (4), it should have been a simple matter to detect in any of our samples the predominance of air which originated in the stratosphere if it had occurred. We found no such indication in twenty-one samples. Since all of them were obtained at latitudes $\lambda \leqslant 30°$, one may consider this result as being consistent with existing views on the rarity or absence of an appreciable downward air transport across the equatorial tropopause. It would now of course be interesting to extend such measurements to the temperate and polar regions.

2. Measurements on Short-Lived Cosmic-ray Produced Isotopes

Cosmic radiation in the atmosphere is composed of a variety of high and low energy particles, capable of producing nuclear transmutations. Some of the reactions lead to radioactive end-products which can be detected in rain water or aerosol and can be observed even after they have reached the surface of the earth, provided their half-lives are sufficiently long. Thus, ^{10}Be whose half-life is 2·7 million years has been isolated in deep-sea sediments, while ^{14}C and tritium have been found not only on the ocean floor but also in ocean water, in inland lakes and in organic materials on land.

All cosmic-ray produced isotopes which have been found to date together with their half-lives and decay energies are listed in Table 1.

Many different nuclear processes contribute to isotope production. Tritium and beryllium isotopes are produced mainly in spallation reactions induced by medium and low energy neutrons in nitrogen and oxygen. Sulphur-35 and phosphorus-32 isotopes come from similar reactions induced in atmospheric argon. Sodium-22 also derives from argon, but its production requires high energy collisions. Photo-nuclear reactions and the capture of negative muons in ^{40}A contribute somewhat to the production of ^{35}S, but not significantly to that of lighter radioelements. Muon capture in argon is the main source of ^{39}Cl, at least in the lower

* The term "air mass" is used here without attempting a precise definition. In fact, it has been a great difficulty in meteorology to find a definition which remains meaningful in a turbulent medium for a period sufficiently long to permit description of even short-term meteorological changes. It is conceivable that the absolute and relative concentration of cosmic-ray produced isotopes in a body of air, which characterizes its radiation history, may lead to a new and meteorologically meaningful definition of the term "air mass".

VOL. 13 1958/5

Table 1. Cosmic-ray produced isotopes

Isotope	Half-life	Decay	Reference
^{10}Be	$2{\cdot}7 \times 10^6$ years	β^-, 550 keV	Peters (1955), Arnold (1956), Goel *et al.* (1957).
^{14}C	5700 years	β^-, 156 keV	Libby (1952).
^{3}H	12·5 years	β^-, 18 keV	Faltings and Harteck (1950), Kaufmann and Libby (1954).
^{22}Na	2·6 years	β^+, 540 keV γ, 1·3 MeV	Marquez *et al.* (1957).
^{35}S	87 days	β^-, 167 keV	Goel (1956).
^{7}Be	53 days	E.C. γ, 480 keV (11%)	Arnold and Al Salih (1955), Goel *et al.* (1956), Cruikshank *et al.* (1956).
^{33}P	25 days	β^-, 250 keV	Lal *et al.* (1957)
^{32}P	14·3 days	β^-, 1·7 MeV	Marquez and Costa (1955).
^{39}Cl	1 hr	β^-, 1·5 MeV	Winsberg (1956).

part of the atmosphere. The capture of slow neutrons by ^{14}N is the principal source of the isotope ^{14}C.

^{35}S, ^{7}Be, ^{33}P and ^{32}P have half-lives suitable for studying the circulation of air masses. The lifetime of ^{10}Be and of ^{14}C is too long and that of ^{39}Cl too short for this particular application. Tritium and ^{22}Na could be useful, but tritium production is now largely dominated by thermonuclear explosions and ^{22}Na activity is so weak that further refinements in detection techniques are required before this isotope can be used for routine activity determinations.

Detection of activity

Methods for the quantitative extraction of ^{35}S, ^{7}Be, ^{33}P and ^{32}P directly from atmospheric air are being developed, but are still in the experimental stage. Until recently we have confined our measurements to the determination of the concentration of isotopes in rain water. The methods for chemical separation and purification which we have found most useful for this purpose have been discussed by Goel *et al.* (1958) for sulphur and by Goel *et al.* (1956) for beryllium. A satisfactory procedure for separating phosphorus has been given by Marquez and Costa (1955) who established the presence of ^{32}P in rain water. The same procedure was followed by Lal *et al.* (1957) when they established the presence of ^{33}P.

The radiation from ^{7}Be and from ^{32}P is very penetrating and its measurement, even at low levels of activity, does not present any particular difficulties. It is convenient to work with rain-water samples of from 25 to 50 liters.

Sulphur-35 emits soft β-rays, and the problem of self-absorption arises especially when the specific activity of the sulphur is low because of appreciable amounts of stable sulphur which are often present in rain. It is usually necessary to work with thick sources. Since specific rather than absolute activity limits the accuracy, there is little advantage in using more than 25 l. of rain water.

It is difficult to determine the activity of ^{33}P, because this isotope emits β-rays of low energy; the activity of ^{33}P must always be measured in the presence of a

similar specific activity of the much harder β-rays of ^{32}P. Only in very thin sources is it possible to get comparable counting rates from both isotopes; non-uniformity of source deposition has so far limited our accuracy. A method which involves depositing the activity on a filter paper impregnated with scintillating material is being developed and may in the near future give results more accurate than those obtained so far with end-window counters.

Annual fall-out rates

The isotope concentration in rain water depends on the amount of water condensed from a given air mass and must, therefore, be expected to vary within wide limits. One does in fact find factors in concentration as high as 40 between different rains and appreciable variations even in precipitations separated by only a few hours. Individual radioactivity determinations of a particular isotope are, therefore, of little value.

Measurements on single isotopes may, however, lead to useful information if they are carried on over a period sufficiently long to average out fluctuations. One can then obtain a long-term average value for the fall-out at a given locality. Because of the strong zonal air circulation it seems reasonable to assume that annual fall-out rates are representative of an entire latitude belt in the sense that the fall-out within the same belt should be simply proportional to the local annual precipitation. Only data from a world-wide long-term programme of measurements can decide whether such a simple assumption is justified. We shall, however, use it as a working hypothesis for interpreting the existing measurements. An indication that this assumption is not strictly valid is contained in the footnote to Table 2.

VOL.
13
1958/5

The deposition rate of ^{7}Be has been measured in Kodaikanal (lat. 10°), and Bombay (lat. 19°), from January 1956 to December 1957. Details of the 1956 measurements have been published by RAMA and ZUTSHI (1958). The average concentration of ^{7}Be in rain water at these two stations is based on analyses which form a representative sample of the total precipitation throughout the 2 years. Another thirty-five less representative samples have been taken during 1957 at various stations in North India between latitudes $25\frac{1}{2}°$ and 34°. The annual fallout rates derived from these results are summarized in Table 2, which also includes measurements made by ARNOLD and AL SALIH (1955) at Chicago.

The deposition rate of radioactive phosphorus and sulphur have also been measured. One can get an average value for the tropics but the number of analyses is not yet sufficiently great to permit a study of the fall-out rate as a function of latitude. Most of the measurements of the sulphur concentrations, whose average value is listed in Table 2, were made on rains which fell at Kodaikanal, Bombay, and in North India (Shillong, Delhi, Mussoorie, Pathankot and Srinagar).* The measurements should be fairly representative of the rains which fell during the second half of 1957.

The question arises whether any substantial part of the observed activity could

* We want to express our gratitude to the officers in charge of various meteorological stations for their co-operation in collecting rain samples. Special thanks are due to Mr. S. BASU and Dr. S. MULL, Director General and Deputy Director General of the Indian Meteorological Department.

Table 2. Average isotope concentration in rain water and estimated annual fall-out

Latitude	Station	No. of samples	Atoms/cm³ of water	Average annual rainfall in the corresponding latitude belt (cm)	Estimated annual fall-out (Atoms/cm² per year)
		Beryllium-7			
10°	Kodaikanal	63	2500	175	$4{\cdot}4 \times 10^5$
19°	Bombay	54	4080	98	$4{\cdot}0 \times 10^5$
$25\frac{1}{2}°$–34°	Various*	19	4200	87	$3{\cdot}65 \times 10^5$
42°	Chicago and Lafayette	22	6000	89	$5{\cdot}3 \times 10^5$
		Phosphorus-33			
19°	Bombay	13	59	98	$5{\cdot}8 \times 10^3$
		Phosphorus-32			
19°	Bombay	13	28	98	$2{\cdot}7 \times 10^3$
		Sulphur-35			
10°–34°	Various	21	316	99	$3{\cdot}1 \times 10^4$

* Sixteen rain samples taken at Shillong averaged only 1000 atoms/cm³. Since the Shillong region has one of the highest annual rainfalls in the world, it is probably not representative of its latitude belt. The sixteen samples have been omitted from Table 2.

be due to nuclear explosions. As far as beryllium is concerned it is possible to give strong arguments to show that this is not the case:

(1) Although the isotope concentration in individual rains varies over a large range (from less than 250 to more than 10,000 atoms/cm³), there is no correlation with changes in the concentration of fission products.

(2) The annual fallout of ^{7}Be and that of the long-lived isotope ^{10}Be estimated from its concentration in deep-sea sediments are both of the same order of magnitude and in the same ratio as one calculates if both were produced by cosmic radiation (Peters, 1957). Since none of the ^{10}Be in ocean sediments can have originated in nuclear explosions, no substantial fraction of ^{7}Be is likely to have originated in that manner.

(3) Analysis of the dust precipitated with rain water shows that no ^{7}Be is embedded in dust; all the ^{7}Be which is carried down with dust goes into solution in water already at a pH = 3 (Rama and Zutshi, 1958).

It is also possible to show that the phosphorus activity in rain water cannot be bomb-produced (the same argument when applied to ^{35}S is, however, not quite conclusive):

Stewart *et al.* (1957) have studied strontium fallout in various parts of the world and have shown that:

(1) Practically all fission activity in rain water comes from a reservoir of radioactive dust in the stratosphere.

(2) The fall-out in the latitude belt of Bombay is almost the same as in England.

(3) The fall-out of ^{89}Sr in the period between May 1956 and May 1957 in England amounted to 45 mc/km^2 or $\sim 9 \times 10^5$ atoms/cm^2.

(4) The ratio in the activity of $^{89}Sr/^{90}Sr$, which directly after fission has the value 154, has only the value 17 in the fall-out. During the relevant period, therefore, the average age of the dust stored in the stratosphere reservoir was approximately 170 days.

The annual fall-out of ^7Be, ^{35}S, ^{33}P and ^{32}P measured in Bombay is smaller than the fall-out of ^{89}Sr by the factors 2, 30, 140 and 300, respectively. If we make the unlikely assumption that most of them are bomb-produced and have an average age of 170 days, the production of ^7Be and ^{32}P during the explosion would have to be of the same order as that of ^{89}Sr. The fall-out of sulphur could be accounted for if it occurred in the fission products with an abundance of about 1 per cent of the abundance of radioactive strontium, and that of ^{33}P, if it occurred with an abundance of 6 per cent. Since strontium lies on the maximum of the fission yield curve while the other isotopes are very far from the maximum, it is clear that fission activity cannot account for the beryllium and phosphorus concentration in the Bombay rains. We have no information on the abundance of ^{35}S in nuclear explosions and, therefore, cannot decide at present the question of its origin.

3. The Production Rate of Various Isotopes

We are interested in the production rate of ^7Be by the spallation of atmospheric nitrogen and oxygen and in that of ^{32}P, ^{33}P and ^{35}S by the spallation of atmospheric argon. A calculation in which these production rates were determined for all latitudes and all altitudes has recently been carried out by LAL *et al.* (1958). In this section it will, therefore, be sufficient to discuss briefly the method which was used for calculating the isotope production in all parts of the atmosphere and to give the main results in graphical form. It turns out that the measured annual fall-out of ^7Be and ^{32}P agrees reasonably well with estimates based on the calculated production rates. The recent fall-out measurements on the isotopes ^{33}P and ^{35}S indicate that their production rates have been underestimated in that paper by factors lying between 2 and 5. We shall return to this point later.

Practically all the isotopes which interest us here are produced by nuclear disintegrations in which one, two or three charged particles are emitted from the target nucleus. In the terminology of cloud-chamber or nuclear-emulsion workers, we are dealing mainly with one-, two- or three-pronged stars. The minimum energy required to produce ^7Be is slightly below 50 MeV, that for producing the other isotopes is lower. Because the number of nucleons in the atmosphere decreases rapidly with increasing energy, most isotopes will be produced by low-energy nucleons ($<$400 MeV), predominantly by low energy neutrons.* High-energy nucleons make appreciable contributions only in the uppermost layers of the atmosphere.

* Protons with less than 400 MeV are quite rare because they rapidly lose energy by ionization and come to the end of their range before producing a nuclear interaction. π-and K-mesons are too short-lived to contribute appreciably to star production. γ-rays and muons are plentiful but their interaction cross-section is small. Their contribution is largest in the production of ^{35}S from ^{40}A where it could amount to a few per cent of the production by nucleons. The capture of slow negative muons by argon and interactions of fast muons also add a few per cent to the ^{35}S production rate (LAL, 1958).

Neither reliable and direct measurements exist of the rate at which one-, two- or three-prong stars are produced in the atmosphere nor reliable theoretical calculations. But there are a large number of experimental results from which, when combined, the desired information can be derived. The lack of direct measurements, however, makes it necessary to proceed in several steps.

The first step is from cloud chamber data to determine the production rate of cosmic-ray stars of various sizes in nitrogen (and oxygen) and in argon at some particular latitude and altitude.

The second step involves extending these production rates to all other latitudes and altitudes with the help of some extensively measured parameters proportional to the flux of the low-energy nucleons which are responsible for these stars. Suitable parameters are the flux of thermal neutrons, the production rate of small stars in nuclear emulsions and small pulses in high-pressure ionization chambers.

The third step is to determine the yield of particular isotopes in various gases in stars with a given number of prongs. These data must be obtained from radiochemical work and cloud chamber experiments carried out with artificially accelerated nucleons.

The production rate of stars

The method of calculating the star production rate in various regions of the atmosphere outlined in steps one and two was adopted in the paper by LAL *et al.* (1958). It differs from that used by other authors in similar calculations dealing with the production of tritium and ^{7}Be in cosmic radiation by the fact that it relies entirely on experimental data obtained in various portions of the atmosphere. It does not make use of the theory of the so-called nucleonic cascades. This cascade theory is still somewhat unreliable because the degree of inelasticity in high energy nuclear collisions, which enters into the theory in a decisive way, has not yet been well established; at the present state of knowledge, it seems likely that the empirical approach of determining the star production rate will give more reliable results.

For details of the calculation we refer to the paper cited above. It is adequate to point out that emulsion, neutron flux and ionization chamber data, together with cloud chamber measurements at mountain altitudes, suffice to determine the production of small and large stars in all parts of the atmosphere as a function of height and geographic location. The star production rates obtained by LAL *et al.* are shown in Fig. 1. For the sake of clarity, curves belonging to different latitudes have been displaced with respect to each other. The figure also shows the position of the tropopause (the mean between summer and winter months), and the average star production rates in the stratosphere ($\bar{S}_s$) and in the troposphere ($\bar{S}_T$). Stars in argon account for 0·63 per cent of the total in all parts of the atmosphere. One observes a very rapid increase in star production with altitude and an appreciable latitude effect at a fixed pressure level between $\lambda = 30°$ and $\lambda = 60°$.

Fig. 2 is obtained by integrating the area under the curves of Fig. 1. The two curves of Fig. 2 represent the number of stars produced per second in a column of air with 1 cm^2 cross section extending from sea level to the tropopause and in another column extending from sea level to the top of the atmosphere. One sees

that troposphere production is practically independent of geographic location; the very appreciable increase in star production with latitude is almost exactly compensated by the decrease in the height of the tropopause. The entire latitude increase of isotope production occurs in the upper layers of the stratosphere.

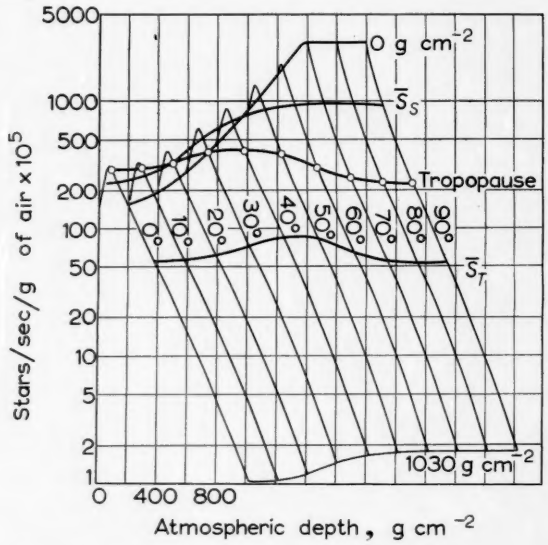

Fig. 1. The number of nuclear disintegrations per gramme of air and per second is plotted against atmospheric pressure. Curves referring to different latitudes have been displaced with respect to each other for the sake of clarity. Intersections of the star-production curves with the lines marked $\bar{S}_S$ and $\bar{S}_T$ represent the average star production at various latitudes in the stratosphere and the troposphere, respectively. Intersections with the line marked "tropopause" give the pressure level of the tropopause at various latitudes averaged between summer and winter months.

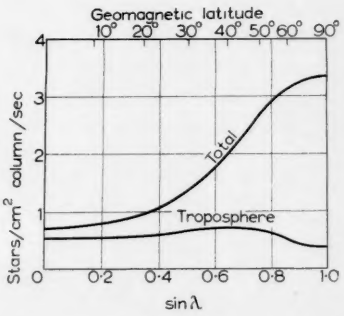

Fig. 2. The number of nuclear disintegrations per second in a column of air extending from sea level to the top of the atmosphere is given as a function of geomagnetic latitude. The lower curve represents the corresponding disintegration rate below the tropopause.

In the polar region, 90 per cent of all isotopes are produced in the stratosphere. In the tropical belt, stratosphere production amounts only to 30 per cent. This distribution of source strength is important for the application of isotopes to meteorology.

Fig. 3 shows the number of nuclear disintegrations in the atmosphere per incident primary cosmic-ray particle and also per incident primary nucleon. This figure differs significantly from the corresponding figure in the paper by LAL *et al.* (1958), because it incorporates the drastic revision in the accepted values for the proton flux at the equator, which has become necessary as a result of the work of MCDONALD (1958). The curves in Fig. 3 show a strong decrease in the number of stars per primary particle with increasing latitude. This reflects the low average primary energy of those particles which are admitted by the earth field at high latitude only. Particles which are admitted only above $\lambda = 60°$ do not contribute any more to isotope production, their energy is so low that they are usually brought to rest by ionization before they have a chance to make a nuclear collision. This

VOL 13 1958/

leads to an important conclusion: The very large changes in cosmic-ray intensity which accompany the sunspot cycle (NEHER and ANDERSON, 1958) have no significant effect on the isotope production; they affect mainly low energy cosmic rays which do not produce many interactions and which are confined to a small

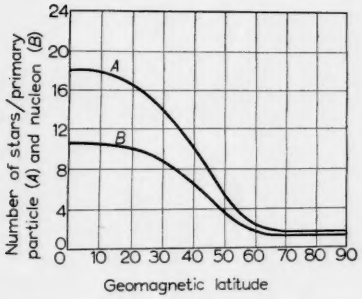

Fig. 3. The number of nuclear disintegrations per incident primary cosmic ray particle (A) and per incident primary nucleon (B) is shown as a function of latitude.

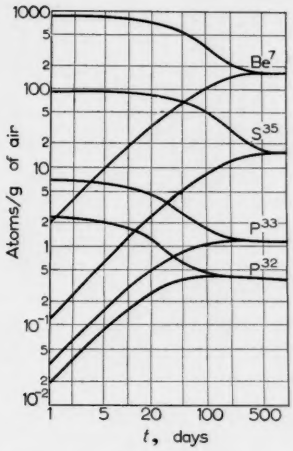

Fig. 4. The number of atoms of various radioisotopes per gramme of air is shown as a function of time for two cases. The lower branches of the curves refer to air which, completely free of activity at time $t = 0$, circulates within a turbulent troposphere. The upper branches refer to air which descended into the troposphere at time $t = 0$, after its radio-activity had come into equilibrium with cosmic radiation of an intensity equal to that encountered slightly above the tropopause.

region around the poles. Although the number of primary cosmic ray particles outside the earth's field seems to vary by more than a factor 2 between sunspot maximum and sunspot minimum, the corresponding increase in isotope production is probably less than 5 per cent.

The yield of various isotopes in nuclear disintegrations

Having determined the rate of nuclear disintegration processes in the atmosphere, it remains to determine the average yield of the various spallation products.

The yield of ^{7}Be produced when bombarding ^{12}C with protons has been measured in the laboratory for all proton energies from threshold to ~5·7 BeV (BENIOFF, 1956). After going through a slight maximum at 50 MeV it becomes nearly independent of energy. The production cross-section of ^{7}Be is also known for nitrogen at 5·7 BeV and for many other elements at various energies. The yields of all possible spallation products were determined with 90 MeV neutrons in carbon by KELLOG (1953) and with 300 MeV neutrons in oxygen by FULLER (1954). As a result, the yield of ^{7}Be in stars of various sizes in nitrogen and oxygen can be calculated reliably. In the atmosphere, the yield is almost independent of latitude or height and has an average value of 4·2 per cent. We shall show that there is

good agreement between the calculated rate of production and the measured rate of fall-out.

Calculations of the yield of phosphorus and sulphur in disintegration of argon is more problematic, since there are no satisfactory direct determinations of the relevant cross-sections. One can make use of the fact that, in medium and heavy nuclei, singly and doubly charged particles are evaporated in a proportion which is close to 4 and does not depend critically on star size. Using this ratio and the corrected star size distribution from cloud chamber work, one can calculate the fraction of phosphorus and suphur produced in stars of various sizes (LAL *et al.*, 1958). In order to distribute this yield between the different isotopes belonging to the same element, one can make use of the semi-theoretical relation of RUDSTAM (1956), whose predictions agree well with spallation experiments carried out in aluminium and in nuclei with atomic number $A \geqslant 51$. For ^{33}P and ^{32}P, the calculated yields per argon star are 4·2 per cent and 3·9 per cent, respectively, and stay fairly constant in all parts of the atmosphere; for ^{35}S the yield is about 7 per cent. While this procedure may be reasonably satisfactory for estimating the yield of lighter isotopes and even perhaps for ^{32}P and ^{33}P, its applicability in the case of ^{35}S is doubtful because this isotope can be reached from ^{40}A by the emission of a single α-particle plus a neutron, a configuration which may be strongly favoured compared to other one-prong stars, especially near threshold. It would be important to determine the yield of ^{35}S in the laboratory by bombarding a ^{40}A target with neutrons of various energies.

VOL
13
1958/

Comparison of the calculated production with the observed annual fall-out

The annual fall-out data which are available so far have already been given in Table 2 (Section 2). We shall first consider the fall-out of ^{7}Be because we have more data than for other isotopes and because we can be sure that bomb-produced activity has played no important part. The fall-out at Chicago (geomagnetic latitude 54°, geographic latitude 42°), listed in Table 2, is only 30 per cent higher than in the equatorial belt. Referring to Fig. 2, one sees that this is the correct ratio if the fall-out is proportional to the isotope production in the troposphere, but that it should be four times higher in Chicago than in the equatorial belt if the fall-out were proportional to the combined production in the troposphere and stratosphere. This means that most of the ^{7}Be produced in the stratosphere decays before reaching cloud level. We, therefore, have here evidence for the well-known fact that the mean residence time of air in the stratosphere is long compared to the half-life of ^{7}Be.

Since the troposphere is a turbulent region, we may assume thorough mixing and calculate the annual fall-out, F, on the basis of the calculated average troposphere production P of ^{7}Be. If τ is the mean life against radioactive decay and τ_F the mean life against fall-out, a steady state requires that

$$F = \frac{P}{1 + \tau_F/\tau}$$

τ_F is not the mean life of moisture in the troposphere, which is much shorter. It is the mean interval between two successive condensations of moisture from the

same air mass. Its value as given by STEWART *et al.* (1957) is 30 days. From Fig. 2, and the average yield of 4·2 per cent, we find that the ^{7}Be production in the troposphere of the equatorial belt has the value $P = 6{\cdot}5 \times 10^{5}$ atoms/cm^{2} per year. Therefore, the expected fall-out F is

$$F = \frac{P}{1 + 30/77} = 4{\cdot}7 \times 10^{5} \text{ atoms/cm}^{2} \text{ per year.}$$

According to Table 2, the yearly fall-out in the tropics, estimated on the basis of rain water analyses at Kodaikanal and Bombay, is $4{\cdot}2 \times 10^{5}$ atoms/cm^{2} per year. The agreement is closer than one was justified to expect in view of the approximate nature of the fall-out data.

In an analogous manner one can calculate the expected fall-out of ^{35}S, ^{33}P and ^{32}P. The results are summarized in Table 3.

Table 3. Fall-out estimates in tropical latitudes (atoms/cm^{2} per year)

Isotope	Based on	
	Rain water analyses	Calculated isotope production
^{7}Be	$4{\cdot}2 \times 10^{5}$	$4{\cdot}7 \times 10^{5}$
^{35}S	31,000	6200
^{33}P	5800	2400
^{32}P	2700	1650

The agreement between calculated and measured fall-out is good for ^{7}Be and tolerable for ^{32}P, but the production of ^{33}P has been underestimated by more than a factor 2 and that of ^{35}S by a factor 5. This is probably connected with the fact that ^{7}Be and ^{32}P require comparable particle energies for production near threshold, while the threshold for the production of ^{33}P is somewhat lower and that of ^{35}S considerably lower. If this interpretation is correct, it implies that the star production calculated by LAL *et al.* (1958) and reproduced in Figs. 1, 2 and 3 refers only to stars in which the energy release exceeds about 40 or 50 MeV and that still smaller stars are very numerous, at least in the argon component. This point requires further investigation.

In any case, no plausible change in the assumed isotopic yield in argon stars or in the mean residence time τ_F of isotopes in the troposphere can account for the discrepancy between the observed fall-out ratio ^{7}Be/^{35}S of 13·5 and the calculated ratio of 75. In order to explain the discrepancy it is necessary to introduce some process which gives rise to ^{35}S without, at the same time, contributing to the production of ^{7}Be.

If the very small stars produced by fairly low energy neutrons are responsible for the excess over the calculated production of ^{35}S and ^{33}P, then the frequency of these stars must be directly proportional to the frequency of the slightly larger stars which give rise to these low-energy neutrons and whose altitude and latitude dependence has already been calculated. One should, therefore, get the correct

production rate of isotopes by simply replacing the calculated yield figures in the paper by LAL *et al.* (1958) by empirical ones which give the correct annual fall-out as deduced from rain water analyses.

We can then use Figs. 1 and 2, which show the star production rate in various parts of the atmosphere, and obtain the corresponding isotope production by multiplying the ordinates by the following yield factors σ_i:

$$\sigma = 4{\cdot}2 \times 10^{-2} \quad \text{for } {}^{7}\text{Be}$$
$$\sigma = 2{\cdot}4 \times 10^{-3} \quad \text{for } {}^{35}\text{S}$$
$$\sigma = 6{\cdot}5 \times 10^{-4} \quad \text{for } {}^{33}\text{P}$$
$$\sigma = 4{\cdot}0 \times 10^{-4} \quad \text{for } {}^{32}\text{P}$$

As far as ^{35}S is concerned, there remains, however, still the possibility mentioned in the earlier section, namely, that some of the fall-out could be due to causes other than cosmic radiation.*

4. THE CONCENTRATION OF ISOTOPES IN DIFFERENT AIR MASSES

In the previous section it was shown that the rate of star production per gramme of air, $S(h,\lambda)$, as a function of altitude h and of latitude λ is known fairly accurately for all values of these variables. Similarly, the average yield σ_i of each isotope i per nuclear disintegration can be estimated reasonably well. The change in the concentration of an isotope C_i in the interval between rains is then described by the differential equation

$$\frac{dC_i}{dt} = -\frac{C_i}{\tau_i} + \sigma_i S(t) \tag{1}$$

where τ_i is its mean life against decay. If we now make the plausible assumption that the last precipitation of moisture (at $t = 0$) removed all the activity previously accumulated, then the concentration at time t is given by

$$C_i(t) = \sigma_i \tau_i \exp(-t/\tau_i) \int_0^t \exp(t'/\tau_i) S[h(t'),\lambda(t')]\, dt' \tag{2}$$

The unknown functions $\lambda(t')$ and $h(t')$ describe the position of the air mass at any time $t' < t$ and, therefore, characterize its trajectory.

The isotope concentrations and also the ratios between the concentrations of isotopes with different half-lives are quite different for air masses which have descended from the stratosphere and for air masses which have remained in the troposphere. These differences are large compared to probable errors of measurement and will persist until the next precipitation.

In order to illustrate this point we shall solve equation (1) under certain simplifying assumptions:

(1) We assume sufficient convection in the troposphere to insure that every air mass spends an appropriate time in the various pressure intervals. We can then replace $S(h,\lambda)$ by its average value $\bar{S}_T$ for all altitudes, h, less than the

* *Note added in proof*—Measurements of the ^{35}S concentrations in rains during 1958 show that they were nearly three times higher than in 1957. On the other hand, the concentrations of ^{7}Be, ^{32}P and ^{33}P were comparable. This shows clearly that most of the ^{35}S observed in rain during the last two years was due to nuclear explosions.

height of the tropopause, h_T. The neglect of latitude dependence is justified because, in the troposphere, S is nearly independent of λ, as shown in Fig. 2. The vertical motions which ordinarily take place in the troposphere probably justify replacing S by its average value.

(2) We assume that any air mass which descends from the stratosphere had been there for a time long compared to the half-lives of the relevant isotopes. This assumption is supported by the data on bomb-produced activity fall-out, which indicate that the mean period of residence of air in the stratosphere must be of the order of several years.

(3) Above the tropopause, we have no justification for replacing $S(h,\lambda)$ by its average value. This region, where at medium and high latitudes most of the isotope production occurs, is stable. It is not known whether an exchange of air takes place between different layers of the stratosphere in a period of the order of or short compared to three months, the longest half-life with which we are concerned at present. Fig. 1 shows that, as long as we confine ourselves to the tropical belt or at any rate to latitudes less than 35°, the question whether or not there is mixing in the stratosphere does not affect the calculations, because the rate of nuclear disintegration in the layer close to the tropopause, $S(h_T)$, is almost the same as $\bar{S}_S$, the rate averaged over the entire stratosphere. At higher latitudes, however, this is no longer the case; there, the isotope production in the layer closest to the tropopause is considerably smaller than the average stratosphere value.

OL.
13
8/59

For the sake of definiteness, we shall assume that there is no appreciable mixing between layers in the stratosphere. (If this assumption is wrong and there is mixing also in the stratosphere, the difference between the radioactive contents of stratosphere and troposphere air will be enhanced over and above our sample calculation, especially in the polar zone.) With the assumption (1) to (3) and the help of Fig. 1 we can set:

$$S(h, \lambda) \simeq \bar{S}_T = 6{\cdot}7 \times 10^{-4} \text{ stars/g per sec for } h < h_T$$
$$S(h, \lambda) \simeq S(h_T) = 4{\cdot}0 \times 10^{-3} \text{ stars/g per sec for } h > h_T$$

Thus

$$S(h_T) \simeq 6\bar{S}_T,$$

We write down two solutions of equation (2):

(a) Air which has come to equilibrium in the stratosphere descends at the time $t = 0$ and spends a time t in the turbulent troposphere will have a concentration of radioisotopes given by:

$$C_i = 6{\cdot}7 \times 10^{-4}\, \sigma_i \tau_i \{1 + 5 \exp(-t/\tau_i)\} \text{ atoms/g}; \tag{3a}$$

(b) Air which does not spend any time in the stratosphere and which after being cleansed of radioactivity at a time $t = 0$ circulates for a time t in a turbulent troposphere, will have a concentration of radioisotopes given by

$$C_i(t) = 6{\cdot}7 \times 10^{-4}\, \sigma_i \tau_i \{1 - \exp(-t/\tau_i)\} \text{ atoms/g}. \tag{3b}$$

In Fig. 4, we have plotted $C_i(t)$ as given by equation (3a) and (3b) for ^{7}Be, ^{35}S, ^{33}P and ^{32}P. In Fig. 5, we have plotted the corresponding concentration ratios ^{7}Be/^{32}P, ^{35}S/^{32}P and ^{33}P/^{32}P.

It is evident from Fig. 4 that even a fairly rough determination of isotope concentration should be adequate for distinguishing between stratosphere and troposphere air and that the corresponding characteristics will be preserved for long periods. Fig. 5 shows that it is similarly possible to make this distinction on the basis of the concentration ratios of isotopes with widely different half-lives ($^{35}S/^{32}P$ and $^{7}Be/^{32}P$). Thus the cosmic-ray produced isotopes have the requisite properties which should make them useful for tracing large scale vertical and meridional motions in the atmosphere.

As a tool for studying air circulation, cosmic-ray produced radioactivity and the activity produced in the atmosphere by nuclear explosions can play complementary roles. The discussion of artificial radioactivity of the air is, however, outside the scope of this paper.

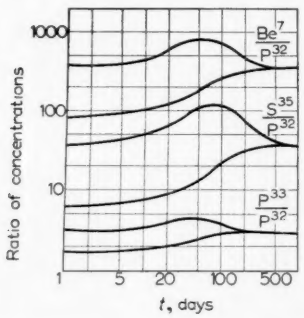

Fig. 5. The ratio in the concentration of different isotopes is given as a function of time for air irradiated under the same conditions which apply to Fig. 4.

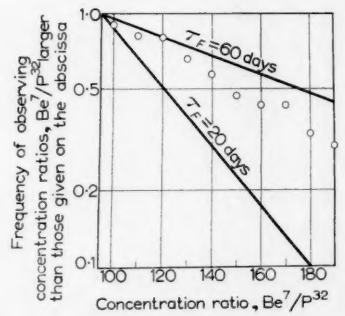

Fig. 6. The frequency distribution of different values of the ratio $^{7}Be/^{32}P$ is shown for rain-water samples collected in 1957.

Experimentally determined isotope ratios

The ratio in the concentration of two isotopes with different half-lives in rain water is a quantity which is of interest because it is independent of local meteorological conditions. In a given air mass, ratios between isotope concentrations are a function only of its radiation history; the same will be true in the moisture condensed from this air mass, not only for the ratio $^{33}P/^{32}P$ but also for the ratio of any other two radioisotopes, provided the scavenging action of the droplet formation is equally effective for both. Measurements of isotope ratios in particular rains may, therefore, be useful.

Table 4 gives a list of results from experiments in which water from individual rains was analysed for two or more isotopes. The measurements were made by GOEL *et al.* (1958). So far there are only twenty-one samples.

When comparing the results listed in Table 4 with the curves in Fig. 5, one sees that, if an appreciable amount of air from the stratosphere had entered into any of our samples, the $^{7}Be/^{32}P$ ratio should have been much higher than the highest ratio observed. The results so far obtained are, therefore, consistent with the well-founded and generally accepted belief that the entrance of large masses of stratosphere air into the equatorial tropopause occurs rarely, if at all.

VOL. 13 1958/5

PROC. INDIAN ACAD. SCI. VOL. XLIX, NO. 6, SECT. A, 1959

Table 4.

Date	Station	Be^7	S^{35} (atoms/cm^3)	P^{32}	Ratios Be^7/S^{35}	Ratios Be^7/P^{32}	Ratios S^{35}/P^{32}	Remarks
20–7–57	Bombay	9000 ± 500 9200 ± 500	690 ± 100	44 ± 4	13 ± 2·5	207 ± 25	15·7 ± 2·5	
22–7–57	Bombay	5700 ± 250 5750 ± 250	690 ± 160	26 ± 3	8·3 ± 2	220 ± 25	26·5 ± 6·5	
26–7–57	Bombay	3500 ± 250 3200 ± 250	—	36 ± 4	—	95 ± 12	—	
5–8–57	Bombay	3400 ± 200 3600 ± 200	—	32 ± 3	—	110 ± 13	—	
11–8–57	Bombay	5000 ± 250 5400 ± 250	—	31 ± 3	—	160 ± 17	—	
16–8–57	Bombay	5900 ± 700 5400 ± 400	—	19 ± 2	—	290 ± 35	—	
18–8–57	Bombay	2700 ± 150 2400 ± 150	—	18 ± 2	—	140 ± 15	—	
20–8–57	Bombay	3300 ± 250 3100 ± 250 3200 ± 250	—	26 ± 2 22 ± 2	—	130 ± 15	—	
22–8–57	Bombay	3500 ± 250 3100 ± 600	—	25 ± 3	—	130 ± 15	—	

Table 4—*continued*

Date	Station	Be^7	S^{35} (atoms/cm^3)	P^{32}	Ratios Be^7/S^{35}	Be^7/P^{32}	S^{35}/P^{32}	Remarks
10–11–57	Bombay	2300 ± 150 2400 ± 150	—	13 ± 1	—	180 ± 20	—	
	Kodaikanal	2300 ± 100	125 ± 15	21 ± 1	18·5 ± 3	110 ± 10	6 ± 1	
11–11–57	Bombay	1700 ± 200 1800 ± 200 1900 ± 200	130 ± 15 110 ± 15	18 ± 1 21 ± 1 17 ± 2 19 ± 1	15 ± 2	95 ± 15	6 ± 1	
20–11–57	Srinagar	3600 ± 300	245 ± 15	—	15 ± 2	—	—	0200–1145 hours
	Pathankot	9500 ± 500	460 ± 50	—	21 ± 3	—	—	1230–1348 hours
	Delhi	7100 ± 300	260 ± 100	—	27 ± 10	—	—	1400–1515 hours
	Mussoorie	5000 ± 300	275 ± 30	—	18 ± 2	—	—	1730 hours
29–11–57	Kodaikanal	1800 ± 100	220 ± 100	17 ± 2	8·2 ± 4	105 ± 15	13 ± 6	
2–12–57	Srinagar	5500 ± 500	420 ± 70	—	13 ± 3	—	—	
4–12–57	Kodaikanal	1250 ± 150	125 ± 40	—	10 ± 3	—	—	
7–12–57	Pathankot	7400 ± 400	650 ± 65	—	11 ± 2	—	—	
11–12–57	Pathankot	3400 ± 300	170 ± 20	—	20 ± 3	—	—	0000–2300 hours
	Delhi	2300 ± 600	140 ± 20	—	16 ± 4	—	—	1515–2130 hours
12–12–57	Mussoorie	2800 ± 240	350 ± 100	—	8 ± 3	—	—	
18–12–57	Kodaikanal	1150 ± 100	125 ± 80	—	9 ± 6	—	—	

Double and triple determinations on the same date and at the same station refer to homogenized samples.

VOL 13 1958/

If we then assume that in all of the rains analysed so far, the corresponding air mass circulated exclusively within the troposphere, we can try to find "τ_F", the average interval between two consecutive precipitations involving the same air mass. One can fit the frequency of occurrence of various ratios $^{7}Be/^{32}P$ to a distribution function of the form $\exp(-t/\tau_F)$, as shown in Fig. 6. The experimental points fit such a distribution best if one choses $\tau_F \simeq 40$ days. τ_F is to be interpreted as the mean interval between successive precipitations and removals of activity involving the same air mass. It is somewhat higher than the value of 30 days deduced by STEWART *et al.* (1957) from the fall-out of bomb-produced activity.

CONCLUSIONS

Existing data on the frequency of cosmic-ray induced nuclear disintegrations and on cross-sections for high-energy nuclear reactions are sufficient to calculate the production of the radioisotopes ^{7}Be and ^{32}P in all parts of the earth's atmosphere. Estimated yearly fall-out rates based on the analysis of rain water over a 2 year period are consistent with the calculated rates of production. Therefore, it is probable that precipitation effectively removes these isotopes from the corresponding air mass and that dry fall-out represents a comparatively small fraction of the total.

The observed fall-out of the radioisotopes ^{33}P and ^{35}S is higher than the value obtained from similar calculations. This is probably due to the fact that their threshold energies for production are lower than those of ^{7}Be and ^{32}P and that the number of very small one- and two-prong stars in argon taken from cloud chamber experiments has been underestimated. In the case of ^{35}S, a contribution of artificially created activity to the fall-out in 1955, 1956 and 1957 cannot be ruled out entirely.*

Isotope production near the tropopause, and also the production averaged over the entire troposphere, is nearly independent of geographic latitude. There is, however, a strong latitude effect in the higher layers of the stratosphere and a rapid increase of production with altitude at all geographic latitudes.

Calculations show that the concentration of ^{7}Be, ^{35}S, ^{33}P and ^{32}P per gramme of air in the stratosphere must be much higher than the highest values which can be reached in air which remains in the troposphere. The long average residence time of air masses in the stratosphere which is generally assumed must lead to ratios between the concentration of long-lived to shorter-lived isotopes, which are much higher than the corresponding ratios in troposphere air.

All these properties of the cosmic-ray induced radioactivity make it useful as a tracer for the study of large scale air circulation. Preliminary results on the rate of isotope concentrations in tropical rains support the view that substantial intrusions of stratosphere air into the tropical troposphere are rare or absent. The results also indicate a mean interval between successive removals of radioactivity of the order of 40 days.

Acknowledgement—I am greatly indebted to Professor K. R. RAMANATHAN for reading the manuscript and for making valuable suggestions.

* See footnote on page 364.

References

Arnold J. R. and Al-Salih H.	1955	*Science* **121,** 451.
Arnold J. R.	1956	*Science* **124,** 584.
Benioff P. A.	1956	*Phys. Rev.* **104,** 1122.
Cruikshank A. J., Cowper G. and Grumitt W. E.	1956	*Canad. J. Chem.* **34,** 214.
Faltings V. and Harteck P.	1950	*Z. Naturf.* **5a,** 438.
Fuller M. O.	1954	*Disintegration of Oxygen by 300-MeV Neutrons.* Thesis, UCRL–2699.
Goel P. S., Jha S., Lal D., Radhakrishna P. and Rama Thor.	1956	*Nucl. Phys.* **1,** 196.
Goel P. S.	1956	*Nature, Lond.* **178,** 1458.
Goel P. S., Kharkar D. P., Lal D., Narasappaya N., Peters B. and Yatirajam V.	1956	*Deep-Sea Res.* **4,** 202.
Goel P. S., Narasappaya N., Prabhakara C., Rama Thor and Zutshi P. K.	1950	*Tellus.* In press.
Kaufmann S. and Libby W. F.	1954	*Phys. Rev.* **93,** 1337.
Kellogg D. A.	1953	*Phys. Rev.* **90,** 224.
Libby W. F.	1952	*Radiocarbon Dating.* University of Chicago Press.
Lal D., Narasappaya N. and Zutshi P. K.	1957	*Nucl. Phys.* **3,** 69.
Lal D.	1958	*Investigations of Nuclear Interactions Produced by Cosmic Rays.* Thesis.
Lal D., Malhotra P. K. and Peters B.	1958	*J. Atmosph. Terr. Phys.* **12,** 306
Marquèz L. and Costa N. L.	1955	*Nuovo Cim.* **2,** 1038.
Marquez L., Costa N. L. and Almeida I. G.	1957	*Nuovo Cim.* **6,** 1292.
McDonald F. B.	1958	*Phys. Rev.* **109,** 1367.
Neher H. V. and Anderson H.	1958	*Phys. Rev.* **109,** 608.
Peters B.	1955	*Proc. Ind. Acad. Sci.* **41,** 67.
Peters B.	1957	*Z. Phys.* **148,** 93.
Rama Thor and Zutshi P. K.	1958	*Tellus* **10.**
Rudstam G.	1956	*Spallation of Medium Weight Elements* p.168. Gustaf Werner Institute for Nuclear Chemistry, University of Uppsala.
Stewart N. G., Osmond R. G. D., Crooks R. N. and Fisher E. M.	1957	*The Worldwide Deposition of Long-Lived Fission Products from Nuclear Test Explosions.* A.E.R.E. HP/R 2354.
Winsberg L.	1956	*Geochim. et Cosmochim. Acta* **9,** 183.

VOL
13
1958/

Journal of Atmospheric and Terrestrial Physics, 1959, Vol. 13, pp. 371 to 381. Pergamon Press Ltd. Printed in Northern Ireland

RESEARCH NOTES

Measurements of magnetic declination during the solar eclipse of 23 October 1957

(*Received* 30 *April* 1958)

IT is well known that the reduction in the electron and ion content of the atmosphere during a solar eclipse should affect the intensity of the electric currents which produce the transient magnetic variations at the earth's surface; CHAPMAN (1956) has concluded that the expected magnetic changes will be small. EGEDAL (1956) has indicated that the comparison

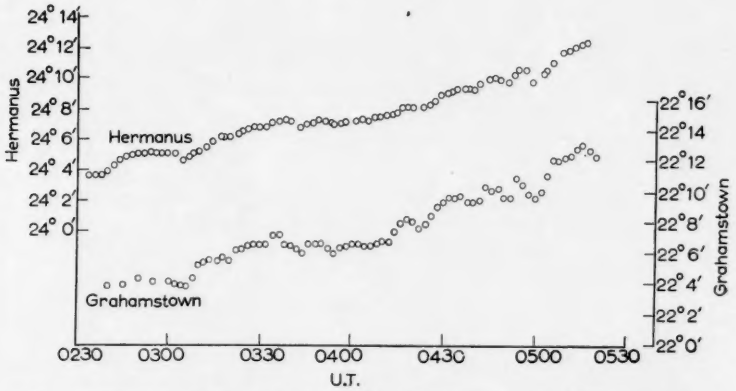

Fig. 1. Westerly declination observed at Grahamstown and Hermanus.

of declination measurements obtained during an eclipse by several observatories is valuable, and has suggested that a study of the magnitude of the area over which eclipse effects are detected might give information concerning the distribution of atmospheric electric currents.

During the eclipse of 23 October 1957 the authors made measurements of magnetic declination at the Union Magnetic Observatory, Hermanus (lat. 34° 25·5′ S, long. 19° 13·5′ E) and at Rhodes University, Grahamstown (lat. 33° 16·8′ S, long. 26° 29·4′ E). They feel that these measurements might provide useful control for investigations carried out by expeditions nearer the centre of the eclipse. The apparatus used could detect changes of the order of one quarter of a minute of arc.

Figure 1 shows the variation of magnetic declination observed at the two stations. Neither curve shows any noticeable eclipse effect and the results resemble those which were obtained on control days. At a point 100 km above Grahamstown sunrise occurred at

02·35 UT; the eclipse began at 02·56 UT, attained its maximum at 03·43 UT (when the fraction of the sun's disc obscured was 46 per cent) and ended at 04·31 UT.

Department of Physics H. Helm
Rhodes University, Grahamstown J. W. King
Union of South Africa
Magnetic Observatory, Hermanus A. M. van Wijk
Union of South Africa

References

Chapman S. 1956 *Solar Eclipses and the Ionosphere* p. 221. Supplement No. 6 to *J. Atmosph. Terr. Phys.*

Egedal J. 1956 *Solar Eclipses and the Ionosphere* p. 228. Supplement No. 6 to *J. Atmosph. Terr. Phys.*

A comparison of the critical frequency of the *F2*-layer between Rarotonga and Maui

(*Received* 16 *June* 1958)

Appleton (1954) first noticed a systematic pattern of behaviour in the *F2*-region by plotting f_0F2 against geomagnetic latitude. Here an attempt is made to answer the question on a purely empirical basis "Is there any systematic difference in diurnal variation of f_0F2 at two magnetically conjugate points?"

The stations at Rarotonga and Maui present an ideal opportunity for such a study as they have similar geomagnetic and geographic co-ordinates. These co-ordinates are:

Station	Geographic		Geomagnetic
	Lat.	Long.	Lat.
Rarotonga	22·0°S	200·0°E	21·7°S
Maui	20·8°N	203·5°E	20·9°N

The data examined were the differences of f_0F2 between Rarotonga and Maui for the years 1950 to 1954. These were found to have two components, an annual and a seasonal.

(1) *Annual*

This was of the form shown in Fig. 1(a). The form of the variation was self-consistent when examined on a yearly basis as shown in Fig. 1(b). There is a possibility that the amplitude is dependent on the sun-spot cycle but not to any great extent.

VOL 13 1958/

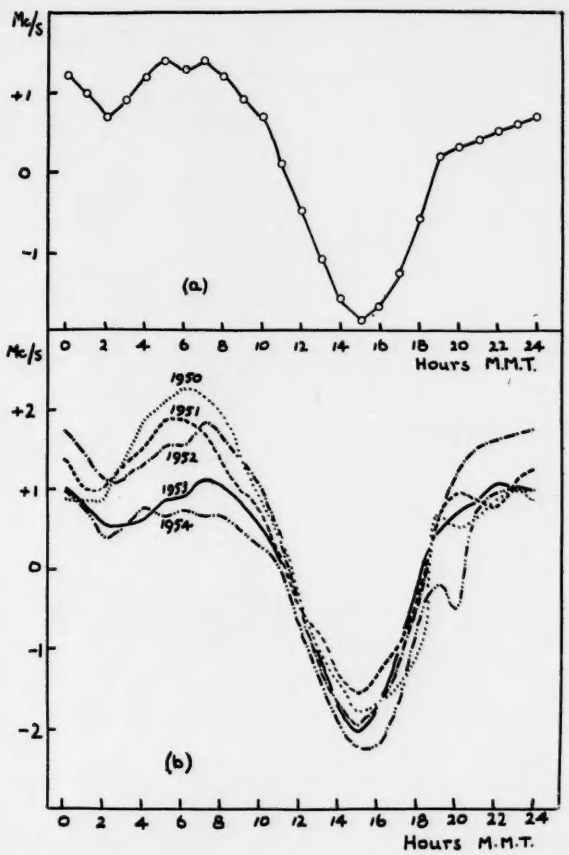

Fig. 1

(a). The mean annual component of f_0F2 Rarotonga minus f_0F2 Maui. Based on data from 1950 to 1954.

(b). The annual component for individual years showing the self-consistency of the component.

(2) *Seasonal*

On subtracting out the annual variation from the monthly variation of the difference, a seasonal component was left. These differences were obtained with a time lag of 6 months between stations in order to eliminate any variation due to solar zenith angle (i.e. the Maui July diurnal variation was subtracted from the Rarotonga January variation and then the mean seasonal diurnal variation of the difference removed.) The resulting variation showed a seasonal dependence, being out of phase at six monthly intervals. The amplitude of the variation depended on solar declination.

An examination of f_0F2 for Tananarive (geographic latitude 18·8°N, longitude 47·8°E; geomagnetic latitude 25°N) showed variations of the same form as Rarotonga suggesting that the differences are part of a general north–south anomaly and do not depend on magnetic declination. Unfortunately there is not another station reasonably close to the fourth singular point where the geographic and geomagnetic co-ordinates are similar.

This line of enquiry has led to the following conclusions, the critical frequency of the

F2-layer appears to be perturbed in two main ways. Firstly an annual component which is part of a general north–south anomaly and secondly a seasonal component which depends on solar declination both in amplitude and phase. It is fully realized that it is dangerous to reduce the diurnal variation of f_0F2 to the sum of independent variations but the striking pattern which emerges by this method gives some vindication of its use.

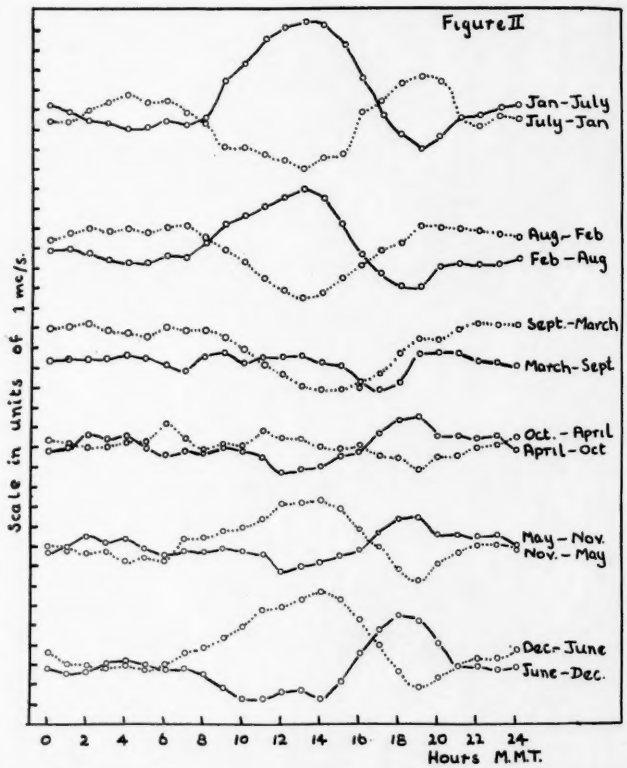

Fig. 2. The seasonal component. The curve marked "Jan.–July" indicates the diurnal variation of f_0F2 Rarotonga for January minus f_0F2 Maui for July after the annual component has been removed. This shows the peculiar progression of the curves throughout the year.

Acknowledgements—I am indebted to Mr. J. W. Beagley, Superintendent of the Christchurch Geophysical Observatory, Department of Scientific and Industrial Research, New Zealand, for suggesting this work.

C. H. Cummack

Geophysical Observatory
Department Scientific and Industrial Research
New Zealand

Reference

Appleton E. V. 1954 *J. Atmosph. Terr. Phys.* **5**, 6.

VOL. 13 1958/5

Earth-current variations of different period in the observatorium near Nagycenk

(*Received* 8 *July* 1958)

THE Geophysical Observatory of the Hungarian Academy of Sciences deals chiefly with the distribution of the earth current variations of different period. For this purpose we divided the frequency spectrum into five bands (the periods are 1:0–2′, 2:2–6′, 3:6–12′, 4:12–24′, 5:24–60′). The activity of the bands is characterized by a telluric index, on the basis of the daily mean amplitudes (i.e., we have not appropriate number of data on the daily mean amplitudes, so we cannot follow the distribution, introduced by BARTELS, with the limits between the indices.) The scale of these indices is approximately logarithmic, but they must be regarded as preliminary ones, because of the unsatisfactory long period of observation. So the mean indices for the single bands are different. Studying the mean daily amplitudes, our attention was attracted by the fact that the maximal activity of bands 2 and 5 occurred 1–2 days before that of bands 3 and 4. Thereupon we made an examination choosing those days on which the index of band 5 reached or exceeded 6. We took into consideration only those days before which the index of band 5 had been smaller than 6 for at least 2 days. We wanted to avoid the same disturbance occurring twice in our calculation. The mean index for each frequency band was calculated for 2 days before and 5 days after those days.

Table 1. Mean indices in the five frequency bands about the chosen days (twenty-four cases in all)

Band	$n-2$	$n-1$	n	$n+1$	$n+2$	$n+3$	$n+4$	$n+5$	$n+6$	Average of 9 months
1	3·1	3·3	3·9	3·8	3·5	3·9	3·4	3·9	3·7	3·92
2	3·7	3·8	4·5	4·3	4·0	4·1	4·0	3·8	4·0	3·95
3	2·6	2·9	3·3	3·5	3·3	3·0	2·7	2·8	2·7	2·91
4	4·2	4·2	4·7	5·1	4·6	4·4	4·4	4·2	4·4	4·11
5	3·5	3·8	6·2	5·3	4·9	4·8	4·5	4·8	4·3	4·34

As Table 1 shows the phenomenon described does appear, the maximal activity of band 3 and 4 appeared 1 day later.

For controlling we calculated similarly the mean indices for those days, on which the index of band 4 reached 6. In this case the results confirm the preceding ones, although not so definitely (Table 1). The maximal activity appears in all bands later than in band 4, but

Table 2. Mean indices about the maximal activity of band 4 (twenty cases in all)

Band	$n-2$	$n-1$	n	$n+1$	$n+2$	$n+3$
1	3·4	3·3	3·6	4·3	4·6	3·6
2	3·2	3·8	4·3	5·2	4·6	3·6
3	2·3	2·2	3·6	3·8	3·6	3·0
4	3·8	3·9	6·5	5·6	5·0	4·4
5	4·2	5·1	5·1	5·2	4·9	4·6

the increase in bands 2 and 5 is already important on the day before the disturbance; in bands 3 and 4, however, it begins only on the day of the disturbance. The maximum of

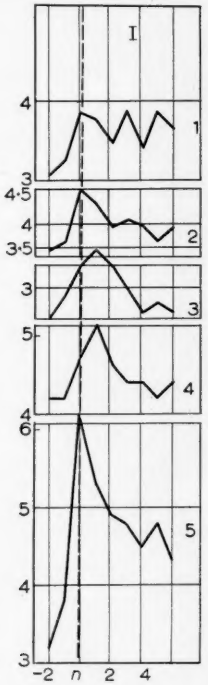

Fig. 1

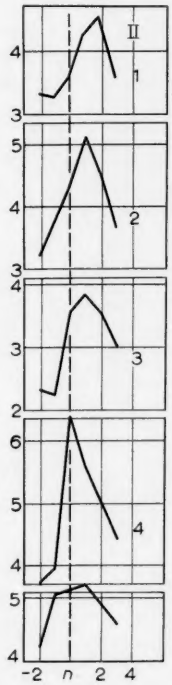

Fig. 2

band 1 occurs 2 days later. (In Table 1 there is a maximum on day $n + 3$ also.) It may be mentioned that, though the time for observation has been relatively short, a similar phenomenon can be concluded in the seasonal distribution. About aequinoctes bands 1, 2 and 5, after them bands 3 and 4 are the most active. Besides bands 2 and 5 often appear together, as bay and pulsation.

J. Verö

Geophysical Research Laboratory
Hungarian Academy of Sciences
Sopron, Hungary

VOL.
13
1958/5

References

Bartels J. 1958 *Z. Geophys.* **14**, 68.
Ádám A. and Verö J. 1958 *Geofis. Pur. Appl.* **39**, 126.
Staff of Geophys. Res. Lab., Hung. Acad. Sci. 1958 *Acta Tech. Hung.* To be published

Satellite Doppler measurements and the ionosphere

(*Received* 31 *July* 1958)

An analysis has been made of the effect of the ionosphere on the simultaneous Doppler frequency shifts of the 20 and 40 Mc/s signals from the artificial satellite *Sputnik* I (1957α).

An outline of the method of analysis and preliminary results are presented here. A detailed account of the investigation will be published shortly.

The Doppler frequency shift Δf of a signal of frequency f_0 from an emitter travelling with velocity V in the ionosphere where the refractive index is μ_s has been shown (HIBBERD, 1958) to be

$$\Delta f = f - f_0 = \frac{f_0 V \mu_s}{c} (\cos \alpha \sin \psi_s - \cos \beta \cos \psi_s) \tag{1}$$

where α is the angle between the velocity vector V and the normal to the earth radial direction that lies in the plane of propagation of the signal from satellite to receiver, β is the angle between V and the outward radial direction, and ψ_s is the angle that the observed ray makes, as it leaves the satellite, with the inward radial direction.

Quantities associated with the 20 and 40 Mc/s signals are denoted by $'$ and $''$ respectively and the subscript $_0$ denotes the frequency of a signal as it is emitted from the satellite transmitter. It is convenient to extract the ionospheric effect from the observed data by considering the difference $2f' - f''$ at each instant. From equation (1) we can write for the frequency f' of the 20 Mc/s signal as it is received:

$$f' = f_0' + \frac{f_0' V \mu_s'}{c} (\cos \alpha \sin \psi_s' - \cos \beta \cos \psi_s')$$

A similar expression can be written for the 40 Mc/s frequency f''. The difference $2f' - f''$ can then be shown to be:

$$2f' - f'' = D + \frac{DV\mu_s'}{c} (\cos \alpha \sin \psi_s' - \cos \beta \cos \psi_s') + \frac{Vf_0''}{c} [\cos \alpha (\mu_s' \sin \psi_s' - \mu_s'' \sin \psi_s'') - \cos \beta (\mu_s' \cos \psi_s' - \mu_s'' \cos \psi_s'')] \tag{2}$$

where $D = 2f_0' - f_0''$. For *Sputnik* I, $D \sim 7$ kc/s and $V \sim 7$ km/sec, so that the second term in (2) does not exceed 0·2 c/s.

In the absence of the ionosphere $\mu_s' = \mu_s''$ and $\psi_s' = \psi_s''$ and then the third term of equation (2) is zero. A graph of $2f' - f''$ against time, if the ionosphere were absent would thus be a straight line at constant frequency D on which is superimposed a small fluctuation not exceeding 0·2 c/s. Graphs of $2f' - f''$ plotted from experimental observations for some night-time transits when the satellite was effectively below the ionosphere yielded such a straight line.

By considering in turn the variation with time of each of the terms in equation (2), it can be shown that when the satellite is travelling in the ionosphere, and rising, the graph of $2f' - f''$ against time should take the form shown in Fig. 1.

A detailed examination has been made of all Doppler measurements made by the British Post Office Frequency Measuring Stations at Baldock and Banbury. Those records which were sufficiently extensive on both frequencies, for which the signals were sufficiently strong for accurate measurements to have been obtained, and which were otherwise smooth and regular, all gave the predicted type of variation of $2f' - f''$. Although these Post Office records were generally very good and are perhaps the best available, because of the very small magnitude of the effect sought, only a few such curves were sufficiently precise and extensive for an analysis of them to be worth attempting.

The transit that has been analysed in detail is that of 0342 hours on 17 October 1957, observed at Baldock. Basically the method consists of adopting a model ionosphere and from this, and the known elements of the orbit, computing in turn each of the quantities

in the third term on the right-hand side of equation (2) for comparison with the observed values of $2f' - f''$.

Because the computations are very lengthy and in the first instance have been done manually, a simple model ionosphere with uniform electron concentration was adopted. The choice of the height of the lower boundary of the model and its electron concentration was guided by the $N(h)$ curves computed by the Radio Section of the Cavendish Laboratory from the $h'(f)$ records taken by the Radio Research Station at Slough at 0300 and 0400

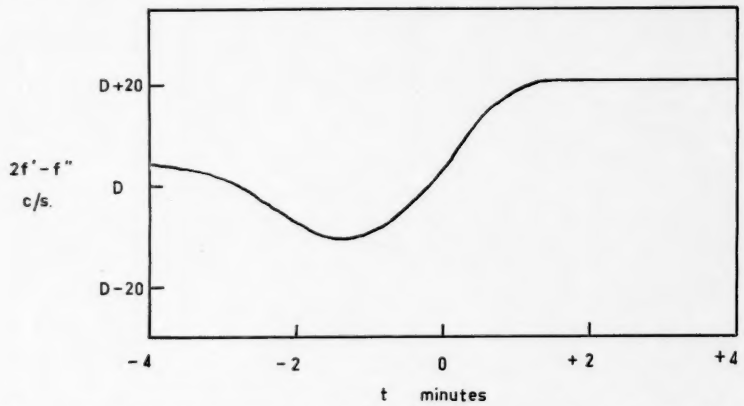

Fig. 1. This shows the manner in which the difference $2f' - f''$, for the observed frequencies f' and f'', varies with time t measured from $t = 0$ at the instant of closest approach to the observer. D is the difference $2f_0' - f_0''$, where f_0 indicates the frequency of the emitter.

VOL
13
1958/

hours. The orbit elements used were those of the Mullard Radio Astronomy Observatory of the Cavendish Laboratory (*Nature*, 1957). From the latter the values of V, α, β and the altitude of the satellite at a number of successive instants near the time of closest approach to Baldock ($t = 0$) were computed. For each of these the value of ψ_s corresponding to minimum optical path between satellite and receiver was calculated.

Because in equation (2) the first term is constant and the second term is less than 0·2 c/s, the third term

$$\frac{Vf_0''}{c}[\cos\alpha(\mu_s'\sin\psi_s' - \mu_s''\sin\psi_s'') - \cos\beta(\mu_s'\cos\psi_s' - \mu_s''\cos\psi_s'')] \qquad (3)$$

differs from $2f' - f''$ solely by an arbitrary constant and (3) varies with time in the same manner as $2f' - f''$. The appropriate values of all quantities computed above for each instant were substituted into equation (3). The computed curve of expression (3) against time was found to be almost the same shape as the observed curve of $2f' - f''$. However, the magnitude of the dip in the computed curve was less than that in the observed curve and there was also a time displacement of the position of the minimum. These differences are associated with the crude ionospheric model used in the computations and primarily to the neglect of the decrease in electron concentration above the F-maximum. This will be discussed further in a later paper. In view of the crudeness of the model, the unjustified assumption that the ionosphere is horizontally uniform over a large distance, and the uncertainties in the orbit data, the agreement is considered satisfactory. It shows that the observed Doppler ionospheric effect is consistent with what is otherwise known of the ionosphere below the F-maximum.

The procedure can be adapted for computation by a digital computer and this would

need to be done for any more detailed analysis. In this way it would be possible to include the known $N(h)$ profile up to the F-maximum and find the model for the upper ionosphere that gives the best agreement with experiment.

Mention should be made of the precision required, for ionospheric purposes, in Doppler measurements at the frequencies used. Each frequency may be changing at a rate of up to 10 c/s per sec and, since one requires to know $2f' - f''$ to within about 1 c/s, it is necessary to measure the two frequencies simultaneously (to within at least 0·1 sec of each other) and each to an accuracy of better than 1 c/s. This is probably near the limit of the present best measuring techniques.

The small departures ($\sim$5 c/s) from the smooth Doppler curves, which are sometimes observed, may not be entirely due to measuring inaccuracy but may possibly be associated with scintillations produced during the passage of the signals through ionospheric irregularities. If this be so, then scintillations will be an important factor limiting the precision attainable.

This work was carried out at the Cavendish Laboratory where we were both fortunate to spend a year's sabbatical leave. We gratefully acknowledge the assistance of a Nuffield Foundation Fellowship (J. A. T.) and a British Council Scholarship (F. H. H.). We thank the Post Office for supplying the Doppler data and the Officers in charge at Baldock and Banbury for their cordial and helpful discussions with us of their methods of measurement and the accuracy of their data.

J. A. Thomas
F. H. Hibberd

University of Queensland, Brisbane, Australia, and
University of New England, Armidale, N.S.W., Australia

VOL. 13 58/59

References

Hibberd F. H. 1958 *J. Atmosph. Terr. Phys.* **12,** 338.
Mullard Radio Astronomy Observatory Staff 1957 *Nature, Lond.* **180,** 879.

Le renforcement du champ en ondes longues et les evanouissements en ondes courtes

(*Received* 28 *July* 1958)

Au Laboratoire Ionosphérique à Rabat, les perturbations ionosphériques à débuts brusques (Pidb ou Sid) sont observées au moyen de l'enregistrement du champ de la station de radiodiffusion d'Allouis (6200 kc/s) et de l'enregistrement du niveau moyen des atmosphériques sur 27 kc/s.

On sait que les éruptions chromosphériques provoquent, dans la majorité des cas, un évanouissement du champ en ondes décamétriques (ici sur Allouis) et, simultanément, un renforcement du champ sur ondes très longues (ici sur environ 10,000 m).

On constate cependant que tous les évanouissements en ondes courtes ne sont pas accompagnés d'un renforcement du niveau moyen des atmosphériques sur ondes longues. Cela peut être attribué soit au comportement différent de l'ionosphère sous l'influence de différentes formes d'éruptions chromosphériques, soit au fait que l'action de l'ionosphère sur la propagation des composantes enregistrées dépend de la distance des foyers d'atmosphériques.

Nous avons tenté d'élucider ce point en effectuant l'enregistrement d'une station de radiodiffusion en ondes longues, par exemple: Droitwich (200 kc/s). Nous avons alors constaté que tous les évanouissements sur Allouis étaient accompagnés d'une variation brutale du champ de Droitwich, variation qui dans la majorité des cas est un renforcement précédé ou non d'une très brève diminution.

Par les études sur le spectre des atmosphériques effectuées par BUREAU, on savait que les éruptions chromosphériques affectaient parfois les enregistrements de niveau moyen jusqu'à la fréquence de 150 kc/s; mais la raréfaction de la corrélation était attribuée à l'élévation de la fréquence par rapport à celle de 27 kc/s considérée comme optimum.

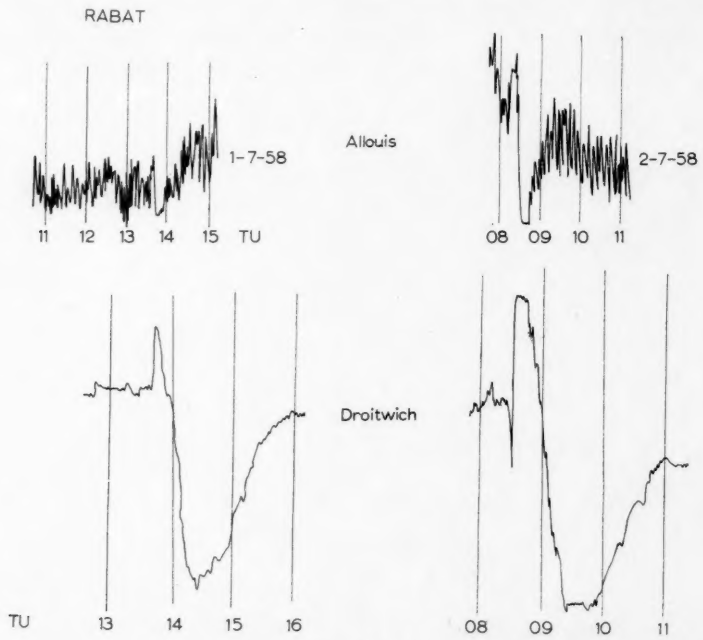

Fig. 1

Au moment d'un évanouissement en ondes courtes, le champ de Droitwich commence parfois par décroître brusquement, puis il remonte aussi brusquement, dans un laps de temps de 1–3 min. Le même phénomène avait été signalé par BUREAU (1947) sur le niveau moyen des atmosphériques sur 150 kc/s, mais le fait que ce niveau était tantôt renforcé, tantôt atténué, avait fait conclure par l'auteur que la fréquence de 150 kc/s était la fréquence de transition entre l'atténuation et le renforcement. Il apparaît, d'après les résultats obtenus ici sur Droitwich, que la fréquence de transition est située encore au-dessus de 200 kc/s et que les alternatives observées par BUREAU sur les atmosphériques paraissent être plutôt la conséquence de la variation de la répartition géographique des sources, par rapport à la station d'observation (un enregistrement récent de champ de Luxembourg montre que les renforcements synchrones avec les évanouissements sur Allouis se manifestent aussi à la fréquence de 236 kc/s).

L'examen des variations de champ de Droitwich fait apparaître de plus les caractères suivants: le renforcement qui suit la variation brusque se développe dans un temps de

VOL
13
1958/

l'ordre du quart d'heure, puis il est suivi d'une décroissance progressive, parfois trés profonde, suivie elle-même d'une remontée également progressive, les durées de ces deux dernières variations étant chacune de l'ordre de l'heure.

Le départ brusque correspond à l'arrivée dans l'ionosphère d'un rayonnement ionisant plus pénétrant que le rayonnement normal; par sa pénétration plus profonde, le gradient d'ionisation peut diminuer et entraîner une réduction du coefficient de réflexion, d'où la diminution rapide du champ; mais très vite il va se former un nouveau maximum à une altitude plus basse, au-dessous de laquelle un gradient élevé va apparaître à nouveau, d'où le renforcement du champ. L'absence d'affaiblissement préalable pourrait être due à la plus ou moins grande brusquerie du phénomène par rapport à la constante de temps de l'appareil (une expérience toute récente paraît confirmer cette façon de voir).

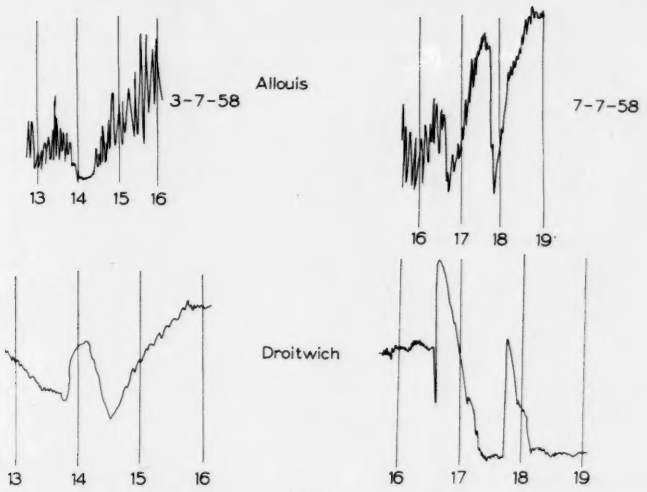

Fig. 2

Par contre, les phénomènes ultérieurs plus lents paraissent être dûs à l'évolution thermodynamique de l'ionosphère elle-même.

Quoi qu'il en soit, nous pensons pouvoir supprimer les enregistrements d'atmosphériques effectués uniquement dans le but de détecter les Pidb et les remplacer par un enregistrement permanent de Droitwich, dont les indications paraissent beaucoup plus sûres et plus prometteuses d'enseignements.

Institut Scientifique Cherifieu,
Laboratorie Ionosphere,
Avenue Biarnay, Rabat, Morocco.

A. Haubert

Reference

Bureau R. 1947 *Onde Electrique*, p. 239.

Journal of Atmospheric and Terrestrial Physics, 1959, Vol. 13, p. 382. Pergamon Press Ltd. Printed in Northern Ireland

LETTER TO THE EDITOR

The origin of the current nomenclature for the ionospheric layers

RECENTLY, I was fortunate enough to uncover some old correspondence between Dr. J. H. DELLINGER and Sir EDWARD APPLETON revealing the manner in which the layers came to be named by Sir Edward. At the time, Dr. Dellinger was chief of the Interservice Radio Propagation Laboratory, National Bureau of Standards, Washington, D.C. and Sir Edward was Secretary of the Department of Scientific and Industrial Research of England.

The following material is presented with the permission of both Dr. Dellinger and Sir Edward Appleton.

On 13 February 1943 Dr. Dellinger stated, in the middle of a letter addressed to Sir Edward Appleton:

> Here is a small question on history. I have often been asked how you happened to start the names *D*, *E* and *F*, for the ionosphere layers. I would be interested to know what was in your mind.

In a letter dated 20 March 1943 Sir EDWARD replied:

> I was very interested to have your question on the early history of the nomenclature for the ionosphere layers. The story of how I came to give them the names *D*, *E* and *F* is really a very simple one. In the early work with our broadcasting wavelengths, I obtained reflections from the Kennelly-Heaviside layer, and on my diagrams I used the letter *E* for the electric vector of the down-coming wave. When therefore in the winter of 1925 I found that I could get reflections from a higher and completely different layer, I used the term *F* for the electric vector of the waves reflected from it. Then at about the same time I got occasional reflections from a very low height and so naturally used the letter *D* for the electric vector of the return waves. Then I suddenly realized that I must name these discrete strata and being rather fearful of assuming any finality about my measurements I felt I ought not to call them layers *A*, *B* and *C* since there might be undiscovered layers both below and above them. I therefore felt that the original designation for the electric vector *D*, *E* and *F* might be used for the layers themselves since there was considerable latitude for the naming of any layers that might come to light as a result of further work. I am afraid that that is all there is in the story.

R. SILBERSTEIN

National Bureau of Standards,
Boulder Laboratories,
Boulder, Colorado, U.S.A.

VOL.
13
1958/5

Journal of Atmospheric and Terrestrial Physics, 1959, Vol. 13, pp. 383 to 384. Pergamon Press Ltd. Printed in Northern Ireland

Book reviews

Handbuch der Physik. *Gasentladungen II.* Band XXII. *Edited by* S. FLÜGGE. (**Encyclopedia of Physics.** *Gas Discharges II.* Vol. XXII). Springer, Berlin, 1956. vii + 652 pp., £10. 12s.

WITHIN the last decade growing numbers of research workers have found their interests drawn to some aspect of gaseous discharges, and many must have been bewildered by the volume and diversity of the literature on this subject which has been accumulating during the last century. One might say that the gas discharge might be easier to understand if less had been written about it, for in the light of recent advances much that has appeared can be disregarded. There has been a growing need for a book where leading authorities in the different regimes of the discharge set down what they themselves regard as being fundamental to the understanding of their particular field. Volume XXII of this new Handbuch does just this and thereby establishes itself as one of the best modern references on the subject which can be recommended to the research worker.

The volume contains seven chapters, contributed by authorities with well-established reputations, three from America, three from Britain and one from Germany. It opens with an account of the basic processes in ionization growth and breakdown, by F. LLEWELLYN JONES. Then follows quite a long section by G. FRANCIS detailing the general properties of the low-pressure gas discharge, and a concise but most valuable chapter by R. G. FOWLER on the mechanisms of radiation from low-pressure discharges. One hundred and ninety pages are then devoted to the physics of arcs and thermal plasmas by W. FINKELNBURG and H. MAEKER, in German, followed by two chapters on what might be called engineering aspects of breakdown: the first, by L. B. LOEB, deals with breakdown under impulse potentials, and the second, by S. C. BROWN, treats breakdown under alternating fields. B. F. J. SCHONLAND contributes the final chapter on the most energetic and spectacular discharge of all, lightning.

In this particular volume not much is said about the influence of magnetic fields, and the astrophysicist will find nothing about the new subject of magnetohydrodynamics. Solar discharges and aurorae are treated in other volumes of the series. It is as well to point out that unlike the earlier *Handbuch der Physik* this new series does not attempt to deal with the details of experimentation.

The volume is expensive for the individual worker, but it contains a wealth of up-to-date information and is beautifully produced and well illustrated with photographs and line diagrams. A large number of references is given in each chapter and the book is provided with an excellent index.

W. E. J. FARVIS

J. W. HORTON: **Fundamentals of Sonar.** U. S. Naval Institute, Annapolis, Md., 1957. 387 pp., $10.00.

THE author of this book has directed his efforts particularly to the needs of engineers and naval officers who are actively engaged in underwater sound operations. In order to use their apparatus effectively, they must be trained in the principles of wave motion and sound, in the properties of the medium in which they operate and the interpretation of the results they obtain by the use of the equipment supplied to then. Research, design and development are only of incidental interest; the understanding of the behaviour of their tools and environment is paramount. The author accomplishes his mission with completeness and distinction.

The first third of the book discusses in detail the nature and propagation of underwater sound. The selection and organization of material are very carefully done; a judicious balance is maintained between theory and practical details; the exposition and diagrams are excellent. Sufficient historical background is presented to orient the subject and actual field conditions are described at times to arouse and maintain interest. The description of the difficulties to the conduct of sound experiments encountered in Chesapeake Bay due to the presence of croakers is fascinating reading. An outstanding characteristic of the writing is the care bestowed on definitions of terms used in sonar. For example, acoustic impedance is defined, initially, wholly in terms of sound and wave motion and is treated as a sound concept complete in itself; it is not until much later in the book, when certain calculations are made, that the analogy is drawn between it and the impedance of an alternative current circuit. The whole subject of reflection, refraction and sound channels in water is covered in an outstanding manner, the presentation being by far the best that I have seen. This part of the book should be required reading by all who teach sound and wave motion. It should appeal too to geophysicists and especially to seismologists.

The remaining two thirds of the book are devoted to practical details of the operation of sonar equipment. The successive chapter headings illustrate the range of topics covered: Transducers; Transducer Systems; Indicators and Recorders; Direct Listening; Fundamental Factors in Echo Ranging. The descriptions and discussions are clear, precise and convincing and embrace all the important aspects of the field.

W. A. LYNCH

VOL.
13
1958/5

Advances in Geophysics, Vol. 4. Edited by H. E. LANDSBERG and J. VAN MIEGHEM. Academic Press Inc., New York, 1958. 456 pp.

THIS volume contains five geophysical monographs by five separate authors. As one of the editors states in the foreword, the International Geophysical Year, and the public interest it has stimulated, has served to promote "a once rather obscure area of science into the limelight". At the same time the IGY has exposed the professional need for up-to-date review articles on different aspects of geophysics, delineating the frontiers which may well be extended as the vast effort of the years 1957/8 is first undertaken and subsequently understood. These five monographs have been prepared to meet just such a need. There is an article on "Atmospheric Chemistry" by CHRISTIAN E. JUNGE; one by JOSEPH W. CHAMBERLAIN on "Theories of the Aurora"; one by LINCOLN LAPAZ on "The Effects of Meteorites upon the Earth (including its Inhabitants, Atmosphere and Satellites)"; one by J. LEITH HOLLOWAY Jr., on the "Smoothing and Filtering of Time Series and Space Fields"; and a final article by PAUL J. MELCHIOR on "Earth Tides". The average extent of each monograph amounts to about 100 pages; and, since mathematics is not evaded, there being no attempt to effect a popular treatment, the articles merit the close attention of specialist workers in these respective fields.

Each article is comprehensive in treatment with a full bibliography and the volume must surely be an essential addition to any geophysical library. Yet the authors have not all succeeded in being entirely judicial. The author of the article on meteorites, for example, gives a biased account of the hyperbolic meteor velocity controversy; while the author of the article on the treatment of geophysical time series studiously omits any mention of the classical work of Bartels, for example, on recurrence tendencies.

E. V. APPLETON

Journal of Atmospheric and Terrestrial Physics, 1959, Vol. 13, pp. 385 to 387. Pergamon Press Ltd. Printed in Northern Ireland

Indices of geomagnetic activity

of the Observatories at HARTLAND (*Ha*), ESKDALEMUIR (*Es*), LERWICK (*Le*)
July to September 1958

The figures give on pages 385 to 387 represent the K-indices for three-hour intervals, beginning with 00–03 hrs for the first and ending with 21–24 hrs for the eighth figure.

July 1958

Day	*Ha* Range for $K = 9 : 500\gamma$		*Es* Range for $K = 9 : 750\gamma$		*Le* Range for $K = 9 : 1000\gamma$		*Day*
	K-Indices	*Sum*	*K-Indices*	*Sum*	*K-Indices*	*Sum*	
1	4333 3331	21	4332 3322	22	5332 3312	22	1
2	0111 2332	13	1111 3232	14	1112 3223	15	2
3	3133 2432	21	2122 3432	19	3222 3433	22	3
4	1333 3533	24	2233 4543	26	2243 5543	28	4
5	3223 3323	21	2222 3234	20	2212 3323	18	5
6	2220 1210	10	2111 1210	9	3312 2220	15	6
7	0123 4343	20	1223 4443	23	1123 3333	19	7
8	2287 7979	51	2277 8999	53	3366 8979	51	8
9	5544 5534	35	7555 5535	40	6776 4426	42	9
10	4322 2223	20	4422 3223	22	6423 3323	26	10
11	3222 2243	20	3223 3343	23	4432 3343	26	11
12	4334 3431	25	4334 3432	26	3334 3432	25	12
13	3342 1414	22	3332 2413	21	3332 3423	23	13
14	3333 2321	20	3333 2321	20	3432 2422	22	14
15	1211 2222	13	1212 2122	13	2222 3222	17	15
16	2221 2323	17	2221 2213	15	3212 3323	19	16
17	4443 2210	20	3443 2320	21	3433 2221	20	17
18	3343 5543	30	2343 5543	29	2343 4444	28	18
19	2342 2244	23	2343 3244	25	3342 3245	26	19
20	4433 3432	26	4433 3432	26	4433 3422	25	20
21	3332 3665	31	3333 3665	32	3232 3576	31	21
22	4332 5431	25	4323 5432	26	3323 3221	19	22
23	1122 3112	13	1122 3122	14	1112 3112	12	23
24	3311 4533	23	2222 4533	23	2212 4433	21	24
25	2233 3444	25	2233 4443	25	2233 5444	27	25
26	4223 2122	18	4322 2132	18	4323 1221	18	26
27	2333 4243	24	2333 4243	24	2333 5355	29	27
28	4231 1123	17	3221 2233	18	4222 2222	18	28
29	2201 2242	15	2212 3342	19	1211 2132	13	29
30	2123 3434	22	2233 3433	23	1222 3433	20	30
31	2122 2532	19	2113 2532	19	2122 2542	20	31

August 1958

Day	*Ha* Range for $K = 9 : 500\gamma$			*Es* Range for $K = 9 : 750\gamma$			*Le* Range for $K = 9 : 1000\gamma$			*Day*
	K-Indices		*Sum*	*K-Indices*		*Sum*	*K-Indices*		*Sum*	
1	2214	4333	22	2114	4343	22	2122	4232	18	1
2	2223	3322	19	2223	4332	21	1223	3332	19	2
3	3322	2210	15	3322	3221	18	3221	3221	16	3
4	1111	1210	8	1222	2221	14	1222	2221	14	4
5	1101	2211	9	1112	3221	13	1122	3111	12	5
6	1201	1222	11	1112	1222	12	1222	2222	15	6
7	1122	3331	16	1132	4331	18	1122	4332	18	7
8	1111	3301	11	1112	2311	12	1112	2211	11	8
9	2211	2323	16	2211	2322	15	2211	2222	14	9
10	2233	3433	23	2133	3443	23	2123	4433	22	10
11	3333	2233	22	3233	2333	22	2223	3332	20	11
12	2223	1133	17	2223	2132	17	2232	2132	17	12
13	3233	2311	18	3233	2321	19	3233	2311	18	13
14	2221	1333	17	2121	1323	15	1122	1334	17	14
15	2322	2321	17	2322	2322	18	4222	2221	17	15
16	4332	3431	23	4222	3431	21	3222	2331	18	16
17	0164	6674	34	1154	6665	34	1143	6677	35	17
18	3343	3321	22	5333	3322	24	6433	3222	25	18
19	3323	2322	20	2333	2332	21	2323	2332	20	19
20	1121	2221	12	1122	3321	15	2222	2211	14	20
21	1103	2222	13	1113	2323	16	1112	2213	13	21
22	5553	4332	30	4444	3331	26	6543	2322	27	22
23	0333	3323	20	1333	3333	22	1332	2332	19	23
24	6655	5432	36	6656	5432	37	8855	5432	40	24
25	4332	4221	21	3333	4231	22	4332	4221	21	25
26	1333	3232	20	2333	3232	21	1333	3232	20	26
27	3555	4453	34	3455	4463	34	3556	4464	37	27
28	1132	2332	17	1133	3332	19	1233	4342	22	28
29	2233	3233	21	2223	3333	21	2223	3233	20	29
30	2223	3222	18	2222	3322	18	2221	3322	17	30
31	1221	2310	12	1111	2310	10	1211	2322	14	31

September 1958

1	0013	3310	11	0023	2311	12	1123	3321	16	1
2	1112	2110	9	1122	2211	12	1222	2211	13	2
3	2244	5555	32	2134	6556	32	3234	5677	37	3
4	4433	5878	42	4333	6998	45	6333	7889	47	4
5	6643	2453	33	9744	3352	37	8843	3453	38	5
6	2222	3211	15	2212	2321	15	3121	2321	15	6
7	1222	2343	19	1222	3344	21	2222	4456	27	7
8	4223	2315	22	4323	2425	25	5532	2416	28	8
9	3223	4334	24	3233	4434	26	5333	5435	31	9
10	3222	3323	20	3222	3323	20	3332	3323	22	10
11	2222	1221	14	2212	2221	14	3212	2222	16	11
12	2112	1210	10	2212	1210	11	2122	2211	13	12

VOL.
13
1958/5

September 1958 (*contd.*)

Day	*Ha* *Range for K = 9 : 500γ*			*Es* *Range for K = 9 : 750γ*			*Le* *Range for K = 9 : 1000γ*			*Day*
	K-Indices		*Sum*	*K-Indices*		*Sum*	*K-Indices*		*Sum*	
13	0011	1211	7	1121	2221	12	0122	2121	11	13
14	0022	1111	8	0133	2221	14	0133	3111	13	14
15	0013	2232	13	0122	2332	15	1123	2232	16	15
16	3334	4444	29	3334	5554	32	2333	5564	31	16
17	3323	3211	18	3332	3211	18	5322	3211	19	17
18	0002	1221	8	1211	2221	13	1112	2221	12	18
19	0012	2011	7	1022	3111	11	1112	2111	10	19
20	1111	1122	10	0111	1122	9	1111	1112	9	20
21	1011	1121	8	1111	1221	10	1011	1111	7	21
22	1001	1121	7	1012	1221	10	1011	1121	8	22
23	1122	0013	10	2112	2113	13	1121	1113	11	23
24	2001	2113	10	3101	2212	12	3111	2113	13	24
25	4454	5556	38	3444	5656	37	3445	6678	43	25
26	4433	3333	26	4332	3323	23	6633	3333	30	26
27	2112	2223	15	1112	2223	14	3122	2223	17	27
28	3322	2200	14	3322	2210	15	3221	1211	13	28
29	0123	2000	8	1122	2000	8	0122	2111	10	29
30	2013	3354	21	1113	3354	21	1013	3454	21	30

OL.
13
8/59

Papers to be published in future issues

W. R. French, Jr. and R. L. Chasson: Atmospheric effects on the hard component of cosmic radiation near sea level

A. A. Weiss: The limitations of narrow-beam radio equipments in the detection of weak meteor showers

R. G. Rastogi: Geomagnetic influence on the *F1*- and *F2*-regions of the ionosphere—Effect of solar activity

J. W. King: Ionospheric self-demodulation and self-distortion of radio waves

J. E. Titheridge: Ray paths in the ionosphere. Approximate calculations in the presence of the earth's magnetic field

G. C. Reid and C. Collins: Observations of abnormal VHF radio wave absorption at medium and high latitudes

L. A. Manning: Oblique echoes from over-dense meteor trails

B. Ramachandra Rao and E. Bhagiratha Rao: Study of horizontal drifts in the *F1*- and *F2*-regions

L. Haring and J. Tröim: Determination of the angle of arrival of auroral echoes

W. N. Abbot and S. Chapman: On the aurora of 19 August 1950, photographed from Greece

L. Thomas: Some measurements of horizontal movements in region-*F2* using widely spaced observing stations

G. McK. Allcock: The electron density distribution in the outer ionosphere derived from whistler data

R. Montalbetti: Photoelectric measurements of hydrogen emissions in aurorae and air glow

C. M. Minnis and G. H. Bazzard: Some indices of solar activity based on ionospheric and radio-noise measurements

C. H. CUMMACK: Chapman behaviour in the lower ionosphere

G. S. KENT: High-frequency fading observed on the 40 Mc/s wave radiated from artificial satellite 1957α

G. S. AITCHISON and K. WEEKES: Some deductions of ionospheric information from the observations of emissions from satellite 1957α 2—I. The theory of the analysis

G. S. AITCHISON *et al.*: Some deductions of ionospheric information from the observations of emissions from satellite 1957α 2—II. Experimental procedure and results

C. A. VENTRICE and E. R. SCHMERLING: Coefficients for the rapid reductions of L'–F records to N–h profiles without computing aids

E. L. HAGG *et al.*: Spiral occurrence of sporadic-E

F. HEPBURN: Interpretation of smooth-type atmospheric wave forms

M. W. McELHINNY: Some further analyses of E-layer measurements in South Africa during the solar eclipse of 25 December 1954

C. S. WARWICK and R. T. HANSEN: Geomagnetic activity following large solar flares

W. H. WARD: On the origin of terrestrial particles from solar flares

V. A. BAILEY: Some possible effects caused by strong gyro waves in the ionosphere—I

M. H. REES: Absolute photometry of the aurora—I

M. H. REES: Absolute photometry of the aurora—II

P. C. CLEMMOW and M. A. JOHNSON: A contribution to the theory of the motion of weak irregularities in the ionosphere

W. J. G. BEYNON and G. M. BROWN: Geomagnetic distortion of region-E

G. F. WALTON: Calculation of the vertical distribution of atmospheric ozone

N. F. BARBER and D. D. CROMBIE: VIF reflections from the ionosphere in the presence of a transverse magnetic field

L. G. H. HUXLEY: A discussion of the motion in nitrogen of free electrons with small energies, with reference to the ionosphere

J. M. MALVILLE: Type B aurorae in the Antarctic

W. BECKER: New methods and some results concerning true ionospheric height calculation

P. BANDYOPADHYAY: The early morning $E2$-layer and some evidence of pre-sunrise F-layer splitting

W. L. PRICE: Anomalous ionospheric reflection during solar eclipses

J. D. WHITEHEAD: Sudden changes in the virtual height of radio waves reflected from the E-region of the ionosphere

M. D. VICKERS: The effect of the $F1$-layer on the calculation of the height of the $F2$-layer

F. MARIANI: A new theoretical model of the composite F-layer

C. A. ONWUMECHILLI and N. S. ALEXANDER: Variations in the geomagnetic field at Ibadan, Nigeria—I. Solar variations

C. A. ONWUMECHILLI and N. S. ALEXANDER: Variations in the geomagnetic field at Ibadan, Nigeria—II. Lunar and luni-solar variations in H and Z

E. WOYK: The refraction of radio waves by a spherical ionized layer

A. J. FERRARO and J. J. GIBBONS: Polarization by means of the multislab approximation

B. N. SINGH and R. L. RAM: Rhythmic fading of short-wave radio signals

A. G. McNAMARA and D. W. R. McKINLEY: The effect of trail irregularities on the interpretation of meteor echoes

K. C. CLARK and A. E. BELON: Spectroscopic observations of the great aurora of 10 February 1958—I. Abnormal vibration of N_2^+

K. C. CLARK and A. E. BELON: Spectroscopic observations of the great aurora of 10 February 1958—II. Unusual atomic features

M. L. MEEKS and J. C. JAMES: Meteor radiant distributions and the radio-echo rates observed by forward scatter

E. A. LYTLE and D. M. HUNTEN: The ratio of sodium to potassium in the upper atmosphere

J. F. NOXON, A. W. HARRISON and A. VALLANCE JONES: The infrared spectrum of the night airglow from 1·4 μ to 4·0 μ

G. KVIFTE: Auroral and nightglow observations at Ås, Norway

VOL
13
1958/

VOL.
13
58/59